# Improvement of Nonlinear Static Seismic Analysis Procedures

## FEMA 440

*June 2005*

FEMA

nehrp

# FEMA 440
# IMPROVEMENT OF NONLINEAR STATIC SEISMIC ANALYSIS PROCEDURES

Prepared by:

ATC

Applied Technology Council (ATC-55 Project)

201 Redwood Shores Parkway, Suite 240
Redwood City, California 94065

Prepared for:

Department of Homeland Security
Federal Emergency Management Agency

Washington, D.C.

*June, 2005*

## Notice

# Forward

One of the primary goals of the Department of Homeland Security's Federal Emergency Management Agency (FEMA) and the National Earthquake Hazards Reduction Program (NEHRP) is to encourage design and building practices that address the earthquake hazard and minimize the resulting damage. This document, *Improvement of Nonlinear Static Seismic Analysis Procedures* (FEMA 440), reaffirms FEMA's ongoing efforts to improve the seismic safety of new and existing structures in this country.

The primary goal of this project was the evaluation and improvement of the nonlinear static procedures (NSPs) contained in the *Prestandard and Commentary for Seismic Rehabilitation of Buildings* (FEMA 356) and in the Applied Technology Council ATC-40 report, *Seismic Evaluation and Retrofit of Concrete Buildings*, and the development of guidance on when and how each methodology should be used to avoid conflicting answers. FEMA initiated this project with ATC based on reports of discrepancies between the two NSP methodologies. However, in the course of this project, several improvements to both procedures were also identified and we thought it in the best interests of the earthquake engineering community to capture those improvements as part of this state-of-the-art resource document.

There are some potential differences between this document and other FEMA-sponsored products, such as the FEMA 356-based *Standard for the Seismic Rehabilitation of Existing Buildings* currently being developed by the American Society of Civil Engineers (ASCE-41) and FEMA's *HAZUS* standardized loss estimation methodology, which uses the procedures of ATC-40 in its fragility functions. Some of this document's recommendations concerning NSPs could bias selection of analysis procedures to linear static procedures (LSPs) unless similar modifications are also made to the LSPs. These differences are primarily for short-period structures, and should not affect the ongoing use of those current products. This document is a resource guide to capture the current state of the art for improved understanding of NSPs and to generate future improvements to those products, and as such, should not take precedence over those products.

Looking ahead, FEMA is already funding ATC to perform additional studies of the cyclic and in-cycle stiffness and strength degradation nonlinear models and their impact on response and response stability. Future FEMA-funded ATC studies will focus on the differences between linear and nonlinear design for short-period buildings and on soil-structure interaction. The results of these studies should be available within the next four years, within the time frame for submittal to a future update of ASCE 41.

FEMA is proud to have sponsored the development of this resource document through ATC. We are particularly grateful for work done by Project Director Craig Comartin, the Project Management Committee, the Project Review Panel, the Project Focus Groups and Working Groups, and all of the other contributors who made this document possible. FEMA also wishes to acknowledge the National Science Foundation (NSF) for their funding provided through the Pacific Earthquake Engineering Research Center (PEER) for the investigation of short-period building response and soil-structure interaction. We also wish to acknowledge the NSF funding of the research of Andrew Guyader on equivalent linearization and the NATO science fellowship from the Scientific Research and Technical Council of Turkey that partially funded research by Sinan Akkar. This project is an excellent example of the interagency cooperation that is made possible through the NEHRP. All of the individuals involved in this project are listed at the end of this document, and FEMA gratefully appreciates their involvement. This product would not have been possible without their dedication and professionalism.

Federal Emergency Management Agency

# Preface

Knowledgeable engineers have long recognized that the response of buildings to strong ground shaking caused by earthquakes results in inelastic behavior. Until recently, most structural analysis techniques devised for practical application relied on linear procedures to predict the seismic behavior of buildings. With the publication of the ATC-40 Report, *Seismic Evaluation and Retrofit of Concrete Buildings*, in 1996, the FEMA 273 Report, *Guidelines for the Seismic Rehabilitation of Buildings*, in 1997, and the FEMA 356 Report, *Prestandard and Commentary for the Seismic Rehabilitation of Buildings* (which replaced FEMA 273), in 2000, nonlinear static analysis procedures became available to engineers providing efficient and transparent tools for predicting seismic behavior of structures.

Both the ATC-40 and FEMA 356 documents present similar performance-based engineering methods that rely on nonlinear static analysis procedures for prediction of structural demands. While procedures in both documents involve generation of a "pushover" curve to predict the inelastic force-deformation behavior of the structure, they differ in the technique used to calculate the inelastic displacement demand for a given ground motion. The FEMA 356 document uses the Coefficient Method, whereby displacement demand is calculated by modifying elastic predictions of displacement demand. The ATC-40 Report details the Capacity-Spectrum Method, whereby modal displacement demand is determined from the intersection of a capacity curve, derived from the pushover curve, with a demand curve that consists of the smoothed response spectrum representing the design ground motion, modified to account for hysteretic damping effects.

The publication of the above cited documents resulted in the widespread use of these two methods, and engineers have since reported that the two procedures often give different estimates for displacement demand for the same building. Hence the Applied Technology Council (ATC) proposed to the Federal Emergency Management Agency (FEMA) in 2000 that a study be conducted to determine the reasons for differing results and to develop guidance for practicing engineers on improved application of these two methods. FEMA agreed to fund the investigation, and in October 2000, ATC commenced a project to provide guidance for improved applications of these two widely used inelastic seismic analysis procedures (ATC-55 Project).

The ATC-55 Project had two objectives: (1) the development of practical recommendations for improved prediction of inelastic structural response of buildings to earthquakes (i.e., guidance for improved application of inelastic analysis procedures) and (2) the identification of important issues for future research. Intended outcomes of the project included:

1. Improved understanding of the inherent assumptions and theoretical underpinnings of existing and proposed updated inelastic analysis procedures.
2. Recognition of the applicability, limitations, and reliability of various procedures.
3. Guidelines for practicing engineers to apply the procedures to new and existing buildings.
4. Direction for researchers on issues for future improvements of inelastic analysis procedures.

The project was conducted in three phases over a 3-year time span. Phase 1 consisted of the assembly and refinement of important issues relating to the improvement of inelastic seismic analysis procedures. Activities included (1) the solicitation of input from researchers and practicing engineers, and (2) the development of study models of typical buildings to stimulate discussion, facilitate analytical studies, and provide example applications. Phase 2 consisted of analytical studies to explore selected key issues, the generation of written discussions on important topics, and the development of examples of the application of inelastic analysis procedures. This phase also included assembly of guidelines for the improved practical implementation of the procedures. Phase 3 consisted of the report development process, under which this document was drafted, reviewed, and finalized.

This report (FEMA 440) is the final and principal product of the ATC-55 Project. The document has three specific purposes: (1) to provide guidance directly applicable to the evaluation and design of actual structures by engineering practitioners; (2) to facilitate a basic conceptual understanding of underlying principles as well as the associated capabilities and limitations of the procedures; and (3) to provide additional detailed information used in the development of the document for future reference and use by researchers and others.

A wide variety of personnel participated in the project. The project was conducted under the direction of ATC Senior Consultant Craig Comartin, who served as Project Director. Technical and management direction were provided by a Project Management Committee consisting of Craig Comartin (Chair), Christopher Rojahn (Ex-Officio member), Ronald O. Hamburger, William T. Holmes, Wilfred D. Iwan, Jack P. Moehle and Jonathan Stewart. A Project Review Panel, identified by ATC with input from FEMA, provided overview and guidance; this Panel consisted of Anthony B. Court (ATC Board Representative), Leonard Joseph, Daniel Shapiro, Steve Sweeney, Chia-Ming Uang, and Michael Valley.

The Project Management Committee created four Focus Groups to assist in developing findings on the following specific subtopics: (1) displacement modification; (2) equivalent linearization; (3) multi-degree-of-freedom effects; and (4) response of short-period buildings, with a specific focus on soil-structure interaction. The purpose of the Focus Groups was to gather fresh perspective from qualified sources that were not directly responsible for the project planning or the resulting recommendations. Focus Group participants reviewed draft materials developed by the project team. They then attended a one-day meeting with representative members of the Project Management Committee and the project team members responsible for the subject materials. The meetings allowed for a constructive discussion of the subject in general and critical feedback – positive and negative – on the draft materials. Focus Group members were also afforded an opportunity to comment on the final draft of materials related to their area of expertise. It is important to note that Focus Group members were not asked to endorse the project process or the recommendations in documents developed as part of the ATC-55 Project. These remain the responsibility of ATC and the Project Management Committee.

Each Focus Group consisted of three members. John Hooper, Gregory A. MacRae, and Stephen A. Mahin were members of the Focus Group on Displacement Modification. The Focus Group on Equivalent Linearization consisted of Terrance Paret, Graham Powell, and Andrew S. Whittaker. Anil K. Chopra, Jon A. Heintz, and Helmut Krawinkler served on the Focus Group on Multi-Degree-of-Freedom Effects, and Jacobo Bielak, Gregory L. Fenves, and James Malley served on the Focus Group on Soil-structure Interaction.

Detailed work on the project was carried out by several Working Groups appointed by the Project Management Committee. The Phase 1 Project Working Group consisted of Joseph R. Maffei (Group Leader), Mark Aschheim, Maureen Coffey, and Mason T. Walters. The Phase 2 Project Working Group consisted of Sinan Akkar, Mark Aschheim, Andrew Guyader, Mehmet Inel, Eduardo Miranda, Junichi Sakai, Jorge Ruiz-Garcia, Tjen Tjhin and Tony Yang. Peter N. Mork produced and formatted the electronic files from which this report was printed.

The affiliations of the project personnel identified above are provided in the list of Project participants.

The Applied Technology Council gratefully acknowledges the cooperation, insight and patience provided by the FEMA Project Officer, Michael Mahoney, and the FEMA Technical Monitor, Robert D. Hanson. ATC also gratefully acknowledges the National Science Foundation (NSF)for supplemental funding provided through the Pacific Earthquake Engineering Research Center to conduct the investigation of the response of short-period buildings, soil-structure-foundation interaction, and application of the proposed methods. NSF also provided funding for the research of Andrew Guyader on equivalent linearization. A NATO science fellowship from the Scientific Research and Technical Council of Turkey provided partial support for research by Sinan Akkar.

Christopher Rojahn
ATC Executive Director

# Executive Summary

This document records in detail an effort to assess current nonlinear static procedures (NSP) for the seismic analysis and evaluation of structures. In addition, the document presents suggestions that were developed to improve these procedures for future application by practicing engineers. The elements of work included several analytical studies to evaluate current procedures and to test potential improvements. An extensive review of existing pertinent technical literature was compiled. A survey of practicing engineers with experience in applying nonlinear static procedures was also conducted. Expert practitioners and researchers in appropriate fields worked together to develop the proposed improvements presented in this document. The context for the work was provided by two existing documents, the FEMA 356 *Prestandard and Commentary for the Seismic Rehabilitation of Buildings,* and the ATC-40 report, *Seismic Evaluation and Retrofit of Concrete Buildings*, each of which contain procedures for nonlinear static analysis. These procedures were both evaluated and suggestions for improvement are made for each. Not all of the portions of the two current documents (FEMA 356 and ATC-40) were evaluated. Conclusions regarding the relative accuracy or technical soundness of these documents should not be inferred beyond the specific material and discussions contained in this document.

## 1. Overview of Inelastic Seismic Analysis Procedures

Nonlinear static procedures are one type of inelastic analysis that can be used to estimate the response of structures to seismic ground shaking. The differences between the various approaches relate to the level of detail of the structural model and the characterization of the seismic ground shaking. Detailed structural models can often be simplified into equivalent multi-degree-of-freedom (MDOF) models; or, in some cases, single-degree-of-freedom (SDOF) oscillator models, as with nonlinear static procedures. The most detailed characterizations of seismic ground motion are actual ground motion records that comprise accelerations, velocities, and displacements expected at the ground surface at a specific site. A simplification can be made by representing the effects ground motion has in the frequency domain with response spectra that plot maximum response of an elastic SDOF oscillator as a function of period. This is the type of characterization normally used for nonlinear static procedures.

The discussion provided in Chapter 2 includes basic descriptions of the two nonlinear static procedures that currently are used in practice. FEMA 356 utilizes a displacement modification procedure (Coefficient Method) in which several empirically derived factors are used to modify the response of a single-degree-of-freedom model of the structure assuming that it remains elastic. The alternative Capacity-Spectrum Method of ATC-40 is actually a form of equivalent linearization. This technique uses empirically derived relationships for the effective period and damping as a function of ductility to estimate the response of an equivalent linear SDOF oscillator.

## 2. Evaluation of Current Nonlinear Static Procedures

In practice, the current procedures can result in estimates of maximum displacement that are significantly different from one another. This has caused concern on the part of practicing engineers. One of the major objectives of the project was to ascertain the reason for these differences and to try to correct both procedures to produce similar results. Chapter 3 documents a comprehensive evaluation of both current procedures. The basic technique was to develop a series of nonlinear single-degree-of-freedom oscillators of varying period, strength, and hysteretic behavior. These were subjected to ground motion representing different site soil conditions. The resulting database of approximately 180,000 predictions of maximum displacement was used as a benchmark to judge the accuracy of the approximate nonlinear static procedures. This was accomplished by comparing the estimates for each oscillator from both nonlinear static procedures to the results of the nonlinear response history analyses. Differences in the two estimates were compiled and compared in a statistical study.

## 3. Strength Degradation

The results of the evaluation of the nonlinear static procedures suggest that both procedures would benefit from greater clarity with respect to the different types of possible degradation in structures subject to seismic shaking. This is particularly critical for degradation in strength. Chapter 4 presents a discussion of the differences between the consequences of strength loss within a single cycle of deformation (in-cycle) and that which occurs in subsequent cycles (cyclic). In-cycle strength degradation, including that associated with $P$-$\Delta$

effects, can lead to dynamic instability. To account for this, a limitation on the strength of a structure is suggested for use with nonlinear static procedures. The limit is a function of the period of the structure and the post-elastic stiffness characteristics as modified for in-cycle strength degradation. If the structure has less strength than the limit, nonlinear dynamic analysis is recommended.

### 4. Improved Procedures for Displacement Modification

Based on the evaluation of nonlinear static procedures, Chapter 5 proposes modifications to the Coefficient Method of FEMA 356. The suggestions relate primarily to the coefficients themselves. Improved relationships for coefficients $C_1$ and $C_2$ are proposed. It is also suggested that the coefficient $C_3$ be replaced with a limitation on minimum strength as suggested in the previous section.

### 5. Improved Procedures for Equivalent Linearization

Chapter 6 presents the results of an effort to improve the practical application of equivalent linearization procedures. The resulting suggestions focus upon improved estimates of equivalent period and damping. This chapter also includes an optional adjustment to generate a modified acceleration-displacement response spectrum (MADRS) that does intersect the capacity spectrum at the Performance Point. Similar to the current ATC-40 procedure, the effective period and damping are both dependent on ductility and consequently an iterative or graphical technique is required to calculate the Performance Point. Several options are outlined in Chapter 6. In application, the improved procedures are similar to the current ATC-40 Capacity-Spectrum Method.

### 6. Evaluation and Comparison of Improved Nonlinear Static Procedures

The improved procedures were evaluated in an independent study. This study, summarized in Chapter 7, utilized nine elastic-perfectly-plastic oscillators with three different periods and three different strengths. These were subjected to thirteen ground motions for class C sites. Estimates of maximum displacements were calculated utilizing both current procedures and the proposed improved procedures.

This study was not comprehensive enough to make broad general conclusions. However, a number of key observations can be made:

- The improved procedures do not exhibit large differences between displacement modification and equivalent linearization approaches.
- The improved procedures also produced more accurate estimates of displacements when compared to response history analysis (also known as time-history analysis) results than those produced by the current nonlinear procedures.
- Improved procedures also seem to work well, at least for the case that was studied, in estimating maximum displacement response in conjunction with a design spectrum.
- The results of the evaluation of the improved nonlinear procedures illustrate the dispersion of results from nonlinear response history analysis using design level ground motions.

### 7. Soil-Structure Interaction Effects

Chapter 8 presents procedures to incorporate soil-structure interaction (SSI) into nonlinear static analyses. The objective is to replace the judgmental limits with rational technical justifications for reducing seismic demand. These SSI techniques address the following issues.

- radiation and material damping in supporting soils;
- response reduction resulting from structure embedment in the ground (i.e., full and partial basements); and
- incoherent ground-motion input to buildings with relatively large plan dimensions.

The basic principles used for the development of the SSI procedures for damping in Chapter 8 have been included in the FEMA 368 *NEHRP Recommended Provisions for Seismic Regulations for New Buildings and Other Structures* (BSSC, 2000)[1] for the linear analysis and design of new buildings for a number of years. They have been adapted for use with inelastic procedures. Both the damping and ground motion procedures are applicable to both the displacement modification and equivalent linearization forms of nonlinear static analysis.

1.Superseded in 2003 with the FEMA 450 *Recommended Provisions for Seismic Regulations for New Buildings and Other Structures.*

## 8. Multiple-Degree-of Freedom Effects

Chapter 9 reviews the accuracy and practical implications of the requirements of ATC-40 and FEMA 356 related to MDOF effects including:

1. current options for load vectors, and
2. the conversion of a MDOF pushover curve to an equivalent SDOF system.

The results of a comprehensive study of five example buildings that examines the differences in response predicted using various options compared to a common nonlinear dynamic analyses benchmark are also summarized. The results are consistent with previous research. Practical implications are:

- Nonlinear static procedures generally provide reliable estimates of maximum floor and roof displacements.
- Nonlinear static procedures are not particularly capable, however, of accurate prediction of maximum story drifts, particularly within flexible structures.
- Nonlinear static procedures are very poor predictors of story forces, including shears and overturning moments.
- The use of the first mode load vector is suggested due to the relatively good displacement estimates made with this assumption.
- Multi-mode pushover analysis consisting of the use of multiple load vectors proportional to the mode shapes of the structure and combining them statistically shows promise in producing better estimates in inter-story drifts over the heights of the buildings.
- The provisions of FEMA 356 as to when higher modes are to be considered significant are not particularly reliable.
- Specific limitations as to when nonlinear static procedures produce reliable results are elusive.
- As a result of the study it was observed that, in many cases, a single time history response of a multi-degree-of-freedom model gave better indications of drifts and story forces than any of the approximate single-degree-of-freedom estimates.

## 9. Important Future Developments

The proposed improvements to nonlinear static analysis procedures in this document will lead to better results in practice. Nonetheless, not all of the shortcomings of NSP's have been addressed. In developing the improvements a number of important observations about the need for future develop and improvement of inelastic seismic analysis procedures have emerged. These include the need for additional developmental work on:

1. Nonlinear Modeling for Cyclic and In-Cycle Degradation of Strength and Stiffness
2. Soil and Foundation Structure Interaction
3. Nonlinear Multi-Degree of Freedom Simplified Modeling

## 10. Application Example

Chapter 10 includes an example application of the recommended nonlinear static analysis procedures on an example building. The application example includes a flowchart describing the implementation process, along with building plans, calculations, and commentary. The example illustrates both the displacement modification and the equivalent linearization procedures to estimate the maximum displacement of a building model.

# Table of Contents

# List of Figures

# List of Tables

# 1. Introduction

This report documents the results of a project for the Department of Homeland Security's Federal Emergency Management Agency (FEMA) by the Applied Technology Council (ATC) to evaluate and improve the application of simplified inelastic analysis procedures for use with performance-based engineering methods for seismic design, evaluation, and upgrade of buildings. Chapters 1 through 9 summarize the developmental efforts and results in concise language to facilitate application of the project findings in practice. Chapter 10 contains a summary and a practical application example using the improved procedures. Supporting information describing the project findings in detail are provided in the appendices.

This document has been published in two formats: (1) a printed version, which summarizes the developmental efforts and project findings and includes the application example (Chapters 1 through 10), and (2) a complete version of the report on CD-ROM (inside back cover), which includes all of the material in the printed version plus six appendices containing project results and findings. The printed version of the report is relatively brief to facilitate use by design professionals.

## 1.1 Background

During the past decade, significant progress has been made in performance-based engineering methods that rely on nonlinear static analysis procedures (NSPs). In 1996, ATC published the ATC-40 report, *Seismic Evaluation and Retrofit of Concrete Buildings*, which was developed with funding from the California Seismic Safety Commission. In a larger project funded by FEMA, ATC (under contract to the Building Seismic Safety Council) prepared the FEMA 273 *Guidelines for the Seismic Rehabilitation of Buildings*, and the companion FEMA 274 *Commentary*, which were published in 1997 by FEMA. Soon thereafter, the American Society of Civil Engineers (ASCE) prepared the FEMA 356 report, *Prestandard and Commentary for the Seismic Rehabilitation of Buildings* (the successor to FEMA 273/274*)*, which was published by FEMA in 2000. All of these documents present similar approaches. FEMA 273 and FEMA 356 use a procedure known as the Coefficient Method, and ATC-40 details the Capacity-Spectrum Method. The two approaches are essentially the same when it comes to generating a "pushover" curve to represent the inelastic force-deformation behavior of a building. They differ, however, in the technique used to calculate the inelastic displacement demand for a given representation of ground motion.

The development of this report was instigated by several factors. The use of NSPs in engineering practice has accelerated since the publication of ATC-40 and FEMA 356. Consequently, there is valuable information available on the practical application of these inelastic analysis procedures. In addition to experience with the initial application of these performance-based methods by practicing professionals, ongoing research promises important modifications, improvements, and alternatives to current NSPs.

There has also been a large national investment in performance-based engineering, because of the tangible prospect of vastly improving seismic design practices. The future effective use of performance-based engineering depends on the continued development of reliable and credible inelastic analysis procedures.

The intent of the ATC-55 project has been to gather the results of practical experience and relevant research and to develop guidance for improving the application of nonlinear static analysis procedures to both existing and new structures.

## 1.2 Project Purpose and Scope

The purpose of the ATC-55 project was to evaluate current NSPs, as described in FEMA 356 and ATC-40 and to develop improvements where feasible. The primary objectives were:

- to improve understanding of the inherent assumptions and theoretical underpinnings of existing and proposed new simplified analysis procedures;
- to recognize the applicability, limitations, and reliability of various procedures;
- to develop guidelines for practicing engineers on how to apply the procedures to new and existing buildings; and
- to provide direction for researchers on issues to consider for future improvements of simplified inelastic analysis procedures.

Project activities also were guided by the fact that engineers and researchers have similar concerns with

respect to inelastic analysis procedures. Some of the more prominent issues considered are listed below.

- In some cases, different nonlinear static procedures produce significantly different results for the same building model and ground motion representation.
- Current procedures for addressing the degradation of stiffness and strength in structures are ambiguous and unclear.
- The predicted response of short-period structures seems to be extreme when compared with observed performance.
- Since they are based on single-degree-of-freedom (SDOF) approximations, nonlinear static procedures may not reliably predict important response parameters for some multi-degree-of-freedom (MDOF) structures.

## 1.3 Report Scope, Organization and Contents

The document is intended to be useful from the practical, educational, and archival standpoints. Its fundamental purpose is to provide guidance that can be used directly by engineering practitioners. From an educational perspective, the report is intended to facilitate a basic conceptual understanding of underlying principles, as well as the associated capabilities and limitations of the procedures, so that practicing structural engineers can apply the procedures appropriately. Finally, the archival aspect recognizes that the development of inelastic procedures will continue, and that it is important to record detailed information from the project for future reference and use.

The scope of the evaluation of inelastic analysis procedures and the development of recommendations for improvement, as presented in this document, focus on nonlinear static procedures (NSPs). In light of the concerns identified by practicing engineers and researchers, the document specifically addresses the following questions:

- How well do current NSPs predict maximum global displacement (elastic plus inelastic)?
- How well do current NSPs predict effects arising from the multiple-degree-of-freedom (MDOF) response of structures?
- What modifications might be incorporated into NSPs to improve accuracy and to reduce uncertainty associated with the first two questions?

The initial phase of the project, during early 2001, focused on the identification and refinement of important issues related to the improvement of inelastic seismic analysis procedures. Activities included the solicitation of input from researchers (see Appendix A.) and practicing engineers (see Appendix B.). This information was used to formulate a plan for the subsequent phases of the project, comprising the evaluation of current procedures and the development of proposed improvements.

Several analytical efforts formed the basis for the evaluation of current procedures and the development of improvements. The first tested the accuracy of the Coefficient Method of FEMA 356 and the Capacity-Spectrum Method of ATC-40 in predicting global displacement demands, when compared to response-history analysis of SDOF oscillators. This effort is described in Chapter 3, with detailed results provided in Appendix C.

During evaluations of both the Coefficient Method and Capacity-Spectrum Method, it became evident that important clarifications regarding strength degradation are applicable to both NSP approaches. This issue is addressed in Chapter 4.

Improved procedures for use with the Coefficient Method are described in Chapter 5. Improved procedures for use with the Capacity-Spectrum Method, are described in Chapter 6. Supplementary information and data on the equivalent linearization approach are provided in Appendix D.

Chapter 7 describes an independent analysis that was implemented to test the accuracy of the procedural improvements described in Chapters 5 and 6. Comparisons with results using the original procedures are provided.

For many years, researchers have observed that the predicted inelastic displacement response of oscillators, with periods in excess of about 1 second, is often very similar to the predicted displacement response of elastic oscillators having the same period. This has led to the so-called “equal displacement approximation.” Researchers have also recognized that the predicted inelastic response of oscillators with short periods, less than approximately 0.5 seconds, are often significantly larger than the predicted response of elastic structures of the same period, particularly if the structures are both very stiff and very weak. When this principle is applied using nonlinear analysis techniques to the performance

evaluation of small, stiff buildings, such as those that comprise much of the building inventory in the United States, very poor performance and extreme damage is often predicted. This has created a paradox, in that such buildings have generally been observed to experience limited damage in past earthquakes. Several factors contribute to this conflict between predicted and observed performance of such structures, including:

- models used to predict performance of such structures commonly neglect many elements that contribute to their strength;
- fixed base models used to predict structural response neglect foundation flexibility, resulting in predictions of smaller periods than that of the actual structures;
- stiff buildings will experience small displacements even at large ductility demand and thus may experience only limited damage; and
- in addition to foundation flexibility, other soil-structure interaction effects can significantly reduce the response of some stiff structures to ground shaking.

In part, these effects can be addressed by more accurate analytical models that incorporate all structural and nonstructural elements significant to structural response as well as the flexibility of foundations. Soil-structure interaction effects are of particular importance. Chapter 8 describes analysis techniques for SSI effects that have been adapted for use with nonlinear static procedures and detailed supporting information on soil-structure interaction is provided in Appendix E.

Multi-degree-of-freedom effects are addressed in Chapter 9, which summarizes a comprehensive analysis of five example buildings to illustrate the application and limitations of simplified techniques to account for MDOF effects within current NSPs. Details are provided in Appendix F.

Finally, Chapter 10 comprises a complete summary of the results of the efforts and the suggested improvements from a practical perspective. Chapter 10 concludes with a detailed example application of the suggested improved procedures to a building structure.

# 2. Overview of Inelastic Seismic Analysis Procedures

Practicing engineers use inelastic analysis procedures for the seismic evaluation and design of upgrades of existing buildings and other structures, as well as design of new construction. The practical objective of inelastic seismic analysis procedures is to predict the expected behavior of the structure in future earthquake shaking. This has become increasingly important with the emergence of performance-based engineering (PBE) as a technique for seismic evaluation and design (ATC, 1996; BSSC, 2000). PBE uses the prediction of performance to inform decisions regarding safety and risk. For this purpose, PBE characterizes performance primarily in terms of expected damage to structural and nonstructural components and contents. Since structural damage implies inelastic behavior, traditional design and analysis procedures that use linear elastic techniques can predict performance only implicitly. By contrast, the objective of inelastic seismic analysis procedures is to directly estimate the magnitude of inelastic deformations and distortions.

The generic process of inelastic analysis is similar to conventional linear procedures in that the engineer develops a model of the building or structure, which is then subjected to a representation of the anticipated seismic ground motion (see Figure 2-1). The results of analysis are predictions of engineering demand parameters within the structural model that are subsequently used to determine performance based on acceptance criteria. The engineering demand parameters normally comprise global displacements (e.g., roof or other reference point), story drifts, story forces, component distortions, and component forces.

There are several basic inelastic analysis procedures that differ primarily on the types of structural models used for analysis and the alternatives for characterizing seismic ground shaking.

## 2.1 Structural Modeling

*Detailed structural models* for inelastic analysis are similar to linear elastic finite-element (component) models (see Figure 2-2). The primary difference is that

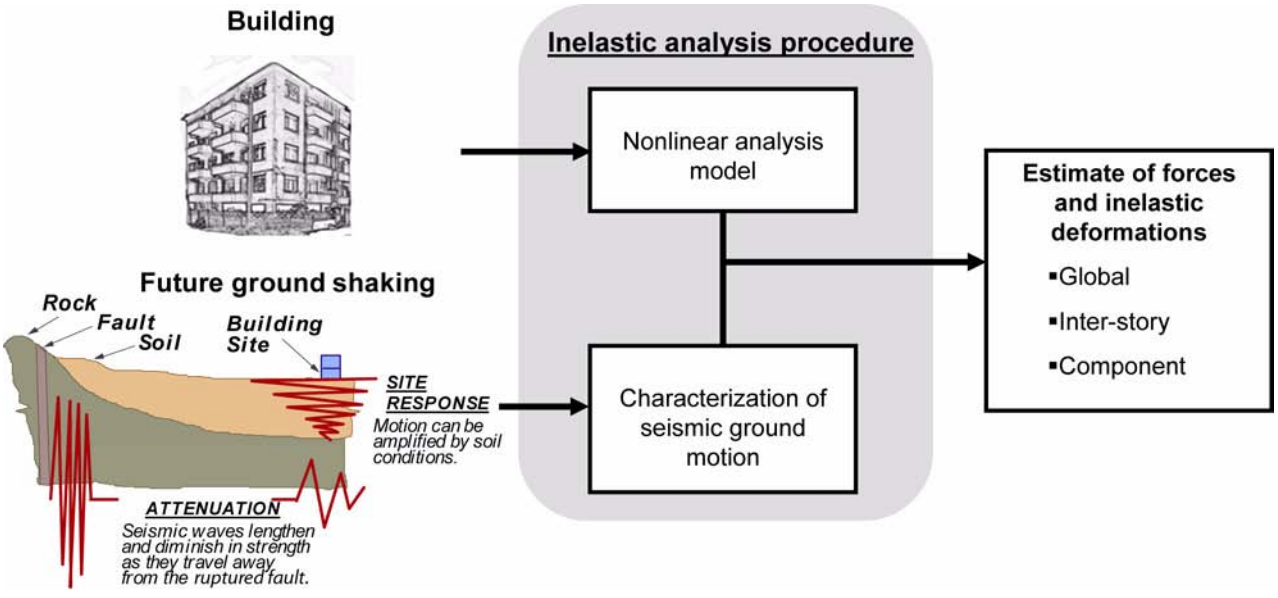


Figure 2-1 Schematic depiction of the use of inelastic analysis procedures to estimate forces and inelastic deformations for given seismic ground motions and a nonlinear analysis model of the building.

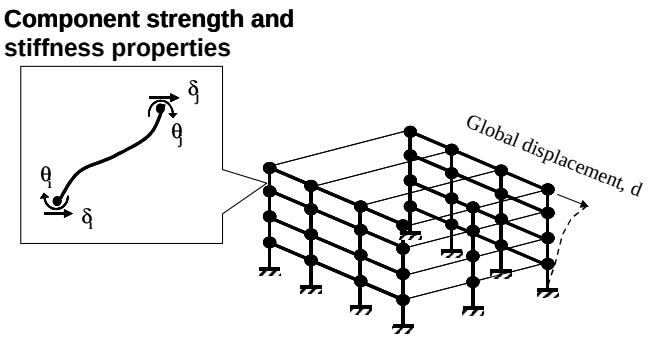


Figure 2-2 Schematic of a detailed 3-dimensional inelastic structural model developed from component properties.

the properties of some or all of the components of the model include post-elastic strength and deformation characteristics in addition to the initial elastic properties. These are normally based on approximations derived from test results on individual components or theoretical analyses (see Figure 2-3). Information of this type is tabulated in ATC-40 and FEMA 356. In many instances, it is important to include the structural and geotechnical components of the foundation in the analysis model.

As detailed as these models may be, they inevitably introduce approximations and associated uncertainties into the analysis process. In most instances with inelastic analysis, it is preferable to base the model on the best estimate of the expected properties of the structure. In this manner, the overall analysis results in the estimate of central values (e.g., median or mean) of engineering demand parameters with minimum bias. Subsequently, the engineer may decide on the appropriate interpretation of the results in light of all the uncertainties involved and the specific decision in question.

In some instances, engineers simplify detailed structural models into *equivalent multi-degree-of-freedom* models. These can be used to consolidate properties into what have been termed “fish bone” models (see Figure 2-4a). In some cases, the model can simplified further. For example, when rotational coupling among various vertical flexural elements is negligible (e.g., cantilever shear walls or braced frames) or when story shear mechanisms are anticipated (e.g., strong beam/weak column frames) a “stick” model can be used (see Figure 2-4b and c). Often, substructuring techniques are helpful in developing simplified models. The purpose of the simplified models is to reduce computational and data management efforts. More importantly, they can also provide an improved visualization tool for the engineer. The negative aspect to simplified models is that they introduce additional approximations and uncertainty into the analysis.

Another important simplification to detailed structural models is what have become known as “pushover” or “capacity” curves. These curves form the basis of nonlinear static procedures discussed below. They are generated by subjecting a detailed structural model to one or more lateral load patterns (vectors) and then increasing the magnitude of the total load to generate a nonlinear inelastic force-deformation relationship for the structure at a global level (see Figure 2-5). The load vector is usually an approximate representation of the relative accelerations associated with the first mode of vibration for the structure. In the Coefficient Method of FEMA 356, the global parameters are normally base shear and roof displacement. For the Capacity-Spectrum Method of ATC-40, these are transformed to spectral acceleration and spectral displacement. Nonlinear static procedures use these force-deformation relationships to represent the behavior of a simple *single-degree-of-freedom* (SDOF) oscillator.

## 2.2 Characterization of Seismic Ground Motion

When an earthquake occurs, the amplitude, phasing, and frequency content of the shaking depend strongly on source characteristics (e.g., magnitude, rupture mechanism, fault plane orientation with respect to site). In addition, the characteristics of shaking are affected by attenuation that occurs as seismic waves propagate through rock from the source to the site and by local site effects. Site characteristics that may be important include potential 3-D basin structure, dynamic properties of relatively shallow sediments, and surface topography. The source, attenuation, and site effects, which are depicted schematically in the left frame of Figure 2-6, affect the character of ground shaking as expressed by *ground motion records* (i.e., plots of the acceleration, velocity and displacement of a point on the ground surface as a function of time (center frame in Figure 2-6)).

Ground motion records can be used to define *elastic response spectra* (right frame in Figure 2-6), which comprise a relationship of the maximum response

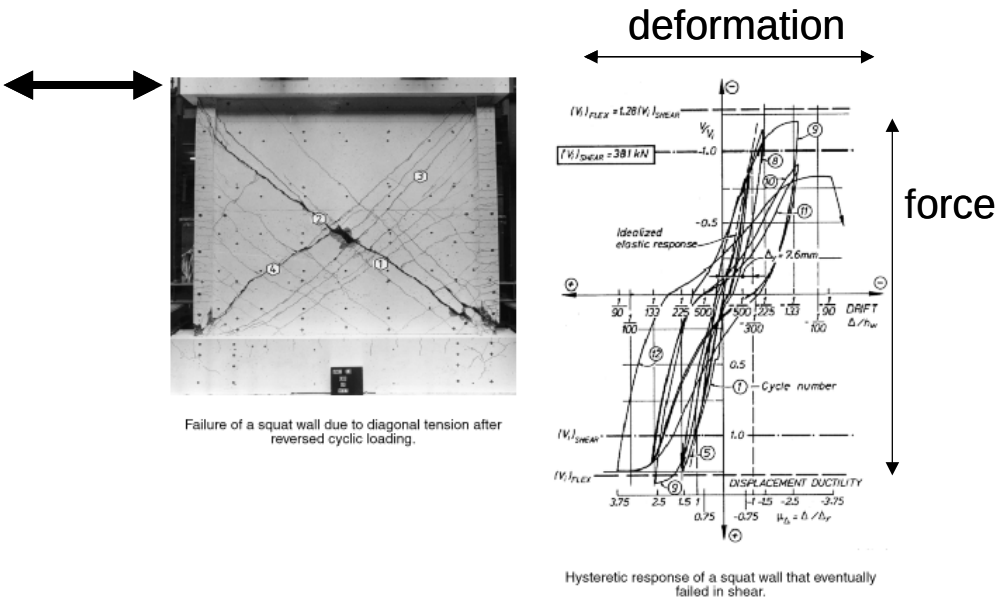


**a) Hysteretic force-deformation behavior from tests**

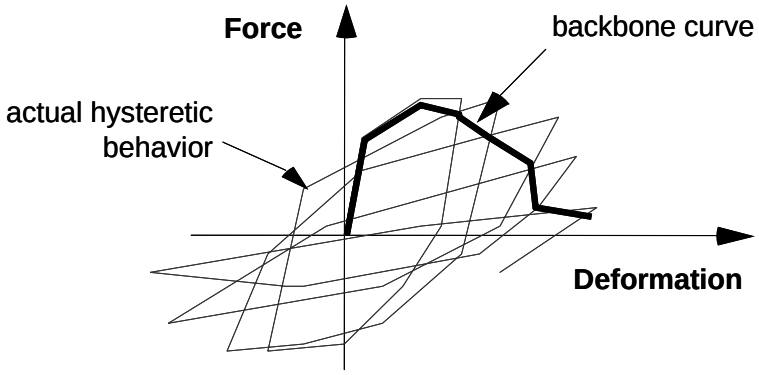


**b) Backbone representation of hysteretic behavior**

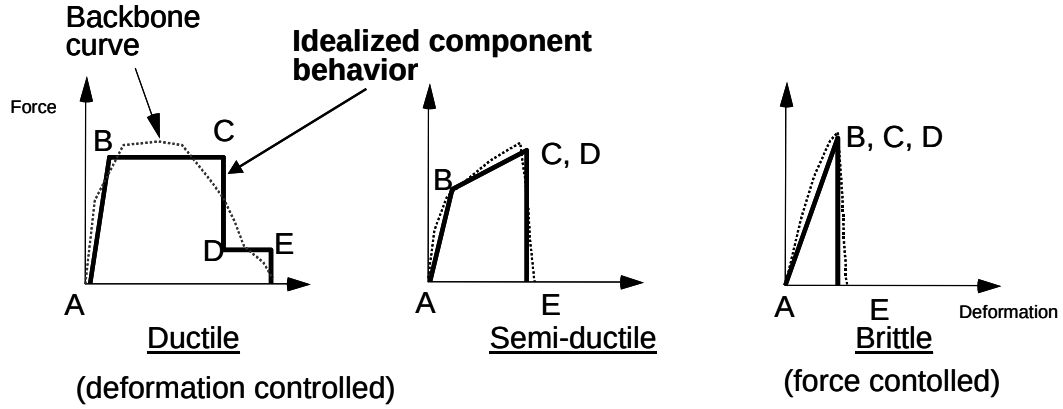


**c) Idealized properties for analysis models**

Figure 2-3 Schematic depictions illustrating how inelastic component strength and stiffness properties from test data are used to create idealized force-deformation relationships.

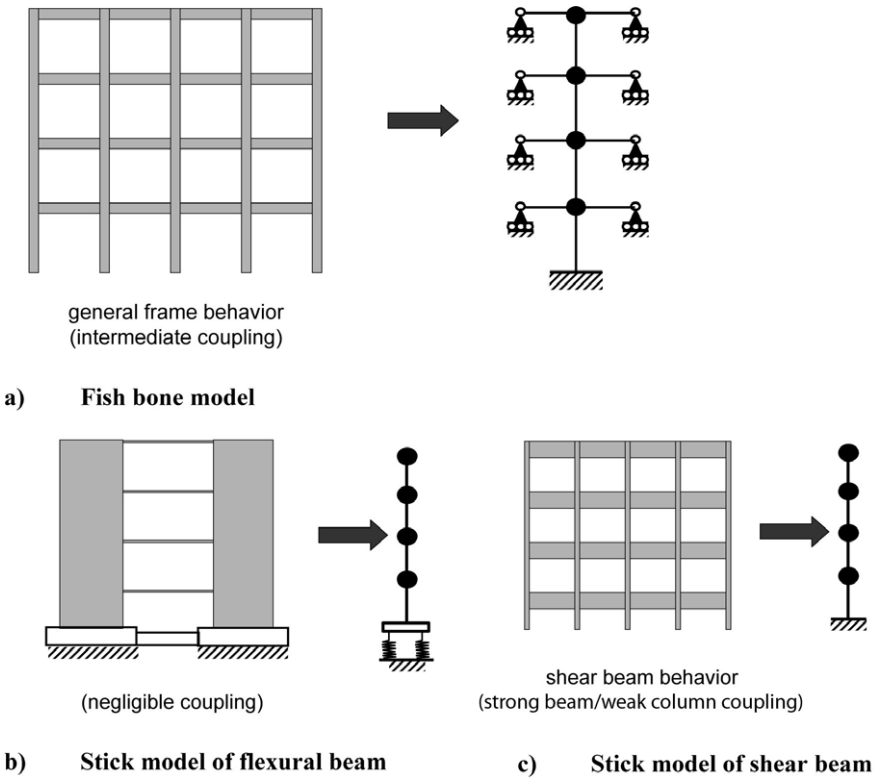


Figure 2-4 Forms of simplified equivalent multiple-degree-of-freedom models.

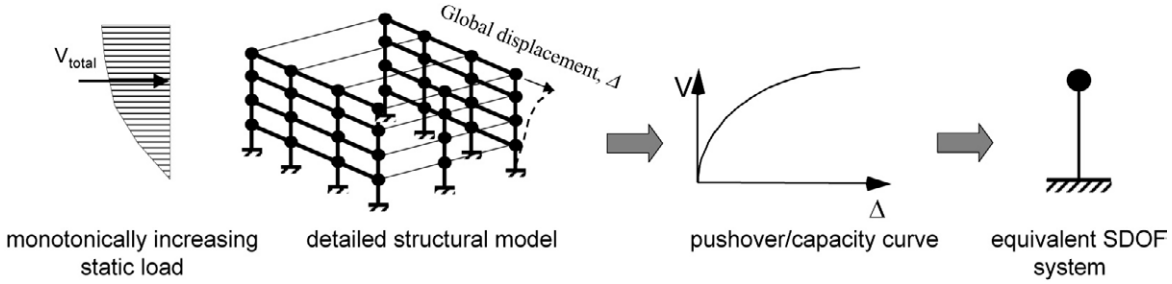


Figure 2-5 Schematics depicting the development of an equivalent SDOF system from a pushover/capacity curve.

(acceleration, velocity, and displacement) over the entire response-history record of a single-degree-of-freedom oscillator and the frequency, or more commonly the period, of the oscillator, for a specified level of damping. Response spectral ordinates are commonly used to represent seismic demand for structural design. It should be noted that in this document, as in conventional structural engineering practice, pseudo-acceleration is used in place of actual spectral acceleration. The notation $S_a$ actually represents the pseudo-acceleration.

The response spectrum for a single ground motion record is typically highly variable (jagged), depending on the assumed level of damping. For this reason, multiple records representative of a single source at a specified distance from the site and of a specified magnitude are often combined and smoothed, as implied in Figure 2-6. The results of this type of seismic

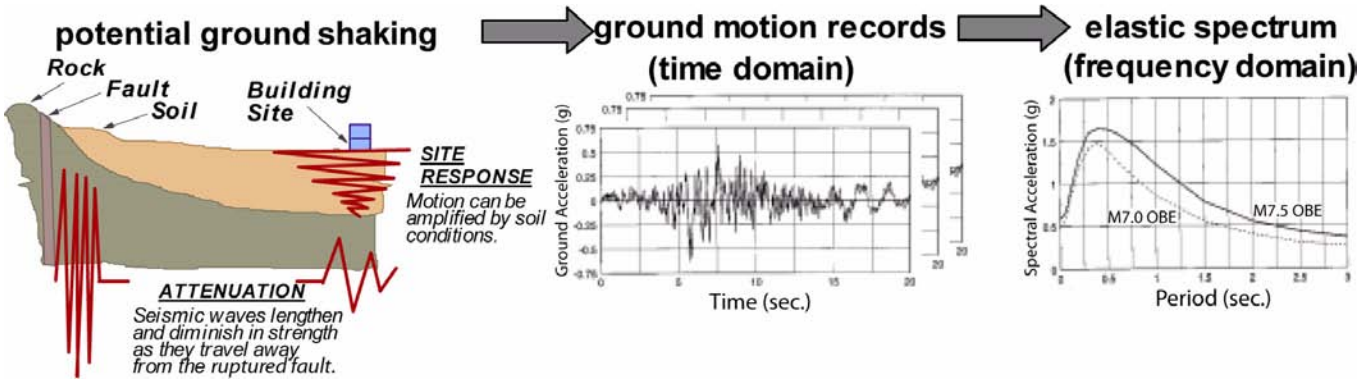


Figure 2-6 Factors affecting seismic ground motion and various ways to characterize ground motions graphically.

hazard analysis that provide an estimate of ground motion for a specified set of source and path parameters is a *deterministic spectrum*.

The level of uncertainty in source, path, and site effects associated with deterministic spectra is relatively poorly defined. These uncertainties are accounted for directly in probabilistic seismic hazard analyses that provide estimates of ground motion parameters (such as response spectral ordinates) with a specified probability of being exceeded within a specified time period. The analysis includes all earthquakes (magnitudes and faults) that potentially could cause significant seismic shaking at a given site. When response spectral ordinates for a range of periods are evaluated for a specified probability of being exceeded, the result is an *equal-hazard spectrum*.

Modern standards and guidelines (FEMA 356, ATC-40, and the *NEHRP Recommended Provisions for New Buildings*), allow the use of approximate *design spectra* that represent a simplification of equal-hazard spectra on a location-specific basis. Design spectra have standardized shapes, and can be evaluated based on nationally mapped values of spectral accelerations for short and long periods.

Deterministic spectra, equal-hazard spectra, and design spectra commonly exhibit smooth shapes with respect to period in contrast with the highly variable (jagged) shape of actual ground motion spectral records (particularly for low levels of damping). Structural response to an actual ground motion record is likely to be sensitive to the complex nature of the resulting spectrum. This uncertainty is not eliminated by the use of smooth spectra.

## 2.3 Options for Inelastic Analysis

Various combinations of structural model types and characterizations of seismic ground motion define a number of options for inelastic analysis. The selection of one option over another depends on the purpose of the analysis, the anticipated performance objectives, the acceptable level of uncertainty, the availability of resources, and the sufficiency of data. In some cases, applicable codes and standards may dictate the analysis procedure.

The primary decision is whether to choose inelastic procedures over more *conventional linear elastic analysis*. In general, linear procedures are applicable when the structure is expected to remain nearly elastic for the level of ground motion of interest or when the design results in nearly uniform distribution of nonlinear response throughout the structure. In these cases, the level of uncertainty associated with linear procedures is relatively low. As the performance objective of the structure implies greater inelastic demands, the uncertainty with linear procedures increases to a point that requires a high level of conservatism in demand assumptions and/or acceptability criteria to avoid unintended performance. Inelastic procedures facilitate a better understanding of actual performance. This can lead to a design that focuses upon the critical aspects of the building, leading to more reliable and efficient solutions.

*Nonlinear dynamic analysis* using the combination of ground motion records with a detailed structural model theoretically is capable of producing results with relatively low uncertainty (see Figure 2-7). In nonlinear dynamic analyses, the detailed structural model subjected to a ground-motion record produces estimates of component deformations for each degree of freedom in the model. Higher-level demands (element

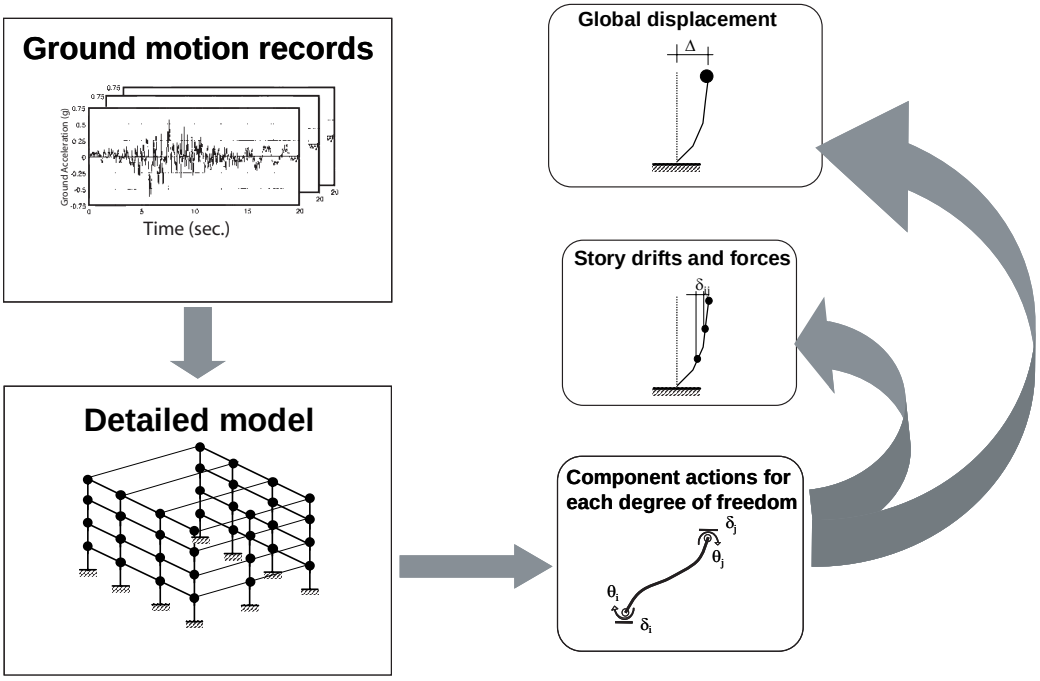


Figure 2-7 Flow chart depicting the nonlinear dynamic analysis process. Note that component actions are used to determine higher-level effects, such as story drifts and roof displacement, Δ.

distortions, story drifts, roof displacement) derive directly from the basic component actions, as illustrated in Figure 2-7. There is still uncertainty with the detailed models, associated primarily with the lack of data on actual component behavior, particularly at high ductilities. In addition, the variability of ground motion results in significant dispersion in engineering demand parameters. This is illustrated in Figure 2-8, which depicts results from a series of nonlinear dynamic analyses for increasingly larger intensities of ground shaking (Vamvatsikos and Cornell, 2002). At each level of intensity, the multiple time histories produce a distribution of results in terms of a selected engineering demand parameter. Note that the dispersion increases with higher shaking intensity and with greater elasticity.

*Simplified nonlinear dynamic analysis with equivalent multi-degree-of-freedom models* also use ground motion records to characterize seismic demand. However, these techniques produce engineering demand parameters above the basic component level only. For example, a "stick" model produces story displacements or drifts. The engineer can estimate corresponding component actions using the assumptions that were originally the basis of the simplified model. Thus the uncertainty associated with the component actions in the simplified model is greater than those associated with the detailed model.

*Simplified nonlinear dynamic analysis with equivalent single-degree-of-freedom (SDOF) models* are a further simplification using ground motion records to characterize seismic shaking (see Figure 2-9). The result of the analysis is an estimate of global displacement demand. It is important to recognize that the resulting lower-level engineering demands (e.g., story drifts, component actions) are calculated from the global displacement using the force-deformation relationship for the oscillator. In contrast to the use of the more detailed model (see Figure 2-7), they are directly related to the assumptions, and associated uncertainties, made to convert the detailed structural model to an equivalent SDOF model in the first place. This adds further to the overall uncertainty associated with the simplified nonlinear dynamic analysis. Note that if the SDOF model is subjected to multiple time histories a statistical representation of response can be generated.

*Nonlinear static procedures (NSPs)* convert MDOF models to equivalent SDOF structural models and represent seismic ground motion with response spectra as opposed to ground-motion records (see Figure 2-10). They produce estimates of the maximum global displacement demand. Story drifts and component actions are related subsequently to the global demand parameter by the pushover or capacity curve that was

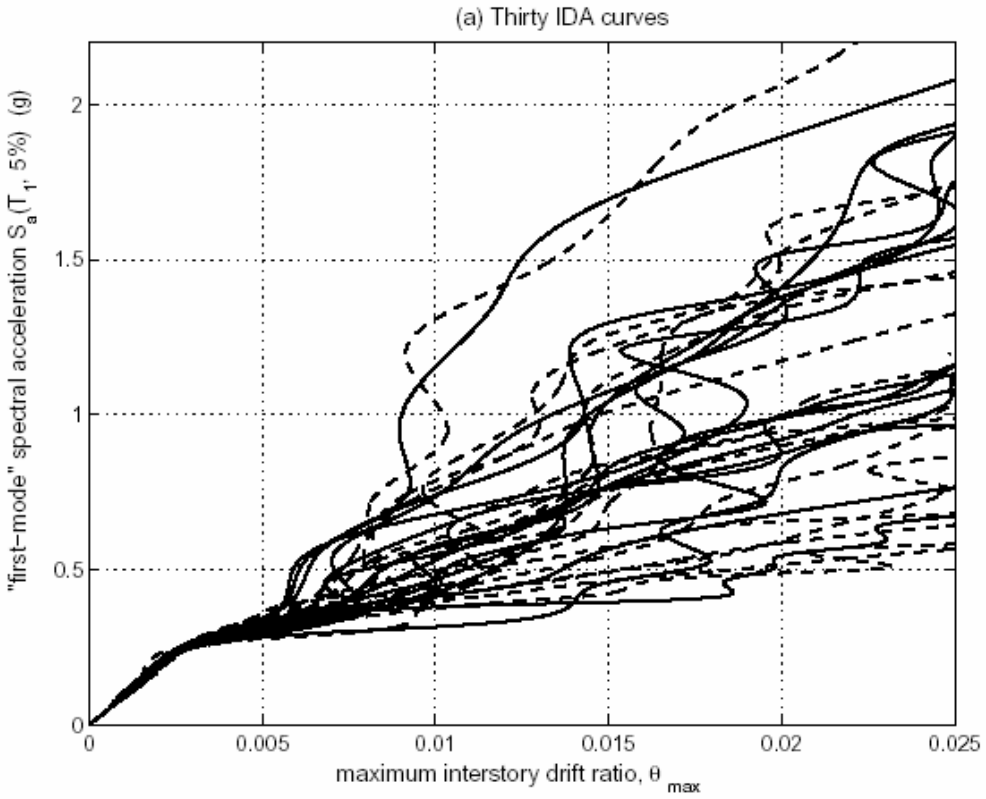


Figure 2-8 Incremental dynamic analysis study for thirty ground motion records for a 5-story steel braced frame (Vamvatsikos and Cornell, 2002)

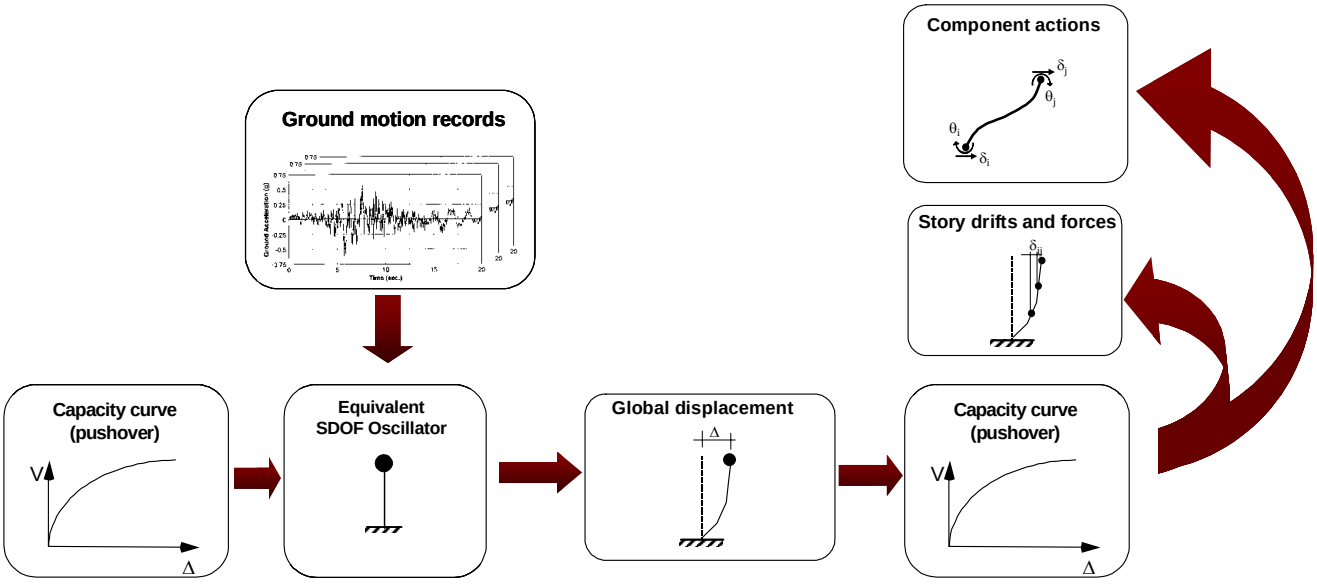


Figure 2-9 Flow chart depicting simplified SDOF nonlinear analysis process. Note that component actions are estimated from global displacement demand using the pushover curve.

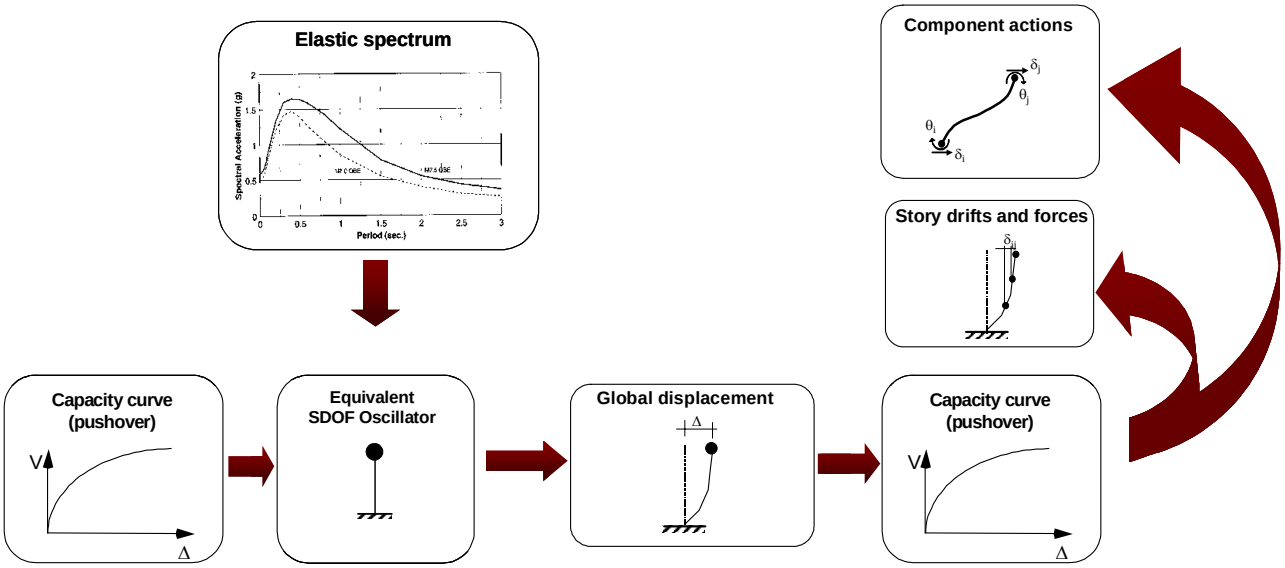


Figure 2-10 Flow chart depicting the process followed in nonlinear static procedures. Note that component actions are based on global displacement demand and a pushover/capacity curve.

used to generate the equivalent SDOF model. This is similar to simplified nonlinear dynamic analyses using SDOF models. In contrast to the use of simplified dynamic analyses using multiple ground motion records, the use of nonlinear static procedures implies greater uncertainty due to the empirical procedures used to estimate the maximum displacement. This is true even if spectra representative of the multiple ground motion records are used in the nonlinear static analysis.

Figure 2-11 summarizes the relationship among the normal options for inelastic seismic analysis procedures with respect to the type of structural model and characterization of ground motion. Also noted in the figure is the relative uncertainty associated with each option. The actual uncertainty inherent in any specific analysis depends on a number of considerations. Nonlinear dynamic analyses can be less uncertain than other techniques if the nonlinear inelastic properties of the components in the detailed structural model are accurate and reliable. If the component properties are poorly characterized, however, the results might not be an improvement over other alternatives. Some analysis options are better than others, depending on the parameter of interest. For example, with simplified dynamic analyses, a SDOF oscillator can be subjected to a relatively large number of ground motion records to provide a good representation of the uncertainty associated with global displacement demand due to the variability of the ground motion. On the other hand, if the engineer is comfortable with the estimate of maximum global displacement from a nonlinear static procedure, a multi-mode pushover analysis might provide improved estimates of inter-story drift that would not necessarily be available from the simplified SDOF dynamic analyses.

## 2.4 Current Nonlinear Static Procedures

Nonlinear static procedures are popular with practicing engineers, as demonstrated by the voluntary state-of-practice internet query results in Appendix B. Two options are used predominantly. Equivalent linearization techniques are based on the assumption that the maximum total displacement (elastic plus inelastic) of a SDOF oscillator can be estimated by the elastic response of an oscillator with a larger period and damping than the original. These procedures use estimates of ductility to estimate effective period and damping. The Coefficient Method is fundamentally a displacement modification procedure that is presented in FEMA 356. Alternatively, displacement modification procedures estimate the total maximum displacement of the oscillator by multiplying the elastic response, assuming initial linear properties and damping, by one or more coefficients. The coefficients are typically derived empirically from series of nonlinear response-history analyses of oscillators with varying periods and strengths.

A form of equivalent linearization known as the Capacity-Spectrum Method is documented in ATC-40. Other variations and versions of these two procedures

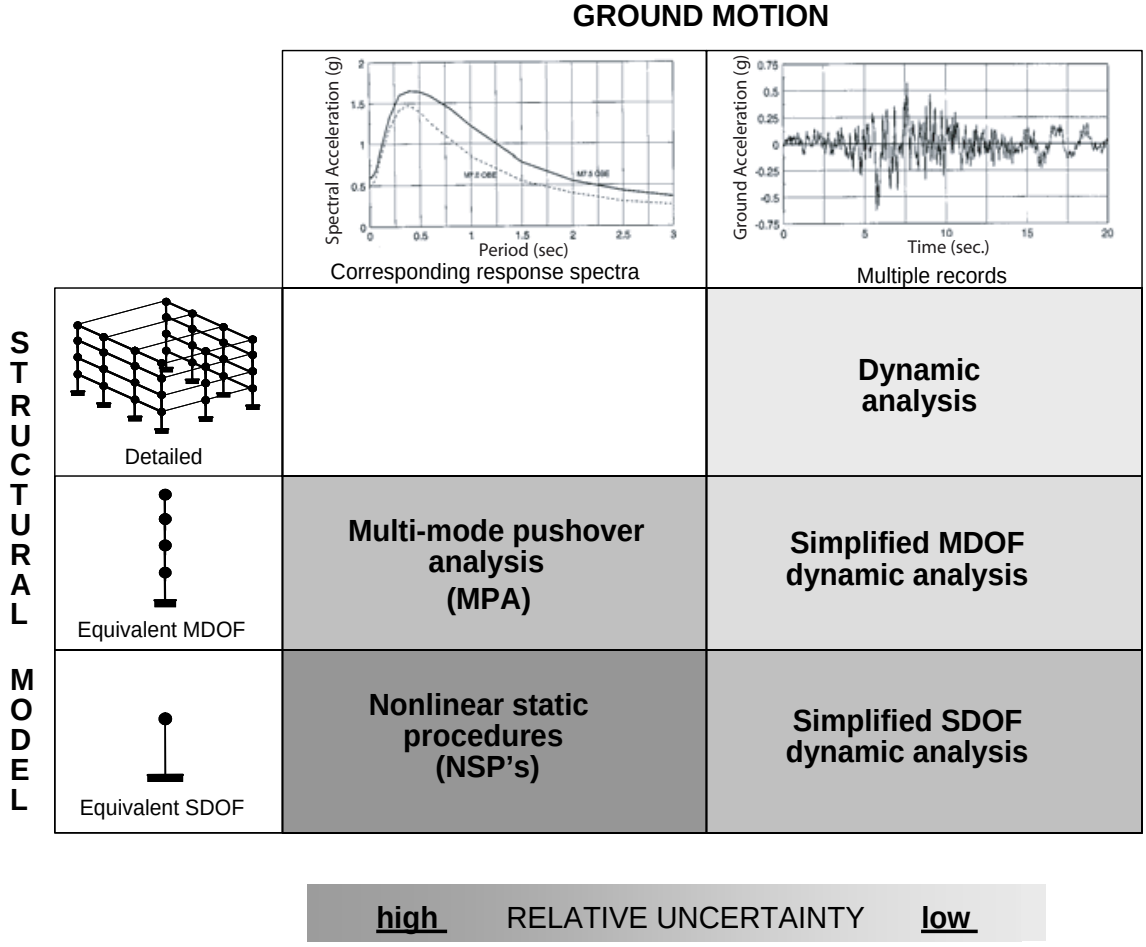


Figure 2-11 Matrix depicting possible inelastic seismic analysis procedures for various structural models and ground-motion characterizations along with trends of uncertainty in the result.

have been suggested (see Appendices A and B), but all are related fundamentally to either displacement modification or equivalent linearization. Both approaches use nonlinear static analysis (pushover analysis) to estimate the lateral force-deformation characteristics of the structure. In both procedures the global deformation (elastic and inelastic) demand on the structure is computed from the response of an equivalent single-degree-of-freedom system having the load-deformation properties determined from the pushover analysis. They differ, however, in the technique used to estimate the maximum deformation demand (elastic and inelastic).

### *2.4.1 The Coefficient Method of Displacement Modification from FEMA 356*

The Coefficient Method is the primary nonlinear static procedure presented in FEMA 356. This approach modifies the linear elastic response of the equivalent SDOF system by multiplying it by a series of coefficients $C_0$ through $C_3$ to generate an estimate of the maximum global displacement (elastic and inelastic), which is termed the target displacement. The process begins with an idealized force-deformation curve (i.e., pushover curve) relating base shear to roof displacement (see Figure 2-12). An effective period, $T_e$, is generated from the initial period, $T_i$, by a graphical procedure that accounts for some loss of stiffness in the transition from elastic to inelastic behavior. The effective period represents the linear stiffness of the equivalent SDOF system. When plotted on an elastic response spectrum representing the seismic ground motion as peak acceleration, $S_a$, versus period, $T$, the effective period identifies a maximum acceleration response for the oscillator. The assumed damping, often five percent, represents a level that might be expected for a typical structure responding in the elastic range.

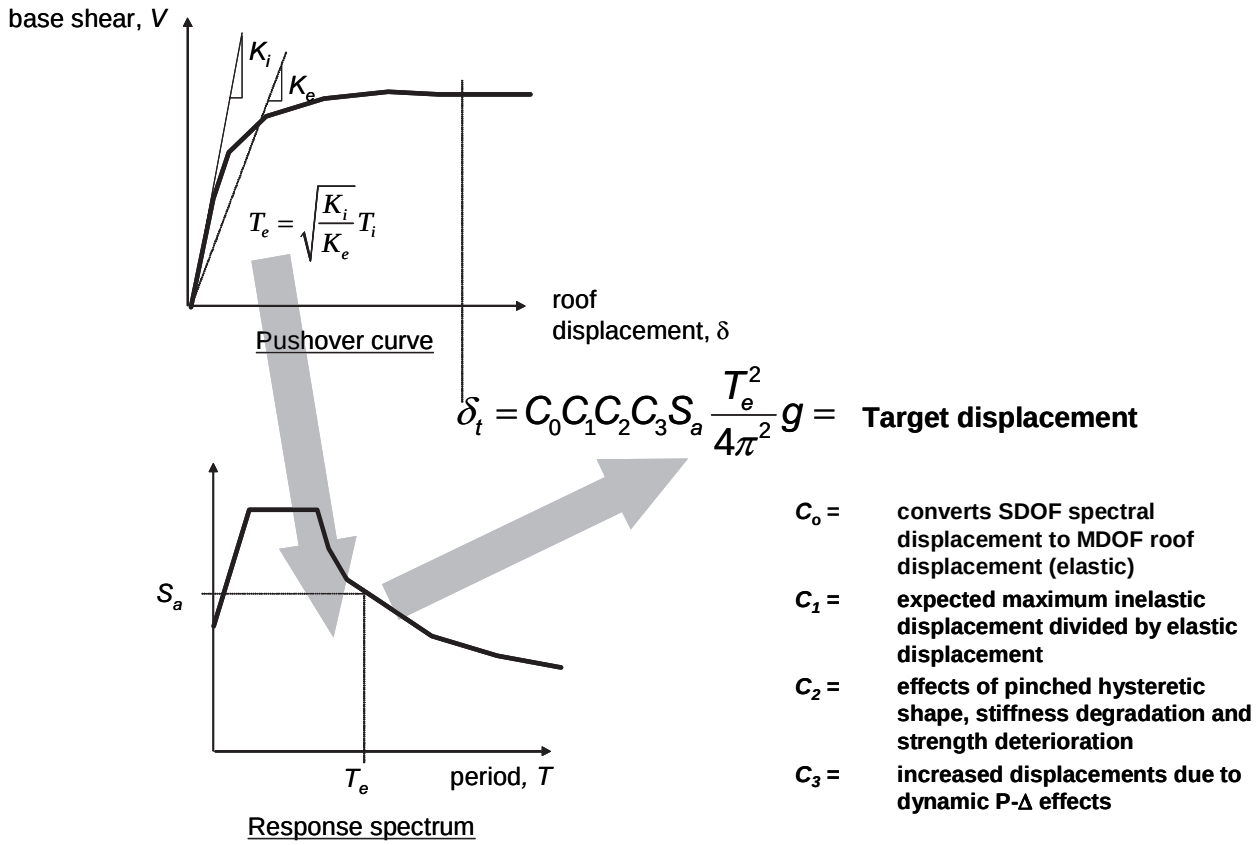


Figure 2-12 Schematic illustrating the process by which the Coefficient Method of displacement modification (per FEMA 356) is used to estimate the target displacement for a given response spectrum and effective period, $T_e$.

The peak elastic spectral displacement is directly related to the spectral acceleration by the relationship

$$S_d = \frac{T_{eff}^2}{4\pi^2} S_a . \qquad (2\text{-}1)$$

The coefficient $C_0$ is a shape factor (often taken as the first mode participation factor) that simply converts the spectral displacement to the displacement at the roof. The other coefficients each account for a separate inelastic effect.

The coefficient $C_1$ is the ratio of expected displacement (elastic plus inelastic) for a bilinear inelastic oscillator to the displacement for a linear oscillator. This ratio depends on the strength of the oscillator relative to the response spectrum and the period of the SDOF system, $T_e$. The coefficient $C_2$ accounts for the effect of pinching in load-deformation relationships due to degradation in stiffness and strength. Finally, the coefficient $C_3$ adjusts for second-order geometric nonlinearity ($P$-$\Delta$) effects. The coefficients are empirical and derived primarily from statistical studies of the nonlinear response-history analyses of SDOF oscillators and adjusted using engineering judgment. The coefficients are described in greater detail in Chapter 3.

### 2.4.2 Capacity-Spectrum Method of Equivalent Linearization in ATC-40

The basic assumption in equivalent linearization techniques is that the maximum inelastic deformation of a nonlinear SDOF system can be approximated from the maximum deformation of a linear elastic SDOF system that has a period and a damping ratio that are larger than the initial values of those for the nonlinear system. In the Capacity-Spectrum Method of ATC-40, the process begins with the generation of a force-deformation relationship for the structure. This process is virtually identical to that for the Coefficient Method of FEMA 356, except that the results are plotted in acceleration-

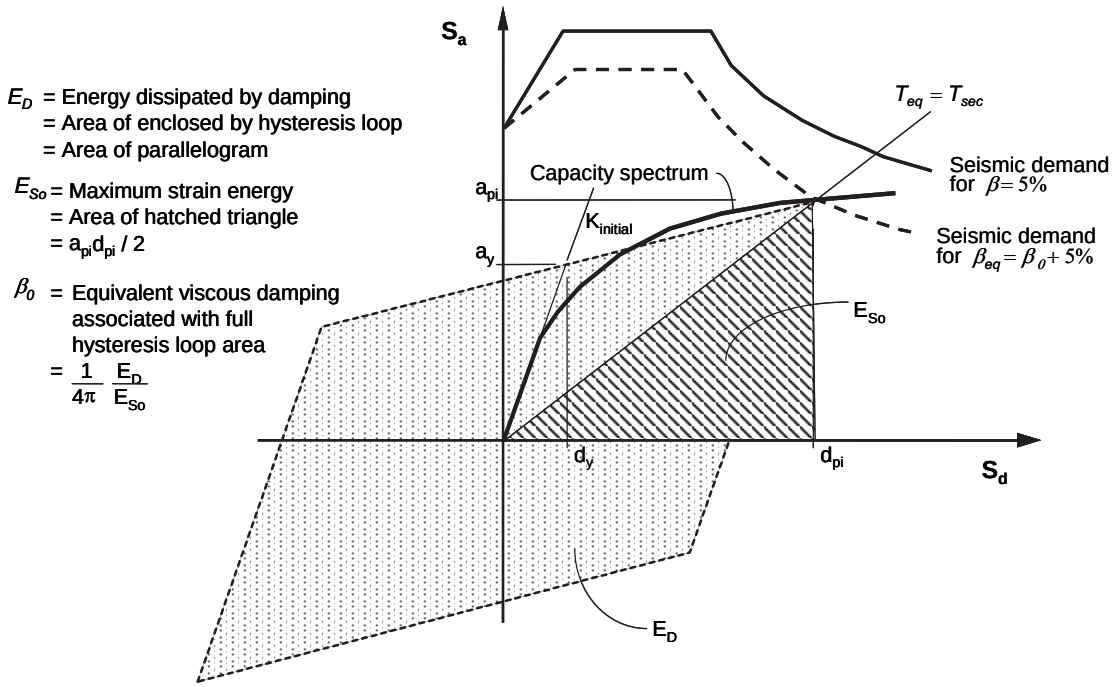


Figure 2-13 Graphical representation of the Capacity-Spectrum Method of equivalent linearization, as presented in ATC-40.

displacement response spectrum (ADRS) format (see Figure 2-13). This format is a simple conversion of the base-shear-versus-roof-displacement relationship using the dynamic properties of the system, and the result is termed a capacity curve for the structure. The seismic ground motion is also converted to ADRS format. This enables the capacity curve to be plotted on the same axes as the seismic demand. In this format, period can be represented as radial lines emanating from the origin.

The Capacity-Spectrum Method of equivalent linearization assumes that the equivalent damping of the system is proportional to the area enclosed by the capacity curve. The equivalent period, $T_{eq}$, is assumed to be the secant period at which the seismic ground motion demand, reduced for the equivalent damping, intersects the capacity curve. Since the equivalent period and damping are both a function of the displacement, the solution to determine the maximum inelastic displacement (i.e., performance point) is iterative. ATC-40 imposes limits on the equivalent damping to account for strength and stiffness degradation. These limits are reviewed in greater detail in Chapter 3.

# 3. Evaluation of Current Nonlinear Static Procedures

## 3.1 Introduction

This chapter summarizes the results of studies to assess the ability of current approximate nonlinear static procedures to estimate the maximum displacement of inelastic structural models. Initial studies evaluated both the Coefficient Method of FEMA 356 and the Capacity-Spectrum Method of ATC-40.

The use of NSPs (nonlinear static procedures) has accelerated in the United States since the publication of ATC-40, FEMA 273/274 and FEMA 356 documents. As a consequence there is valuable information available on the practical application of these inelastic analysis procedures (see Appendix B, "Summary of Practice using Inelastic Analysis Procedures"). Various researchers and practicing engineers have found that, in some cases, different inelastic analysis methods give substantially different estimates for displacement demand for the same ground motion and same SDOF oscillator (Aschheim et al., 1998; Chopra and Goel 1999a,b, 2000; Albanessi et al., 2000; Kunnath and Gupta, 2000; Lew and Kunnath, 2000; Yu et al, 2001; Zamfirescu and Fajfar, 2001; MacRae and Tagawa, 2002). The disparities in displacement predictions highlight the need for comparison and further study of these different approaches (see Appendix A, "Summary of Research on Inelastic Analysis Procedures").

The objective of this evaluation was to study the accuracy of the approximate methods described in ATC-40 and FEMA 356 for estimating the maximum displacement demand of inelastic single-degree-of-freedom (SDOF) systems. This global displacement is a spectral displacement, termed the Performance Point in ATC-40. It is the roof displacement, termed the Target Displacement in FEMA 356. In particular, this study was aimed at identifying and quantifying the errors in these procedures when applied to SDOF systems. For this purpose, approximate total displacements computed with ATC-40 and with FEMA 356 were compared with the results of nonlinear response-history analyses of SDOF oscillators. The nonlinear response-history analyses are "exact" for the assumptions made for the properties of the oscillator (damping ratio and type of hysteretic behavior) and for the particular ground motion record. Thus these results are a useful benchmark to evaluate the approximate procedures.

Of particular interest is the extent to which the approximate methods might tend to overestimate or underestimate displacement demands (introduce bias) and the spectral regions or strength levels for which these biases are likely to occur. Errors were quantified through statistical analyses. A large number of SDOF systems (with a wide range of periods of vibration, lateral strengths, and hysteretic behavior) were subjected to a relatively large number of recorded earthquake ground motions. Ground motions included near-fault and far-fault records representative of site conditions ranging from rock to very soft soil. However, it is recognized that there may be some situations that deviate from those used in this investigation. Caution should be used when extrapolating the results presented in this evaluation for ground motions and site conditions that differ substantially.

Section 3.2 describes the period of vibration, damping ratio, lateral strength, and hysteretic behavior of the SDOF systems that were considered in this investigation. This section also describes the types and characteristics of the recorded ground motion records that were used as well as the error measures computed in this study. Section 3.3 describes the evaluation of the simplified inelastic analysis procedure in ATC-40 to estimate the maximum displacement of inelastic systems using equivalent linearization. Section 3.4 provides a corresponding evaluation of the simplified analysis procedure in FEMA 356. In particular, this chapter provides an evaluation of coefficients $C_1$, $C_2$ and $C_3$ in this method. Finally, Section 3.5 summarizes the dynamic response of nonlinear elastic, or rocking, oscillators. A complete compilation of the evaluation study data is provided in Appendix C, "Supplemental Data on the Evaluation of Current Procedures."

## 3.2 Evaluation Procedures

### *3.2.1 Hysteretic Characteristics*

SDOF systems with initial periods of vibration between 0.05 s and 3.0 s were used in this investigation. A total of 50 periods of vibration were considered (40 periods between 0.05 s and 2.0 s, equally spaced at 0.05 s, and 10 periods between 2.0 s and 3.0 s, equally spaced at 0.1 s intervals). The initial damping ratio, $\beta$, was assumed to be equal to 5% for all systems.

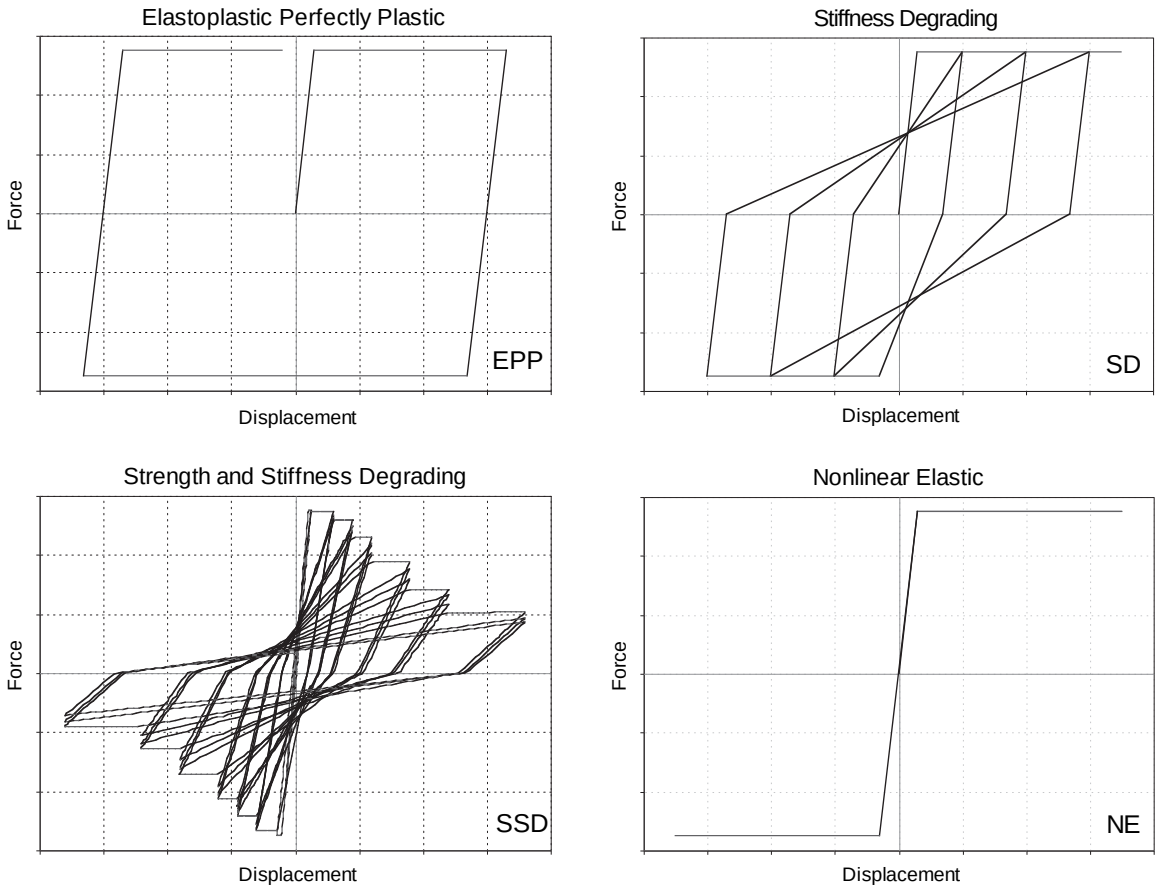


Figure 3-1 Basic hysteretic models used in the evaluation of current procedures: elastic perfectly plastic (EPP); stiffness-degrading (SD); strength and stiffness degrading (SSD), and nonlinear elastic (NE).

In this study the lateral strength is normalized by the strength ratio *R*, which is defined as

$$R = \frac{mS_a}{F_y} \tag{3-1}$$

where $m$ is the mass of the SDOF oscillator, $S_a$ is the spectral acceleration ordinate corresponding to the initial period of the system, and $F_y$ is the lateral yield strength of the system. The numerator in Equation 3-1 represents the lateral strength required to maintain the system elasticity, which sometimes is also referred to as the elastic strength demand. *Note that this R-factor is not the same as the response-modification coefficient conventionally used for design purposes.* This *R*-factor is the design *R*-factor divided by the overstrength factor, omega sub-zero. This is discussed on page 105 of FEMA 450-2, *NEHRP Recommended Provisions for Seismic Regulations for New Buildings and Other Structures, Part 2: Commentary* (BSSC, 2003). Nine levels of normalized lateral strength were considered, corresponding to $R$ = 1, 1.5, 2, 3, 4, 5, 6, 7 and 8.

Four different hysteretic behaviors were used in this study (see Figure 3-1):

- The *elastic perfectly plastic (EPP)* model is used as a reference model. This model has been used widely in previous investigations and therefore it represents a benchmark to study the effect of hysteretic behavior. Furthermore, recent studies have shown that this is a reasonable hysteretic model for steel beams that do not experience lateral or local buckling or connection failure (Foutch and Shi, 1998).
- The *stiffness-degrading (SD)* model corresponds to the modified-Clough model, as originally proposed by Clough (1966) and as modified by Mahin and Lin (1983). This model was originally proposed as

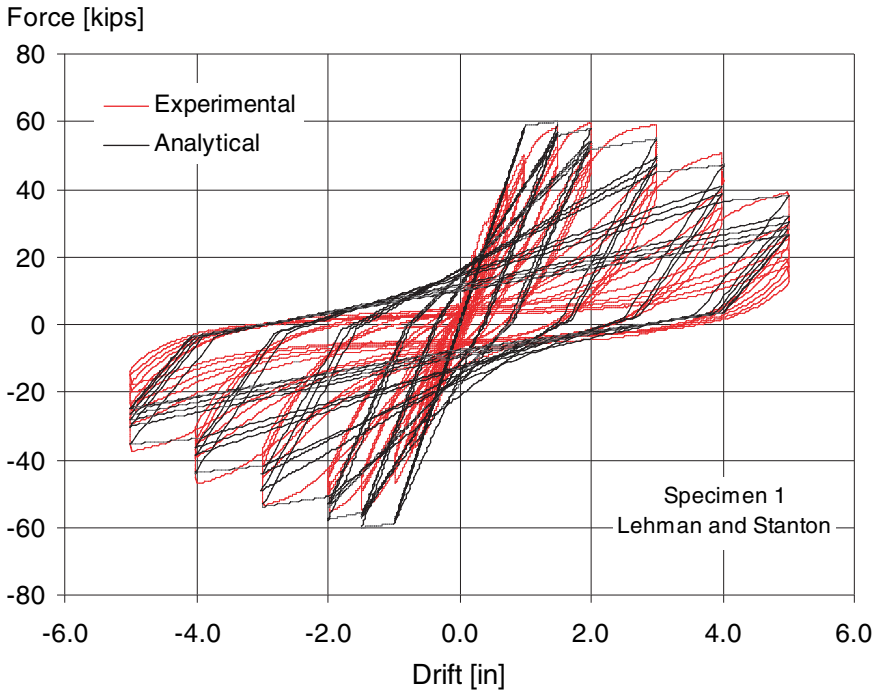


Figure 3-2 Comparison of experimental results (after Lehman et al., 2000) with the hysteretic response computed with the SSD model.

representative of well detailed and flexurally controlled reinforced concrete structures in which the lateral stiffness decreases as the level of lateral displacement increases.

- The *strength and stiffness-degrading (SSD)* model is aimed at approximately reproducing the hysteretic behavior of structures in which lateral stiffness and lateral strength decrease when subjected to cyclic reversals. In this model, the amount of strength and stiffness degradation is a function of the maximum displacement in previous cycles as well as a function of the hysteretic energy dissipated. This model is similar to the three-parameter model implemented in IDARC (Kunnath et al., 1992). When properly calibrated, this model can reproduce the response of poorly detailed reinforced concrete structures relatively well. An example is shown in Figure 3-2, in which the load-deformation relationship of a poorly detailed beam-column joint tested at the University of Washington (Lehman et al., 2000) is compared with the response computed with the SSD model. A single set of parameters representing severe strength and stiffness degradation was used for this model. The type of degradation that is captured by this model only includes cyclic degradation. Note that the post-elastic stiffness in any cycle is always equal to zero or greater. Thus, the strength never diminishes in the current cycle of deformation. The degradation of strength occurs in subsequent cycles (or half-cycles) of deformation. Oscillators that have in-cycle negative post-elastic stiffnesses and in-cycle degradation of strength can be prone to dynamic instability. They are covered in Section 3.4.4 and in Chapter 4.
- The *nonlinear elastic (NE)* model unloads on the same branch as the loading curve and therefore exhibits no hysteretic energy dissipation. This model approximately reproduces the behavior of pure rocking structures. Most instances of rocking in real structures are a combination of this type of behavior with one of the other hysteretic types that include hysteretic energy losses.

In summary, the combinations of period of vibration, lateral strength, and hysteretic behavior represent a total of 1,800 different SDOF systems.

### 3.2.2 Earthquake Ground Motions

A total of 100 earthquake ground motions recorded on different site conditions were used in this study. Ground motions were divided into five groups with 20 accelerograms in each group. The first group consisted of earthquake ground motions recorded on stations located on rock with average shear wave velocities between 760 m/s (2,500 ft/s) and 1,525 m/s (5,000 ft/s).

These are representative of site class B, as defined by the *NEHRP Recommended Provisions for Seismic Regulations for New Buildings and Other Structures, Part I, Provisions* (BSSC, 2000)[1]. The second group consisted of records obtained on stations on very dense soil or soft rock with average shear wave velocities between 360 m/s (1,200 ft/s) and 760 m/s, while the third group consisted of ground motions recorded on stations on stiff soil with average shear wave velocities between 180 m/s (600 ft/s) and 360 m/s. These are consistent with site class C and D respectively. The fourth group corresponds to ground motions recorded on very soft soil conditions with shear wave velocities smaller than 180 m/s, which can be classified as site class E. Finally, the fifth group corresponds to 20 ground motions influenced by near-field forward-directivity effects. Detailed listings of the ground motions are presented in Appendix C.

### 3.2.3 Error Measures and Statistical Study

The maximum displacement of each inelastic SDOF system was estimated with the simplified inelastic procedures in ATC-40 and FEMA 356 when subjected to each of the ground motions. The maximum displacement of each inelastic SDOF system was then computed using nonlinear response-history analyses. The maximum displacement is defined as the maximum of the absolute value of the displacement response. A total of 180,000 nonlinear response-history analyses were run as part of this investigation. In this study, the results computed with nonlinear response-history analyses are the benchmark maximum displacements, $(\Delta_i)_{ex}$. The maximum displacements estimated with simplified inelastic procedures of ATC-40 and FEMA 356 are the approximate maximum displacements, $(\Delta_i)_{app}$ of the inelastic system. It should be noted that the nonlinear response-history analyses are "exact" only for the SDOF oscillator with the assumed properties and for the particular ground motion. The uncertainty of the modeling assumptions with respect to the actual building is not included in either the nonlinear response-history analyses or the approximate analyses. The nonlinear response-history results are a convenient benchmark.

In order to evaluate the accuracy of these approximate procedures, an error measure was defined as the ratio of approximate, $(\Delta_i)_{app}$, to benchmark, $(\Delta_i)_{ex}$, maximum displacement as follows:

$$E_{T,R} = \left[ \frac{(\Delta_i)_{\text{app}}}{(\Delta_i)_{\text{ex}}} \right]_{T,R} \tag{3-2}$$

This error measure was computed for each period of vibration $T$ and each level of normalized lateral strength $R$. Values of $E_{T,R}$ larger than one indicate that the approximate method overestimates the maximum displacement of the SDOF system and values smaller than one indicate underestimation. A total of 320,000 individual errors were computed in this study.

In order to identify whether the approximate methods, on average, tend to overestimate or underestimate maximum displacements of inelastic systems, mean errors were computed as follows:

$$\bar{E}_{T,R} = \frac{1}{n} \sum_{i=1}^{n} \left( E_{T,R} \right)_i \tag{3-3}$$

where $n$ is the number of records in each group of ground motions. Mean errors were computed for each hysteretic behavior type, each period of vibration (or for each normalized period of vibration as will be explained later) and each level of normalized lateral strength. Therefore, mean errors computed with Equation 3-3 do not allow for underestimations in a spectral region to be compensated by overestimations in another spectral region. Information on the bias for each period, for each type of hysteretic behavior, for each level of normalized lateral strength, and for each site class is retained.

The sample mean error computed with Equation 3-3 is an unbiased estimator of the mean error of the population. Therefore, it provides an estimate of the average error produced by the approximate methods. However, it provides no information on the dispersion of the error. In order to obtain a measure of the dispersion of the errors produced by the approximate methods, the standard deviation of the error was computed as

$$\sigma_{T,R} = \sqrt{\frac{1}{n-1} \sum_{i=1}^{n} \left[ \left( E_{T,R} \right)_i - \bar{E}_{T,R} \right]^2} \tag{3-4}$$

The square of the sample standard deviation of the error computed with Equation 3-4 is an unbiased estimator of the variance of the error in the population. The standard deviation of the error was computed for each period, for

1. Superseded in 2003 with the FEMA 450 *Recommended Provisions for Seismic Regulations for New Buildings and Other Structures.*

each type of hysteretic behavior, for each level of normalized lateral strength, and for each site class.

## 3.3 Evaluation of Capacity-Spectrum Method of ATC-40

### *3.3.1 Summary of the Approximate Method*

The simplified inelastic analysis procedure in ATC-40, a version of the Capacity-Spectrum Method (CSM), is based on equivalent linearization. The basic assumption in equivalent linear methods is that the maximum displacement of a nonlinear SDOF system can be estimated from the maximum displacement of a linear elastic SDOF system that has a period and a damping ratio that are larger than those of the initial values for the nonlinear system. The elastic SDOF system that is used to estimate the maximum inelastic displacement of the nonlinear system is usually referred to as the equivalent or substitute system. Similarly, the period of vibration and damping ratio of the elastic system are commonly referred to as equivalent period and equivalent damping ratio, respectively.

The concept of equivalent viscous damping was first proposed by Jacobsen (1930) to obtain approximate solutions for the steady forced vibration of damped SDOF systems with linear force-displacement relationships but with damping forces proportional to the *n*th power of the velocity of motion when subjected to sinusoidal forces. In this pioneering study, the stiffness of the equivalent system was set equal to the stiffness of the real system and the equivalent viscous damping ratio was based on equating the dissipated energy per cycle of the real damping force to that of the equivalent damping force. Years later, the same author extended the concept of equivalent viscous damping to yielding SDOF systems (Jacobsen, 1960). Since then, there have been many methods proposed in the literature. Review of the earlier equivalent linear methods can be found in Jennings (1968), Iwan and Gates (1979), Hadjian (1982), Fardis and Panagiatakos (1996), while a review of some recent methods can be found in Miranda and Ruiz-García (2003). The Capacity Spectrum Method as documented in ATC-40 is based primarily on the work of Freeman et al. (1975).

In equivalent linear methods, the equivalent period is computed from the initial period of vibration of the nonlinear system and from the maximum displacement ductility ratio, $\mu$. Similarly, the equivalent damping ratio is computed as a function of damping ratio in the nonlinear system and the displacement ductility ratio. The main differences among the many equivalent linear methods that are available in the literature stem primarily from the functions used to compute the equivalent period and equivalent damping ratio.

As discussed in Section 2.4.2, the Capacity-Spectrum Method according to ATC-40 uses the secant stiffness at maximum displacement to compute the effective period and relates effective damping to the area under the hysteresis curve (see Figure 2-13).These assumptions result in an equivalent period, $T_{eq}$, and equivalent damping ratio (referred to as effective viscous damping, $\beta_{eq}$, in ATC-40) given by

$$T_{eq} = T_0 \sqrt{\frac{\mu}{1+\alpha\mu-\alpha}} \tag{3-5}$$

$$\beta_{eq} = \beta_{eff} = 0.05 + \kappa \frac{2}{\pi} \frac{(\mu-1)(1-\alpha)}{\mu(1+\alpha\mu-\alpha)} \tag{3-6}$$

where $T_0$ is the initial period of vibration of the nonlinear system, $\alpha$ is the post-yield stiffness ratio and $\kappa$ is an adjustment factor to approximately account for changes in hysteretic behavior in reinforced concrete structures. ATC-40 proposes three equivalent damping levels that change according to the hysteretic behavior of the system. Type A hysteretic behavior denotes structures with reasonably full hysteretic loops, similar to the EPP oscillator in Figure 3-1. The corresponding equivalent damping ratios take the maximum values. Type C hysteretic behavior represents severely degraded hysteretic loops (e.g., SSD), resulting in the smallest equivalent damping ratios. Type B hysteretic behavior is an intermediate hysteretic behavior between types A and C (e.g., SD). The value of $\kappa$ decreases for degrading systems (hysteretic behavior types B and C). ATC-40 suggests an initial elastic viscous damping ratio (first term on the right hand side of Equation 3-6) of 0.05 (5%) for reinforced concrete buildings. The terms to the right of $\kappa$ in Equation 3-6 represent the equivalent hysteretic viscous damping for an idealized bilinear system designated as $\beta_0$ in ATC-40 documentation. Table 3-1 shows the variation of $\kappa$ with respect to $\beta_0$ for different hysteretic behaviors types.

The equivalent period in Equation 3-5 is based on a lateral stiffness of the equivalent system that is equal to the secant stiffness at the maximum displacement. It only depends on the displacement ductility ratio and the

**Table 3-1 Variation of $\kappa$-Value in ATC-40**

| *Hysteretic Behavior* | $\beta_0$ | $\kappa$ |
|---|---|---|
| Type A | $\leq 0.1625$ | 1.0 |
| | $> 0.1625$ | $1.13 - 0.51 \times (\pi/2) \times \beta_0$ |
| Type B | $\leq 0.25$ | 0.67 |
| | $> 0.25$ | $0.845 - 0.446 \times (\pi/2) \times \beta_0$ |
| Type C | Any value | 0.33 |

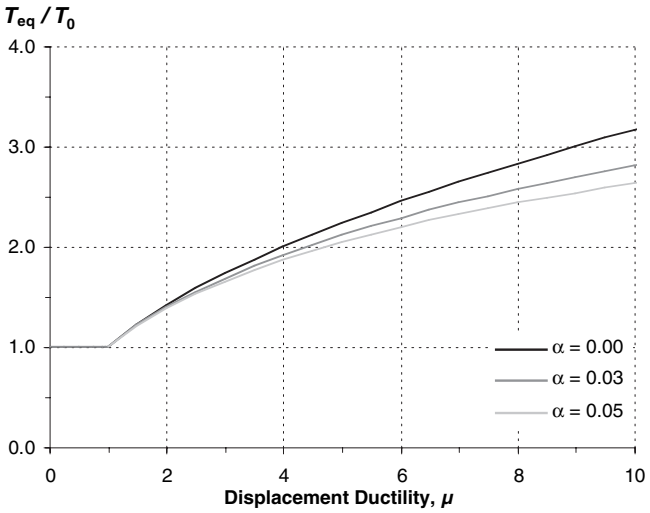


Figure 3-3 Variation of period shift based on secant stiffness.

post-yield stiffness ratio of the inelastic system. Figure 3-3 shows the variation of equivalent periods for different post-yield stiffness ratios for a wide range of displacement ductility ratios. The equivalent period becomes longer as the displacement ductility ratio increases and as the post-yield stiffness ratio decreases.

Figures 3-4 and 3-5 present the variation of $\kappa$ and effective damping value, $\beta_{eq}$, with changes in the ductility ratio, respectively. The calculations were done assuming elastic perfectly plastic (EPP) behavior to represent a system that has full hysteretic loops (i.e., a non-degrading system). It can be seen that for structures with type A behavior (systems having full hysteretic loops), the $\kappa$ value is 1.0 for displacement ductility ratios less than 1.3. For ductility ratios larger than 1.3, $\kappa$ decreases up to a value of 0.77 at a displacement ductility ratio of 3.4 and remains constant at 0.77 for larger ductilities. Similarly, for structures with type B hysteretic behavior, the value of $\kappa$ is constant and equal to 0.67 for displacement ductility ratios less than 1.6,

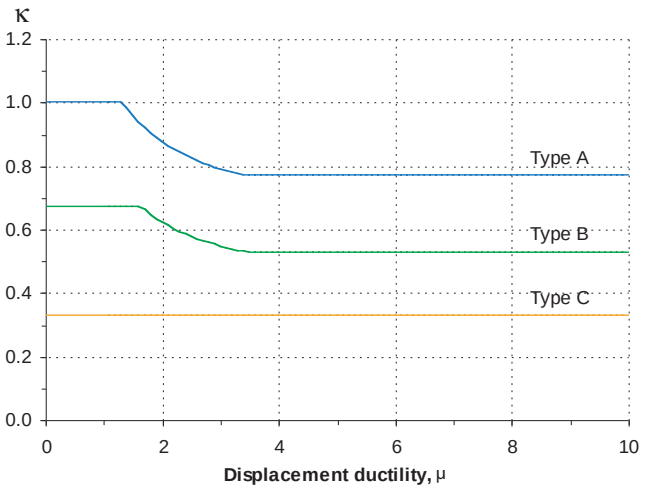


Figure 3-4 Variation of $\kappa$-factor with the displacement ductility ratio, $\mu$.

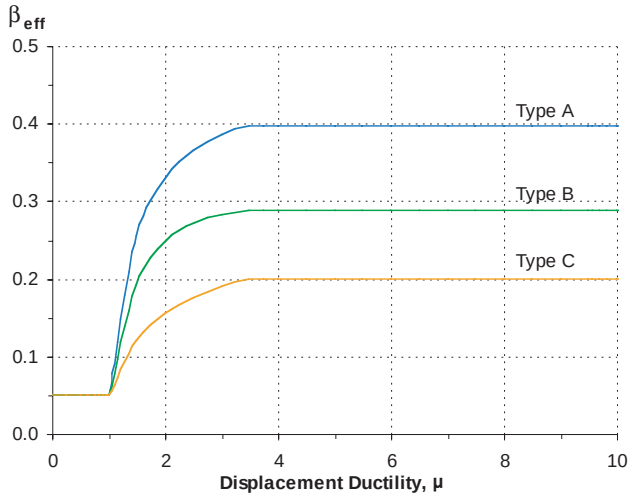


Figure 3-5 Variation of equivalent (effective) damping ratios with changes in the displacement ductility ratio, $\mu$.

decreases to 0.53 for ductility ratio of 3.4, and remains constant for larger ductilities. For structures with type C hysteretic behavior, the κ factor is equal to 0.33 regardless of the level of ductility demand.

The equivalent damping ratio in the equivalent linear spectrum method documented in ATC-40 rapidly increases once the structures yields and remains constant for ductility ratios higher than 3.4. The maximum equivalent damping ratios for hysteretic behavior types A, B, and C are 0.40, 0.29 and 0.20, respectively. According to Equations 3-5 and 3-6, structures with hysteretic behaviors type B and C will

have much larger displacement demands because of the

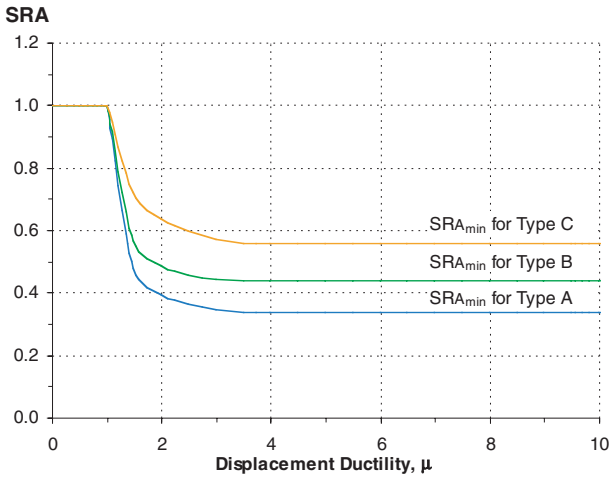


Figure 3-6 Variation of spectral reduction factors SRA for different hysteretic behaviors as a function of the displacement ductility ratio, $\mu$.

reduced hysteretic energy dissipation capacity produced by narrower hysteretic loops.

When applied to design spectra, ATC-40 provides reduction factors to reduce spectral ordinates in the constant-acceleration region and constant-velocity region as a function of the effective damping ratio. These spectral reduction factors are given by

$$SR_A = \frac{3.21 - 0.68\ln\left(100\beta_{\text{eff}}\right)}{2.12} \qquad (3\text{-}7)$$

$$SR_V = \frac{2.31 - 0.41\ln\left(100\beta_{\text{eff}}\right)}{1.65} \qquad (3\text{-}8)$$

where $\beta_{\text{eff}}$, is the effective or equivalent damping ratio computed with Equation 3-6. $SR_A$ is the spectral-reduction factor to be applied to the constant-acceleration region in the linear elastic design spectrum, and $SR_V$ is the spectral reduction factor to be applied to the constant-velocity region (descending branch) in the linear elastic design spectrum. These spectral-reduction factors are shown in Figures 3-6 and 3-7. It can be seen that for displacement ductility demands larger than 3.4, the spectral ordinates no longer decrease. Consequently, the ATC-40 procedures impose limits on the amount of hysteretic damping-related reduction in spectral response that can be achieved. Table 3-2 shows these limiting values.

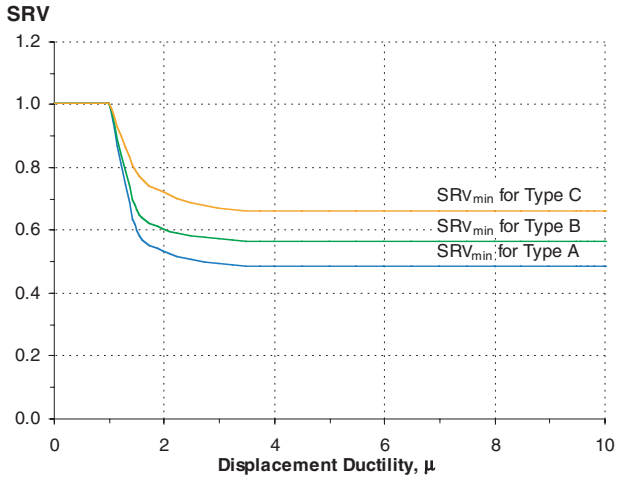


Figure 3-7 Variation of spectral reduction factors SRV for different hysteretic behaviors as a function of the displacement ductility ratio, $\mu$.

**Table 3-2 Minimum Allowable Spectral Reduction Factors for Displacement Ductility Ratios Larger than 3.4**

| *Behavior Type* | $SR_A$ | $SR_V$ |
|---|---|---|
| Type A | 0.33 | 0.50 |
| Type B | 0.44 | 0.56 |
| Type C | 0.56 | 0.67 |

### *3.3.2 Iteration Procedures*

Equivalent linearization equations, in general, require prior knowledge of the displacement ductility ratio in order to compute the equivalent period of vibration and equivalent damping ratio, $\mu$, which are then needed to estimate the maximum inelastic displacement demand on a SDOF system when subjected to a particular ground motion. Specifically, in Equations 3-5 and 3-6, $\mu$ must be known in order to compute $\beta_{\text{eff}}$ and $T_{eq}$. However, when evaluating a structure, the maximum displacement ductility ratio is not known. Consequently, iteration is required in order to estimate the maximum displacement.

ATC-40 describes three iterative procedures to reach a solution for the approximation. Procedures A and B are described as the most transparent and most convenient for programming, as they are based on an analytical method. Procedure C is a graphical method that is not convenient for spreadsheet programming. ATC-40 presents Procedure A as the most straightforward and

easy in application among the three procedures. In a recent study, Chopra and Goel (1999a,b, 2000) investigated the iteration methods implemented in ATC-40. By using various SDOF examples, they showed that Procedure A did not always converge when using actual earthquake spectra, as opposed to smooth design spectra. They also concluded that the displacement computed with Procedure B was unique and the same as that determined with Procedure A, provided that the latter converged. In a more recent study, Miranda and Akkar (2002) provide further discussion of the convergence issues in equivalent linearization procedures. They also note that equivalent linearization procedures can lead to multiple results for some specific earthquake ground motions.

An iteration procedure based on secant iteration that is guaranteed to converge was used for the evaluation study. As noted in the previous section, multiple equivalent linearization solutions may exist for actual ground motion records that were used for the study, as opposed to smoothed spectra normally used by engineers. For the purposes of this investigation, the first computed displacement encountered within 1% of the assumed displacement was taken as the approximate inelastic displacement without verifying whether this was the only possible solution.

### *3.3.3 Evaluation Using Ground Motion Records*

In order to evaluate the Capacity-Spectrum Method when applied to structures with hysteretic behavior type A, approximate results were compared with response-history analysis (RHA) benchmark results computed with the EPP hysteretic model. Similarly, the approximate results computed for behavior type B were compared with RHA benchmark results of the stiffness degrading (SD) model, and the approximate results computed for behavior type C were compared with RHA benchmark results of the strength-and-stiffness-degrading (SSD) model. Mean errors corresponding to ground motions recorded in site class C and for hysteretic behaviors type A, B, and C are shown in Figure 3-8. Based on the complete results presented in Appendix C, it was found that the Capacity-Spectrum Method implemented in ATC-40 leads to very large overestimations of the maximum displacement for relatively short-period systems (periods smaller than about 0.5 s). Approximate maximum displacements in this period range can be, on average, larger than twice the RHA benchmark displacements. These large overestimations of displacement in the short-period range have also been reported previously for other

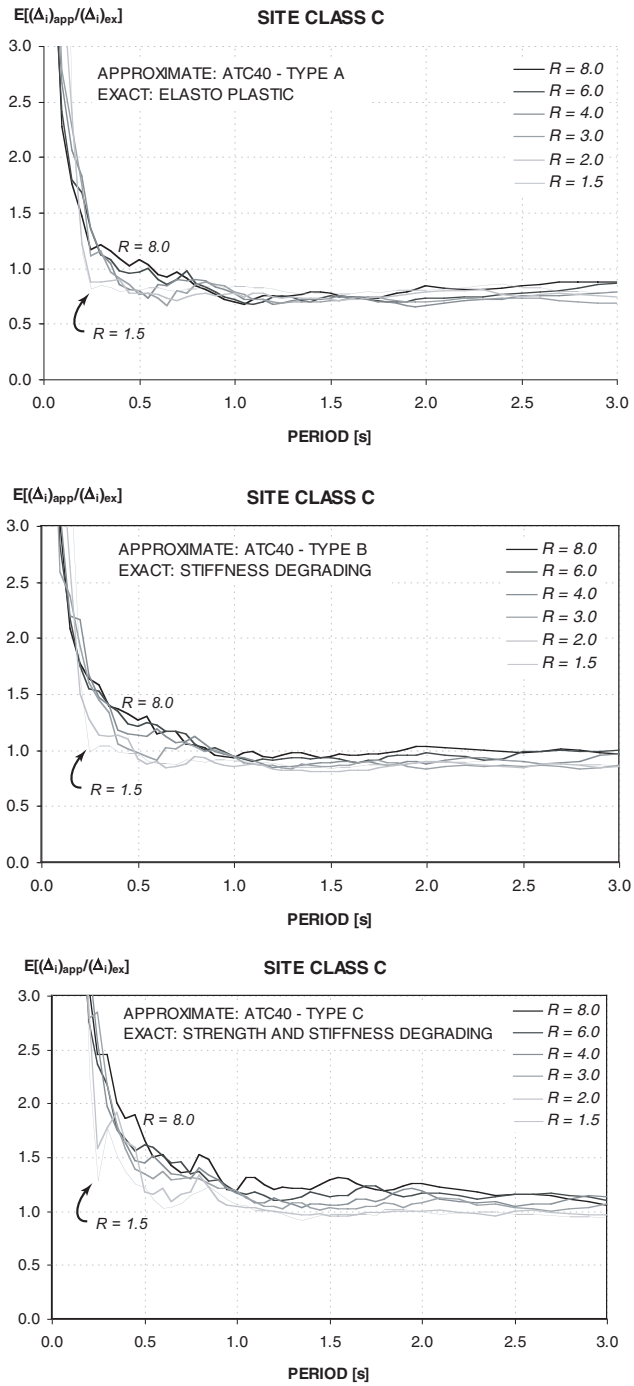


Figure 3-8 Mean error associated with the Capacity-Spectrum Method of ATC-40 for hysteretic behaviors types A, B, and C for site class C.

equivalent linearization methods that are based on secant stiffness (Miranda and Ruiz-García, 2003; Akkar and Miranda, 2005).

The complete results indicate that, for periods longer than about 0.6 s, ATC-40 behavior type A tends to underestimate the maximum displacements. Maximum displacements computed with the ATC-40 procedure are, on average, about 25% to 35% smaller than those computed with RHA using elasto-plastic systems. Underestimations are slightly smaller for site class B and slightly larger for site class D. Mean errors for ATC-40 behavior type A are not significantly influenced by changes in the normalized lateral strength *R*.

For systems with ATC-40 hysteretic behavior type B and periods longer than about 0.8 s, the Capacity-Spectrum Method tends to underestimate displacements compared with those of inelastic systems with stiffness-degrading (SD) models for site class B. Underestimations are small and tend to decrease as *R* increases. Average underestimations range from 5% to 25%. For site classes C and D, ATC-40 may underestimate or overestimate lateral deformation of systems with type B hysteretic behavior depending on the normalized lateral strength, *R*.

In the case of systems with hysteretic behavior type C, the approximate ATC-40 procedure tends to overestimate inelastic displacements for practically all periods when compared to those computed for inelastic systems with strength-and-stiffness-degrading (SSD) hysteretic models. Overestimations increase as *R* increases. The level of overestimation varies from one site class to another. Detailed information on the actual errors are contained in Appendix C.

Dispersion of the error is very large for periods smaller than about 0.5 s and is moderate and approximately constant for periods longer than 0.5 s. In general, dispersion increases as *R* increases. Mean errors computed with ground motions recorded on very soft soil sites or with near-fault ground motions are strongly influenced by the predominant period of the ground motion. Detailed results of dispersion for site classes B, C, and D and behavior types A, B, and C are also presented in Appendix C.

## 3.4 Evaluation of Coefficient Method (FEMA 356)

### *3.4.1 Summary of the Approximate Method*

The determination of the target displacement in the simplified nonlinear static procedure (NSP) known as the displacement Coefficient Method is primarily described in the FEMA 356 document (Section 3.3.3.3.2). According to this document, the target displacement, $\delta_t$, which corresponds to the displacement at roof level, can be estimated as

$$\delta_t = C_0 C_1 C_2 C_3 S_a \frac{T_e^2}{4\pi^2} g \tag{3-9}$$

where:

$C_0$ = Modification factor to relate spectral displacement of an equivalent SDOF system to the roof displacement of the building MDOF system. It can be calculated from

- the first modal participation factor,
- the procedure described in Section 3.3.3.2.3 in FEMA 356, or
- the appropriate value from Table 3.2 in FEMA 356.

$C_1$ = Modification factor to relate the expected maximum displacements of an inelastic SDOF oscillator with EPP hysteretic properties to displacements calculated for the linear elastic response.

$$C_1 = \begin{cases} 1.0 & \text{for } T_e \geq T_s \\ 1.0 + \dfrac{(R-1)T_s}{T_e} & \\ \dfrac{}{R} & \text{for } T_e < T_s \end{cases}$$

but not greater than the values given in Section 3.3.1.3.1 (Linear Static Procedure, LSP section) nor less than 1. Values of $C_1$ in Section 3.3.1.3.1 are

$$C_1 = \begin{cases} 1.5 \text{ for } T_e < 0.1 \text{ s} \\ 1.0 \text{ for } T_e \geq T_s \end{cases}$$

with linear interpolation used to calculate $C_1$ for the intermediate values of $T_e$.

The limit imposed on $C_1$ by Section 3.3.1.3.1 is often referred to as "$C_1$ *capping*."

$C_2$ = Modification factor to represent the effect of pinched hysteretic shape, stiffness degradation, and strength deterioration on the maxi-

mum displacement response. Values of $C_2$ for different framing systems and structural performance levels (i.e., immediate occupancy, life safety, and collapse prevention) are obtained from Table 3.3 of the FEMA 356 document. Alternatively, $C_2$ can take the value of one in nonlinear procedures.

$C_3$ = Modification factor to represent increased displacements due to dynamic *P-Δ* effects. For buildings with positive post-yield stiffness, $C_3$ is set equal to 1. For buildings with negative post-yield stiffness, values of $C_3$ are calculated using the following expression:

$$C_3 = 1.0 + \frac{|\alpha|(R-1)^{3/2}}{T_e} \qquad (3\text{-}10)$$

where:

$T_e$ = Effective fundamental period of the building computed in accordance with section 3.3.3.2.5.

$T_s$ = Characteristic period of the response spectrum, defined as the period associated with the transition from the constant-acceleration segment of the spectrum to the constant-velocity segment of the spectrum.

$R$ = Ratio of elastic strength demand to calculated strength capacity.

$S_a$ = Response spectrum acceleration, at the effective fundamental period and damping ratio of the building.

$g$ = Gravitational acceleration.

### 3.4.2 Maximum Displacement Ratio (Coefficient $C_1$)

Coefficient $C_1$ is the ratio of the maximum displacement for inelastic response of a SDOF oscillator with non-degrading hysteretic behavior to the maximum displacement had the oscillator remained elastic. Figure 3-9 shows the variation of $C_1$ for site class B using a characteristic period $T_s$ equal to 0.4 s. This characteristic period value is computed by applying the procedure described in Sections 1.6.1.5 and 1.6.2.1 of the FEMA 356 document. For the evaluation of the FEMA 356 Coefficient Method, this study utilized characteristic periods equal to 0.4 s,

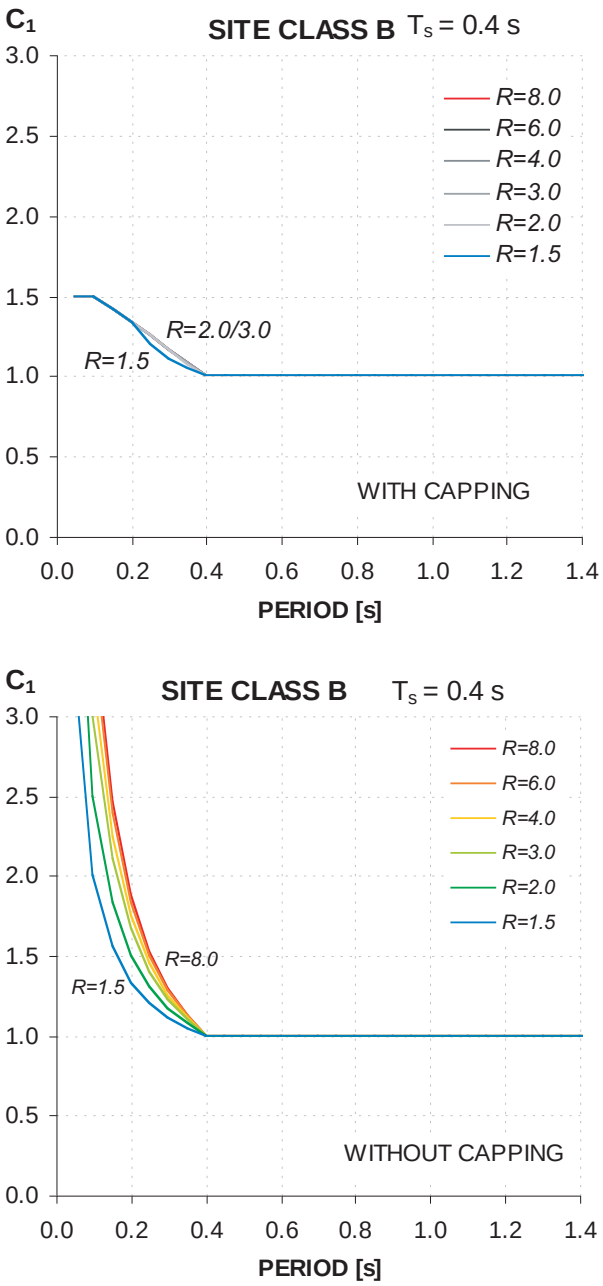


Figure 3-9 Comparison of coefficient $C_1$ in FEMA 356 with and without capping.

0.55 s, 0.6 s and 1.0 s for site classes B, C, D, and E, respectively. These characteristic periods are representative of the periods computed according to FEMA 356 when using large ground motion intensities for which the system is expected to behave nonlinearly. Figure 3-9 shows a comparison between the values of $C_1$ with the limitation (capping), as defined in FEMA 356 Section 3.3.3.3.2, and without the limitation.

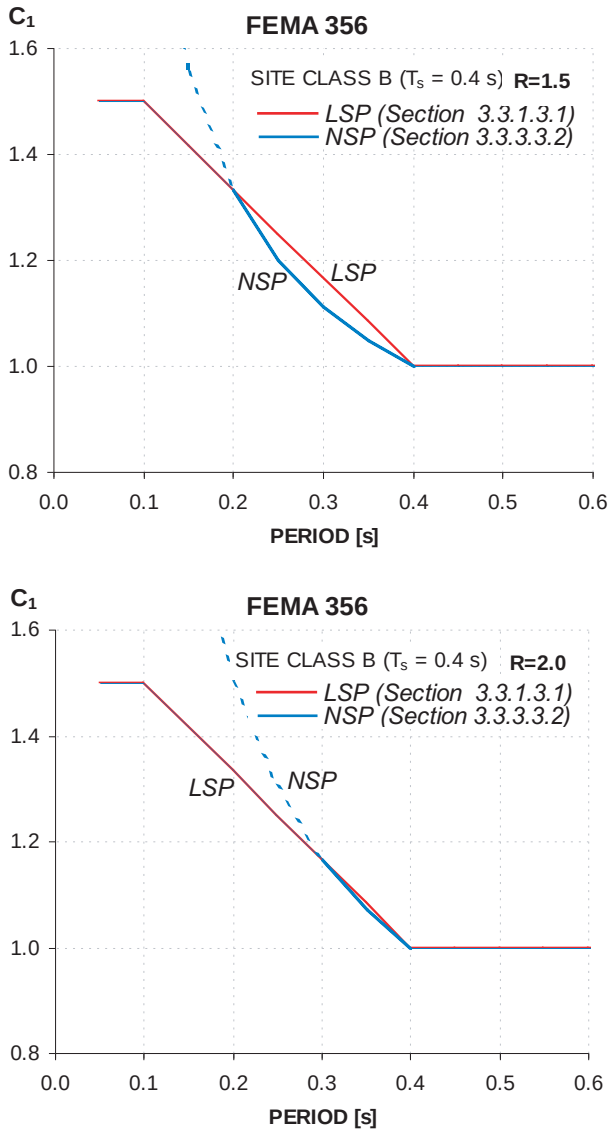


Figure 3-10 A close up view of the effect of the capping limitation of $C_1$ coefficient.

The most important observation that can be made from Figure 3-9 is that with the limitations on $C_1$ imposed by FEMA 356 for structures with short periods of vibration (often referred to as "capping"), the $C_1$ coefficient becomes independent of the lateral strength of the structure. This means that changes in $R$ do not produce changes in lateral displacement demand. Figure 3-10 shows a close-up view of the $C_1$ coefficients for site class B as a function of period. For $R$ = 1.5 (top graph) the equation specified in the NSP will control this coefficient for periods between 0.2 and 0.4 s, while for $R$ = 2.0 (bottom graph) the NSP equation has only a minimal effect for periods between 0.3 and 0.4 s. For

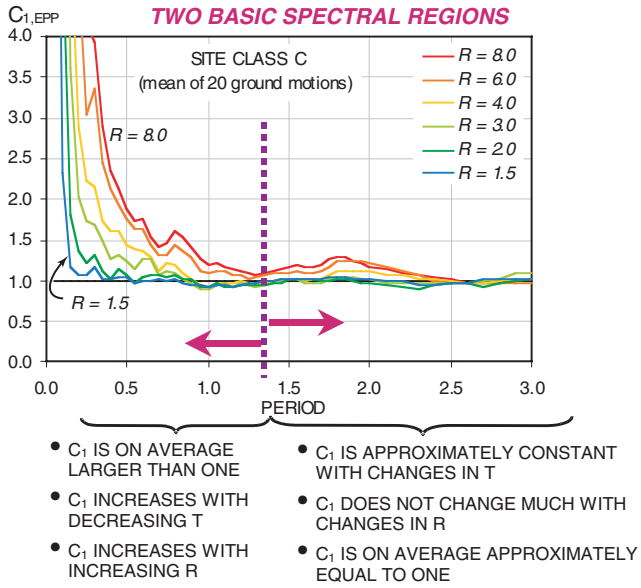


Figure 3-11 Variation of mean $C_1$ computed for the elastic perfectly plastic (EPP) model when subjected to ground motions recorded on site class C.

values of $R$ approximately larger than 2.5, the capping equation will always control the value of $C_1$.

Mean values of the computed ratio of the maximum displacement for inelastic response of a SDOF oscillator with non-degrading hysteretic behavior, to the maximum displacement had the oscillator remained elastic when subjected to 20 ground motions recorded on site class C, is shown in Figure 3-11. It can be seen that this ratio is clearly different in two spectral regions. Based on this figure, the following observations can be made:

- For periods longer than about 1.0 s, the computed $C_1$ ratio is on average fairly insensitive to the level of strength (i.e., the value of $C_1$ does not change much with changes in $R$).
- In the long-period spectral region, the computed $C_1$ ratio is on average independent of the period of vibration (i.e., the value of $C_1$ does not change much with changes in $T$).
- The equal-displacement approximation is a relatively good approximation of the expected value of $C_1$ in the long-period spectral region (i.e., the value of $C_1$ is approximately equal to one when $T >$ 1.3).

- In the short-period region, inelastic displacements are on average larger than elastic displacements (i.e., $C_1$ is larger than one).
- In the short-period region, the value of $C_1$ is highly dependent (i.e., very sensitive) on the level of lateral strength. In general, $C_1$ increases as $R$ increases (i.e., as the lateral strength decreases).
- In the short-period region, the value of $C_1$ is sensitive to changes in the period of vibration. In general, for a given $R$, a decrease in period produces an increase in $C_1$.
- The transition period dividing the region in which the equal-displacement approximation underestimates displacement, from the region in which this approximation applies (short- versus long-period region), increases as the lateral strength decreases (as $R$ increases).

Figure 3-12 presents a comparison of mean values of coefficient $C_1$ generated from the nonlinear response-history analyses for site classes B, C, and D. The transition period dividing the region in which the equal-displacement approximation underestimates displacements, from the region in which this approximation is valid, increases as the site becomes softer. For site classes B and $R$ smaller than 8, this period is approximately 1.0 s; for site class C it is approximately 1.1 s; and for site class D it is approximately 1.4 s.

Figure 3-13 compares mean values of the computed ratio of the maximum displacement for inelastic response of a SDOF oscillator with elasto-plastic hysteretic behavior to the maximum displacement had the oscillator remained elastic when subjected to 20 ground motions recorded on site B to the approximate coefficient $C_1$ specified in FEMA 356.

The FEMA 356 transition period, dividing the region in which the equal-displacement approximation underestimates displacements, from the region in which this approximation is valid, is shorter than that observed for the ground motions used in this study. For example, for site class B, the transition period in FEMA 356 is 0.4 s while results from nonlinear response-history analyses suggest that this period should be about twice as long. The transition periods that can be observed from these nonlinear response-history analyses in Figure 3-12 (approximately 1.0 s, 1.1 s and 1.4 s for site classes B, C and D, respectively) are all significantly longer than those specified in FEMA 356 (0.4 s, 0.55 s, 0.6 s, for site classes B, C, and D, respectively).

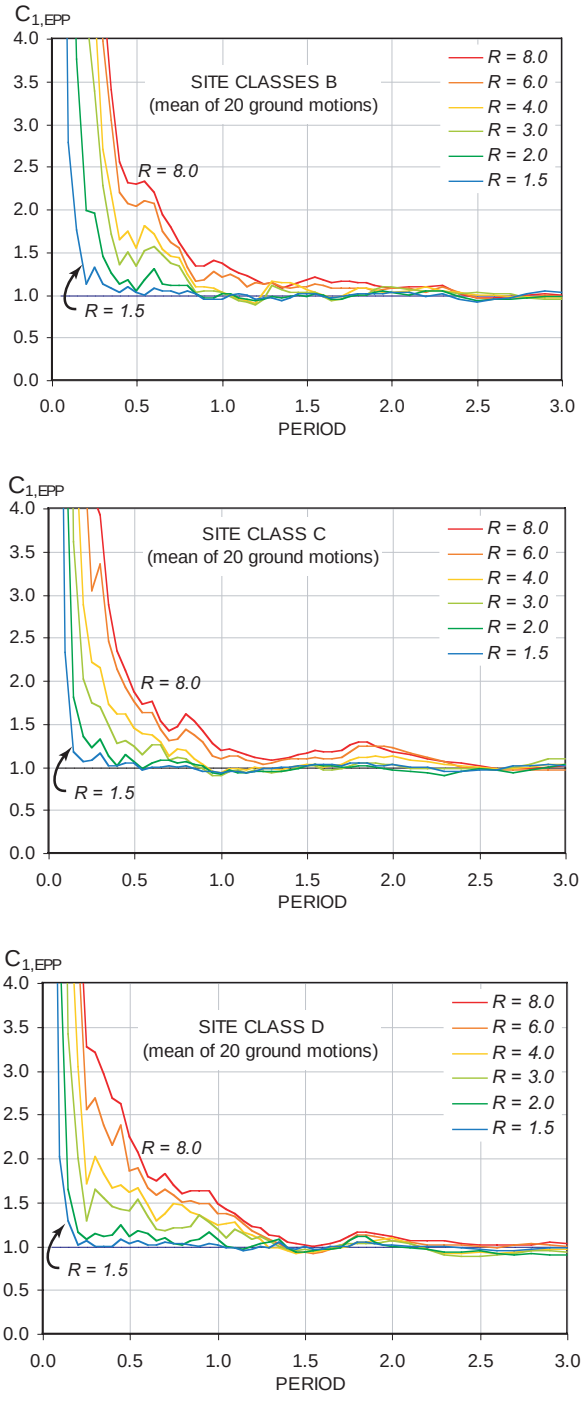


Figure 3-12 Mean coefficient $C_1$ for site classes B, C and D.

While results from nonlinear response-history analyses indicate a strong sensitivity of the computed $C_1$ ratio with changes in $R$ for short periods, the capping in FEMA 356 practically eliminates this sensitivity to lateral strength. For example, mean inelastic displacement ratios computed from response-history analyses for a period of 0.3 s suggest that a change in $R$

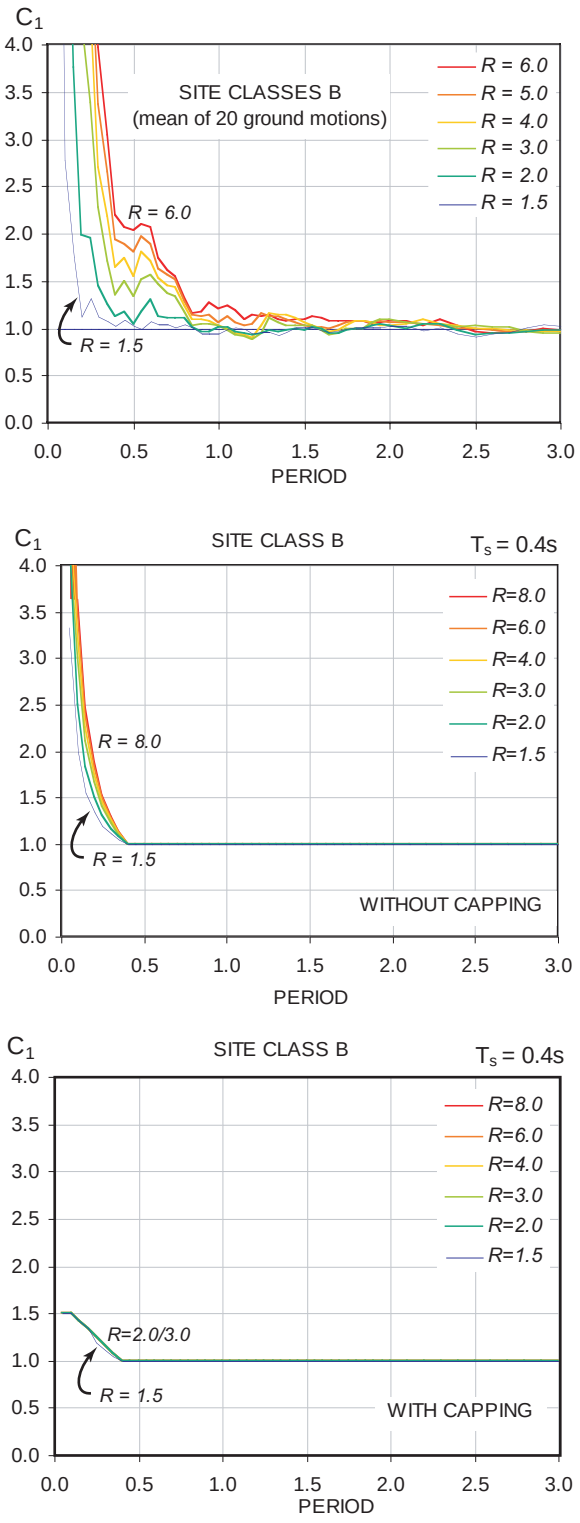


Figure 3-13 Comparison between the mean $C_1$ computed from nonlinear response-history analyses to $C_1$ in FEMA 356 (non-capped and capped).

from 2 to 8 almost triples the value of $C_1$, while the capped coefficient in FEMA 356 leads to the conclusion that the displacement of these systems is the same regardless of the lateral strength of the structure.

In the absence of the cap on $C_1$, the equation currently used in FEMA 356 to estimate this coefficient in section 3.3.3.3.2 does not capture the effect of changes in lateral strength on displacement demands. For example, for SDOF systems with periods of 0.3 s, one with $R = 2$ and the other with $R = 8$, the expression in FEMA 356 would indicate that the displacement demand in the weaker system would be only about 15% larger than the displacement demand in the stronger system, while response-history analyses indicate a much larger sensitivity to lateral strength.

Figure 3-14 shows inelastic displacement ratios computed for two ground motions recorded in very soft soil sites in the San Francisco Bay Area during the 1989 Loma Prieta earthquake. It can be seen that despite being in the same site class, the inelastic displacement ratios can be very different. For example, for a structure with a 1 s period and $R = 6$ at the Larkspur site $C_1$ can reach 2.8 (displacement for the inelastic oscillator 2.8 times larger than the maximum elastic), while at the Emeryville site it is 0.65 (displacement for the inelastic oscillator smaller than the maximum elastic). In order to obtain a better characterization of maximum displacement ratios, periods of vibration were normalized by the predominant period of the ground motion, as first proposed by Miranda (1991, 1993). The predominant period, $T_g$, of the ground motion is computed as the period of vibration corresponding to the maximum 5% damped relative-velocity spectral ordinate. Examples of the computation of $T_g$ for these two recording stations are shown in Figure 3-15. The resulting inelastic displacement ratios are shown in Figure 3-16, where it can be seen that when the periods of vibration are normalized, a better characterization of displacement demands is obtained. As shown, inelastic displacement ratios at soft soil sites are characterized by values larger than one for normalized periods smaller than about 0.7, values smaller than one for normalized periods between 0.7 and 1.5 s, and values approximately equal to one for longer normalized periods.

Mean inelastic ratios computed for 20 ground motions for site class E are shown in Figure 3-17. The same trend observed in individual records is preserved for the mean. Additional information on inelastic displacement demands of structures on very soft soil can be found in Ruiz-García and Miranda (2004).

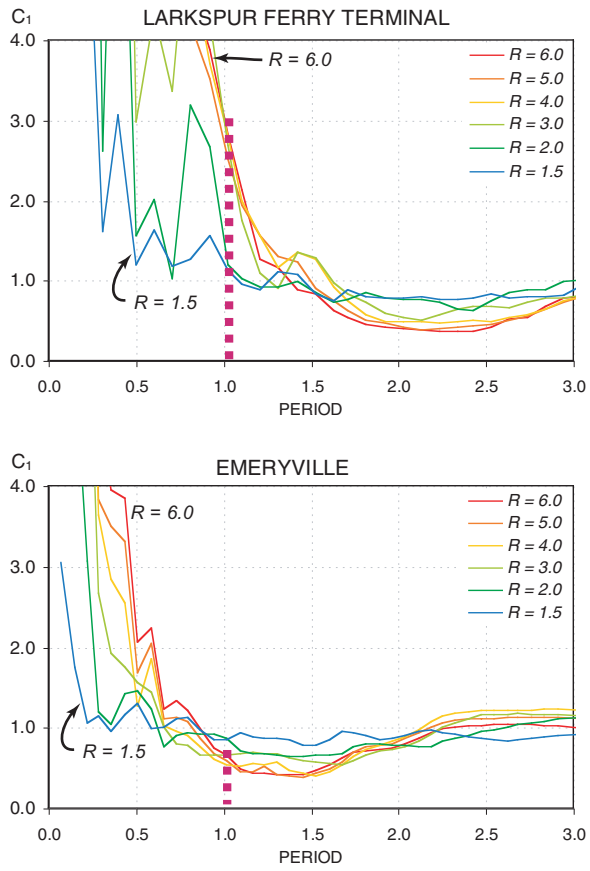


Figure 3-14 Variation of $C_1$ for two individual ground motions recorded on soft soil E.

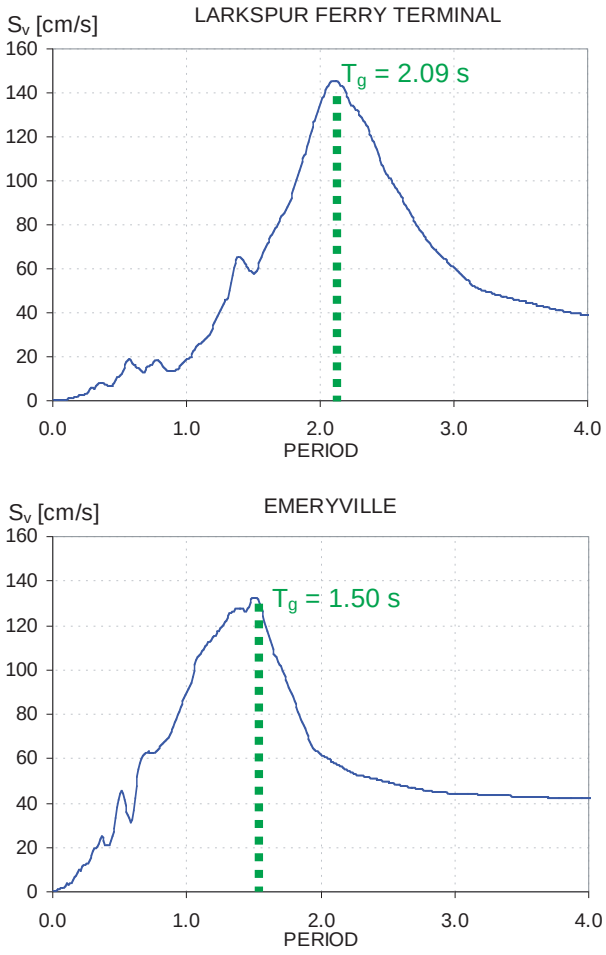


Figure 3-15 Predominant ground motion periods for the soft soil records obtained at Larkspur Ferry Terminal and Emeryville during the 1989 Loma Prieta earthquake.

Inelastic displacement ratios for near-fault ground motions influenced by forward directivity effects can be computed in an analogous manner by normalizing the periods of vibration by the pulse period, which was computed using the same procedure as for soft soils (refer to Figure 3-15).

The procedure described in Section 3.2 was used to calculate mean errors associated with the FEMA 356 specifications for the coefficient $C_1$ when compared with the nonlinear response-history benchmark. Figure 3-18 shows mean errors corresponding to maximum displacement demands computed using FEMA 356 with and without capping when subjected to ground motions recorded on site classes B and C. These mean errors correspond to displacements computed with $C_2 = C_3 = 1$, normalized by the benchmark displacement demands computed with an EPP hysteretic model. It can be seen that, in general, the results are very good for periods of vibration larger than 1.0, where the equal-displacement approximation provides acceptable results with only small overestimations.

In Figure 3-18, it is evident that for site class B and periods between 0.4 s and 1.0 s, the underestimation of the transition period leads to underestimation of maximum displacement. Underestimation increases as $R$ increases. For example, for a period of 0.4 s, benchmark displacements are on average 1.8 times larger than approximate displacements for $R = 8$. Similar underestimations are produced for site class C.

For periods smaller than 0.4 s in the case of site class B, and for periods smaller than 0.55 s in the case of site class C, the use of capping on $C_1$ leads to large underestimation of displacements when $R$ is larger than 2. When the capping is removed, in some cases large

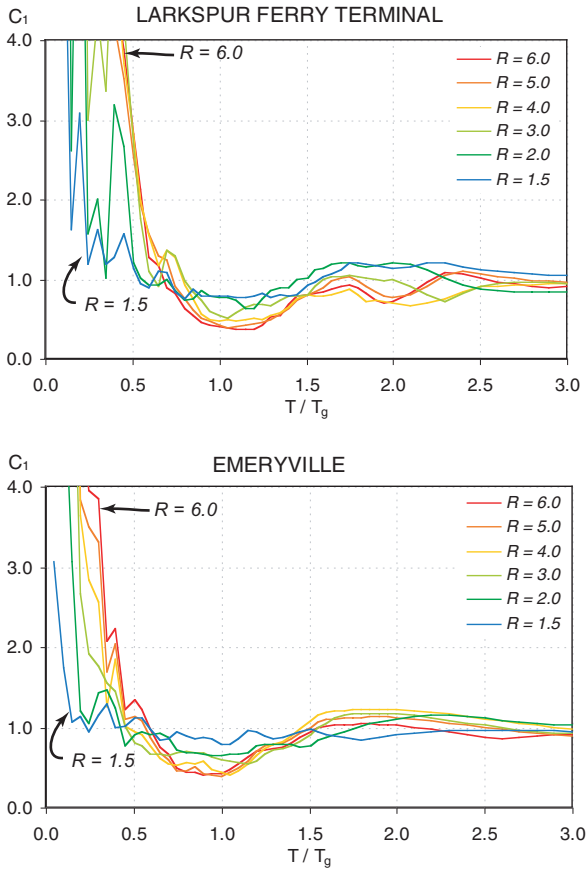


Figure 3-16 $C_1$ values of Larkspur Ferry Terminal and Emeryville soft soil records for normalized periods of vibration with respect to dominant ground motion periods of each record.

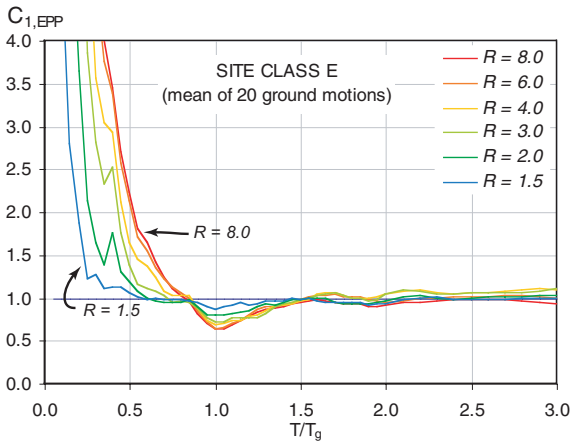


Figure 3-17 The variation of mean $C_1$ values for site class E.

underestimations of displacements are produced while in other cases large overestimations of displacements are computed. This suggests that the variation of $C_1$ with changes in period and lateral strength as specified in FEMA 356 could be improved.

### 3.4.3 *Degrading System Response (Coefficient $C_2$)*

The coefficient $C_2$ is a modification factor to represent the effect of pinched hysteretic shape, stiffness degradation, and strength deterioration on the maximum displacement response according to FEMA 356. Values of $C_2$ for implementation in FEMA 356 depend on the type of structural framing system and structural performance levels being considered (i.e., immediate occupancy, life safety, and collapse prevention). Values of coefficient $C_2$, computed according to Table 3-3 in FEMA 356, are shown in Figure 3-19.

Benchmark ratios of the maximum displacement demand were calculated by dividing the maximum displacement for the stiffness-degrading oscillator (SD) model by that for the EPP model when both were subject to actual ground motions. This ratio thus corresponds with the coefficient $C_2$. Mean ratios were calculated for the different site classes. An example for ground motions recorded on site class D is shown in Figure 3-20. With the exception of periods of vibration smaller than about 0.6 s, the maximum displacements of SD models are on average slightly smaller (3% to 12%) than that of the EPP systems. Although this may seem surprising considering the smaller hysteresis loops of the SD model, the results shown in this figure are consistent with previous investigations (Clough, 1966; Clough and Johnston, 1966; Chopra and Kan, 1973; Powell and Row, 1976; Riddel and Newmark, 1979; Mahin and Bertero, 1981; Gupta and Kunnath, 1998; Foutch and Shi, 1998; and Gupta and Krawinkler, 1998). The coefficient $C_2$ specified in FEMA 356, in contrast, increases lateral displacements in this period range.

For periods of vibration smaller than about 0.6 s, lateral displacement of SD systems are generally larger than those of non-degrading EPP systems. Differences increase with increasing $R$. This observation is similar to observations of several of the studies mentioned previously. Values of $C_2$ in the period range specified in FEMA 356 are generally higher than those computed for relatively strong SD systems ($R < 3$) but smaller than those computed for relatively weak SD systems.

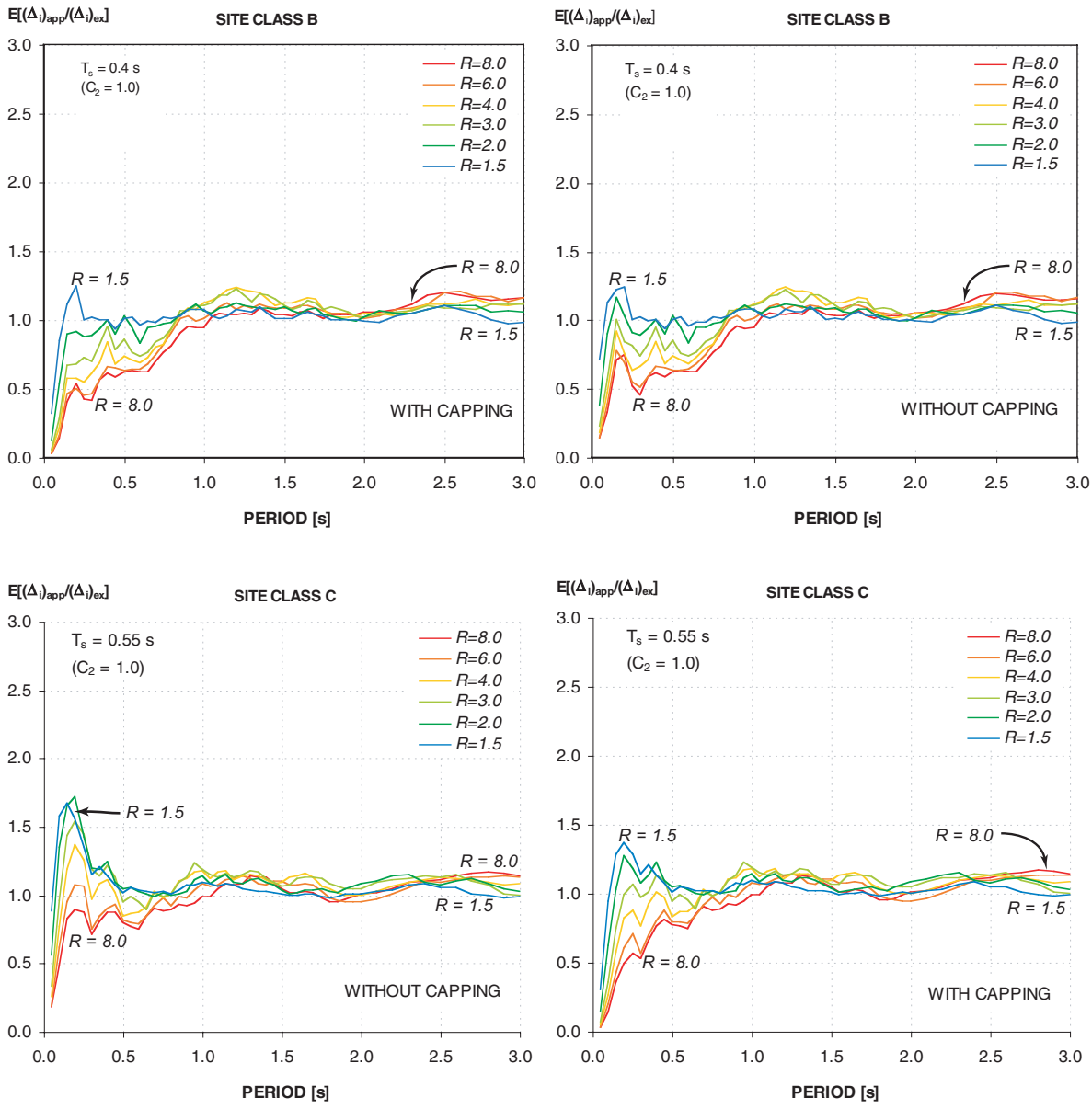


Figure 3-18 Mean error statistics of capped and not capped $C_1$ values for the ground motions recorded in site classes B and C, respectively.

Mean ratios of maximum displacements of strength-and-stiffness degrading (SSD) systems to those of EPP systems are shown in Figure 3-21, which shows very similar trends. However, in the case of periods shorter than 0.8 s, the increase in lateral displacement produced by SSD behavior is larger than that produced by stiffness degradation only. For periods longer than 0.8 s, the maximum displacement of SSD systems is on average equal to that of EPP systems. It should be noted that displacement ratios shown in Figures 3-20 and 3-21 only correspond to mean (average) values and that a very large uncertainty exists, particularly for periods smaller than 0.6 s.

Figure 3-22 presents mean errors calculated from the ratio of the displacements computed with FEMA 356 (with and without capping of $C_1$) for $C_2$ computed assuming a life safety structural performance level to the maximum displacements computed with nonlinear response-history analyses using the SD model. Results

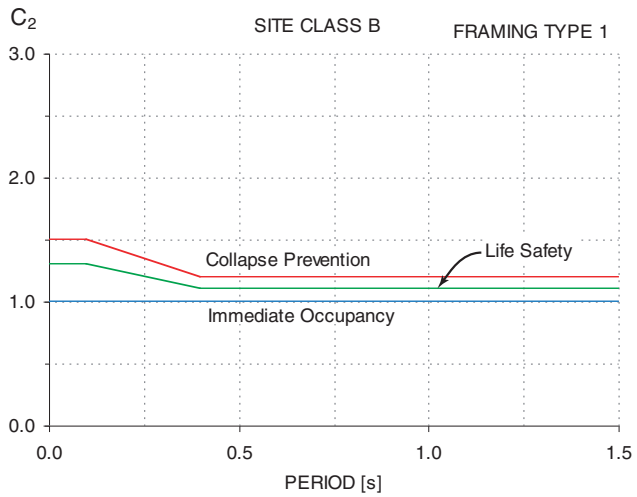


Figure 3-19 A sample variation of $C_2$ values in accordance with FEMA-356

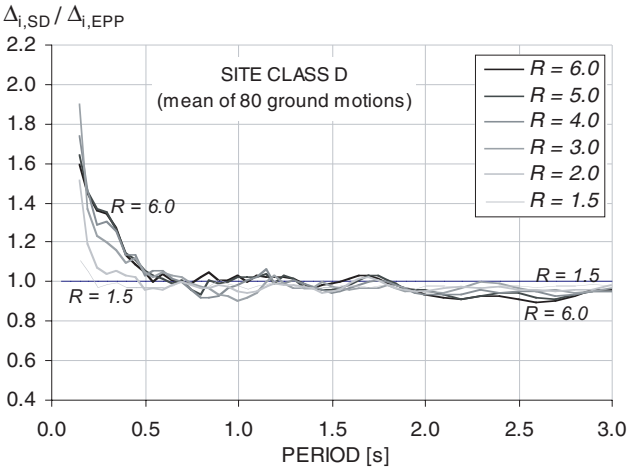


Figure 3-20 Mean displacement ratio of SD to EPP models computed with ground motions recorded on site class D.

presented in this figure are for site class B. For periods of vibration larger that 1.0 s, the simplified method in FEMA 356 overestimates displacements by about 25%. For short periods of vibration, maximum displacements tend to be overestimated for small values of *R* and underestimated for large values of *R*. This trend is more pronounced when capping is included.

Figure 3-23 presents mean errors calculated from the ratio of the displacements computed using $C_1$ and $C_2$ as determined from FEMA 356 to maximum displacements computed with nonlinear response-history analyses for the SSD model. Results in this case

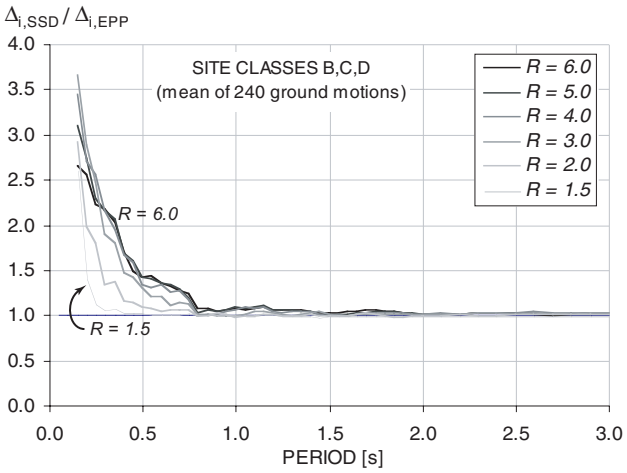


Figure 3-21 Mean displacement ratio of SSD to EPP models computed with ground motions recorded on site classes B, C, and D.

correspond to site class C. The trends are in general similar to those presented in Figure 3-22; however, in this case overestimations are larger and underestimations are smaller.

### 3.4.4 *P-Δ Effects (Coefficient $C_3$)*

The displacement modification factor $C_3$ is intended to account for increased displacements due to dynamic *P-Δ* effects. Displacement modification factors ($C_3$) computed using Equation 3-10 of FEMA 356 are shown in Figure 3-24. Displacement amplifications increase as the post-yield negative stiffness ratio $\alpha$ decreases (becomes more negative), as *R* increases, and as the period of vibration decreases.

In order to evaluate this coefficient, the model shown in Figure 3-25 was considered. Several studies have shown that systems with negative post-elastic stiffness may exhibit dynamic instability when subjected to earthquake ground motions (Jennings and Husid, 1968; Husid, 1969; Bernal 1987, 1992; MacRae, 1994; and Miranda and Akkar, 2003). An example from Miranda and Akkar (2003) is shown in Figure 3-26. In this figure, the ratio of maximum displacement of the system with negative post-yield stiffness to the maximum displacement in an elastic system is plotted for two systems with a period of 1.0 s as a function of *R* when subjected to a recorded earthquake ground motion. The darker line represents a system with relatively severe negative post-elastic stiffness, while the light line represents a system with more moderate negative post-elastic stiffness. It can be seen that in the system with moderate negative stiffness ($\alpha = -0.06$), *R*

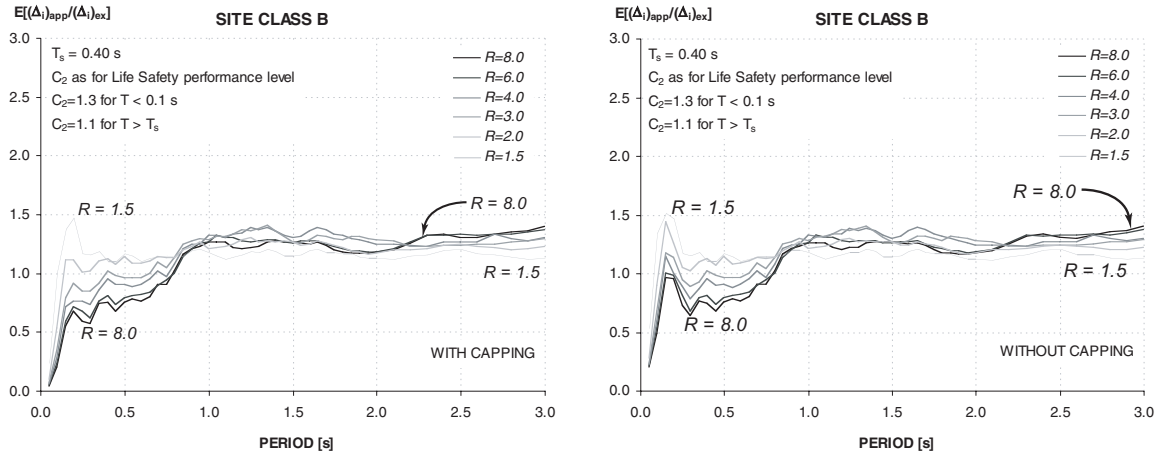


Figure 3-22 The mean error statistics associated with $C_1$ and $C_2$ assuming a Life Safety performance level in accordance with FEMA 356 for stiffness degrading (SD) systems.

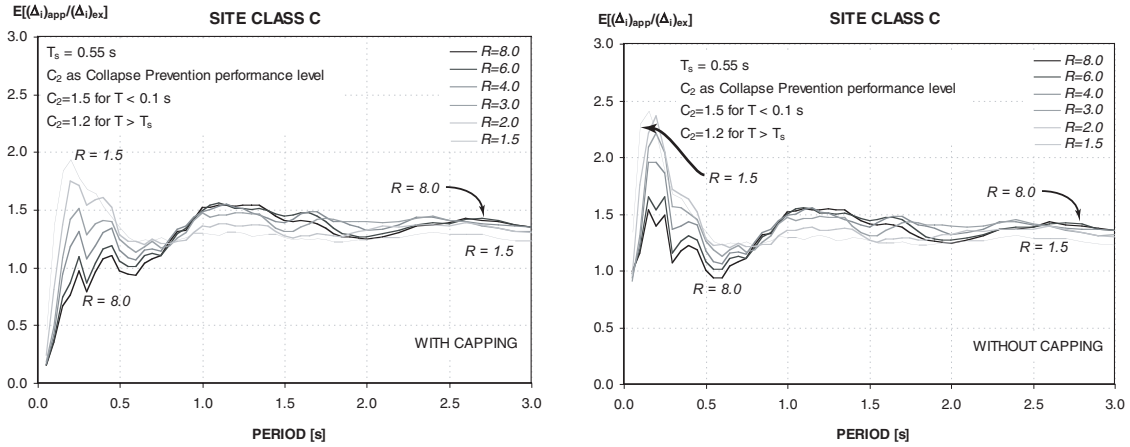


Figure 3-23 The mean error statistics associated with $C_1$ and $C_2$ assuming a Collapse Prevention performance level in accordance with FEMA 356 for stiffness and strength (SSD) degrading systems.

can be increased to approximately 4 without any significant increase in lateral displacement. Note that $\alpha$ is a ratio of the post-elastic stiffness to the elastic stiffness. Thus, a negative value of $\alpha$ indicates an effective decrease of strength with increasing displacement. If the lateral strength is further decreased ($R$ is further increased), a large, abrupt increase in lateral displacements is produced, and soon after dynamic instability occurs. For the system with more severe negative stiffness ($\alpha = -0.21$), $R$ can only be increased to about 1.8. From this and other similar data, it is clear that systems that may exhibit negative stiffness need to have a minimum lateral strength (an $R$ smaller than a maximum critical value) in order to avoid collapse. Comparison of Figures 3-24 and 3-26 illustrates that this phenomenon is not adequately captured by coefficient $C_3$ in FEMA 356.

It should be noted that $P$-$\Delta$ effects are equivalent to a type of strength degradation that occurs in a single cycle (in-cycle) of vibratory motion. This differs from cyclic strength degradation that occurs in subsequent cycles modeled with the SSD type oscillator. These two types of strength degradation have different implications with respect to dynamic behavior. Further discussion of this subject is contained in Chapter 4.

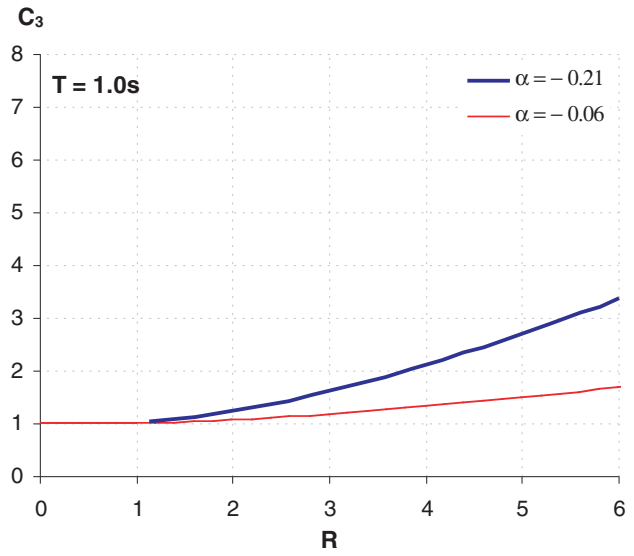


Figure 3-24 The variation of $C_3$ from FEMA 356 with respect to R for different negative post-elastic stiffness values.

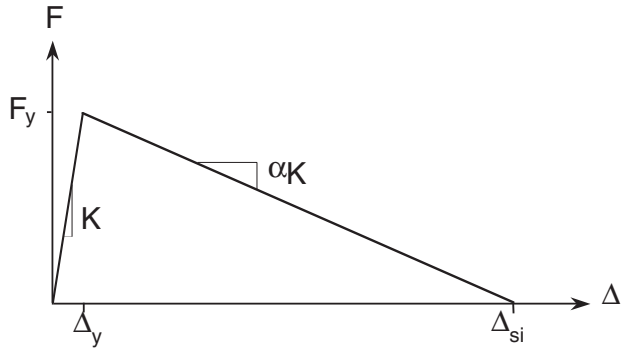


Figure 3-25 Bilinear system with in-cycle negative post-elastic stiffness due to *P-Δ* effects.

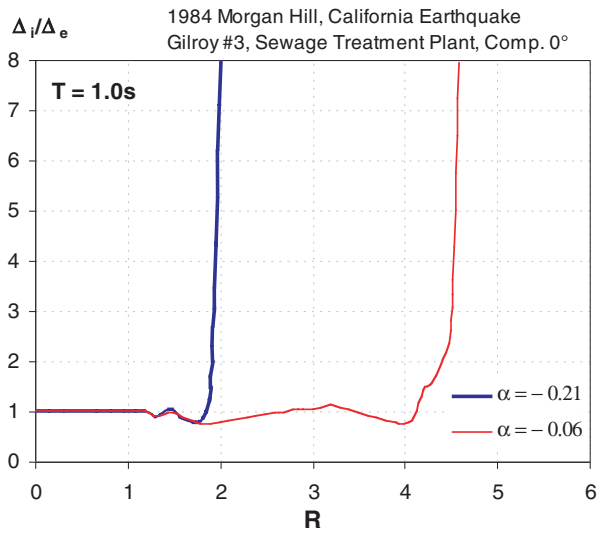


Figure 3-26 Displacement modification factors in SDOF that exhibit in-cycle negative post-yield stiffness.

## 3.5 Nonlinear Elastic Behavior

The results of the response-history analyses for the nonlinear elastic (NE) model are illustrated in Figure 3-27. Comparison with Figure 3-12 indicates that the maximum nonlinear elastic (NE) response is generally greater than the EPP. The difference varies with both period and strength and can exceed 40% in some cases. Neither ATC-40 nor FEMA 356 explicitly address nonlinear elastic behavior. In reality, it is not found often for typical structural systems. It represents a pure rocking response. Virtually all structures exhibit some hysteretic damping that tends to reduce response from that predicted for pure rocking.

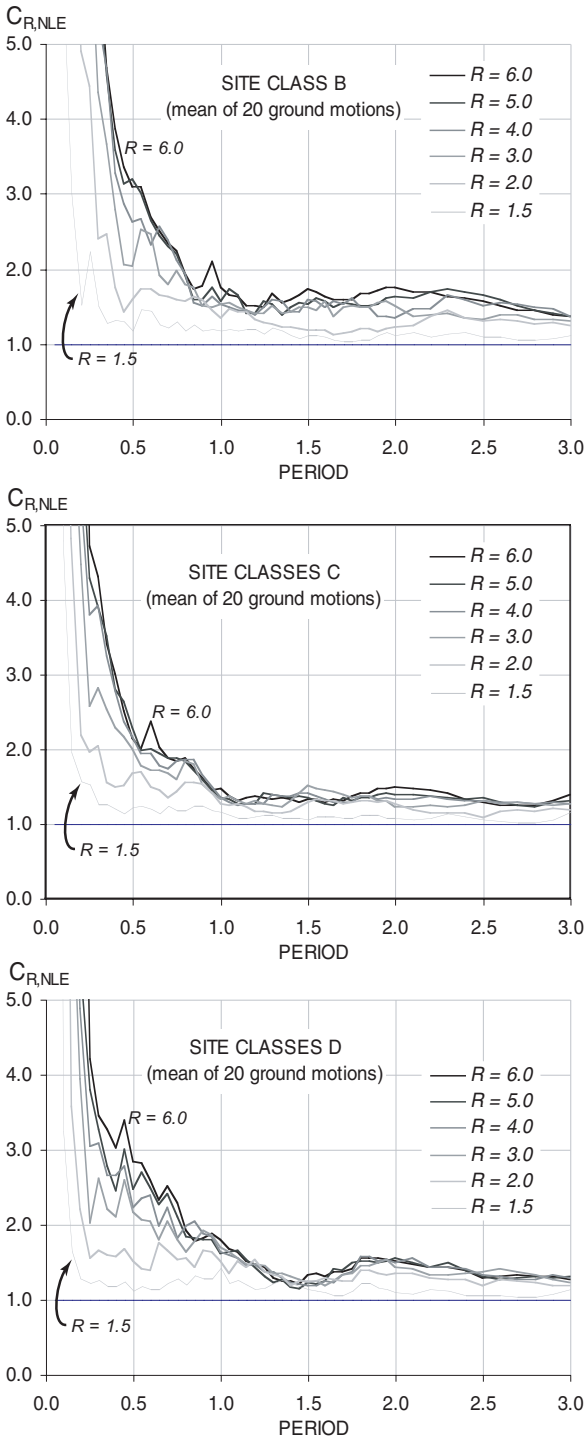


Figure 3-27 Ratio of maximum displacement for a nonlinear elastic (NE) oscillator to elastic response for site classes B, C, and D.

# 4. Strength Degradation

Loss of lateral strength in structures during an earthquake is an issue of concern for engineers. In general, the nonlinear hysteretic characteristics of most buildings include both stiffness degradation and strength degradation to some extent. Strength degradation, including *P-Δ* effects, can lead to an apparent negative post-elastic stiffness in a force-deformation relationship for a structural model using nonlinear static procedures. The performance implications depend on the type of strength degradation. For structures that are affected by component strength losses, including *P-Δ* effects, occurring in the same cycle as yielding, the negative post-elastic slope can lead to dynamic instability of the structural model. For this reason, a suggestion for a minimum strength for such structures is presented in Section 4.4

## 4.1 Types of Strength Degradation

Two types of strength degradation during hysteretic response are shown in Figure 4-1. Both oscillators exhibit inelastic stiffness and strength degradation. The oscillator in Figure 4-1a (*cyclic* strength degradation) maintains its strength during a given cycle of deformation, but loses strength in the subsequent cycles. The effective stiffness also decreases in the subsequent cycles. The slope of the post-elastic portion of the curve during any single cycle of deformation is not negative. Figure 4-1b (*in-cycle* strength degradation) illustrates a different type of strength degradation. Note that the degradation occurs during the same cycle of deformation in which yielding occurs, resulting in a negative post-elastic stiffness. This can be due to actual degradation in the properties of the component due to damage. It is also the consequence of *P-Δ* effects that increase demand on components and effectively reduce strength available to resist inertial loads.

## 4.2 Strength Degradation and SDOF Performance

The strength and stiffness degrading (SSD) oscillators used to evaluate current nonlinear static procedures (see Section 3.2) were similar to those in Figure 4-1a. The results of the evaluation demonstrate that these cyclic strength-degrading oscillators often exhibit maximum displacements that are comparable with those that do not exhibit strength degradation. More importantly, responses are dynamically stable in general, even for relatively weak systems and large ductility.

The in-cycle strength-degrading counterpart discussed in Section 3.4.4, in contrast, can be prone to dynamic instability. Velocity pulses often associated with near-

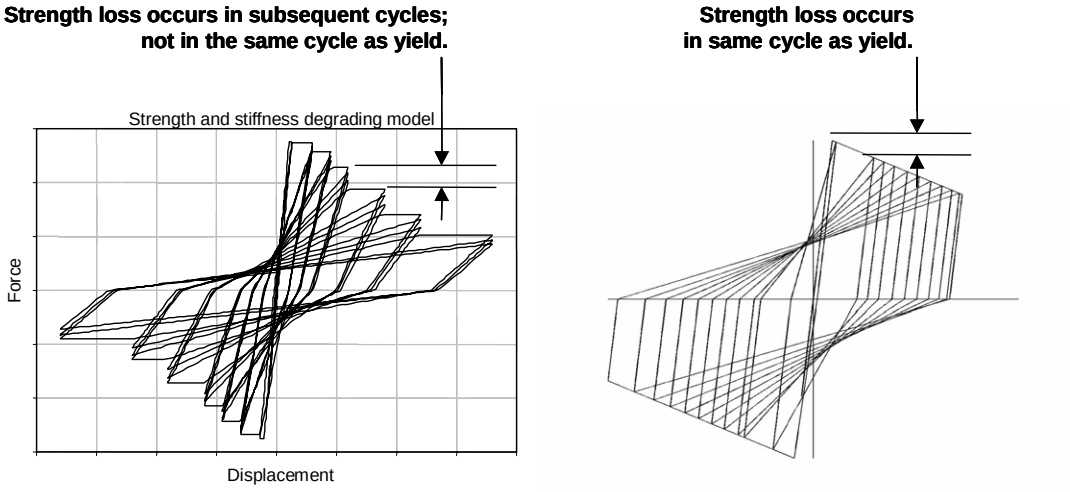


**a) Cyclic strength degradation** **b) In-cycle strength degradation**

Figure 4-1 Two types of strength degradation.

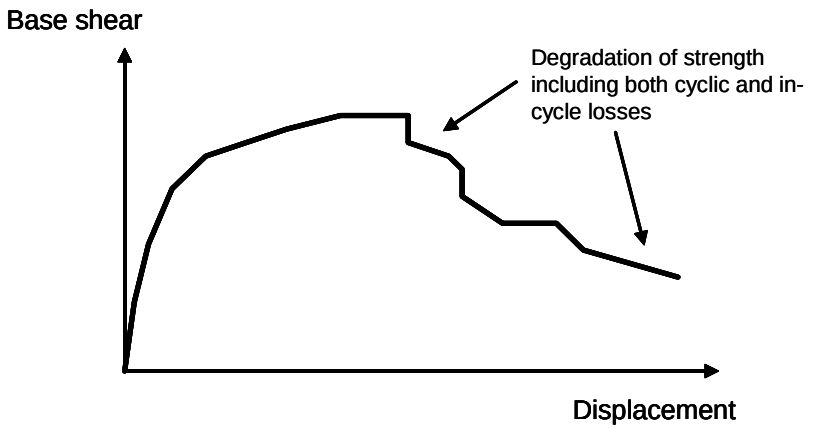


Figure 4-2 Example capacity curve for a medium rise concrete structure

field ground motion records can exacerbate the problem. These pulses can drive the oscillator far into the post-elastic, strength-degrading branch in a single cycle of motion.

## 4.3 Global Force-Deformation Behavior with Strength Degradation

In many structures, strength degradation is complex. A pushover curve for an example medium-rise reinforced concrete building is shown in Figure 4-2. There is an apparent negative post-elastic stiffness. This might be due to three effects. First, there could be cyclic (that is, from cycle to cycle) strength degradation associated with low-cycle fatigue damage of various components in the lateral-force-resisting system. Interspersed might be in-cycle strength losses due to component damage as deformations increase monotonically. Superimposed on this is the negative slope associated with $P$-$\Delta$ effects, which may or may not be significant. Unfortunately, it is not possible to distinguish between cyclic and in-cycle strength losses solely from information normally available from a nonlinear static analysis. The $P$-$\Delta$ effects are always present and contribute to real negative post-elastic stiffness. The $P$-$\Delta$ effects are simple to separate from the others. Precise separation of the remaining constituents of strength degradation cannot be inferred directly, since the distribution depends on the nature of individual ground motions and the sequence of inelastic behavior among the various components as a lateral mechanism develops.

For purposes of nonlinear static analysis, the calculated relationship between base shear and displacement of a control node (e.g. roof) may be replaced with an idealized relationship to calculate the effective lateral stiffness ($K_e$), effective yield strength ($V_y$), and effective positive ($\alpha_1$) and/or negative ($\alpha_2$) stiffnesses of the building model, as shown in Figure 4-3. The initial linear portion of the idealized force-displacement curve begins at the origin. A second linear portion ends at a point on the calculated force-displacement curve at the calculated target displacement, or the point of maximum base shear ($V_d$), whichever is least. The intersection of the two idealized segments defines effective lateral stiffness ($K_e$), the effective yield strength ($V_y$), and effective positive post-yield stiffness ($\alpha_1 K_e$). The intersection point is determined by satisfying two constraints. First, the effective stiffness, $K_e$, must be such that the first segment passes through the calculated curve at a point where the base shear is 60% of the effective yield strength. Second, the areas above and below the calculated curve should be approximately equal. For models that exhibit negative post-elastic stiffness, a third idealized segment can be determined by the point of maximum base shear on the calculated force-displacement curve and the point at which the base shear degrades to 60% of the effective yield strength [the same strength that was used to establish $K_e$]. This segment defines the maximum negative post-elastic stiffness ($\alpha_2 K_e$). This negative slope approximates the effects of cyclic and in-cycle degradation of strength. Note that the selection of 60% of the yield strength to define this slope is based purely on judgement.

As noted, nonlinear static procedures are not capable of distinguishing completely between cyclic and in-cycle strength losses. However, insight can be gained by separating the in-cycle $P$-$\Delta$ effects from $\alpha_2$ (see Figure 4-3). An effective post-elastic stiffness can then be determined as

$$\alpha_e = \alpha_{P-\Delta} + \lambda(\alpha_2 - \alpha_{P-\Delta}) \quad (4\text{-}1)$$

where $0 \le \lambda \le 1.0$ .

Current knowledge of component behavior as well as unknown characteristics of the future ground motion make it impossible at present to know the correct value of $\lambda$. For the present, it is recommended that $\lambda$ be assigned a value of 0.2 for sites not subject to near field effects and 0.8 for those that are. These values, solely based on judgment, are intended to recognize the potential for dynamic instability that might arise from in-cycle strength losses associated with large impulsive near-field motions while, at the same time, avoid penalizing structures with predominantly cyclic strength loss associated with non-impulsive motions.

## 4.4 Limitation on Strength for In-Cycle Strength Degradation Including *P-Δ* Effects

When using displacement modification techniques similar to the coefficient method of FEMA 356, it is recommended that the displacement prediction be modified to account for cyclic degradation of stiffness and strength. Chapter 5 presents an improved procedure for calculating the coefficient $C_2$ for this purpose. It is also suggested that the current coefficient $C_3$ be eliminated and replaced with a limit on minimum strength (maximum value of $R$) required to avoid dynamic instability. The same limitation on $R_{max}$ is recommended for the equivalent linearization alternative in ATC-40 as modified in Chapter 6 of this document.

The recommended limitation on the design force reduction, $R_{max}$, is as follows (see also Figure 4-3 for notation):

$$R_{\max} = \frac{\Delta_d}{\Delta_y} + \frac{|\alpha_e|^{-t}}{4} \quad (4\text{-}2)$$

where

$$t = 1 + 0.15 \ln T \quad (4\text{-}3)$$

If this limitation is not satisfied, then a nonlinear dynamic analysis using representative ground motion records for the site should be implemented to investigate the potential for dynamic instability. The structural model must appropriately model the strength degradation characteristics of the structure and its components.

Equation 4-2 is a simplification of an expression derived by Miranda and Akkar (2003), which was obtained using single-degree-of-freedom systems. It should be noted that significant variability exists in the strength required to avoid dynamic instability; hence, this equation is aimed only at identifying cases where dynamic instability should be further investigated using response history analyses and not as an accurate measure of the lateral strength required to avoid dynamic instability in MDOF structures.

The use of the equivalent linearization techniques (see Chapter 6) can provide initial insight into whether the

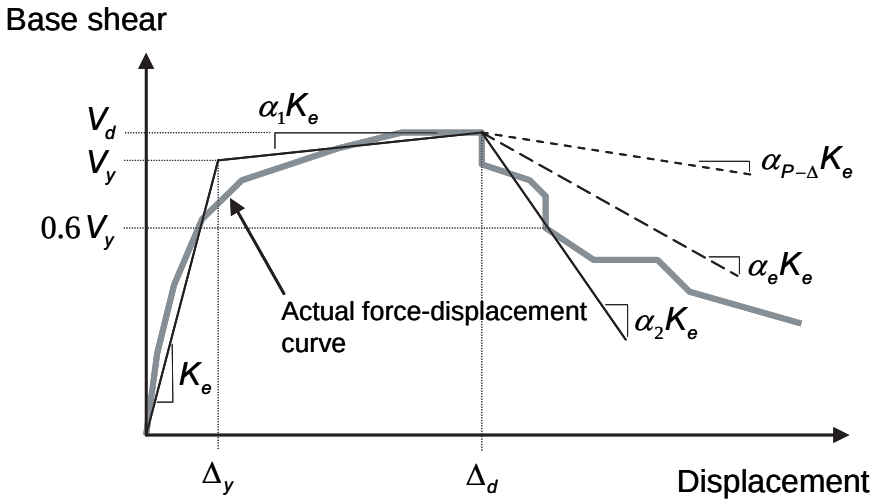


Figure 4-3 Idealized force-displacement curve for nonlinear static analysis

nonlinear dynamic analysis is worthwhile. In particular, solution procedure C produces a locus of potential performance points. If this locus tends to be parallel to and above the capacity curve, then dynamic instability is indicated according to that procedure. However, if the locus intersects the capacity curve, instability is not indicated; nonlinear dynamic analysis may be fruitful in demonstrating this stability.

# 5. Improved Procedures for Displacement Modification

## 5.1 Introduction

Based on the evaluation summarized in Chapter 3 and available research data, suggested improvements to the Coefficient Method of FEMA 356 have been developed and are presented in this chapter. Recommendations include several improved alternatives for the basic ratio of the maximum displacement (elastic plus inelastic) for an elastic perfectly plastic SDOF oscillator to the maximum displacement for a completely linear elastic oscillator that is designated as the coefficient $C_1$ in FEMA 356. This chapter also recommends that the current limitations (capping) allowed by FEMA 356 to the coefficient $C_1$ be abandoned. In addition, a distinction is recognized between two different types of strength degradation that have different effects on system response and performance, as discussed in Chapter 4. This distinction leads to recommendations for the coefficient $C_2$ to account for cyclic degradation in strength and stiffness. It is also suggested that the coefficient $C_3$ be eliminated and replaced with a limitation on strength in accordance with Section 4.4.

The proposed expressions for coefficients in this section are based on empirical data. They have been formulated to provide estimates of expected values based on available analytical results on the response of SDOF oscillators subjected to ground motion records. As noted in the subsequent text, there is dispersion, at times large, in the data. The user should be cognizant of this when applying these procedures in practice.

## 5.2 Maximum Displacement Ratio (Coefficient $C_1$)

The coefficient $C_1$ in FEMA 356 is used along with other coefficients in a nonlinear static procedure known as the Coefficient Method. This form of displacement modification is described in more detail in Section 3.4.1 of this document and in Chapter 3 of FEMA 356. As a result of the work summarized in Chapter 3 and a review of available pertinent research, improvements to the coefficient $C_1$ can be made. A relatively simple expression is proposed here. As noted in Section 3.4.1, FEMA 356 currently allows the coefficient $C_1$ to be limited (capped) for relatively short-period structures. It is suggested that this limitation not be used. This may increase estimates of displacement for some structures. However, Chapter 8 presents rational procedures to account for some of the characteristics of short-period structures that may reduce their response to ground motions in lieu of the current limitations on the coefficient $C_1$.

### *5.2.1 Simplified Expression*

For most structures the following simplified expression may be used for the coefficient $C_1$:

$$C_1 = 1 + \frac{R-1}{a T_e^2} \tag{5-1}$$

where $T_e$ is the effective fundamental period of the SDOF model of the structure in seconds and $R$ is the strength ratio computed with Equation 3-16 of the FEMA 356 document. The constant $a$ is equal to 130, 90, and 60 for site classes B, C, and D, respectively. For periods less than 0.2 s, the value of the coefficient $C_1$ for 0.2 s may be used. For periods greater than 1.0 s, $C_1$ may be assumed to be 1.0.

This expression provides improved estimation of the ratio of peak deformations of inelastic SDOF systems with elasto-plastic behavior to peak deformations of linear single-degree-of-freedom systems. Equation 5-1 is plotted in Figure 5-1. This equation estimates mean values of this ratio. Considerable dispersion (scatter) exists about the mean. For information and discussion of the dispersion of $C_1$ see Ruiz-Garcia and Miranda (2003). When interpreting results and assessing structural performance, engineers should consider the implications of these uncertainties. For example, the expression can be used with $a$ = 60 for softer sites (class E and F) to estimate displacements, but it is less reliable due to very high dispersion of results in studies of SDOF oscillators for soft sites. Similarly, this equation may not provide completely adequate results for ground motions strongly influenced by forward directivity effects, for the same reason.

Systems with nonlinear elastic hysteretic behavior (e.g. rocking) can have deformation ratios larger than those computed with Equation 5-1. Results of the studies for nonlinear elastic systems (NE) summarized in Section 3.5 indicate that these oscillators can exhibit displacements up to 40% larger than their elasto-plastic counterparts. However, most systems that exhibit rocking also have some hysteretic energy dissipation (as

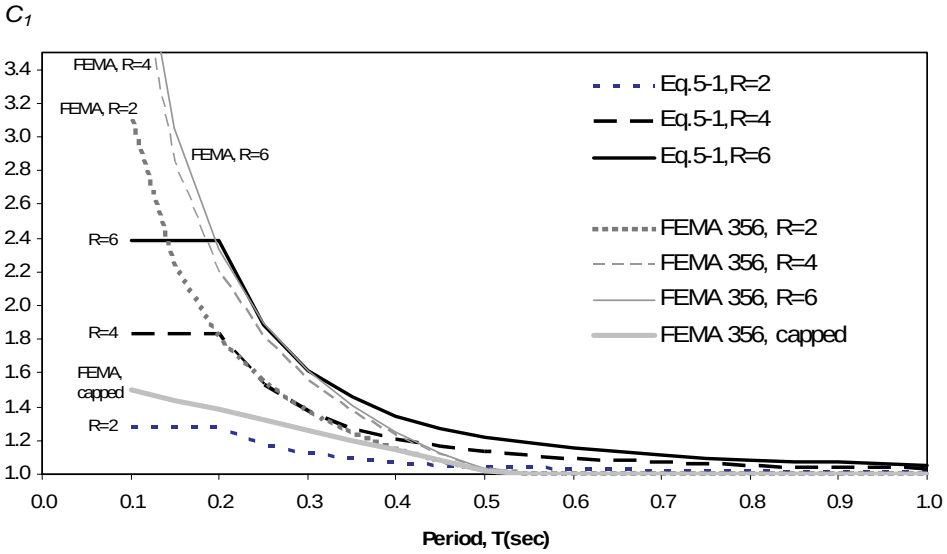


Figure 5-1 Expression for coefficient $C_1$ (Eqn.5-1 with $a = 90$ for site class C) and current FEMA 356 expression.

opposed to the "pure" rocking of the NE oscillator) that would likely reduce this tendency. Specific recommendations cannot be made at this point and further study is warranted.

Recently, various studies have proposed simplified expressions for $C_1$. Figure 5-2 compares the $C_1$ computed with Equation 5-1 assuming site class C to that proposed by other investigators (Aydinoglu and Kacmaz, 2002; Ramirez et al., 2002; Ruiz-Garcia and Miranda, 2003; Chopra and Chintanapakdee, 2003). With exception of the study by Ramirez et al., all deformation ratios plotted in Figure 5-2 are for EPP hysteretic behavior. Deformation ratios by Ramirez et al. shown in Figure 5-2 were computed using constants recommended for systems with post-elastic stiffnesses of 5% of the elastic. The simplified equation proposed here leads to results that are similar to those of previous investigations.

### 5.2.2 *Limits on Maximum Displacements for Short Periods*

FEMA 356 currently contains a limitation (cap) on the maximum value of the coefficient $C_1$ as described in Section 3.4.1. As noted in Appendix B, the limitation is used by many engineers. The evaluation of the Coefficient Method in Chapter 3 demonstrates that the limitation contributes to inaccuracy in the prediction of maximum displacements. The authors of FEMA 356 included the limitations for two related reasons. First, there is a belief in the practicing engineering community that short, stiff buildings do not respond to seismic shaking as adversely as might be predicted using simplified analytical models. Indeed, there may be logical explanations for this phenomenon, including various aspects of soil-structure interaction. These factors are often cited qualitatively, along with the observed good performance of such buildings in past earthquakes, as justification for less onerous demand parameters in codes and analytical procedures. Traditional design procedures have evolved accordingly, giving rise to a second reason. The authors of FEMA 356 felt that the required use of the empirical equation without relief in the short-period range would motivate practitioners to revert to the more traditional, and apparently less conservative, linear procedures. FEMA 357, *Global Topics Report on the Prestandard and Commentary for the Seismic Rehabilitation of Buildings* (ASCE, 2000b), has a discussion of the issue and addresses the concern about the limitations (capping) on $C_1$ and the potential for underestimating the displacement response of weak structures.

In an effort to deal more logically with the characteristics of short-period structures that may reduce their response to strong ground motions from that predicted by current analysis procedures, this document includes the development of rational procedures in Chapter 8. It is suggested that these be used in lieu of the limitation in FEMA 356 to estimate the response of short-period structures.

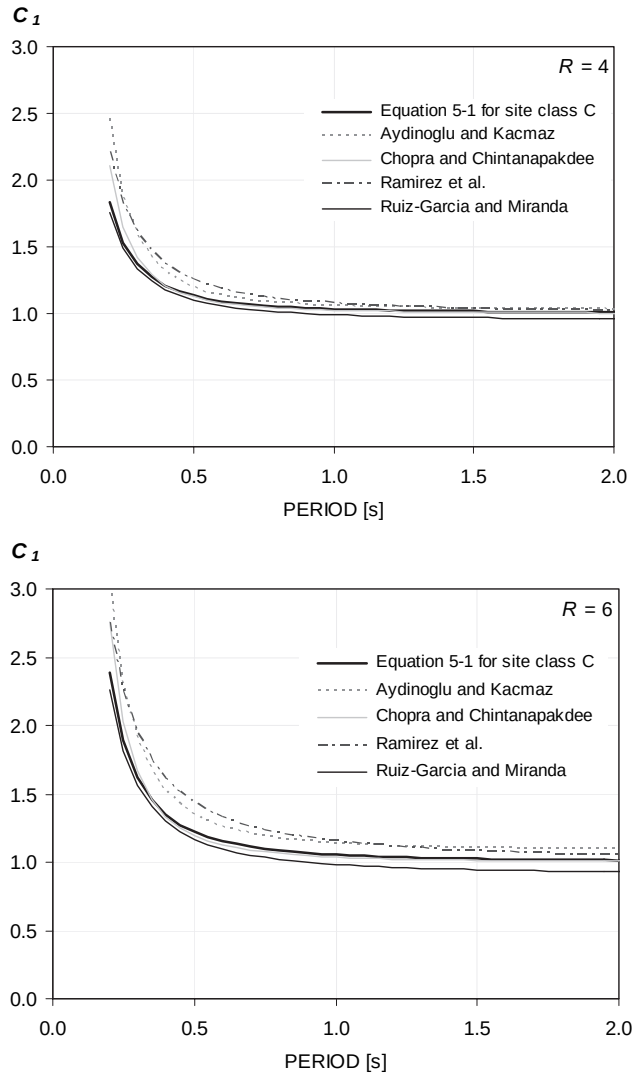


Figure 5-2 Comparison of alternative expressions for the coefficient $C_1$ for $R = 4$ and $R = 6$ for site class C.

## 5.3 Adjustment for Cyclic Degradation (Coefficient $C_2$)

As discussed in Chapter 4, two types of degradation of stiffness and/or strength can affect response. Also, the effects of each type differ from one another. For the purposes of displacement modification procedures in accordance with FEMA 356, it is suggested that the $C_2$ coefficient represent the effects of stiffness degradation only. The effects of strength degradation are addressed by the suggested limitation presented in Chapter 4. It is recommended that the $C_2$ coefficient be as follows:

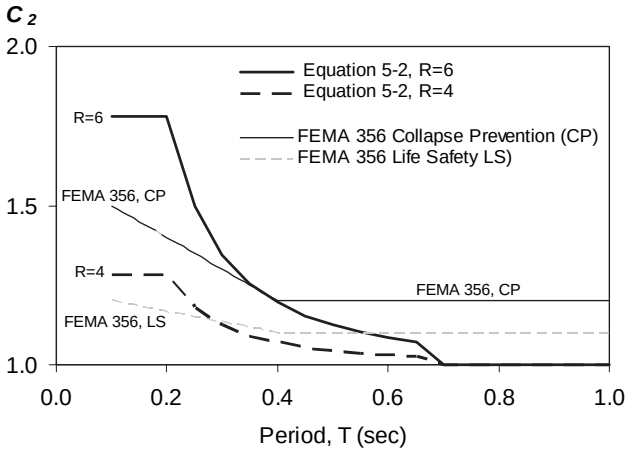


Figure 5-3 Coefficient $C_2$ from Eq. 4-2 and FEMA 356 for site classes B, C, and D.

$$C_2 = 1 + \frac{1}{800}\left(\frac{R-1}{T}\right)^2 \qquad (5\text{-}2)$$

For periods less than 0.2 s, the value of the coefficient $C_2$ for 0.2 s may be used. For periods greater than 0.7 sec, $C_2$ may be assumed equal to 1.0. The expression is plotted in Figure 5-3. The coefficient $C_2$ need only be applied to structures that exhibit significant stiffness and/or strength degradation.

The degree by which deformation demands are increased by cyclic degradation depends on the characteristics of the hysteretic behavior, which are very sensitive to the structural material, detailing, and ground motion characteristics. Because of the many parameters involved, it is difficult to capture the effects of all possible types of cyclic degradation with a single modifying factor. Equation 5-2 represents a simplification and interpretation of many statistical results with various kinds of cyclically degrading systems. The dispersion of results of SDOF oscillator studies used to formulate the $C_2$ factor is larger than that of the $C_1$ factor. It is important to consider this large dispersion when interpreting the results obtained from simplified procedures recommended in this document, particularly for structures with periods of vibration smaller than 0.5s.

## 5.4 Limitation on Strength to Avoid Dynamic Instability for Nonlinear Static Procedures

The studies of the Coefficient Method in Chapter 3 indicate that global displacement demand is not significantly amplified by degrading strength until a critical point at which dynamic instability may occur. This point is related to the initial strength and period of the oscillator as well as the magnitude of the negative post-elastic stiffness caused by in-cycle strength degradation.

It is suggested that the current coefficient $C_3$ be eliminated and replaced with a limit on minimum strength (maximum $R$) required to avoid dynamic instability. The proposed limitation is presented in Section 4.4.

# 6. Improved Procedures for Equivalent Linearization

## 6.1 Introduction

This chapter presents an improved equivalent linearization procedure as a modification to the Capacity-Spectrum Method (CSM) of ATC-40. The CSM is a form of equivalent linearization briefly summarized in Sections 2.4 and 3.3.1. Detailed information on equivalent linearization in general and the derivation of the improved procedures are included in Appendix D.

When equivalent linearization is used as a part of a nonlinear static procedure that models the nonlinear response of a building with a SDOF oscillator, the objective is to estimate the maximum displacement response of the nonlinear system with an "equivalent" linear system using an effective period, $T_{\text{eff}}$, and effective damping, $\beta_{\text{eff}}$ (see Figure 6-1). The global force-deformation relationship shown in Figure 6-1 for a SDOF oscillator in acceleration-displacement response spectrum (ADRS) format is termed a capacity curve. The capacity curve shown in Figure 6-1 is developed using the conventional procedures of FEMA 356 or ATC-40. The effective linear parameters are functions of the characteristics of the capacity curve, the corresponding initial period and damping, and the ductility demand, $\mu$, as specified in the following sections.

Recommendations for the improved equivalent linearization procedures rely on the previous procedures in ATC-40, and much of the process remains the same. This chapter focuses on the parts that change. The following section presents new expressions to determine effective period and effective damping. It also includes a technique to modify the resulting demand spectrum to coincide with the familiar CSM technique of using the intersection of the modified demand with the capacity curve to generate a performance point for the structural model. The reduction in the initial demand spectrum resulting from the effective damping may be determined using conventional techniques outlined in Section 6.3. The previous limits on effective damping of ATC-40 should not be applied to these new procedures. However, the user must recognize that the results are an estimate of median response and imply no factor of safety for structures that may exhibit poor performance and/or large uncertainty in behavior. The effective parameters for equivalent linearization are functions of ductility. Since ductility (the ratio of maximum displacement to yield displacement) is the object of the analysis, the solution must be found using iterative or graphical techniques. Three of these are presented in Section 6.4. They have been developed to be similar to those of ATC-40.

Finally, it should be noted that these procedures may not be reliable for extremely high ductilities (e.g., greater than 10 to 12).

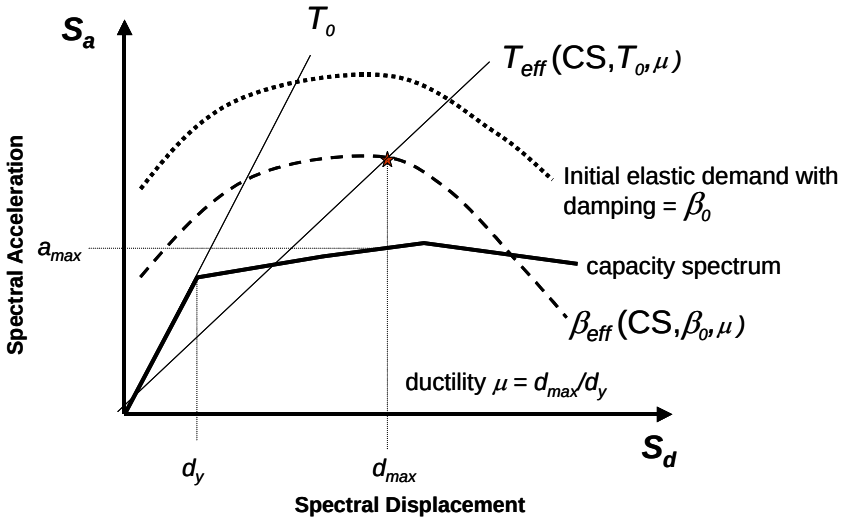


Figure 6-1 Acceleration-displacement response spectrum (ADRS) showing effective period and damping parameters of equivalent linear system, along with a capacity curve.

## 6.2 Basic Equivalent Linearization Parameters

Optimal equivalent linear parameters (i.e., effective period, $T_{\text{eff}}$, and effective damping, $\beta_{\text{eff}}$) are determined through a statistical analysis that minimizes, in a rigorous manner, the extreme occurrences of the difference (i.e., error) between the maximum response of an actual inelastic system and its equivalent linear counterpart. Conventionally, the measurement of error has been the mean of the absolute difference between the displacements. Although this seems logical, it might not lead to particularly good results from an engineering standpoint in which the difference between conservative or unconservative estimates is important. This is illustrated in Figure 6-2. It is possible to select linear parameters for which the mean error is zero, as for the broad, flat distribution. However, the narrower curve might represent equivalent linear parameters that provide better results from an engineering standpoint, since the chance of errors outside a –10% to +10% range, for example, are much lower, even accounting for the –5% mean error. This is owing to the smaller standard deviation. See Appendix D for details on the optimization process.

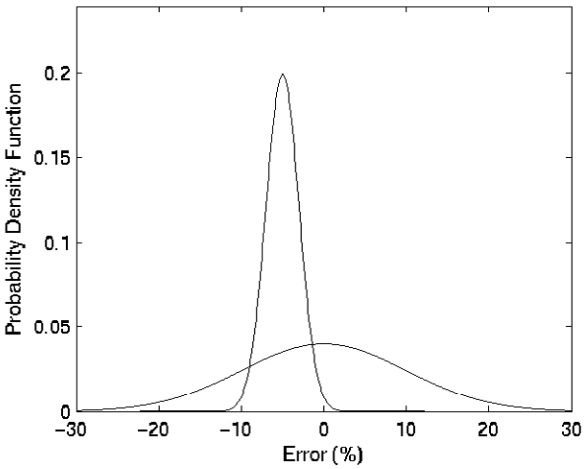


Figure 6-2 Illustration of probability density function of displacement error for a Gaussian distribution.

A variety of different inelastic hysteretic systems have been studied including bilinear hysteretic (BLH), stiffness- degrading (STDG), and strength-degrading behavior as shown in Figure 6-3. Note that the bilinear model (BLH) is the same as the elastic perfectly plastic (EPP) discussed in Chapter 3. Similarly, the stiffness degrading model (STDG) is the same as the SD model in Chapter 3. In contrast, the strength-degrading model (STRDG) differs from the SSD model of Chapter 3. A negative value of the post-elastic stiffness ratio, $\alpha$, is indicative of in-cycle degradation (see Chapter 4). Also included are parameters that have been optimized for all types of behavior.

### *6.2.1 Effective Damping*

Effective viscous damping values, expressed as a percentage of critical damping, for all hysteretic model types and alpha values have the following form:

For $1.0 < \mu < 4.0$:

$$\beta_{\text{eff}} = A(\mu - 1)^2 + B(\mu - 1)^3 + \beta_0 \qquad (6\text{-}1)$$

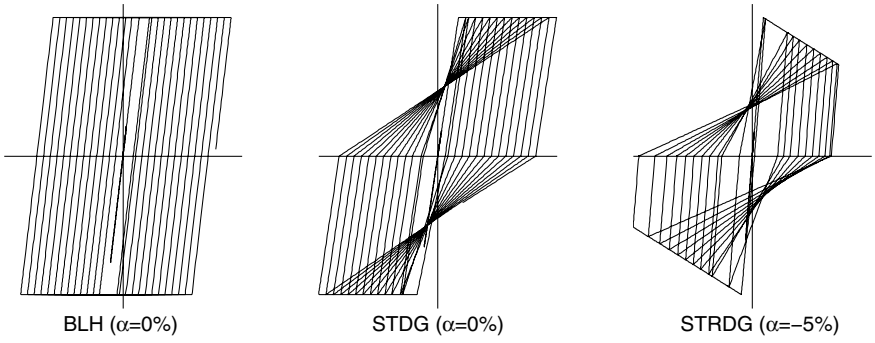


Figure 6-3 Types of inelastic behavior considered. BLH=Bilinear Hysteretic STDG=Stiffness Degrading, and STRDG=Strength Degrading.

For $4.0 \le \mu \le 6.5$:

$$\beta_{\text{eff}} = C + D(\mu - 1) + \beta_0 \qquad (6\text{-}2)$$

For $\mu > 6.5$:

$$\beta_{\text{eff}} = E\left[\frac{F(\mu-1)-1}{[F(\mu-1)]^2}\right]\left(\frac{T_{\text{eff}}}{T_0}\right)^2 + \beta_0 \qquad (6\text{-}3)$$

Values of the coefficients in the equations for effective damping of the model oscillators are tabulated in Table 6-1. Note that these are a function of the characteristics of the capacity curve for the oscillator in terms of basic hysteretic type and post-elastic stiffness, $\alpha$.

The coefficients in Table 6-1 have been optimized to fit the empirical results for idealized model oscillators having well defined hysteretic behavior designated earlier in this document as Elastic Perfectly Plastic (EPP), Stiffness Degrading (SD) and Strength and Stiffness Degrading (SSD). Real buildings, comprised of a combination of many elements, each of which may have somewhat different strength and stiffness characteristics, will seldom display hysteretic behaviors that match those of the oscillators, exactly. Adaptation of these coefficients to building models with a number of components may be done with caution. If all components exhibit similar behavior (e.g., flexurally controlled concrete with stiffness degradation and strain hardening), then it is reasonable to infer that hysteretic behavior of the overall building will be similar to the behavior of the simple idealized oscillators on which this table is based. For building models in which components exhibit disparate force-deformation behavior, it is less clear which coefficients to use. When in doubt, the practitioner should use the more generally optimized equations presented in the following paragraph.

The following approximate equations for the effective damping value have been optimized for application to any capacity curve, independent of hysteretic model type or alpha value used for the study:

For $1.0 < \mu < 4.0$:

$$\beta_{\text{eff}} = 4.9(\mu - 1)^2 - 1.1(\mu - 1)^3 + \beta_0 \qquad (6\text{-}4)$$

For $4.0 \le \mu \le 6.5$:

$$\beta_{\text{eff}} = 14.0 + 0.32(\mu - 1) + \beta_0 \qquad (6\text{-}5)$$

**Table 6-1 Coefficients for use in Equations for Effective Damping**

| *Model* | $\alpha$ *(%)* | *A* | *B* | *C* | *D* | *E* | *F* |
|---|---|---|---|---|---|---|---|
| Bilinear hysteretic | 0 | 3.2 | –0.66 | 11 | 0.12 | 19 | 0.73 |
| Bilinear hysteretic | 2 | 3.3 | –0.64 | 9.4 | 1.1 | 19 | 0.42 |
| Bilinear hysteretic | 5 | 4.2 | –0.83 | 10 | 1.6 | 22 | 0.40 |
| Bilinear hysteretic | 10 | 5.1 | –1.1 | 12 | 1.6 | 24 | 0.36 |
| Bilinear hysteretic | 20 | 4.6 | –0.99 | 12 | 1.1 | 25 | 0.37 |
| Stiffness degrading | 0 | 5.1 | –1.1 | 12 | 1.4 | 20 | 0.62 |
| Stiffness degrading | 2 | 5.3 | –1.2 | 11 | 1.6 | 20 | 0.51 |
| Stiffness degrading | 5 | 5.6 | –1.3 | 10 | 1.8 | 20 | 0.38 |
| Stiffness degrading | 10 | 5.3 | –1.2 | 9.2 | 1.9 | 21 | 0.37 |
| Stiffness degrading | 20 | 4.6 | –1.0 | 9.6 | 1.3 | 23 | 0.34 |
| Strength degrading | -3[a] | 5.3 | –1.2 | 14 | 0.69 | 24 | 0.90 |
| Strength degrading | –5[a] | 5.6 | –1.3 | 14 | 0.61 | 22 | 0.90 |

a. Negative values of post-elastic stiffness should be limited to $\alpha_e$, as discussed in Section 4.3

**Table 6-2 Coefficients for use in Equations for Effective Period**

| Model | $\alpha$(%) | G | H | I | J | K | L |
|---|---|---|---|---|---|---|---|
| Bilinear hysteretic | 0 | 0.11 | –0.017 | 0.27 | 0.090 | 0.57 | 0.00 |
| Bilinear hysteretic | 2 | 0.10 | –0.014 | 0.17 | 0.12 | 0.67 | 0.02 |
| Bilinear hysteretic | 5 | 0.11 | –0.018 | 0.09 | 0.14 | 0.77 | 0.05 |
| Bilinear hysteretic | 10 | 0.13 | –0.022 | 0.27 | 0.10 | 0.87 | 0.10 |
| Bilinear hysteretic | 20 | 0.10 | –0.015 | 0.17 | 0.094 | 0.98 | 0.20 |
| Stiffness degrading | 0 | 0.17 | –0.032 | 0.10 | 0.19 | 0.85 | 0.00 |
| Stiffness degrading | 2 | 0.18 | –0.034 | 0.22 | 0.16 | 0.88 | 0.02 |
| Stiffness degrading | 5 | 0.18 | –0.037 | 0.15 | 0.16 | 0.92 | 0.05 |
| Stiffness degrading | 10 | 0.17 | –0.034 | 0.26 | 0.12 | 0.97 | 0.10 |
| Stiffness degrading | 20 | 0.13 | –0.027 | 0.11 | 0.11 | 1.0 | 0.20 |
| Strength degrading | –3[a] | 0.18 | –0.033 | 0.17 | 0.18 | 0.76 | –0.03 |
| Strength degrading | –5[a] | 0.20 | –0.038 | 0.25 | 0.17 | 0.71 | –0.05 |

a.Negative values of post-elastic stiffness may be limited to $\alpha_e$, as discussed in Section 4.3

For $\mu > 6.5$:

$$\beta_{\text{eff}} = 19\left[\frac{0.64(\mu-1)-1}{\left[0.64(\mu-1)\right]^2}\right]\left(\frac{T_{\text{eff}}}{T_0}\right)^2 + \beta_0 \qquad (6\text{-}6)$$

### 6.2.2 Effective Period

Effective period values for all hysteretic model types and alpha values have the following form:

For $1.0 < \mu < 4.0$:

$$T_{\text{eff}} = \left[G(\mu-1)^2 + H(\mu-1)^3 + 1\right]T_0 \qquad (6\text{-}7)$$

For $4.0 \le \mu \le 6.5$:

$$T_{\text{eff}} = \left[I + J(\mu-1) + 1\right]T_0 \qquad (6\text{-}8)$$

For $\mu > 6.5$:

$$T_{eff} = \left\{K\left[\sqrt{\frac{(\mu-1)}{1+L(\mu-2)}} - 1\right] + 1\right\}T_0 \qquad (6\text{-}9)$$

Values of the coefficients in the equations for effective period of the model oscillators are tabulated in Table 6-2. Note that these are a function of the characteristics of the capacity spectrum for the oscillator in terms of basic hysteretic type and post-elastic stiffness, $\alpha$.

The use of these coefficients in Table 6-2 for actual buildings is subject to the same limitations as for effective damping, as discussed in Section 6.2.1. When in doubt, the practitioner should use the following equations for the effective period value that have been optimized for application to any capacity spectrum, independent of the hysteretic model type or alpha value:

For $1.0 < \mu < 4.0$:

$$T_{\text{eff}} = \left\{0.20(\mu-1)^2 - 0.038(\mu-1)^3 + 1\right\}T_0 \qquad (6\text{-}10)$$

For $4.0 \le \mu \le 6.5$:

$$T_{\text{eff}} = \left[0.28 + 0.13(\mu-1) + 1\right]T_0 \qquad (6\text{-}11)$$

For $\mu > 6.5$:

$$T_{eff} = \left\{0.89\left[\sqrt{\frac{(\mu-1)}{1+0.05(\mu-2)}} - 1\right] + 1\right\}T_0 \qquad (6\text{-}12)$$

Note that these expressions apply only for $T_0 = 0.2$ to 2.0 s.

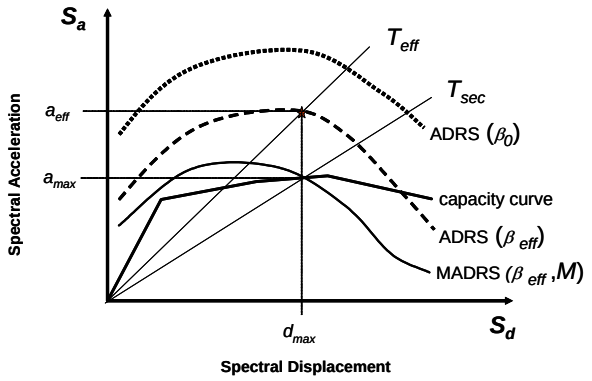


Figure 6-4 Modified acceleration-displacement response spectrum (MADRS) for use with secant period, $T_{sec}$.

### 6.2.3 MADRS for Use with Secant Period

The conventional Capacity-Spectrum Method (ATC-40) uses the secant period as the effective linear period in determining the maximum displacement (performance point). This assumption results in the maximum displacement occurring at the intersection of the capacity curve for the structure and a demand curve for the effective damping in ADRS format. This feature is useful for two reasons. First, it provides the engineer with a visualization tool by facilitating a direct graphical comparison of capacity and demand. Second, there are very effective solution strategies for equivalent linearization that rely on a modified ADRS demand curve (MADRS) that intersects the capacity curve at the maximum displacement.

The use of the effective period and damping equations in Sections 6.2.1 and 6.2.2 generate a maximum displacement that coincides with the intersection of the radial effective period line and the ADRS demand for the effective damping (see Figure 6-4). The effective period of the improved procedure, $T_{\text{eff}}$, is generally shorter than the secant period, $T_{\text{sec}}$, defined by the point on the capacity curve corresponding to the maximum displacement, $d_{\max}$. The effective acceleration, $a_{\text{eff}}$, is not meaningful since the actual maximum acceleration, $a_{\max}$, must lie on the capacity curve and coincide with the maximum displacement, $d_{\max}$. Multiplying the ordinates of the ADRS demand corresponding to the effective damping, $\beta_{\text{eff}}$, by the modification factor

$$M = \frac{a_{\max}}{a_{\text{eff}}} \tag{6-13}$$

results in the modified ADRS demand curve (MADRS) that may now intersect the capacity curve at the performance point. Since the acceleration values are directly related to the corresponding periods, the modification factor can be calculated as:

$$M = \left(\frac{T_{\text{eff}}}{T_{\text{sec}}}\right)^2 = \left(\frac{T_{\text{eff}}}{T_0}\right)^2 \left(\frac{T_0}{T_{\text{sec}}}\right)^2, \tag{6-14}$$

using the equations in Section 6.2.2 for the effective period and recognizing from Equation 3-5 that

$$\left(\frac{T_0}{T_{\text{sec}}}\right)^2 = \frac{1+\alpha(\mu-1)}{\mu} \tag{6-15}$$

where $\alpha$ is the post-elastic stiffness from Equation 6-18.

## 6.3 Spectral Reduction for Effective Damping

Equivalent linearization procedures applied in practice normally require the use of spectral reduction factors to adjust an initial response spectrum to the appropriate level of effective damping, $\beta_{\text{eff}}$. They are also a practical way to adjust for foundation damping as presented in Chapter 8. In the case of foundation damping, the initial damping value, $\beta_0$, for a flexible-base structural model is modified from the fixed-base linear value, $\beta_i$ (e.g., 5%). These factors are a function of the effective damping and are termed damping coefficients, $B(\beta_{\text{eff}})$. They are used to adjust spectral acceleration ordinates as follows:

$$(S_a)_\beta = \frac{(S_a)_0}{B(\beta_{\text{eff}})} \tag{6-16}$$

There are a number of options in current procedures for determining $B(\beta_{\text{eff}})$. Some of these are plotted in Figure 6-5. Also shown in the figure is the following expression:

$$B = \frac{4}{5.6 - \ln \beta_{\text{eff}}\,(\text{in \%})} \tag{6-17}$$

This simple expression is very close to equations specified in both the *NEHRP Recommended Provisions for Seismic Regulations for New Buildings and Other Structures* and the ATC-40 document. It is suggested that Equation 6-17 replace the current specifications.

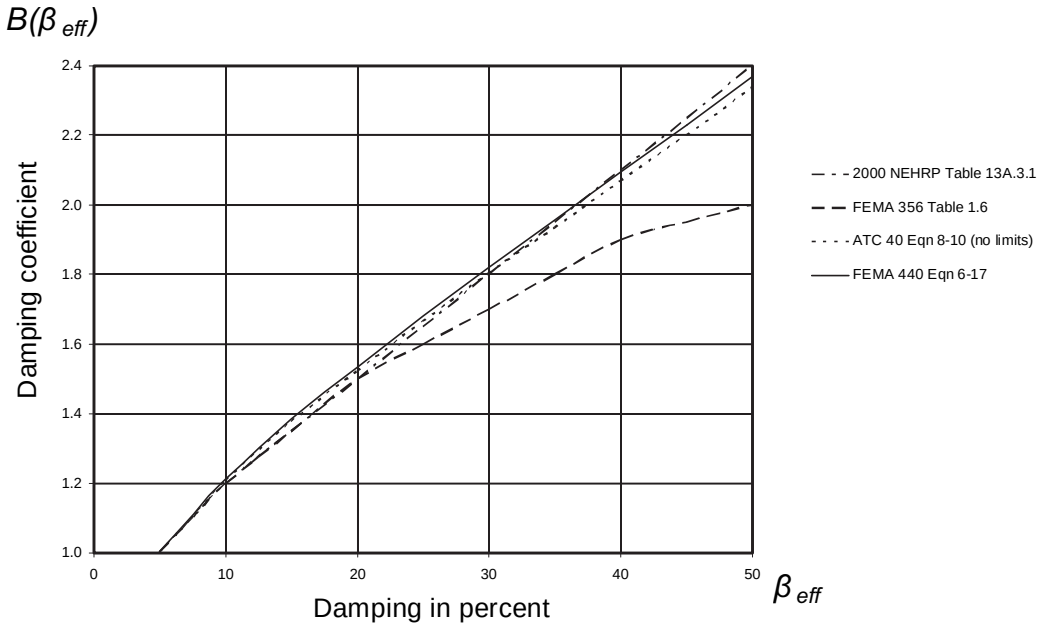


Figure 6-5 Damping coefficients, $B$, as a function of damping, $\beta_{\text{eff}}$, from various resource documents.

Note that if the ATC-40 equations are used, then the limits on the reduction should not be applied.

## 6.4 Solution Procedures

Since the effective period, $T_{\text{eff}}$, and effective damping, $\beta_{\text{eff}}$, are both functions of ductility demand, the calculation of a maximum displacement using equivalent linearization is not direct and requires an iterative or graphical solution procedure. This is the same as the previous situation with the Capacity-Spectrum Method of ATC-40. This section presents three alternate procedures. Other procedures are possible.

All of the solution procedures presented here require initial steps listed below.

1. Select a spectral representation of the ground motion of interest with an initial damping, $\beta_i$ (normally 5%). This may be a design spectrum from ATC-40 or FEMA 356, a site-specific deterministic spectrum, or an equal hazard probabilistic spectrum.
2. Modify the selected spectrum, as appropriate, for soil-structure interaction (SSI) in accordance with the procedures in Chapter 9. This involves both potential reduction in spectral ordinates for kinematic interaction and a modification in the system damping from the initial value, $\beta_i$ to $\beta_0$, to account for foundation damping. If foundation damping is ignored, $\beta_0$ is equal to $\beta_i$.
3. Convert the selected spectrum, modified for SSI when appropriate, to an acceleration-displacement response spectrum format in accordance with the guidance in ATC-40. This spectrum is the initial ADRS demand (see Figure 6-6).
4. Generate a capacity curve for the structure to be analyzed. This is a fundamental relationship for a SDOF model of the structure between spectral acceleration and spectral displacement (see Figure 6-6). Detailed guidance is available in ATC-40 and FEMA 356. Note that the FEMA 356 procedures result in a relationship between base shear and roof displacement. This requires conversion to ADRS format for equivalent linearization procedures (see ATC-40).

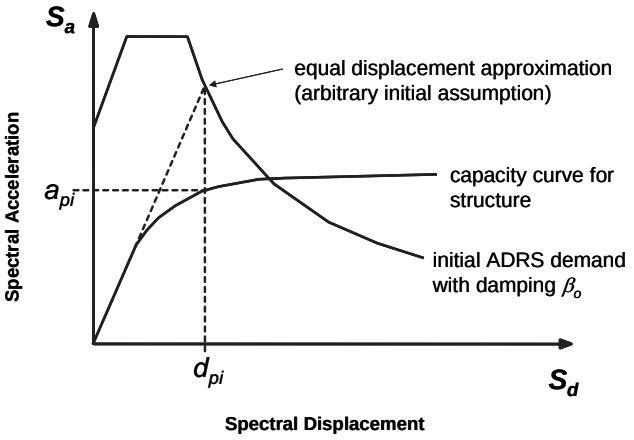


Figure 6-6 Initial ADRS demand and capacity spectrum.

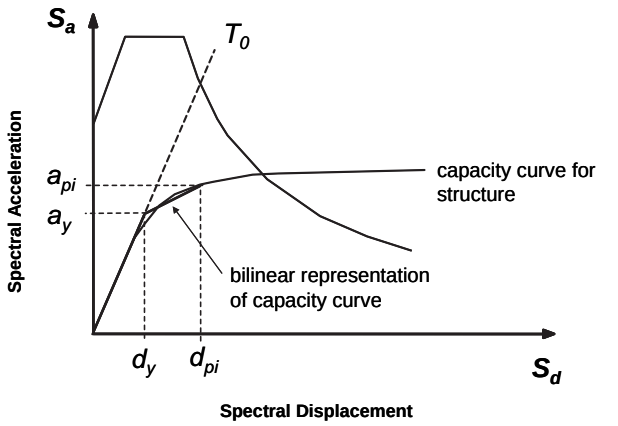


Figure 6-7 Bilinear representation of capacity spectrum.

5. Select an initial performance point (maximum acceleration, $a_{pi}$, and displacement, $d_{pi}$). This may be based on an equal-displacement approximation as shown in Figure 6-6 or any other point based on engineering judgment.
6. Develop a bilinear representation of the capacity spectrum in accordance with the procedures in ATC-40. This defines the initial period, $T_0$, yield displacement, $d_y$, and yield acceleration, $a_y$. (see Figure 6-7). Note that these parameters may vary for differing assumptions $a_{pi}$ and $d_{pi}$
7. For the bilinear representation developed in Step 6, calculate the values of post-elastic stiffness, $\alpha$, and ductility, $\mu$, as follows:

$$\alpha = \frac{\left(\frac{a_{pi} - a_y}{d_{pi} - d_y}\right)}{\left(\frac{a_y}{d_y}\right)} \tag{6-18}$$

$$\mu = \frac{d_{pi}}{d_y} \tag{6-19}$$

8. Using the calculated values for post-elastic stiffness, $\alpha$, and ductility, $\mu$, from Step 7, calculate the corresponding effective damping, $\beta_{\text{eff}}$, (see Section 6.2.1). Similarly calculate the corresponding effective period, $T_{\text{eff}}$, (see Section 6.2.2).

After this step in the procedures, a number of options are available for identifying a single solution. Three possible procedures are described below.

**Procedure A (Direct Iteration).** In this procedure, the iteration is done to converge directly on a performance point. The ADRS demand spectra generated for the various values of effective damping are not modified to intersect the capacity spectrum, as outlined in Section 6.2.3.

A9. Using the effective damping determined from Step 8, adjust the initial ADRS to $\beta_{\text{eff}}$ (see Section 6.3).

A10. Determine the estimated maximum displacement, $d_i$, using the intersection of the radial effective period, $T_{\text{eff}}$, with the ADRS for $\beta_{\text{eff}}$. The estimated maximum acceleration, $a_i$, is that corresponding to $d_i$ on the capacity curve (see Figure 6-8).

A11. Compare the estimated maximum displacement, $d_i$, with the initial (or previous) assumption. If it is within acceptable tolerance, the performance point corresponds to $a_i$ and $d_i$. If it is not within acceptable tolerance, then repeat the process from Step 5 using $a_i$ and $d_i$, or some other selected assumption (see Section 6.6), as a starting point.

**Procedure B (Intersection with MADRS).** In this procedure, the performance point is defined as the intersection of the capacity spectrum with the modified ADRS (MADRS). The MADRS demand spectrum is generated by modifying the ADRS for the various values of effective damping, as outlined in Section 6.2.3.

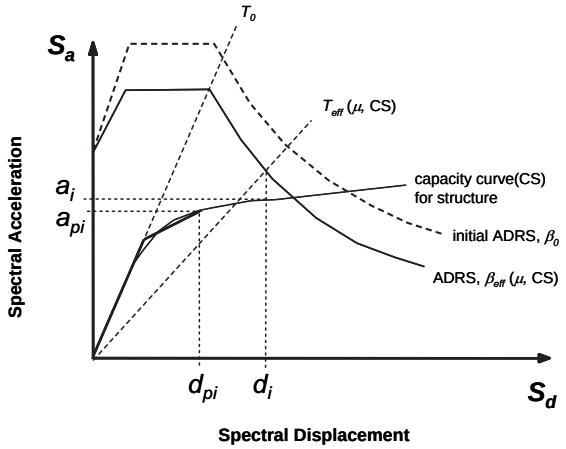


Figure 6-8 Determination of estimated maximum displacement using direct iteration (Procedure A)

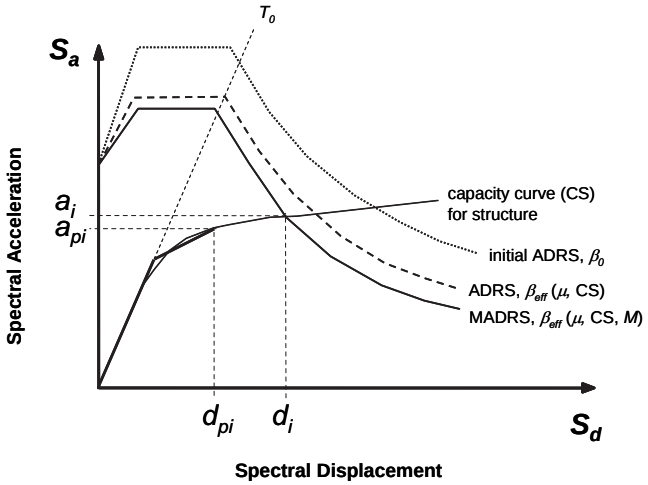


Figure 6-9 Determination of estimated maximum displacement using intersection of capacity spectrum with MADRS (Procedure B)

B9. Using the effective damping determined from Step 8, adjust the initial ADRS to $\beta_{\text{eff}}$ (see Section 6.3).

B10. Multiply the acceleration ordinates only (i.e., not the displacement ordinates) of the ADRS for $\beta_{\text{eff}}$ by the modification factor, $M$, determined using the calculated effective period, $T_{\text{eff}}$, in accordance with Section 6.2.3 to generate the modified acceleration-displacement response spectrum (MADRS).

B11. Determine the estimate of the maximum acceleration, $a_i$, and displacement, $d_i$, as the intersection of the MADRS with the capacity curve (see Figure 6-9).

B12. Compare the estimated maximum displacement, $d_i$, with the initial (or previous) assumption, $d_{pi}$. If it is within acceptable tolerance, the performance point corresponds to $a_i$ and $d_i$. If it is not within acceptable tolerance, then repeat the process from Step 5 using $a_i$ and $d_i$, or some other selected assumption (see Section 6.6), as a starting point.

**Procedure C (MADRS Locus of Possible Performance Points).** This approach uses the modified acceleration-response spectrum for multiple assumed solutions ($a_{pi}$, $d_{pi}$) and the corresponding ductilities to generate a locus of possible performance points. The actual performance point is located at the intersection of this locus and the capacity spectrum.

C9. Using the effective damping determined from Step 8, adjust the initial ADRS to $\beta_{\text{eff}}$ (see Section 6.3).

C10. Multiply the acceleration ordinates of the ADRS for $\beta_{\text{eff}}$ by the modification factor, $M$, determined using the calculated effective period, $T_{\text{eff}}$, in accordance with Section 6.2.3 to generate the modified acceleration-displacement response spectrum (MADRS).

C11. A possible performance point is generated by the intersection of the radial secant period, $T_{\text{sec}}$, with the MADRS (see Figure 6-10).

C12. Increase or decrease the assumed performance point and repeat the process to generate a series of possible performance points.

C13. The actual performance point is defined by the intersection of the locus of points from Step 12 and the capacity spectrum.

Note that Procedure C is conducive to an automated process wherein the initial solution is assumed to correspond to a ductility of 1.0 and subsequent trials are set as incrementally greater ductilities (e.g., 2, 3, 4, 5,….).

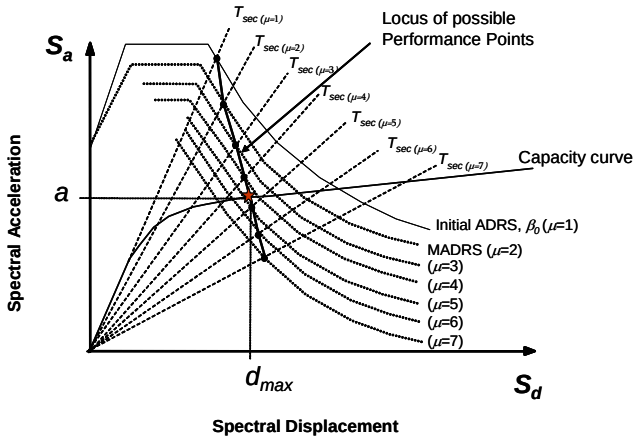


Figure 6-10 Locus of possible performance points using MADRS.

## 6.5 Approximate Solution Procedure

The following procedure is a simplified MADRS approach based on approximations to the equations in Section 6.2. It uses a MADRS solution procedure similar to that of Section 6.4. The approximations are based upon an EPP single-degree-of freedom system. The results of the approximate procedure are compared to the more rigorous procedures for various types of hysteretic behavior in Figure 6-11. The first seven steps in the procedure are the same as Steps 1 through 7 in the beginning of Section 6.4. The next steps in the approximate procedure are given below.

D8. Using the calculated values for ductility, $\mu$, from Step 7, calculate the corresponding spectral response-reduction factors as

$$\left[\frac{6}{\mu+5}\right] \quad \text{for } 1 \le \mu \le 4 \tag{6-20}$$

$$\left[\frac{75}{\mu+110}\right] \quad \text{for } \mu > 4 \tag{6-21}$$

D9. Using the spectral response-reduction factors from Step 8, multiply both the spectral accelerations and corresponding spectral displacements by the response-reduction factor to generate a reduced ADRS corresponding to the assumed ductility, $\mu$.

D10. Multiply the spectral acceleration ordinates (not the spectral displacement ordinates) of the reduced ADRS by a simplified modification factor

$$M = \frac{1}{\mu} \ge 0.64 \tag{6-22}$$

to generate the approximate modified acceleration-displacement response spectrum (MADRS). It should be noted that for ductilities greater than 1.6 the bounding limit of 0.64 controls this step.

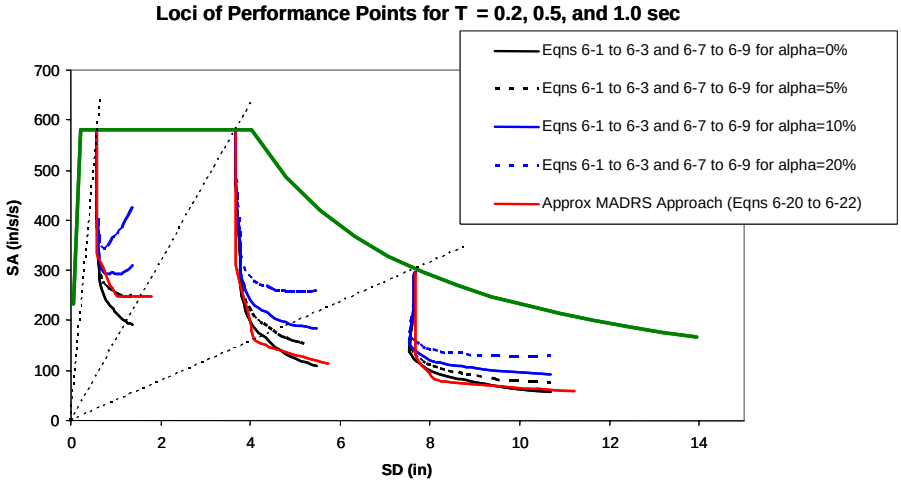


Figure 6-11 Comparison of approximate solution results with results from more detailed procedures.

D11. A possible performance point is generated by the intersection of the radial effective period, $T_{eff}$, with the MADRS (see Figure 6-9).

D12. Increase or decrease the assumed performance point and repeat the process to generate a series of possible performance points.

D13. The actual performance point is defined by the intersection of the locus of points from Step 12 and the capacity curve. For this approximate procedure, the calculated target displacement must be equal to or greater than the elastic target displacement.

## 6.6 Iterative Strategy

Subsequent assumptions for the performance point can be calculated by averaging the previous value of the initial assumption $d_{pi}$ and the calculated result $d_i$, then choosing the corresponding acceleration value from the capacity curve. However, this is not required and some educated guessing and judgment can improve solution time. For example, the initial assumption, $d_{pi}$, and the resulting estimated maximum displacement, $d_i$, can be plotted as a point, as shown in Figure 6-12. Note that the actual performance point will fall along the line where the two values are equal. By tracking the subsequent trial point with this type of plot, it is easy to see solution trends. An example with three iterations is shown in Figure 6-12. After the second trial, it is apparent that the performance point is larger than the estimate, as the track of the trial points has not crossed the line of equal displacement. So the third trial assumes a relatively large displacement. The results of the third trial indicate a solution somewhere between the assumptions of Trial 2 and Trial 3.

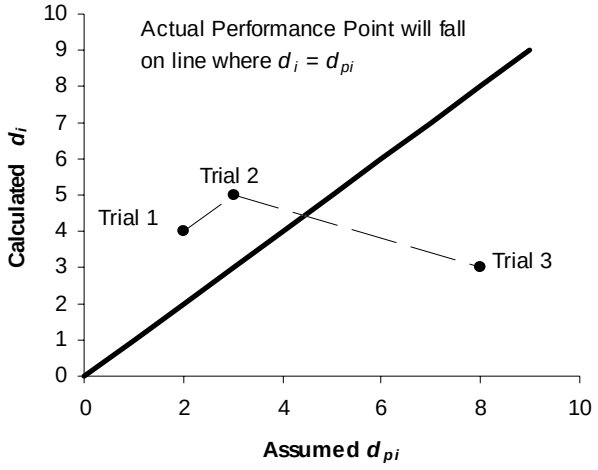


Figure 6-12 Tracking iteration for equivalent linearization by comparing assumed displacement to calculated displacement.

## 6.7 Limitation on Strength to Avoid Dynamic Instability for Nonlinear Static Procedures

The evaluation of current procedures summarized in Chapter 3 revealed that oscillators that exhibit in-cycle strength degradation can be prone to dynamic instability during strong shaking. The subject is covered in detail in Chapter 4. When using equivalent linearization procedures, the strength of the structural model should be checked in accordance with Section 4.4.

# 7. Evaluation and Comparison of Improved Nonlinear Static Procedures

## 7.1 Introduction

Previous chapters have introduced improvements to nonlinear static procedures that are useful for estimating the peak displacement amplitude for a SDOF oscillator subjected to earthquake ground motion. This chapter compares results of those methods with results obtained using nonlinear response-history analyses for ground motion records selected and scaled to be representative of a specific hazard level and site conditions. The ground motion selection and scaling procedures are similar to those specified in the 2000 *NEHRP Recommended Provisions for Seismic Regulations for New Buildings and Other Structures* (BSSC, 2000),[1] and therefore provide an example of the types of results one might obtain in a practice-related application.

Several nonlinear oscillators were selected, having different vibration periods and strengths. The oscillators were assumed to be sited on ground classified as NEHRP Site Class C, with ground motions generated by a fault capable of a strike-slip earthquake of magnitude $M_S = 7$. Smooth design response spectra were established using the 2000 *NEHRP Recommended Provisions for New Buildings*, scaled for the design-basis earthquake. Furthermore, ground motion records from representative sites and earthquakes were selected and scaled. Displacement amplitudes of the oscillators were calculated by both the nonlinear static procedures and nonlinear dynamic response-history analysis, for comparison purposes.

The scope of the study reported in this chapter is limited by the periods, strengths, and hysteretic behavior of the SDOF oscillators, as well as the number and nature of the ground motions used. The results do not represent a large statistical sample and broad general conclusions should not be drawn solely from these data. Nonetheless, they are illustrative of the types of errors and variations among procedures that should be anticipated when using these simplified analysis techniques.

1.Superseded in 2003 with the FEMA 450 *Recommended Provisions for Seismic Regulations for New Buildings and Other Structures.*

## 7.2 Summary of Evaluation Procedures

### 7.2.1 NEHRP Design Response Spectrum

Procedures similar to the 2000 *NEHRP Recommended Provisions for New Buildings* were used to define design response spectra. Values for short- and 1-second period spectral accelerations at the Maximum Considered Earthquake (MCE) level were read from the pertinent maps for 5% damping and site class C, resulting in values $S_S = 1.5$ g and $S_1 = 0.6$ g. Following the 2000 NEHRP procedures, the short- and long-period values were modified for site class C to $S_{MS} = F_a S_S$ and $S_{M1} = F_v S_1$, where $F_a = 1.0$ and $F_v = 1.3$. Design-basis ordinates then were obtained as $S_{DS} = (2/3)S_{MS}$ and $S_{D1} = (2/3)S_{M1}$. These values were used with the spectral shape defined in the *NEHRP Recommended Provisions for New Buildings* (Figure 7-1) to derive the NEHRP design response spectrum. Note that the acceleration values in Figure 7-1 and in the rest of the document are actually pseudo-acceleration values.

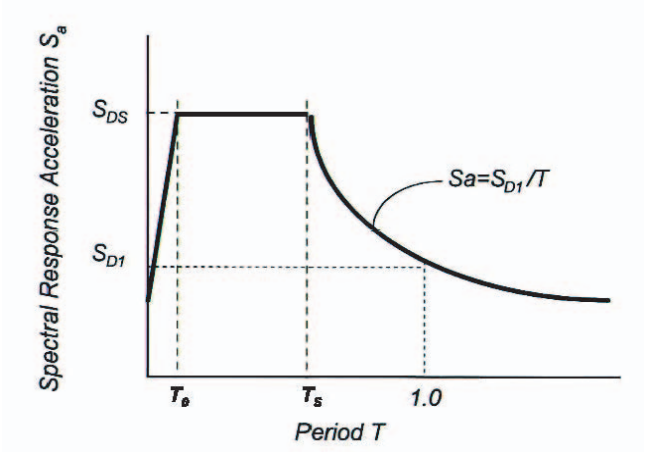


Figure 7-1 NEHRP design response spectrum.

### 7.2.2 Ground Motions and Ground-Motion Scaling

Ground motions were intended to be representative of design-level motions for a facility located approximately 10 km from a fault rupturing with strike-slip mechanism at magnitude $M_S$ 7. The soil at the site corresponds to NEHRP Site Class C. Ground motions were selected from the Pacific Earthquake Engineering Research (PEER) Center strong ground motion

**Table 7-1 Ground Motion Records**

| *Earthquake* | *Magnitude* | *Record* | *PGA (g)* | *PGV (cm/s)* | *PGD (cm)* | *Distance closest to fault rupture (km)* |
|---|---|---|---|---|---|---|
| Imperial Valley 1979/ 10/15 23:16 | *M* 6.5, $M_l$ 6.6, $M_s$ 6.9 | IMPVALL/H-PTS315 | 0.204 | 16.1 | 9.94 | 14.2 |
| | | IMPVALL/H-CPE147 | 0.169 | 11.6 | 4.25 | 26.5 |
| | | IMPVALL/H-CPE237 | 0.157 | 18.6 | 7.95 | 26.5 |
| Landers 1992/06/28 11:58 | *M* 7.3 $M_s$ 7.4 | LANDERS/CLW-LN | 0.283 | 25.6 | 13.74 | 21.2 |
| | | LANDERS/CLW-TR | 0.417 | 42.3 | 13.76 | 21.2 |
| | | LANDERS/MVH000 | 0.188 | 16.6 | 9.45 | 19.3 |
| | | LANDERS/MVH090 | 0.14 | 20.2 | 6.33 | 19.3 |
| | | LANDERS/DSP000 | 0.171 | 20.2 | 13.87 | 23.2 |
| | | LANDERS/DSP090 | 0.154 | 20.9 | 7.78 | 23.2 |
| | | LANDERS/JOS000 | 0.274 | 27.5 | 9.82 | 11.6 |
| | | LANDERS/JOS090 | 0.284 | 43.2 | 14.51 | 11.6 |
| | | LANDERS/NPS000 | 0.136 | 11 | 4.97 | 24.2 |

PGA: peak ground acceleration; PGV: peak ground velocity; PGD: peak ground displacement

database (*http://peer.berkeley.edu*), and were scaled to be representative of design-level motions at the site.

The *NEHRP Recommended Provisions for New Buildings* prescribe a scaling procedure to be used when ground motion records are used directly for time-domain dynamic analysis. According to this procedure, ground motions should be selected that are from similar site conditions, rupture mechanism and magnitude, and epicentral distance. For the present study, the selected records were for sites classified as NEHRP Site Class C, having strike-slip mechanism, magnitude $M_s$ ranging from 6.3 to 7.5, and closest distance to fault rupture ranging from 5 to 25 km.

The SDOF oscillators were to be analyzed as planar structures subjected to a single horizontal component of ground motion. Therefore, records were scaled individually rather than scaling them as pairs as is recommended by the *NEHRP Recommended Provisions for New Buildings* for three-dimensional structures. The *Provisions* stipulate that the ground motions be scaled such that the average of the ordinates of the five-percent-damped linear response spectra does not fall below the design spectrum for the period range $0.2T_i$ to $1.5T_i$, where $T_i$ is the fundamental period of vibration of the structure modeled as a linear system. The period $0.2T_i$ is selected as the lower bound to ensure that important higher modes of vibration are adequately excited. This lower bound is not relevant for the present study because the structure is an oscillator with a single vibration mode. Rather, for the present study, it is more important that the average approximate the design spectrum in the period range just below $T_i$ to values higher than $T_i$, such that as the oscillator yields, it will, on average, experience ground motion intensities close to that represented by the design spectrum. Also, because this is a study of the procedures, rather than a building design, it is preferable to scale the motions so that the average of the spectral ordinates follows the design spectrum closely, rather than conservatively scaling the motions to be above the design spectrum as might be done for design purposes.

Sixteen ground motion records were selected for consideration. Each was examined to be certain it did not contain obvious near-fault directivity effects. Each motion was scaled so that the five-percent-damped spectral ordinate at the period of the oscillator matched that of the NEHRP response spectrum at the same period. Ground motions were eliminated selectively to avoid motions with unacceptably large scaling factors and motions whose response spectra did not appear consistent with the NEHRP response spectrum. The process of elimination continued until there were ten records available for each oscillator. Note that the oscillators had three different vibration periods (0.2, 0.5, and 1.0 s). Within the criteria stated above, it was not feasible to use the same ten motions for each oscillator. In total, 13 ground motions were used for the study. The ground motion records are identified in Table 7-1. The response spectra of the scaled ground

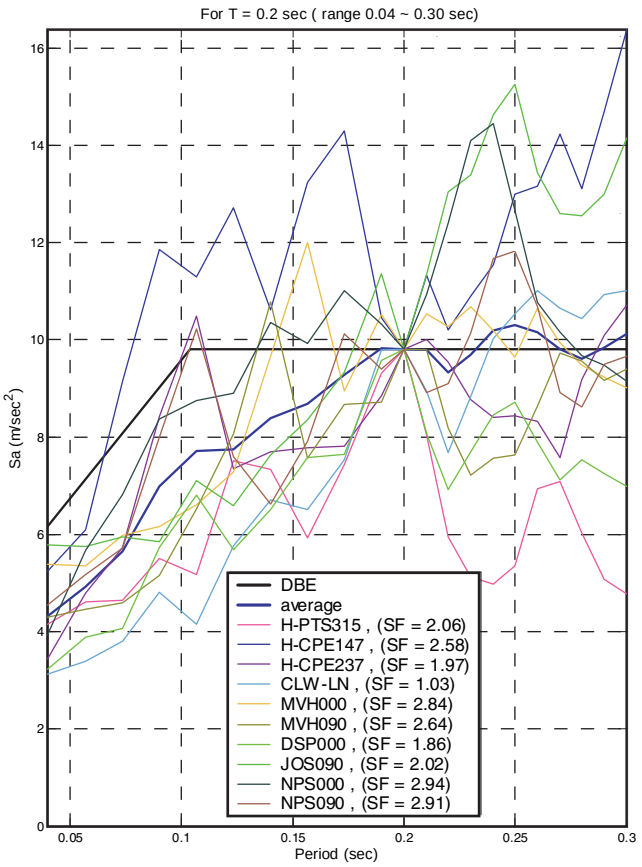


Figure 7-2 NEHRP response spectrum and 5%-damped response spectra of scaled motions, used for oscillators having $T = 0.2$ s.

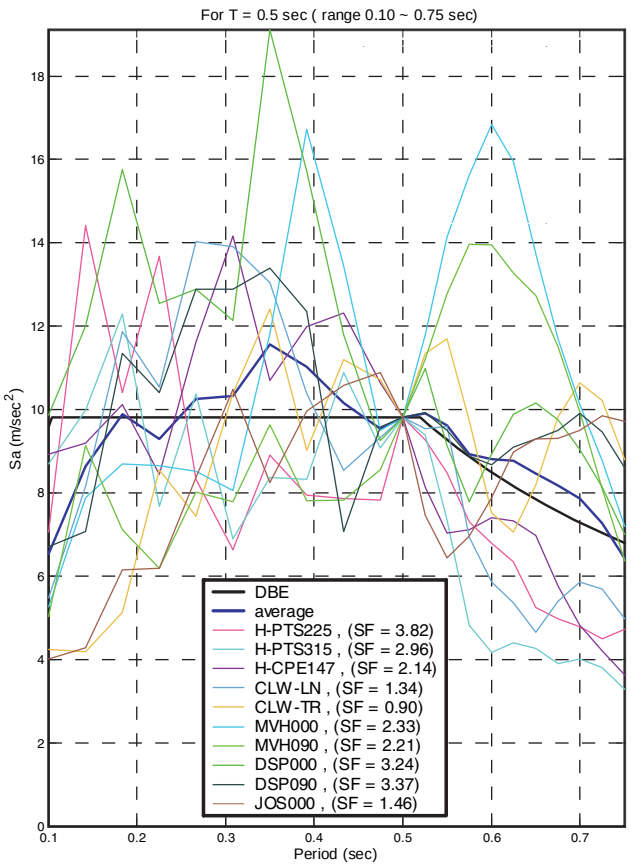


Figure 7-3 NEHRP response spectrum and 5%-damped response spectra of scaled motions, used for oscillators having $T = 0.5$ s.

motions used for oscillators having periods 0.2, 0.5, and 1.0 s are shown in Figures 7-2, 7-3, and 7-4, respectively.

### 7.2.3 Characteristics of Oscillators

Nine SDOF oscillators were used for this study. The oscillators had bilinear load-displacement relationships with post-elastic stiffness equal to five percent of the initial elastic stiffness. Loading and unloading characteristics are shown in Figure 7-5 without strength or stiffness degradation. Initial damping was five percent of critical damping. The oscillators had three different yield strengths and three different periods. For each period, the spectral acceleration was read from the NEHRP response spectrum. The yield strengths were then defined as the elastic base shear demand (product of the mass and spectral acceleration) divided by a strength reduction factor $R$. $R$ values of 2, 4, and 8 were considered. Figure 7-6 summarizes the elastic vibration periods and $R$ values selected.

### 7.2.4 Nonlinear Static Procedure Estimates Using Smoothed or Average Spectra

The improved nonlinear static procedures of Chapters 5 and 6 were applied to the NEHRP response spectra, as well as to the average of the 5%-damped response spectra. The former represents more closely how the procedures would be used with the NEHRP response spectra, whereas the latter represents more closely how the procedures might be used when a site-specific response spectrum is defined by the average of the response spectra for a series of design ground motions selected for a site.

For application of the displacement modification method of Chapter 5, the displacement amplitude was defined as

$$C_1 C_2 S_d = C_1 C_2 S_a \left( \frac{T_i}{2\pi} \right)^2 ,$$

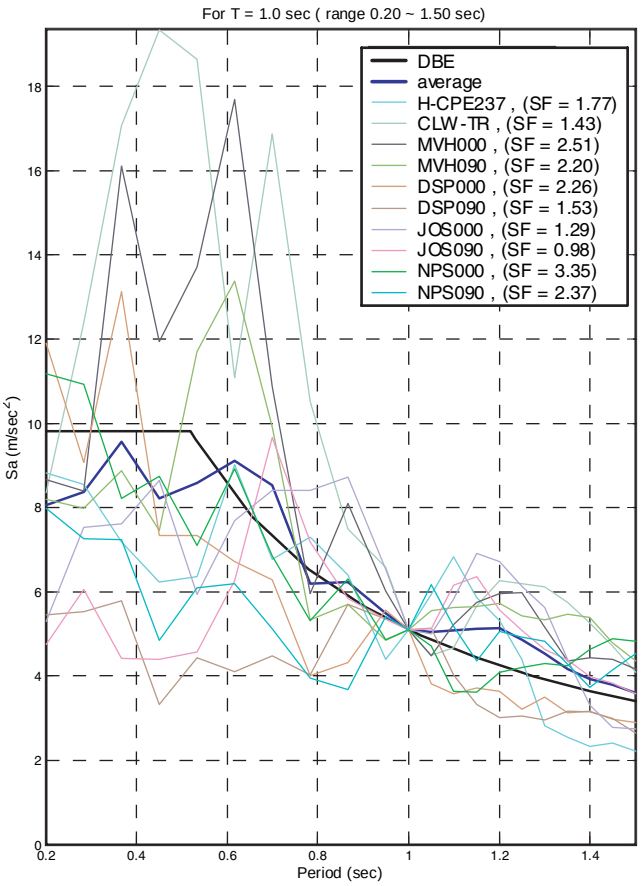


Figure 7-4 NEHRP response spectrum and 5%-damped response spectra of scaled motions, used for oscillators having $T = 1.0$ s.

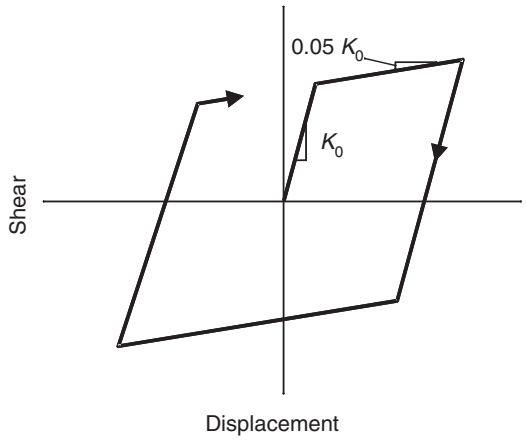


Figure 7-5 Bilinear load-displacement relation of oscillators.

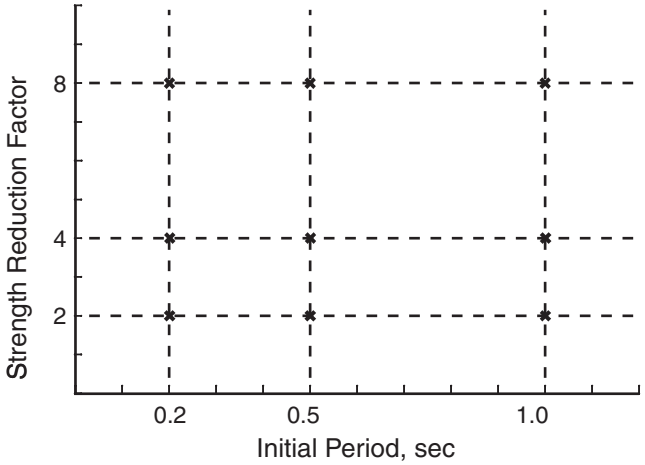


Figure 7-6 Linear vibration periods and strength reduction factors for oscillators.

in which $S_a$ = pseudo-spectral acceleration ordinate at the period of the oscillator $T_i$. The coefficient $C_1$ was defined as

$$C_1 = 1 + \frac{R-1}{90T_i^2}.$$

Coefficient $C_2$ was taken equal to 1.0, as it was assumed that there was no stiffness or strength degradation.

For application of the equivalent linearization procedure of Chapter 6, response spectra were converted to the spectral acceleration-spectral displacement format. In studies using the average response spectra, the spectral ordinates were calculated for each ground motion for each of several different damping ratios. The results for a given damping ratio were averaged for the different ground motions to obtain the average response spectrum for that damping ratio. In studies using the NEHRP smooth design response spectra, spectral ordinates for damping exceeding 5% of critical damping were calculated using the spectral reduction factors of ATC-40; however, the limits on the reductions (ATC-40 Tables 8-1 and 8-2) were not imposed. Damping factors and effective periods were calculated using the equations and tabulated quantities in FEMA 440 Chapter 6, specific to the bilinear oscillator behavior with 5% post-elastic stiffness, rather than the more generally applicable equations. Iteration Procedure A was used with the average spectra, while iteration Procedure B was used for the smooth spectra, in general accordance with Section 6.4. Convergence was assumed when the

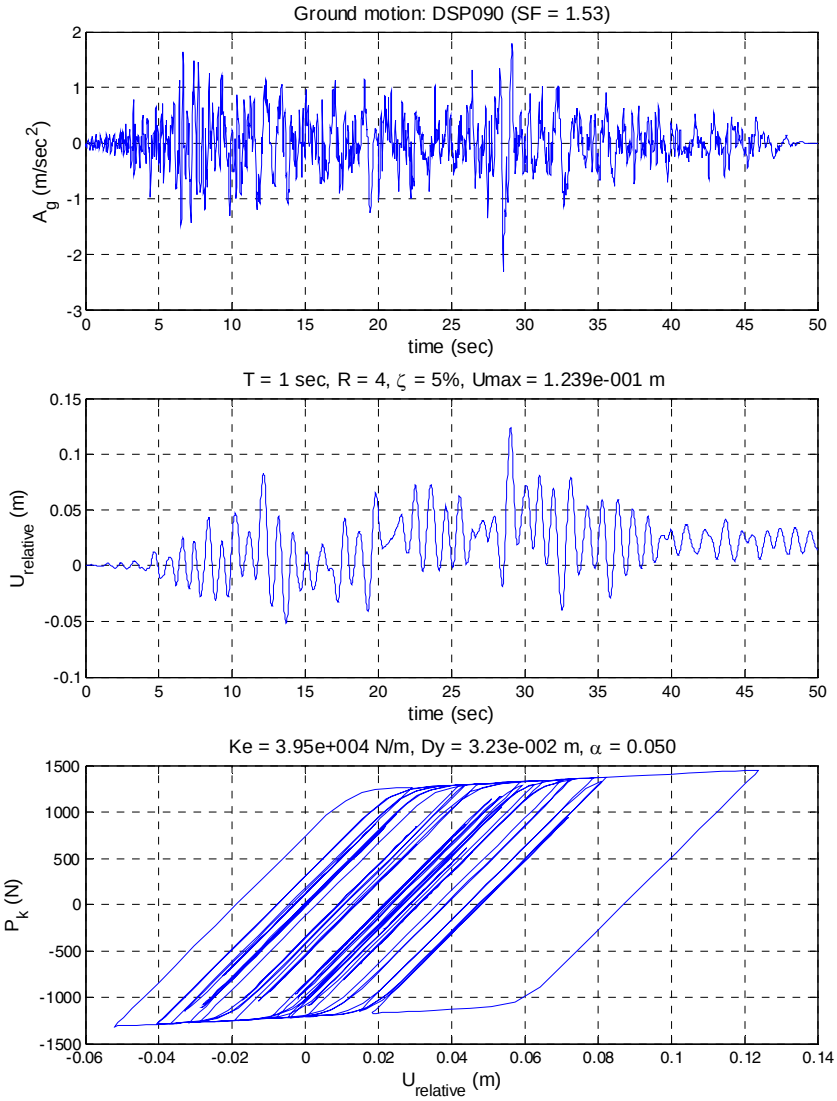


Figure 7-7 Representative nonlinear response-history analysis result (this example is for oscillator period $T = 1$ s, ground motion DSP090 scaled by factor 1.53, and strength-reduction factor $R = 4$).

calculated displacement was not more than 5% different from the assumed displacement. Also, solutions were generated using the approximate MADRS approach of Section 6.5.

Results also are presented using the Coefficient Method of FEMA 356 and the Capacity-Spectrum Method of ATC-40. For the Coefficient Method, the coefficients for the nonlinear static procedure were used with a cap on $C_1$ equal to 1.5, as permitted, and all other coefficients set equal to 1.0. For the Capacity-Spectrum Method, the procedures of ATC-40 were followed explicitly, using the response spectra in the same manner as for the improved procedure.

### *7.2.5 Response-History Analyses*

Inelastic responses of the single-degree-of-freedom oscillators, with different periods and strength-reduction factors, were calculated for each of the ground motion histories. Figure 7-7 presents a representative result.

## 7.3 Results of the Study

Figure 7-8 presents results of the study using ground motions scaled to match the NEHRP design response spectrum, with the nonlinear static results calculated for the NEHRP design response spectrum. Data are presented in three sequential graphs, one each for oscillator of the initial periods: 0.2 s 0.5 s, and 1.0 s.

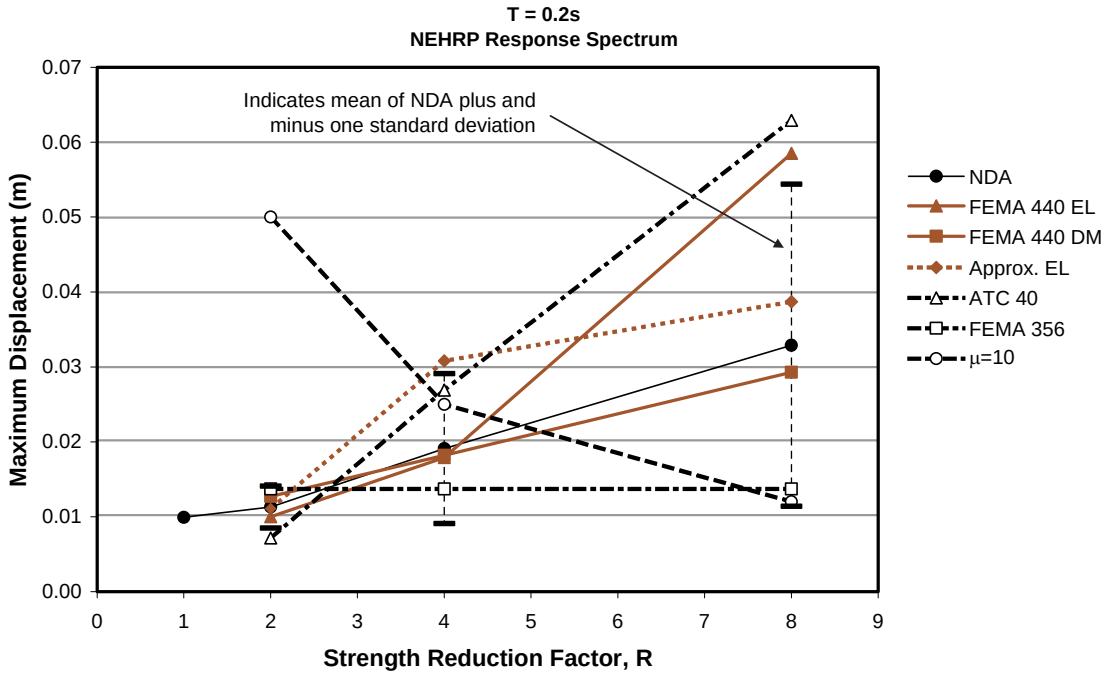


Figure 7-8 Comparison of responses for an oscillator with $T = 0.2$ s calculated using various procedures, response spectra scaled to the NEHRP spectrum, and values calculated for the NEHRP spectrum

Each graph plots maximum relative displacement amplitude as a function of the strength-reduction factor *R*. The legend to the right of each graph identifies the data in the graph, as follows:

1. NDA mean is the mean of the maximum displacement response amplitudes calculated using nonlinear dynamic analysis (time-domain) for the ten ground motions. Each graph also includes a representation of the NDA results for each strength value, consisting of the mean plus and minus one standard deviation.
2. FEMA 440 EL is the result obtained by the improved equivalent linearization method (Section 6.4)
3. FEMA 440 DM is the result obtained by the improved displacement modification method of Chapter 5.
4. Approximate EL is the result obtained by the approach given in Section 6.5.
5. ATC-40 is the result obtained by the Capacity-Spectrum Method of ATC-40.
6. FEMA 356 is the result obtained by the displacement modification method of FEMA 356.
7. $\mu = 10$ plots the displacement corresponding to displacement ductility of 10.

In Figures 7-8, 7-9, and 7-10, the results of primary interest are those for which the actual displacement is less than approximately10 times the yield displacement. Displacements near or beyond this level are unrealistic for most actual structures, because their vertical- and lateral-force-resisting systems are unlikely to be able to sustain such large deformations without failure. The coefficients of the FEMA 440 EL method were optimized for solutions with displacement ductility less than this limit.

The results obtained using nonlinear dynamic analysis (NDA) indicate that for short-period oscillators, the maximum displacement response amplitude increases with decreasing strength (increasing *R*), while for longer-period oscillators the peak displacement response is less sensitive to strength. NDA results reflect wider dispersion for shorter-period oscillators and for lower strength values. This observation is partly because the response spectra (Figures 7-2, 7-3, and 7-4) show increasing dispersion as the period elongates (as occurs for structures with lower strengths). Previous studies, including those summarized in Chapter 3, also have shown that dispersion of response generally

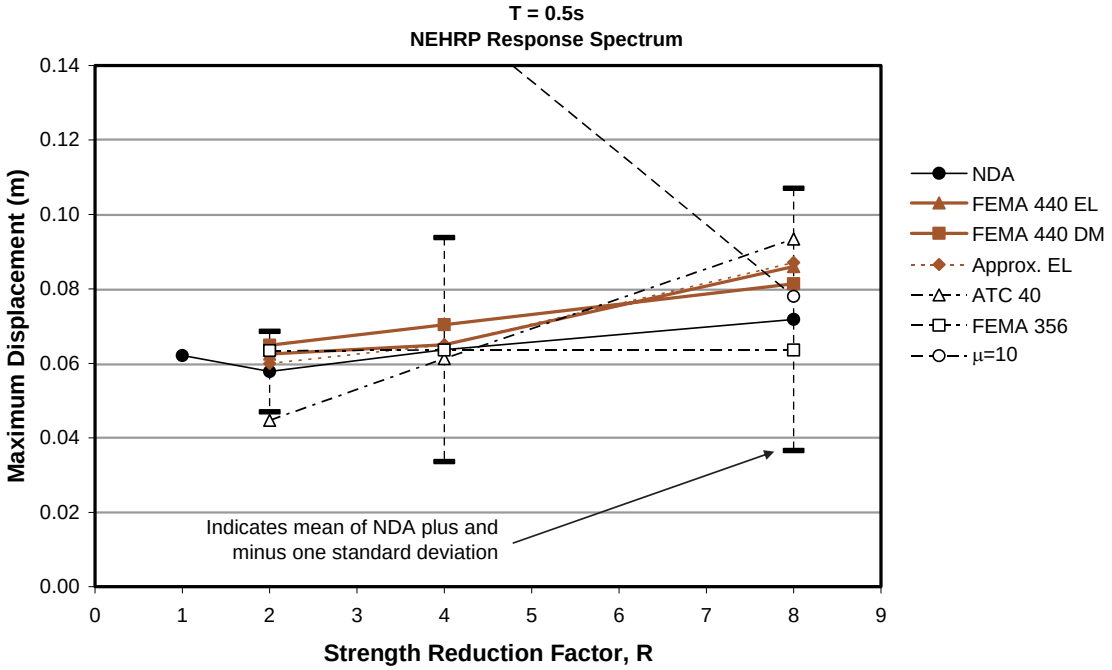


Figure 7-9 Comparison of responses for an oscillator with $T = 0.5$ s calculated using various procedures, response spectra scaled to the NEHRP spectrum, and values calculated for the NEHRP spectrum.

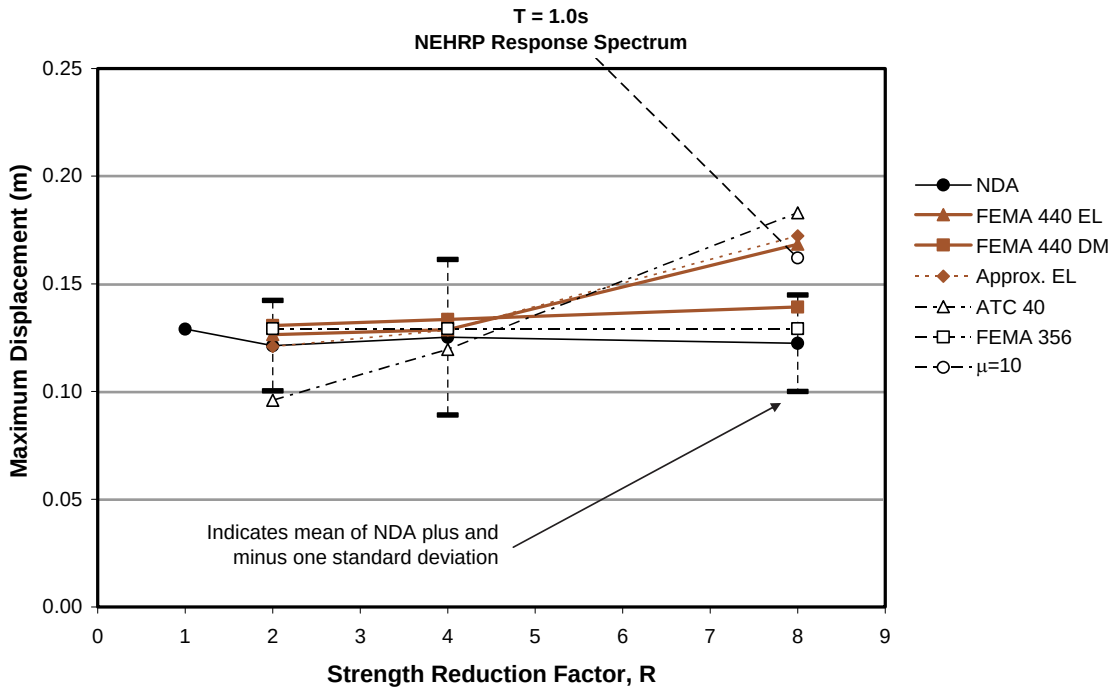


Figure 7-10 Comparison of responses for an oscillator with $T = 1.0$ s calculated using various procedures, response spectra scaled to the NEHRP spectrum, and values calculated for the NEHRP spectrum.

increases for shorter periods and higher *R* values, regardless of the tendency of the response spectra.

The proposed improved procedures generally follow the observed mean trends for the NDA results, provided that the displacement ductilities remain within reasonable bounds. Unreasonable ductility values are the cause of overestimates of displacement in some instances, using the FEMA 440 EL and the approximate EL procedures (e.g., Figure 7-8 with $T = 0.2$ s and $R = 8$, Figure 7-10 with $T = 1.0$ s and $R = 8$). This tendency is not apparent when the average spectrum is used, as noted below.

As expected, the FEMA 356 procedure does not predict the increase in displacement response with increasing *R* for short-period oscillators. The ATC-40 procedure tends to underestimate the displacement response for small *R* and overestimate the response for large *R*. These results are again consistent with the previous studies (Chapter 3).

Figures 7-11, 7-12, and 7-13 present data similar to those of Figures 7-8, 7-9, and 7-10. The ground motions are identical, having been scaled to match the *NEHRP* smooth design response spectrum, and oscillator strengths also are identical. However, the nonlinear static procedures all are applied using the average of the response spectra for the scaled ground motions. For the displacement modification methods, the ordinate of the 5% damped response spectrum at period *T* of the oscillator is unchanged from the previous analyses, so the results shown in Figures 7-11, 7-12, and 7-13 for those methods are the same as those shown in Figures 7-8, 7-9, and 7-10. For the equivalent linearization methods, the analysis required the calculation of the average of the linear response spectra for each scaled ground motion record for each of several different damping values. Results for these methods therefore differ from those presented in Figures 7-8, 7-9, and 7-10. Data are presented in three sequential graphs, separated by the oscillator initial periods of 0.2, 0.5, and 1.0 s. Each graph plots maximum relative displacement amplitude as a function of strength-reduction factor, *R*. The legend to the right of each graph identifies the data in the graph, defined as described above.

Results for the improved equivalent linearization methods using the average spectrum (Figure 7-8) are somewhat improved over those using the NEHRP spectrum (Figures 7-8, 7-9, and 7-10), especially for larger ductilities. This improvement might be expected for two reasons. First, the equivalent linearization methods were derived using response spectra calculated for individual motions for various specific values of

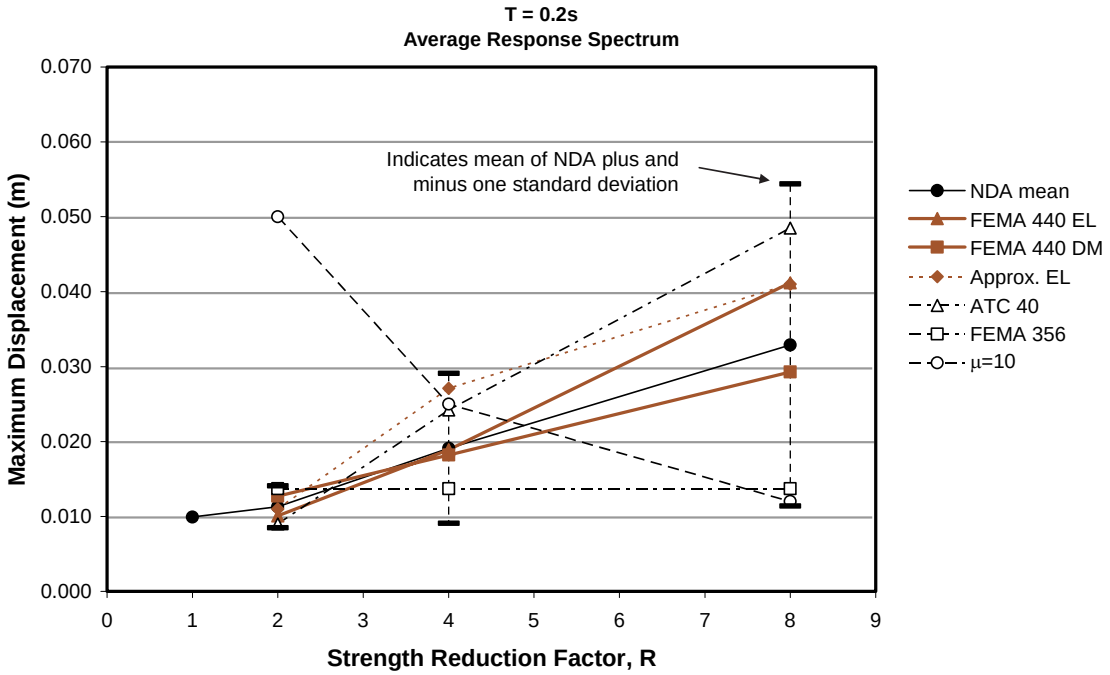


Figure 7-11 Comparison of responses of an oscillator with $T = 0.2$ s calculated using various procedures, response spectra scaled to NEHRP spectrum, and values calculated for the average spectrum.

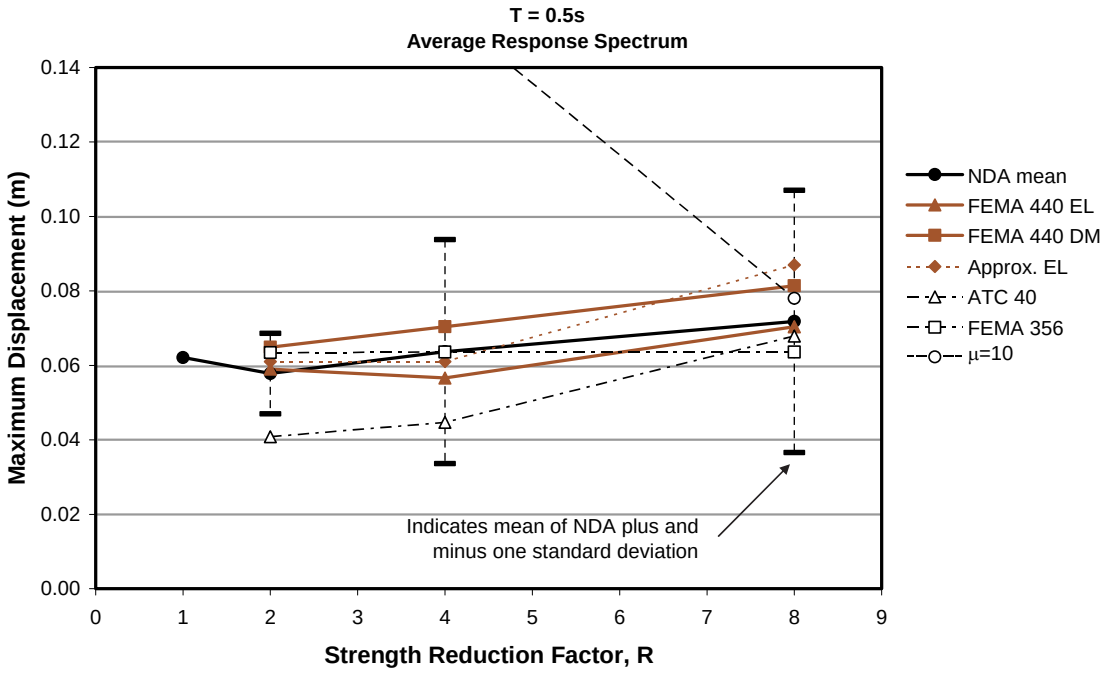


Figure 7-12 Comparison of responses of an oscillator with $T = 0.5$ s calculated using various procedures, response spectra scaled to the NEHRP spectrum, and values calculated for the average spectrum.

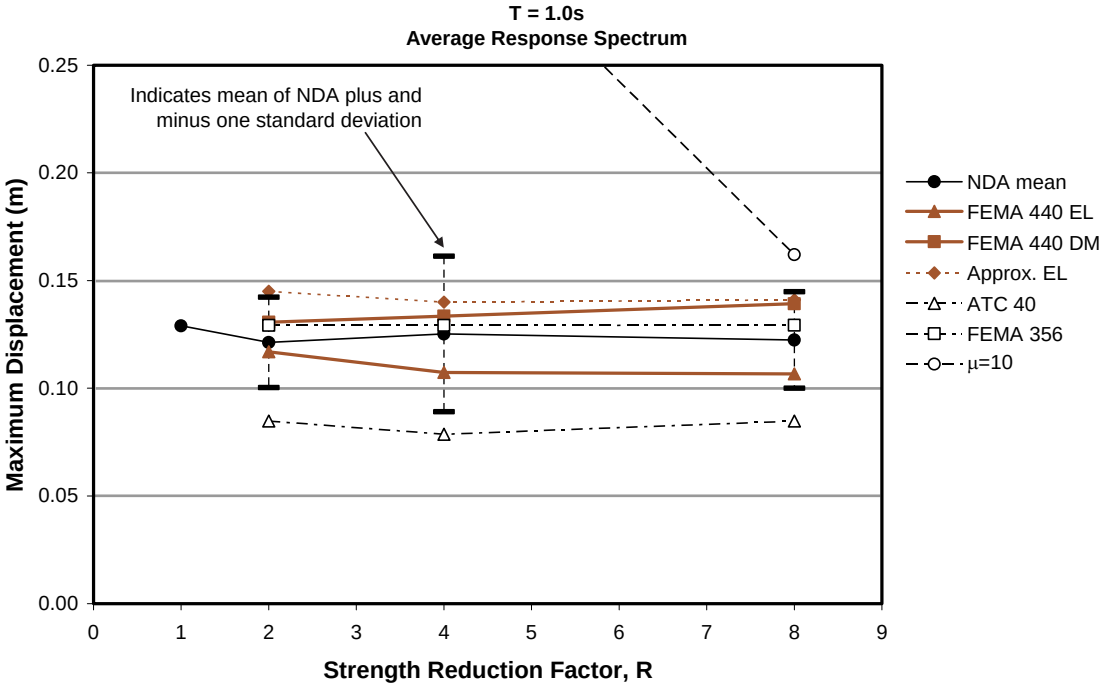


Figure 7-13 Comparison of responses of an oscillator with $T = 1.0$ s calculated using various procedures, response spectra scaled to the NEHRP spectrum, and values calculated for the average spectrum

damping. When used with the NEHRP design spectrum, it was necessary to estimate the effect of damping on spectral ordinates using approximate spectral reduction factors. Additionally, the effective period relationships were optimized from actual spectra as opposed to an assumed shape (e.g., NEHRP spectrum).

## 7.4 Summary of Implications of the Results of the Study

As noted elsewhere in this document, the dispersion of maximum displacement responses for nonlinear oscillators subjected to earthquake ground motions is relatively large, such that a relatively large number of analyses with different oscillators and ground motions may be required to reach statistically meaningful conclusions regarding response statistics. The results reported in this chapter based on a relatively small number of ground motions and oscillators are insufficient to serve as the basis for broad conclusions for all cases. Nonetheless, some general observations can be made from the results.

Engineers using the Capacity-Spectrum Method of ATC-40 and the Coefficient Method of FEMA 356 have observed that sometimes the two methods give widely different displacement estimates. This observation is evident from the results reported in Section 7.3. In some cases, the results of the methods differ by as much as a factor of two (Figures 7-8 through 7-13). One of the objectives of the effort to develop improved nonlinear static procedures, reported here, was to reduce the discrepancy in the results obtained by the two methods. As shown in Figures 7-8 through 7-13, this objective has been met for the ground motions and oscillators that were studied.

Another objective in developing the improved procedures in the frequency domain was to improve the accuracy of the methods relative to results for maximum global displacements obtained using nonlinear dynamic analysis. For this particular sample of ground motions and oscillators, the improved nonlinear static procedures provide generally better estimates of the mean maximum displacement response than do the current procedures. For displacement ductility less than about 10, which is deemed an excessive value for most structures to which these procedures would be applied, the improved nonlinear static procedures produced results within about one standard deviation of mean responses obtained by nonlinear dynamic analysis.

Another objective was to investigate whether the improved simplified static procedures could be applied to design spectra commonly used in practice, with sufficient accuracy. As shown in Figures 7-8, 7-9, and 7-10, for the ground motions, scaling procedure, and oscillators considered, the improved simplified static procedures effectively estimated the mean of maximum displacement response in conjunction with smooth design spectra. Again, the procedures probably should not be used for excessive displacement ductility values.

Finally, the results reported in this chapter illustrate the dispersion typical of nonlinear dynamic analysis using design-level ground motions. Actual response for a real design-level event may differ significantly from the estimate given by the simplified procedures using a NEHRP-like design spectrum. The same is true even if the spectrum is derived from specific ground motions records and even if the simplified procedures are capable of reasonably matching the median response. When interpreting results and assessing structural performance, engineers must consider the implications of these uncertainties.

# 8. Procedures for Including Soil-Structure Interaction Effects

## 8.1 Introduction

This chapter presents simplified procedures for including the effects of interaction between a structure and the supporting soils in a structural model for nonlinear static analysis procedures. There are three primary categories of soil-structure interaction (SSI) effects. These include:

- introduction of flexibility to the soil-foundation system (flexible foundation effects),
- filtering of the ground motions transmitted to the structure (kinematic effects), and
- dissipation of energy from the soil-structure system through radiation and hysteretic soil damping (foundation damping effects).

Current analysis procedures in FEMA 356 and ATC-40 partially address the flexible foundation effect through guidance on including the stiffness and strength of the geotechnical (soil) components of the foundation in the structural analysis model. However, these procedures do not address the reduction of the shaking demand on the structure relative to the free-field motion caused by kinematic interaction or the foundation damping effect. Guidance on including these effects in NSPs is provided in this section. A simple example illustrates the application of these procedures. Appendix E provides detailed information on these soil-structure interaction effects.

Figure 8-1a illustrates the assumption that the structural model is mounted on a rigid base that is excited by the free-field motion. The free-field motion is the theoretical movement of a single point on the surface of the ground, assuming that there is no structure near it. The fixed-base modeling assumption is inappropriate for many structures though. Structural systems that incorporate stiff vertical elements for lateral resistance (e.g., shear walls, braced frames) can be particularly sensitive to even small base rotations and translations that are neglected with a fixed base assumption. Relatively flexible vertical elements (e.g., moment frames) are often not significantly affected by SSI.

Figure 8-1b illustrates the incorporation of foundation flexibility into the structural model directly. ATC-40 and FEMA 356 include provisions for estimating the flexibility and strength of the foundation (i.e., the properties of the springs indicated in Figure 8-1b) in a structural model for inelastic analysis. Those provisions normally use the free-field motion as the seismic demand with 5% damping as the conventional initial value. This approach is capable of modeling both the structural and geotechnical (soil) components of the foundation. The result is that the response of the overall structural system includes deformations (elastic and inelastic) in the structural and geotechnical parts of the foundation system. These deformations are sometimes referred to as an inertial SSI effect. These improvements in modeling can lead to significant departures from fixed-base results and more accurate representation of probable structural response. Compared with the fixed-base modeling approach, the predicted period of the structure lengthens, the distribution of forces among various elements changes, the sequence of inelasticity and the modes of inelastic behavior can change, and foundation mechanisms (e.g., rocking, soil bearing failure, and pier/pile slip) can be directly evaluated and considered. All of these effects result in more realistic evaluation of the probable structural behavior and performance.

Figure 8-1c illustrates the filtering effects that soil-structure interaction can have on the character and intensity of ground motion experienced by the structural model. Kinematic interaction results from the presence of relatively stiff foundation elements on or in soil that cause foundation motions to deviate from free-field motions. Two effects are commonly identified: base-slab averaging and embedment effects. The base-slab averaging effect can be visualized by recognizing that the instantaneous motion that would have occurred in the absence of the structure within and below its footprint is not the same at every point. Placement of a structure and foundation across these spatially variable motions produces an averaging effect in which the overall motion is less than the localized maxima that would have occurred in the free field. The embedment effect is associated with the reduction of ground motion that tends to occur with depth in a soil deposit. Both base-slab averaging and embedment affect the character of the foundation-level motion (sometimes called the foundation input motion, or FIM) in a manner that is independent of the superstructure (i.e., the portion of the structure above the foundation), with one exception. The effects are strongly period-dependent, being maximized at small periods. The effects can be visualized as a filter

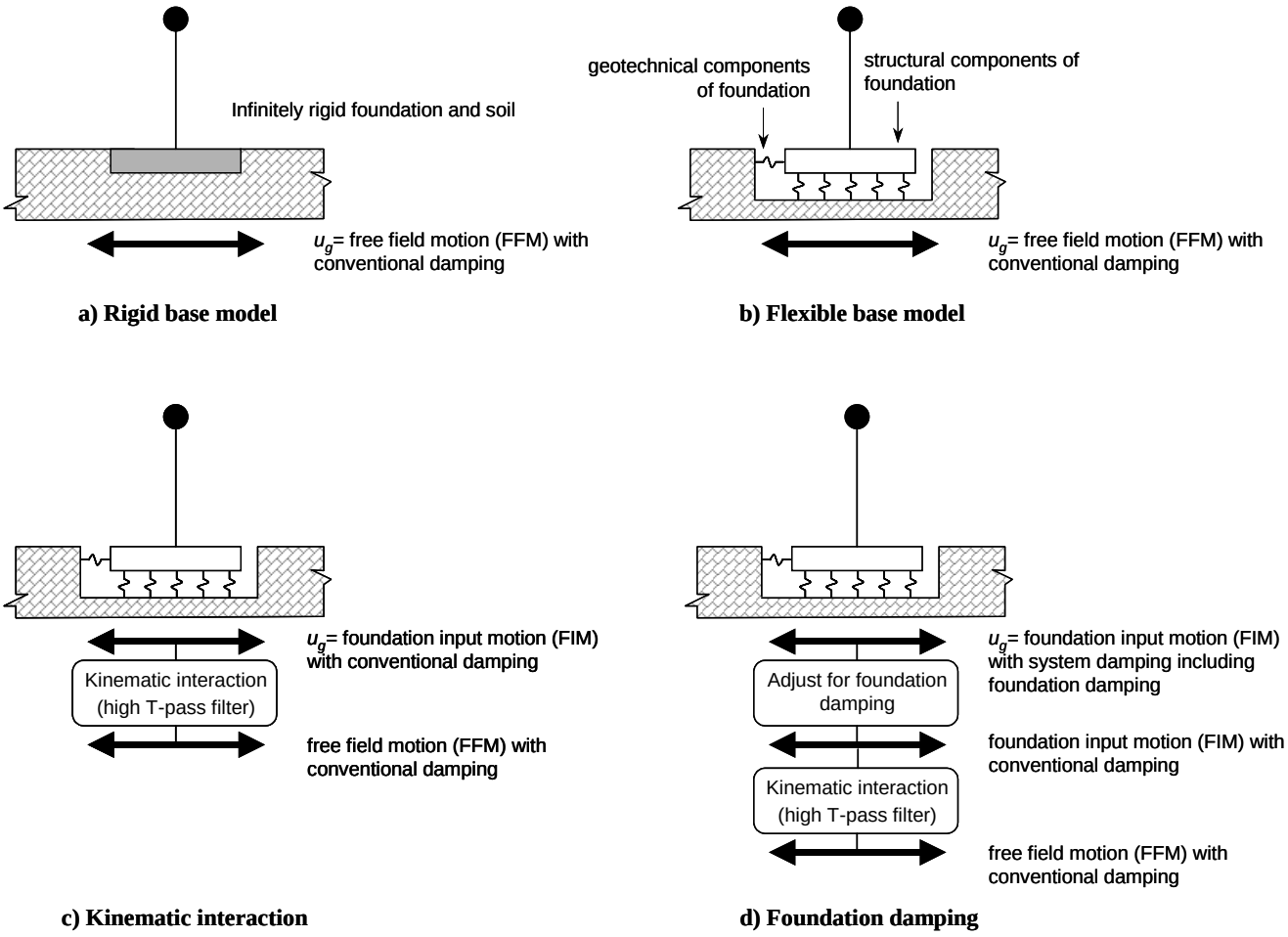


Figure 8-1 Foundation modeling assumptions.

applied to the high-frequency (short-period) components of the free-field ground motion. The impact of those effects on superstructure response will tend to be greatest for short-period buildings. A simplified procedure to apply these principles for reduction of the spectral amplitudes of the free-field motion to generate the FIM spectrum is presented in Section 8.2. The foundation input motion can be applied to a fixed-base model or, as depicted in Figure 8-1c, can be combined with a flexible-base model.

Figure 8-1d illustrates foundation damping effects that are another result of inertial soil-structure interaction in addition to foundation flexibility. Foundation damping results from the relative movements of the foundation and the supporting soil. It is associated with radiation of energy away from the foundation and hysteretic damping within the soil. The result is an effective decrease in the spectral ordinates of ground motion experienced by the structure. Although seldom used in practice the *NEHRP Recommended Provisions for Seismic Regulations for New Buildings and Other Structures* (BSSC, 2000),[1] as well as the ASCE-7 *Standard for Minimum Design Loads for Buildings and Other Structures* (ASCE, 2002) include procedures to account for this effect when using linear analysis procedures. Section 8.3 incorporates similar, although updated, procedures for use with NSPs. In the procedure, the foundation damping is linked to the ratio of the fundamental period of the system on the flexible-foundation to that of a fixed-base model. Other factors affecting foundation damping are the foundation size and embedment. The foundation damping is combined with the conventional initial structural damping to generate a revised damping ratio for the entire system, including the structure, foundation, and soil. This system damping ratio then modifies the foundation

1.Superseded in 2003 with the FEMA 450 *Recommended Provisions for Seismic Regulations for New Buildings and Other Structures.*

input motion imparted to the system model as seismic shaking demand.

## 8.2 Procedures for Kinematic Effects

The ground motions imposed at the foundation of a structure can differ from those in the free field due to averaging of variable ground motions across the foundation slab, wave scattering, and embedment effects. These effects are referred to here as kinematic interaction effects, and they tend to be important for buildings with relatively short fundamental periods (i.e., periods < ~ 0.5 s), large plan dimensions, or basements embedded 10 feet or more in soil materials. This section presents procedures to account for kinematic effects on building structures.

A ratio of response spectra (RRS) factor can be used to represent kinematic interaction effects. An RRS is simply the ratio of the response spectral ordinates imposed on the foundation (i.e., the foundation input motion, FIM) to the free-field spectral ordinates. Two phenomena should be considered in evaluating RRS: base slab averaging and foundation embedment, both of which are introduced in the preceding section. Base-slab averaging occurs to some extent in virtually all buildings. The slab-averaging effect occurs at the foundation level for mats or spread footings interconnected by either grade beams or reinforced concrete slabs. Even if a laterally stiff foundation system is not present, averaging can occur at the first elevated level of buildings with rigid diaphragms. The only case in which base-slab averaging effects should be neglected is in buildings without a laterally connected foundation system and with flexible floor and roof diaphragms. Foundation embedment effects should be considered for buildings with basements. Such effects should not be considered for buildings without basements, even if the footings are embedded. Embedment effects tend to be significant when the depth of basements is greater than about 10 feet. The following simplified procedure (adapted from Kim and Stewart (2003) and other sources) is recommended for analysis of these two kinematic interaction effects as a function of period, *T*, of the structural model:

1. Evaluate the effective foundation size $b_e = \sqrt{ab}$, where *a* and *b* are the full footprint dimensions (in feet) of the building foundation in plan view.
2. Evaluate the RRS from base-slab averaging ($RRS_{bsa}$) as a function of period (see Figure 8-2). An approximation to the curves in Figure 8-2 is given by the following:

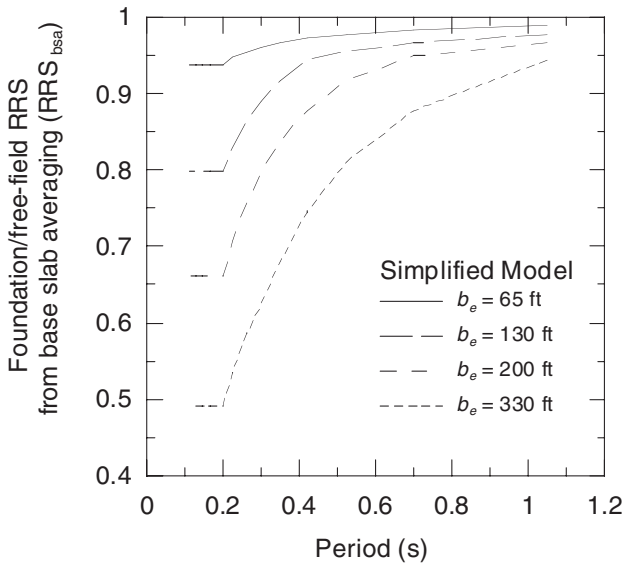


Figure 8-2 Ratio of response spectra for base slab averaging, $RRS_{bsa}$, as a function of period, *T*, and effective foundation size, $b_e$.

$$RRS_{bsa} = 1 - \frac{1}{14{,}100}\left(\frac{b_e}{T}\right)^{1.2} \geq \text{the value for } T = 0.2 \text{ s} \quad (8\text{-}1)$$

3. If the structure has a basement embedded a depth *e* from the ground surface, evaluate an additional RRS from embedment ($RRS_e$) as a function of period (see Figure 8-3). The curves in Figure 8-3 are described by the following:

$$RRS_e = \cos\left(\frac{2\pi e}{T n v_s}\right) \geq \text{ the larger of 0.453 or the } RRS_e \text{ value for } T = 0.2 \text{ s.} \quad (8\text{-}2)$$

where

$e$ = foundation embedment (in feet)

$v_s$ = shear wave velocity for site soil conditions, taken as average value of velocity to a depth of $b_e$ below foundation (ft/s)

$n$ = shear wave velocity reduction factor for the expected PGA as estimated from Table 8-1.

4. Evaluate the product of $RRS_{bsa}$ times $RRS_e$ to obtain the total RRS for each period of interest. The spectral ordinate of the foundation input motion at each period is the product of the free-field spectrum and the total RRS.

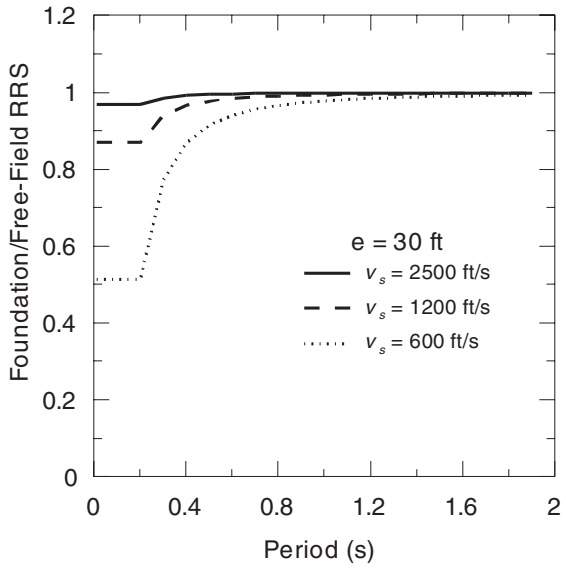


Figure 8-3 Ratio of response spectra for embedment $RRS_e$, for an embedment, e, of 30 feet as a function of period, *T*, and shear wave velocity, $v_s$.

**Table 8-1 Approximate Values of Shear Wave Velocity Reduction Factor, *n***

| | *Peak Ground Acceleration (PGA)* | | | |
|---|---|---|---|---|
| | *0.10g* | *0.15g* | *0.20g* | *0.30g* |
| *n* | 0.90 | 0.80 | 0.70 | 0.65 |

5. Repeat steps 2 through 4 for other periods if desired to generate a complete spectrum for the foundation input motion (FIM).

If desired, more detailed procedures can also be used, which are described in Appendix E.

Limitations associated with application of this approach include the following, each of which is explained in Appendix E:

- Kinematic interaction effects should be neglected for soft clay sites such as Site Class E.
- Embedment effects can be neglected for foundations embedded in firm rock (Site Classes A and B).
- The base-slab averaging model:
  a. underestimates reductions in ground motions for foundation materials that consist of firm rock (Site Classes A and B).
  b. has not been rigorously studied for structures without large in-plane stiffness (continuous mat foundation or footings interconnected with a reinforced slab and/or grade beams); however, it is considered reasonable to extend its application to all structures except those without both an interconnected foundation and rigid floor and roof diaphragms.
  c. has not been rigorously studied for structures with plan dimensions greater than 200 ft.; however, it is considered reasonable to extend the application to these conditions, provided that the foundation elements are laterally connected.
  d. has not been rigorously studied for structures with pile-supported foundations; however it is considered reasonable to extend application to pile-supported structures in which the cap and soil are in contact or in which the caps are laterally connected to one another by a slab or grade beams.

## 8.3 Procedures for Foundation Damping

Damping related to foundation-soil interaction can significantly supplement damping that occurs in a structure due to inelastic action of structural components. The damping from foundation-soil interaction is associated with hysteretic behavior of soil (not to be confused with hysteretic action in structural components) as well as radiation of energy into the soil from the foundation (i.e., radiation damping). These foundation damping effects tend to be important for stiff structural systems (e.g., shear walls, braced frames), particularly when the foundation soil is relatively soft (i.e., Site Classes D-E).

The effects of foundation damping are represented by a modified system-damping ratio. The initial damping ratio for the structure neglecting foundation damping is referred to as $\beta_i$, and is generally taken as 5%. The damping attributed to foundation-soil interaction alone (i.e., the foundation damping) is referred to as $\beta_f$. Finally, the damping ratio of the complete structural system, accounting for foundation-soil interaction, as well as structural damping, is referred to as $\beta_0$. The change in damping ratio from $\beta_i$ to $\beta_0$ modifies the elastic response spectrum. The spectral ordinates are reduced if $\beta_0 > \beta_i$.

A number of factors influence the foundation damping factor $\beta_f$ (see Appendix E). Subject to the limitations noted below, the following simplified procedure can be used to estimate $\beta_f$ and the subsequent spectral ordinate change due to the modified damping ratio of the complete structural system, $\beta_0$.

1. Evaluate the linear periods for the structural model assuming a fixed base, $T$, and a flexible base, $\tilde{T}$ using appropriate foundation modeling assumptions. Guidelines for the evaluation of soil spring stiffnesses are provided in FEMA 356 and ATC-40. In those calculations, the strain-degraded shear modulus should be used to represent the soil stiffness.

2. Calculate the effective structural stiffness of the SDOF oscillator for fixed base conditions as

$$K^*_{\text{fixed}} = M^* \left( \frac{2\pi}{T} \right)^2 \tag{8-3}$$

where $M^*$ is the effective mass for the first mode calculated as the total mass times the effective mass coefficient (see ATC-40 Eqn. 8-21).

3. Determine the equivalent foundation radius for translation as

$$r_x = \sqrt{\frac{A_f}{\pi}} \tag{8-4}$$

where $A_f$ is the area of the foundation footprint if the foundation components are inter-connected laterally.

4. Calculate the translational stiffness of the foundation, $K_x$. This can be evaluated using the procedures in FEMA 356 (Chapter 4) or ATC-40 (Chapter 10). For many applications, the translational stiffness can be estimated as

$$K_x = \frac{8}{2-\upsilon} G r_x \tag{8-5}$$

where $G$ = effective, strain-degraded soil shear modulus (see FEMA 356, Table 4.7) and $\upsilon$ = soil Poisson's ratio (~0.3 for sand, ~0.45 for clay).

5. Calculate the equivalent foundation radius for rotation, $r_\theta$, by first evaluating the effective rotational stiffness of the foundation, $K_\theta$, as

$$K_\theta = \frac{K^*_{\text{fixed}} \left( h^* \right)^2}{\left( \frac{\tilde{T}}{T} \right)^2 - 1 - \frac{K^*_{\text{fixed}}}{K_x}} \tag{8-6}$$

Where $h^*$ is the effective structure height taken as the full height of the building for one-story structures, and as the vertical distance from the foundation to the centroid of the first mode shape for multi-story structures. In the latter case, $h^*$ can often be well-approximated as 70% of the total structure height. The quantity $K_x$ is often much larger than $K^*_{\text{fixed}}$, in which case an accurate evaluation of $K_x$ is unnecessary and the ratio, $K^*_{\text{fixed}}/K_x$, can be approximated as zero.

The equivalent foundation radius for rotation is then calculated as

$$r_\theta = \left( \frac{3(1-\upsilon) K_\theta}{8G} \right)^{\frac{1}{3}} \tag{8-7}$$

The soil shear modulus, $G$, and soil Poisson's ratio, $\upsilon$, should be consistent with those used in the evaluation of foundation spring stiffness.

6. Determine the basement embedment, $e$, if applicable.

7. Estimate the effective period-lengthening ratio, $\tilde{T}_{\text{eff}} / T_{\text{eff}}$, using the site-specific structural model developed for nonlinear pushover analyses. This period-lengthening ratio is calculated for the structure in its degraded state (i.e., accounting for structural ductility and soil ductility). An expression for the ratio is

$$\frac{\tilde{T}_{\text{eff}}}{T_{\text{eff}}} = \left\{ 1 + \frac{1}{\mu} \left[ \left( \frac{\tilde{T}}{T} \right)^2 - 1 \right] \right\}^{0.5} \tag{8-8}$$

where the term $\mu$ is the expected ductility demand for the system (i.e., including structure and soil effects). Thus, the ductility must be estimated prior to the actual solution and subsequently verified.

8. Evaluate the initial fixed-base damping ratio for the structure ($\beta_i$), which is often taken as 5%.

9. Determine foundation damping due to radiation damping, $\beta_f$, based on $\tilde{T}_{\text{eff}} / T_{\text{eff}}$, $e/r_x$, and $h/r_\theta$, using the plots in Figures 8-4 and 8-5. An approximation to those curves is given by the following:

$$\beta_f = a_1 \left( \frac{\tilde{T}_{\text{eff}}}{T_{\text{eff}}} - 1 \right) + a_2 \left( \frac{\tilde{T}_{\text{eff}}}{T_{\text{eff}}} - 1 \right)^2 \tag{8-9}$$

where $\beta_f$ is in percent and

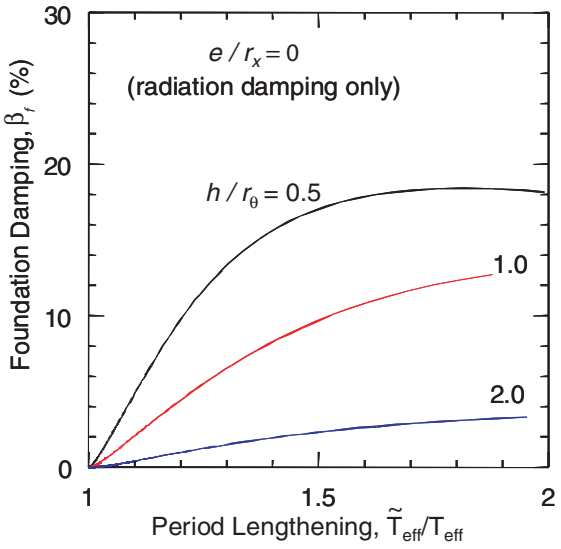


Figure 8-4 Example of foundation damping, $\beta_f$, as a function of effective period lengthening ratio, $\tilde{T}_{\text{eff}} / T_{\text{eff}}$, for constant embedment, $e/r_x = 0$, and various values of foundation stiffness rotational stiffness, $h/r_\theta$.

$$a_1 = c_e \exp\left(4.7 - 1.6h / r_\theta\right) \quad \text{(8-9a)}$$

$$a_2 = c_e \left[25 \ln\left(h / r_\theta\right) - 16\right] \quad \text{(8-9b)}$$

$$c_e = 1.5\left(e / r_x\right) + 1 \quad \text{(8-9c)}$$

The above equations are most applicable for $\tilde{T}_{\text{eff}} / T_{\text{eff}} < 1.5$, and generally provide conservative (low) damping estimates for higher $\tilde{T}_{\text{eff}} / T_{\text{eff}}$.

10. Evaluate the flexible-base damping ratio ($\beta_0$) from $\beta_i$, $\beta_f$, and $\tilde{T}_{\text{eff}} / T_{\text{eff}}$ as follows:

$$\beta_0 = \beta_f + \frac{\beta_i}{\left(\tilde{T}_{\text{eff}} / T_{\text{eff}}\right)^3} \quad \text{(8-10)}$$

11. Evaluate the effect on spectral ordinates of the change in damping ratio from $\beta_i$ to $\beta_0$ (in accordance with Section 6.3); then modify the spectrum of the foundation input motion (recall that foundation input motion is equal to the free-field motion if kinematic effects are neglected).

From this point, the maximum expected displacement of the nonlinear SDOF oscillator model can be estimated using the displacement modification

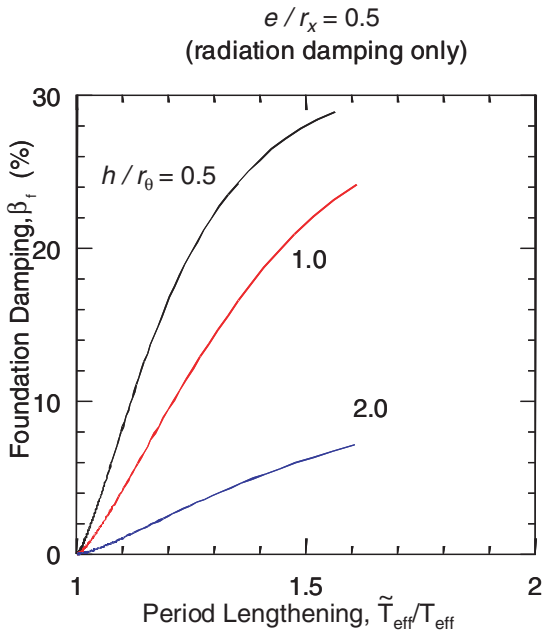


Figure 8-5 Example of foundation damping, $\beta_f$, as a function of effective period lengthening ratio, $\tilde{T}_{\text{eff}} / T_{\text{eff}}$, for constant embedment, $e/r_x = 0.5$, and various values of foundation stiffness rotational stiffness, $h/r_\theta$.

procedures of FEMA 356 and Chapter 5 or the equivalent linearization procedures of ATC-40 and Chapter 6. The ductility demand should be checked against the value assumed in Step 7 above.

The damping ratios determined in accordance with this section represent radiation damping effects only. Hysteretic soil damping effects are neglected, since ductility in soil springs is included as part of structural pushover analysis.

Limitations on the damping analysis described above include the following:

- The procedure above should not be used when shear walls or braced frames are spaced sufficiently closely that waves emanating from distinct foundation elements will destructively interfere with each other across the period range of interest. This can effectively decrease the energy dissipated in the soil material, and the above formulation could overestimate the related damping. Unfortunately, this effect has not been investigated sufficiently to justify definitive limits. In the absence of such limits, a reasonable approximation might be to neglect the effect of softly-coupled foundation

components spaced at a distance less than the larger dimension of either component in the corresponding direction. Further discussion is presented in Appendix E, Section E.3.1.5.

- The analysis can be conservative (underpredicting the damping) when foundation aspect ratios exceed about 2:1. Further discussion is presented in Appendix E, Section E.3.1.4.
- The analysis is conservative when foundations are deeply embedded, $e/r_x > 0.5$. Further discussion is presented in Appendix E, Section E.3.1.3.
- The analysis is unconservative (overpredicting the damping) if $v_s T/r_x > 2\pi$ (where $v_s$ = average shear wave velocity to a depth of about $r_x$) and the foundation soils have significant increases of shear stiffness with depth. Further discussion is presented in Appendix E, Section E.3.1.2.
- The analysis is unconservative if the foundation soil profile consists of a soil layer overlying a very stiff material (i.e., there is a pronounced impedance contrast within the soil profile), and if the system period is greater than the first-mode period of the layer. Further discussion is presented in Appendix E, Section E.3.1.2.

# 9. Multiple-Degree-of-Freedom Effects

## 9.1 Introduction

One of the primary assumptions of nonlinear static analysis procedures is that the behavior of a structure with multiple degrees of freedom (MDOF) subject to seismic ground motion can be estimated from the response of an oscillator with a single degree of freedom (SDOF). In order to generate the SDOF model, the engineer generates a global force-deformation relationship for the structure by subjecting a MDOF model to a predetermined lateral load vector. This relationship is then converted to an equivalent SDOF representation to estimate the maximum global displacement of the model using displacement-modification or equivalent linearization techniques. The global displacement is typically monitored at the roof level or center of mass. The magnitude of localized demand in the MDOF model (e.g., story drifts and forces or component deformations) are directly related to the global displacement. The actual maximum global displacement for the MDOF system can differ from the equivalent SDOF approximation. The distribution of localized demand depends on the assumptions associated with the load vector used to generate the equivalent SDOF model. The distribution of forces on the structure changes continuously during an earthquake. In the elastic range, this is attributable to the fact that the response comprises contributions from multiple modes of vibration. The actual distribution is difficult to assess since the dynamic characteristics of the ground motion itself are a major influence. Inelasticity further complicates the situation. The combined deviations of the actual distribution of forces and deformations from those associated with the equivalent SDOF system and the assumed load vector are termed MDOF effects. They can result in maximum inelastic response in components or elements that differ from the SDOF model predictions in nonlinear static analysis.

This section reviews the accuracy and practical implications of the requirements of ATC-40 and FEMA 356 related to MDOF effects including:

1. current options for load vectors, and
2. the conversion of a MDOF pushover curve to an equivalent SDOF system.

The results of a comprehensive study of five example buildings that examines the differences in response predicted using various options compared to a common nonlinear dynamic analyses benchmark are also summarized. Finally, this chapter provides recommendations for practical applications and identifies promising developments for the future.

## 9.2 Review of Current Simplified Procedures

There are a number of options for the form of the load vector used to generate the SDOF model of a structure. Some are based on a single vector and one uses several vectors applied to comprise a multi-mode pushover approach. In all the options, lateral forces are applied incrementally to a nonlinear structural model to generate a "pushover" or capacity curve representing the relationship between the applied lateral force and the global displacement at the roof or some other control point. The applied lateral force at any level in the structure is proportional to the mass at that level and an acceleration determined from a specific shape vector assumption. The various options are summarized below, as are the specifications of ATC-40 and FEMA 356 related to MDOF effects.

### *9.2.1 Single-Mode Load Vectors*

**Concentrated Load.** The simplest assumption for a load vector is a single concentrated load located normally at the top of the structure.

**Uniform.** A uniform load vector assumes that the acceleration in the MDOF model is constant over its height. This alternative is sometimes termed "rectangular."

**Triangular.** A triangular-shaped vector assumes that the acceleration increases linearly from zero at the base to a maximum at the top of the MDOF model.

**Code Distribution.** The "code" load pattern appears in many documents. The acceleration pattern varies from the triangular shape for periods less than 0.5 s to a parabolic shape for periods greater than 2.5 s, as a means to account for higher-mode effects.

**First Mode.** The first-mode technique applies accelerations proportional to the shape of the first mode of the elastic MDOF model.

**Adaptive.** The adaptive procedure uses the first mode and recognizes that softening of the capacity curve

reflects a reduction in stiffness, which, in turn, causes a change in the mode shape. Thus, lateral forces are applied in proportion to the amplitude of an evolving first-mode shape and the mass at each level within the MDOF model.

**SRSS.** The square-root-of-the-sum-of-the-squares (SRSS) technique is based on elastic modal responses. The response in each mode has a lateral force pattern, which can be summed to obtain story shears associated with each mode. An SRSS combination of the modal story shears results in a particular shear profile, referred to as the SRSS story shears. The lateral forces required to generate the SRSS story shear profile are applied to the MDOF model in this pushover technique. The elastic spectral amplitudes and modal properties are used even when nonlinear response is anticipated. A sufficient number of modes to represent at least 90% of the mass is generally included.

### *9.2.2 Multi-Mode Pushover Procedures*

Multi-mode pushover analysis procedures consider response in several modes. Approaches have been described by various investigators such as Sasaki et al. (1998), Reinhorn (1997), Chopra and Goel (2002), and Jan et al. (2004). Chopra and Goel (2001b) describe an approach in which pushover analyses are conducted independently in each mode, using lateral-force profiles that represent the response in each of the first several modes. Response values are determined at the target displacement associated with each modal pushover analysis. Response quantities obtained from each modal pushover normally are combined using the SRSS method. Although response in each mode may potentially be nonlinear, the mode shapes and lateral-force profiles are assumed to be invariant in this analysis procedure. Target displacement values may be computed by applying displacement modification or equivalent linearization procedures to an elastic spectrum for an equivalent SDOF system representative of each mode to be considered. Chopra and Goel (2001d) and Yu et al. (2001) illustrate the method using SRSS combinations of floor displacement, interstory drift, and component deformation (plastic hinge rotations).

### *9.2.3 Summary of Current Provisions*

**FEMA 356.** FEMA 356 (Section 3.3.3.2.3) requires that two separate nonlinear static analyses be done, each using different load vectors. For each response quantity of interest, the larger value of the two analyses is compared to the applicable acceptability criteria.

One load vector is selected from the following list.

- Code distribution—Restricted to the cases in which more than 75% of mass participates in first mode, and the second vector must be the uniform distribution.
- First mode—Restricted to the cases in which more than 75% of mass participates in first mode.
- SRSS of modal story loads – This option must be used if $T_e > 1$ s.

A second load vector is selected from the following options.

- Uniform distribution or
- Adaptive load distribution.

In FEMA 356 (Section 2.4.2.1), the use of NSPs must be supplemented with a linear dynamic analysis if any SRSS story shear from a response-spectrum analysis including modes representing 90% of the mass exceeds 130% of the corresponding story shear from a first-mode response-spectrum analysis.

The yield displacement, $\Delta_y$, of the equivalent SDOF system is effectively determined as

$$\Delta_y = \frac{\Delta_{y,\text{roof}}}{\Gamma_1} \tag{9-1}$$

where $\Delta_{y,\text{roof}}$ = the roof displacement at yield, and $\Gamma_1$ = the first-mode participation factor.

In the FEMA 356 approximation, it can be shown that the yield strength coefficient of the equivalent SDOF system is approximated as

$$C_y = \frac{S_a}{g} = \frac{V_{mdof}}{W}\Gamma_1 \tag{9-2}$$

where $S_a$ = the pseudo-acceleration associated with yield of the ESDOF (Equivalent SDOF) system, $g$ = the acceleration of gravity, $V_{mdof}$ = the yield strength of the MDOF system, $W$ = the weight of the MDOF system. This simplification relies on the approximation $\Gamma_1 \approx 1/\alpha_1$, where $\alpha_1$ is the modal mass coefficient.

**ATC-40.** The primary recommendation in ATC-40 (Section 8.2.1) for load vectors is to use the first mode. However, the guidelines recognize a hierarchy of other options, arranged here in order of preference.

1. Concentrated load
2. Code distribution
3. First mode
4. Adaptive
5. Multi-mode pushover

The guidelines also note that pushover analyses using the first-mode shape are generally valid for structures with fundamental periods up to about one second. They suggest that the engineer might want to consider multi-mode pushover for structures with longer periods.

In the ATC-40 method, the yield displacement of the equivalent SDOF is the same as that of FEMA 356; however the yield strength coefficient of the equivalent SDOF system is given by

$$C_y = \frac{S_a}{g} = \frac{V_{mdof}/W}{\alpha_1} \quad (9\text{-}3)$$

where $S_a$ = the pseudo-acceleration associated with yield of the ESDOF system, $g$ = the acceleration of gravity, $V_{y,\,mdof}$ = the yield strength of the MDOF system, $W$ = the weight of the MDOF system, and $\alpha_1$ = the modal mass coefficient.

## 9.3 Summary of Illustrative Examples

In order to compare and illustrate the effects of the various options with NSPs related to the effects of higher modes, five example buildings were analyzed. Detailed information and results of the analyses are contained in Appendix F. The basic description of the example buildings and the other features of the analysis are listed below.

**Example Buildings**

- Three-story, steel frame (SAC LA Pre-Northridge M1 Model)
- Three-story, weak-story steel frame (lowest story at 50% of strength)
- Eight-story, shear wall (Escondido Village)
- Nine-story, steel frame (SAC LA Pre-Northridge M1 Model)
- Nine-story, weak-story steel frame (lowest story at 60% of strength)

**Ground Motions**

- Eleven site Class C motions, 8-20 km from the fault rupture, five events
- Four near-field motions: Erzincan, Northridge (Rinaldi Receiving Station & Sylmar County Hospital), and Landers earthquakes

**Global Drift Levels**

Ordinary motions (scaled to result in specified global drift)

- 0.5, 2, 4% drift, as a percentage of building height, for frames
- 0.2, 1, 2% drift, as a percentage of building height, for wall

Near-field (unscaled)

- 1.8 to 5.0% for 3-story frames, 1.7-2.1% for 9-story frames
- 0.6 – 2.1% drift, as a percentage of building height, for wall

**Load Vectors**

- Triangular
- Uniform
- Code
- First mode
- Adaptive
- SRSS
- Multi-mode pushover

**Response Parameters**

- Floor and roof displacement
- Interstory drift
- Story shear
- Overturning moment

**Error Measurements**

- Mean over all floors
- Maximum over all floors

### *9.3.1 Load Vectors*

For analyses using the ordinary ground motions, each motion was scaled to result in the pre-determined levels of total drift at the roof for each example building in the

nonlinear response-history analysis of the MDOF models. The resulting response parameters served as the basis for comparison with nonlinear static analyses using the various options for load vectors. Observations from the comparisons are summarized as follows:

- Anomalous capacity curves resulted because the roof displacements reversed in two of the higher-mode pushover analyses. Consequently, the Modal Pushover Analysis procedure described by Chopra and Goel (2001b) could not be applied without modification to the examples. In order to represent higher-mode contributions, a multiple mode calculation procedure was introduced in the ATC-55 project. In this procedure, response quantities for the 2nd and 3rd mode were determined under the assumption that the response in these modes is elastic. A conventional inelastic pushover analysis was used for response in the first mode. Floor displacement, interstory drift, story shear, and overturning moments were determined as an SRSS combination of the modal responses in the first three modes. Motivated by review of early results of these analyses, Chopra et al. (2004) have investigated this approach, described as a "modified MPA," in comparison with the original MPA procedure.
- All the simplified procedures evaluated resulted in good estimates of peak displacements over the height of the five example buildings (Figure 9-1) when compared with nonlinear dynamic response-history analysis results. Estimates made using the first-mode, triangular, and adaptive load vectors were best. A multiple mode procedure may be warranted for structures in which displacement response is suspected to be predominantly in a higher mode.
- The dispersion in the displaced shapes of the weak-story buildings was pronounced at the moderate drift levels. This is likely due to the fact that weak-story mechanisms did not always develop at these levels of roof drift. This is illustrated by comparing the dispersion in floor displacements of the nine-story, weak story frame building at 2% roof drift (Figure 9-2a) that is actually greater than that for the same building at 4% drift (Figure 9-2b).
- Good estimates of interstory drift were obtained over the height of the three-story frames and eight-story wall using the first-mode, triangular, code, adaptive, and SRSS load vectors, as well as with the modified MPA procedure (Figure 9-3).
- Interstory drifts estimates over the height of the nine-story buildings were poor for the single-mode load vectors (see Figure 9-4). The results using the modified MPA procedure were consistently better than those obtained with the single load vectors, although the interstory drift values were still underestimated at some locations in the nine-story frames. Similar results are reported by Goel and Chopra (2004).
- The maximum interstory drift over the height of each building model, determined using the single-mode load vectors (excluding the uniform load vector), was a reasonable estimate of the maximum interstory drift occurring at that particular location in the nonlinear dynamic analyses. This drift was also a reasonable estimate of the maximum interstory drift that developed over the height of each building model in the nonlinear dynamic analyses (Figures 9-3 and 9-4), although these estimates depended to some extent on the load vector selected. Also, drifts at other locations predicted with the load vectors often did not correspond to those from the nonlinear dynamic analyses.
- Estimates of story shear and overturning moment for the three-story frames (Figure 9-5) were not as accurate as the displacement and interstory drift estimates (Figure 9-3a). These quantities typically were underestimated using the single load vectors and overestimated using the modified MPA procedure. The tendency for the modified MPA procedure to overestimate forces and moments is not surprising, as SRSS combinations of these quantities can exceed limits associated with the development of an inelastic mechanism and depend on the number of modes included in the combination.
- Estimates were inconsistent and often poor for story shears and overturning moment for the eight-story wall and nine-story frames (Figure 9-6). Although the overall pattern of overturning moments was often correct, errors in the estimates of overturning moment were often substantial, particularly for the upper floors. Similar results are reported by Krawinkler and Seneviratna (1998) and Gupta and Krawinkler (2003).
- The accuracy of the simplified procedures was similar for the set of Site Class C motions and for the set of near-field motions that was considered.

### *9.3.2 Equivalent SDOF Estimates of Global Displacement*

For each example building, the force-displacement relationship generated with the first-mode vector was converted to an equivalent SDOF system using the

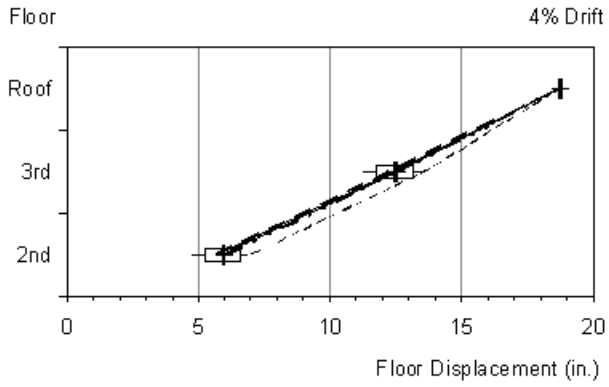


**(a) Three-story frame building at 4% drift**

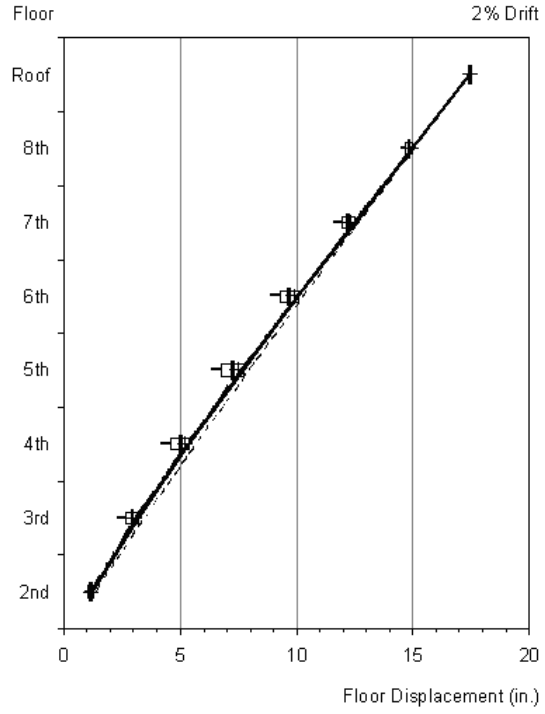


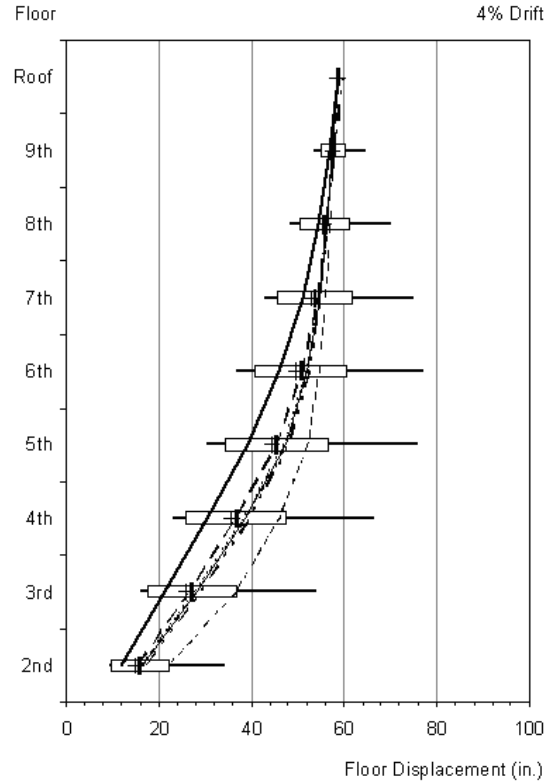


**(b) Eight-story wall building at 2% drift** **(c) Nine-story frame at 4% drift**

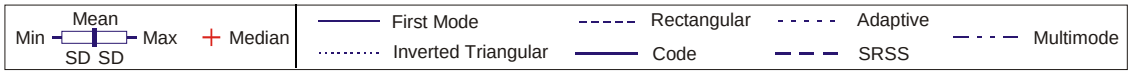


**NDA** **NSP Load Vectors**

Figure 9-1 Example results for displacements predicted by nonlinear static procedures (NSP) compared to nonlinear dynamic response-history analyses (NDA).

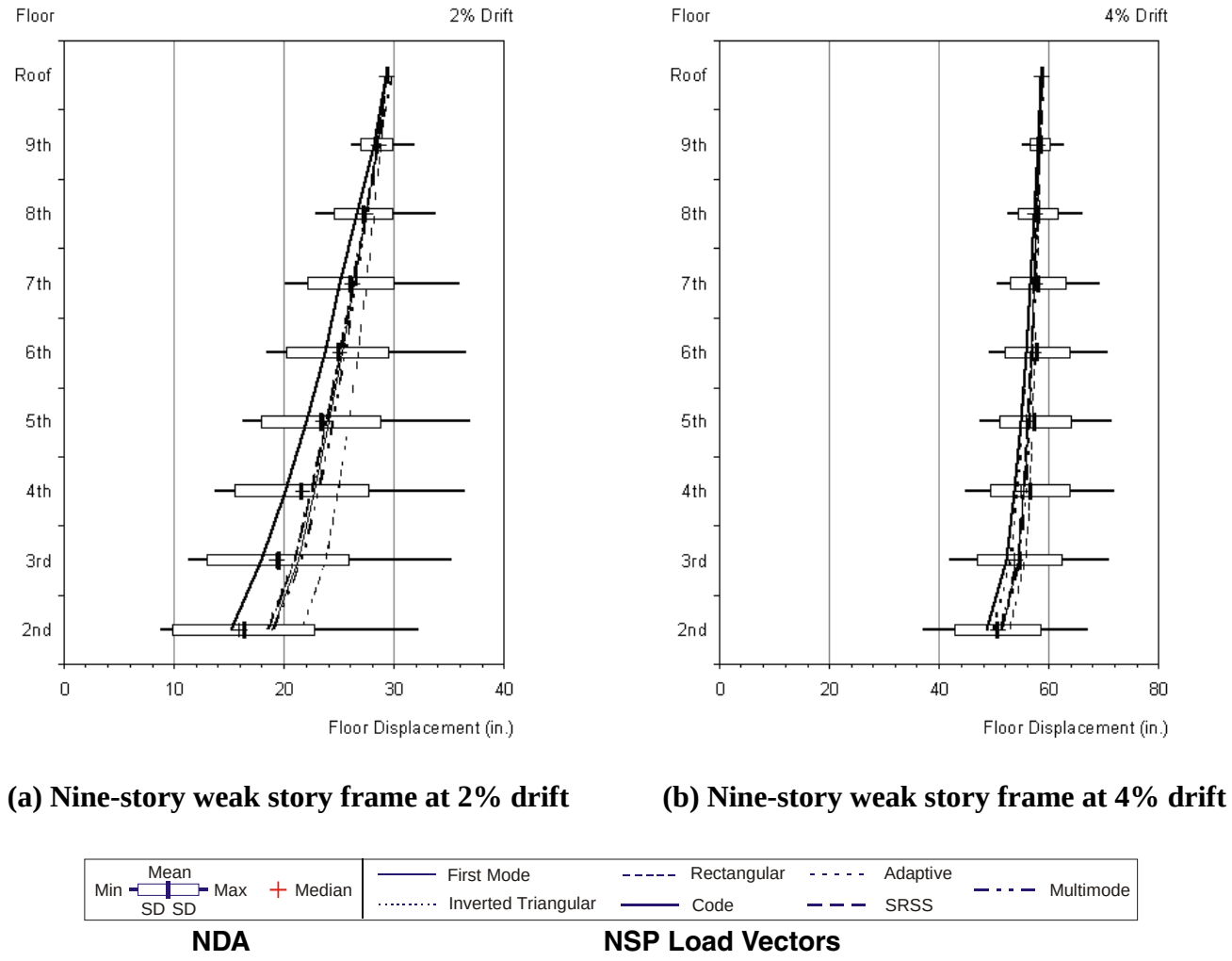


**(a) Nine-story weak story frame at 2% drift** **(b) Nine-story weak story frame at 4% drift**

Figure 9-2 Dispersion in results for displacement for two levels of global drift.

procedures of both FEMA 356 and ATC-40. These models were then subjected to scaled ground-motion records. A displacement ratio was defined as the ratio of the estimated roof displacement and the peak roof displacement obtained in the nonlinear response-history analysis. Results are reported in detail in Appendix F and summarized below.

- In cases in which the post-yield stiffness of the capacity curve is positive (with or without *P-Δ* effects present), mean displacement ratios obtained using the ATC-40 formulation were between approximately 0.95 and 1.25 for the five buildings. Within this range, mean displacement ratios tended to increase with increasing roof drift.
- Similar mean displacement ratios were obtained with the FEMA 356 formulation, although dispersions were larger for this formulation. Accuracy was similar for the near-field motions.
- In cases in which the post-yield stiffness of the capacity curve is negative (due to *P-Δ* effects), equivalent SDOF systems can have excessive displacement response, leading to overestimates of the peak roof displacement. For such cases, nonlinear dynamic analysis of the MDOF structure may be more accurate.

## 9.4 Practical Implications

NSPs can provide reliable estimates of maximum displacement. They are also capable of providing reasonable estimates of the largest interstory drift that may occur at any location over the height, but are

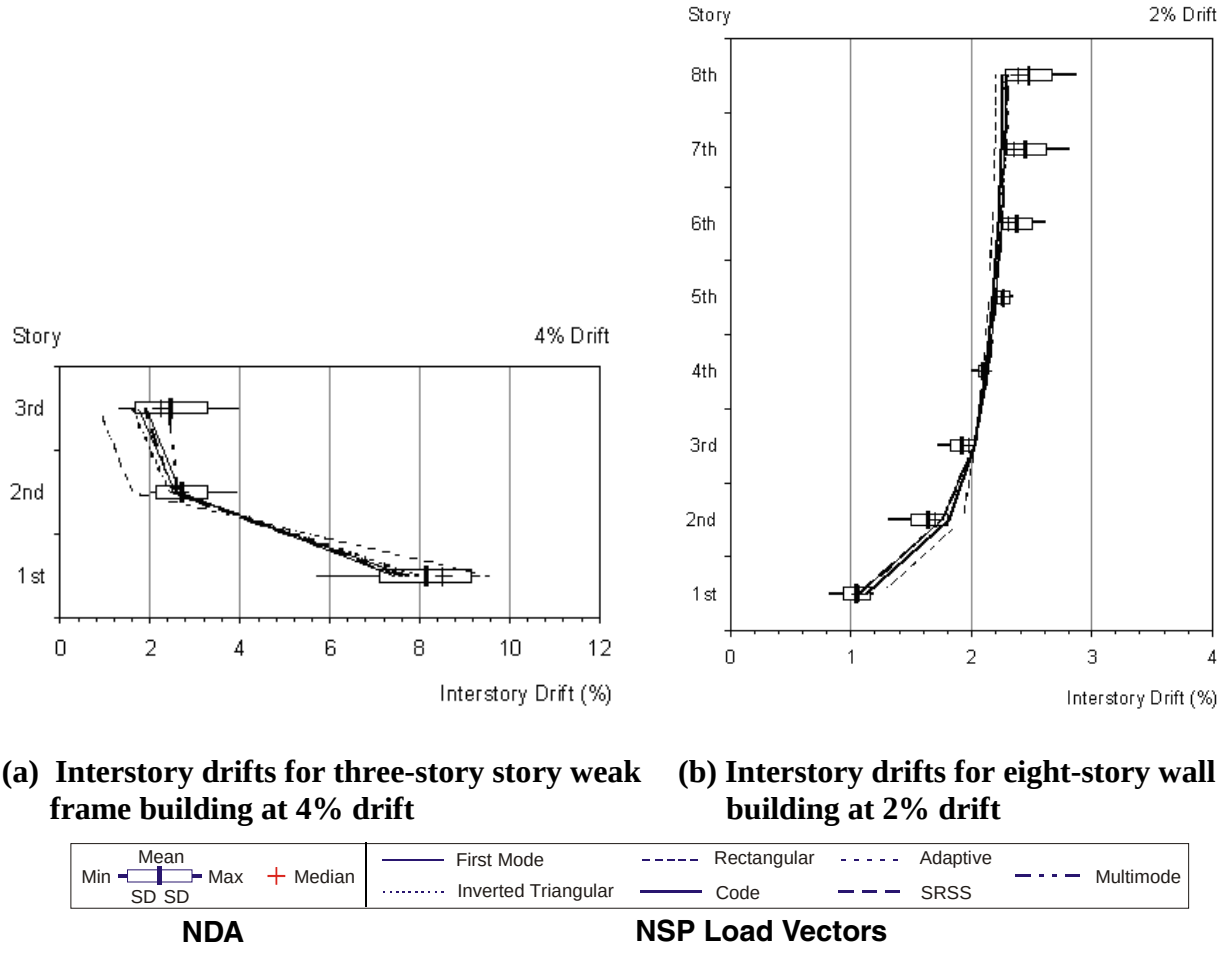


**(a) Interstory drifts for three-story story weak frame building at 4% drift**

**(b) Interstory drifts for eight-story wall building at 2% drift**

Figure 9-3 Relatively good results for interstory drift predicted using nonlinear static procedures (NSP), as compared to nonlinear dynamic response-history analyses (NDA).

limited in the capability to predict drift accurately over the full height of relatively tall, flexible MDOF structures. In contrast, interstory drift over the height of the three-story frames and eight-story shear wall example buildings were estimated well. Nonlinear static procedures that combine contributions from independent modal analyses appear to be poor predictors of story shear and overturning moment. These observations are consistent with the results of a number of other research efforts (Seneviratna and Krawinkler, 1994; Krawinkler and Seneviratna, 1998; Kunnath and Gupta, 2000; Lew and Kunnath, 2000; Yu et al., 2001; Chopra and Goel, 2001b; Gupta and Krawinkler, 2003; Goel and Chopra, 2004; and Jan et al., 2004). This situation raises a number of questions with regard to the practical application of NSPs in cases in which MDOF effects are important. First, is there any preference for any one load vector over the others? Second, when should results of NSPs not be relied upon for MDOF effects? Finally, what should be done now and in the future?

### *9.4.1 Single Load Vectors*

The first-mode load vector is recommended because of the low error obtained for displacement estimates made with this assumption and to maintain consistency with the derivations of equivalent SDOF systems. The code distribution and the triangular vectors may be used as alternatives, typically with little increase in error.

Mean and maximum errors were sometimes smaller and sometimes larger using the adaptive load vector. The adaptive method requires more computational effort and fails for systems exhibiting a negative tangent stiffness.

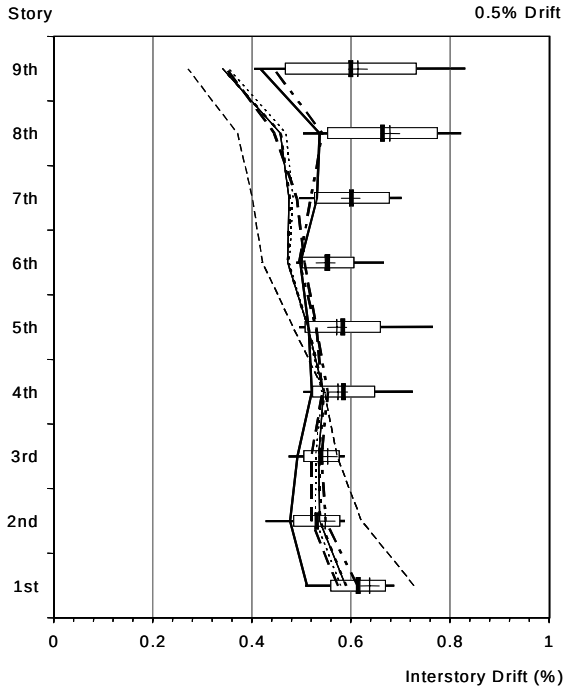


(a) Nine story regular building at 0.5% roof drift

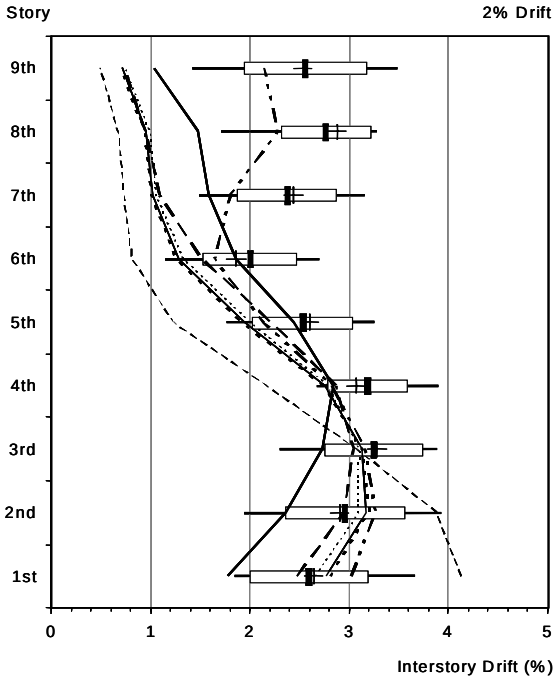


(b) Nine story regular building at 2% roof drift

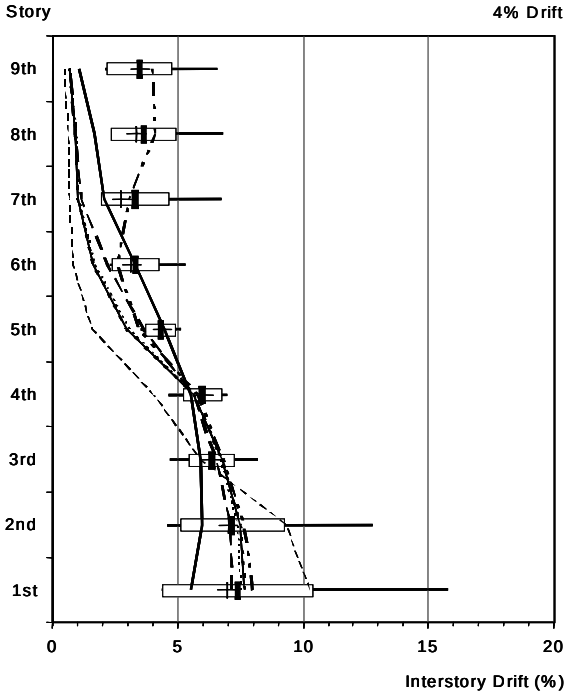


(c) Nine story regular building at 4% roof drift

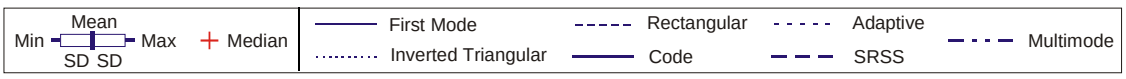


**NDA** **NSP Load Vectors**

Figure 9-4 Relatively poor results for interstory drift predicted using nonlinear static procedures (NSP) compared to nonlinear dynamic response-history analyses (NDA).

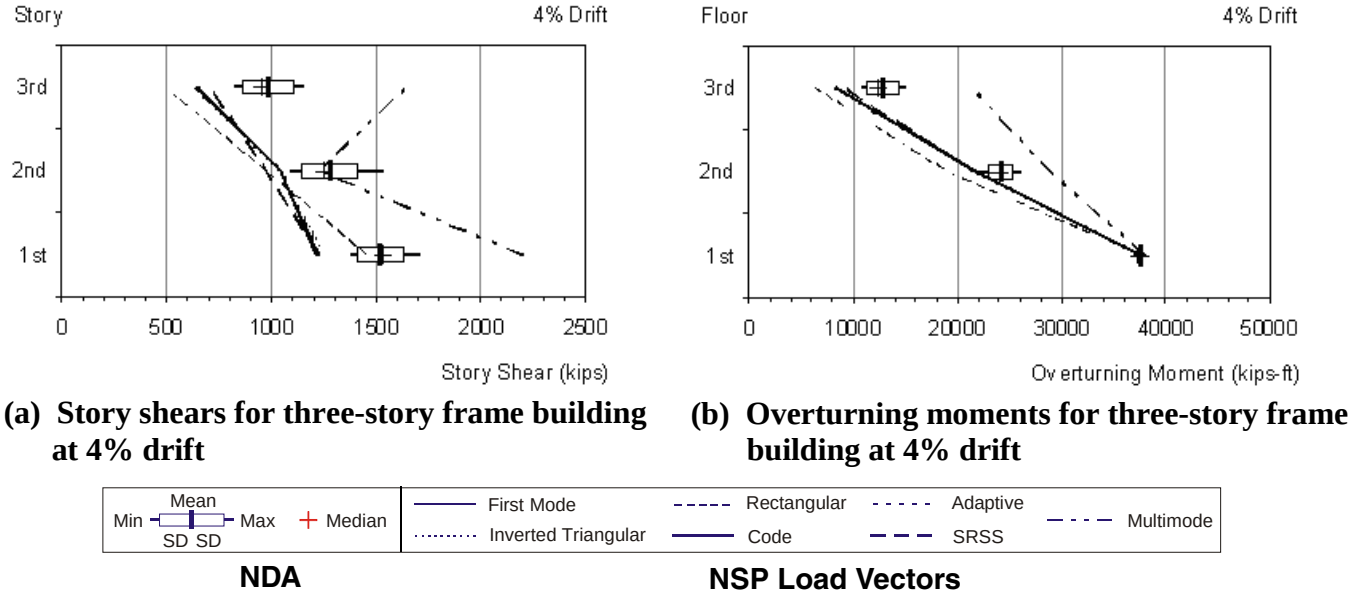


**(a) Story shears for three-story frame building at 4% drift**

**(b) Overturning moments for three-story frame building at 4% drift**

Figure 9-5 Story forces and overturning moments in the example three-story frame building when different load vectors are used.

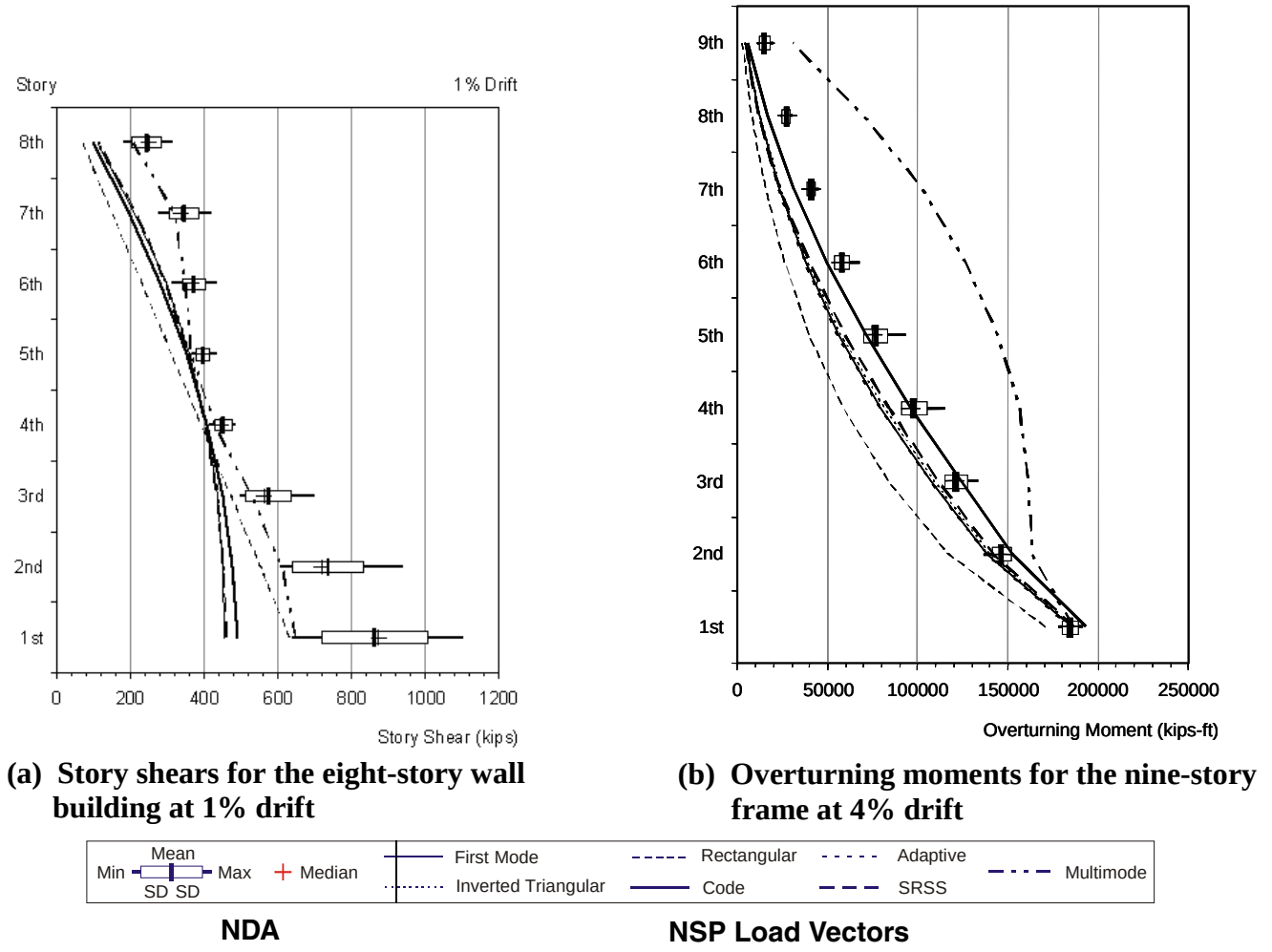


**(a) Story shears for the eight-story wall building at 1% drift**

**(b) Overturning moments for the nine-story frame at 4% drift**

Figure 9-6 Story forces and overturning moments in eight-story wall and nine-story frame example buildings, using various load vectors.

The SRSS load vector led to small improvements in story shear and overturning moment for the example frames, had minor and mixed effects for interstory drift, and sometimes was worse for estimates of displacement, when compared to the first-mode load vector. It requires greater computational effort for inconsistent improvements.

The uniform load vector led to notably worse errors for all four response quantities in the example buildings, relative to the first-mode load vector. Thus, it is not recommended as a stand-alone option. Although the use of the uniform load vector in conjunction with another vector as a bounding function (e.g., in the case of a shear wall building to ensure flexurally controlled behavior) is appealing, peak response quantities often exceeded the estimates made with the uniform vector.

The use of multiple load vectors in FEMA 356 implies unwarranted accuracy and does not provide reliable results. A single first-mode vector is sufficient for displacement estimates and for the estimate of response quantities that are not significantly affected by higher modes.

### *9.4.2 Multi-Mode Pushover Analysis*

It is apparent and logical that the use of multiple mode pushover techniques (MPA) should produce generally better estimates of interstory drift than single load vectors. Although higher modes typically contribute little to displacement, multiple mode pushover analyses may be useful for identifying cases in which displacement responses are dominated by a higher mode.

The application of the multi-mode pushover analysis (MPA) procedure in the ATC-55 project was encumbered by the reversals observed in two of the higher-mode pushover curves. Seeking a single approach capable of representing higher-mode contributions, a modified MPA procedure was introduced in these studies. Although often improved over the single-mode vectors, estimates of interstory drift over the full height of buildings made with the modified MPA procedure may not be consistently reliable. However, it is important to note that researchers are devoting significant effort to the further development of MPA procedures. Some of these are briefly described below.

- Chopra and Goel (2001b) found the original MPA provided good estimates of floor displacement and story drift, but did not estimate plastic hinge rotations with acceptable accuracy for a nine-story steel moment-frame building.
- Chintanapakdee and Chopra (2003) applied the MPA procedure to estimate interstory drift for so-called "generic" frames having 3, 6, 9, 12, 15, and 18 stories. They found that the accuracy of interstory drift estimates depend on the story level and degree of inelasticity. Accuracy was best for shorter buildings and for the lower and middle stories of taller buildings. For the upper stories of tall frames, the MPA procedure was not able to provide a reasonable estimate of interstory drift for many ground motions. The procedure was not used to determine shear, bending moment, axial force, or component deformation.
- Yu et al. (2002) applied the original MPA and two modified versions of MPA to estimate the interstory drift and plastic hinge rotation for an instrumented 13-story steel frame building. When target displacements were estimated by applying the displacement Coefficient Method to the median elastic response spectrum, the MPA method tended to underestimate story drifts in the upper stories and to overestimate drifts in the lower stories; beam and column plastic hinge rotations were often overestimated, while panel zone deformations were estimated reasonably well.
- Chopra et al. (2004) compared interstory drift estimates obtained using the original and modified MPA methods for a set of "generic" frames and SAC frames and found the modified MPA method is an attractive alternative to the original MPA, because it leads to a larger estimate of seismic demand, thereby improving the accuracy of the MPA results in some cases and increasing their conservatism in others.
- Goel and Chopra (2004) describe an "improved" version of the MPA, which considers $P$-$\Delta$ effects in all modes considered and which adds a specialized step for estimating plastic hinge rotation on the basis of the estimated interstory drift and an assumed inelastic mechanism. The "improved" MPA procedure, although better than single-mode estimates, is found to lack accuracy for estimating plastic hinge rotation, overestimating the rotation in the lower stories and underestimating it in the upper stories of the 9- and 20-story moment-resisting frames that were studied.
- Jan et al. (2004) propose an alternative technique in which potentially inelastic contributions from the first two modal pushover analyses are added together. Estimates of displacement, interstory drift,

and plastic hinge rotation were compared with those made using a triangular load profile and the original MPA procedure for a set of 2-, 5-, 10-, 20-, and 30-story moment-resisting frames. The triangular load profile and the original MPA produced very good estimates of interstory drift for the 2- and 5-story frames. The proposed technique provided better estimates of interstory drift for the 20- and 30-story frames, and it was the only technique of those considered it that could provide reasonable estimates of the location and severity of plastic hinge rotations in these frames.

- Hernández-Montes et al. (2004) developed an energy-based pushover technique that overcomes the problems observed with reversals of the higher-mode pushover curves that were observed in the application of the original MPA procedure in the ATC-55 studies.

The MPA procedures seem to produce results that are somewhat more reliable than those obtained from single load vectors. However, it is readily apparent from the literature that the adequacy of these results depends upon the parameter of interest (e.g., drift, plastic hinge rotation, force), the characteristics of the structure, and the details of the specific procedure. It is also possible that future development of the basic MPA procedure may improve predictions further. If these improvements can be realized with transparent and computationally efficient procedures, then they may very well be worthwhile. On the other hand, MPA procedures are fundamentally limited, as are NSPs more generally. From a broader perspective, it is important to develop practical versions of nonlinear dynamic response-history analyses of detailed and, perhaps, simplified MDOF models.

Until other practical nonlinear alternatives are available, the recommendation is that experienced practitioners, who interpret results with an appropriate degree of caution, can utilize MPA procedures for comparison with, and possible improvement over, the static load vector procedures.

### *9.4.3 Roof Displacement Estimation*

The results for the estimate of maximum global displacement of the example building models are consistent with the results of other studies (e.g., Miranda, 1991; Collins et al., 1995; Seneviratna and Krawinkler, 1997; Cuesta and Aschheim, 2001; Chopra et al., 2003). The ATC-40 formulation for the yield strength coefficient of an equivalent SDOF (Equation 9-3) is recommended, because it resulted in smaller dispersions, accurately reflected the frequency content of the excitation for elastic response, and maintains consistency with derivations of "equivalent" SDOF systems. Where the hazard is described by smoothed elastic design spectra, displacement estimates should make use of the improved procedures that are described in Chapters 5 and 6.

### *9.4.4 Limitation of Simplified Procedures*

Nonlinear static pushover procedures appear to be reliable for the design and evaluation of low-rise buildings. However, MDOF effects associated with the presence of significant higher-mode response in relatively tall frame buildings, can cause interstory drift, story shear, overturning moment, and other response quantities to deviate significantly from estimates made on the basis of single-mode pushover analyses. Multi-mode pushover procedures appear capable of more reliable estimates than do single-mode procedures; however, they cannot be deemed completely reliable based on currently available data. The dividing line between buildings for which reliable results can be obtained using NSPs and those for which the results cannot be relied upon is nebulous. The sufficiency of nonlinear static procedures and the need for nonlinear dynamic analysis depend on a number of related considerations.

- *Response quantity of interest.* As illustrated in the examples, current simplified procedures are often adequate for estimating displacements. They seem to produce reasonable estimates of interstory drift for low-rise frame buildings and wall buildings. However, for virtually all cases, the simplified procedures produce unreliable estimates of story shear and overturning moments. If required for evaluation or design, accurate estimates of these parameters require more detailed analyses.
- *Degree of inelasticity.* The example buildings indicate that the importance of MDOF effects increases with the amount of inelasticity in the structure. NSPs may be adequate for situations in which the performance goals for a structure are such that only slight or moderate levels of inelasticity are expected.
- *Periods of vibration of the fundamental and higher modes relative to the spectral demands at these periods.* Higher-mode contributions become more significant for structures with fundamental periods that fall in the constant-velocity portion of the response spectrum. It appears that accurate estimates of the distribution of interstory drift over the height of moment-resisting frames cannot be obtained with

NSPs alone when the fundamental period of the structure exceeds approximately twice the characteristic site period, $T_S$. A significantly lower limit applies to the determination of story forces in both wall and frame structures, however.

- *Structural system type.* Shear walls and frames have different higher-mode periods relative to their fundamental modal periods. These systems have characteristically different percentages of mass participating in the first and higher modes and develop characteristically different types of mechanisms. As noted previously, NSPs do not predict story forces reliably, and more sophisticated analytical techniques may be required for systems sensitive to these parameters.
- *Post-elastic strength.* Both the studies on the response of SDOF oscillators (Chapter 3) and the SDOF examples (Appendix F) demonstrate that systems with a critical level of negative post-elastic strength degradation are prone to dynamic instability. This has been documented in other recent research as well. As discussed in Chapter 4, the critical post-elastic stiffness should be based on $P$-$\Delta$ effects and other types of in-cycle degradation. Systems with strength values less than those specified in Chapter 4 require nonlinear response-history analysis.
- *Inelastic mechanism*. Forces associated with response in other modes may influence the development of an inelastic mechanism, and thus, pushover analyses may not always identify the governing mechanism (Krawinkler and Seneviratna, 1998).
- *Multi-mode pushover analysis procedures.* SRSS combinations of force quantities can exaggerate the effects of gravity loads and can exceed the limits associated with the development of an inelastic mechanism. Typically, algebraic signs of the modes can be expected to influence the intensity of component demands. The use of uniform hazard spectra presents inconsistencies, because different portions of the spectrum may be driven by vastly different events, rather than representing a single event.
- *FEMA 356 provisions.* This document requires supplementary linear dynamic analysis if higher-mode effects are significant. Higher modes are considered significant if the SRSS of story shears from modes that incorporate at least 90% of the mass exceeds 130% of story shear from a first-mode response-spectrum analysis. It is important to note that all the example buildings, with the minor exception of the upper floor of the 9-story frame, would have qualified for the nonlinear static procedure alone without the linear dynamic procedure (LDP) for a NEHRP design spectrum in an area of high seismicity and Site Class C site conditions. The potential for the NSP to significantly underestimate response quantities for structures that satisfy this limitation indicates that the current limitation is not adequate.

## 9.5 Potential Future Improvements

Based on the studies conducted in conjunction with this document and results from current research, it is apparent that there is a need for improved inelastic analysis techniques that can be used to reliably address MDOF effects. As noted previously, research on multi-mode pushover analysis procedures is ongoing. There are two examples of potential improvements that have not been discussed earlier and that warrant mention here.

### *9.5.1 Incremental Response-Spectrum Analysis*

Aydinoglu (2003) describes a multi-modal incremental response-spectrum analysis method, in which contributions of multiple modes are considered in an incremental pushover analysis. The incremental nature of the analysis allows the effects of softening due to inelasticity in one mode to be reflected in the properties of the other modes. An example was used to illustrate application of the method to a generic frame model of the nine-story SAC building (neglecting gravity loads and $P$-$\Delta$ effects), comparing estimates based on four modes with those determined by nonlinear dynamic analysis. Very good agreement is shown for floor displacement, interstory drift, story shear, floor overturning moment, and beam plastic hinge rotation. Further study is required to establish the generality of the findings and potential limitations of the approach.

### *9.5.2 Nonlinear Dynamic Procedure Using Scaled Response Histories*

The MDOF example studies summarized in Section 9.3 revealed that the estimates of response quantities obtained by nonlinear static pushover analyses often were less accurate than the results obtained by any single nonlinear dynamic analysis when comparing both to the mean results for all ground motions. This observation suggests the possibility of an analytical procedure in which response quantities are determined by nonlinear dynamic analysis using ground motion records that are scaled so that the peak roof

displacement matches a predetermined target displacement. In effect, the seismic hazard would be characterized by the maximum inelastic displacement at the roof level. This displacement could be estimated for a structure using nonlinear static procedures in conjunction with the NEHRP maps, for example. Thus, nonlinear response-history analyses would be used to investigate MDOF effects through nonlinear dynamic analyses using a relatively small number of ground motion records scaled to give the same roof displacement. Such a procedure could avoid both the necessity of generating a series of spectrum-compatible records and the difficulty of combining the results of the analyses for practical use. This potential method, termed the "Scaled NDP" method, is summarized here, with supporting information provided in Appendix F

The basic suggested procedure is outlined below.

**Step 1.** Given a spectrum representative of the site hazard of interest, estimate the peak displacement of the roof (or more generally, a "control point") using the displacement modification or equivalent linearization procedures, described in Chapters 5 and 6, respectively.

**Step 2.** Select $n$ ground motion records that reflect the characteristics of the hazard (e.g., magnitude, distance, and site class) and for each record, conduct a nonlinear dynamic analysis, with the record scaled iteratively until the peak displacement of the control point is equal to the estimate determined in Step 1. Extract peak values of the response quantities of interest from the results of each analysis and compute the sample mean, $\overline{x_n}$, of each peak quantity of interest. At least three analyses ($n \geq 3$) are suggested.

**Step 3.** Although the sample mean is the best estimate of the true mean, sampling error may be present. Furthermore, estimates of some response quantities may be desired at the mean plus $\kappa$ standard deviation level. Thus, the sample mean could be multiplied by a coefficient that depends on the coefficient of variation of the sample, in order to estimate a response quantity at the mean plus $\kappa$ standard deviation level with a desired level of confidence. A derivation of such a coefficient is provided in Appendix F

**Discussion**

The proposed analysis method retains the benefits of the pushover method, in that the engineer can use the pushover to quickly identify the likely nonlinear mechanism of the system and the expected peak displacement response. The method makes use of currently available spectral descriptions of seismic hazard as well as the improvements described in Chapters 5 and 6 of this document. The dynamic analyses indicate the variability in response quantities associated with the randomness in the higher mode amplitudes and timing relative to the first mode. In effect, the static load vector of traditional pushover analysis, used to determine the peak of global displacement demand, is augmented by a dynamic load, represented by the scaled ground motion record.

Within the limitations of the nonlinear model, each analysis faithfully represents the influence of higher modes on response quantities such as interstory drift, story shear, and overturning moment, and does so in a manner that accounts for capacity limits on force and moment quantities. Any single dynamic analysis is a valid representation of actual response of the model, and each analysis helps to establish the central tendency and range of peak response quantities.

Refinements and improvements may potentially be made in the areas of (1) characterizing and selecting site-specific ground motions, (2) determining the confidence levels and numbers of standard deviations above the mean that should be used in the estimation of various response quantities, and (3) improvement of the precision of the NSP estimates of peak roof displacement. The conservatism of current pushover techniques, in their tendency to overestimate the peak roof displacements of structures responding inelastically, may provide a desirable level of conservatism to the method at this stage in its development.

# 10. Summary and Application Example

This document records in detail an effort to assess current nonlinear static procedures (NSPs) given in FEMA 356 and ATC-40 for the seismic analysis and evaluation of structures. In addition, the document presents approaches that were developed to improve these procedures for future application by practicing engineers. Not all of the portions of the two documents were evaluated. Conclusions regarding the relative accuracy or technical soundness of these documents should not be inferred beyond the specific material and discussions contained in this document.

The purpose of this summary is to present a practical overview of the results and to illustrate the application of NSPs, that include the proposed improvements for an example building. Sections 10.1 through 10.8 contain key results of analytical studies conducted as part of this project and resulting suggestions for specific changes to existing procedures for nonlinear static analysis procedures. Section 10.9 discusses some important aspects of uncertainty and reliability of nonlinear static procedures and the suggestions for improvement. Section 10.10 summarizes some key observations with respect to shortcomings of inelastic seismic analysis procedures that were not fully resolved in this project. These are areas in which significant improvement might be made in the future. Section 10.11 is the application example.

## 10.1 Overview of Inelastic Seismic Analysis Procedures

Nonlinear static procedures are one type of inelastic analysis that can be used to estimate the response of structures to seismic ground shaking. The differences among the various approaches to inelastic analysis in general relate to the level of detail of the structural model and the characterization of the seismic ground shaking. Detailed structural models can often be simplified into equivalent multi-degree-of-freedom models; or, in some cases, single-degree-of-freedom oscillator models, as with nonlinear static procedures. The most detailed characterizations of seismic ground motion are actual ground motion records that comprise accelerations, velocities, and displacements expected at the ground surface at a specific site. A simplification can be made by representing the effects ground motion has in the frequency domain with response spectra that plot maximum response of an elastic SDOF oscillator as a function of period. This is the type of characterization normally used for nonlinear static procedures.

The discussion in Chapter 2 includes basic descriptions of the two nonlinear static procedures that are currently used in practice. FEMA 356 uses a displacement modification procedure (Coefficient Method) in which several empirically derived factors are used to modify the response of a single-degree-of-freedom model of the structure, assuming that it remains elastic. The alternative Capacity-Spectrum Method of ATC-40 is actually a form of equivalent linearization. This technique uses empirically derived relationships for the effective period and damping as a function of ductility to estimate the response of an equivalent linear SDOF oscillator.

## 10.2 Evaluation of Current Nonlinear Static Procedures

In practice, the current procedures can result in estimates of maximum displacement that are significantly different from one another. This has caused concern on the part of practicing engineers. One of the major objectives of the project was to ascertain the reasons for these differences and to try to correct both procedures to produce similar results. Chapter 3 documents a comprehensive evaluation of both procedures. The basic technique was to develop a series of nonlinear single-degree-of-freedom oscillators of varying period, strength, and hysteretic behavior. These were subjected to ground motion representing different site soil conditions. The resulting database of approximately 180,000 predictions of maximum displacement was used as a benchmark to judge the accuracy of the approximate NSPs. This was accomplished by comparing the estimates for each oscillator from both NSPs to the results of the nonlinear response-history analyses. Differences in the two estimates were compiled and compared in a statistical study.

### *10.2.1 Key Observations: ATC-40 Version of Capacity-Spectrum Method*

**Longer-period response.** The ATC-40 procedures for structures with hysteretic behavior type A tended to underestimate the maximum displacement response for inelastic systems. The underestimation averages 25% to 35% for systems with periods longer than about 0.7 s.

For structures with hysteretic behavior type B, the ATC-40 procedures led to small underestimations or small overestimations of lateral displacement of systems with periods longer than about 0.6 s. Whether

ATC-40 underestimates or overestimates depends on the level of lateral strength and on the site class.

For structures with hysteretic behavior type C, the ATC-40 procedures led to overestimations of the maximum displacement for all periods. The overestimation increases as $R$ increases. Average overestimations for periods greater than 0.5 s range from approximately 5% for systems with $R = 1.5$ to about 35% for systems with $R = 8$.

**Shorter-period response.** The ATC-40 procedures can lead to significant overestimations of the maximum displacements of inelastic oscillators for periods shorter than those noted above. The overestimations increase with decreasing strength. Estimated displacements in the short-period range can be, on average, up to two times larger than the benchmark displacements from response-history analyses.

**Degrading stiffness and strength.** ATC-40 assumes that the inelastic deformation demands in structures with behavior type B will be larger than those in structures with behavior type A, while results of nonlinear response-history analyses show that the deformations are actually approximately the same or slightly larger for the elastic-perfectly-plastic (EPP) model as compared to the stiffness-degrading (SD) model. The current provisions of ATC-40 do not address the potential dynamic instability that can arise in systems with in-cycle strength degradation and/or P-delta effects.

**Limitations on damping and spectral reduction factors.** ATC-40 specifies limits on effective damping that result in the imposition of minimum spectral-reduction factors based on the anticipated performance of building types. These limitations were based on engineering judgment that has not been borne out in the analytical studies reported here. While the intention of these limitations may have been to provide some conservatism for degrading structures, the resulting estimates of displacement exceed expected mean values when compared with actual behavior for many cases.

### *10.2.2 Key Observations: FEMA 356 and the Coefficient Method*

**Transition period for the equal-displacement approximation.** Nonlinear dynamic analyses demonstrate that the total displacement experienced by long-period structures that undergo inelastic response tends to be about the same as structures of the same period, responding in an elastic manner, leading to the so-called equal displacement approximation. Short-period structures do not behave in this manner. FEMA-356 defines a characteristic site period to differentiate between these two types of behavior. Characteristic site periods of FEMA 356 are based on the period at the intersection of the constant-acceleration spectral region and the constant-velocity spectral region. These characteristic periods are shorter than the transition periods observed from nonlinear response-history analyses. This can result in underestimation of inelastic deformations for periods between the characteristic site period and periods that are approximately 1.5 times the characteristic site period.

**Ratio of inelastic to elastic deformation, coefficient $C_1$.** The use of the equal displacement approximation to compute the coefficient $C_1$ for systems with periods longer than the characteristic periods leads to relatively good approximations of maximum inelastic deformations for systems with EPP behavior for periods longer than about 1 s. Only small overestimations in the order of 5% or 10% are produced with this approximation. Note that for very soft soil sites and near-fault records, this is only true for systems with periods of vibration that are approximately 1.5 times longer than the predominant period and the pulse periods, respectively.

For systems with $R$ larger than about 2.5, the limiting values (capping) of $C_1$ imposed by Section 3.3.1.3.1. of the LSP of FEMA 356 will control the estimate of maximum inelastic deformation. This can lead to theoretically large underestimates of displacements in short-period structures, particularly on soft sites.

If capping is not used, and if the transition period is lengthened, the FEMA 356 equation to calculate $C_1$ does not adequately capture the changes in inelastic deformation demands that are produced with changes in $R$ for short-period structures. The magnification of inelastic displacement demands with decreasing lateral strength for short-period structures was found to be larger than that implied by FEMA 356.

**Degradation of stiffness and strength (Coefficients $C_2$ and $C_3$).** There is not a clear division of the intent of coefficients $C_2$ and $C_3$. This problem was documented in FEMA 357. In particular, $C_2$ is supposed to account for changes in lateral displacement produced by departures of the hysteretic behavior from an EPP hysteretic model (such as pinching, stiffness degradation and strength degradation.). $P$-$\Delta$ effects are accounted for by $C_3$ in the current provisions of FEMA 356. FEMA 356 does not distinguish between cyclic strength degradation and in-cycle strength degradation.

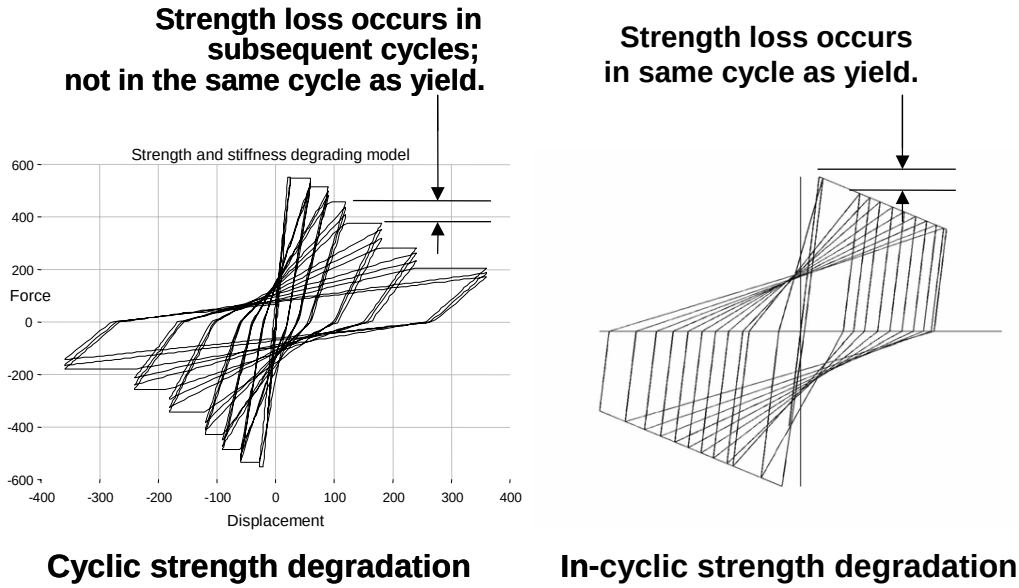


Figure 10-1 Differences between cyclic and in-cycle strength degradation

In-cycle degradation produces effects similar to $P$-$\Delta$, which can lead to dynamic instability in weak structures.

The $C_2$ coefficient of FEMA 356 implies that inelastic displacement should increase for stiffness degrading systems as compared with EPP systems. With the exception of periods of vibration smaller than about 0.7 s, the maximum displacement of stiffness-degrading systems is actually very similar to or slightly smaller (5% to 10%) than the maximum displacement of EPP systems.

FEMA 356 introduced an alternative recommendation for $C_2$ that was not in FEMA 273, as follows: "Alternatively, use of $C_2 = 1$ shall be permitted for nonlinear procedures". The ambiguity of conflicting recommendations is confusing to users of FEMA 356.

Coefficient $C_3$ does not adequately address the possibility of dynamic instability.

## 10.3 Strength Degradation

The results of the evaluation of the NSPs suggest that both procedures would benefit from greater clarity with respect to the different types of possible degradation in structures subject to seismic shaking. This is particularly critical for degradation in strength. Chapter 4 discusses the differences between the consequences of strength loss within a single cycle of deformation (in-cycle) and that which occurs in subsequent cycles (cyclic). This important distinction illustrated in Figure 10-1. In-cycle strength degradation, including that associated with $P$-$\Delta$ effects, can lead to dynamic instability. To account for this, a lower limit on the strength of structures that exhibit strength-degrading behavior is suggested for use with nonlinear static procedures. The limit is a function of the period of the structure and the post-elastic stiffness characteristics, as modified for in-cycle strength degradation. If the structure has less strength than the limit, nonlinear dynamic analysis is recommended.

## 10.4 Improved Procedures for Displacement Modification

Based on the evaluation of NSPs, Chapter 5 proposes modifications to the Coefficient Method of FEMA 356. The suggestions relate primarily to the coefficients themselves. These are tabulated along with the current specifications in Table 10-1. The changes are briefly summarized as follows:

### *10.4.1 Summary of Findings Pertaining to Coefficient $C_1$*

This coefficient represents the approximate ratio of the maximum displacement of an EPP SDOF oscillator model to that of a fully elastic counterpart. The proposed modification is based on the results of the simplified dynamic analyses conducted as a part of the

**Table 10-1 Coefficients for Use in Equations for Effective Damping**

| *Coefficient* | *Current Specification* | *Modification* | *Purpose of Coefficient* |
|---|---|---|---|
| $C_1$ | 1.0 for $T_e \geq T_s$<br>$[1.0 + (R\text{-}1)T_s/T_e]/R$ for $T_e < T_s$ | $C_1 = 1 + \frac{R-1}{aT^2}$<br>where a =<br>130 for site class B<br>90 for site class C<br>60 for site class D | Convert max. elastic displacement to estimate for inelastic system |
| $C_1$<br>(with short $T$ "cap") | 1.5 for $T_e < 0.1$s<br>interpolating to<br>1.0 for $T_e \geq T_s$ | Not recommended | |
| $C_2$<br>(degrading systems) | Immediate Occupancy<br>1.0<br>Life Safety<br>1.3 for $T \leq 0.1$<br>interpolating to<br>1.1 for $T \geq T_s$<br>Collapse Prevention<br>1.5 for $T \leq 0.1$<br>interpolating to<br>1.2 for $T \geq T_s$ | $C_2 = 1 + \frac{1}{800}\left[\frac{R-1}{T}\right]^2$<br>recommended only for structures with significant stiffness and/or strength degradation | Hysteretic pinching<br>Cyclic degradation |
| $C_2$<br>(non-degrading systems) | 1.0 | 1.0 | |
| $C_3$ | $1.0 + \frac{\lvert\alpha\rvert(R-1)^{3/2}}{T_e}$ | Eliminate in favor of strength limit | *P-Δ*<br>In-cycle degradation |

evaluation database. The proposed relationship is a function of strength ($R$), period ($T$), and site class.

The current provisions of FEMA 356 allow the $C_1$ coefficient to be limited for short-period structures. Although this limitation was intended to recognize that short-period buildings do not respond as often predicted by analysis, the basis of the limitation is subjective. For this reason, the use of the "cap" on $C_1$ is not recommended. However, the effects of soil-structure interaction can have a mitigating effect on maximum inelastic displacements of short-period structures. Some rational procedures for including the SSI effect in nonlinear static analyses are presented in Chapter 8.

### *10.4.2 Summary of Findings Pertaining to Coefficient $C_2$*

This coefficient accounts for the change in maximum inelastic displacement for systems that exhibit cyclic degradation of stiffness and strength. The proposed modification is based on the results of the simplified dynamic analyses conducted as a part of the evaluation database. In many cases, the data suggest that cyclic degradation does not increase maximum displacements. However, there are exceptions, especially for short-period, low-strength structures.

### *10.4.3 Summary of Findings Pertaining to Coefficient $C_3$*

This coefficient was intended to account for *P-Δ* effects. Review of related research and results of detailed analyses indicate that maximum inelastic

displacements tend to increase abruptly, leading to dynamic instability and implied collapse for relatively weak structures. The point at which this transition occurs is related to the strength, period, and post-elastic stiffness of the structure. Although the current expression includes these variables, it does not predict the instability. The recommendation is for a limit on minimum strength (maximum $R$) for structural models that exhibit strength degradation. This limit eliminates the need for the $C_3$ coefficient.

## 10.5 Improved Procedures for Equivalent Linearization

Many engineers favor working with the Capacity-Spectrum Method, a form of equivalent linearization. This is likely due, at least in part, to the intuitive nature of the procedure that graphically relates "capacity" to "demand." Chapter 6 presents the results of an effort to improve the practical application of equivalent linearization procedures. The resulting suggestions focus on improved estimates of equivalent period and damping. These differ from the assumptions in ATC-40. Generally, the optimal effective period is less than the secant period (see Figure 10-2). The optimal

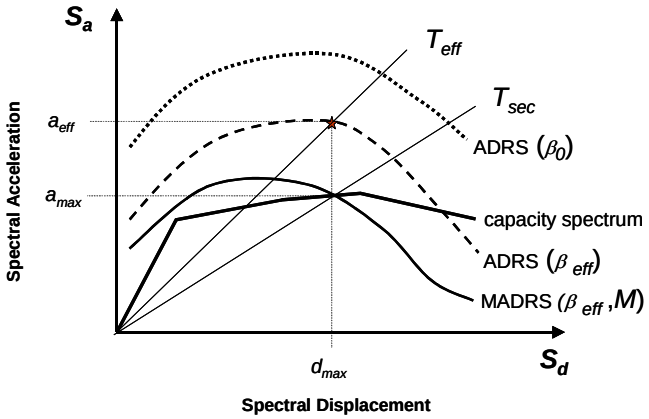


Figure 10-2 Acceleration-displacement response spectrum (ADRS) showing effective period and damping parameters of equivalent linear system, along with a capacity curve.

effective damping is also less than that specified in ATC-40. Note also in Figure 10-2 that the optimal effective period does not intersect the capacity spectrum for the structure at the maximum inelastic displacement or Performance Point. In order to preserve this useful visualization feature, Chapter 6 also includes an optional adjustment to generate a modified acceleration-displacement response spectrum (MADRS) that does intersect the capacity spectrum at the Performance Point. Similar to the current ATC-40 procedure, the effective period and damping are both dependent on ductility and consequently, an iterative or graphical technique is required to calculate the Performance Point. Several options are outlined in Chapter 6.

## 10.6 Evaluation and Comparison of Improved Nonlinear Static Procedures

The improved procedures were evaluated in an independent study. This study utilized nine EPP oscillators with three different periods and three different strength values. These were subjected to thirteen ground motions for class C sites. The motions were scaled in accordance with the *NEHRP Recommended Provisions for Seismic Regulations for New Buildings and Other Structures* to match a *NEHRP* design-response spectrum. Estimates of maximum displacements were calculated utilizing both current procedures and the proposed improved procedures. This was done using both the NEHRP design spectrum and the average spectrum for the scaled ground motions. This study was not comprehensive enough to make broad general conclusions. However, a number of key observations were made:

- The improved procedures do not exhibit large differences between displacement modification and equivalent linearization approaches. This differs from previous experience with the ATC-40 Capacity-Spectrum Method and the FEMA 356 Coefficient Method.
- The improved procedures also produced more accurate estimates of displacements when compared to response-history analysis results than those produced by the current nonlinear procedures. For displacement ductility of less than ten, the new procedures produced estimates that were within one standard deviation of the response-history results.
- Improved procedures also seem to work well, at least for the case that was studied, in estimating maximum displacement response in conjunction with a design spectrum. Further investigations are warranted to assess the uncertainty involved with this approach on a more general basis.
- The results of the evaluation of the improved nonlinear procedures illustrate the dispersion of results from nonlinear response-history analysis using design level ground motions. This dispersion is the result of the many uncertainties involved in inelastic seismic analysis. It is important for practitioners to keep this in mind when interpreting the results of inelastic analyses.

## 10.7 Soil-Structure Interaction Effects

There is a perception among many in the practicing engineering community that short, stiff buildings do not respond to seismic shaking as adversely as might be predicted analytically. There are several reasons why short-period structures may not respond as conventional analysis procedures predict. Among these are:

- radiation and material damping in supporting soils;
- structures with basements that experience reduced levels of shaking;
- incoherent input to buildings with relatively large plan dimensions; and
- inaccuracies in modeling, including lumping of masses, neglecting foundation flexibility and some elements that contribute to strength.

These factors are often cited qualitatively, along with the observed good performance of such buildings in past earthquakes, as justification for less onerous seismic demand parameters in codes and analytical procedures. Traditional design procedures have evolved accordingly. Consequently, FEMA 356 currently contains limitations (caps) on the maximum value of the coefficient $C_1$ for short-period buildings. Many practicing engineers routinely use the limitations on $C_1$. Capping leads to prediction of maximum inelastic displacements that are less than predicted by the current empirical relationship by a margin that varies widely depending on period, strength, and site conditions. For periods of interest for most buildings (> 0.2 sec. or so), the margin ranges from relatively small (< 20%) for firm (Class B) sites to rather large (> 200%) for soft (Class E) sites.

Chapter 8 presents procedures to incorporate soil-structure interaction (SSI) into nonlinear static analyses. The objective is to replace the subjective limits with rational technical justifications for reducing seismic demand. These SSI techniques address the first three items listed above. The distribution of mass is not addressed in this document; however, it is worthy of future investigation to further improve inelastic analysis procedures.

FEMA 356 and ATC-40 contain similar procedures for incorporating the strength and stiffness of foundations into structural models for inelastic analyses. These procedures result in changes in response compared to fixed base assumptions that can be very significant for some structures. These changes include:

- lengthening of period of the system;
- distribution of forces and displacements among elements;
- sequence of inelastic behavior; and
- potential foundation modes of inelastic behavior (e.g. rocking, soil crushing, pier/pile slip).

Relatively stiff foundation elements on, or in, soil tend to average overall shaking effects to an intensity that is lower than localized maximums. These kinematic effects depend on the plan dimensions of the structure, its embedment into the soil, and its period. They can be visualized as a low-pass frequency (high-pass period) filter on the free-field ground motion. (see Figure 10-3). For nonlinear static procedures this leads to a reduced spectrum representing a foundation input motion. That is, this effect tends to minimize the amplitude of high frequency motion experienced by the structure.

Relative movements in the soil beneath structures dissipate energy through both radiation damping and hysteretic damping. Hysteretic damping is implied in the nonlinear force-deformation properties of the geotechnical components of foundation models, when these elements are modeled. Radiation damping can be incorporated into inelastic analysis procedures by estimating foundation damping and combining it with the conventional assumption for the structure to generate an initial system damping ratio for the system. For NSPs, the result is a further modification in initial spectral ordinates, depending primarily upon the foundation area and effective moment of inertia.

The basic principles used for the development of the SSI procedures in Chapter 8 have been included in the *NEHRP Recommended Provisions for New Buildings* (BSSC, 2000)[1] for the linear analysis and design of new buildings for a number of years. They have been adapted for use with inelastic procedures. They are applicable to both the displacement modification and equivalent linearization forms of nonlinear static analysis.

## 10.8 Multiple-Degree-of Freedom Effects

Whether evaluating performance or designing a structure, the engineer makes decisions primarily based on component forces and deformations. These are typically compared to some type of acceptability criteria. The intensity of component deformations and

1.Superseded in 2003 with the FEMA 450 *Recommended Provisions for Seismic Regulations for New Buildings and Other Structures.*

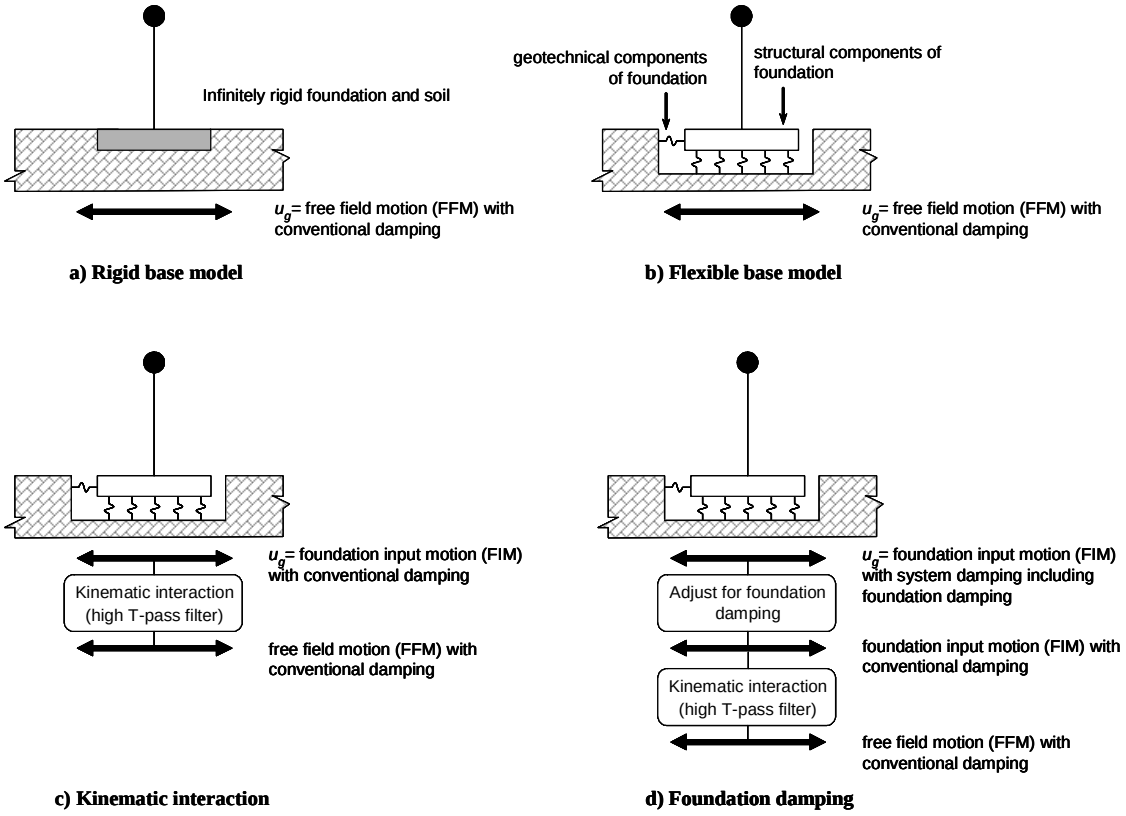


Figure 10-3 Foundation modeling alternatives

forces are directly related to a global displacement parameter (i.e., roof displacement or first-mode spectral displacement) in NSPs. The approximate relative distribution of elastic and inelastic forces and deformations for the multiple-degree-of-freedom (MDOF) structure are controlled by the characteristics of the single-degree-of-freedom (SDOF) model pushover curve assumed in the analysis. The variations of these parameters in a true multi-degree-of-freedom system from those of the SDOF approximation are known as MDOF effects. The adequacy of simplified procedures to address MDOF effects has been questioned by a number of researchers.

Chapter 9 summarizes the options for different load vectors used to generate SDOF pushover curves for structures. In order to investigate and illustrate these various options for evaluating MDOF effects, a comprehensive study of five buildings compared approximate estimates from NSPs for several parameters to those obtained from nonlinear MDOF response-history analyses. The results are consistent with previous research. Practical implications for structures with significant MDOF effects are:

- NSPs generally provide reliable estimates of maximum floor and roof displacements. They also are capable of providing reasonable estimates of the largest inter-story drifts that may occur at any location over the height.
- NSPs are not particularly capable, however, of accurately predicting maximum drifts at each story, particularly within tall flexible structures.
- NSPs are very poor predictors of story forces, including shear forces and overturning moments in taller structures.
- The use of the first-mode load vector is suggested due to the relatively good displacement estimates made with this assumption. Other single-load vectors were less consistent in producing reliable results. The use of two single-load vectors to try to envelope response parameters is not particularly useful.
- Multi-mode pushover analysis consisting of the use of multiple load vectors proportional to the mode shapes of the structure that are statistically combined shows promise in producing better estimates in inter-

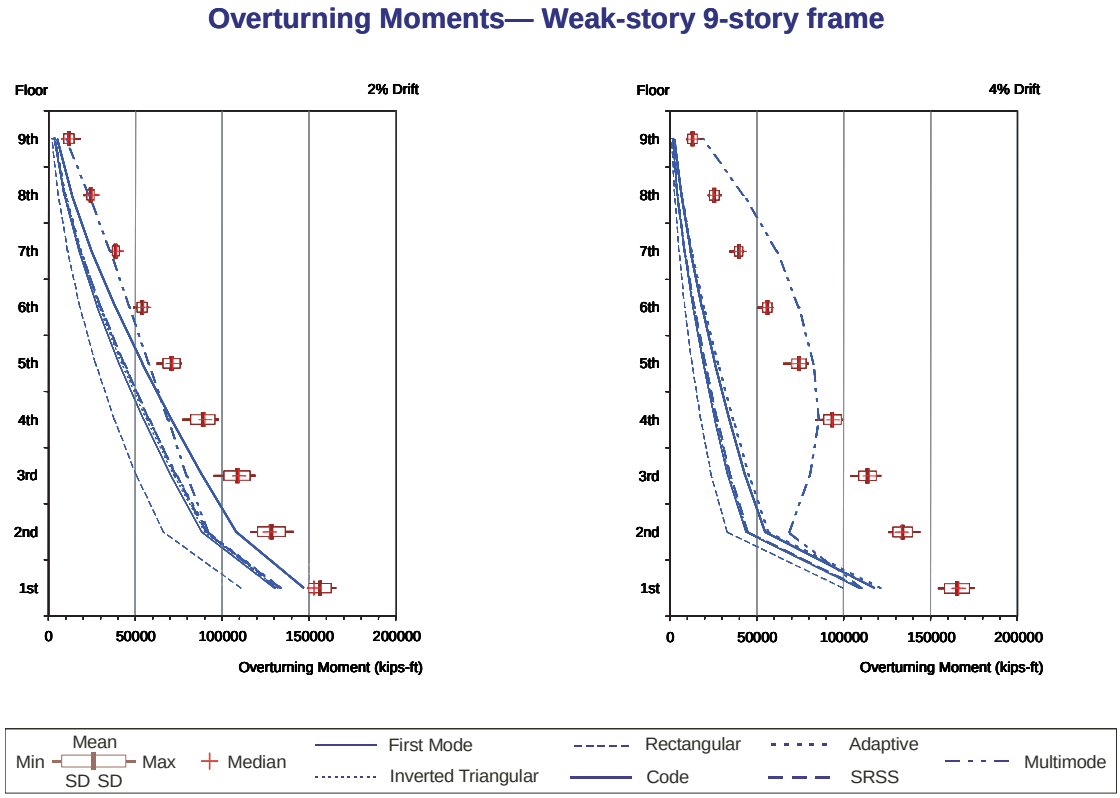


Figure 10-4 Overturning moments in example 9-story building using various load vectors.

story drifts over the heights of the buildings. Current results documented in the literature conclude that the adequacy of results from multi-mode pushover analyses depends on the parameter of interest. It seems that future developments may further improve multi-mode pushover analysis.

- The provisions of FEMA 356 as to when higher modes are to be considered significant are not particularly reliable. All of the example buildings in Chapter 9 would have satisfied the criteria (i.e., higher modes would not have been significant). This is in spite of the fact that all of the buildings, in one way or another, showed sensitivity to higher-mode effects.
- Specific limitations as to when NSPs produce reliable results for MDOF structures are elusive. Chapter 9 provides a discussion of important considerations, but at this time considerable judgment on the part of the practicing engineer is required.
- As a result of the study, it was observed that, in many cases, a single time history response of a multi-degree-of-freedom model gave better indications of drifts and story forces than any of the approximate single-degree-of-freedom estimates (see Figure 10-4). This suggests that a future procedure might be developed that utilizes a small number of response histories to estimate variation and MDOF response parameters.

## 10.9 Uncertainty and Reliability

NSPs are an important part of performance-based engineering. Performance-based engineering departs from traditional practices in a number of ways. One of the more important departures relates to the treatment of uncertainty and reliability. Uncertainty arises from the seismic ground motion, the structural model, and the analysis technique utilized. Traditional prescriptive analysis and design procedures (e.g., working stress design, load and resistance factor methods) incorporate margins of safety in the calculation of demand and capacity. These procedures treat uncertainty implicitly and they are appropriately conservative with respect to the actual potential consequences. In contrast, performance-based procedures can be used to predict

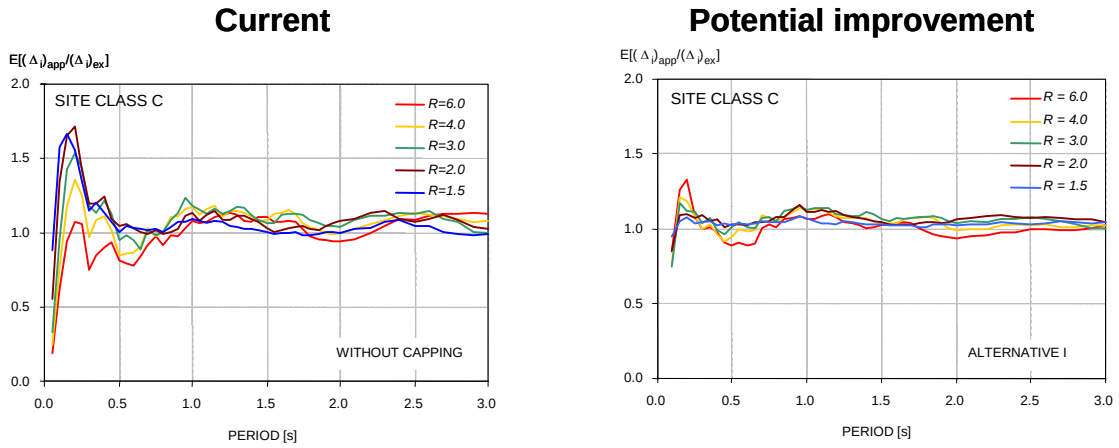


Figure 10-5 Error associated with the Coefficient $C_1$ as formulated in FEMA 356 (left) and the potential improved formulation (right).

the expected consequences of future ground motions. When used in this manner, the results of the analysis are central (i.e., mean or median) values. This means that they represent the most likely, or "expected," response. However, this also means that the actual response has roughly a 50% chance of being greater and a 50% chance of being less than the predicted response.

The improvements to existing procedures proposed in the document have been developed to optimize predictions of expected values. An example is illustrated in Figure 10-5 showing the error associated with the current FEMA 356 value for coefficient $C_1$ and a potential improved formulation. The error is determined by dividing the approximate prediction of displacement by the expected value from the response history analyses. The expected value in this case is the mean of results for twenty different ground motion records for each period ($T$) and for each strength ($R$). The closer the error is to 1.0, the better the approximate result. Thus the potential improvement clearly provides more accurate results than the current procedure. However, the dispersion of the results for the twenty ground motions is not apparent in this illustration.

The independent evaluation of the proposed improvements is summarized in Chapter 7. In this study, a series of bilinear EPP oscillators with post-elastic stiffness equal to 5% of the initial stiffness were subject to thirteen ground motion records. The results of the nonlinear dynamic (response-history) analyses for an oscillator with a period of 0.5 s are shown in Figure 10-6 for several different strengths. Note the dispersion of the results on either side of the mean (expected) value. Note also that the dispersion increases with lower strength (higher $R$), as is typical in most cases.

In general, it is important to recognize the empirical nature of the improved expressions for the proposed modifications in this document. They are formulated by attempting to match actual analysis data. They may appear complex, but they do not imply accuracy beyond that associated with the statistical variation in the underlying data. Scrutiny of the detailed characteristics of the data indicates significant uncertainties in expected values. The degree of uncertainty increases for:

a. shorter period;

b. lower strength (higher $R$);

c. degrading hysteretic behavior; and

d. near-source ground motion.

When applying these procedures, it is important to estimate basic parameters as carefully as possible. For example, using a conservative (low) estimate of the strength of a structure may lead to a conservative (high) estimate of displacement. It is suggested that realistic estimates for all parameters be used to generate expected values as a result of the analysis. Then engineering judgment may be applied to inject the appropriate degree of conservatism, considering the

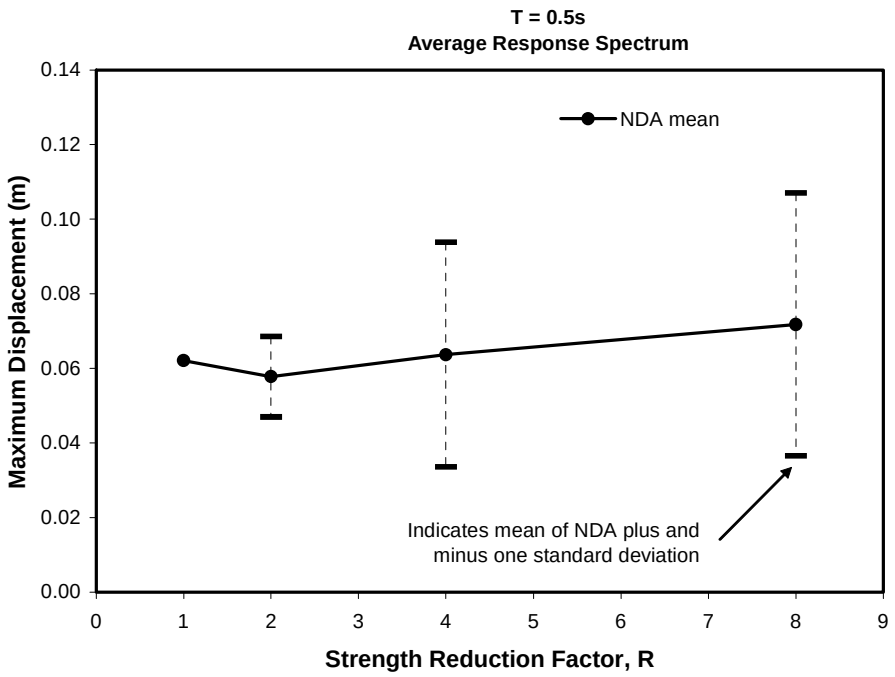


Figure 10-6 Dispersion of results for the nonlinear dynamic analysis (NDA) of a SDOF oscillator subject to thirteen NEHRP Site Class C ground motions

particular circumstances. With this in mind, it should be noted that traditional design equations, including some of those in FEMA 356 and ATC-40, are conservative and may underestimate strength capacities and deformation acceptability for some structures and components. More accurate supplemental information is available from other sources (FEMA 306/307/308, FEMA 355C).

## 10.10 Important Future Developments

The proposed improvements to nonlinear static analysis procedures in this document will lead to better results in practice. Nonetheless, not all of the shortcomings of NSPs have been addressed. In developing the improvements, a number of important observations about the need for future improvement of inelastic seismic analysis procedures have emerged. These are summarized in the following sections.

### *10.10.1 Nonlinear Modeling for Cyclic and In-Cycle Degradation of Strength and Stiffness*

FEMA 440 makes a distinction between two types of degradation of stiffness and strength of inelastic single degree-of-freedom oscillators (see Figure 10-1). This distinction had not previously been addressed explicitly by guidelines for nonlinear static procedures. Independent studies demonstrate that if strength degradation occurs cyclically, then dynamic response of SDOF systems is stable. In contrast, in-cycle loss of strength can lead to dynamic instability. It is vitally important to be able to differentiate between these two types of structural degradation. Current nonlinear static pushover procedures cannot fully distinguish between cyclic and in-cycle strength degradation. FEMA 440 includes interim recommendations based solely on judgment for this purpose.

Important questions include:

- What current data exist on force-deformation behavior and strength degradation of components subjected to large ductility demands in a single cycle of loading?

- How does in-cycle strength loss in components affect the global dynamic stability of structural models?
- Can this effect be adequately incorporated into NSPs?
- What practical guidance can be provided for the incorporation of in-cycle degradation into nonlinear response-history analysis procedures?
- How can these effects be incorporated into simplified models?

### *10.10.2 Soil and Foundation Structure Interaction*

While some advances are made in FEMA 440, there is not completely adequate guidance for addressing the effects of the interaction between structures and supporting foundations and soils. This is particularly important for short-period or large-footprint structures, where current models may over-predict the input ground motion. Furthermore, additional guidance on force-deformation relationships and damping characteristics of foundations is needed. Finally, there is an important need for adequate guidance on the effect of foundation rocking on structural response.

FEMA 440 supplements existing NSPs with preliminary recommendations for the inclusion of soil-structure-interaction effects (see Figure 10-3). These recommendations augment the existing guidelines in FEMA 356 and ATC-40 for soil-foundation stiffness and strength with approximate procedures to account for kinematic SSI and soil damping. The provisions for soil load-deformation behavior provide a framework primarily with some default values for typical materials. The documents recommend site-specific studies if performance is significantly affected by soil properties.

Important issues include:

- Is the adaptation of linear SSI procedures for nonlinear analysis presented in FEMA 440 adequate as is, or are further adjustments warranted?
- What information is available on soil load-deformation characteristics that might be adopted for general practical application?
- What analytical procedures are available to geotechnical engineers to estimate critical soil properties for inelastic seismic analysis?
- What are the effects of foundation rocking on inelastic seismic response and how can these effects be incorporated into practical analysis procedures?
- What are the effects of foundation sliding on inelastic seismic response and how can these effects be incorporated into practical analysis procedures?

### *10.10.3 Nonlinear Multi-Degree of Freedom Simplified Modeling*

Current nonlinear static procedures are based on single-degree-of-freedom models, which, while simple to understand, are very limited in their ability to address complex structures and multiple-degree-of-freedom effects from input seismic ground motions. As noted, FEMA 440 recognizes that current NSPs are limited in the ability to reliably predict the effects of inelastic behavior of MDOF systems. Specifically, predictions of maximum story drifts, story forces, and inelastic component demands (i.e., plastic hinge rotations) are not reliable using a single-load vector. FEMA 440 also notes that current procedures for using multiple-load vectors representative of the fundamental mode and one or more higher modes (multi-mode pushover analysis) can improve results somewhat, particularly for prediction of maximum story drifts. Ongoing research suggests that multi-mode pushover procedures might be modified to provide better estimates of other demand parameters as well. These improvements come at the expense of greater computational effort and less transparency, however. These barriers have been cited as obstacles to the practical application of nonlinear analysis techniques (i.e., using response-history analysis). This raises the question: why not devote the effort to simplified nonlinear response-history analysis?

One of the interesting observations about MDOF effects during the preparation of the FEMA 440 report was that, in spite of significant dispersion among records, any single nonlinear response-history analysis result often produced better estimates of maximum engineering demand parameters than any of the approximate analyses (see Figure 10-4). This observation suggests that there may be an analysis procedure that characterizes global engineering demand as the maximum displacement response of a structural model subject to shaking hazard represented by currently available regional maps (i.e., by the maps currently prepared by the U.S. Geological Survey for the National Earthquake Hazards Reduction Program). Maximum displacements might be estimated using nonlinear static procedures. Story-level and component-level engineering demand could then be estimated using a simplified MDOF response-history analysis for a small number of ground motion records, scaled to result in the previously estimated global

displacement demand. This approach could greatly simplify nonlinear response-history analysis.

Nonlinear response-history analysis might be facilitated further by the use of simplified structural models. Detailed structural models often can require hundreds of degrees of freedom, making the process prone to error and complicating the interpretation of results. As noted in FEMA 440, many practitioners have used innovative sub-structuring techniques to generate "stick" or "fishbone" models that greatly simplify data management, computational effort, and visualization of results.

In summary, this issue presents the following critical questions:

- What are the limits (e.g. periods, separation of modes, mass participation) for building models when MDOF effects must be considered significant?
- Can multi-mode pushover procedures provide adequate results for systems with significant MDOF effects?
- Can maximum engineering demand below the global level (i.e., story and component levels) be predicted using a limited number of nonlinear response-history analyses?
- How should ground motion records be scaled to produce global maximum displacement demands that are representative of a specific shaking hazard?
- How can MDOF structural models be simplified while still providing reliable results for practical application?
- How can strength and stiffness degradation (see Section 10.10.1) be adequately represented in MDOF structural models?
- How can improved methods for modeling foundations and soil structure interaction (see Section 10.10.2) be incorporated into MDOF structural models?
- What is the effect of concentrating masses at story levels on inelastic response, particularly for relative short structures?

## 10.11 Application Example

This section contains structural analysis calculations, and related commentary, utilizing nonlinear static procedures for the analysis of an example building. The steps in this process are presented in the flowchart in Figure 10-7. On the flowchart, tags have been used to identify pertinent sections of FEMA 440 (this document), and also FEMA 356 and ATC-40. The calculations also include similar tags for ease of reference to these three documents. The example illustrates use of both the displacement modification and the equivalent linearization procedures to estimate the maximum displacement of a building model.

### *10.11.1 Example Building Description*

In order to illustrate the application of NSPs, including the suggested improvements in this document, an example building has been developed. It is depicted and described on calculation Sheet 1. This type of construction is typical for relatively small commercial office and/or retail uses. It is assumed to be located in an area of relatively high seismicity. This example is very simple from an analysis perspective since all of the walls are assumed to be identical and the floor and roof diaphragms are assumed to be rigid. The building is also completely regular and symmetrical. Although some actual buildings might be this simple, it is not always the case and the user should not infer that all structures may be reduced to this level of simplicity.

### *10.11.2 Basic Ground Motion*

The basic ground motion spectrum for the example is illustrated on calculation Sheet 2. The selection of the basic ground motion does not differ from current procedures of FEMA 356, ATC-40 and the 2000 *NEHRP Recommended Provisions for New Buildings*. The same assumptions used for the evaluation study summarized in Chapter 7 are used for the example. Values for short- and 1-second period spectral accelerations at the Maximum Considered Earthquake (MCE) level were assumed for 5% damping and site class C, resulting in values $S_S$ = 1.5g and $S_1$ = 0.6g. Following the procedures in the *2000 NEHRP Recommended Provisions for New Buildings*, the short- and long-period values were modified for site class C to $S_{XS} = F_a S_S$ and $S_{X1} = F_v S_1$, where $F_a$ = 1.0 and $F_v$ = 1.3. Design-basis ordinates then were obtained as $S_{DS} = 2/3 S_{XS}$ and $S_{D1} = 2/3 S_{X1}$. These values were used with the spectral shape defined in the *NEHRP Recommended Provisions for New Buildings*.

### *10.11.3 Kinematic Soil-structure Interaction*

The next step, also illustrated on Sheet 2, is to modify the initial spectrum to account for kinematic soil-structure interaction in accordance with Chapter 8. Note that the kinematic effect associated with the base-slab averaging is considered, but not the effect related to embedment. This is due to the fact that the building,

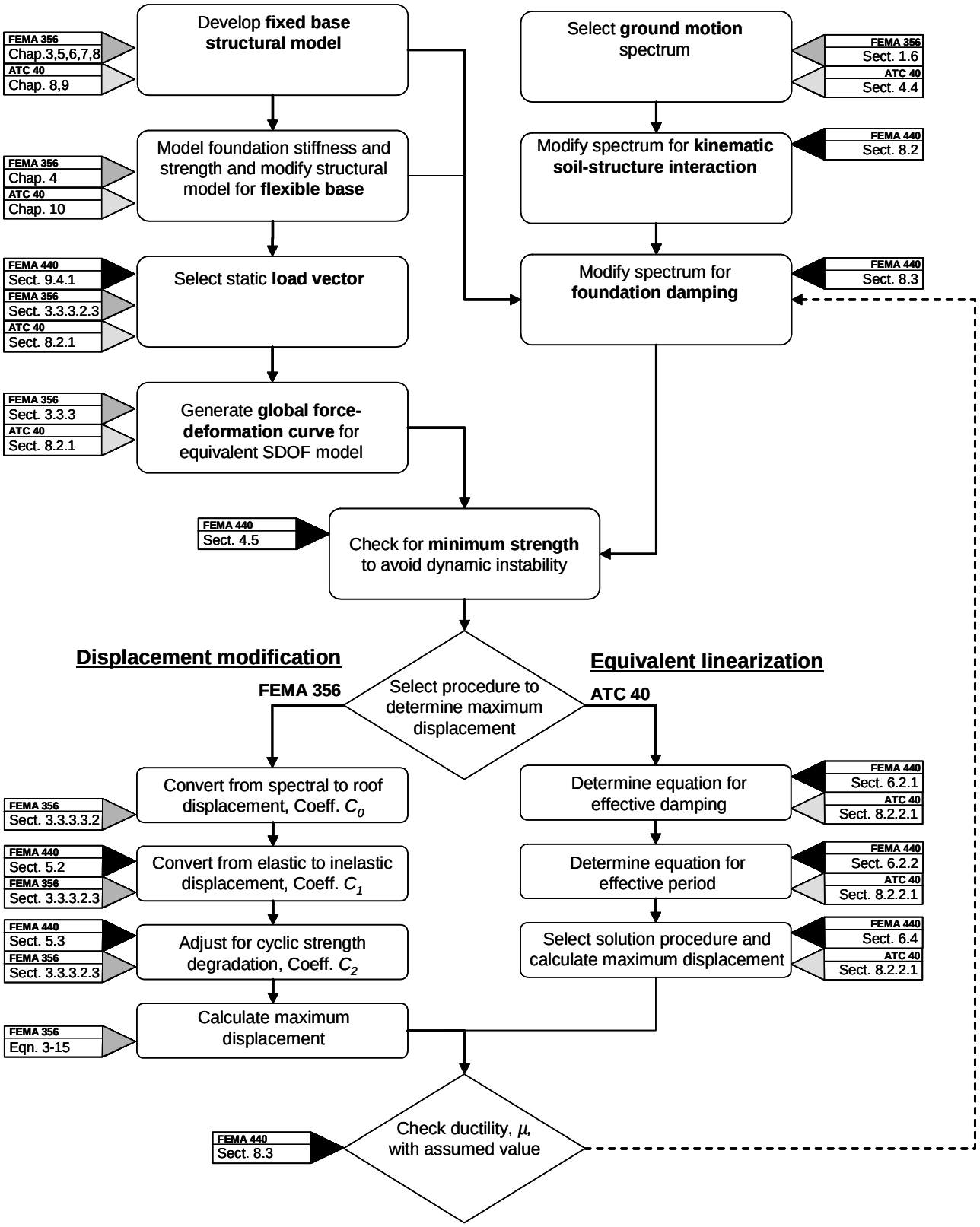


Figure 10-7 Application flowchart for nonlinear static seismic analysis

although supported three feet below grade, does not have a basement. The result of this step is a reduced spectrum representing the foundation input motion.

### 10.11.4 Fixed-Base Model

The basic procedures to develop a structural model and determine a lateral force and deformation relationship (pushover curve) for a structure remain essentially the same as in ATC-40 and FEMA 356. For the example building, a fixed-based model is relatively simple, as shown on Sheet 3. The fixed-based model is necessary, even if the intention is to include a flexible foundation, due to the fact that foundation damping procedures rely on an estimate of the change in period from a fixed base to a flexible model. The total masses for the building are calculated assuming that the roof weight is approximately 140 psf and that the floors are approximately 160 psf. These estimates are intended to include not only the weight of the structural components of the buildings, but also other dead loads and actual live loads. In an actual application, the weights would be determined in a more detailed take-off. The effective rigidities of the walls are calculated in accordance with the requirements of FEMA 356 and ATC-40 for walls that are cracked. The requirements in this case are identical in both documents.

The linear dynamic properties for the model shown on Sheet 3 are calculated utilizing the basic equations in ATC-40, Section 8.5. In many practical applications, these calculations are done using computer software. The determination of the linear dynamic properties can be simplified by using Rayleigh's method to reduce the number of degrees of freedom in the model to the lateral displacement at the roof and that at the floor level. The process is initiated by estimating a mode shape assuming a uniform acceleration acting on the story masses. Then the deflections at the roof and the floor are calculated. In this case, moment-area calculations were used for this purpose. These displacements are then normalized to a unit displacement at the roof to determine an initial estimate of the fundamental mode shape. Then a first-mode participation factor is calculated. Utilizing the participation factor, modal story forces for unit spectral acceleration can be calculated. This essentially revises the loads that were initially assumed using uniform acceleration. Application of these revised forces to the model results in a change in the displacement at the roof and the floor. These are once again normalized to the roof displacement to generate a revised mode shape. The process continues until the calculated mode shape is essentially equal to that which was assumed. Then the period may be calculated as shown at the end of the calculations on Sheet 3.

### 10.11.5 Flexible-Base Model

The process continues by repeating the calculations with the assumption of a flexible base, as shown on calculation Sheet 4. The stiffness of the foundation in this case is assumed to be controlled by the soil properties (i.e., foundation structure assumed to be rigid compared to the supporting soil). The initial shear modulus of the soil material is calculated based on the shear wave velocity for the material. For a Class C site, this ranges from 1200 to 2500 feet per second. The effective shear modulus is calculated by reducing the initial value, depending on the severity of shaking at the site. In this case a ratio was determined in accordance with the recommendations of FEMA 356.

Both FEMA 356 and ATC-40 contain equations for calculating rotational and translational stiffness of foundations assuming a rigid plate acting on a homogeneous elastic half space representing the soil. The equations in FEMA 356 differ from those in ATC-40 in their formulation. The equations shown Sheet 4 are from FEMA 356. Essentially the same values can be determined by using the equations in ATC-40. Note that both the rotational stiffness and the translational stiffness are increased due to the embedment of the foundation. It should be noted that the translational stiffness in this case is calculated only for the six shear walls acting in each direction. In reality, the stiffness is probably higher, due to the effect of the foundations beneath the walls acting in the orthogonal direction, as well as the slab on grade that ties all the footings together.

Once the foundation stiffness values are calculated, Rayleigh's method can be used once again to reduce the degrees of translational freedom to two. The calculations to determine dynamic properties for the flexible based model as shown on Sheet 4 are then analogous to those for a fixed base.

### 10.11.6 Foundation Damping

The next step is to modify the ground motion spectrum further for the effects of foundation damping. The calculations to determine foundation damping are illustrated on calculation Sheet 5. This process begins with an estimate of the effective stiffness of the fixed-base model. Note that the mass must be modified by the effective mass coefficient. The equation for this may be found in ATC-40. The equivalent foundation

radius for translation is calculated for the entire footprint of the building. Using this radius, the translational stiffness of the foundation can be estimated using FEMA 440. Note that this estimate corresponds well with that calculated using the actual soil properties on Sheet 4.

The effective height of the building is required to estimate the rotational stiffness of the foundation. This parameter is essentially the centroid of the first-mode shape measured from the base. As noted in Chapter 8, 70% of the total height of the building is often a good approximation. In this example the dynamic properties are used to calculate the actual value. Rotational stiffness of the foundation can then be estimated. Note again that the estimate on Sheet 5 compares reasonably well with that calculated for the flexible-base model using the soil properties of the foundation directly. This leads to an equivalent foundation radius for rotation, which can be visualized as a radius of gyration representing the effective moment of inertia of the foundation.

The actual amount of foundation damping depends on the relative amount of inelasticity in the foundation compared with that in the structure. The procedures in Chapter 8 essentially assume that the inelasticity is concentrated in the structure, which leads to a conservative estimate of foundation damping. The calculation requires an estimate of the system ductility demand. An initial assumption of 3.0 is made for the example. Combining this with an initial damping of 5% leads to an effective damping for the flexible-base model. Combining the foundation damping with the initial assumed damping value (5%) leads to an estimate of the total flexible-base system damping. The foundation input motion calculated, including the effects of kinematic interaction, is based on the initial assumption of 5% damping. The foundation input motion is then modified to reflect the flexible based damping as shown on calculation Sheet 6.

### *10.11.7 Force-Displacement Relationships (Pushover Curves)*

The next step in the process is the selection of a lateral load vector. FEMA 356 and ATC-40 both require and/or suggest a number of options for this selection. Based on the recommendation in Chapter 8, a vector proportional to the first-mode shape is sufficient and preferable to the others; thus the first-mode shape for the flexible-base model is used to generate the basic load-deformation characterizations for the model (see calculation Sheet 7). Two different possibilities are considered. The first case involves an arbitrary assumption that the strength is approximately 0.4 W, resulting in an *R*-factor of 1.52. If the governing inelastic mechanism were foundation rocking or some other ductile mechanism, the pushover curve might be as shown on Sheet 7 for the positive post-elastic stiffness model. Note that a positive post-elastic stiffness of 5% reflects some strain hardening and participation of the slab and columns. If the mechanism included modes of behavior that imply the loss of strength, the post-elastic portion of the curve would have a negative slope for such a degrading system. For the second model, this is assumed to be -25% of the initial oscillator stiffness for the strength-degrading model, as also illustrated in the pushover diagrams on Sheet 7. Each of these cases is examined further.

### *10.11.8 Check on Minimum Strength for Strength Degrading Model*

The model with degrading strength must be checked to determine if there is a potential for dynamic instability, as shown on calculation Sheet 8. The maximum negative post elastic stiffness evident from the pushover curve could be due to cyclic and/or in-cycle loss of strength (including $P$-$\Delta$ effects). As noted in Chapter 4, there is currently no practical means of separating these effects. The suggestion in this document is to assume that the effective post-elastic stiffness, for sites located in the near field, is equal to that attributable to $P$-$\Delta$ effects plus 80% of the balance evident from the pushover curve. For non-near-field sites the percentage drops to 20%. This is strictly a subjective provision and further research is needed on this issue. For the strength-degrading model in the example, dynamic analysis would not be required for the building in either case. However, as noted on Sheet 8, the assumed design level ground motions equal 2/3 of MCE ground motions. Larger motions would imply lower relative strength (higher *R*) for the model. In fact, the MCE motion likely would result in an *R* greater than the maximum allowable and the potential for dynamic instability. This is discussed further below in conjunction with equivalent linearization procedures.

### *10.11.9 Target Displacement for Displacement Modification*

The target displacement for the positive post-elastic stiffness model is calculated using the displacement modification as shown on calculation Sheet 9. The procedure is the Coefficient Method of FEMA 356 modified with the suggested changes for the coefficients $C_1$ and $C_2$. The coefficient $C_2$ is included in the calculation since a concrete structure is likely to

have stiffness degradation and pinching hysteretic behavior. Note that the solution for maximum displacement for the strength-degrading model (near- and non-near field) would be the same as the case on Sheet 9, since the displacement-modification procedure does not directly consider negative post-elastic stiffness in the calculation of the coefficients.

### *10.11.10 Calculation of the Performance Point Using Equivalent Linearization*

The solution for the maximum displacement of the positive post-elastic stiffness model using equivalent linearization procedures is shown on calculation Sheets 10 and 11. The effective damping and period calculations for a stiffness-degrading oscillator with positive post-elastic stiffness of 5% are shown on Sheet 10. The selected solution procedure is the construction of the locus of performance points, as shown on Sheet 11. A check using the general equations for effective damping (Equations 6-4, 6-5, and 6-6) and effective period (Equations 6-10, 6-11, and 6-12) produced essentially the same performance point.

### *10.11.11 Check on Assumed Ductility*

The solutions for the positive post elastic-stiffness model are essentially equivalent for displacement modification and equivalent linearization. The resulting ductility demand is approximately 1.8, as opposed to the assumed value of 3.0. This would result in an increase from 6.9% to 7.9% in initial flexible-base damping for the model. This reduces the maximum displacement slightly, but not significantly, in this case.

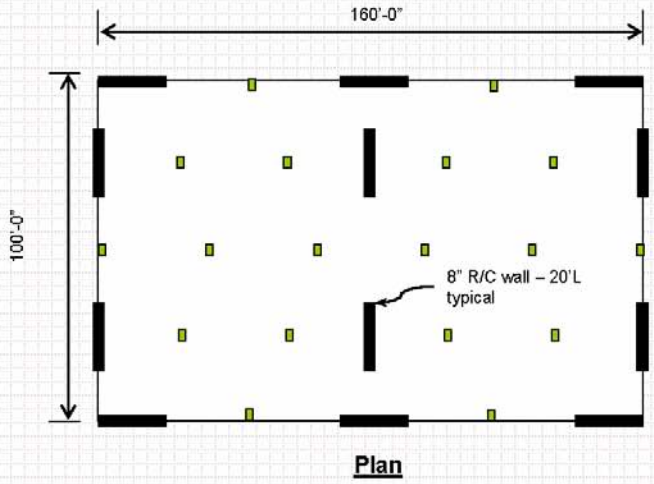


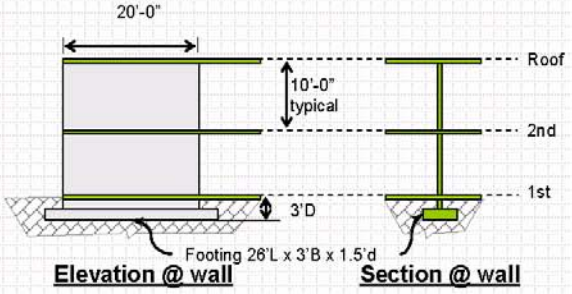


- **Two story concrete structure:** *FEMA* model buildng Type C2
- **Story to story heights 10 ft:** total building height of 20 ft.
- **Plan dimensions:** 100 ft. by 160 ft.
- **Floors and roof construction:** two-way reinforced concrete flat slab
  - Roof DL = 140 psf
  - Floor DL = 160 psf
- **Vertical support:** concrete columns and interior and exterior reinforced concrete bearing walls
- **Lateral system:** six shear walls in each direction, 12 total – L=20 ft., t=8 in.
- **Foundations:** spread footings bearing 3 ft. below grade and reinforced concrete slab on grade
- **Soils conditions:** very stiff alluvium, $v_s$ = 1200 fps, *NEHRP* Site Class C
- **Ground motion:** shaking with a 10% chance of being exceed in 50 yrs.
- **Analysis objective:** Maximum global displacement for specified ground motion

The analysis procedure is based upon nonlinear static procedures. Both the Coefficient Method of *FEMA 356* and the Capacity Spectrum Method *of ATC 40* are used to estimate the displacement. Both procedures incorporate suggested improvements from *FEMA 440.*

| PROJECT: | TITLE: | SHEET: |
|---|---|---|
| **FEMA 440**<br>**Example Building Analysis** | **Building description** | 1 |

**Select ground motion spectrum**

FEMA 356 Sect. 1.6
ATC 40 Sect. 4.4

Site class C and shear wave velocity, $v_s = 1200$ fps

Acceleration parameters for MCE shaking

| | | |
|---|---|---|
| short period | $S_s =$ | 1.5 g |
| long period | $S_1 =$ | 0.6 g |

Damping coefficients for initial $\beta = 5\%$

$B_s = 1.0$

$B_1 = 1.0$

Adjustment for site class C

| | | |
|---|---|---|
| short period | $S_{xs} = F_a S_s = (1)1.5 = 1.5g$ | $F_a = 1.0$ |
| long period | $S_{x1} = F_v S_1 = (1.3)0.6 = 0.78g$ | $F_v = 1.3$ |

To reduce to design level motions (e.g.10% chance of being exceeded in 50 years), multiply accelerations by 2/3

| | | |
|---|---|---|
| short period | $S_{DS} = \frac{2}{3} S_{xs} =$ | 1.00 g |
| long period | $S_{D1} = \frac{2}{3} S_{x1} =$ | 0.52 g |

**Modify kinematic soil-structure interaction**

Effective foundation size:

$a =$ 100 ft.

$b =$ 160 ft.

$b_e = \sqrt{ab} =$ 126 ft.

Embedment:

$e =$ 0 no basement

$RRS_e = 1.0$

Ratio of response spectra for base slab averaging

$$RRS_{bsa} = 1 - \frac{1}{14100}\left(\frac{b_e}{T}\right)^{1.2} \geq \text{the value for } T = 0.2 \text{ sec.}$$

FEMA 440 Eqn. 8-1

Foundation input motion (FIM)

$$(S_a)_{FIM} = RRS_{bsa}\, RRS_e\, (S_a)_{FFM}$$

| $T$ | $(S_a)_{FFM}$ | $RRS_{bsa}$ | $(S_a)_{FIM}$ |
|---|---|---|---|
| 0.00 | 0.52 | 0.84 | 0.44 |
| 0.10 | 1.00 | 0.84 | 0.84 |
| 0.15 | 1.00 | 0.84 | 0.84 |
| 0.20 | 1.00 | 0.84 | 0.84 |
| 0.30 | 1.00 | 0.90 | 0.90 |
| 0.40 | 1.00 | 0.93 | 0.93 |
| 0.50 | 1.00 | 0.95 | 0.95 |
| 0.60 | 0.87 | 0.96 | 0.83 |
| 0.70 | 0.74 | 0.96 | 0.72 |
| 0.80 | 0.65 | 0.97 | 0.63 |
| 0.90 | 0.58 | 0.97 | 0.56 |
| 1.00 | 0.52 | 0.98 | 0.51 |
| 1.10 | 0.47 | 0.98 | 0.46 |
| 1.20 | 0.43 | 0.98 | 0.43 |
| 1.30 | 0.40 | 0.98 | 0.39 |
| 1.40 | 0.37 | 0.98 | 0.37 |
| 1.50 | 0.35 | 0.99 | 0.34 |

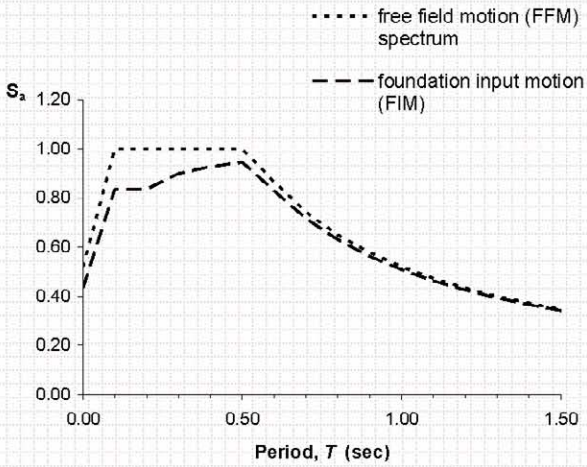


| PROJECT: | TITLE: | SHEET: |
|---|---|---|
| **FEMA 440 Example Building Analysis** | **Basic response spectrum and modification for kinematic effects** | 2 |

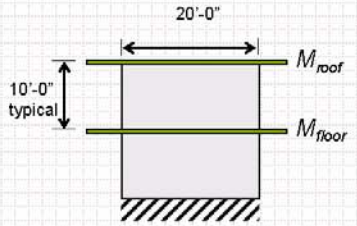


**Total masses**

$$M_{roof} = \frac{W_{roof}}{g} = \frac{\text{width(ft.)} \times \text{length(ft.)} \times \text{roof weight(ksf)}}{386.4\ \text{in./sec}^2} =$$ 5.80 k-sec$^2$/in

width= 100 ft
length= 160 ft
roof weight= 0.140 ksf

$$M_{floor} = \frac{W_{floor}}{g} = \frac{\text{width(ft.)} \times \text{length(ft.)} \times \text{floor weight(ksf)}}{386.4\ \text{in./sec}^2} =$$ 6.63 k-sec$^2$/in

width= 100 ft
length= 160 ft
floor weight= 0.160 ksf

## Fixed base model

**Effective rigidities** — FEMA 356, Table 6-5; ATC 40, Table 9-3

Flexural $0.5E_c I_g = 0.5 \times 3{,}000(\text{ksi}) \times \frac{t_w\,(\text{in}) \times l_w(\text{in})^3}{12} \times 6\ \text{walls} =$ 8.3E+10 k-in$^2$

Shear $0.4E_c A_w = 0.4 \times 3{,}000 \times t_w\,(\text{in}) \times l_w(\text{in}) \times 6\ \text{walls} =$ 1.38E+07 k

$t_w$ = 8 in $l_w$ = 240 in

**Fixed base linear dynamic properties**

First-mode load vector — FEMA 440, Sect. 9.4.1
(estimate with uniform acceleration acting on masses)

$F_{roof}$ = 2240 k $\Delta_{roof}$ = 0.23 in.
$F_{floor}$ = 2560 k $\Delta_{floor}$ = 0.10 in.

Normalize to unit displacement at roof for mode shape $\bar{\phi} = \begin{Bmatrix} \phi_{roof} \\ \phi_{floor} \end{Bmatrix} = \begin{bmatrix} 1.0 \\ 0.4 \end{bmatrix}$

First mode participation factor $PF_m = \left[ \frac{\sum_{i=1}^{N} (w_i \phi_{im})/g}{\sum_{i=1}^{N} (w_i \phi_{im}^2)/g} \right] =$ 1.23 — ATC 40, Eqn 8-20

Modal story forces for unit $S_a$ $F_{im} = PF_m \phi_{im} S_a w_i =$ [ 2758 k @ roof; 1348 k @ floor ] — ATC 40, Eqn 8-23

Displacements due to modal story forces $\delta_{im} =$ [ 0.24 in @ roof; 0.08 in @ floor ]

Normalize to unit displacement at roof for revised mode shape $\bar{\phi} = \begin{Bmatrix} \phi_{roof} \\ \phi_{floor} \end{Bmatrix} = \begin{bmatrix} 1.0 \\ 0.3 \end{bmatrix}$

Revise modal participation factor

$PF_m = \left[ \frac{\sum_{i=1}^{N} (w_i \phi_{im})/g}{\sum_{i=1}^{N} (w_i \phi_{im}^2)/g} \right] =$ 1.22 — ATC 40, Eqn 8-20

Revise modal story forces for unit $S_a$ $F_{im} = PF_m \phi_{im} S_a w_i =$ [ 2744 k @ roof; 1038 k @ floor ] — ATC 40, Eqn 8-23

Displacements due to modal story forces $\delta_{im} =$ [ 0.23 in @ roof; 0.07 in @ floor ]

Normalize to unit displacement at roof for revised mode shape (same as assumed) $\bar{\phi} = \begin{Bmatrix} \phi_{roof} \\ \phi_{floor} \end{Bmatrix} = \begin{bmatrix} 1.0 \\ 0.3 \end{bmatrix}$

Period $T = 2\pi \sqrt{\left(\sum w_i \delta_i^2\right) / \left(g \sum F_{im} \delta_{im}\right)} =$ 0.14 sec — ATC 40, Eqn 8-27

| PROJECT: | TITLE: | SHEET: |
|---|---|---|
| **FEMA 440 Example Building Analysis** | **Fixed base structural model** | 3 |

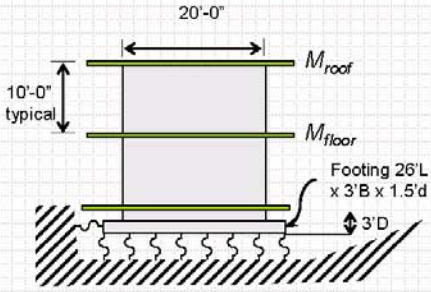


**Flexible base model**

**Soil properties** — ATC 40, Sect. 10.4.1.2

initial shear modulus $G_0 = \frac{\gamma}{g} v_s^2 =$ 31 ksi

unit wt. of soil, $\gamma =$ 100 pcf

shear wave velocity, $v_s =$ 1200 fps

effective shear modulus $G/G_0 =$ 0.75 — FEMA 356, Table 4.7

$G =$ 23 ksi

Poisson's ratio $\upsilon =$ 0.3

**Foundation dimensions**

| | |
|---|---|
| length, L= | 26 ft |
| width, B= | 3 ft |
| thickness, | 1.5 ft |
| depth, D= | 3 ft |

**Rotational stiffness**

at surface $K_{\theta,sur} = \frac{GB^3}{1-\upsilon}\left[0.47\left(\frac{L}{B}\right)^{2.4} + 0.034\right] X\ 6 walls =$ 780,342,531 k-in/rad — FEMA 356, Fig. 4.4; ATC 40, Table 10.2&3

embedment factor $\beta_\theta = 1 + 1.4\left(\frac{d}{L}\right)^{0.6}\left[1.5 + 3.7\left(\frac{d}{L}\right)^{1.9}\left(\frac{d}{D}\right)^{-0.6}\right] =$ 1.39

at depth $K_\theta = K_{\theta,sur}\beta_\theta =$ 1,081,161,315 k-in/rad

**Translational stiffness**

at surface $K_{x,sur} = \frac{GB}{2-\upsilon}\left[3.4\left(\frac{L}{B}\right)^{0.65} + 1.2\right] X\ 6 walls =$ 44,505 k/in — FEMA 356, Fig. 4.4; ATC 40, Table 10.2&3

embedment factor $\beta_x = \left(1 + 0.21\sqrt{\frac{D}{B}}\right)\left[1 + 1.6\left(\frac{Dd(B+L)}{BL^2}\right)^{0.4}\right] =$ 1.86

at depth $K_x = K_{x,sur}\beta_x =$ 82,607 k/in

**Linear dynamic properties**

First-mode load vector (estimate with uniform acceleration acting on masses) — FEMA 440, Sect. 9.4.1

$F_{roof} =$ 2240 k $\quad \Delta_{roof} =$ 0.48 in.

$F_{floor} =$ 2560 k $\quad \Delta_{floor} =$ 0.25 in.

Normalize to unit displacement at roof for mode shape $\bar{\phi} = \begin{Bmatrix} \phi_{roof} \\ \phi_{floor} \end{Bmatrix} = \begin{bmatrix} 1.0 \\ 0.5 \end{bmatrix}$

First mode participation factor $PF_m = \left[\frac{\sum_{i=1}^{N}(w_i\phi_{im})/g}{\sum_{i=1}^{N}(w_i\phi_{im}^2)/g}\right] =$ 1.22 — ATC 40, Eqn 8-20

Modal story forces for unit $S_a$ $F_{im} = PF_m\phi_{im}S_a w_i =$ [2725 k @ roof; 1638 k @ floor] — ATC 40, Eqn 8-23

Displacements due to modal story forces $\delta_{im} =$ [0.48 in @ roof; 0.23 in @ floor]

Normalize to unit displacement at roof for revised mode shape (same as assumed) $\bar{\phi} = \begin{Bmatrix} \phi_{roof} \\ \phi_{floor} \end{Bmatrix} = \begin{bmatrix} 1.0 \\ 0.5 \end{bmatrix}$

Period $\bar{T} = 2\pi\sqrt{\left(\sum w_i\delta_i^2\right)/\left(g\sum F_{im}\delta_{im}\right)} =$ 0.20 sec — ATC 40, Eqn 8-27

| PROJECT: | TITLE: | SHEET: |
|---|---|---|
| **FEMA 440 Example Building Analysis** | **Flexible base structural model** | 4 |

Effective stiffness for fixed base model

$$K^*_{fixed} = M^* \left(\frac{2\pi}{T}\right)^2 = \alpha_m M \left(\frac{2\pi}{T}\right)^2 = 17{,}889 \text{ k/in}$$ FEMA 440 Eqn. 8-3

where $$\alpha_m = \frac{\left[\sum_{i=1}^{N} w_i \phi_{im} / g\right]^2}{\left[\sum_{i=1}^{N} w_i / g\right]\left[\sum_{i=1}^{N} w_i \phi_{im}^2 / g\right]} = 0.77$$ ATC 40 Eqn 8-21

Determine equivalent foundation radius for translation

$$r_x = \sqrt{A_f / \pi} = 71 \text{ ft.} = 856 \text{ in.}$$ FEMA 440 Eqn. 8-4

Determine translational stiffness of the foundation

$$K_x = \frac{8}{2-\upsilon} G r_x = 93{,}867 \text{ k/in}$$ FEMA 440 Eqn. 8-5

Calculate effective building height

$$h^* = \frac{h\sum_{i=1}^{N} M_i \varphi_i}{\sum_{i=1}^{N} M_i} = 174 \text{ in.}$$ FEMA 440 Sect. 8-3

Rotational stiffness of foundation

$$K_\theta = \frac{K^*_{fixed}\left(h^*\right)^2}{\left(\frac{\tilde{T}}{T}\right)^2 - 1 - \frac{K^*_{fixed}}{K_x}} = 6.0\text{E+08 k-in/rad}$$ FEMA 440 Eqn.8-6

Effective foundation radius for rotation

$$r_\theta = \left(\frac{3(1-\upsilon)K_\theta}{8G}\right)^{\frac{1}{3}} = 189 \text{ in}$$ FEMA 440 Eqn. 8-7

Effective period lengthening

Assume $\mu =$ 3

$$\frac{\tilde{T}_{eff}}{T_{eff}} = \left\{1 + \frac{1}{\mu}\left[\left(\frac{\tilde{T}}{T}\right)^2 - 1\right]\right\}^{0.5} = 1.2$$ FEMA 440 Eqn. 8-8

Calculate foundation damping

$$\beta_f = a_1\left(\frac{\tilde{T}_{eff}}{T_{eff}} - 1\right) + a_2\left(\frac{\tilde{T}_{eff}}{T_{eff}} - 1\right)^2 = 3.73 \%$$ FEMA 440 Eqn. 8-9a

where

$$a_1 = c_e \exp(4.7 - 1.6 h / r_\theta) = 25.19$$ FEMA 440 Eqn. 8-9b

$$a_2 = c_e\left[25 \ln(h / r_\theta) - 16\right] = -18.06$$ FEMA 440 Eqn. 8-9c

$$c_e = 1.5(e / r_x) + 1 = 1.00$$ FEMA 440 Eqn 8-9d

Calculate flexible base damping

$$\beta_0 = \beta_f + \frac{\beta_i}{\left(\tilde{T}_{eff} / T_{eff}\right)^3} = 6.9 \%$$ FEMA 440 Eqn. 8-10

where $\beta_i =$ 5 %

| PROJECT: | TITLE: | SHEET: |
|---|---|---|
| **FEMA 440**<br>**Example Building Analysis** | **Determine effect of foundation damping on flexible base damping** | 5 |

Adjust spectrum for flexible base damping

$\beta_0 =$ 6.9 % flexible base damping including effect of foundation damping

$$(S_a)_{\beta_0} = \frac{(S_a)_{5\%}}{B(\beta_0)} = \frac{(S_a)_{FIM}}{B(\beta_0)}$$ FEMA 440 Eqn.6-16

$$B = \frac{4}{(5.6 - \ln \beta_0(\text{in \%}))} = 1.09$$ FEMA 440 Eqn.6-17

| | Free field motion with $\beta$=5% | | Foundation input motion with $\beta$=5% | | | Foundation input motion with $\beta = \beta_0$ | |
|---|---|---|---|---|---|---|---|
| $T$ | $(S_a)_{FFM}$ | $(S_d)_{FFM}$ | $RRS_{bse}$ | $(S_a)_{FIM}$ | $(S_d)_{FIM}$ | $(S_a)_{\beta}$ | $(S_d)_{\beta}$ |
| 0.00 | 0.52 | 0.00 | 0.84 | 0.44 | 0.00 | 0.40 | 0.00 |
| 0.10 | 1.00 | 0.10 | 0.84 | 0.84 | 0.08 | 0.77 | 0.08 |
| 0.15 | 1.00 | 0.22 | 0.84 | 0.84 | 0.18 | 0.77 | 0.17 |
| 0.20 | 1.00 | 0.39 | 0.84 | 0.84 | 0.33 | 0.77 | 0.30 |
| 0.30 | 1.00 | 0.88 | 0.90 | 0.90 | 0.79 | 0.83 | 0.73 |
| 0.40 | 1.00 | 1.57 | 0.93 | 0.93 | 1.46 | 0.85 | 1.34 |
| 0.50 | 1.00 | 2.45 | 0.95 | 0.95 | 2.32 | 0.87 | 2.13 |
| 0.60 | 0.87 | 3.06 | 0.96 | 0.83 | 2.92 | 0.76 | 2.68 |
| 0.70 | 0.74 | 3.57 | 0.96 | 0.72 | 3.44 | 0.66 | 3.16 |
| 0.80 | 0.65 | 4.08 | 0.97 | 0.63 | 3.95 | 0.58 | 3.63 |
| 0.90 | 0.58 | 4.59 | 0.97 | 0.56 | 4.46 | 0.52 | 4.10 |
| 1.00 | 0.52 | 5.09 | 0.98 | 0.51 | 4.97 | 0.47 | 4.57 |
| 1.10 | 0.47 | 5.60 | 0.98 | 0.46 | 5.49 | 0.42 | 5.04 |
| 1.20 | 0.43 | 6.11 | 0.98 | 0.43 | 6.00 | 0.39 | 5.51 |
| 1.30 | 0.40 | 6.62 | 0.98 | 0.39 | 6.51 | 0.36 | 5.98 |
| 1.40 | 0.37 | 7.13 | 0.98 | 0.37 | 7.02 | 0.34 | 6.45 |
| 1.50 | 0.35 | 7.64 | 0.99 | 0.34 | 7.53 | 0.31 | 6.92 |

Acceleration-displacement response spectra

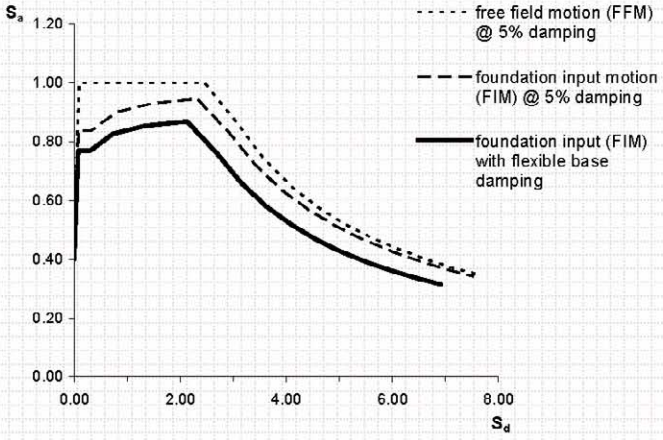


Acceleration vs. period

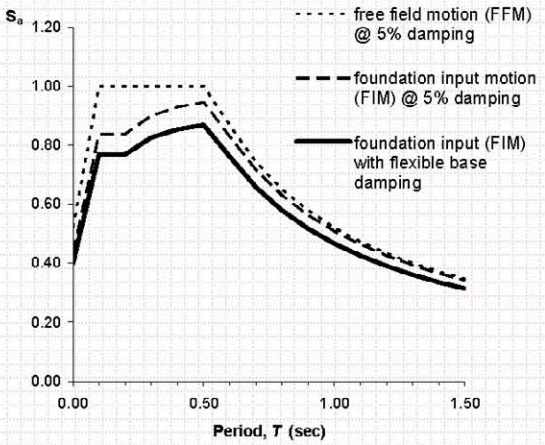


| PROJECT: | TITLE: | SHEET: |
|---|---|---|
| **FEMA 440 Example Building Analysis** | **Adjust ground motion spectrum for flexible base damping** | 6 |

**Non-strength degrading evaluation model**

Actual expected base shear strength 0.38 $W$

**Pushover curve**

Assuming first mode response determine
associated spectral acceleration and associated displacements

| $V$ | $\Delta_{roof}$ | |
|---|---|---|
| 0 | 0 | |
| 0.38 | 0.23 | expected strength |
| 0.48 | 1.5 | a =+5% |

ATC 40 Eqn 8-24: $V_m = \alpha_m S_{am} W$

$$S_{am} = \frac{V_m}{\alpha_m W} = \quad 0.49 \text{ g}$$

where $\alpha_m$ is the effective mass coefficient for the first mode and $S_{am}$ is the spectral acceleration that results in a base shear equal to the expected strength.
Note that $\alpha_m$ is equivalent to $C_m$ in *FEMA 356*.

ATC 40 Eqn 8-26: $\delta_{im} = PF_m \phi_{im} S_{am} \left(\frac{T_m}{2\pi}\right)^2 g =$ 0.23 in. at roof, 0.11 in. at floor

$R = \frac{S_a}{v_y / W} C_m =$ 1.56 (FEMA 356 Eqn 3-16)

where $PF_m$ is the first mode participation factor and $\phi_{im}$ is the first mode shape.

**Strength degrading model**

Same strength with post-elastic stiffness= -25%

**Pushover curve**

| $V$ | $\Delta_{roof}$ | |
|---|---|---|
| 0 | 0 | |
| 0.38 | 0.23 | expected strength |
| 0.03 | 1.10 | a = -25% |

$R = \frac{S_a}{v_y / W} C_m =$ 1.56 (FEMA 356 Eqn 3-16)

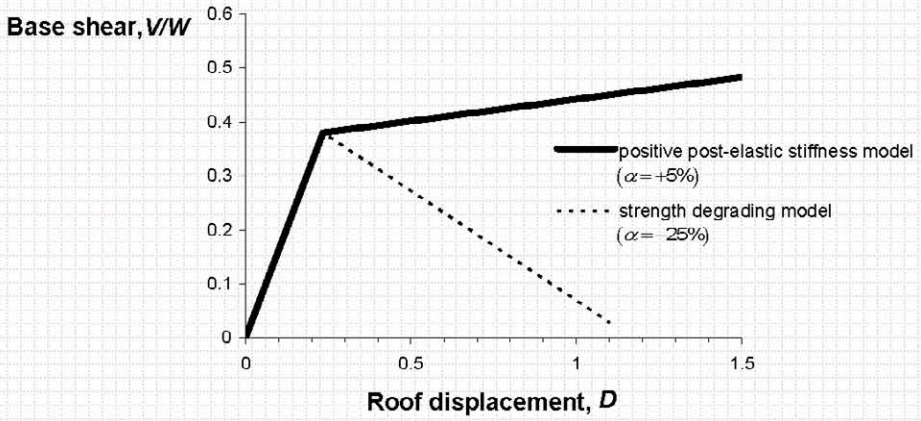


| PROJECT: | TITLE: | SHEET: |
|---|---|---|
| **FEMA 440**<br>**Example Building Analysis** | **Force-displacement relationships** | 7 |

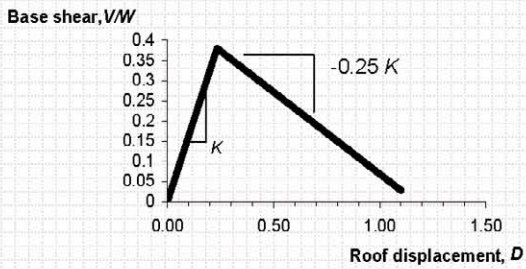


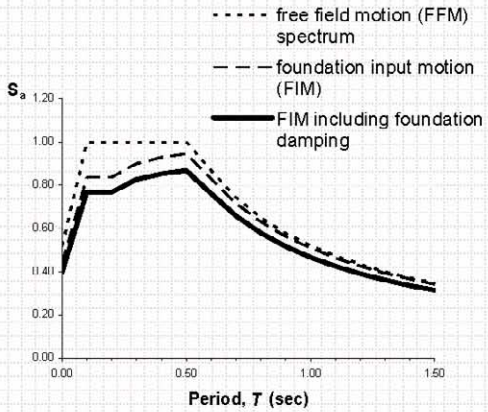


$\alpha_{max} =$ -25%

**Strength degrading model**

$$R = \frac{S_a}{V_y / W} C_m =$$ 1.56 — FEMA 356 Eqn 3-16

**Check for effective post-elastic stiffness**

$$\alpha_e = \alpha_{P-\Delta} + \lambda(\alpha_2 - \alpha_{P-\Delta})$$ — FEMA 440 Eqn. 4-1

where $\lambda =$ 0.8 near field
0.2 non-near field

assuming that $\alpha_{P-\Delta} \approx 0$ and $\alpha_2 = -25\%$

$\alpha_e =$ -20% near field
-5% non-near field

**Check minimum strength**

$$R_{max} = \frac{\Delta_u}{\Delta_y} + \frac{|\alpha_e|^{-t}}{4}$$ — FEMA 440 Eqn. 4-2

where

$$t = 1 + 0.15 \ln T =$$ 0.76 — FEMA 440 Eqn. 4-3

$R_{max} =$

| | | | |
|---|---|---|---|
| 1.85 | near field: greater than | 1.56 | dynamic analysis not required |
| 3.42 | non-near field: greater than | 1.56 | dynamic analysis not required |

Note: Since the ground motion is for the design 2/3 MCE motion, caution is warranted for possible instability in MCE. This would be particularly critical in the near field.

| PROJECT: | TITLE: | SHEET: |
|---|---|---|
| **FEMA 440 Example Building Analysis** | **Check strength degrading model for minimum strength** | 8 |

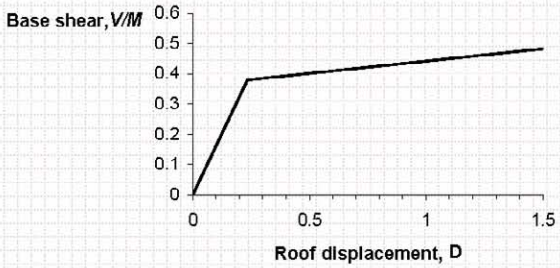


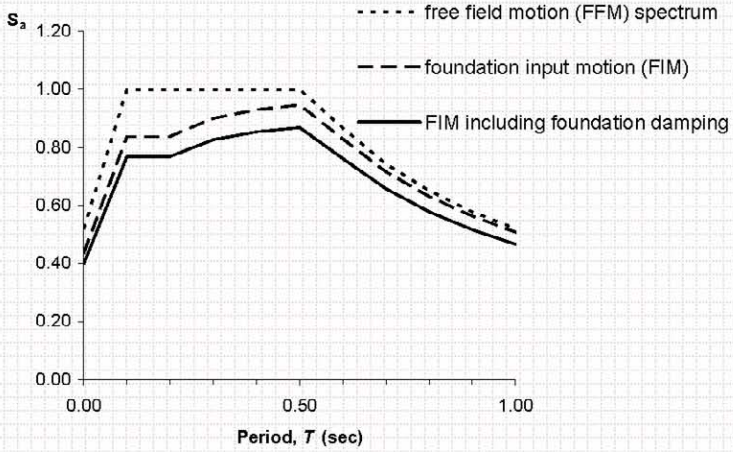


**Non-strength degrading evaluation assumption**

$$R = \frac{S_a}{v_y / W} C_m = \quad 1.56$$

$C_0 =$ 1.22

$$C_1 = 1 + \frac{R-1}{aT_e^2} = \quad 1.16$$ FEMA 440 Eqn. 5-1

where $a$ = 90 for Site Class C

$$C_2 = 1 + \frac{1}{800}\left(\frac{R-1}{T_e}\right)^2 = \quad 1.01$$ FEMA 440 Eqn. 5-2

Calulate target displacement

$$\delta_t = C_0 C_1 C_2 S_a \frac{T_e^2}{4\pi^2} g = \quad 0.4 \text{ in.}$$ FEMA 356 Eqn 3-15

| PROJECT: | TITLE: | SHEET: |
|---|---|---|
| **FEMA 440 Example Building Analysis** | **Calculate target displacement using displacement modification (*FEMA 356*)** | 9 |

Effective damping

$$\beta_{eff} = A(\mu-1)^2 + B(\mu-1)^3 + \beta_0 \quad \text{For} \quad \mu < 4.0$$ FEMA 440 Eqn. 6-1

$$\beta_{eff} = C + D(\mu-1) + \beta_0 \quad \text{For} \quad 4.0 \le \mu < 6.5$$ FEMA 440 Eqn. 6-2

$$\beta_{eff} = E\left[\frac{F(\mu-1)-1}{[F(\mu-1)]^2}\right]\left(\frac{T_{eff}}{T_o}\right)^2 + \beta_0 \quad \text{For} \quad \mu \ge 6.5$$ FEMA 440 Eqn. 6-3

Effective period

$$T_{eff} = \left[G(\mu-1)^2 + H(\mu-1)^3 + 1\right]T_o \quad \text{For} \quad \mu < 4.0$$ FEMA 440 Eqn. 6-7

$$T_{eff} = \left[I + J(\mu-1) + 1\right]T_o \quad \text{For} \quad 4.0 \le \mu < 6.5$$ FEMA 440 Eqn. 6-8

$$T_{eff} = \left\{K\left[\sqrt{\frac{(\mu-1)}{1+L[(\mu-2]}} - 1\right] + 1\right\}T_o \quad \text{For} \quad \mu \ge 6.5$$ FEMA 440 Eqn. 6-9

Coefficients for stiffness degrading (STDG) behavior with 5% positive post-elastic stiffness

Damping — FEMA 440 Table 6-1

| α(%) | A | B | C | D | E | F |
|---|---|---|---|---|---|---|
| 5 | 5.60 | -1.30 | 10.00 | 1.80 | 20.00 | 0.38 |

Period — FEMA 440 Table 6-2

| α(%) | G | H | I | J | K | L |
|---|---|---|---|---|---|---|
| 5 | 0.18 | -0.037 | 0.15 | 0.16 | 0.92 | 0.05 |

Effective damping and period as functions of μ

$\beta_0 =$ 7.5 %  $T_0 =$ 0.20 sec

| $\mu$ | $\beta_{eff}$ | $T_{eff}$ | $T_{sec}$ | $M$ | B |
|---|---|---|---|---|---|
| 1 | 7.5 | 0.20 | 0.20 | 1.00 | 1.12 |
| 2 | 11.8 | 0.23 | 0.28 | 0.69 | 1.28 |
| 3 | 19.5 | 0.28 | 0.33 | 0.74 | 1.52 |
| 4 | 22.8 | 0.32 | 0.37 | 0.76 | 1.62 |

| PROJECT: | TITLE: | SHEET: |
|---|---|---|
| **FEMA 440**<br>**Example Building Analysis** | **Calculate performance point using equivalent linearization (*ATC 40*)** | 10 |

**Procedure C (MADRS locus of Performance Points)** — FEMA 440 Sect. 6.4

Foundation input motion @ 5% damping

MADRS for various $\mu$

| $T$ | $(S_a)_{5\%}$ | $(S_d)_{5\%}$ | $\mu=1$ $(S_a)_{\beta_{eff}}$ | $(S_d)_{\beta_{eff}}$ | MADRS | $\mu=2$ $(S_a)_{\beta_{eff}}$ | $(S_d)_{\beta_{eff}}$ | MADRS | $\mu=3$ $(S_a)_{\beta_{eff}}$ | $(S_d)_{\beta_{eff}}$ | MADRS | $\mu=4$ $(S_a)_{\beta_{eff}}$ | $(S_d)_{\beta_{eff}}$ | MADRS |
|---|---|---|---|---|---|---|---|---|---|---|---|---|---|---|
| 0.00 | 0.44 | 0.00 | 0.40 | 0.00 | 0.40 | 0.35 | 0.00 | 0.24 | 0.29 | 0.00 | 0.22 | 0.27 | 0.00 | 0.21 |
| 0.10 | 0.84 | 0.08 | 0.77 | 0.08 | 0.77 | 0.67 | 0.07 | 0.46 | 0.56 | 0.05 | 0.41 | 0.52 | 0.05 | 0.40 |
| 0.15 | 0.84 | 0.18 | 0.77 | 0.17 | 0.77 | 0.67 | 0.15 | 0.46 | 0.56 | 0.12 | 0.41 | 0.52 | 0.12 | 0.40 |
| 0.20 | 0.84 | 0.33 | 0.77 | 0.30 | 0.77 | 0.67 | 0.26 | 0.46 | 0.56 | 0.22 | 0.41 | 0.52 | 0.21 | 0.40 |
| 0.30 | 0.90 | 0.79 | 0.83 | 0.73 | 0.83 | 0.72 | 0.63 | 0.49 | 0.60 | 0.53 | 0.45 | 0.56 | 0.50 | 0.43 |
| 0.40 | 0.93 | 1.46 | 0.85 | 1.34 | 0.85 | 0.74 | 1.16 | 0.51 | 0.62 | 0.97 | 0.46 | 0.58 | 0.91 | 0.44 |
| 0.50 | 0.95 | 2.32 | 0.87 | 2.13 | 0.87 | 0.75 | 1.85 | 0.52 | 0.63 | 1.54 | 0.47 | 0.59 | 1.45 | 0.45 |
| 0.60 | 0.83 | 2.92 | 0.76 | 2.68 | 0.76 | 0.66 | 2.33 | 0.45 | 0.55 | 1.95 | 0.41 | 0.52 | 1.83 | 0.39 |
| 0.70 | 0.72 | 3.44 | 0.66 | 3.16 | 0.66 | 0.57 | 2.74 | 0.39 | 0.48 | 2.29 | 0.35 | 0.45 | 2.15 | 0.34 |
| 0.80 | 0.63 | 3.95 | 0.58 | 3.63 | 0.58 | 0.50 | 3.15 | 0.34 | 0.42 | 2.63 | 0.31 | 0.39 | 2.47 | 0.30 |
| 0.90 | 0.56 | 4.46 | 0.52 | 4.10 | 0.52 | 0.45 | 3.56 | 0.31 | 0.37 | 2.97 | 0.28 | 0.35 | 2.79 | 0.27 |
| 1.00 | 0.51 | 4.97 | 0.47 | 4.57 | 0.47 | 0.40 | 3.96 | 0.28 | 0.34 | 3.31 | 0.25 | 0.32 | 3.11 | 0.24 |
| 1.10 | 0.46 | 5.49 | 0.42 | 5.04 | 0.42 | 0.37 | 4.37 | 0.25 | 0.31 | 3.65 | 0.23 | 0.29 | 3.43 | 0.22 |
| 1.20 | 0.43 | 6.00 | 0.39 | 5.51 | 0.39 | 0.34 | 4.78 | 0.23 | 0.28 | 3.99 | 0.21 | 0.27 | 3.75 | 0.20 |
| 1.30 | 0.39 | 6.51 | 0.36 | 5.98 | 0.36 | 0.31 | 5.19 | 0.21 | 0.26 | 4.33 | 0.19 | 0.25 | 4.07 | 0.19 |
| 1.40 | 0.37 | 7.02 | 0.34 | 6.45 | 0.34 | 0.29 | 5.59 | 0.20 | 0.24 | 4.67 | 0.18 | 0.23 | 4.39 | 0.17 |
| 1.50 | 0.34 | 7.53 | 0.31 | 6.92 | 0.31 | 0.27 | 6.00 | 0.19 | 0.23 | 5.01 | 0.17 | 0.21 | 4.71 | 0.16 |

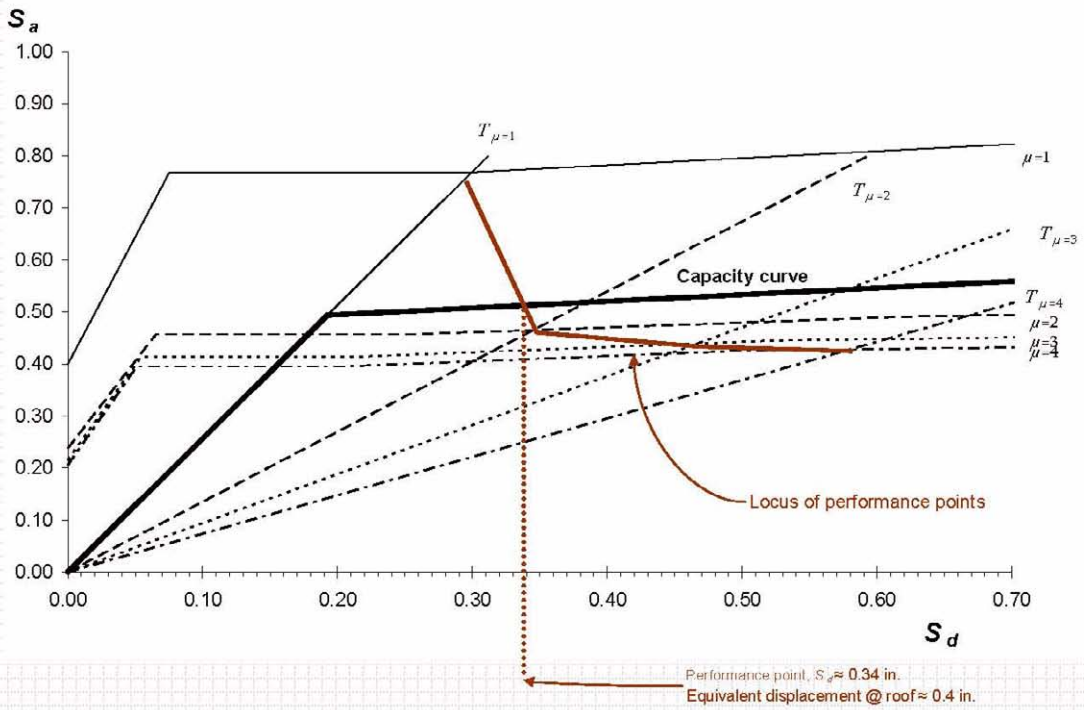


Pushover curve

| $V$ | $\Delta_{roof}$ |
|---|---|
| 0.00 | 0.00 |
| 0.38 | 0.23 |
| 0.48 | 1.50 |

Convert to ADRS coordinates for Capacity Curve

$S_a = \frac{V}{W\alpha}$ $S_d = \frac{\Delta_{roof}}{PF}$

| $S_a$ | $S_d$ |
|---|---|
| 0.00 | 0.00 |
| 0.49 | 0.19 |
| 0.98 | 4.00 |

| PROJECT: | TITLE: | SHEET: |
|---|---|---|
| **FEMA 440**<br>**Example Building Analysis** | **Locus of performance points for equivalent linearization** | 11 |

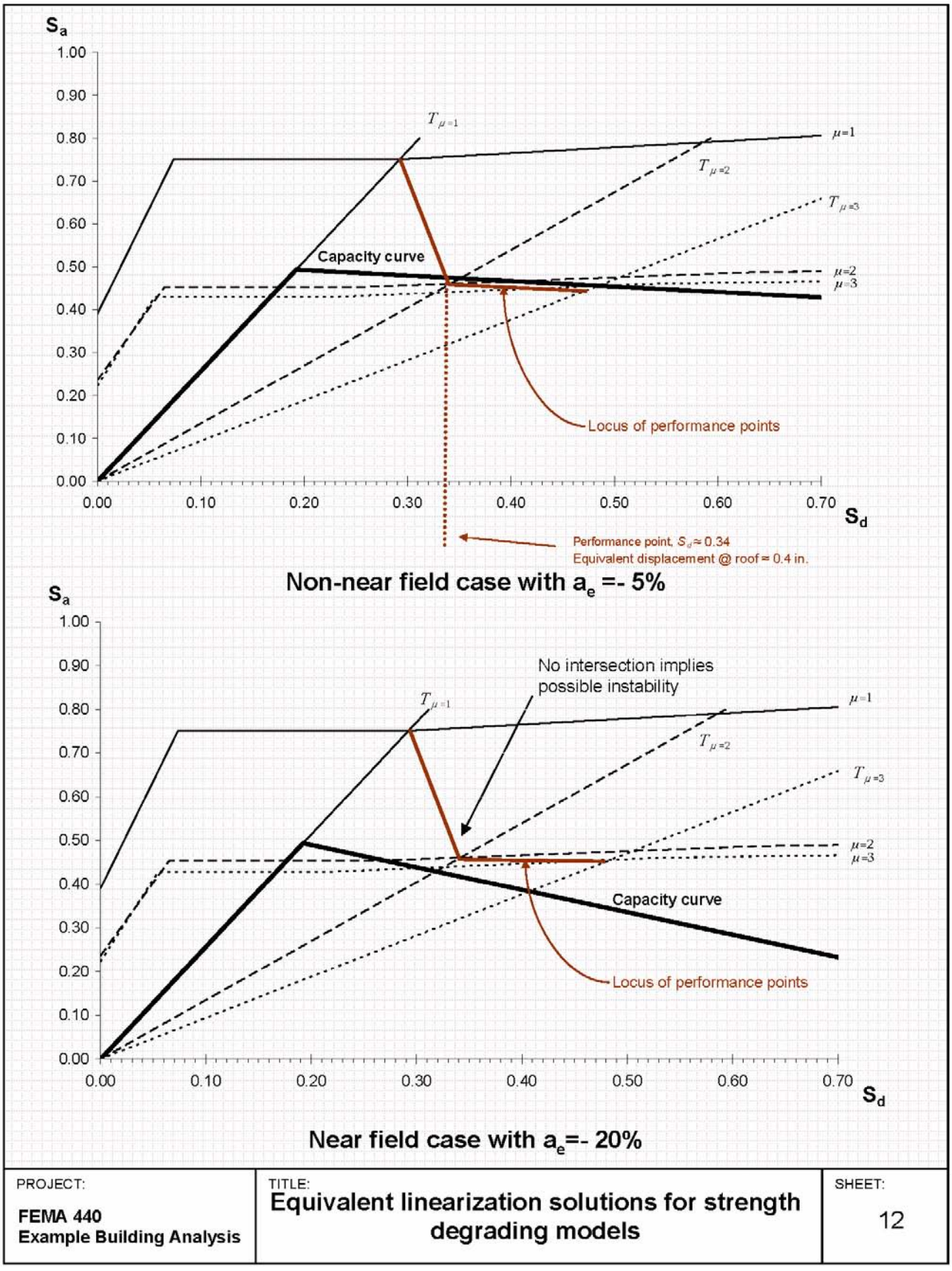
Sa
1.00
0.90
0.80
0.70
0.60
0.50
0.40
0.30
0.20
0.10
0.00
0.00
0.10
0.20
0.30
0.40
0.50
0.60
0.70
Sd
$T_{\mu=1}$
$T_{\mu=2}$
$T_{\mu=3}$
μ=1
μ=2
μ=3
Capacity curve
Locus of performance points
Performance point, $S_d \approx 0.34$
Equivalent displacement @ roof ≈ 0.4 in.
Non-near field case with $a_e$ =- 5%
Sa
No intersection implies
possible instability
$T_{\mu=1}$
$T_{\mu=2}$
$T_{\mu=3}$
μ=1
μ=2
μ=3
Capacity curve
Locus of performance points
Sd
Near field case with $a_e$=- 20%
PROJECT:
FEMA 440
Example Building Analysis
TITLE:
Equivalent linearization solutions for strength degrading models
SHEET:
12

# References and Bibliography

This section contains references, additional bibliography, and acronyms. Following the references and bibliography section is a list of FEMA reports cited in this document.

## References and Additional Bibliography


Akkar S.D. and Miranda, E., 2005, "Statistical evaluation of approximate methods for estimating maximum deformation demands on existing structures," *Journal of Structural Engineering*, American Society of Civil Engineers, Vol. 131, No. 1.

Akkar, S., and Gulkan, P., 2000, "Comparative performance evaluation of displacement based design procedures for near field earthquakes," *Proceedings of the 12th World Conference on Earthquake Engineering*, New Zealand Society for Earthquake Engineering, Upper Hutt, New Zealand.

Albanesi, T., Nuti, C. and Vanzi, I., 2000, "A simplified procedure to assess the seismic response of nonlinear structures," *Earthquake Spectra*, Vol. 16, No. 4, Earthquake Engineering Research Institute, Oakland, California, pp. 715-734.

ASCE, 2000a, *Prestandard and Commentary for the Seismic Rehabilitation of Buildings*, FEMA 356 Report, prepared by the American Society of Civil Engineers, published by the Federal Emergency Management Agency, Washington, D.C.

ASCE, 2000b, *Global Topics Report on the Prestandard and Commentary for the Seismic Rehabilitation of Buildings*, FEMA 357 Report, prepared by the American Society of Civil Engineers, published by the Federal Emergency Management Agency, Washington, D.C.

ASCE, 2002, *Minimum Design Loads for Buildings and Other Structures*, ASCE 7-02 Report, American Society of Civil Engineers, Reston, Virginia.

ATC, 1996, *Seismic Evaluation and Retrofit of Concrete Buildings*, ATC-40 Report, Volumes 1 and 2, Applied Technology Council, Redwood City, California.

ATC/BSSC, 1997, *NEHRP Guidelines for the Seismic Rehabilitation of Buildings*, FEMA 273 Report *(Guidelines)* and FEMA 274 Report *(Commentary)*, prepared by the Applied Technology Council for the Building Seismic Safety Council, published by the Federal Emergency Management Agency, Washington, D.C.

Aschheim, M.A., Maffei, J., and Black, E.F., 1998, "Nonlinear static procedures and earthquake displacement demands," *6th U.S. National Conference on Earthquake Engineering, Seattle, Washington*, Earthquake Engineering Research Institute, Oakland, California.

Aschheim, M., and Black, E.F., 2000, "Yield point spectra for seismic design and rehabilitation," *Earthquake Spectra*, Vol. 16, No. 2, Earthquake Engineering Research Institute, Oakland, California, pp. 317-335.

Aschheim, M.A., Maffei, J., and Black, E.F., 1998, "Nonlinear static procedures and earthquake displacement demands," *Proceedings, 6th U.S. National Conference on Earthquake Engineering, Seattle, Washington*, CD-ROM, Paper 167, Earthquake Engineering Research Institute, Oakland, California.

Aydinoğlu, N.M., 2003, "An incremental response spectrum analysis procedure based on inelastic spectral displacements for multi-mode seismic performance evaluation," *Bulletin of Earthquake Engineering*, Vol. 1, Kluwer Academic Publishers, pp.3-36.

Aydinoglu, N.M., and Kacmaz, U., 2002, *Strength Based Displacement Amplification Spectra For Inelastic Seismic Performance Evaluation*, Department of Earthquake Engineering Report, No. 2002/2, Kandilli Observatory and Earthquake Research Institute, Bogazici University, Istanbul, Turkey, 32 pages.

Baez, J.I., and Miranda, E., 2000, "Amplification factors to estimate inelastic displacement demands for the design of structures in the near field," *Proceedings of the 12th World Conference on Earthquake Engineering*, New Zealand Society for Earthquake Engineering, Upper Hutt, New Zealand.

Benjamin, J.R. and Cornell, C.A., 1970, *Probability, Statistics, and Decision for Civil Engineers*, McGraw Hill, New York, 684 pp.

Bernal, D., 1987, "Amplification factors for inelastic dynamic P-delta effects in earthquake analysis," *Earthquake Engineering and Structural Dynamics*, Vol. 15, pp. 635-651.

Bernal, D., 1992, "Instability of buildings subjected to earthquakes," *Journal of Structural Engineering*, Vol. 118, No. 8, American Society of Civil Engineers, pp. 2239-2260.

Black, E.F., and Aschheim, M., 2000, *Seismic Design and Evaluation of Multistory Buildings using Yield Point Spectra*, CD Release 00-04, Mid-America Earthquake Center, University of Illinois, Urbana.

Blume, J.A., Newmark, N.M., and Corning, L.H., 1961, *Design of Multistory Reinforced Concrete Buildings for Earthquake Motions*, Portland Cement Association, Skokie, Illinois.

Bracci, J.B., Kunnath, S.K., and Reinhorn, A.M., 1997, "Seismic performance and retrofit evaluation of reinforced concrete structures," *Journal of Structural Engineering*, Vol. 123, American Society of Civil Engineers, pp. 3-10.

Browning, J., 2000, "Implications of a proportioning method for earthquake-resistant RC frames subjected to strong ground motion," *Proceedings of the 12th World Conference on Earthquake Engineering*, New Zealand Society for Earthquake Engineering, Upper Hutt, New Zealand.

Browning, J., Li, R., Lynn, A., and Moehle, J.P., 2000, "Performance assessment for a reinforced concrete frame building," *Earthquake Spectra*, Vol. 16, No. 3, Earthquake Engineering Research Institute, Oakland, California, pp. 541-555.

BSSC, 2000, *NEHRP Recommended Provisions for Seismic Regulations for New Buildings and Other Structures*, Part 1, *Provisions*, and Part 2, *Commentary*, FEMA 368 and 369, prepared by the Building Seismic Safety Council, published by the Federal Emergency Management Agency, Washington, D.C.

BSSC, 2003, *NEHRP Recommended Provisions for Seismic Regulations for New Buildings and Other Structures*, Part 1, *Provisions*, and Part 2, *Commentary*, FEMA 450-1 and 450-2, prepared by the Building Seismic Safety Council, published by the Federal Emergency Management Agency, Washington, D.C.

Chintanapakdee, C., and Chopra, A.K., 2003, "Evaluation of modal pushover analysis using generic frames," *Earthquake Engineering and Strucural Dynamics*, Vol. 32, Wiley Publishers, Hoboken, New Jersey, pp. 417–442.

Chopra, A.K., and Chintanapakdee, C., 2004, "Inelastic deformation ratios for design and evaluation of structures: single-degree-of-freedom bilinear systems," *Journal of Structural Engineering.*, Vol. 130, No. 9, American Society of Civil Engineers, Reston, Virginia, pp. 1309-1319.

Chopra, A.K., and Goel, R.K., 1999a, *Capacity-Demand Diagram Methods for Estimating Seismic Deformation of Inelastic Structure: SDF Systems*, Report No. PEER-1999/02, Pacific Earthquake Engineering Center, University of California, Berkeley, California.

Chopra, A.K., and Goel, R.K., 1999b, "Capacity-demand diagram methods based on inelastic design spectrum," *Earthquake Spectra*, Vol. 15, No. 4, Earthquake Engineering Research Institute, Oakland, California, pp. 637-656.

Chopra, A.K. and Goel, R.K., 2000, "Evaluation of NSP to estimate seismic deformation: SDF systems," *Journal of Structural Engineering*, Vol. 126, No. 4, American Society of Civil Engineers, pp. 482-490.

Chopra, A.K., and Goel, R.K., 2001a, "Direct displacement based design: Use of inelastic vs. elastic design spectra," *Earthquake Spectra*, Vol. 17, No. 1, Earthquake Engineering Research Institute, Oakland, California, pp. 47-64.

Chopra, A.K., and Goel, R.K., 2001b, *A Modal Pushover Analysis Procedure to Estimate Seismic Demands for Buildings: Theory and Preliminary Evaluation*, Report No. PEER 2001/03, Pacific Earthquake Engineering Research Center, University of California, Berkeley.

Chopra, A.K., and Goel, R.K., 2001c, "Modal pushover analysis of SAC buildings," *Third U.S.-Japan Workshop on Performance-Based Earthquake Engineering Methodology for Reinforced Concrete Building Structures, August 16-18*, Seattle, Washington.

Chopra, A.K., and Goel, R.K., 2001d, *A Modal Pushover Analysis Procedure to Estimate Seismic Demands for Buildings: Theory and Preliminary Evaluation*, PEER-2001/03, Berkeley: Pacific Earthquake Engineering Research Center, University of California, 87 pages.

Chopra, A.K., and Goel, R.K., 2002, "A modal pushover analysis procedure for estimating seismic demands for buildings," E*arthquake Engineering and Structural Dynamics*, Vol. 31, pp. 561-582.

Chopra, A.K. and Kan, C., 1973, "Effect of stiffness degradation on ductility requirements for multistory buildings," *Earthquake Engineering and Structural Dynamics*, Vol. 2, pp. 35-45.

Chopra, A.K., Goel, R.K., and Chintanapakdee, C., 2003, "Statistics of single-degree-of-freedom estimate of displacement for pushover analysis of

buildings," *Journal of Structural Engineering*, Vol. 129, No. 4, pp. 459-469.

Chopra A.K., Goel, R.K., and Chintanapakdee, C., 2004, "Evaluation of a modified MPA procedure assuming higher modes as elastic to estimate seismic demands," *Earthquake Spectra*, Vol. 20, No. 3, Earthquake Engineering Research Institute, Oakland, California, pp. 757-778.

Clough, R.W., 1966, *Effect of Stiffness Degradation on Earthquake Ductility Requirements*, University of California, Dept. of Civil Engineering, Berkeley, California.

Clough, R.W. and Johnston, S.B., 1966, "Effects of stiffness-degradation on earthquake ductility requirements," *Proceedings Japan Earthquake Engineering Symposium*, Tokyo, Japan, pp. 227-232.

Collins, K.R., Wen, Y.K., and Foutch, D.A., 1995, *Investigation of Alternative Seismic Design Procedures for Standard Buildings*, UILU-ENG-95-2003 Report, Civil Engineering Studies, Structural Research Series No. 600, Dept. of Civil Engineering, University of Illinois at Urbana-Champaign, 187 pages.

Cornell, C.A., Vamvatsikos, D., Jalayer, F., and Luco, N., 2000, "Seismic reliability of steel frames," *Proceedings of the 9th IFIP WG 7.5 Working Conference on Reliability and Optimization of Structural Systems*, Ann Arbor, Michigan.

Cuesta, I., and Aschheim, M., 2001, *Using Pulse R-Factors to Estimate Structural Response to Earthquake Ground Motions*, CD Release 01-03, Mid-America Earthquake Center, University of Illinois, Urbana, Illinois.

Cuesta, I., Aschheim, M., and Fajfar, P., 2003, "Simplified R-factor relationships for strong ground motions," *Earthquake Spectra*, Vol. 19, No. 1, Earthquake Engineering Research Institute, Oakland, California, pp. 25-45.

Elnashai, A.S., 2000, "Advanced inelastic static (push-over) analysis for seismic design and assessment," *G. Penelis International Symposium on Concrete and Masonry Structures*, Aristotle University of Thessaloniki, Thessaloniki, Greece, pp 23-34.

Fajfar, P., 1999, "Capacity-spectrum method based on inelastic demand spectra," *Earthquake Engineering and Structural Dynamics*, Vol. 28, pp. 979-993.

Fajfar, P., and Gaspersic, P., 1996, "The N2 method for the seismic damage analysis of RC buildings," *Earthquake Engineering and Structural Dynamics*, Vol. 25, No. 1, pp. 31-46.

Fardis, M.N. and Panagiotakos, T.B., 1996, "Hysteretic damping and reinforced concrete elements," *Proceedings, 11*th *World Conference on Earthquake Engineering*, CD-ROM, Paper 464, Acapulco, Mexico.

Filiatrault, A., and Folz, B., 2001, "Performance-based seismic design of wood framed buildings," accepted for publication in *Journal of Structural Engineering*, American Society of Civil Engineers.

Foutch, D.A., and Shi, S., 1998, "Effects of hysteresis type on the seismic response of buildings," *Proceedings, 6th U.S. National Conference on Earthquake Engineering*, CD-ROM, Paper 409, Earthquake Engineering Research Institute, Oakland, California.

Freeman, S.A., Nicoletti, J.P. and Tyrell, J.V., 1975, "Evaluations of existing buildings for seismic risk - a case study of Puget Sound Naval Shipyard, Bremerton, Washington," *Proceedings of U.S. National Conference on Earthquake Engineering*, Berkeley, California, pp. 113-122.

Goel, R.K., and Chopra, A.K., 2004, "Evaluation of modal and FEMA pushover analysis: SAC buildings," *Earthquake Spectra*, Vol. 20, No. 1, Earthquake Engineering Research Institute, Oakland, California, pp. 225-254.

Gulkan P., and Sozen, M.A., 1974, "Inelastic responses of reinforced concrete structures to earthquake motions," *Proceedings of the American Concrete Institute*, Vol. 71, No. 12, pp. 605-610.

Gupta, A., and Krawinkler, H., 1998, "Effect of stiffness degradation on deformation demands for SDOF and MDOF structures," *Proceedings, 6th U.S. National Conference on Earthquake Engineering*, CD-ROM, Paper 225, Earthquake Engineering Research Institute, Oakland, California.

Gupta, A., and Krawinkler, K., 2000a, "Estimation of seismic drift demands for frame structures," *Earthquake Engineering and Structural Dynamics*, Vol. 29, pp. 1287-1305.

Gupta, A., and Krawinkler, K., 2000b, "Dynamic P-delta effects for flexible inelastic structures," *Journal of Structural Engineering*, Vol. 126, No. 1, American Society of Civil Engineers.

Gupta, A., and Krawinkler, H., 2003, "Feasibility of pushover analysis for estimation of strength demands," in *STESSA 2003: Proceedings of the*

*Conference on Behavior of Steel Structures in Seismic Areas*, June 9-12, 2003, Naples, Italy.

Gupta, B. and Kunnath, S.K., 1998, "Effect of hysteretic model parameters on inelastic seismic demands," *Proceedings, 6th U.S. National Conference on Earthquake Engineering*, CD-ROM, Paper 358, Earthquake Engineering Research Institute, Oakland, California.

Gupta, B., and Kunnath, S.K., 2000, "Adaptive spectra-based pushover procedure for seismic evaluation of structures," *Earthquake Spectra*, Vol. 16, No. 2, Earthquake Engineering Research Institute, Oakland, California, pp. 367-391.

Hadjian, A.H., 1982, "A re-evaluation of equivalent linear models for simple yielding systems," *Earthquake Engineering and Structural Dyn*amics, Vol. 10, pp. 759-767.

Han, S.W., and Wen, Y.K., 1997, "Method of reliability-based seismic design. I: Equivalent nonlinear system," J*ournal of Structural Engineering*, Vol. 123, American Society of Civil Engineers, pp. 256-265.

Hanson, R.D., Aiken, I., Nims, D.K., Richter, P.J., and Bachman, R.E., 1993, "State-of-the-art and state-of-the-practice in seismic energy dissipation," *Proceedings of Seminar on Seismic Isolation, Passive Energy Dissipation, and Active Control*, ATC 17-1 Report, Applied Technology Council, Redwood City, California, pp. 449-471.

Hanson, R.D., and Soong, T.T., 2001, *Seismic Design with Supplemental Energy Dissipation Devices*, Publication No. MNO-8, Earthquake Engineering Research Institute, Oakland, California.

Heintz, J.A., Poland, C.D., and Low, W.A., 1999, "Improvements to the FEMA 273 linear static procedure," *U.S.-Japan Workshop on Performance-Based Earthquake Engineering Methodology for Reinforced Concrete Building Structures*, PEER-1999/10 Report, Pacific Earthquake Engineering Research Center, University of California, pp. 267-276.

Hernández-Montes, E., Kwon, O-S, and Aschheim, M., 2004, "An energy-based formulation for first- and multiple-mode nonlinear static (pushover) analyses," *Journal of Earthquake Engineering*, Vol. 8, No. 1, pp. 69-88.

Hudson, D.E., 1965, "Equivalent viscous friction for hysteretic systems with earthquake-like excitations," *Proceedings, 3rd World Conference on Earthquake Engineering*, New Zealand, pp. II:185-201.

Husid, R., 1969, "The effect of gravity on the collapse of yielding structures with earthquake excitation," *Proceedings, 4th World Conference on Earthquake Engineering*, Vol. 2, Chilean Association of Seismology and Earthquake Engineering, Santiago, Chile, pp. A4-31 to A4-43.

Islam, M.S., Gupta, B., and Kunnath, S., 1998, "A critical review of state-of-the-art analytical tools and acceptance criterion in light of observed response of an instrumented nonductile concrete frame building," *Proceedings, 6th U.S. National Conference on Earthquake Engineering*, Earthquake Engineering Research Institute, Oakland, California.

Iwan, W.D., 1980, "Estimating inelastic response spectra from elastic spectra," *Earthquake Engineering and Structural Dynamics*, Vol. 8, pp. 375-388.

Iwan, W.D., and Chen, X.D., 1995, "Important near-field ground motion data from the Landers earthquake," P*roceedings, 10th European Conference on Earthquake Engineering*, Vol. 1, A. A. Balkema, Rotterdam, pp. 229-234.

Iwan, W.D. and N.C. Gates, 1978, "The effective period and damping of a class of hysteretic structures," *Earthquake Engineering and Structural Dynamics*, Vol. 7, pp. 199-211.

Iwan, W.D., and Gates, N.C., 1979, "Estimating earthquake response of simple hysteretic structures," *Journal of the Engineering Mechanics Division*, Vol. 105, EM3, American Society of Civil Engineers, pp. 391-405.

Iwan, W.D. and Guyader, A.C., 2001, "A study of the accuracy of the capacity-spectrum method in engineering analysis," *Proceedings of the Workshop on Performance-Based Earthquake Engineering Methodology*, Seattle, Washington.

Iwan, W.D., Huang, C-T., and Guyader, A.C., 1999, *Evaluation of the Effects of Near-Source Ground Motions*, Earthquake Engineering Research Laboratory Report 99-01, California Institute of Technology, Pasadena.

Iwan, W.D., Huang, C-T., and Guyader, A.C., 2000, "Important features of the response of inelastic structures to near-field ground motion," *Proceedings of the 12th World Conference on Earthquake Engineering*, New Zealand Society for Earthquake Engineering, Upper Hutt, New Zealand.

Jacobsen, L.S., 1930, "Steady forced vibrations as influenced by damping," *Transactions ASME*, Vol. 52 (APM), pp. 169-181.

Jacobsen, L.S., 1960, "Damping in composite structures," *Proceedings 2nd World Conference on Earthquake Engineering, Tokyo and Kyoto, Japan*, Vol. 2, pp. 1029-1044.

Jan, T.S., Liu, M.W., and Kao, Y.C., 2004, "An upper bound pushover analysis procedure for estimating the seismic demands of high rise buildings," *Engineering Structures*, Vol. 26, pp. 117-128.

Jennings, P., 1968, "Equivalent damping for yielding structures," *Journal of Engineering Mechanics*, Vol. 94, American Society of Civil Engineers, pp. 103-116.

Jennings, P.C. and Husid, R., 1968, "Collapse of yielding structures during earthquakes," *Journal of Engineering Mechanics*, Vol. 94, No. 5, American Society of Civil Engineers, pp. 1045-1065.

Judi, H.J., Davidson, B.J., and Fenwick, R.C., 2000, "The direct displacement based design method: a damping perspective," *Proceedings of the 12th World Conference on Earthquake Engineering*, Auckland, New Zealand Society for Earthquake Engineering, Upper Hutt, New Zealand.

Kim, S. and Stewart, J.P., 2003, "Kinematic soil-structure interaction from strong motion recordings," *J. Geotech. & Geoenv. Engrg.*, Vol. 129, No. 4, American Society of Civil Engineers, pp. 323-335.

Kowalsky, M.J., 1994, *Displacement-Based Design–a Methodology for Seismic Design Applied to RC Bridge Columns*, Master's Thesis, University of California San Diego, La Jolla, California.

Krawinkler, H., and Alavi, B., 1998, "Development of improved design procedures for near fault ground motions," *Proceedings, SMIP98 Seminar on Utilization of Strong-Motion Data*, Oakland, California.

Krawinkler, H., and Seneviratna, G.D.P.K., 1998, "Pros and cons of a pushover analysis of seismic performance evaluation," *Engineering Structures*, Vol. 20, No. 4-6, pp. 452-464.

Kunnath, S.K., Reinhorn, A.M., and Lobo, R.F., 1992, *IDARC: Inelastic Damage Analysis of RC Structures - Version 3.0*, Report NCEER-92-0022, State University of New York at Buffalo, New York.

Kunnath, S.K. and Gupta, B., 2000, "Validity of deformation demand estimates using nonlinear static procedures," *Proceedings of the U.S.-Japan Workshop on Performance-Based Engineering of Reinforced Concrete Building Structures*, Sapporo, Hokkaido, Japan.

Kunnath, S.K., Nghiem, Q., John Jr., A., and El-Tawil, S., 2000, "Validation of evaluation methods and acceptance criteria in evolving performance-based seismic codes," *Proceedings, SMIP2000 Seminar on Utilization of Strong-Motion Data*, California Division of Mines and Geology, Sacramento, pp. 39-63.

Lehman, D.E., Mosier, W.G. and Stanton, J.F., 2000, "Seismic performance of reinforced concrete beam-column joints," *Proceedings, the Second U.S.-Japan Workshop on Performance-Based Earthquake Engineering Methodology for Reinforced Concrete Building Structures*, September 11-13, Sapporo, Japan, Report PEER-2000/10, Pacific Earthquake Engineering Research Center, University of California, pp. 365-376.

Lepage, A., 1998, "Nonlinear drift of multistory RC structures during earthquakes," *Proceedings, 6th U.S. National Conference on Earthquake Engineering*, Earthquake Engineering Research Institute, Oakland, California.

Lew, H.S. and Kunnath, S.K., 2000, "Evaluation of analysis procedures for performance-based seismic design of buildings," *Proceedings, 12th World Conference on Earthquake Engineering, Auckland*, CD-ROM, Paper 1005, New Zealand Society for Earthquake Engineering, Upper Hutt, New Zealand.

Lin, Y.Y. and Chang, K.C., 2002, "A study on damping reduction factor for buildings under earthquake ground motions," accepted for publication in *Journal of Structural Engineering*, American Society of Civil Engineers.

MacRae, G.A., 1994, "P-delta effects on single-degree-of-freedom structures in earthquakes," *Earthquake Spectra*, Vol. 10, No. 3, Earthquake Engineering Research Institute, Oakland, California, pp. 539-568.

MacRae, G.A., Morrow, D.V., and Roeder, C.V., 2001, "Near-fault ground motion effects on simple structures," *Journal of Structural Engineering*, Vol. 127, No. 9, American Society of Civil Engineers, pp. 996-1004.

MacRae, G., and Tagawa, H., 2001, *Methods to Estimate Displacements of PG&E Structures*, draft report on research conducted under PGE/PEER Task No. 505, University of Washington, Seattle, Washington.

MacRae, G. and Tagawa, H., 2002, *Methods to Estimate Displacements of PG&E Structures*, Report PGE/

PEER Task No. 505, University of Washington, Seattle, Washington.

Mahin, S.A. and Bertero, V.V., 1981, "An evaluation of seismic design spectra," *Journal of Structural Engineering*, Vol. 107 (ST9), American Society of Civil Engineers, pp. 1777-1795.

Mahin, S.A. and Lin, J., 1983, *Construction of Inelastic Response Spectra for Single Degree of Freedom Systems*, Report No. UCB/EERC-83/17, Earthquake Engineering Research Center, University of California at Berkeley, Berkeley, California.

Miranda, E., 1991, *Seismic Evaluation and Upgrading of Existing Buildings*, PhD Thesis, University of California at Berkeley, Berkeley, California.

Miranda, E., 1993, "Evaluation of site-dependent inelastic seismic design spectra," *Journal of Structural Engineering*, Vol. 119, No. 5, American Society of Civil Engineers, pp. 1319-1338.

Miranda, E., 2000, "Inelastic displacement ratios for structures on firm sites," *Journal of Structural Engineering*, Vol. 126, No. 10, American Society of Civil Engineers, pp. 1150-1159.

Miranda, E., 2001, "Estimation of inelastic deformation demands of SDOF systems," *Journal of Structural Engineering*, Vol. 127, No. 9, American Society of Civil Engineers, pp. 1005-1012.

Miranda, E. and Akkar, S.D., 2002, "Evaluation of iterative schemes in equivalent linear methods," submitted for review and possible publication to *Earthquake Spectra*, Earthquake Engineering Research Institute, Oakland, California.

Miranda, E. and Akkar, S.D., 2003, "Dynamic instability of simple structural systems," *Journal of Structural Engineering*, American Society of Civil Engineers, Vol. 129, No. 12, pp. 1722-1726.

Miranda, E., and Bertero, V., 1994, "Evaluation of strength reduction factors for earthquake-resistant design", *Earthquake Spectra*, Vol. 10, No. 2, Earthquake Engineering Research Institute, Oakland, California, pp. 357-379.

Miranda, E., and Ruiz-García, J., 2002, "Evaluation of approximate methods to estimate maximum inelastic displacement demands," *Earthquake Engineering and Structural Dynamics*, Vol. 31, pp. 539-560.

Mwafy, A.M., and Elnashai, A.S., 2001, "Static pushover versus dynamic collapse analysis of RC buildings," *Engineering Structures*, Vol. 23, pp. 407-424.

Naeim, F., Skliros, K, and Reinhorn, A.M., 2000, "Influence of hysteretic deteriorations in seismic response of multistory steel frame buildings," *Proceedings of the 12th World Conference on Earthquake Engineering*, Auckland, New Zealand Society for Earthquake Engineering, Upper Hutt, New Zealand.

Nakaki, S., 2000, *Developing Design Guidelines for Precast Concrete Diaphragms*, Earthquake Engineering Research Institute, Oakland, California.

Nakashima, M., Ogawa, K., and Inoue, K., 2002, "Generic frame model for simulation of earthquake responses of steel moment frames," *Earthquake Engineering and Structural Dynamics*.

Newmark, N.M., and Hall, W.J., 1982, *Earthquake Spectra and Design*, Earthquake Engineering Research Institute, Berkeley, California.

Otani, S., 2000, "New seismic design provisions in Japan," *Proceedings of the U.S.-Japan Workshop on Performance-Based Earthquake Engineering for Reinforced Concrete Building Structures*, Sapporo, Japan.

Paparizos, L.G., and W.D., Iwan, 1988, "Some observations on the random response of an elasto-plastic system," *Journal of Applied Mechanics*, Paper No. 88-WA/APM-64, American Society of Civil Engineers.

Paret, T.F., Freeman, S.A., and Dameron, R.A, 2002, "Rethinking the earthquake engineering paradigm: from response reduction to response suppression," *Proceedings, Seventh U.S. National Conference on Earthquake Engineering*, Earthquake Engineering Research Institute, Oakland, California.

Porter, K.A., Beck, J.L., and Shaidhutdinov, R.V., 2002, "Sensitivity of building loss estimates to major uncertain variables," *Earthquake Spectra*, Vol. 18 No. 4, Earthquake Engineering Research Institute, Oakland, California.

Powell, G.H., 1993, *Drain-2DX Element Description and User Guide for Element Type01, Type02, Type04, Type06, Type09, and Type15 Version 1.10*, Report No. UCB/SEMM-93/18, Structural Engineering Mechanics and Materials, University of California, Berkeley, California.

Powell, G.H., and Row, D.G., 1976, "Influence of analysis and design assumptions on computed inelastic response of moderately tall frames," Report No. UCB/EERC-76/11, Earthquake Engineering Research Center, University of California at Berkeley, Berkeley, California.

Prakash, V., Powell, G.H., and Campbell, S., 1993, *Drain-2DX Base Program Description and User Guide Version 1.10*, Report No. UCB/SEMM-93/17, Structural Engineering Mechanics and Materials, University of California, Berkeley, California.

Qi, X., and Moehle, J.P., 1991, *Displacement Design Approach for Reinforced Concrete Structures Subjected to Earthquakes*, Report No. UCB/EERC-91/02, Earthquake Engineering Research Center, University of California, Berkeley.

Ramirez, O. M., Constantinou, M. C., Whittaker, A. S., Kircher, C. A., Johnson, M. W., and Chrysostomou, C. Z., 2003, "Validation of the 2000 NEHRP Provisions' equivalent lateral force and modal analysis procedures for buildings with damping systems, *Earthquake Spectra*, Vol. 19, No. 4, Earthquake Engineering Research Institute, Oakland, California, pp. 981-999.

Reinhorn, A., 1997, "Inelastic techniques in seismic evaluations," in *Seismic Design Methodologies for the Next Generation of Codes*, Fajfar, P., and Krawinkler, H., eds., Bled, Slovenia.

Riddell, R. and Newmark, N.M., 1979, *Statistical Analysis of the Response of Nonlinear Systems Subjected to Earthquakes*, Structural Research Series, Report No. UILI-ENG79-2016, Dept. of Civil Engineering, University of Illinois, Urbana, Illinois.

Rothe, D., and Sozen, M.A., 1983, A *SDOF Model to Study Nonlinear Dynamic Response of Large- and Small-Scale R/C Test Structures*, Structural Research Series, No. 512, Department of Civil Engineering, University of Illinois at Urbana-Champaign, Urbana, Illinois.

Ruiz-Garcia, J., and Miranda, E., 2003, "Inelastic displacement ratios for evaluation of existing structures," *Earthquake Engineering & Structural Dynamics*, Vol. 32, No. 8, pp. 1237-1258.

Ruiz-Garcia, J., and Miranda, E., 2004, "Inelastic displacement ratios for design of structures on soft soils sites," *Journal of Structural Engineering*, Vol. 130, No. 12, American Society of Civil Engineers, Reston, Virginia, pp. 2051-2061.

SAC, 2000, *State of the Art Report on Systems Performance of Steel Moment Frames Subject to Earthquake Ground Shaking*, FEMA 355C Report, prepared by the SAC Joint Venture (a partnership of the Structural Engineers Association of California, the Applied Technology Council, and California Universities for Research in Earthquake Engineering) for the Federal Emergency Management Agency, Washington, D.C.

Sasaki, K.K., Freeman, S.A., and Paret, T.F., 1998, "Multi-mode pushover procedure (MMP) -- a method to identify the effects of higher modes in a pushover analysis," *Proceedings, Sixth U.S. National Conference on Earthquake Engineering, Seattle, Washington*, Earthquake Engineering Research Institute, Oakland, California.

Seneviratna, G.D.P.K. and Krawinkler, H., 1994, "Strength and displacement demands for seismic design of structural walls," *Proceedings of the 5th U.S. National Conference on Earthquake Engineering*, Chicago, Vol. II, pp. 181-190.

Seneviratna, G.D.P.K., and Krawinkler, H., 1997, *Evaluation of Inelastic MDOF Effects for Seismic Design*, BLUME-120 Report, John A. Blume Earthquake Engineering Center, Stanford, California, 177 pages.

Song, J.K., and Pincheira, J.A., 2000, "Spectral displacement demands of stiffness and strength degrading systems," *Earthquake Spectra*, Vol. 16 No. 4, Earthquake Engineering Research Institute, Oakland, California, pp. 817-851.

Tagawa, H., and MacRae, G., 2000, "Capacity spectra method for estimating SDOF oscillator demands," *Proceedings of the 2001 Structures Congress & Exposition, American Society of Civil Engineers, Washington, D.C., May 21-23*.

Tsopelas, P., Constantinou, M.C., Kircher, C.A., and Whittaker, A. S., 1997, *Evaluation of Simplified methods of Analysis of Yielding Structures*, Technical Report NCEER-97-0012, National Center for Earthquake Engineering Research, State University of New York, Buffalo.

Uetani, K., and Tagawa, H., 1998, "Criteria for suppression of deformation concentration of building frames under severe earthquakes," *Engineering Structures*, Vol. 20, No. 4-6, pp. 372-383.

Valley, M.T., and Harris, J.R., 1998, "Application of modal techniques in a pushover analyses," *Proceedings, Sixth U.S. National Conference on Earthquake Engineering*, Seattle, Washington, Earthquake Engineering Research Institute, Oakland, California.

Vamvatsikos, D., and Cornell, C.A., 2002, "Incremental dynamic analysis," submitted to E*arthquake Engineering and Structural Dynamics*, John Wiley & Sons, Ltd.

Villaverde, R., 1996, "Simplified response spectrum analysis of nonlinear structures," *Journal of Engi-*

*neering Mechanics*, Vol. 122, American Society of Civil Engineers, pp. 282-285.

Wen, Y.K., and Wu, C.L., 2001, "Uniform hazard ground motions for mid-America cities," *Earthquake Spectra*, Vol. 17, No. 2, Earthquake Engineering Research Institute, Oakland, California, pp. 359-384.

Wu, J., and Hanson, R.D., 1989, "Study of inelastic spectra with high damping," *Journal of Structural Engineering*, American Society of Civil Engineers, Vol. 115, No. 6, pp. 1412-1431.

Yu, K., Heintz, J., and Poland, C., 2001, "Assessment of nonlinear static analysis procedures for seismic evaluation of building structures," *Proceedings U.S.-Japan Joint Workshop and Third Grantees Meeting, U.S.-Japan Cooperative Research on Urban Earthquake Disaster Mitigation, 15-16 August 2001*, University of Washington, Seattle, Washington, pp. 431-450.

Zamfirescu, D. and Fajfar, P., 2001, "Comparison of simplified procedures for nonlinear seismic analysis of structures," *Proceedings, 3rd U.S. Japan Workshop on Performance-Based Earthquake Engineering Methodology for Reinforced Concrete Buildings*, Seattle, Washington.

## FEMA Reports

FEMA reports are listed by report number.

FEMA 306, 1998, *Evaluation of Earthquake Damaged Concrete and Masonry Wall Buildings, Basic Procedures Manual*, prepared by the Applied Technology Council for the Partnership for Response and Recovery, published by the Federal Emergency Management Agency, Washington D.C.

FEMA 307, 1998, *Evaluation of Earthquake Damaged Concrete and Masonry Wall Buildings, Technical Resources*, prepared by the Applied Technology Council for the Partnership for Response and Recovery, published by the Federal Emergency Management Agency, Washington D.C.

FEMA 308, 1998, *Repair of Earthquake Damaged Concrete and Masonry Wall Buildings*, prepared by the Applied Technology Council for the Partnership for Response and Recovery, published by the Federal Emergency Management Agency, Washington D.C.

FEMA 355C, 2000, *State of the Art Report on Systems Performance of Steel Moment Frames Subject to Earthquake Ground Shaking*, prepared by the SAC Joint Venture (a partnership of the Structural Engineers Association of California, the Applied Technology Council, and California Universities for Research in Earthquake Engineering) for the Federal Emergency Management Agency, Washington, D.C.

FEMA 356, 2000, *Prestandard and Commentary for the Seismic Rehabilitation of Buildings*, prepared by the American Society of Civil Engineers for the Federal Emergency Management Agency, Washington, D.C.

FEMA 357, 2000, *Global Topics Report on the Prestandard and Commentary for the Seismic Rehabilitation of Buildings*, prepared by the American Society of Civil Engineers for the Federal Emergency Management Agency, Washington, D.C.

FEMA 368, 2000, *NEHRP Recommended Provisions for Seismic Regulations for New Buildings and Other Structures, Part 1 - Provisions*, prepared by the Building Seismic Safety Council for the Federal Emergency Management Agency, Washington, D.C.

FEMA 369, 2000, *NEHRP Recommended Provisions for Seismic Regulations for New Buildings and Other Structures, Part 2 - Commentary*, prepared by the Building Seismic Safety Council for the Federal Emergency Management Agency, Washington, D.C.

FEMA 450-1, 2003, *NEHRP Recommended Provisions for Seismic Regulations for New Buildings and Other Structures, Part 1 - Provisions*, prepared by the Building Seismic Safety Council for the Federal Emergency Management Agency, Washington, D.C.

FEMA 450-2, 2003, *NEHRP Recommended Provisions for Seismic Regulations for New Buildings and Other Structures, Part 2 - Commentary*, prepared by the Building Seismic Safety Council for the Federal Emergency Management Agency, Washington, D.C.

# Project Participants

## Project Management

Christopher Rojahn (Principal Investigator)
Applied Technology Council
201 Redwood Shores Parkway, Suite 240
Redwood City, California 94065-1175

Bernadette Mosby (Project Coordinator)
Applied Technology Council
201 Redwood Shores Parkway, Suite 240
Redwood City, California 94065-1175

Craig D. Comartin (Project Director)
CDComartin, Inc.
7683 Andrea Avenue
Stockton, California 95207-1705

## FEMA Oversight

Michael Mahoney (Project Officer)
Federal Emergency Management Agency
500 "C" Street, SW, Room 416
Washington, DC 20472

Robert D. Hanson (Technical Monitor)
2926 Saklan Indian Drive
Walnut Creek, California 94595

## Project Management Committee

Craig D. Comartin (Chair)
Christopher Rojahn (Ex-officio)

Ronald O. Hamburger
Simpson Gumpertz & Heger
The Landmark @ One Market, Suite 600
San Francisco, California 94105

William T. Holmes
Rutherford & Chekene
427 Thirteenth Street
Oakland, California 94612

Wilfred D. Iwan
California Institute of Technology
Earthquake Engineering Research Lab.
MC 104-44
Pasadena, California 91125

Jack P. Moehle
(University of California at Berkeley)
3444 Echo Springs Road
Lafayette, California 94549

Jonathan P. Stewart
University of California, Los Angeles
Dept. of Civil & Environmental Engineering
5731 Boelter Hall
Los Angeles, California 90095

## Project Review Panel

Anthony B. Court*
Curry Price Court
444 Camino Del Rio South, #201
San Diego, California 92108

Daniel Shapiro
SOHA Engineers
48 Colin P. Kelley Street
San Francisco, California 94107

Leonard Joseph
Thornton-Tomasetti Group
2415 Campus Drive, Suite 110
Irvine, California 92612

Steve Sweeney
US Army Engineer Research and Development Center
Construction Engineering Research Laboratory
2902 Farber Drive
Champaign, Illinois 61821

*ATC Board Representative

Chia-Ming Uang
University of California, San Diego
Structural Engineering Department
409 University Center
La Jolla, California 92093-0085

Michael Valley
Magnusson Klemencic Associates
1301 Fifth Avenue, Suite 3200
Seattle, Washington 98101

## Phase 1 Project Working Group

Joseph R. Maffei (Group Leader)
Consulting Structural Engineer
Rutherford & Chekene Consulting Engrs.
427 Thirteenth Street
Oakland, California 94612

Mark Aschheim
Santa Clara University
Department of Civil Engineering
500 El Camino Real
Santa Clara, California 95053

Maureen Coffey
Rutherford & Chekene
427 Thirteenth Street
Oakland, California 94612

Mason T. Walters
Forell/Elsesser, Inc.
160 Pine Street, Suite 600
San Francisco, California 94111

## Phase 2 Project Working Group

Sinan Akkar
Department of Civil Engineering
Middle East Technical University
06531 Ankara, Turkey

Mark Aschheim
Santa Clara University
Department of Civil Engineering
500 El Camino Real
Santa Clara, California 95053

Andrew Guyader
California Institute of Technology
Earthquake Engineering Research Lab.
MC104-44
Pasadena, California 91125

Mehmet Inel
Pamukkale University
Denizli, Turkey

Eduardo Miranda
Stanford University
Civil & Environmental Engineering
Terman Room 293
Stanford, California 94305-3707

Jorge Ruiz-Garcia
Stanford University
52D Escondido Village
Dudley Lane
Stanford, California 94306

Junichi Sakai
Pacific Earthquake Engineering Research Center
University of California at Berkeley
1301 South 46th Street
Richmond, California 94804-4698

Tjen Tjhin
Department of Civil and Environmental Engineering
University of Illinois
Urbana, Illinois 61820

Tony Yang
Pacific Earthquake Engineering Research Center
University of California at Berkeley
1301 South 46th Street
Richmond, California 94804-4698

## Phase 2 Focus Groups

### *Focus Group on Displacement Modification*

John Hooper
Magnusson Klemencic Associates
1301 Fifth Avenue, Suite 3200
Seattle, Washington 98101

Gregory A. MacRae
Assistant Professor
University of Washington
Department of Civil Engineering
Seattle, Washington 98195-2700

Stephen A. Mahin
University of California at Berkeley
Dept. of Civil Engineering
777 Davis Hall,
Berkeley, California 94720

### *Focus Group on Equivalent Linearization*

Terrence Paret
Wiss, Janey, Elstner Associates, Inc.
2200 Powell Street, Suite 925
Emeryville, California 94608-1836

Graham Powell
Graham H. Powell, Inc.
140 Birchbark Place
Danville, California 94506

Andrew S. Whittaker
University at Buffalo, SUNY
Department of Civil, Structural, and
Environmental Engineering
212 Ketter Hall
Buffalo, New York 14260-4300

### *Focus Group on Multi-Degree-of-Freedom (MDOF) Effects*

Anil K. Chopra
University of California at Berkeley
Department of Civil Engineering
Berkeley, California 94720

Jon A. Heintz
Degenkolb Engineers
225 Bush Street, Suite 1000
San Francisco, California 94104

Helmut Krawinkler
Stanford University
Civil Engineering Department
Stanford, California 94305-4020

### *Focus Group on Soil-Structure Interaction*

Jacobo Bielak
Carnegie Mellon University
Dept. of Civil Engineering
Pittsburgh, Pennsylvania 15213-3890

Gregory L. Fenves
University of California at Berkeley
Dept. of Civil Engineering
729 Davis Hall, #1710
Berkeley, California 94820-1710

James O. Malley
Degenkolb Engineers
225 Bush Street, Suite 1000
San Francisco, California 94104

## Applied Technology Council

The Applied Technology Council (ATC) is a nonprofit, tax-exempt corporation established in 1971 through the efforts of the Structural Engineers Association of California. ATC's mission is to develop state-of-the-art, user-friendly engineering resources and applications for use in mitigating the effects of natural and other hazards on the built environment. ATC also identifies and encourages needed research and develops consensus opinions on structural engineering issues in a non-proprietary format. ATC thereby fulfills a unique role in funded information transfer.

ATC is guided by a Board of Directors consisting of representatives appointed by the American Society of Civil Engineers, the National Council of Structural Engineers Associations, the Structural Engineers Association of California, the Western Council of Structural Engineers Associations, and four at-large representatives concerned with the practice of structural engineering. Each director serves a three-year term.

Project management and administration are carried out by a full-time Executive Director and support staff. Project work is conducted by a wide range of highly qualified consulting professionals, thus incorporating the experience of many individuals from academia, research, and professional practice who would not be available from any single organization. Funding for ATC projects is obtained from government agencies and from the private sector in the form of tax-deductible contributions.

### 2005-2006 Board of Directors

Lawrence G. Griffis, President
Christopher P. Jones, Vice President
Pat Buscovich, Secretary/Treasurer
David C. Breiholz
Gregory G. Deierlein
Ramon Gilsanz
James R. Harris
Eve Hinman
David A. Hutchinson
Mark H. Larsen
Ugo Morelli
H. John Price
Charles Thornton

# A. Summary of Research on Inelastic Analysis Procedures

## A.1 Introduction

Inelastic analysis of structures is a field with a number of active researchers. In order to gauge the current situation with respect to information and data that might be used to evaluate and improve procedures, ATC solicited information from investigators on relevant published research as well as on research in progress and unpublished insights and perspectives. The purpose was to obtain insight for the direction of the project. This section summarizes the information obtained from these investigators including limited review of literature relevant to the objectives of the project. Announcements in professional newsletters informed the engineering community of the project and directed interested persons to the ATC web site. There they found a description of the project and a form for initial researcher input. Project team members met with investigators in face-to-face meetings from March through June 2001. This effort was supplemented by interviews and e-mail discussions. In total, the project team members contacted over fifty researchers in the United States, Europe, and Japan. Over thirty in structural engineering, risk and reliability; geotechnical engineering, and engineering seismology provided input, for which ATC, FEMA and PEER are most thankful. Table A-1 contains a partial list of the researchers contacted, along with an indication of the format in which information was collected.

**Table A-1 Investigator Research Data**

| *Researchers Contacted* | *Researcher Input Form* | *Discussion Notes* | | | |
|---|---|---|---|---|---|
| | | *Meeting Notes* | *Telephone Notes* | *E-mail* | *Other* |
| *Risk and Reliability* | | | | | |
| Allin Cornell | ✓ | ✓ | | | |
| Y.K. Wen | | ✓ | | | |
| *Structural Engineering* | | | | | |
| Mark Aschheim | | | | | ✓ |
| John Bonacci | | | | ✓ | |
| Joe Bracci | | ✓ | | | |
| Anil Chopra | | ✓ | | ✓ | |
| Michael Constantinou | | ✓ | | | |
| Greg Deierlein | | ✓ | | | |
| Amr Elnashai | | ✓ | | | |
| Peter Fajfar | | | | | ✓ |
| Greg Fenves | | ✓ | | | |
| Andre Filiatrault | | ✓ | | | |
| Doug Foutch | | ✓ | | | |
| Sig Freeman | | ✓ | | | |
| Rakesh Goel | | | ✓ | | |

**Table A-1 Investigator Research Data (continued)**

| *Researchers Contacted* | *Researcher Input Form* | *Discussion Notes* | | | |
|---|---|---|---|---|---|
| | | *Meeting Notes* | *Telephone Notes* | *E-mail* | *Other* |
| Ron Hamburger | | | | ✓ | |
| Bill Iwan | ✓ | | | | |
| Mervyn Kowalsky | | ✓ | | | |
| Helmut Krawinkler | | ✓ | | | |
| Sashi Kunnath | | | ✓ | | |
| Andres Lepage | | | ✓ | | |
| Greg MacRae | | | ✓ | | |
| Joe Maffei | | ✓ | | | |
| Eduardo Miranda | | ✓ | | | |
| Jose Pincheira | | ✓ | | | |
| Graham Powell | | ✓ | | ✓ | |
| Nigel Priestley | | | | | ✓ |
| Andrei Reinhorn | | | ✓ | | |
| Mete Sozen | | | | | |
| John Stanton | | ✓ | | | |
| Masaomi Teshigawara | ✓ | | | | |
| Mike Valley | | ✓ | | | |
| Ed Wilson | | | | ✓ | |
| *Geotechnical Engineering and Site Effects* | | | | | |
| Youssef Hashash | | ✓ | | | |
| *Engineering Seismology and Ground Motions* | | | | | |
| Bruce Bolt | | | ✓ | | |
| Mehmet Celebi | | | ✓ | | |

The summary that follows is a composite of information submitted by or obtained from interviews of researchers, and the results of literature review by project team members. Last name references are used to attribute thoughts and opinions of individual researchers contacted. In a few instances, the work of other researchers not contacted is mentioned without a formal citation. Information from published and pending articles and reports is cited by lead author and date as listed in the References section.

## A.2 Classification of Analysis Methods

The research summary addresses various methods of inelastic analysis, but focuses upon the nonlinear static procedures known as the Capacity-Spectrum Method, as described in ATC-40 (ATC, 1996), and the Displacement Coefficient Method, as described in FEMA 273 (ATC/BSSC, 1997) and FEMA 356 (ASCE, 2000). Inelastic analysis methods differ based in the approximations used to model the structural system (e.g. “equivalent” single-degree-of-freedom (SDOF)

considering one or more modes, stick models, "fishbone" models, 2D planar models, 3D models) and the form of the representation of demand (e.g. elastic spectra, approximate inelastic spectra, one or more elastic or nonlinear time histories, or energy-based methods). Both the Capacity-Spectrum Method and Displacement Coefficient Method use "equivalent" SDOF systems to estimate the response of an inelastic system from the response of an elastic system to an elastic response spectrum.

MacRae and Maffei observe that methods for estimating the response of inelastic systems based on elastic response spectra may be classified further based on the assumption used for the elastic period in the estimate of peak inelastic displacement response. Lateral force reduction factors, R-μ-T relations, and the Displacement Coefficient Method are similar in their adoption of the initial elastic period in this regard. In contrast, one of the fundamental features of equivalent linearization techniques is the use of a period longer than the initial to reflect inelastic effects. The Capacity-Spectrum Method, for example, uses the secant period corresponding to the maximum inelastic displacement. Notably, there is a simple algebraic relationship relating the initial and periods if they are both known. Consequently, the graphic representation of a method can be de-coupled from the underlying relationships that are used to estimate displacements. For example the use of inelastic spectra in a Capacity-Spectrum Method format allows secant stiffnesses to be used with R-μ-T relations based on the initial, elastic stiffness for estimating displacements. A variant of the Capacity-Spectrum Method known as Yield Point Spectra (Aschheim) allows initial stiffnesses to be used with the same R-μ-T relations. In both cases, the underlying displacement estimate is based on the initial stiffness, because the initial stiffness is used in the definition of the R-μ-T relationships. The original Capacity-Spectrum Method bases the displacement estimate on the elastic response of an oscillator having the secant stiffness of the nonlinear system.

## A.3 Nonlinear Static Procedures

### *A.3.1 Overview of Current Procedures*

#### A.3.1.1 Capacity-Spectrum Method

**Description.** The peak displacement of a nonlinear system is estimated as the intersection of the capacity curve and an elastic response spectrum that is reduced to account for energy dissipated by the yielding structure. The underlying basis of the Capacity-Spectrum Method (CSM) is the concept of an "equivalent linear" system, wherein a linear system having reduced stiffness ($K_{eff} = K_{secant}$), and increased damping proportional to hysteretic energy, is used to estimate the response of the nonlinear system. The CSM is documented thoroughly in ATC-40. It is also described in further detail in Section 7 of this document.

**Advantages**

1. The intersection of "capacity" and "demand" curves implies a sense of dynamic equilibrium.
2. The influence of strength and stiffness on peak displacement is represented by the graphic nature of the procedure.
3. As currently presented in ATC-40, the procedure equates viscous damping to hysteretic damping providing an appealing link to the actual characteristics of the structure.
4. The interpretation of the graphic solution can provide insight for an effective retrofit strategy.

**Drawbacks**

1. There is a controversy over the accuracy of displacement estimates.
2. The iterative procedure is time-consuming and may sometimes lead to no solution or multiple solutions (Chopra).
3. The equating of hysteretic energy dissipation to viscous damping energy dissipation provides a somewhat specious sense that the procedure is "theoretically" based on fundamental physical properties.

**Accuracy.** Some investigators find the CSM overestimates displacement response while others find the CSM underestimates displacement response. Albanesi et al. (2000) find significant disparities between estimates of response made with the CSM, equal energy, and equal displacement assumptions when compared to the results from nonlinear response history analyses. Chopra and Goel (1999a, 1999b) report that the CSM procedure significantly underestimates displacement response for a wide range of periods and ductility values, relative to the Newmark Hall and other R-μ-T relations. Tsopelas et al. (1997) finds that the CSM either accurately estimates or overestimates the mean displacements obtained from nonlinear reponse history analysis. MacRae observes that the CSM both overestimates the effective damping for a given ductility and reduces the 5% damped

spectrum too much for a given level of damping. Iwan reports that the CSM is accurate in a mean sense for some cases, but the scatter in displacement estimates is large because the combination of effective stiffness and damping used in the CSM is not optimal. Iwan et al. (2000) report that the use of equivalent viscous damping to account for inelastic behavior in the CSM yields satisfactory results for the limited period ranges where a resonance type of response occurs; but the CSM is not generally valid for near-field ground motions. Akkar and Gulkan (2000) also report that the CSM underestimates response to near field earthquakes. Freeman notes the intersection point is least ambiguous when the capacity and demand curve form a sharp intersection; whereas when the curves approach each other gradually, the expected displacement may be less certain.

The range of findings on the accuracy of the CSM reflect the various strategies and assumptions used in the evaluation studies. The assessment of the accuracy of the method is likely to vary with the ground motions used to evaluate it, with clear differences emerging, for example, for near-field motions relative to far-field motions. As a part of the current work the Capacity-Spectrum Method as presented in ATC-40 was evaluated for a wide range of parametric values (see Chapter 3)

**Theory .** The apparent theoretical basis of the Capacity-Spectrum Method of ATC-40 is a strength and a weakness. In reality the underpinnings of the current procedure are obscure. As discussed in Section A.3.2.1, the CSM is a form of the empirically based equivalent linearization. Also the need for empirically-determined coefficients (e.g. to account for structure framing type [Valley]) adds an element of empiricism to the method. The use of spectral reduction factors to be applied to a designated spectral shape makes it unclear if the method is even applicable to site specific spectra that depart from the designated spectral shape (Iwan).

**Enhancements.** Improvements and modifications to the basic CSM have been suggested by some investigators. For example, Albanesi et al. (2000) suggest the use of a variable damping response spectrum, in which the damping level increases as the ductility of the system increases. Potential enhancements to the method involve using re-calibrated ductility/damping spectral reduction factor relationships or, more directly, ductility-related spectral reduction factor relationships in:

1. The so-called Direct Capacity Spectra Method (MacRae and Tagawa, 2001).
2. The use of inelastic spectra based on R-μ-T relationships.
3. Using a graphic representation in which an intersection of a “demand curve” and a “capacity curve” defines the maximum displacement similar to the Capacity-Spectrum Method (Chopra and Fajfar).
4. The use of inelastic spectra based on R-μ-T relationships, plotted with yield displacement on the abscissa, in a format known as Yield Point Spectra (Aschheim).

Further discussion may be found in Sections A.3.2.1 and A.3.2.2. Finally, Direct Displacement Based Design is a design version of the CSM (Kowalsky) and is discussed in Section A.3.1.4

#### A.3.1.2 Displacement Coefficient Method

**Description.** The peak displacement of a nonlinear system is estimated as the peak displacement of an elastic system ($K_{eff} = K_{initial}$) multiplied by a series of coefficients. Of primary interest here are the coefficients $C_1$, the ratio of the peak displacement of the inelastic system and the peak displacement of the elastic system having the same period of vibration; $C_2$, which accounts for the effect of pinching in the load-deformation relation; and $C_3$, which accounts for second-order (P-Delta) effects. FEMA 356 is the primary source of documentation for the Displacement Coefficient Method (DCM). It is described further in Chapter 5 of this document. The coefficients are empirical and derived primarily from statistical studies of the nonlinear response history analyses of SDOF oscillators. In particular, $C_1$ is conventionally characterized in terms of strength, ductility, and period ($R$-μ-$T$ relationships). The coefficient $C_1$ usually is greater than 1.0 for relatively short periods and converges to approximately 1.0 as period increases (equal displacement approximation). In the DCM, initial stiffness has a predominant effect on peak displacement response, while strength has little effect.

**Advantages.** The principal advantages of the method are that it is direct and simple to apply. It is also based on empirical parameters ($R$-μ-$T$ relationships) that have been studied and generally accepted in the technical community for some time, leading to relatively little controversy.

**Drawbacks.** The Displacement Coefficient Method has received little scrutiny in recent literature, at least relative to the Capacity-Spectrum Method. Thus, potential drawbacks of the method may not be as apparent. The product formulation for representing the effects of strength, pinching, and P-Delta effects may be questioned. Krawinkler stated that P-Delta effects in multistory structures can not be accounted for accurately using simplified procedures, and realistic spectra should be used for soft soil sites, rather than using a coefficient approach.

**Accuracy.** Many compromises were required to transform research results into the FEMA 273/356 nonlinear static procedure (Krawinkler). The $C_1$ factor as defined in FEMA 356 is smaller than research indicates, as noted in FEMA 274. Miranda (2001) points out that the $C_1$ term should be derived from oscillator response values and not from the R-μ-T relations that are based on these responses, to avoid statistical bias in the results. MacRae and Tagawa (2001) note that the coefficient $C_2$ should approach unity as the strength of the pinched system approaches the strength required for elastic response.

Song and Pincheira (2000) find that the FEMA 273 recommendations provide conservative estimates of the displacement amplification factors for degrading oscillators with periods greater than 0.3 sec on firm soils, and are unconservative at shorter periods.

Lew and Kunnath (2000) compare demands computed using the LSP, LDP, NSP, and NDP of FEMA 273 with the acceptance criteria of the document for an instrumented 7-story reinforced concrete frame building (the Holiday Inn, Van Nuys, California) subjected to ground motions having a 10% probability of exceedance in 50 years, as developed for the FEMA-funded SAC[1] project. A triangular load pattern was used in the pushover analysis, and member plastic rotations were calculated from chord rotations as suggested in FEMA 273. The beam plastic rotation demands determined in this way were similar to the mean beam plastic rotations determined by nonlinear dynamic analysis, with pushover analysis underestimating the plastic rotation demands in the columns relative to those determined by nonlinear dynamic analysis, particularly in the upper stories.

1. SAC: a joint venture partnership of the Structural Engineers Association of California, the Applied Technology Council, and California Universities for Research in Earthquake Engineering

As a part of the current work for the ATC-55 project, the Displacement Coefficient Method as presented in FEMA 356 was evaluated for a wide range of parametric values (see Appendix B).

**Enhancements.** The Displacement Coefficient Method could be improved by deriving $C_1$ factors directly from nonlinear response data. The expression for $C_1$ could be made a function of the degree of degradation of the oscillator load-deformation response and the degree of P-Δ effects present. MacRae and Tagawa (2001) suggest improved $C_1$ factors to account for near-field effects. See the discussion in Section A.3.3 below.

#### A.3.1.3 Drift-Based Approaches

Simple methods to consider drift in the design of multistory buildings have been put forward by Sozen and his coworkers. Lepage (1998) describes a method for estimating peak drift, in which an effective period and an elastic displacement spectrum determined for 2% damping are used with a linear model of the structure. Browning (2000) uses the technique to determine a target period to limit the expected roof drift and interstory drifts during a design level event.

#### A.3.1.4 Direct Displacement-Based Design

Kowalksy considers Direct Displacement Based Design to be a design-oriented implementation of CSM. Rather than estimating peak displacements, a limit on displacement is used to determine the required properties of the system. Lepage noted that this method has been criticized for overestimating the effective damping present, but at the same time, Fenwick finds that uncracked properties make individual components stiffer than is considered in the method. As a result, the higher damping tends to compensate for the use of a more flexible building, resulting in the apparently reasonable displacement estimates. Chopra and Goel (2001,a,b,c) report that the use of linear elastic spectra with increased damping, as recommended by Priestley, does not work well in comparison with an inelastic design spectrum derived using the Newmark-Hall relations.

Filiatrault and Folz (2001) have adapted this procedure to wood frame construction. Because wood softens gradually, a sharp yield point does not exist. This makes the use of *R*-μ-*T* relationships very difficult, while approaches that use the CSM format can handle softening more easily.

### *A.3.2 Fundamental Bases and Relationships*

The Capacity-Spectrum Method and Displacement Coefficient Method rely on different underlying relationships to estimate the response of nonlinear systems based on an elastic response spectrum. The Capacity-Spectrum Method relies on the concept of equivalent linearization while the Displacement Coefficient Method uses R-μ-T relationships (where *R* = the strength required for elastic response divided by the effective yield strength of the system and μ= the displacement ductility response of the system). These fundamental relations are reviewed in the following sections. As presented and utilized currently, the graphical characteristics of the two procedures are also different. However, these differences are not fundamental and results from either approach may be readily transformed into various graphical representations.

#### A.3.2.1 Equivalent Linearization

The basis of the Capacity-Spectrum Method is the premise that the peak response of an inelastic system can be estimated as the peak response of a linear elastic system having reduced stiffness and increased damping. Different approaches have been used to determine the properties of the "equivalent" linear system. In some cases, relationships between the energy dissipated by material nonlinearity and the energy dissipated by viscous damping are used, while in others, empirical calibrations are used to identify the viscous damping (and, in some cases, stiffness) that result in the best estimates of peak displacement response. This section reviews various conceptual approaches that have been taken and discusses empirical observations that bear on the hypothesis that viscous damping is a suitable surrogate for the energy dissipated by hysteretic behavior in nonlinear systems. More discussion of equivalent linearization is included in Chapter 6.

**Empirical Methods.** Equivalent linearization requires that the stiffness and viscous damping of the equivalent linear system be established. A nonlinear system having μ=4, for example, can be represented by a linear system having stiffness equal to the secant stiffness and sufficient damping to cause the peak displacement response to equal the peak displacement of the nonlinear system. Iwan observes that the secant stiffness is a lower bound to the stiffnesses that could potentially be selected, and that for each admissible stiffness, there is an associated damping level that results in the desired peak displacement. Thus, the challenge is to identify the optimal combination of stiffness and damping that results in a least biased estimate of the peak response and minimizes the dispersion in the estimates.

Tagawa and MacRae (2001) identify effective damping values by adjusting the damping of an elastic system, having a period based on the secant stiffness, to obtain peak displacements equal to the peak displacement of the inelastic system. MacRae reports that negative values of substitute damping are required for some combinations of oscillator characteristics and ground motion records to match the peak displacement of an inelastic oscillator, although the mean values tend to be somewhere between the ATC-40 and Japanese Building Standard Law versions of CSM.

The Building Research Institute of Japan studied the CSM for adoption into the Japanese building code. The Japanese implementation (Otani, 2000) uses a lower amount of damping, $h_{eq}$, than the ATC-40 implementation. The effective damping is a function of ductility, μ. For reinforced concrete and steel members in flexure,

$$h_{eq} = \frac{1}{4}\left(1 - \frac{1}{\sqrt{\mu}}\right) + 0.05 \qquad \text{(A-1)}$$

and for reinforced concrete members with pinching or slip related to shear cracking or bar slip,

$$h_{eq} = \frac{1}{5}\left(1 - \frac{1}{\sqrt{\mu}}\right) + 0.05 \qquad \text{(A-2)}$$

**Energy Methods.** Judi et al. (2000) summarize the concepts of equivalent damping and substitute damping. Equivalent damping comes from Jacobsen (1930) and is applicable to nonlinear systems subjected to sinusoidal displacement histories. Substitute damping was defined by Gulkan and Sozen (1974) as the viscous damping needed in an elastic structure to dissipate the same amount of energy input to a structure responding inelastically to an earthquake ground motion, where the elastic system has a fundamental period based on the secant stiffness of the inelastic structure at its peak displacement. Gulkan and Sozen worked with stiffness-degrading systems. Hudson, working with bilinear systems responding to earthquake ground motions reportedly found (in 1965) that substitute damping values were approximately a third of the counterpart equivalent damping values. This observation may reflect the smaller amount of energy dissipation associated with the relatively few cycles of

earthquake shaking oscillations at or near the peak displacements compared to a uniform sinusoidal displacement history.

The Capacity-Spectrum Method assumes that the energy dissipated by nonlinear behavior can be equated to the energy dissipated by a linear elastic system undergoing simple harmonic oscillations at the peak displacement response. The stiffness of the linear elastic system is set equal to the secant stiffness of the nonlinear system at the peak displacement.

Following the same concept employed for evaluating nonlinear site response in the SHAKE program, Powell suggests that the secant stiffness be evaluated at 70-80% of the maximum displacement, since there may be only one or two cycles at or near the peak displacement, with most cycles having peak displacements that are substantially less than the peak displacement. Powell suggests this would result in a smaller period and smaller effective damping relative to the ATC-40 Capacity-Spectrum Method, and therefore would result in larger displacement estimates. The *Perform-2D* computer program allows the equivalent linear stiffness to be set to a proportion of the peak displacement.

Several observations diminish the hypothesis that equivalent damping should be obtained by equating hysteretic energy dissipation to viscous energy dissipation:

1. Oscillators with different hysteretic properties can have the same peak displacement (Kowalsky).
2. As the post-yield stiffness changes from positive to negative, there is a disproportionate increase in displacement response amplitudes (Aschheim).
3. Nonlinear elastic systems (e.g. rocking walls) have no hysteretic energy dissipation, yet peak displacements are not much greater than systems with full energy dissipation (Miranda).
4. Initially undamaged and initially damaged oscillators were found to have nearly identical peak displacements, indicating that differences in the energy dissipated through hysteretic losses has little effect on peak displacement response (Aschheim and Black, 2000).
5. Changes in stiffness associated with nonlinear response interrupts the build up of resonance that drives the elastic spectral ordinates to their peaks (Paret, 2002).

**Accuracy of Effective Damping Relationships.** Iwan notes there may be some sensitivity of the optimal effective stiffness and damping values to the suite of ground motions used. Miranda reports that he is finding that Iwan and Gates (1979) relationships are very good, and the Gulkan and Sozen damping is not very accurate. Fenves, however, reports that the Gulkan and Sozen damping is good for reinforced concrete structures. Kowalsky indicates that effective damping may differ for near-field motions containing significant velocity pulses. R. Goel reports that the Japanese Building Standard Law underestimates damping and leads to overestimates of displacements. Stanton expressed concern that the baseline value of damping, to which the equivalent or substitute damping is added, is not necessarily 5% and might be lower. MacRae has recalibrated the Capacity-Spectrum Method and finds the scatter is similar to a recalibrated version of the Displacement Coefficient Method, except for periods above 1.5 sec, where the recalibrated CSM has greater scatter.

**Spectral Reduction Factors.** Reduction factors to be applied to smoothed elastic design spectra to establish spectral amplitudes for larger amounts of effective damping are tabulated for the Capacity-Spectrum Method. Tagawa and MacRae (2001) find the actual reduction associated with elastic response for a given damping level is not as large as is determined in ATC-40. While the Capacity-Spectrum Method specifies (a) a ductility-effective damping relationship and (b) an effective damping-spectral reduction factor relationship, it is possible to establish a direct relationship between ductility and the spectral reduction factor (MacRae and Tagawa, 2001). MacRae reports that less scatter results when this single relationship is used, in the so-called Direct Capacity Spectra Method.

#### A.3.2.2 Displacement Modification

The coefficient $C_1$ of the Displacement Coefficient Method as currently is derived from $R$-$\mu$-$T$ relationships. Such relationships are usually determined by statistical analysis of the computed response of a large number of SDOF oscillators having prescribed load-deformation relationships to actual ground motion records. There is general agreement on the form of the $R$-$\mu$-$T$ relationship (e.g. Miranda and Bertero, 1994), although there are some differences in the relationships determined by various investigators. There is significant variability in the $R$-factors determined for individual records. Larger $R$-factors generally can be expected for long-duration motions that allow resonance to build up the elastic response, and smaller

*R*-factors can generally be expected for systems subjected to predominantly pulse-type motions.

Most investigators have determined *R*-μ-*T* relationships based on statistics computed on *R*, and have further determined displacement ratios such as $C_1$ by algebraic manipulation of *R*-μ-*T* relationships. Miranda observes that when required strengths are determined by applying *R* factors to elastic spectral amplitudes, the parameter of interest is $R^{-1}$. Furthermore if one assumes a given ductility for an oscillator, then the "required" *R* can be determined statistically from the analysis of the oscillator response to a suite of ground motions. If one then assumes the "required" *R* and calculates the ductility demand, it is not necessarily equivalent to that assumed in the first instance. Since the expected *R* factor for a given ductility level is not precisely correlated to the expected ductility that results from a given *R* factor, coefficients such as $C_1$ should be determined from the oscillator response data and not by algebraic manipulation of the *R*-μ-*T* relationship. This is further complicated by the non-monotonic nature of the strength-ductility relationship, in which different strengths may result in the same ductility response. Recommended *R* factors are usually based on the largest strength associated with a desired ductility level. Cuesta et al. (2001) minimize the error in estimated strengths, and find that *R*-factors should be expressed in relation to a characteristic period of the ground motion (i.e. *R*-μ-$T/T_g$ relationships). This is an observation also made by Vidic et al. (1994). Even so, there is some ambiguity in the identification of the characteristic period of a site, because ground motions recorded in different horizontal directions or in different earthquakes may display different characteristic periods.

#### A.3.2.3 Choosing Between Equivalent Linearization and Displacement Modification

While some investigators find the computation of *R*-factors to be more direct than the use of equivalent linearization, Fenves observed that the averaging of *R*-factors over many ground motions to obtain *R*-μ-*T* relationships separates the relationships from the actual dynamics, and effective damping relationships may be as good. Fajfar noted that both approaches involve approximations, but *R*-μ-*T* relationships are easier to use, in part because no iteration is required, and most people accept the equal displacement approximation that is expressed in many *R*-μ-*T* relationships for periods greater than $T_g$. Fajfar (1999) and Chopra and Goel (1999a, 1999b) have recommended *R*-μ-*T* relationships be used for reducing the elastic response spectra in the CSM. Aschheim and Black (2000) have also recommended the use of these relationships with smoothed elastic design spectra or the display of the actual, jagged, constant ductility spectra of a suite a ground motions, in the Yield Point Spectra format.

The choice between the two procedures is largely a matter of personal preference as opposed to relative accuracy. The comparisons of relative accuracy prior to the ATC 55 project are very limited. There have been no comprehensive studies that simultaneously incorporate the relevant scope (strength, period, hysteretic characteristics, site conditions, etc.) and range of parameters required to make conclusive judgements or recommendations for improvement. This fact is the motivation for the comparisons made in ATC 55 as summarized in Section 5.

### *A.3.3 Near-Field Effects on SDOF Systems*

Near field motions are those that contain one or more large velocity pulses, usually originating from the superposition of waves emanating from the fault as the rupture progresses towards a site (i.e. directivity effect). Short-period systems experience the near-field effects as impulses. The large velocity pulses can cause the elastic spectra to be larger. The R factors associated with such pulses are smaller, in general, than those associated with motions in which resonance contributes to the elastic spectral amplitudes. It is now appreciated that structures with periods less than the characteristic period of the pulse may be severely affected (Krawinkler). Long-period structures may experience large interstory drifts associated with the large amplitude ground motion reversals

Iwan et al. (2000) observe that larger displacement amplification factors and smaller strength reduction factors are indicated for structures having fundamental periods less than the predominant period of the near field ground motion, relative to far-field cases. Baez and Miranda (2000) find that displacement amplification factors (the peak displacement of an inelastic system having a specified ductility divided by the peak displacement of an elastic system having the same initial stiffness) are up to about 20% larger for near field sites, with fault normal amplifications being larger than fault parallel amplifications. MacRae and Tagawa (2001) recommend an *R*-μ-*T* relation for near field motions that changes with directivity.

### *A.3.4 Equivalent SDOF Systems*

Both the Capacity-Spectrum Method and the Displacement Coefficient Method use an "equivalent" SDOF model to represent the resistance of the structure to deformation as it responds in its predominant "mode." Various techniques have been recommended for determining the properties of the "equivalent" SDOF system. Specifically, the relationships used in FEMA 356 and ATC-40 result in different SDOF systems. In many cases the period of the SDOF analogue differs from the natural period of vibration of the structure (Aschheim). For structures in which the predominant mode of response involves a change in the shape vector (e.g. once a plastic hinge develops at the base of a slender structural wall), further adjustments in the post-yield capacity curve of the SDOF analogue may be warranted, although such refinements may be overly precise given the approximate nature of the displacement estimate. Several alternative "equivalent" SDOF techniques have been proposed including those by Rothe and Sozen (1983), Miranda and Bertero, Qi and Moehle (1991), Fajfar and Gaspersic, (1996), Villaverde (1996), Han and Wen (1997), and Chopra and Goel (2001b).

### *A.3.5 Behavior Mode Effects*

Many structures will not exhibit the full hysteretic loops that are often used in analytical research studies. The presence of stiffness degradation, pinching, strength deterioration, and foundation rocking may influence peak displacement estimates. The general consensus appears to be that moderate levels of stiffness degradation and pinching will cause peak displacements of short period systems (below 0.3 to 0.5 sec) to increase slightly above those determined for bilinear systems. Negative values of post-yield stiffness, arising either due to the load-deformation behavior of the component or the presence of P-Delta effects, can cause increases in peak displacement, as can rapid strength deterioration.

Gupta and Kunnath (1998) investigated stiffness degradation and pinching, and found that "severe" degradation causes only structures with periods less than about 0.5 sec to have mean displacements substantially greater than elastic values. Gupta and Krawinkler (1998) find that peak displacements increase with the introduction of pinching, with the increase becoming larger with decreasing initial period. The ratio of peak displacement for a pinching model to the peak displacement without pinching seems to be nearly independent of the ductility of the system. This study finds that peak displacements increase substantially as the post-yield stiffness becomes increasingly negative, and the increase is larger for weaker systems. However, the effect of negative post-yield stiffness on increasing peak displacement is reduced in the presence of pinching.

Song and Pincheira (2000) discuss effects of pinching, stiffness degradation, and negative post-yield stiffness on displacement response. They find that the equal displacement approximation is generally applicable to degrading systems for periods greater than a characteristic period ($T_g$) of the ground motion. Peak displacements were generally larger than those of non-degrading systems for periods less than $T_g$. For systems on rock or firm soil, displacement amplification factors of 2 were found at $T$=0.3 sec, with even larger values possible at shorter periods or on soft soils. Fischinger reports that the shape of the hysteretic loop is important for short-period systems and for cases with negative post-yield stiffness or strength deterioration. Otani agreed that loop shape will not affect peak response amplitudes in the displacement-controlled portion of the spectrum.

Miranda reports that the period $T_c$ that represents a breakpoint in the $R$-$\mu$-$T$ relationship depends on $\mu$, as provided for in the Vidic et al. (1994). $R$ factor relationship. Miranda reports that the shifting of the period at which the $R$ factors change is moderate for cases of pinching and stiffness degradation, but is large for strength deterioration. Miranda (2000) has developed $C_1$ values for oscillators having bilinear load-deformation relations located on firm sites, and has developed $C_1$ values for stiffness degrading systems. Sause reportedly is determining similar parameters for nonlinear elastic systems.

### *A.3.6 MDOF and Inelastic Mechanism Effects*

The use of "equivalent" SDOF systems to characterize the nonlinear response of multistory structures potentially may be misleading if higher modes play a significant role in the response or if inelastic mechanisms develop that were not identified in the nonlinear static (pushover) analysis. Higher modes may influence the mechanisms that develop, and different excitations potentially may cause different mechanisms to develop. This may be more pronounced in buildings in which mechanism strengths or modes of failure are not well separated in a dynamic sense. An example of the latter case would be the development of shear failures in beams or columns due to higher mode forces, in a structure that developed a ductile

mechanism in a pushover analysis. Analytical studies have focused on only a limited number of case study buildings. Sufficient research to address these mechanism issues conclusively is not presently available.

Gupta and Krawinkler (2000a) relate the peak inelastic drifts observed in steel frame buildings to the elastic response of a SDOF oscillator through a series of factors that account separately for roof drift relative to SDOF response, the development of inelasticity, the presence of P-delta effects, the ratio of interstory to average roof drift, and the relation between element deformations and interstory drift. Three-, nine-, and twenty story steel moment frame buildings were subjected to the components of the SAC ground motions having a 2% probability of exceedance (PE) in 50 years, a 10% PE in 50 years and a 50% PE in 50 years, oriented at 45 degrees to the fault-normal and fault-parallel directions. They report that a good estimate of the ratio of elastic roof drift to the first mode spectral displacement is given by the first mode participation factor, but for structures with periods greater than 2 sec they advise use of 1.1 times the first mode participation factor. The effects of inelasticity on roof drift for the MDOF structures are consistent with and similar to the effects observed for SDOF systems. For the period range considered, inelasticity tended to cause peak drifts to be about 70 to 80% of the elastic values, at the median level. The MDOF inelasticity factor tended to become smaller with an increase in roof drift. This was explained as possibly being the result of a concentration of interstory drift demand in a few stories leading to a reduction in roof drift. Gupta and Krawinkler (2000b) find that P-Delta is a relatively benign phenomenon except in the instance when the ground motion drives the structure into the range of global negative post-yield stiffness, at which point large increases in displacement may occur. The ratio of peak story drift to peak roof drift is strongly dependent on the ground motion and structure characteristics. Median values of this ratio increase from about 1.2 for low-rise structures to 2.0 for mid-rise structures to about 2.5 to 3.0 for tall structures, for the structures and motions considered. The drift patterns observed for these structures suggest that a common drift distribution that can be generalized does not exist.

Foutch and Shi (1998) report the results of nonlinear dynamic analyses of steel frame buildings for the SAC steel program in which the beam plastic hinges were modeled with different load-deformation models. Steel moment frame buildings were analyzed that ranged from 3 to 9 stories in height. Eight hysteretic models were considered for the beam plastic hinges: bilinear (with and without strength degradation), stiffness degrading (with and without strength degradation), pinched stiffness degrading (with and without strength degradation), fracturing, and bilinear elastic. The plastic hinge model did affect response histories at the connections. The effect on the maximum story ductility demand relative to the maximum story ductility demand for the non-degrading bilinear model is as follows: a maximum increase of 10-20% for the non-pinching hysteretic models, a maximum increase of 20-30% for the pinching hysteretic models, and a maximum increase of 30-50% for the bilinear elastic model (which has no hysteretic energy dissipation). The Foutch and Shi results may be applicable to buildings that develop desirable mechanisms. Aschheim expects that a weak-story system having degrading column hinges would have much worse performance than the buildings described above.

Naeim et al (2000) also investigated the response of steel moment frame buildings for the SAC steel project. Three-, nine-, and twenty-story steel moment frame structures were investigated using a variety of hysteretic models. Stiffness degradation with slip or pinching was modeled in addition to bilinear response. Strength deterioration was modeled but results were not described. Severe stiffness deterioration increased interstory drifts and residual interstory drifts, with interstory drifts often increasing in the upper stories, and sometimes reducing in the lower stories. The authors suggest this may be attributed to higher modes causing the upper stories to go through many more cycles of sufficient amplitude to be affected by deterioration of the load-deformation response. The observed increases tended to be larger than those observed by Foutch and Shi. Stiffness degradation generally reduced force demands. Slip often reduced lower- and upper-story interstory drift demands, although increases were observed for some combinations of building height, city, and ground motion intensity level. Slip tended to decrease story shears and overturning moments.

Iwan et al. (2000) used a shear beam building model to compare the Capacity-Spectrum Method with nonlinear dynamic analysis for near-field motions. They find that for structural periods shorter than the ground pulse duration, the MDOF model exhibits a fundamental mode type of response, and higher mode contributions to drift and shear demands are negligible. For long period structures, the large displacement and velocity pulses of near field records cause greater participation of the higher modes, resulting in the potential for very

misleading results if a single mode analysis is used. Large interstory drifts were observed at the base, during the forward movement of the ground motion, and were again observed at the upper stories during a large reversal of the ground motion, associated with wave propagation through the structure. This latter case is not associated with the development of the maximum roof drift and does not correspond to a first mode shape. Thus, a fundamental mode analysis would not detect these effects. The investigators conclude that the use of a single-mode "equivalent" system provided a reasonable estimate of the maximum roof displacement regardless of building period, degree of nonlinearity, or distribution of stiffness, even for pulse type motions; but estimates of interstory drift for tall buildings (fundamental period significantly greater than the ground pulse duration) were poor, particularly in the upper stories.

### *A.3.7 Pushover Analysis*

Nonlinear static (pushover) analysis is used to quantify the resistance of the structure to lateral deformation and to gauge the mode of deformation and intensity of local demands. Various techniques have been recommended, including the use of constant lateral force profiles and the use of adaptive and multimodal approaches. Pushover techniques provide useful information on the overall characteristics of the structural system and can be used to identify some (but not necessarily all) of the likely mechanisms. Because the prescribed loading used in pushover analyses can not represent the potential range of loading experienced in dynamic response, the results obtained by pushover analyses at best represent an approximation of the nonlinear behavior expected to develop in the response to earthquake ground motions. The applicability of pushover analyses is less clear for systems having discontinuities in strength and stiffness. Results may be misleading where multiple collapse mechanisms potentially may develop because mechanism strengths are not well separated, or where different modes of behavior potentially may develop (higher modes cause demands to approach or exceed the capacities of strength-controlled components).

Pushover techniques are useful to estimate peak displacement response in conjunction with the use of "equivalent" SDOF systems. While higher modes typically have a small or negligible contribution to displacements, higher modes can significantly affect interstory drifts, plastic hinge rotations, story shears, and overturning forces. The contribution to interstory drifts stems directly from the higher mode shapes being more tortuous and therefore having a greater contribution to interstory drift. Consequently, estimates of interstory drift based on a first mode pushover analysis is prone to be inaccurate as the number of stories and period increases. Pushing to a target displacement will not necessarily develop the maximum interstory drifts in each story because the maximum values in each story do not occur simultaneously, and the sum of the individual maximum interstory drifts may be twice the peak roof displacement, depending on the mechanism that develops (Krawinkler). Some evidence suggests that pushovers tend to overestimate weak story drifts.

The application of lateral forces in a pushover analysis is preferred to applying a prescribed displacement pattern because the former allows softening of the structure to develop and allows story collapse mechanisms to develop. Many techniques involving application of lateral forces have been used. The simplest technique uses a fixed lateral force profile, with lateral forces being proportional to the mass and mode shape amplitude at each floor. An updated load vector would be more likely to identify concentrations of damage, although this presumes that first mode response is dominant. These techniques update the lateral force profile to adapt to the softening structure by using a step-wise lateral force profile that is modified from the first mode pattern to account for higher modes or by combining the results obtained from independent pushover analyses in each of several modes. Adaptive techniques that update the lateral load vector can make the updated load vector be proportional to the current displaced shape or to the current first mode (based on the current stiffness properties of the structure) or may make the increment in lateral loads proportional to the current displaced shape or mode shape. The displaced shape changes more quickly than does the mode shape (Valley). Inconsistencies can be introduced if the load vector is updated without updating the mode participation and mass participation factors used for determining the properties of the "equivalent" SDOF system. Methods that consider higher modes must contend with uncertainty in the amplitudes and algebraic signs of the higher modes, along with their timing relative to the first mode peaks. The question of how simple or complex a pushover technique to use depends on one's analysis objectives. Simple techniques can provide very valuable but incomplete information, while techniques that are more complex are still unable to represent the full range of response that potentially may develop.

Valley and Harris (1998) describe the development of a static pushover curve by repeated elastic analyses, with members removed sequentially as deformations exceed the member yield or ultimate capacities, and with loads reapplied in accordance with updated Ritz vectors. Reinhorn describes multimodal procedures (1997) that rely on updated modal properties. Bracci et al. (1997) also determined demand estimates based on the instantaneous dynamic properties of the structure. Gupta and Kunnath (2000) coupled the use of the instantaneous dynamic properties and the elastic spectral ordinates of the ground motion to determine incremental lateral forces to be applied in the pushover analysis. More recently, Kunnath has looked at sums and differences of modes. Elnashai (2000) also has applied adaptive techniques that make use of the instantaneous modal properties, and is able to follow the $S_a$ vs $S_d$ plot obtained in Incremental Dynamic Analysis reasonably well. Reinhorn suggests that the multi-mode pushover force distribution can be simplified to a linear distribution that is unique for each structure. Kunnath reports that even adaptive pushover techniques fail to capture the response of some stories in some buildings.

Sasaki et al. (1998) perform pushover analyses independently in each of several modes using invariant lateral force distributions, to identify the potential for higher modes to cause mechanisms to develop. Black and Aschheim (2000) combined the peak displacements and interstory drifts determined independently for the first two modes using square-root-of-the-sum-of-the squares (SRSS) combinations, and observed significant disparities between the peak interstory drifts and the SRSS estimates. This procedure is termed a Modal Pushover Analysis (MPA) by Chopra and Goel (2001b), who consider up to three or five modes. Chopra suggests that SRSS combination rules may be used for all computed quantities (e.g. member forces and moments), not just displacements and interstory drifts. Chopra and Goel (2001c) demonstrate that median estimates of interstory drift of the SAC buildings are improved by the use of three modes for the 9-story buildings and five modes for the 20-story buildings, with baseline values established by nonlinear dynamic analysis. Errors in the interstory drift estimates were larger, in general, than the errors associated with response spectrum analysis of linear elastic buildings and were largest for the "Los Angeles" buildings, which generally had larger interstory drift responses than the "Seattle" and "Boston" buildings. Patterns of the distribution of median interstory drifts of the "Los Angeles" and "Seattle" 9- and 20- story buildings differed. Chopra and Goel (2001b) also put forward an Uncoupled Modal Response History Analysis (UMRHA), in which dynamic response histories determined for each "equivalent" SDOF system are summed algebraically in time, and maximum values are determined from the summed response history. If nonlinearities are absent, the MPA and UMRHA approaches are equivalent to the traditional response spectrum and linear dynamic analysis methods, respectively.

Iwan is working on load profiles to better predict spatial distribution of damage. Carr also is reported to be working on improved pushover techniques. Bracci recently has been doing pushovers on frames one story at a time. Deierlein suggested that one could apply a perturbation to a first mode load pattern, consisting of an additional force that is allowed to change its location over the height of the structure, to identify sensitivity in the development of the mechanism.

## A.4 Nonlinear Dynamic Procedures

### *A.4.1 Simplified Models*

Nakashima has described the use of simplified models for nonlinear dynamic analysis. Much like the "notional frames" used by Sozen and Lepage, the generic frame or "fishbone" model consists of a single column with beams at every floor level extending halfway towards an adjacent column, with a roller supporting each beam at midspan. The model allows beam plastic hinges and story mechanisms to develop, much as they can in complete frames. The generic frame model, however, does not determine actions on individual members of the frame (Otani).

### *A.4.2 Incremental Dynamic Analysis*

Incremental Dynamic Analysis (IDA) determines peak response quantities (e.g. roof drift) by a series of independent nonlinear dynamic analyses of a structure subjected to one or more scaled ground motions. The scale factor is increased successively from a small initial value, and peak response quantities are plotted against a measure of the ground motion intensity. Data from such analyses has been represented in two ways. Cornell and Krawinkler plot peak interstory drift as a function of the scaled $S_a$ at the fundamental period of the building ($S_a(T_1)$). Elnashai plots the peak roof displacement versus $S_a(T_1)$. Both investigators plot $S_a$ on the vertical axis and the response measure on the horizontal axis, to be consistent with the conventional plotting of deformations and displacements on the

abscissa and forces on the ordinate. Cornell has developed relationships between the nonlinear static pushover capacity curve and the IDA curve that are implemented in a spreadsheet, allowing an engineer to observe the influence of changes in the capacity curve on response parameters, based on relationships embedded in the spreadsheet. Because these relationships reflect the behavior of the structure, it seems they must change as the relative distributions of strength, stiffness, and mass of the structure vary.

The strength of the IDA is that it captures aspects of the dynamic behavior of the system, and when done for a sufficient number of ground motions, reflects a range of response that may result. Although investigators apparently have not used the technique to characterize the range of mechanisms that may potentially occur under different excitations, the ability to recover this information seems to be another benefit of this form of analysis. Interstory drifts are observed to increase dramatically when the intensity measure is large enough. Such an increase suggests the structure has reached its "capacity". This capacity might be viewed as the collapse limit as defined essentially by loss of dynamic stability as the intensity measure reaches higher levels. This is analogous to the capacity of a steel bar being measured by its ultimate strength, except that the capacity is expressed in terms of the spectral acceleration of a specific excitation waveform. Typically, there is substantial scatter in the capacities determined in this way, reflecting variability in the response of the structure to different excitations.

Concern has been expressed regarding (1) the validity of scaling the ground motion amplitude uniformly (because high frequencies attenuate more rapidly as distance from the fault increases), (2) the uncertainty in establishing an accurate structural model, (3) ambiguity in the definition of "capacity," with Cornell focusing on the interstory drifts and Krawinkler now focusing on the value of the intensity measure ($S_a(T_1)$) at which the response parameter seems to increase without limit, and (4) whether interstory drift is an appropriate parameter to monitor collapse, when collapse may be due to gravity loads acting, for example, after columns have failed in shear.

The IDA curves are interesting because of the peculiar dynamic response characteristics that are apparent in this representation, and may be useful for identifying variability in demands, the "capacity" of the structure, as well as the onset of collapse, subject to limitations on modeling. The usefulness of IDA for design verification has not been investigated as yet.

## A.5 Modeling Limitations

Accuracy in the estimate of response of a given structural model is of little value if the structural model itself is inaccurate. Issues relating to the accuracy of mathematical models used for estimating response include:

1. Evaluation of initial stiffness and strength.
2. Uncertainty and variation in the actual material properties and dimensions of the as-built structure.
3. Variation of the actual component strengths from calculated estimates.
4. The complexity of behaviors to be represented.
5. Limitations in the understanding and modeling of response to complex, inelastic loading histories.

Uncertainty in the initial stiffness and strength of a structure leads to further dispersion in the accuracy of the displacements estimated using the Capacity Spectrum and Displacement Coefficient Methods (Miranda). For reinforced concrete structures, there is ambiguity in how the period of vibration of the structure should be computed (Otani). An additional difficulty relates to actual compressive strengths exceeding the specified strength, leading to likely increases in the modulus of elasticity (Otani). Valley noted that of three tuned-mass-damper buildings that his firm designed, the estimate of period for one was sufficiently off that they had to redesign the tuned mass damper after construction. The Mexico City Building Code of 1976 reportedly considered a range of possible periods, in response to concerns raised by Rosenblueth (Chopra).

Choices made by structural engineers in modeling of a structure can affect computed response. Krawinkler recalled that in the SAC project, a centerline model of a 20-story building was found to collapse in the presence of P-Delta, but had drifts of no more than about 5% when panel zones and gravity columns were modeled. Krawinkler noted that different investigators using different computer codes obtained very different results when first modeling buildings for the SAC project. Only when assumptions were made consistent were the results more or less identical. Diaphragm flexibility generally has not been incorporated into simplified inelastic procedures; an approximate method is described by Nakaki (2000).

There are relatively few instances in which models have been developed of instrumented buildings that were heavily damaged by ground shaking. Kunnath et al. (2000) considered four instrumented buildings, of which two were moderately damaged. He finds that calibrating structural models to observed response is sensitive to mass and stiffness modeling assumptions. Kunnath reports that linear and nonlinear static procedures did not adequately predict interstory drift estimates, and no one procedure consistently gave good results. Islam et al. (1998) modeled the 7-story instrumented reinforced concrete building in Van Nuys, and found that extensive flexural cracking in the beams observed in the pushover analysis at the measured roof drift did not occur; the actual building had only minor flexural cracking at the lower level beams. Browning et al. (2000) report on the ability of various analysis procedures to estimate peak drifts and interstory drifts of this building, and the difficulty in matching locations of column shear failure.

Multiple actions (e.g. axial, shear, and flexural) result in inelastic behaviors that are not well-understood and represented poorly in analysis software. Modeling of collapse requires careful attention to component degradation and may require that the assumptions of small displacement theory be supplanted by large displacement theory. The accuracy of computed predictions of collapse has not been established; even the definition of a collapse limit state is ambiguous.

## A.6 Demand Characterization

The lack of an accepted and clearly-defined relationship between smoothed design spectra and the actual motions they ostensibly represent creates difficulties in (1) evaluating the accuracy of inelastic procedures, (2) assessing variability in response estimates, and (3) establishing design ground motions for use in performance-based earthquake engineering. Traditionally, smoothed design spectra were fit by judgment to the jagged elastic response spectra computed for real ground motions. Current approaches fit a smoothed design spectrum at $T = 1$ sec and at "short" periods, using values determined from a seismic hazard curve. The degree to which actual spectra may, and should, depart from a smoothed spectrum is not defined, yet the degree of variability surely affects the statistical distribution of peak displacements relative to estimates based on smoothed elastic response spectra. Scaling ground motions to precisely match a target design spectrum has been found to result in a systematic underestimate of inelastic response, because response amplitudes to the stronger ground motions are often disproportionately higher than those to weaker ground motions (Wen).

Cornell notes that demand is not a design spectrum but a set of earthquake events that cannot be collapsed into a single spectrum. Particularly for uniform hazard spectra, there does not seem to be a clear answer on how to choose records (Cornell). However, to represent record-to-record variability, it appears to be necessary to use recorded ground motions rather than synthetic motions. For design applications, Wen and Wu (2001) suggests using records based on regional seismicity—perhaps a Magnitude (M) 8 earthquake at 40 km, a few M7.5 earthquakes at 20 km, a few M6 earthquakes at closer distances, etc.

## A.7 Applicability for Performance-Based Earthquake Engineering and Design

### *A.7.1 Role for Inelastic Procedures*

Many researchers have focused on improving simplified analysis procedures with the goal of accurately representing response quantities determined in nonlinear dynamic analyses, with some operating under the notion that analysis and design are so intertwined that they cannot be separated. Other researchers view the role of analysis is to enable good design, acknowledging that even the best analyses are approximate and that approximate analyses are sufficient. Given uncertainty in the accuracy of the mathematical model of a structure and uncertainties in future ground motions, engineers often must rely on their judgment to interpret analytical results. There is a fundamental uncertainty in response amplitudes that applies to all analysis techniques because of variability in the $R$-$\mu$-$T$ relationship from one motion to another, and variability in the elastic spectral ordinates, timing, and algebraic signs of the higher modes. Because even the best analysis techniques are prone to uncertainty with regard to performance under future earthquakes, there may be a role to be played by simplified analysis techniques.

Simplified inelastic procedures can be used for preliminary proportioning and may also be useful for characterizing performance. Simple inelastic procedures can give good estimates of peak roof displacement, at least for regular structures in which response is dominated by the first mode under conditions where P-Delta effects are negligible. Estimates of interstory drift indices, story shears, and plastic rotations in relatively flexible buildings are prone to be inaccurate, due to higher mode

contributions. Therefore, inelastic analysis procedures may be useful as a first approximation and to indicate when analyses of higher precision are needed. Elastic analysis procedures also can serve this purpose, although one would expect inelastic procedures to provide higher fidelity. Inelastic analysis procedures could be used to encourage capacity design approaches in new design.

The profession is in the midst of a transition from force-based design approaches to displacement-based design approaches. A complete implementation of a displacement-based approach involves (1) determining displacement demand, (2) breaking down overall demand into local components, and (3) comparing local capacity to demand (Bonacci). Simplified inelastic procedures can be used to move from force-based approaches (which are very imprecise but were useful for proportioning structures) to displacement-based approaches. Bonacci urges caution in rushing too rapidly to compare local demands and capacities, and cites as an example the difficulty in evaluating whether a stiffener will buckle when we may be 50% off on $T_g$ and PGA (peak ground acceleration). The desire for accurate analytical results must be balanced against the significant uncertainties in deformation capacities (Krawinkler). Furthermore, complicated techniques may be misused by engineers that are unfamiliar with them (Krawinkler).

Foutch suggested that if inelastic analysis techniques are used, they should be simple enough to be useful for conceptual design. Reinhorn suggested that one might use a simple technique to proportion the structure, then iteratively adjust the relative distributions of strength to ensure undesirable mechanisms will not form, and then follow with a more complex procedure to develop statistics on response. Miranda suggested that a simplified static procedure would be useful with estimates of dispersion, followed by nonlinear dynamic analyses to assess simulated response statistics. Aschheim suggests a simple inelastic analysis technique could be used for preliminary design, with nonlinear dynamic analysis being used to develop response statistics only for those structures where this comparison is deemed necessary (e.g. substantial irregularities, high importance, or to satisfy client requirements).

Because of uncertainties in the effects of higher modes, any simple procedure will require that prescriptive provisions are used to ensure that (1) desirable mechanisms form, with plastic hinges having sufficient ductility capacity to absorb uncertainties in plastic rotation demands arising from the presence of higher modes, (2) undesirable mechanisms (e.g. weak story mechanisms) will not form, even under the influence of higher modes, and (3) force-controlled components or modes of behavior have sufficient strength that forces associated with higher modes do not cause brittle failures to result. Variability due to higher modes can be expected to be a function of the number of stories as well as the spectral amplitudes at the higher mode periods. The separation of strengths required to prevent brittle modes of failure and undesirable mechanisms depends in part on the variability of material strengths in the as-built structure and the variability of actual strengths relative to calculated estimates.

Otani expressed concern about safety in view of the scatter in displacement estimates. The Japanese are using a modified form of the Capacity-Spectrum Method for checking the performance of designs that satisfy other criteria. Wilson expressed concern that nonlinear response spectra are 1not applicable to multi-degree-of-freedom (MDOF) systems; response of 2D and 3D structures can and should be determined by nonlinear dynamic analysis, in part because only nonlinear dynamic analysis can really inform the engineer about the behavior of the systems being designed.

Lepage suggested that an iterative procedure could be used, wherein a variety of load patterns are used to determine a variety of deflected shapes and possibly a number of different mechanisms. If similar deflected shapes result, then the deflected shape would be used to determine the “equivalent” SDOF system for each of a suite of ground motions, recognizing that iteration will be required to identify the right shape to be used for different drift levels. Lepage also suggested an alternate approach in which linear estimates of roof displacement are coupled with a collapse mechanism analysis—if drifts concentrate in just a few stories, then all of the estimated drift would be assigned to those stories.

Otani notes that one could use a nonlinear static procedure to get design moments for beam hinge regions, and then apply a factor of safety to design the columns to prevent or limit the development of plastic hinges in the columns.

### *A.7.2 Design Formats*

Design procedures have been formulated for use with three different types of spectral representations. Direct

Displacement Based Design uses the concept of effective damping to establish response spectra that are plotted on the same axes (ADRS) used in the Capacity-Spectrum Method. The period of vibration (or stiffness) required to satisfy a performance objective is determined, along with a required strength. The use of effective damping is supplanted in design procedures recommended by Fajfar and by Chopra and Goel, who use inelastic spectra (based on $R$-$\mu$-$T$ relations) plotted on the same axes used in the Capacity-Spectrum Method to estimate peak displacements and to determine required strengths. Black and Aschheim (2000) used Yield Point Spectra (based on $R$-$\mu$-$T$ relations or the actual jagged spectra associated with design ground motions) to determine the strength required to satisfy multiple performance objectives using admissible design regions. An iterative approach was suggested in which nonlinear static analyses are avoided entirely by relying only on design strengths and elastic properties.

### *A.7.3 Quantities to be Determined and Measures of Performance*

There is uncertainty in estimates of both demands and capacities. Rather than compare very approximate values of local demands and capacities, some suggest that it may be preferable to focus on quantities that are of a more global nature, such as interstory drift (Goel). Estimates of deformation capacity are fairly crude. Krawinkler observed that the best measure of inelastic deformation capacity (e.g., total or plastic rotation, curvature ductility) has not even been identified yet.

One approach is to estimate peak interstory drifts as a factor times the average global roof drift. For regular buildings, the factor varies with the number of stories and may not follow a consistent pattern over the height of the building (Gupta and Krawinkler, 2000a), and may depend on the ground motion (MacRae). Uetani and Tagawa (1998) reportedly find that interstory drifts concentrate less in structures in which the eigenvalues obtained during the nonlinear response are more positive. Fenwick reportedly has introduced into the New Zealand Code an estimate of interstory drift equal to twice the drifts determined by elastic analysis. Interstory drifts for near-field motions appear to be related to ground motion reversals (Iwan), and might be better estimated using concepts of wave propagation theory rather than conventional modal response approaches.

The actual shears in a building can be significantly higher that those associated with development of capacity in the predominant mode. Dynamic shears, therefore, may be significantly higher than estimated by pushover analysis. Rodriguez, Restrepo, and Carr (2002) reportedly found the second and higher modes respond essentially elastically, contributing to the shears associated with inelastic first mode response. Forces in reinforced concrete collectors may be poorly estimated by typical procedures because their larger stiffness in compression causes greater force to be carried in compression than in tension.

Kunnath notes that plastic hinge rotation demands are calculated differently in different software programs. The post-yield stiffness, hinge lengths, and use of distributed or concentrated plasticity affects the values, as do the different solution strategies used by the programs. Estimates of yield and plastic rotation are often based on assuming points of inflection occur at midspan, leading to errors of 50 to 100%. The approximate nature of the demands estimated by any procedure makes comparison with estimated capacities less certain; significant improvements are needed to improve the reliability of estimates of local demands and capacities, to make their comparison more meaningful.

### *A.7.4 Statistical Measures and Treatment of Uncertainty*

Performance may be evaluated in different ways and may include or exclude various types of uncertainties. For example, Wen determines the annual probability of exceeding drifts of various levels. Cornell's work for SAC focuses on the level of confidence in the hypothesis that the structure will satisfy a given performance objective, for ground motions that have a stated probability of exceedance. Uncertainty in the hazard is neglected in the SAC work, although Cornell et al. (2000) presents a theoretical formulation that accounts for uncertainty in the hazard. While it stands to reason that variations in capacities (strengths, deformation capacities) should have an influence on demands, current formulations neglect such interaction.

## A.8 References and Bibliography

Akkar, S., and Gulkan, P., 2000, "Comparative performance evaluation of displacement based design procedures for near field earthquakes," *Proceedings of the 12th World Conference on Earthquake Engineering*, New Zealand Society for Earthquake Engineering, Upper Hutt, New Zealand.

Albanesi, T., Nuti, C., and Vanzi, I., 2000, "A simplified procedure to assess the seismic response of nonlinear structures," *Earthquake Spectra*, Vol. 16, No. 4, Earthquake Engineering Research Institute, Oakland, California, pp. 715-734.

ASCE, 2000, *Prestandard and Commentary for the Seismic Rehabilitation of Buildings*, FEMA 356 Report, prepared by the American Society of Civil Engineers for the Federal Emergency Management Agency, Washington, D.C.

Aschheim, M., and Black, E.F., 2000, "Yield Point Spectra for seismic design and rehabilitation," *Earthquake Spectra*, Vol. 16, No. 2, Earthquake Engineering Research Institute, Oakland, California, pp. 317-335.

Aschheim, M.A., Maffei, J., and Black, E.F., 1998, "Nonlinear static procedures and earthquake displacement demands," *6th US National Conference on Earthquake Engineering, Seattle, Washington*, Earthquake Engineering Research Institute.

ATC, 1996, *Seismic Evaluation and Retrofit of Concrete Buildings*, ATC-40 Report, Volumes 1 and 2, Applied Technology Council, Redwood City, California.

ATC/BSSC, 1997, *NEHRP Guidelines for the Seismic Rehabilitation of Buildings*, FEMA 273 Report *(Guidelines)* and FEMA 274 Report *(Commentary)*, prepared by the Applied Technology Council for the Building Seismic Safety Council, published by the Federal Emergency Management Agency, Washington, D.C.

Baez, J.I., and Miranda, E., 2000, "Amplification factors to estimate inelastic displacement demands for the design of structures in the near field," *Proceedings of the 12th World Conference on Earthquake Engineering*, New Zealand Society for Earthquake Engineering, Upper Hutt, New Zealand.

Black, E.F., and Aschheim, M., 2000, *Seismic Design and Evaluation of Multistory Buildings using Yield Point Spectra*, CD Release 00-04, Mid-America Earthquake Center, University of Illinois, Urbana.

Blume, J.A., Newmark, N.M., and Corning, L.H., 1961, *Design of Multistory Reinforced Concrete Buildings for Earthquake Motions*, Portland Cement Association, Skokie, Illinois.

Bracci, J.B., Kunnath, S.K., and Reinhorn, A.M., 1997, "Seismic performance and retrofit evaluation of reinforced concrete structures," *Journal of Structural Engineering*, Vol. 123, American Society of Civil Engineers, pp. 3-10.

Browning, J., 2000, "Implications of a proportioning method for earthquake-resistant RC frames subjected to strong ground motion," *Proceedings of the 12th World Conference on Earthquake Engineering*, New Zealand Society for Earthquake Engineering, Upper Hutt, New Zealand.

Browning, J., Li, R., Lynn, A., and Moehle, J.P., 2000, "Performance assessment for a reinforced concrete frame building," *Earthquake Spectra*, Vol. 16, No. 3, Earthquake Engineering Research Institute, Oakland, California, pp. 541-555.

Chopra, A.K., and Goel, R.K., 1999a, *Capacity-Demand Diagram Methods for Estimating Seismic Deformation of Inelastic Structure: SDF Systems*, Report No. PEER-1999/02, Pacific Earthquake Engineering Center, University of California, Berkeley.

Chopra, A.K., and Goel, R.K., 1999b, "Capacity-demand diagram methods based on inelastic design spectrum," *Earthquake Spectra*, Vol. 15, No. 4, Earthquake Engineering Research Institute, Oakland, California, pp. 637-656.

Chopra, A.K., and Goel, R.K., 2001a, "Direct displacement based design: use of inelastic vs. elastic design spectra," *Earthquake Spectra*, Vol. 17, No. 1, Earthquake Engineering Research Institute, Oakland, California, pp. 47-64.

Chopra, A.K., and Goel, R.K., 2001b, *A Modal Pushover Analysis Procedure to Estimate Seismic Demands for Buildings: Theory and Preliminary Evaluation*, Report No. PEER 2001/03, Pacific Earthquake Engineering Research Center, University of California, Berkeley.

Chopra, A.K., and Goel, R.K., 2001c, "Modal pushover analysis of SAC buildings," *Third U.S.-Japan Workshop on Performance-Based Earthquake Engineering Methodology for Reinforced Concrete Building Structures*, August 16-18, Seattle, Washington.

Cornell, C.A., Vamvatsikos, D., Jalayer, F., and Luco, N., 2000, "Seismic reliability of steel frames," *Proceedings of the 9th IFIP WG 7.5 Working Conference on Reliability and Optimization of Structural Systems*, Ann Arbor, Michigan.

Cuesta, I., and Aschheim, M., 2001, *Using Pulse R-Factors to Estimate Structural Response to Earthquake Ground Motions*, CD Release 01-03, Mid-

America Earthquake Center, University of Illinois, Urbana.

Cuesta, I., Aschheim, M., and Fajfar, P., 2003, "Simplified R-factor relationships for strong ground motions," *Earthquake Spectra*, Vol. 19, No. 1, Earthquake Engineering Research, pp. 22-45

Elnashai, A.S., 2000, "Advanced inelastic static (push-over) analysis for seismic design and assessment," *G. Penelis International Symposium on Concrete and Masonry Structures*, Aristotle University of Thessaloniki, Thessaloniki, Greece, pp. 23-34.

Fajfar, P., 1999, "Capacity-Spectrum Method based on inelastic demand spectra," *Earthquake Engineering and Structural Dynamics*, Vol. 28, pp. 979-993.

Fajfar, P., and Gaspersic, P., 1996, "The N2 method for the seismic damage analysis of RC buildings," *Earthquake Engineering and Structural Dynamics*, Vol. 25, No. 1, pp. 31-46.

Filiatrault, A., and Folz, B., 2001, "Performance-based seismic design of wood framed buildings," accepted for publication in *Journal of Structural Engineering*, American Society of Civil Engineers.

Foutch, D.A, and Shi, S., 1998, "Effects of hysteresis type on the seismic response of buildings," *Proceedings of 6th U.S. National Conference on Earthquake Engineering*, Seattle, Washington, Earthquake Engineering Research Institute, Oakland, California.

Gulkan P., and Sozen, M.A., 1974, "In-elastic responses of reinforced concrete structures to earthquake motions," *Proceedings of the American Concrete Institute*, Vol. 71, No. 12, pp. 605-610.

Gupta, A., and Krawinkler, K., 1998, "Effect of stiffness degradation on deformation demands for SDOF and MDOF structures," *6th US National Conference on Earthquake Engineering*, Seattle, Washington, Earthquake Engineering Research Institute, Oakland, California.

Gupta, A., and Krawinkler, K., 2000a, "Estimation of seismic drift demands for frame structures," *Earthquake Engineering and Structural Dynamics*, Vol 29, pp. 1287-1305.

Gupta, A., and Krawinkler, K., 2000b, "Dynamic p-delta effects for flexible inelastic structures," *Journal of Structural Engineering*, Vol. 126, No. 1, American Society of Civil Engineers.

Gupta, B., and Kunnath, S.K., 1998, "Effect of hysteretic model parameters on inelastic seismic demands," *6th US National Conference on Earthquake Engineering, Seattle, Washington*, Earthquake Engineering Research Institute.

Gupta, B., and Kunnath, S.K., 2000, "Adaptive spectra-based pushover procedure for seismic evaluation of structures," *Earthquake Spectra*, Vol. 16, No. 2, Earthquake Engineering Research Institute, Oakland, California, pp. 367-391.

Han, S.W., and Wen, Y.K., 1997, "Method of reliability-based seismic design. I: Equivalent nonlinear system," *Journal of Structural Engineering*, Vol. 123, American Society of Civil Engineers, pp. 256-265.

Hudson, D.E., 1965, "Equivalent viscous friction for hysteretic systems with earthquake-like excitations," *3rd World Conference on Earthquake Engineering, New Zealand*, pp. II:185-201.

Islam, M.S., Gupta, B., and Kunnath, S., 1998, "A critical review of state-of-the-art analytical tools and acceptance criterion in light of observed response of an instrumented nonductile concrete frame building," *Proceedings of* 6th *U.S. National Conference on Earthquake Engineering*, Seattle, Washington, Earthquake Engineering Research Institute, Oakland, California.

Iwan, W.D., and Gates, N.C., 1979, "Estimating earthquake response of simple hysteretic structures," *Journal of the Engineering Mechanics Division*, Vol. 105, EM3, American Society of Civil Engineers, pp. 391-405.

Iwan, W.D., Huang, C.T., and Guyader, A.C., 2000, "Important features of the response of inelastic structures to near-field ground motion," *Proceedings of the 12th World Conference on Earthquake Engineering*, New Zealand Society for Earthquake Engineering, Upper Hutt, New Zealand.

Jacobsen, L.S., 1930, "Steady forced vibrations as influenced by damping," *Transactions ASME*, Vol. 52 (APM), pp. 169-181.

Judi, H.J., Davidson, B.J., and Fenwick, R.C., 2000, "The direct displacement based design method: a damping perspective," *Proceedings of the 12th World Conference on Earthquake Engineering*, Auckland, New Zealand Society for Earthquake Engineering, Upper Hutt, New Zealand.

Krawinkler, H., and Alavi, B, 1998, "Development of improved design procedures for near fault ground motions," *Proceedings, SMIP98 Seminar on Utilization of Strong-Motion Data*, Oakland, California.

Kunnath, S. K., and Gupta, B., 2000, "Validity of deformation demand estimates using nonlinear static procedures," *Proceedings of the U.S.-Japan Workshop on Performance-Based Engineering of Reinforced Concrete Building Structures*, Sapporo, Hokkaido, Japan.

Kunnath, S.K., Nghiem, Q., John Jr., A., and El-Tawil, S., 2000, "Validation of evaluation methods and acceptance criteria in evolving performance-based seismic codes," *Proceedings, SMIP2000 Seminar on Utilization of Strong-Motion Data:* Sacramento, California, September 14, 2000, California Division of Mines and Geology, Sacramento, pp. 39-63.

Lepage, A., 1998, "Nonlinear drift of multistory RC structures during earthquakes," *Proceedings, 6th U.S. National Conference on Earthquake Engineering*, Earthquake Engineering Research Institute, Oakland, California.

Lew, H.S., and Kunnath, S.K., 2000, "Evaluation of analysis procedures for performance-based seismic design of buildings," *Proceedings of the 12th World Conference on Earthquake Engineering*, Auckland, New Zealand Society for Earthquake Engineering, Upper Hutt, New Zealand.

MacRae, G., and Tagawa, H., 2001, *Methods to Estimate Displacements of PG&E Structures*, draft report on research conducted under PGE/PEER Task No. 505, University of Washington.

Miranda, E., 2000, "Inelastic displacement ratios for structures on firm sites," *Journal of Structural Engineering*, Vol. 126, No. 10, American Society of Civil Engineers, pp. 1150-1159.

Miranda, E., 2001, "Estimation of Inelastic Deformation Demands of SDOF Systems," *Journal of Structural Engineering*, Vol. 127, No. 9, American Society of Civil Engineers, pp, 1005-1012.

Miranda, E., and Bertero, V., 1994, "Evaluation of strength reduction factors for earthquake-resistant design", *Earthquake Spectra*, Vol. 10, No. 2, Earthquake Engineering Research Institute, Oakland, California, pp. 357-379.

Mwafy, A.M., and Elnashai, A.S., 2001, "Static pushover versus dynamic collapse analysis of RC buildings," *Engineering Structures*, Vol 23, pp. 407-424.

Naeim, F., Skliros, K., and Reinhorn, A.M., 2000, "Influence of hysteretic deteriorations in seismic response of multistory steel frame buildings," *Proceedings of the 12th World Conference on Earthquake Engineering, Auckland*, New Zealand Society for Earthquake Engineering, Upper Hutt, New Zealand.

Nakaki, S., 2000, *Developing Design Guidelines for Precast Concrete Diaphragms*, Earthquake Engineering Research Institute, Oakland, California.

Nakashima, M., Ogawa, K., and Inoue, K., 2002, "Generic frame model for simulation of earthquake responses of steel moment frames," *Earthquake Engineering and Structural Dynamics.*

Otani, S., 2000, "New seismic design provisions in Japan," *Proceedings of the U.S.-Japan Workshop on Performance-Based Earthquake Engineering for Reinforced Concrete Building Structures*, Sapporo, Japan.

Paret, T.F., Freeman, S.A., and Dameron, R.A, 2002, "Rethinking the earthquake engineering paradigm: from response reduction to response suppression," *Proceedings, Seventh U.S. National Conference on Earthquake Engineering*, Earthquake Engineering Research Institute, Oakland, California.

Qi, X., and Moehle, J.P., 1991, *Displacement Design Approach for Reinforced Concrete Structures Subjected to Earthquakes*, Report No. UCB/EERC-91/02, Earthquake Engineering Research Center, University of California, Berkeley.

Reinhorn, A., 1997, "Inelastic techniques in seismic evaluations," in *Seismic Design Methodologies for the Next Generation of Codes*, Fajfar, P., and Krawinkler, H., eds., Bled, Slovenia.

Rodriguez, M.E., Restrepo, J.I., and Carr, A.J., 2002, "Earthquake-induced acceleration in buildings," *Earthquake Engineering and Structural Dynamics*, Vol. 31, pp. 693-718.

Rothe, D., and Sozen, M.A., 1983, *A SDOF Model to Study Nonlinear Dynamic Response of Large- and Small-Scale R/C Test Structures*, Structural Research Series No. 512, Department of Civil Engineering, University of Illinois at Urbana-Champaign, Urbana, Illinois.

Sasaki, K.K. Freeman, S.A., and Paret, T.F., 1998, "Multi-Mode pushover procedure (MMP) -- a method to identify the effects of higher modes in a pushover analysis," *Proceedings, Sixth U.S. National Conference on Earthquake Engineering*, Seattle, Washington, Earthquake Engineering Research Institute, Oakland, California.

Song, J.K., and Pincheira, J.A., 2000, "Spectral displacement demands of stiffness and strength degrading systems," *Earthquake Spectra*, Vol. 16,

No. 4, Earthquake Engineering Research Institute, Oakland, California, pp. 817-851.

Tagawa, H., and MacRae, G., 2001, "Capacity spectra method for estimating SDOF oscillator demands," *Proceedings of the 2001 Structures Congress & Exposition*, American Society of Civil Engineers, Washington, D.C.

Tsopelas, P., Constantinou, M.C., Kircher, C.A., and Whittaker, A.S., 1997, *Evaluation of Simplified Methods of Analysis of Yielding Structures*, Technical Report NCEER-97-0012, National Center for Earthquake Engineering Research, State University of New York, Buffalo, New York.

Uetani, K., Tagawa, H., 1998, "Criteria for suppression of deformation concentration of building frames under severe earthquakes," *Engineering Structures*, Vol. 20, No. 4-6, pp. 372-383.

Vidic, T., Fajfar, P., and Fischinger, M., 1994, "Consistent inelastic design spectra: strength and displacement," *Earthquake Engineering and Structural Dynamics*, Vol. 23, pp. 507-521.

Villaverde, R., 1996, "Simplified response spectrum analysis of nonlinear structures," *Journal of Engineering Mechanics*, Vol. 122, American Society of Civil Engineers, pp. 282-285.

Valley, M.T., and Harris, J.R., 1998, "Application of modal techniques in a pushover analyses," *Proceedings, Sixth U.S. National Conference on Earthquake Engineering*, Seattle, Washington, Earthquake Engineering Research Institute, Oakland, California.

Vamvatsikos, D., and Cornell, C.A., 2001, "Incremental dynamic analysis," submitted to *Earthquake Engineering and Structural Dynamics*.

Wen, Y. K., and Wu, C.L., 2001, "Uniform Hazard Ground Motions for Mid-America Cities," *Earthquake Spectra*, Vol. 17, No. 2, Earthquake Engineering Research Institute, Oakland, California, pp. 359-384.

# B. Summary of Practice using Inelastic Analysis Procedures

## B.1 Introduction

The state of practice inquiry conducted under Phase I of the ATC-55 Project sought information about the use of inelastic analysis procedures for a broad sample of building applications from different practicing structural engineering firms. Respondees were asked to provide information on the following:

- types of buildings and structural systems for which the procedures are used;
- procedures used;
- software used for analysis, if any; and
- Engineers' thoughts about the implementation of procedures, including problems encountered.

This appendix summarizes the information obtained from practicing engineers who responded to the state of practice inquiry, and the relation of their responses to the issues identified by the ATC-55 project team. The information was solicited through three primary means. First, a project web page was established and advertised to practitioners through e-mail and notices in professional newsletters. The website contained a "Summary of Practice Building Data" questionnaire form for completion by each respondent for each building example to be submitted. Second, the ATC-55 project team appealed directly by e-mail to a number of engineering firms, some of whom were known to have experience with inelastic analysis procedures. Finally, the e-mail requests were followed with personal telephone calls. The solicitations took place during the spring and summer of 2001. Information on over 60 examples was obtained from 23 respondents in 12 different structural engineering offices.

## B.2 Typical Buildings and Structural Systems

The example buildings submitted by engineers who responded to the ATC solicitation encompassed a broad range of building types, structural systems, and foundation systems. Following are the percentages of the total example building population by ownership type, purpose of analysis, year of construction, height, and floor area. The percentages of example buildings by seismic (lateral-force resisting) system, by gravity force resisting system, and by foundation type are provided in Table B-1, Table B-2, and Table B-3, respectively.

Ownership Type

| | |
|---|---|
| Private: | 42% |
| Institutional | 52% |
| Unspecified | 6% |

Purpose of Analysis

| | |
|---|---|
| Evaluation only | 32% |
| Upgrade or Evaluation/Upgrade | 41% |
| New | 27% |

Year of Construction

| | |
|---|---|
| Earliest | 1916 |
| Latest | 2001 |
| Mean | 1935 |

Height (stories)

| | |
|---|---|
| 1-2 | 15% |
| 3-6 | 36% |
| 7-11 | 28% |
| 12+ | 21% |

Floor Area (sf)

| | |
|---|---|
| < 10,000 | 3% |
| 10,000 – 50,000 | 14% |
| 50,000 – 100,000 | 19% |
| 100,000 – 200,000 | 60% |
| 200,000 – 500,000 | 2% |
| > 500,000 | 2% |

## B.3 Inelastic Analysis Procedures

The procedures used by the respondents included the following:

- FEMA 273/356 (Coefficient Method)
- Nonlinear response history analysis

**Table B-1 Seismic Systems of Example Buildings Submitted by Respondees**

| *Seismic System(s)* | *Number* | *Percentage of Total* |
|---|---|---|
| Concrete shear walls | 17 | 29% |
| Concrete moment frame | 9 | 15% |
| Concrete frame/brick infill | 6 | 10% |
| Steel CBF (concrete braced frame) | 3 | 5% |
| Steel EBF (eccentric braced frame) | 4 | 7% |
| Steel BRBF (unbonded braced frame) | 2 | 3% |
| Steel moment frame | 6 | 10% |
| Steel frame/brick infill | 3 | 5% |
| Steel truss moment frame | 1 | 2% |
| Plywood or OSB shear walls | 3 | 5% |
| Reinforced masonry walls | 1 | 2% |
| Passive damped frame | 1 | 2% |
| Other | 3 | 5% |

**Table B-2 Gravity Systems of Example Buildings Submitted by Respondees**

| *Gravity System(s)* | *Number* | *Percentage of Total* |
|---|---|---|
| Concrete columns/ beams and/or slab | 22 | 37% |
| Concrete bearing walls | 2 | 3% |
| Wood frame | 5 | 8% |
| Steel frame /wood infill | 2 | 3% |
| Steel frame/concrete slab | 24 | 41% |
| Other | 4 | 7% |

- FEMA 351/SAC method
- ATC-40 (Capacity-Spectrum Method)
- Unspecified nonlinear static

A number of the respondents used two or more procedures for the same building example. The number of primary uses of each procedure (i.e., not accounting for secondary procedures), and the respective percentage of the total number of buildings are listed in Table B-4.

**Table B-3 Foundation Systems of Example Buildings Submitted by Respondees**

| *Foundation System(s)* | *Number* | *Percentage of Total* |
|---|---|---|
| Spread Footings | 32 | 55% |
| Mat | 9 | 15% |
| Piles | 13 | 22% |
| Drilled Piers | 3 | 5% |
| Unknown/Other | 2 | 3% |

**Table B-4 Inelastic Analysis Procedures**

| *Primary Procedure* | *Number* | *Percentage of Total* |
|---|---|---|
| FEMA 273/356 (Coefficient Method) | 21 | 36% |
| Nonlinear response history analysis | 12 | 20% |
| FEMA 351/SAC method | 3 | 5% |
| ATC-40 (Capacity-Spectrum Method) | 8 | 14% |
| Unspecified nonlinear static[1] | 15 | 25% |
| Multiple of above procedures | 8 | 14% |

1. The heading "Unspecified nonlinear static" indicates entries such as "NSP," "CSM," and "Equal Displacement." It was noted that most such entries were associated with analyses that were implemented prior to the publication of ATC-40 and FEMA 273. Several examples cited the use of the Miranda-Bertero procedure, and one example cited the Army TM-5-809-10-1 document.

## B.4 Software

With one exception, the inelastic procedures were implemented with the aid of computer analysis software. Table B-5 lists the programs used, the number of listings of each program name, and the percentage of listings of the total number of program usage listings.

Several examples utilized multiple linear elastic analyses with sequential stiffness modification to represent progressive yielding and degradation. These applications utilized extensive spreadsheet bookkeeping to sum member forces and check member demands against capacities from one analysis to the next.

**Table B-5 Computer Program Usage**

| *Program Name* | *Number of Listings* | *Percentage of Listings* |
|---|---|---|
| ABAQUS | 1 | 1% |
| ANSYS | 3 | 5% |
| CASHEW / RUAUMOKO | 3 | 5% |
| (Custom software) | 6 | 9% |
| DRAIN 2D | 9 | 14% |
| DRAIN 2DX | 8 | 12% |
| ETABS | 3 | 5% |
| FEM-I | 2 | 3% |
| FEM-II | 1 | 1% |
| SAP 90 | 6 | 9% |
| SAP 2000 | 24 | 35% |
| Other | 1 | 1% |
| **Total Listings** | **66** | |

## B.5 Implementation Issues

A total of 65 comments were submitted relating to the implementation of the inelastic procedures. A synopsis of the respondents' comments on major issues follows:

The majority of the comments submitted were related to the relative accuracy of procedures. Engineers' preoccupation with the topic of relative accuracy was indicated by the techniques used, such as variation of parameters (or "bounding"), by comments about the sensitivity of procedures to various assumptions, and by the implementation of comparative analyses using multiple procedures for the same building. Significantly, the large variation in ground motion parameters was not mentioned in any of the practitioners' comments, although one respondent expressed doubt in the validity of using a static procedure to represent the effect of ground motion at a near-field location. Three of the example buildings were full-scale test specimens of wood buildings that were shaken on a simulator and evaluated using a nonlinear response history analysis procedure, for the purpose of research and comparison. Several of the respondents commented on the difficulty of reasonably accounting for cyclic degradation and P-delta effects with existing procedures and/or software. Also, difficulty in establishing a suitable target displacement or ultimate drift was mentioned in two examples.

It is evident that some respondents question the appropriateness of procedures to determine the target displacement. One respondent wrote "FEMA 273 shear strain ratios [were] exceeded in local areas – deemed not to be hazardous." Another wrote "Immediate Occupancy provisions [of FEMA 273] are too conservative." A third wrote "Analysis was straightforward. Determination of target displacement was problematic."

There were several comments regarding the complexity of the procedures. For example, one respondent wrote "The most troublesome problem in implementing the FEMA [273] procedures was developing nonlinear hinge properties (strength and ductility)." Another wrote: "The shear capacity of the concrete columns was difficult to evaluate by the FEMA 273 methods (Eq. 6-4) due to constantly changing parameters." A third wrote: "Convergence was difficult to achieve even for a relatively simple model and depended greatly on the method of solution used."

Several respondents commented during verbal discussions that the established analysis procedures did not allow the evaluation of behavior in the range of severe damage prior to collapse, such as damage to many structures observed in postearthquake reconnaissance.

Several respondents indicated that the results of inelastic procedures are very sensitive to assumptions regarding such parameters as initial stiffness, and pushover loading profile. There is also recognition among respondents that the dynamic and multi-degree-of-freedom (MDOF) effects that would be captured in a nonlinear response history analysis procedure could be quite different from the results of a nonlinear static procedure. Several respondents attempted to account for dynamic behavior, yielding, and MDOF effects by such techniques as adapting pushover loading profiles and use of simplified dynamic analysis.

One respondent discussed the inability of static procedures to represent the response of structures to near-field earthquake pulse-type motions.

Two other respondents collaborated in a comparison of the Capacity Spectrum approach for a single-degree-of-freedom system with nonlinear response history analysis. They identified that the differences in results between the two methods could be largely explained by the dynamic response of the structure to the predominant velocity pulses in the time-history records. They developed a simplified technique to calculate the single-

degree-of-freedom (SDOF) dynamic displacement response for a single velocity pulse, and applied this technique to several structures, evaluating the response of each structure to various pulses for site-specific ground motion records.

One respondent questioned the validity of static procedures for high-rise buildings that would experience significant higher mode components in their response.

There seems to be a lack of understanding among practitioners about how to represent MDOF effects for static procedures. Only one respondent commented about the sensitivity of the static solution to such parameters as initial period and pushover profile. Another used an adaptive load pattern based on modal response at each significant step in the analysis process. A third simply assumed that all stories experienced equal drift.

## B.6 Use of Limitations on Coefficient $C_1$ in FEMA 356

FEMA 356 currently contains arbitrary limitations (caps) on the maximum value of the coefficient $C_1$. This cap tends to reduce the predicted inelastic displacement of relatively short period structures. At an early stage of the second phase of the ATC-55 project, it became apparent that the cap might influence the accuracy of the Coefficient Method. While there may be valid reasons that the response of short-period structures varies from that predicted by current analysis procedures, it seemed that the arbitrary nature of the cap conflicted with the goals of the project. In an effort to gauge qualitatively how this issue affected current practice, the project team contacted twelve practicing engineers from seven different firms from the respondents to the Phase I Practice Study. These individuals and firms are representative of a relatively high level of seismic expertise among practitioners. Three basic questions were posed:

a. Do you use the cap?

b. Why, or why not?

c. What are your thoughts and understanding on this choice?

All but a few engineers follow the same procedure. First they calculate $C_1$ using the empirical equation. If this value is less than 1.5, they use it. If it is higher, they use 1.5. Thus the practice is to neglect the interpolation allowed between 0.10 sec and $T_s$. The pervasive attitude was that they use the cap because it is allowed. Very few were aware of the discussion on this issue in FEMA 273/274/356/357. These were the same few who tended not to use the cap.

## B.7 Practical Guidance and Education

Respondents provided feedback (either in writing, verbally, or implicitly) about the following topics or questions related to the issue of practical guidance and education:

- *The various methods lead to different results. Why?*

It is evident that practicing engineers do not necessarily know why the various NSP methods result in different answers, or why the answers may differ significantly from those resulting from the use of nonlinear response history analysis. Consequently, engineers may lack a way to answer the next item:

- *Which method is the most effective for a given project?*

Respondents indicated that there is a general lack of understanding about how to select a method. In numerous cases, the methods had been dictated by the owner/client. For instance, FEMA 273 is quickly being adopted as the governing guideline by government agencies and is therefore required for evaluations and design of government-funded retrofits.

- *Certain guidelines or evaluation techniques require an impractical amount of effort.*

Some engineers indicated that they chose to adopt an approach using sequential elastic analyses to developing a "backbone" resistance curve for their pushover analysis. In some cases a cumbersome amount of "bookkeeping" was required to keep track of individual member stresses, and to compare these stresses with estimated stress or strain capacities as they changed the model to simulate yielding or degradation.

- *What is the most efficient way to compute results for a given method?*

Based on responses received, it is evident that practicing engineers have searched for efficient ways to handle the large amount of computational effort required for nonlinear analysis.

- *More effective software tools are needed.*

Some respondents indicated that the software programs they currently use for inelastic analysis are sometimes

difficult to use, or do not allow the user to model important aspects of the structure, such as degradation.

Other issues identified related to practical guidance and education, including the following:

- Clients who require these evaluations need to be educated about effort and fees required. Normally, this information comes from the engineer. However, without sufficient experience, the engineer would not be able to accurately estimate the required effort. This relates to the next issue:
- Some practicing engineers have embraced these methods as an improvement. Others have avoided them as requiring a steep learning curve and more effort, with an uncertain outcome. The methods are therefore more risky for the owner as well as the engineer.

# C. Supplemental Data on the Evaluation of Current Procedures

This appendix supplements Chapter 3 on the evaluation of current nonlinear static procedures. The contents are summarized as follows: Section C.1 tabulates the ground-motion data used for the evaluation; Section C.2 presents the results of the response history analyses of the oscillators; Section C.3 presents data on the results of the evaluation of the ATC-40 version of the Capacity Spectrum Method; and Section C.4 presents data on the results of the evaluation of the Coefficient Method of FEMA 356.

## C.1 Ground Motions

**Table C-1 Ground Motions Recorded on Site Class B**

| *Date* | *Earthquake Name* | *Magnitude (Ms)* | *Station Name* | *Station Number* | *Component (deg)* | *PGA ($cm/s^2$)* |
|---|---|---|---|---|---|---|
| 06/28/92 | Landers | 7.5 | Silent Valley, Poppet Flat | 12206 | 0 | 48.9 |
| 06/28/92 | Landers | 7.5 | Twentynine Palms Park Maintenance Bldg | 22161 | 0 | 78.7 |
| 06/28/92 | Landers | 7.5 | Amboy | 21081 | 90 | 146.0 |
| 10/17/89 | Loma Prieta | 7.1 | Point Bonita | 58043 | 297 | 71.4 |
| 10/17/89 | Loma Prieta | 7.1 | Piedmont, Piedmont Jr. High Grounds | 58338 | 45 | 81.2 |
| 10/17/89 | Loma Prieta | 7.1 | San Francisco, Pacific Heights | 58131 | 270 | 60.2 |
| 10/17/89 | Loma Prieta | 7.1 | San Francisco, Rincon Hill | 58151 | 90 | 88.5 |
| 10/17/89 | Loma Prieta | 7.1 | San Francisco, Golden Gate Bridge | 1678 | 360 | 228.6 |
| 10/17/89 | Loma Prieta | 7.1 | Hollister-SAGO vault | 1032 | 360 | 60.1 |
| 10/17/89 | Loma Prieta | 7.1 | South San Francisco, Sierra Point | 58539 | 205 | 102.7 |
| 10/17/89 | Loma Prieta | 7.1 | Berkeley, Lawrence Berkeley Lab. | 58471 | 90 | 114.8 |
| 10/17/89 | Loma Prieta | 7.1 | Coyote Lake Dam, Downstream | 57504 | 285 | 175.6 |
| 01/17/94 | Northridge | 6.8 | Mt Wilson, CIT Seismic Station | 24399 | 90 | 228.5 |
| 01/17/94 | Northridge | 6.8 | Antelope Buttes | 24310 | 90 | 99.7 |
| 01/17/94 | Northridge | 6.8 | Los Angeles, Wonderland | 90017 | 185 | 168.7 |
| 01/17/94 | Northridge | 6.8 | Wrightwood, Jackson Flat | 23590 | 90 | 54.5 |
| 01/17/94 | Northridge | 6.8 | Littlerock-Brainard Can | 23595 | 90 | 7.2 |
| 01/17/94 | Northridge | 6.8 | San Gabriel, E. Grand Ave. | 90019 | 180 | 256.0 |
| 10/01/87 | Whittier Narrows | 6.1 | Los Angeles, Gritfith Park Observatory | 141 | 0 | 133.8 |
| 10/15/79 | Imperial Valley | 6.8 | Superstition Mountain | 286 | 135 | 189.2 |

**Table C-2 Ground Motions Recorded on Site Class C**

| *Date* | *Earthquake Name* | *Magnitude (Ms)* | *Station Name* | *Station Number* | *Component (deg)* | *PGA ($cm/s^2$)* |
|---|---|---|---|---|---|---|
| 10/15/79 | Imperial Valley | 6.8 | El Centro, Parachute Test Facility | 5051 | 315 | 200.2 |
| 02/09/71 | San Fernando | 6.5 | Pasadena, CIT Athenaeum | 80053 | 90 | 107.9 |
| 02/09/71 | San Fernando | 6.5 | Pearblossom Pump | 269 | 21 | 133.4 |
| 06/28/92 | Landers | 7.5 | Yermo, Fire Station | 12149 | 0 | 167.8 |
| 10/17/89 | Loma Prieta | 7.1 | APEEL 7, Pulgas | 58378 | 0 | 153.0 |
| 10/17/89 | Loma Prieta | 7.1 | Gilroy #6, San Ysidro Microwave site | 57383 | 90 | 166.9 |
| 10/17/89 | Loma Prieta | 7.1 | Saratoga, Aloha Ave. | 58065 | 0 | 494.5 |
| 10/17/89 | Loma Prieta | 7.1 | Gilroy, Gavilon College Phys Sch Bldg | 47006 | 67 | 349.1 |
| 10/17/89 | Loma Prieta | 7.1 | Santa Cruz, University of California | 58135 | 360 | 433.1 |
| 10/17/89 | Loma Prieta | 7.1 | San Francisco, Diamond Heights | 58130 | 90 | 110.8 |
| 10/17/89 | Loma Prieta | 7.1 | Fremont, Mission San Jose | 57064 | 0 | 121.6 |
| 10/17/89 | Loma Prieta | 7.1 | Monterey, City Hall | 47377 | 0 | 71.60 |
| 10/17/89 | Loma Prieta | 7.1 | Yerba Buena Island | 58163 | 90 | 66.70 |
| 10/17/89 | Loma Prieta | 7.1 | Anderson Dam, Downstream | 1652 | 270 | 239.40 |
| 04/24/84 | Morgan Hill | 6.1 | Gilroy, Gavilon College Phys Sci Bldg | 47006 | 67 | 95.0 |
| 04/24/84 | Morgan Hill | 6.1 | Gilroy #6, San Ysidro Microwave Site | 57383 | 90 | 280.4 |
| 07/08/86 | Palmsprings | 6.0 | Fun Valley | 5069 | 45 | 129.0 |
| 01/17/94 | Northridge | 6.8? | Littlerock, Brainard Canyon | 23595 | 90 | 70.60 |
| 01/17/94 | Northridge | 6.8 | Castaic, Old Ridge Route | 24278 | 360 | 504.2 |
| 01/17/94 | Northridge | 6.8 | Lake Hughes #1, Fire station #78 | 24271 | 0 | 84.9 |

**Table C-3 Ground Motions Recorded on Site Class D**

| *Date* | *Earthquake Name* | *Magnitude (Ms)* | *Station Name* | *Station Number* | *Component (deg)* | *PGA (cm/s$^2$)* |
|---|---|---|---|---|---|---|
| 6/28/92 | Landers | 7.5 | Yermo, Fire Station | 22074 | 270 | 240.0 |
| 6/28/92 | Landers | 7.5 | Palm Springs, Airport | 12025 | 90 | 87.2 |
| 6/28/92 | Landers | 7.5 | Pomona, 4th and Locust, Free Field | 23525 | 0 | 65.5 |
| 01/17/94 | Northridge | 6.8 | Los Angeles, Hollywood Storage Bldg. | 24303 | 360 | 381.4 |
| 01/17/94 | Northridge | 6.8 | Santa Monica City Hall | 24538 | 90 | 866.2 |
| 01/17/94 | Northridge | 6.8 | Los Angeles, N. Westmoreland | 90021 | 0 | 393.3 |
| 10/17/89 | Loma Prieta | 7.1 | Gilroy 2, Hwy 101 Bolsa Road Motel | 47380 | 0 | 394.2 |
| 10/17/89 | Loma Prieta | 7.1 | Gilroy 3, Sewage Treatment Plant | 47381 | 0 | 531.7 |
| 10/17/89 | Loma Prieta | 7.1 | Hayward, John Muir School | 58393 | 0 | 166.5 |
| 10/17/89 | Loma Prieta | 7.1 | Agnews, Agnews State Hospital | 57066 | 0 | 163.1 |
| 10/01/87 | Whittier Narrows | 6.1 | Los Angeles, 116th St School | 14403 | 270 | 288.4 |
| 10/01/87 | Whittier Narrows | 6.1 | Downey, County Maintenance Bldg | 14368 | 180 | 193.2 |
| 10/15/79 | Imperial Valley | 6.8 | El Centro #13, Strobel Residence | 5059 | 230 | 136.2 |
| 10/15/79 | Imperial Valley | 6.8 | Calexico, Fire Station | 5053 | 225 | 269.6 |
| 04/24/84 | Morgan Hill | 6.1 | Gilroy #4, 2905 Anderson Rd | 57382 | 360 | 341.4 |
| 04/24/84 | Morgan Hill | 6.1 | Gilroy #7, Mantnilli Ranch, Jamison Rd | 57425 | 0 | 183.0 |
| 04/24/84 | Morgan Hill | 6.1 | Gilroy #2, Keystone Rd. | 47380 | 90 | 207.9 |
| 04/24/84 | Morgan Hill | 6.1 | Gilroy #3 Sewage Treatment Plant | 47381 | 90 | 189.8 |
| 02/09/71 | San Fernando | 6.5 | Los Angeles, Hollywood Storage Bldg. | 135 | 90 | 207.0 |
| 02/09/71 | San Fernando | 6.5 | Vernon, Cmd Terminal Building 4814 Loma Vista | 288 | 277 | 104.6 |

**Table C-4 Ground Motions Recorded on Very Soft Soil Sites Used in This Study**

| *Date* | *Earthquake Name* | *Magnitude (Ms)* | *Station Name* | *Station Number* | *Component (deg)* | *PGA ($cm/s^2$)* |
|---|---|---|---|---|---|---|
| 10/17/89 | Loma Prieta | 7.1 | Foster City (APEEL 1; Redwood Shores) | 58375 | 90 | 277.6 |
| 10/17/89 | Loma Prieta | 7.1 | Foster City (APEEL 1; Redwood Shores) | 58375 | 360 | 63.0 |
| 10/17/89 | Loma Prieta | 7.1 | Larkspur Ferry Terminal | 1590 (USGS) | 270 | 134.7 |
| 10/17/89 | Loma Prieta | 7.1 | Larkspur Ferry Terminal | 1590 (USGS) | 360 | 94.6 |
| 10/17/89 | Loma Prieta | 7.1 | Redwood City (APEEL Array Stn. 2) | 1002 (USGS) | 43 | 270.0 |
| 10/17/89 | Loma Prieta | 7.1 | Redwood City (APEEL Array Stn. 2) | 1002 (USGS) | 133 | 222.0 |
| 10/17/89 | Loma Prieta | 7.1 | Treasure Island (Naval Base Fire Station) | 58117 | 0 | 112.0 |
| 10/17/89 | Loma Prieta | 7.1 | Treasure Island (Naval Base Fire Station) | 58117 | 90 | 97.9 |
| 10/17/89 | Loma Prieta | 7.1 | Emeryville, 6363 Christie Ave. | 1662 (USGS) | 260 | 254.7 |
| 10/17/89 | Loma Prieta | 7.1 | Emeryville, 6363 Christie Ave. | 1662 (USGS) | 350 | 210.3 |
| 10/17/89 | Loma Prieta | 7.1 | San Francisco, International Airport | 58223 | 0 | 231.5 |
| 10/17/89 | Loma Prieta | 7.1 | San Francisco, International Airport | 58223 | 90 | 322.7 |
| 10/17/89 | Loma Prieta | 7.1 | Oakland, Outer Harbor Wharf | 58472 | 35 | 281.4 |
| 10/17/89 | Loma Prieta | 7.1 | Oakland, Outer Harbor Wharf | 58472 | 305 | 265.5 |
| 10/17/89 | Loma Prieta | 7.1 | Oakland, Title & Trust Bldg. (2-story) | 58224 | 180 | 191.3 |
| 10/17/89 | Loma Prieta | 7.1 | Oakland, Title & Trust Bldg. (2-story) | 58224 | 270 | 239.4 |
| 10/15/79 | Imperial Valley | 6.8 | El Centro Array 3, Pine Union School | 5057 | 140 | 260.9 |
| 10/15/79 | Imperial Valley | 6.8 | El Centro Array 3, Pine Union School | 5057 | 230 | 216.8 |
| 04/24/84 | Morgan Hill | 6.1 | Foster City (APEEL 1; Redwood Shores) | 58375 | 40 | 45.1 |
| 04/24/84 | Morgan Hill | 6.1 | Foster City (APEEL 1; Redwood Shores) | 58375 | 310 | 66.7 |

**Table C-5 Near-Fault Records with Forward Directivity Used in this Study**

| *Date* | *Earthquake Name* | *Magnitude (Ms)* | *Station Name* | *NEHRP Site Class* | *PGA ($cm/s^2$)* |
|---|---|---|---|---|---|
| 10/17/89 | Loma Prieta | 7.1 | Los Gatos | D | 704.0 |
| 10/17/89 | Loma Prieta | 7.1 | Lexington Dam | D | 673.0 |
| 01/16/95 | Hyogo-Ken-Nanbu, Kobe | 6.9 | Takatori Station | D | 771.0 |
| 01/16/95 | Hyogo-Ken-Nanbu, Kobe | 6.9 | Kobe Station | D | 1067.0 |
| 01/16/95 | Hyogo-Ken-Nanbu, Kobe | 6.9 | Port Island | D | 426.0 |
| 03/13/92 | Erzican, Turkey | 6.9 | Erzican Station | D | 424.0 |
| 01/17/94 | Northridge | 6.8 | Rinaldi Receiving Station | D | 873.0 |
| 01/17/94 | Northridge | 6.8 | Sepulveda | D | 715.0 |
| 01/17/94 | Northridge | 6.8 | Sylmar County Hospital | D | 718.0 |
| 01/17/94 | Northridge | 6.8 | Newhall, LA County Fire Station | D | 709.0 |
| 10/15/79 | Imperial Valley | 6.8 | Meloland | D | 372.0 |
| 10/15/79 | Imperial Valley | 6.8 | El Centro Array 6 | D | 424.0 |
| 04/24/84 | Morgan Hill | 6.1 | Coyote Dam | D | 712.0 |
| 04/24/84 | Morgan Hill | 6.1 | Anderson Dam | D | 436.0 |
| 08/17/99 | Kocaeli, Turkey | 7.8 | YPT | D | 311.5 |
| 08/17/99 | Kocaeli, Turkey | 7.8 | DZC1 | D | 390.1 |
| 11/12/99 | Duzce, Turkey | 7.8 | DZC2 | D | 404.2 |
| 08/17/99 | Kocaeli, Turkey | 7.8 | IZT1 | AB | 164.3 |
| 11/12/99 | Duzce, Turkey | 7.8 | BOL2 | D | 755.9 |
| 08/17/99 | Kocaeli, Turkey | 7.8 | GBZ1 | AB | 240.2 |

## C.2 Response History Results

### *C.2.1 Effect of Site Class on $C_1$ of SDOF Systems with Elastoplastic Perfectly Plastic (EPP) Hysteretic Behavior*

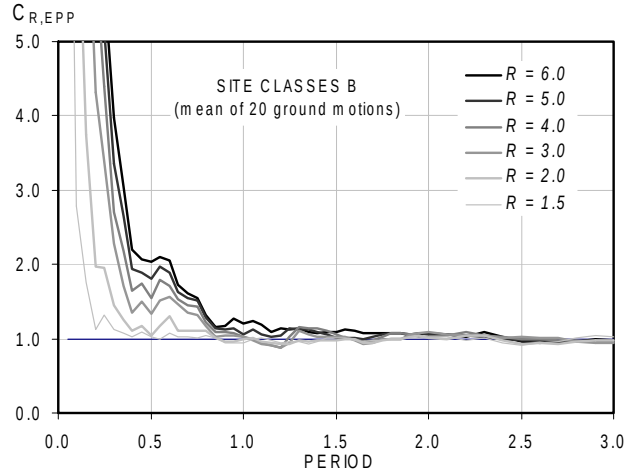


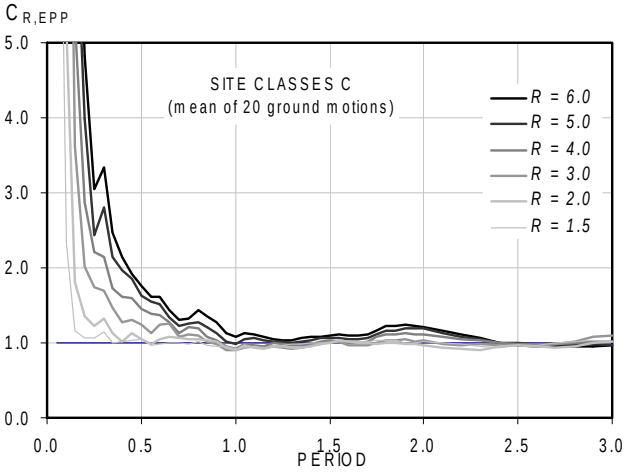


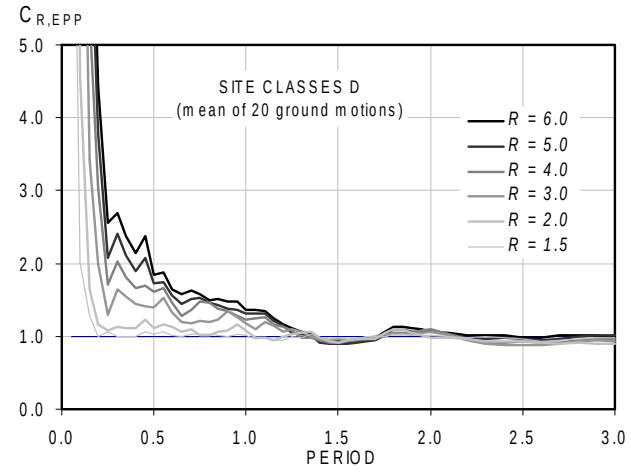


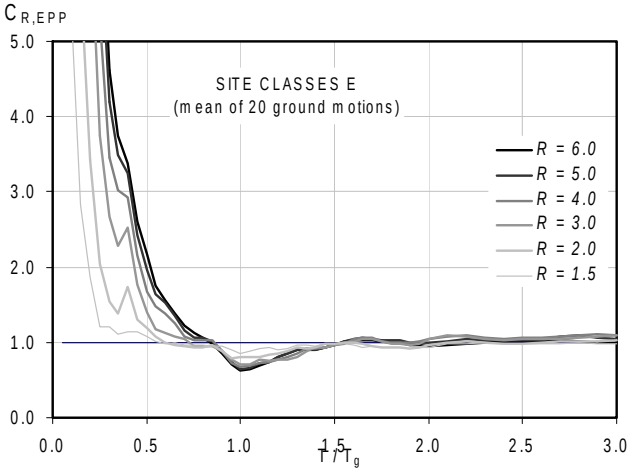


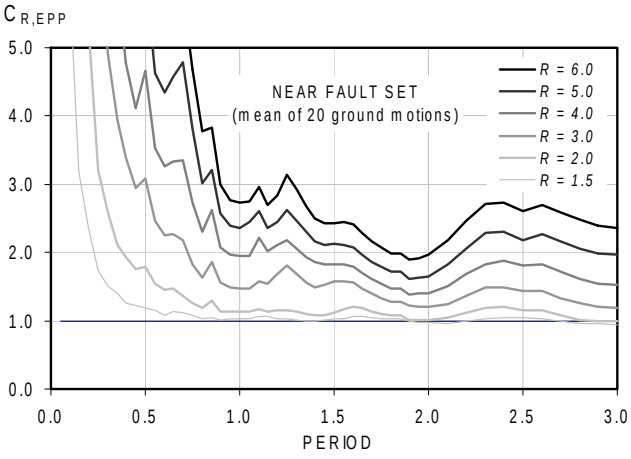


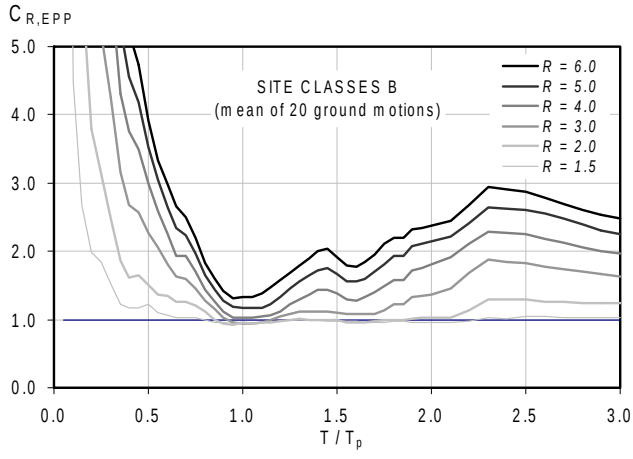

### *C.2.2 Effect of Site Class on $C_1$ of SDOF Systems with Stiffness Degrading (SD) Hysteretic Behavior*

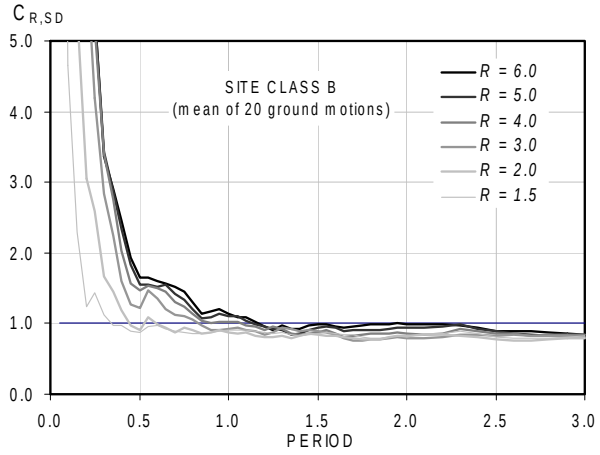


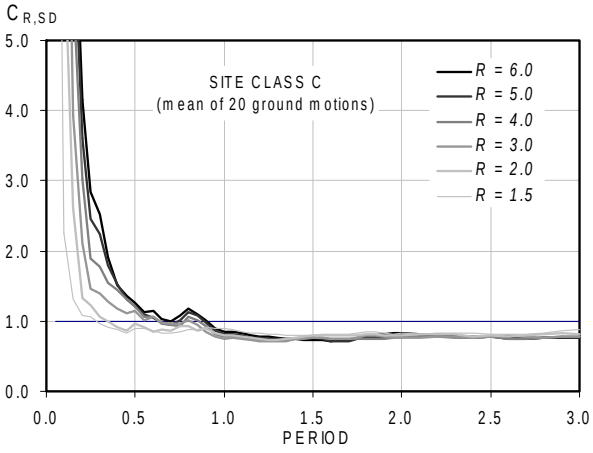


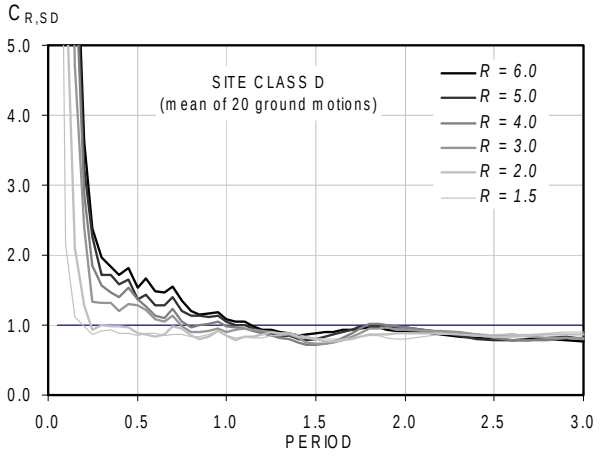


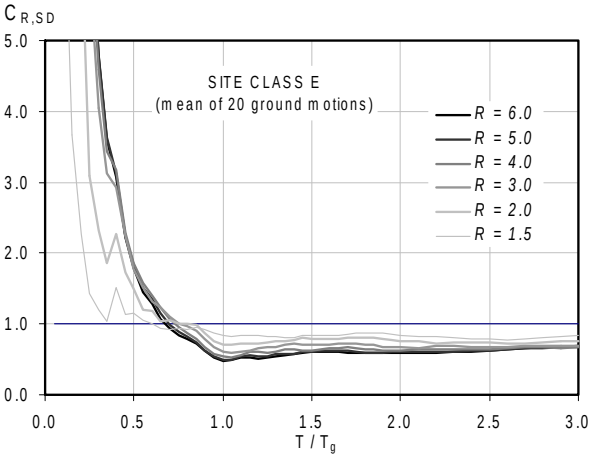


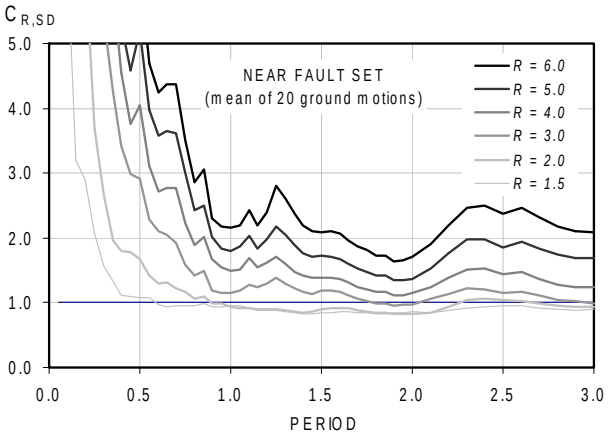


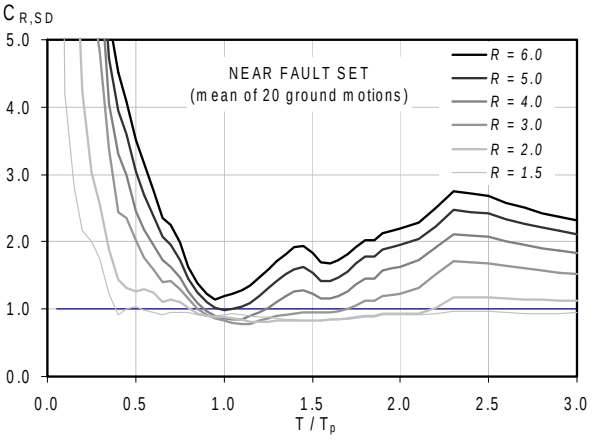

### C.2.3 *Effect of Site Class on $C_1$ of SDOF Systems with Strength and Stiffness Degrading (SSD) Hysteretic Behavior*

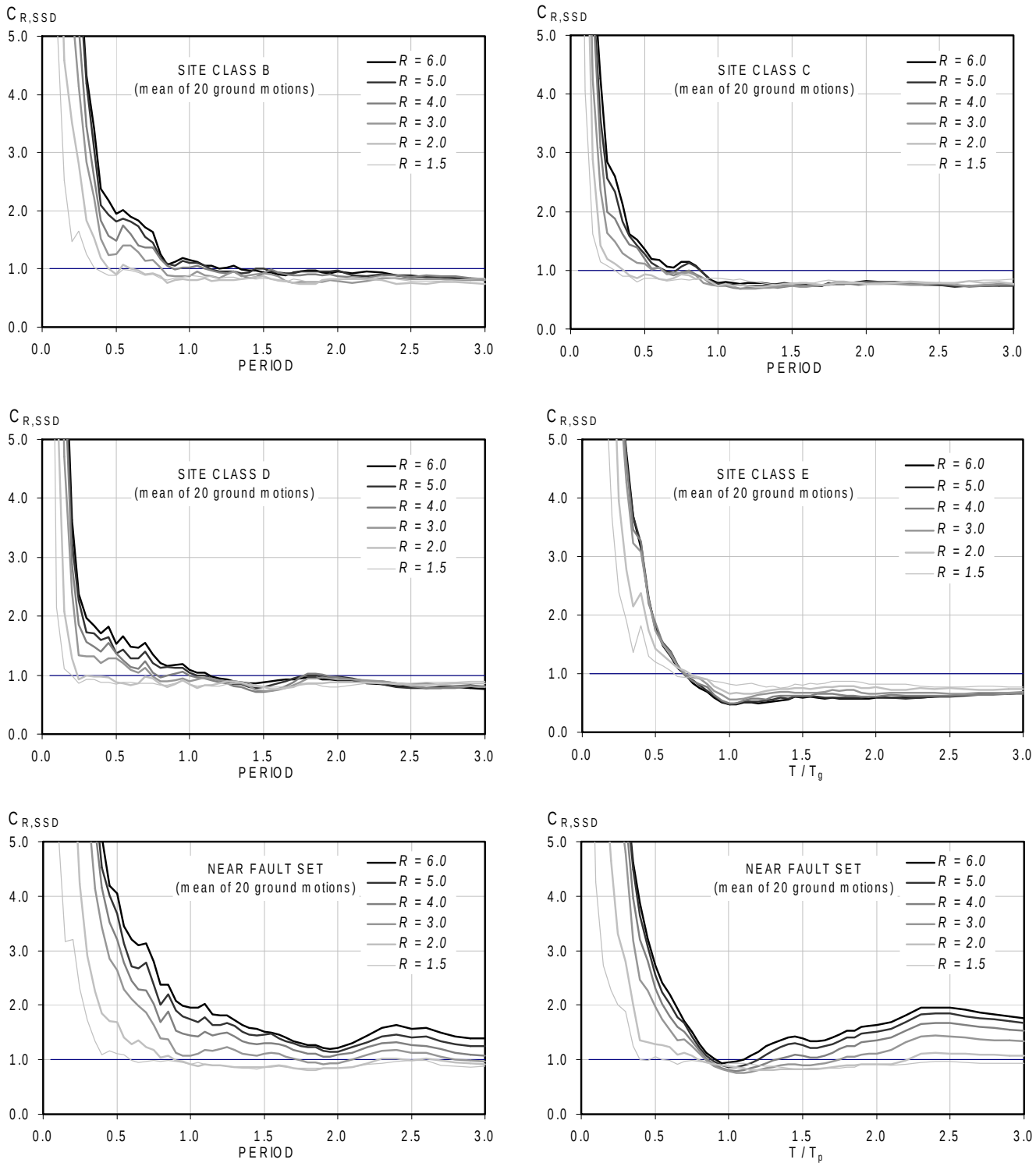

### *C.2.4 Effect of Site Class on $C_1$ of SDOF Systems with Nonlinear Elastic Hysteretic Behavior*

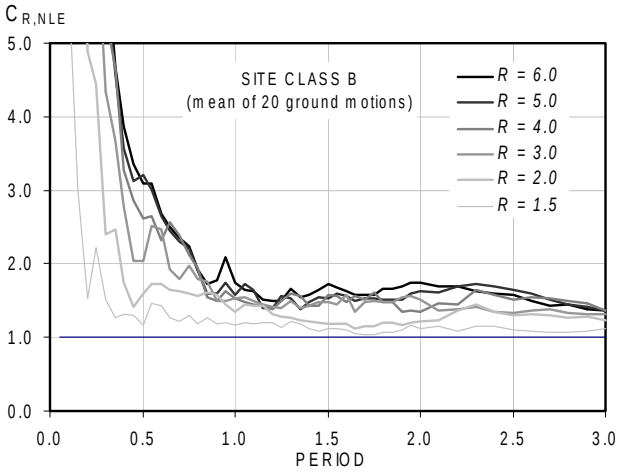


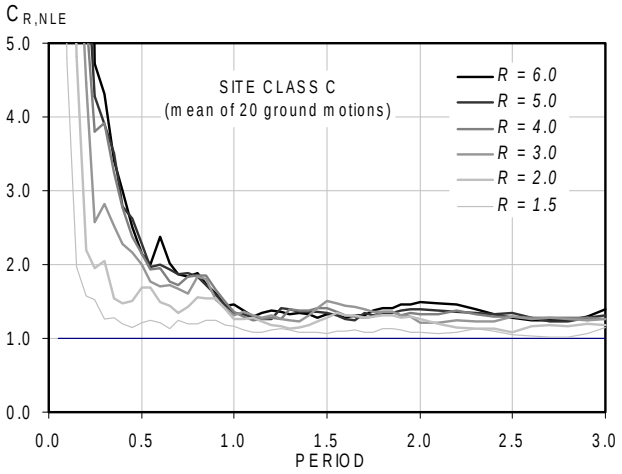


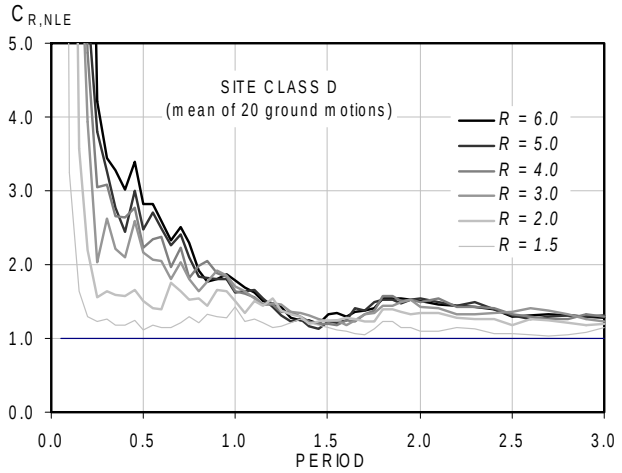


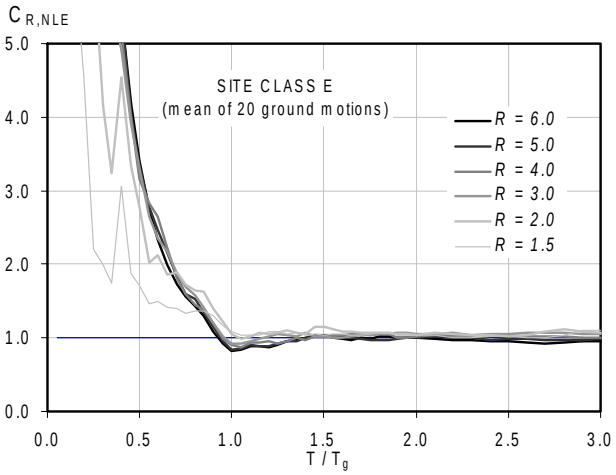


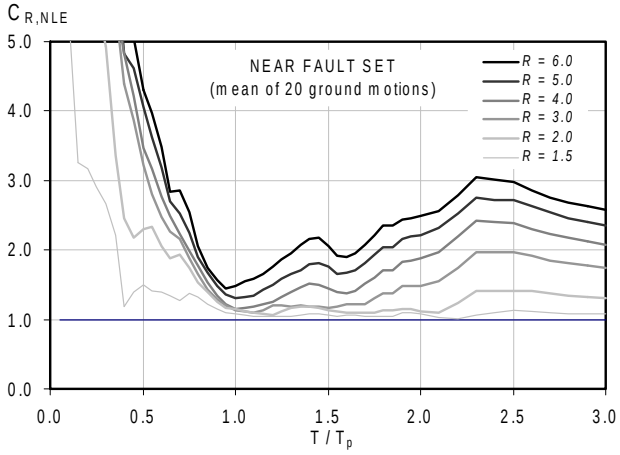

### *C.2.5 Evaluation of Coefficient $C_2$ for Site Class B*

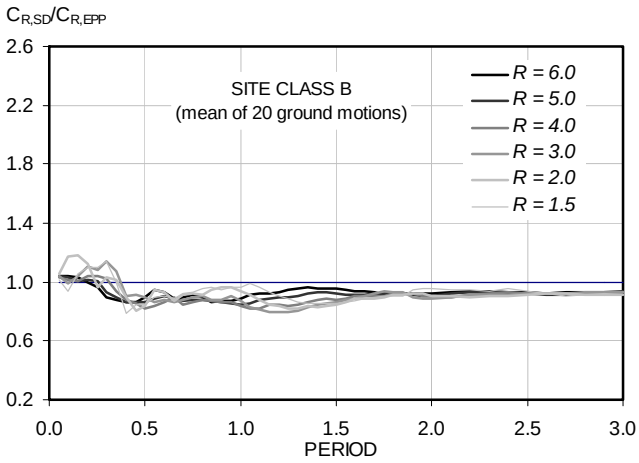


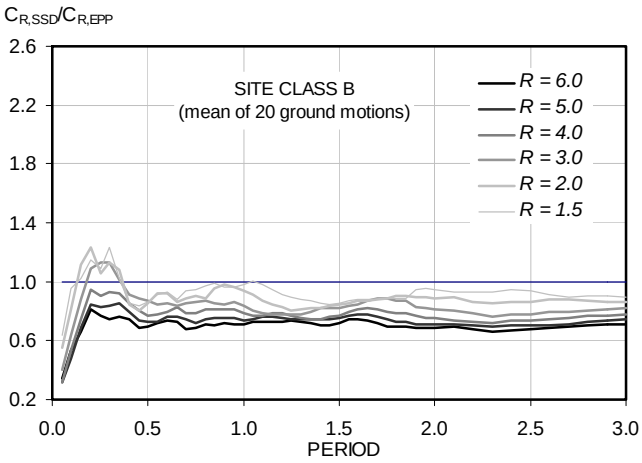


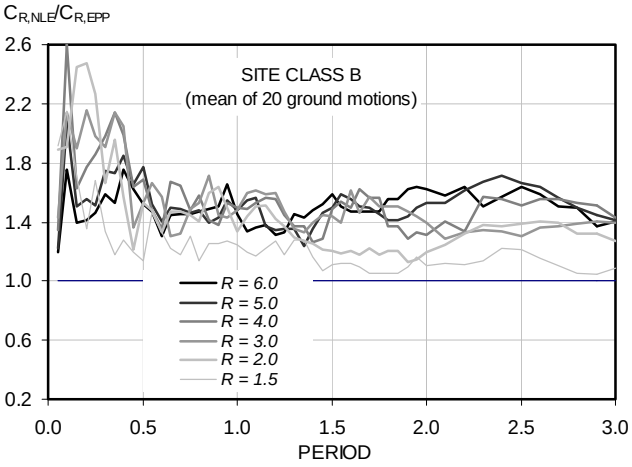

### *C.2.6 Evaluation of Coefficient $C_2$ for Site Class C*

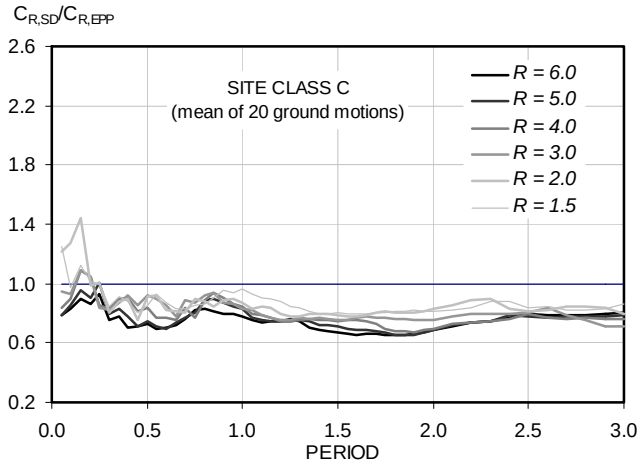


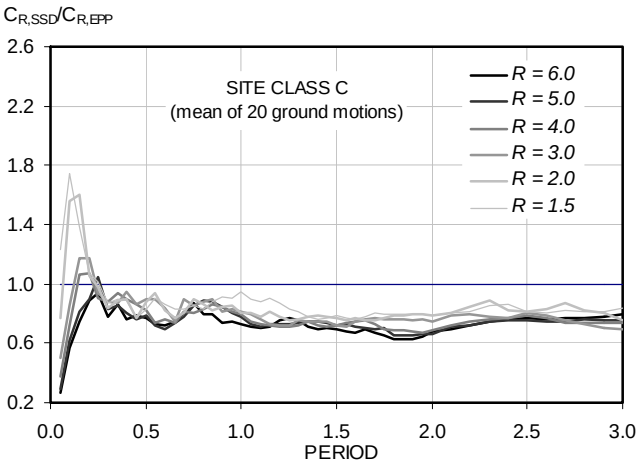


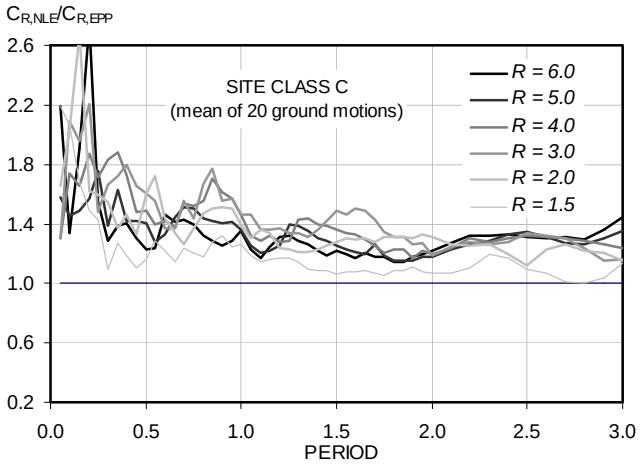

### *C.2.7 Evaluation of Coefficient $C_2$ for Site Class D*

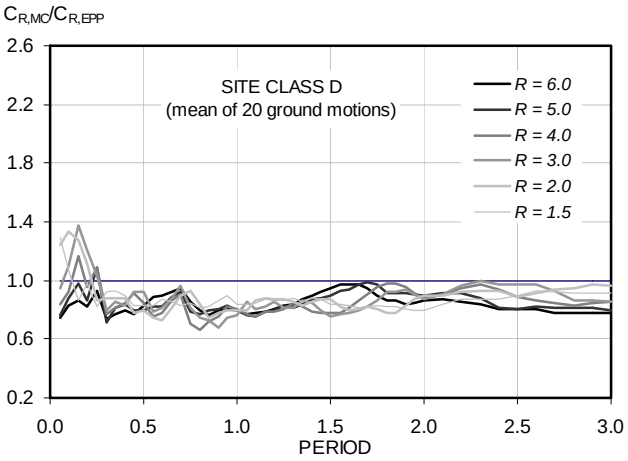


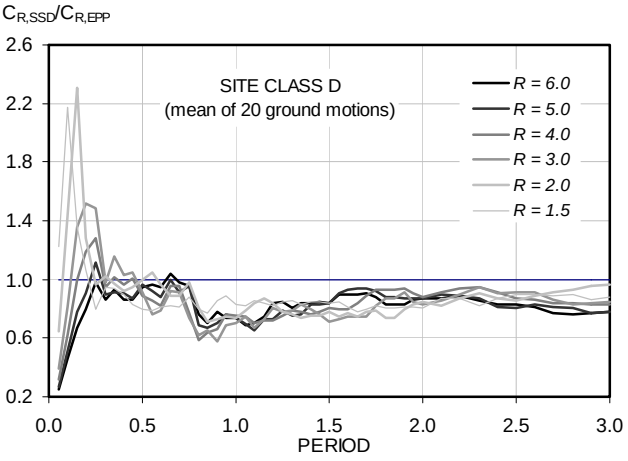


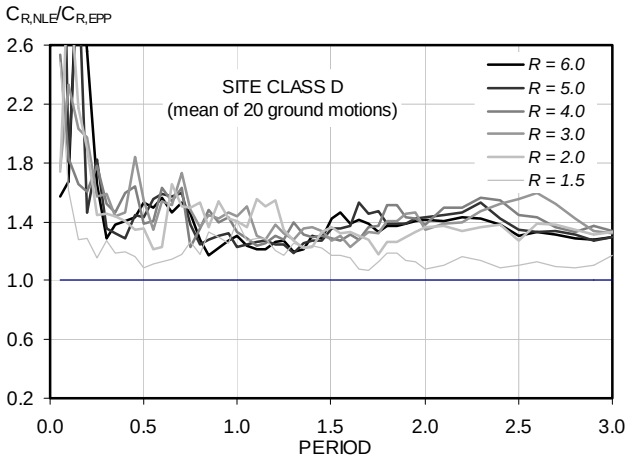

### *C.2.8 Evaluation of Coefficient $C_2$ for Site Class E*

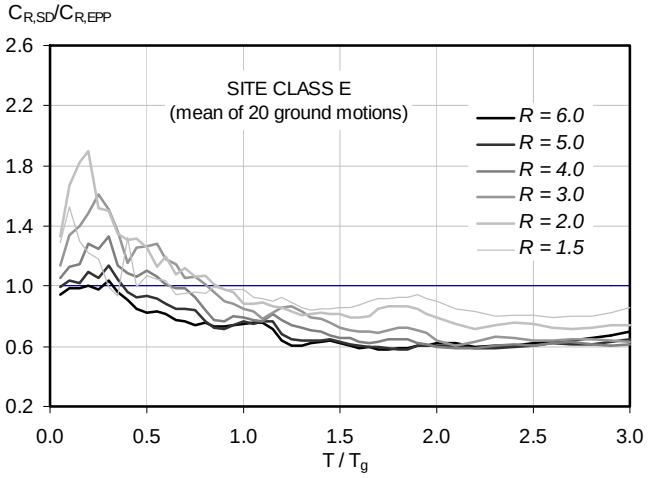


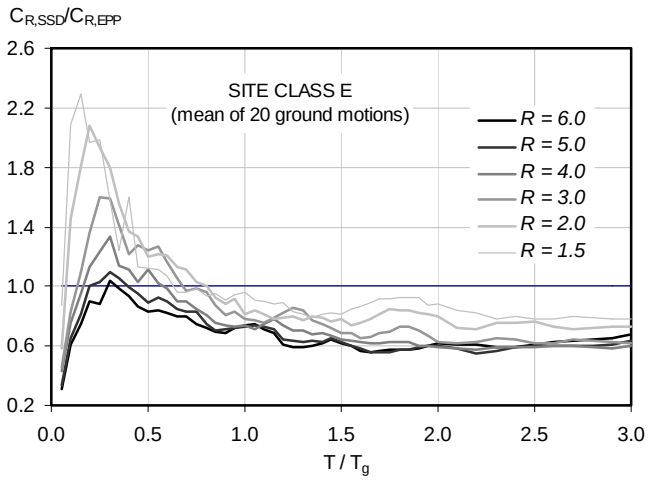


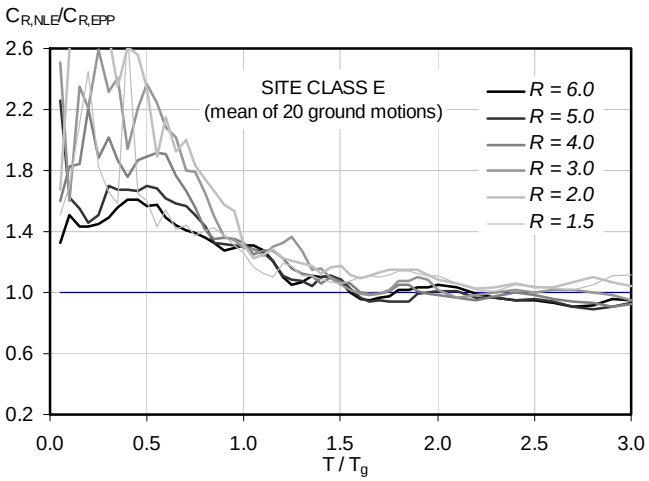

### *C.2.9 Evaluation of Coefficient $C_2$ for Near Fault Set*

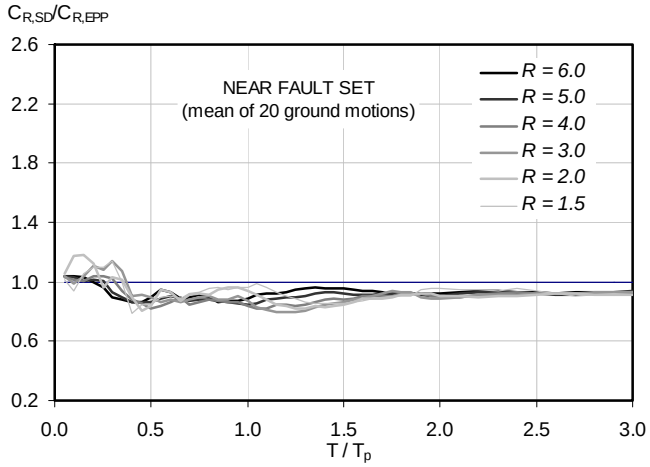


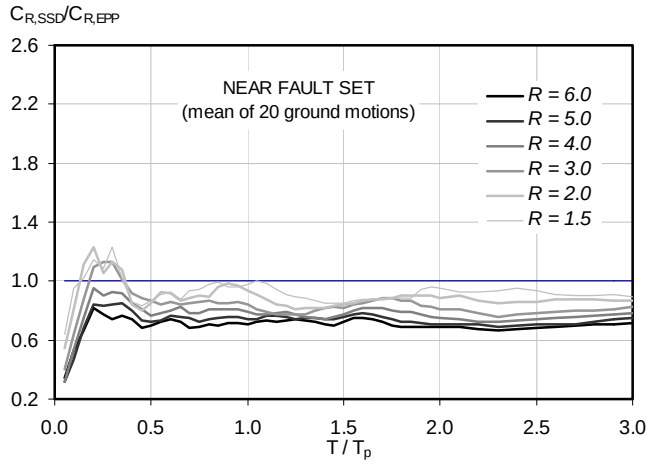


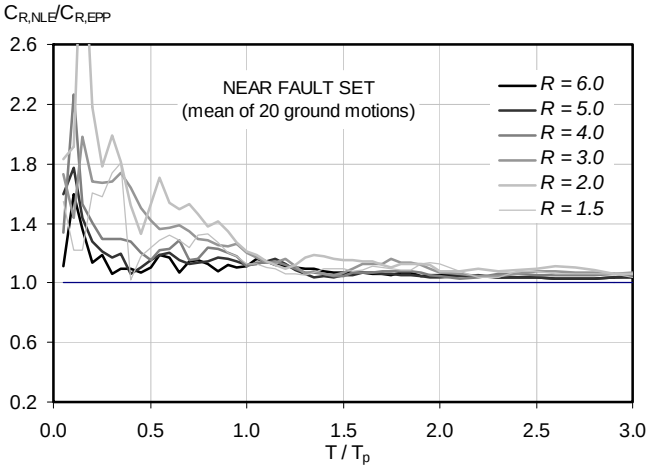

### *C.2.10 Effect of Site Class on Coefficient $C_2$ (Stiffness Degrading Hysteretic Behavior)*

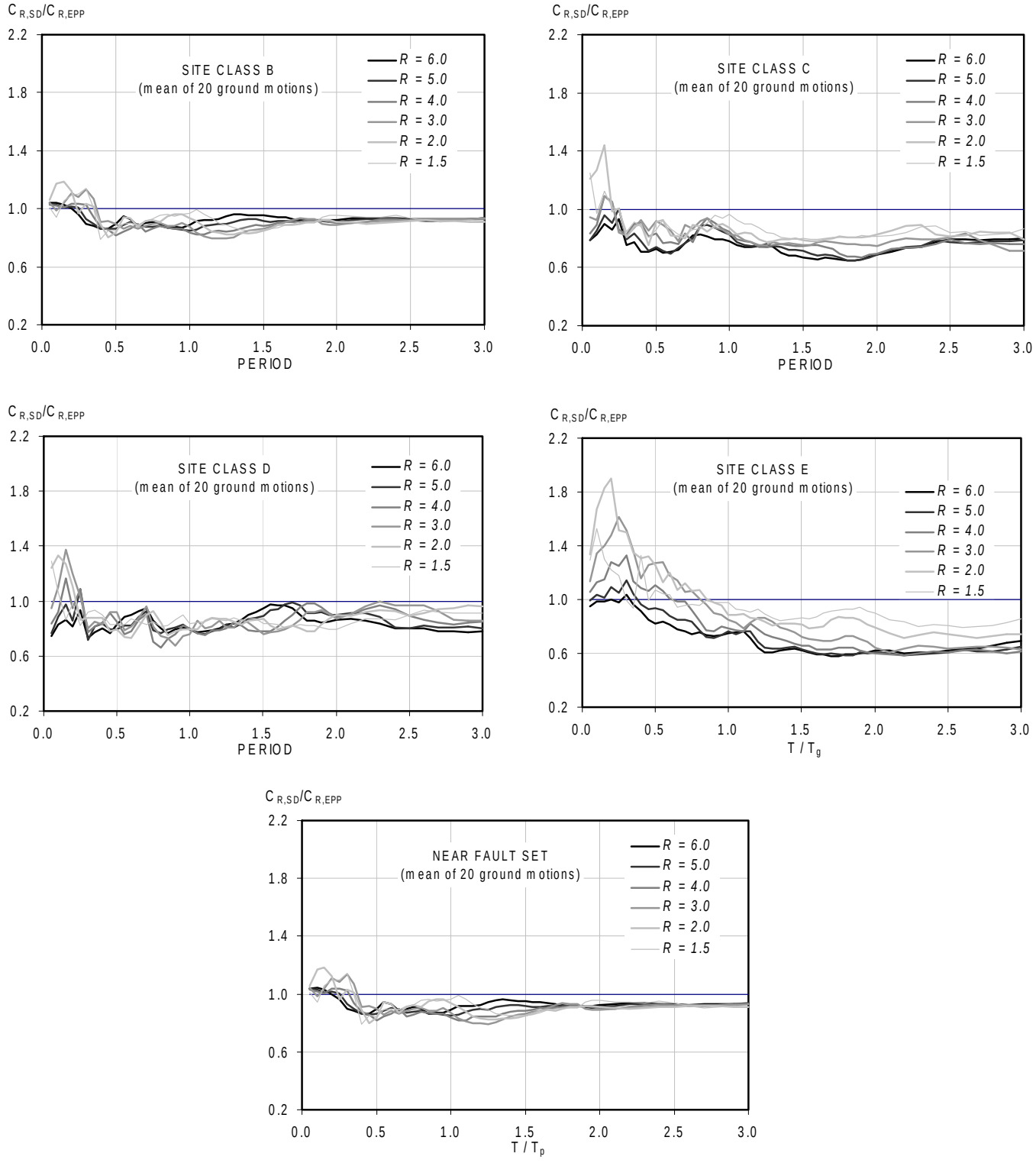

### *C.2.11 Effect of Site Class on Coefficient $C_2$ (Strength-Stiffness Degrading Hysteretic Behavior)*

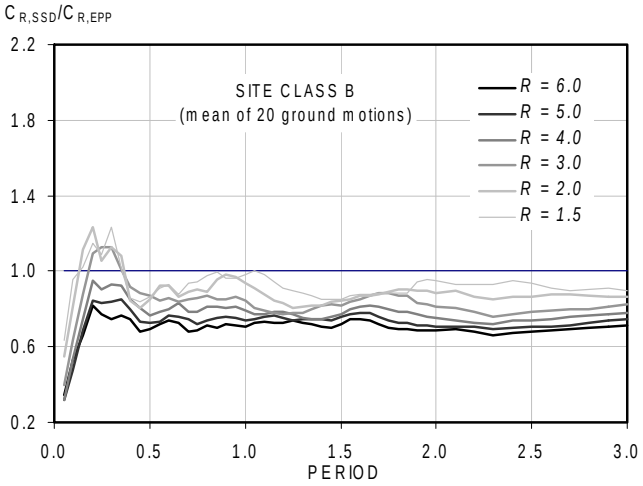


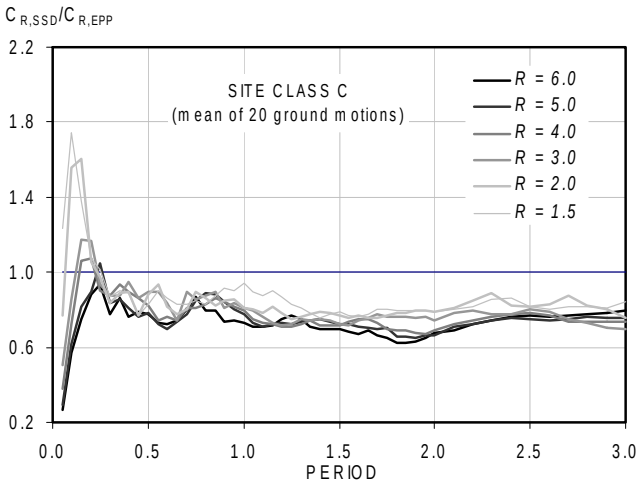


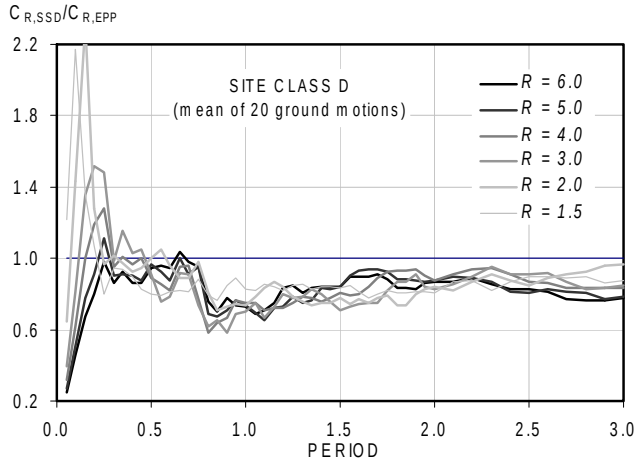


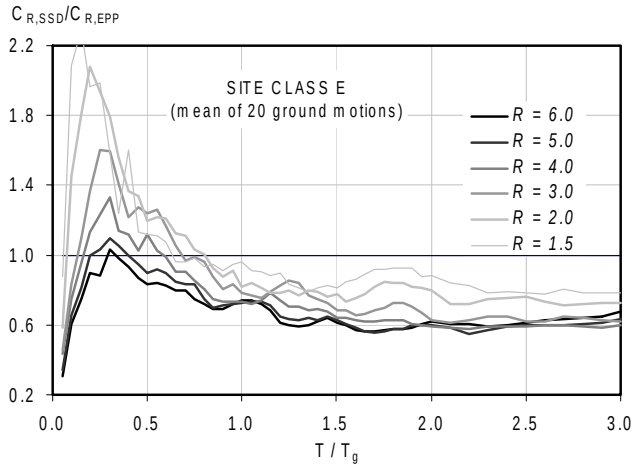


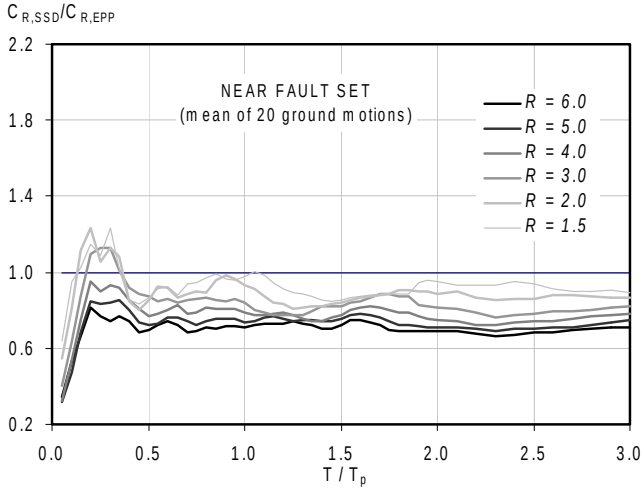

### *C.2.12 Effect of Site Class on Coefficient $C_2$ (Nonlinear Elastic Hysteretic Behavior)*

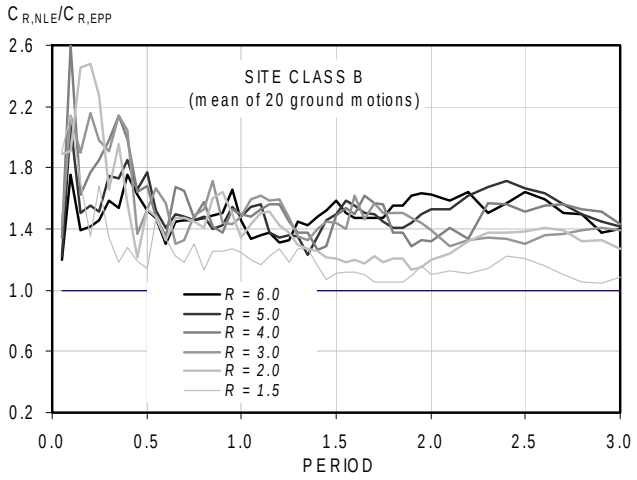


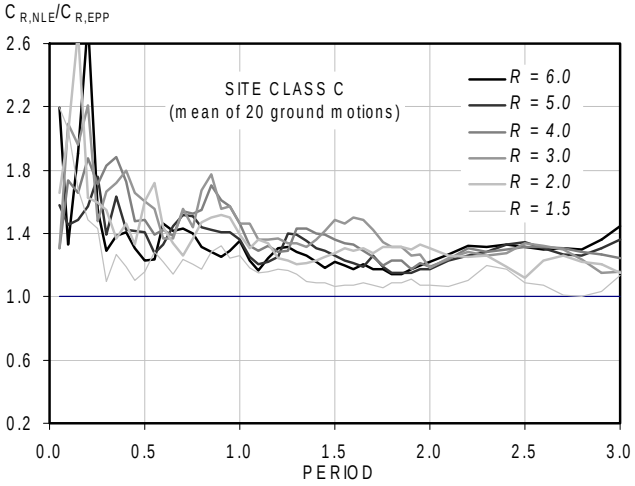


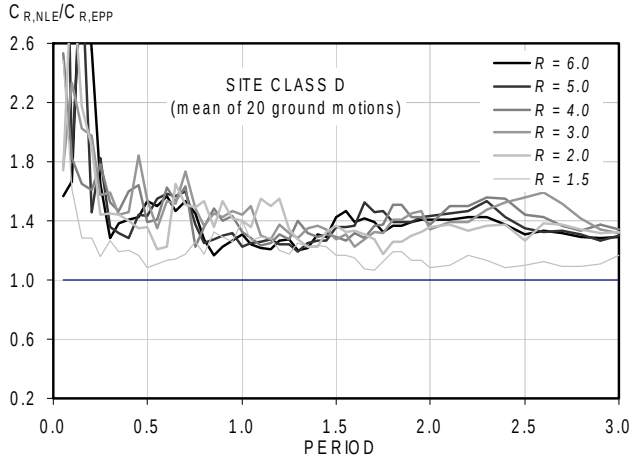


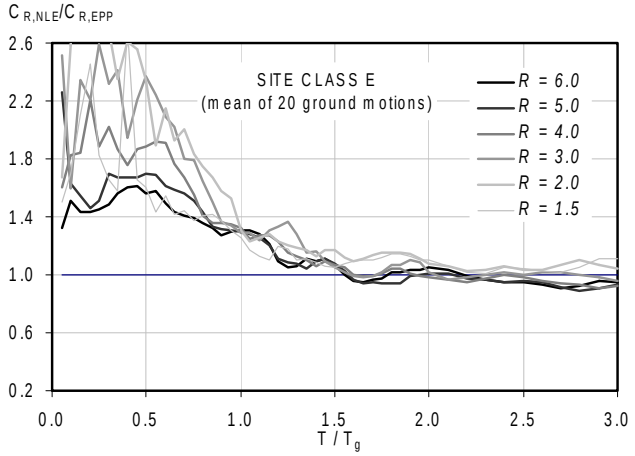


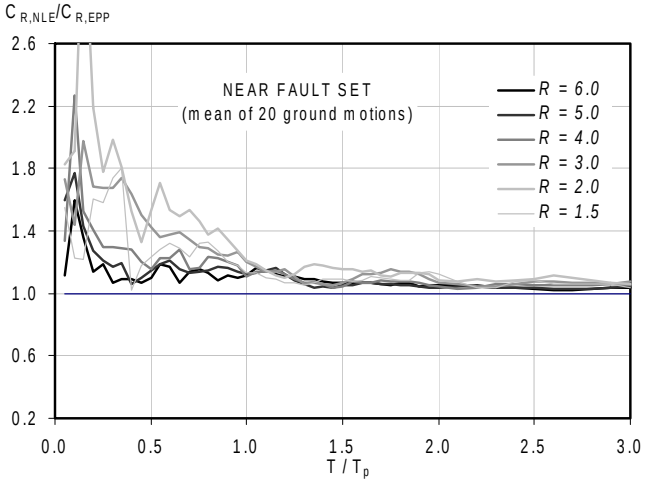

### *C.2.13 Effect of Hysteretic Behavior on $C_1$ of SDOF Systems (Site Class B)*

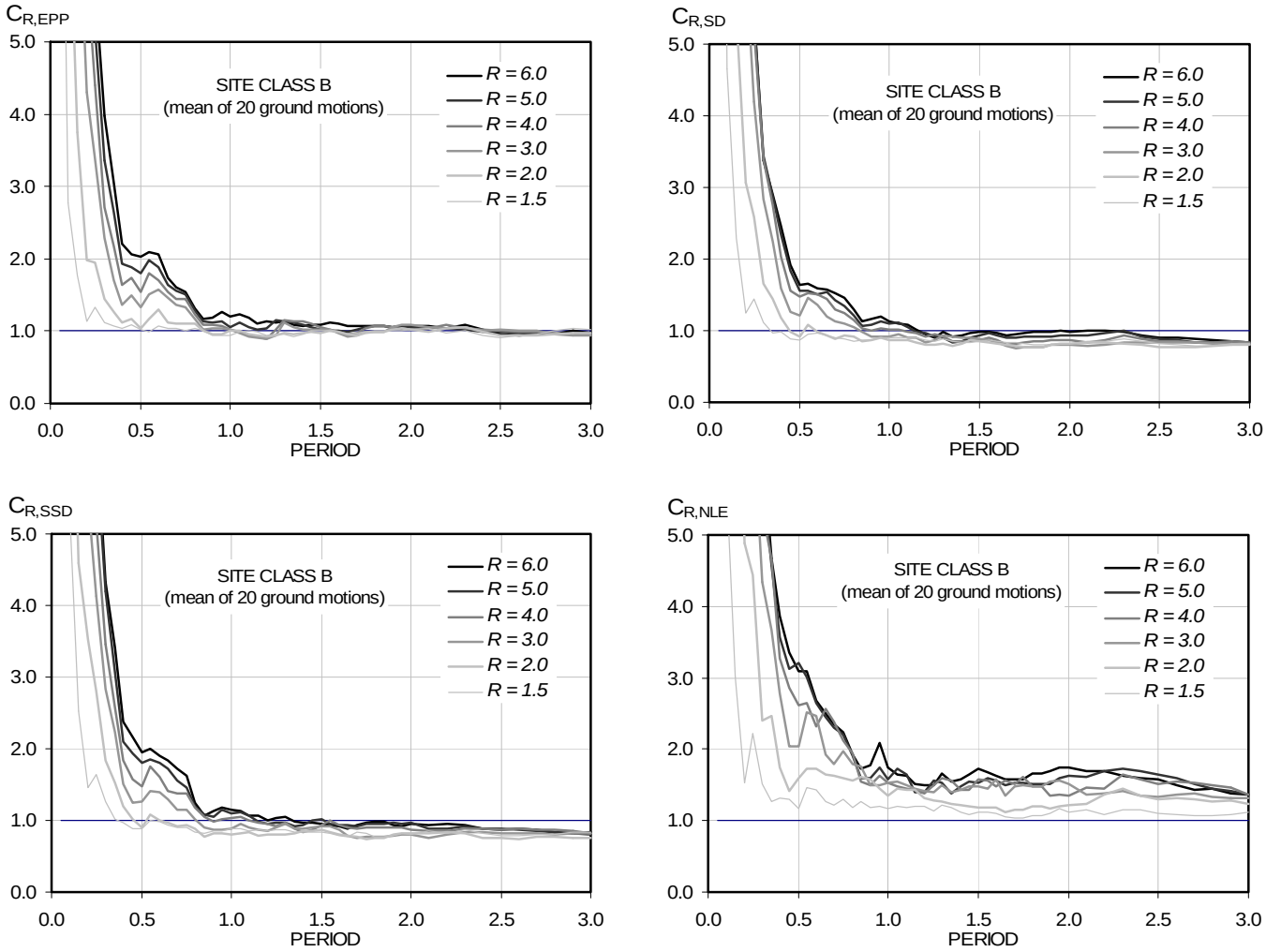

### *C.2.14 Effect of Hysteretic Behavior on $C_1$ of SDOF Systems (Site Class C)*

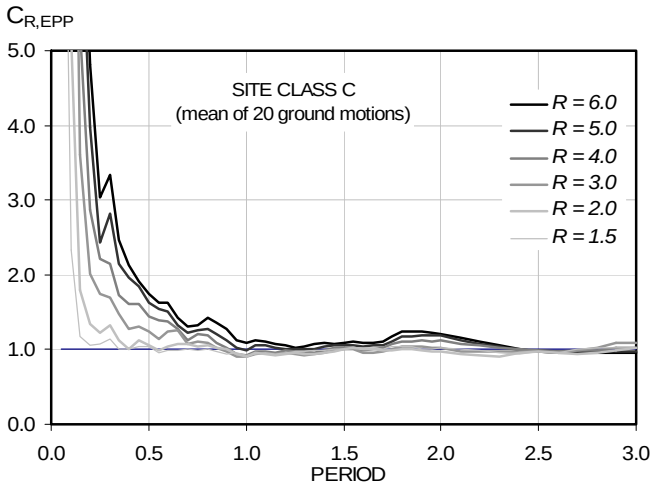


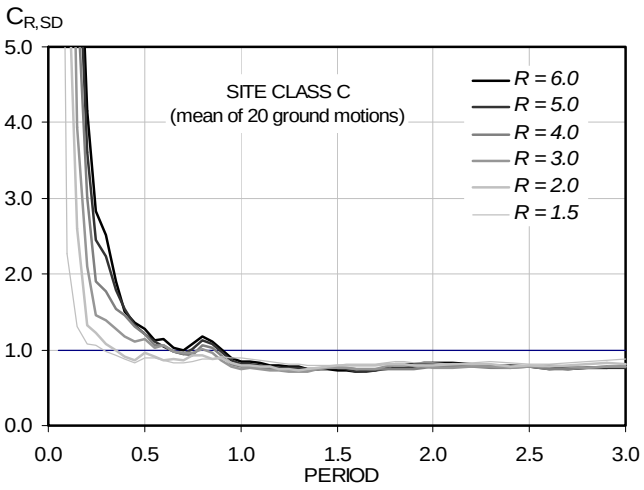


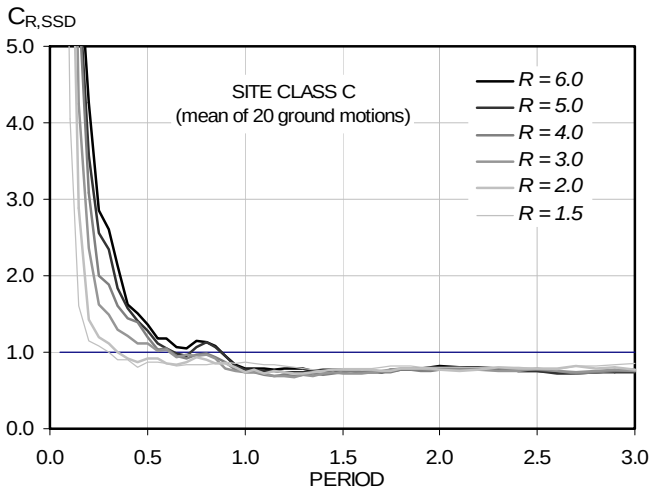


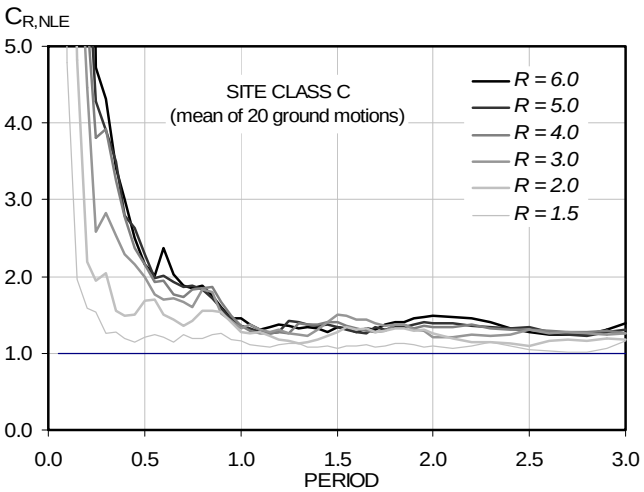

### *C.2.15 Effect of Hysteretic Behavior on $C_1$ of SDOF Systems (Site Class D)*

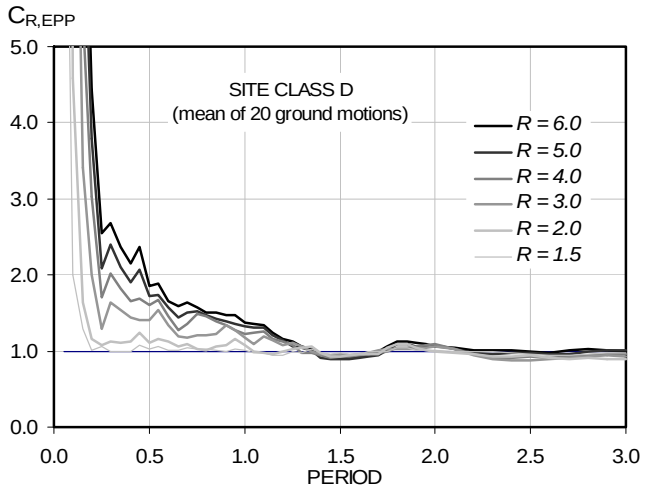


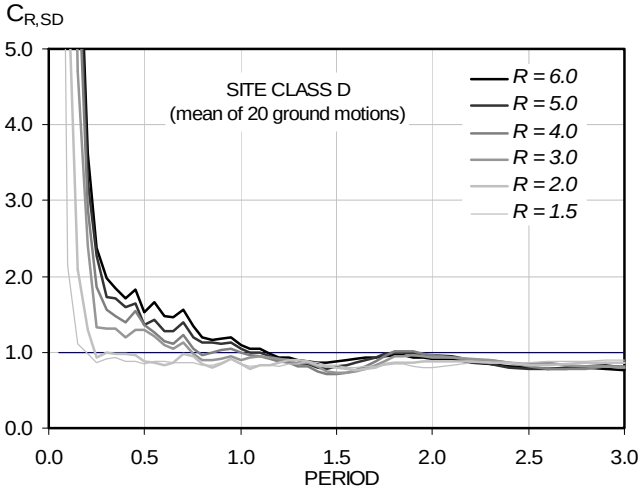


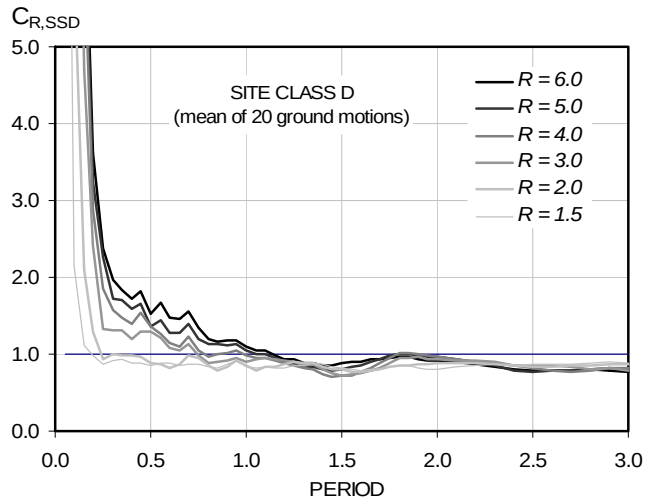


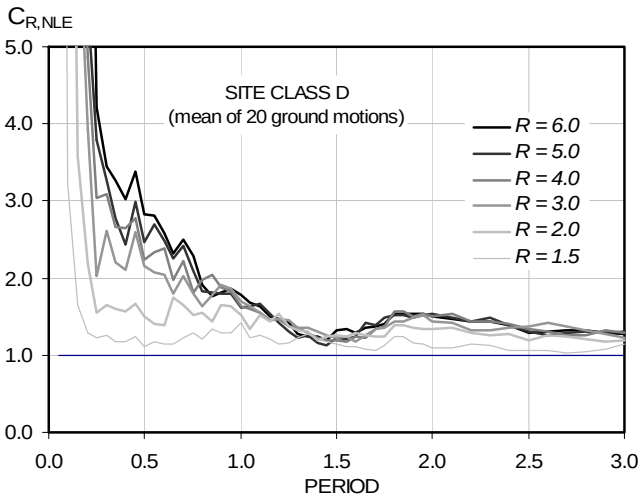

### *C.2.16 Effect of Hysteretic Behavior on $C_1$ of SDOF Systems (Site Class E)*

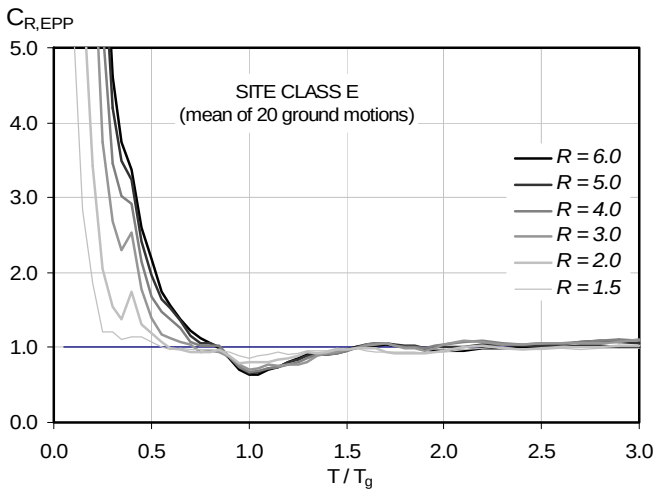


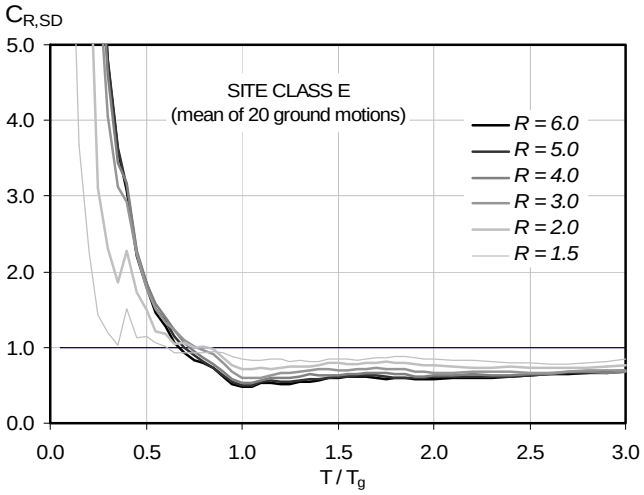


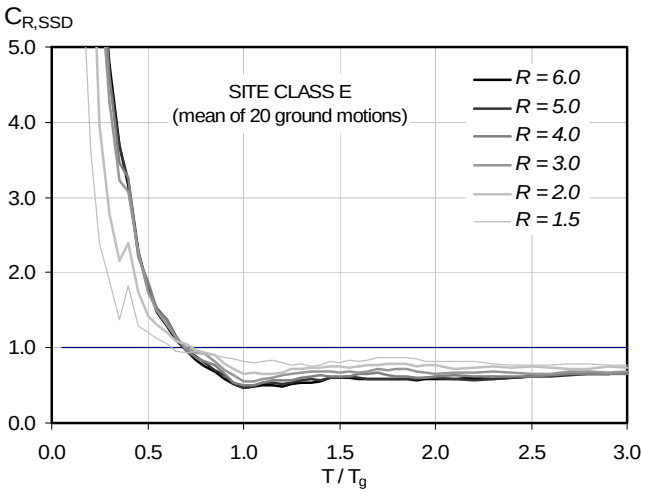


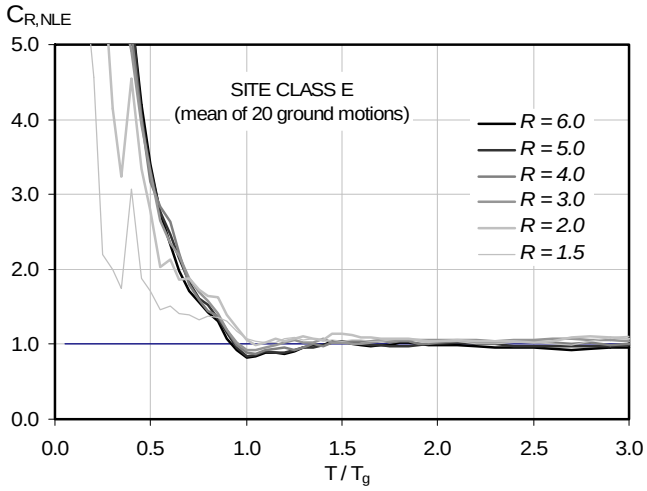

### *C.2.17 Effect of Hysteretic Behavior on $C_1$ of SDOF Systems (Near Fault Set)*

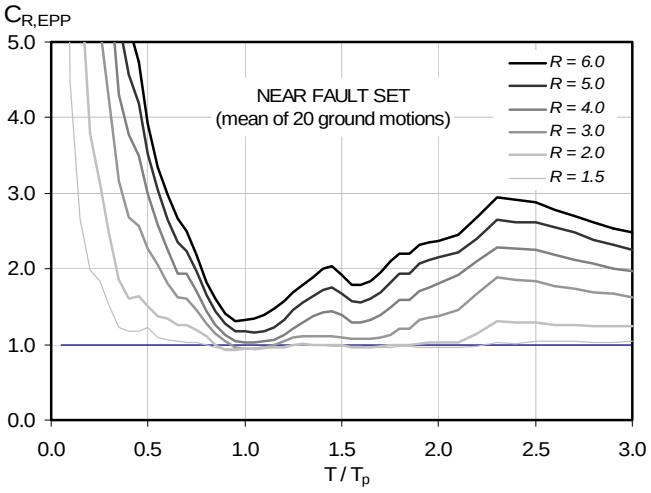


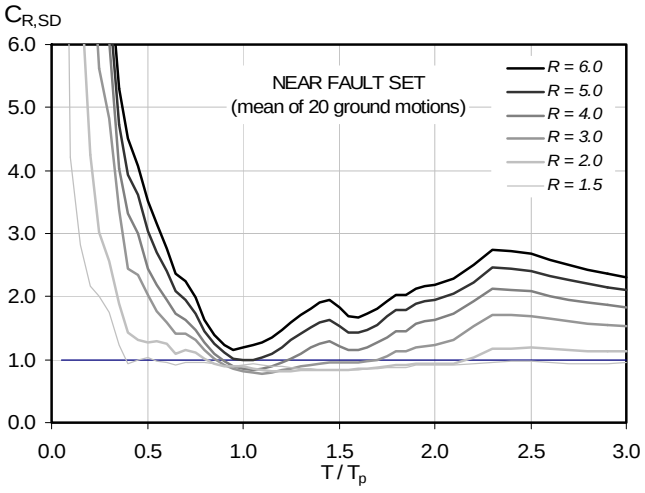


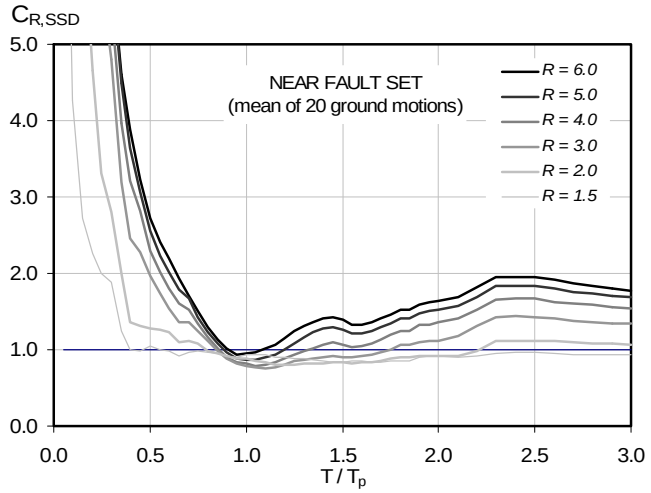


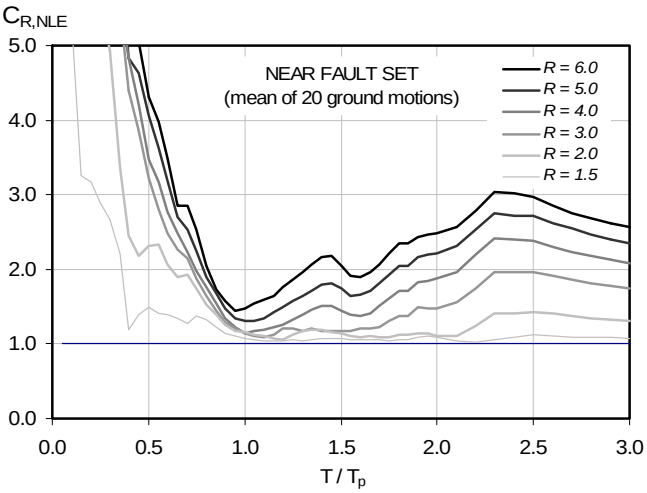

## C.3 Evaluation of ATC-40 Version of Capacity Spectrum Method: Summary Results

### *C.3.1 Comparisons for Site Class B:*

**MEAN ERROR** **ERROR DISPERSION**

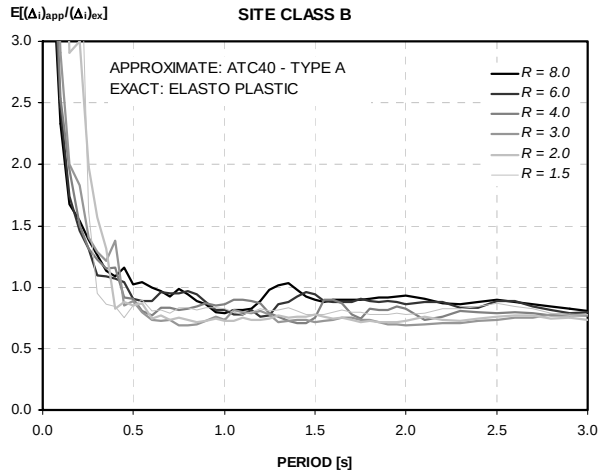


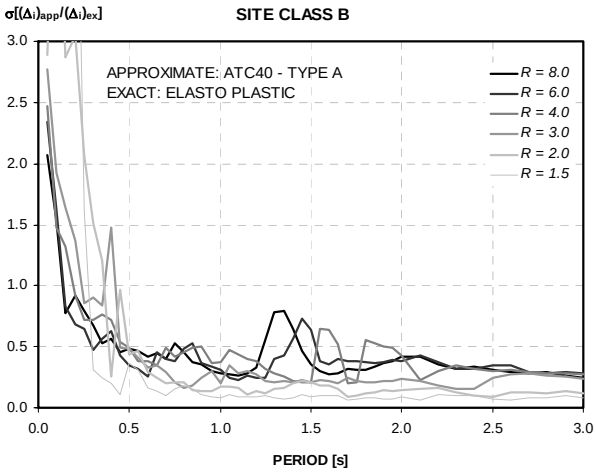


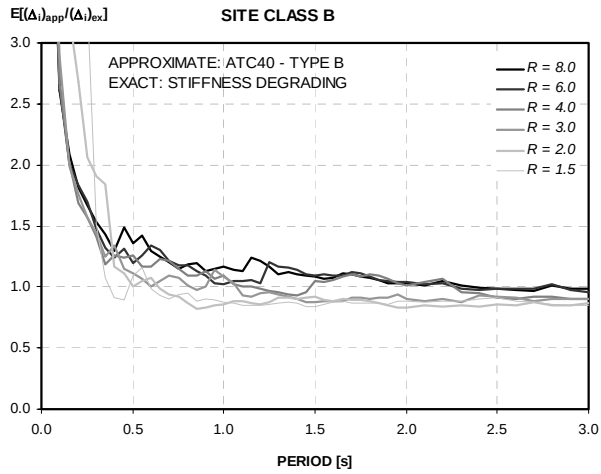


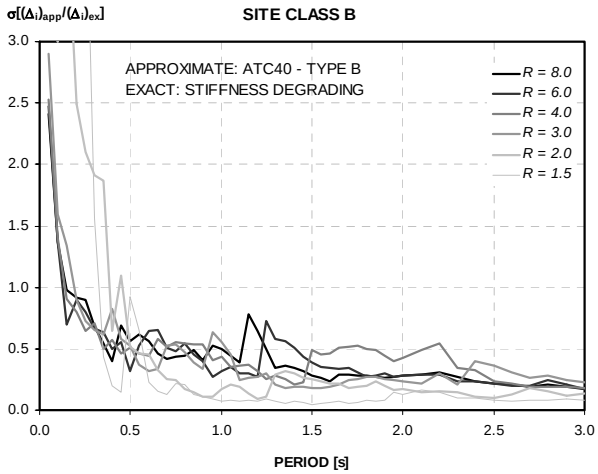


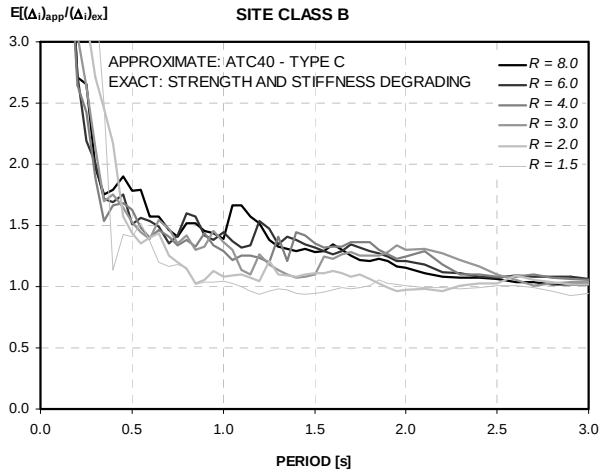


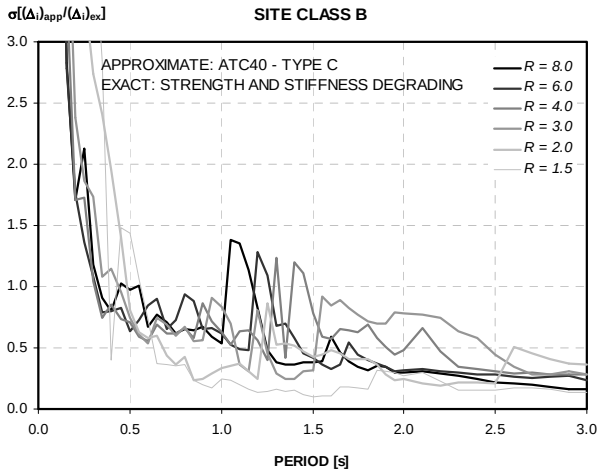

### *C.3.2 Comparisons for Site Class C:*

## MEAN ERROR

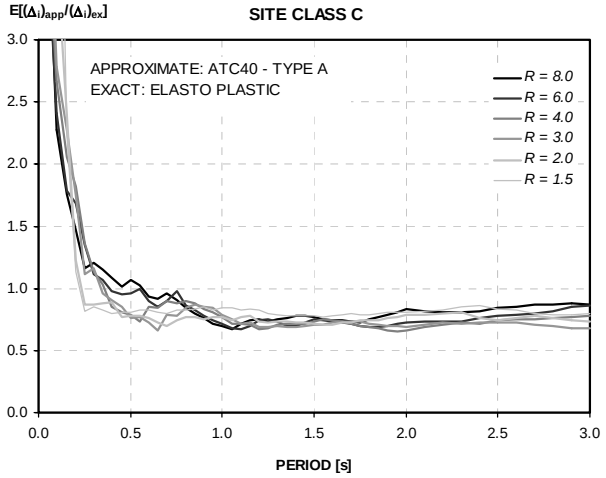


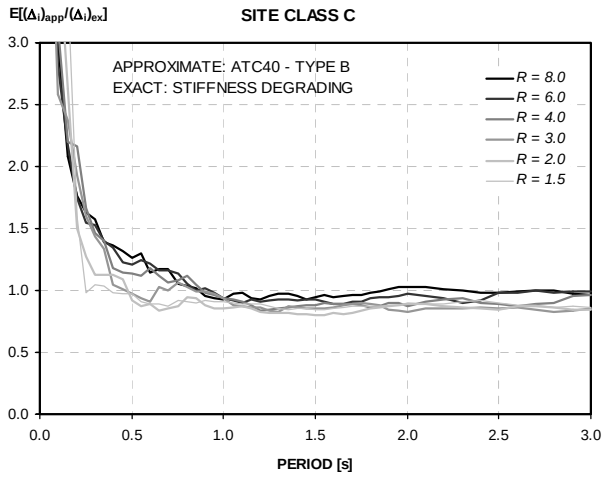


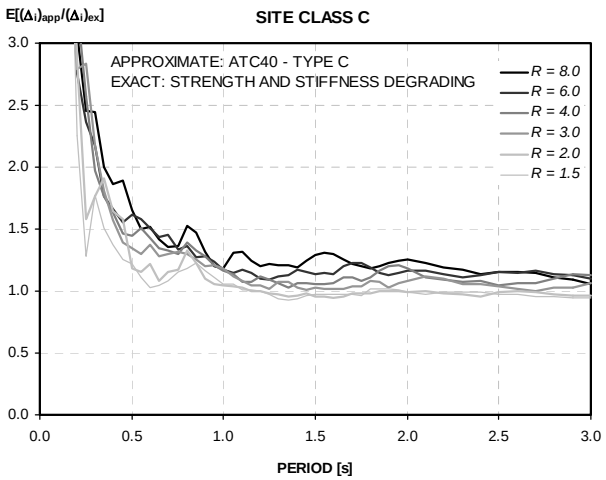


## ERROR DISPERSION

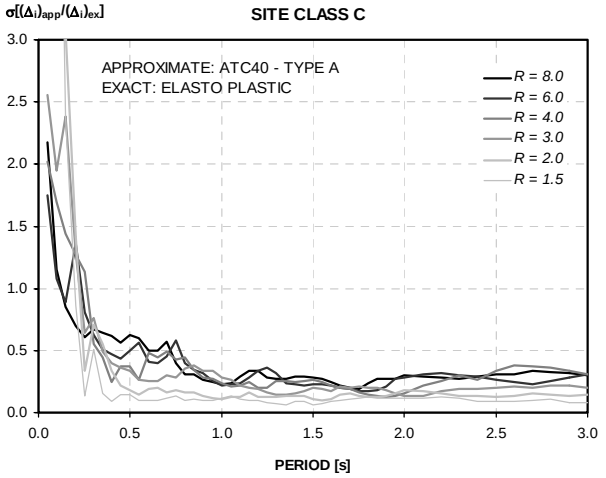


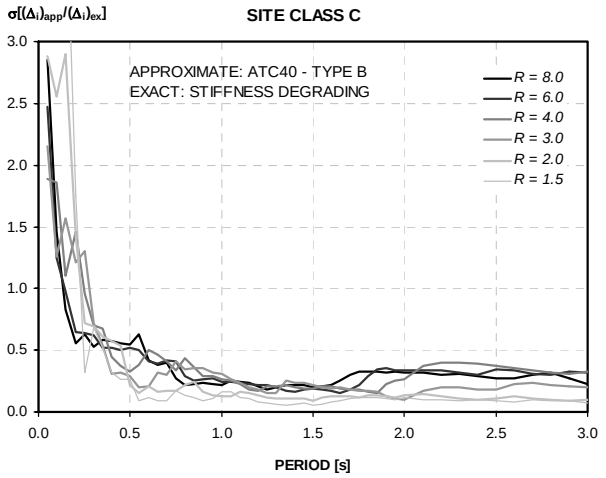


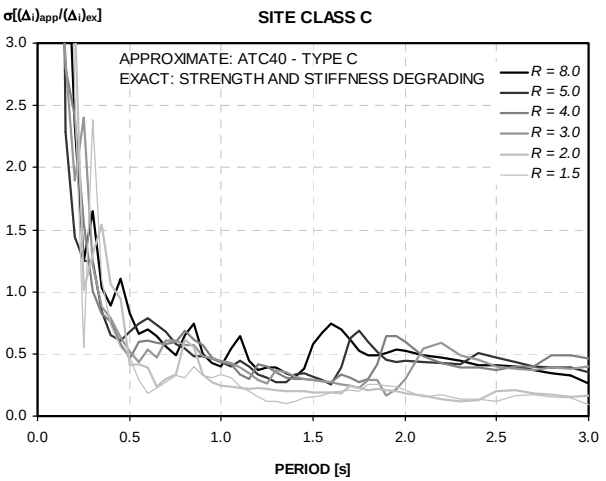

### *C.3.3 Comparisons for Site Class D:*

## MEAN ERROR

## ERROR DISPERSION

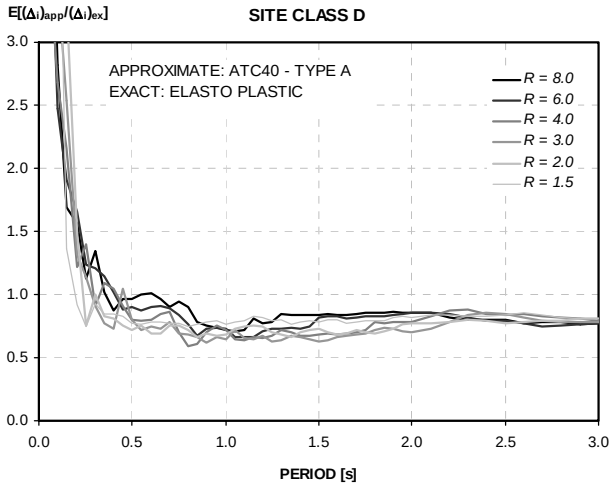


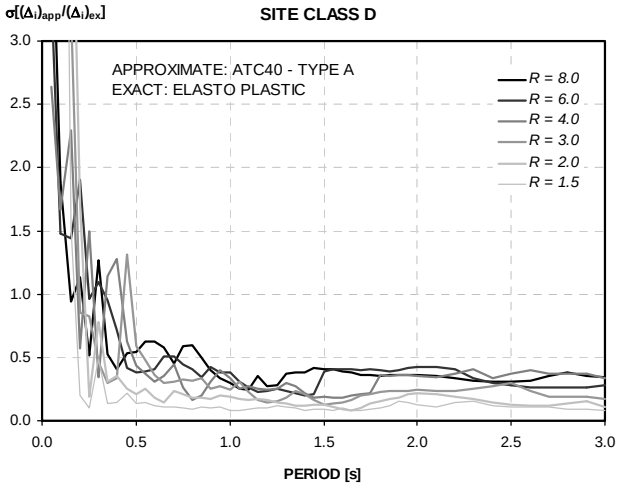


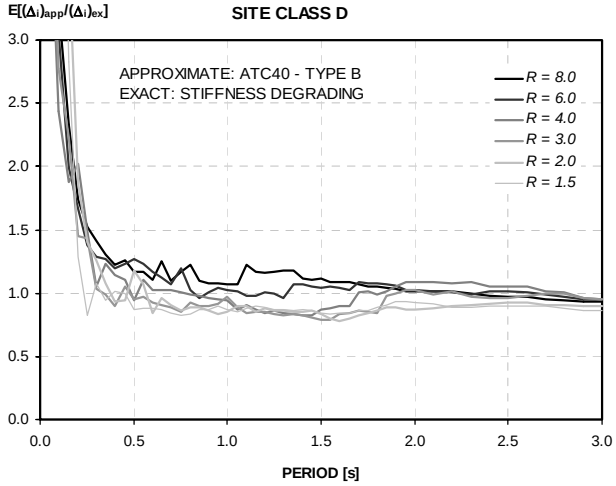


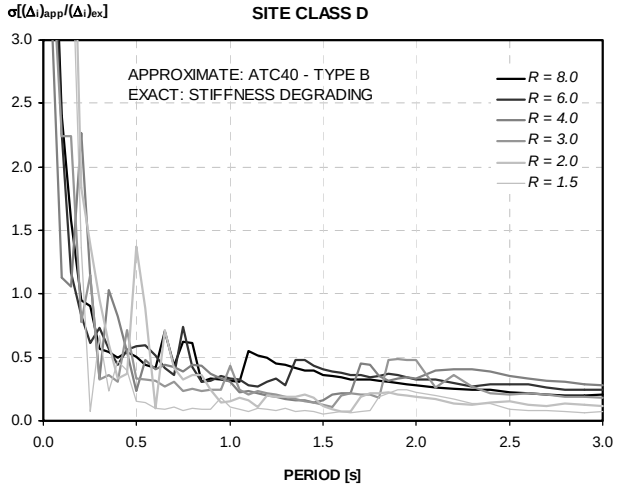


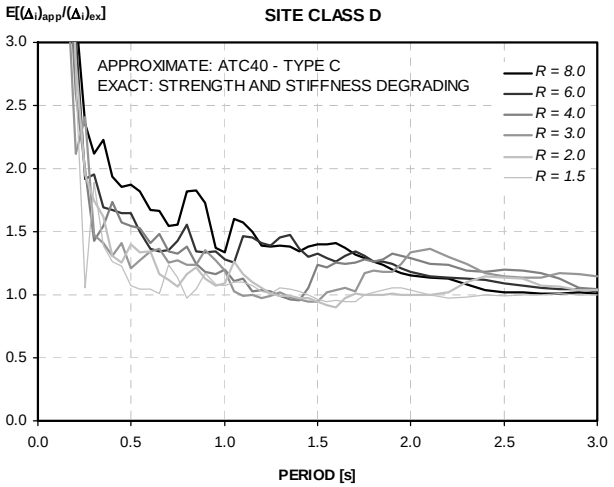


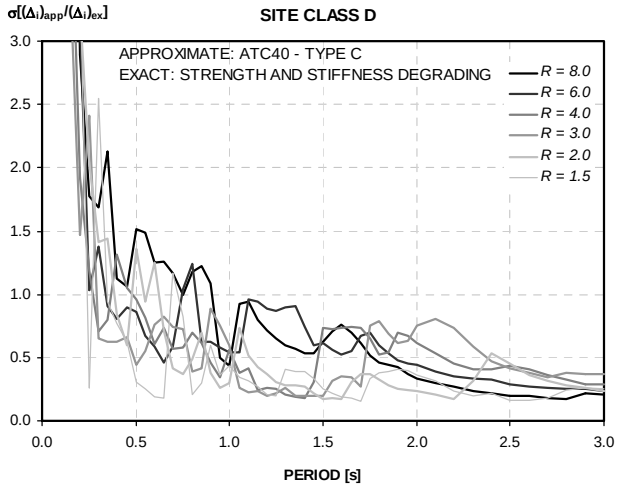

### *C.3.4 Comparisons for Site Class E:*

## MEAN ERROR

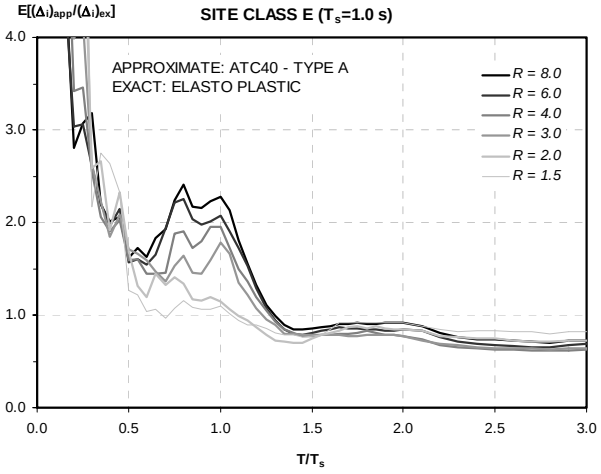


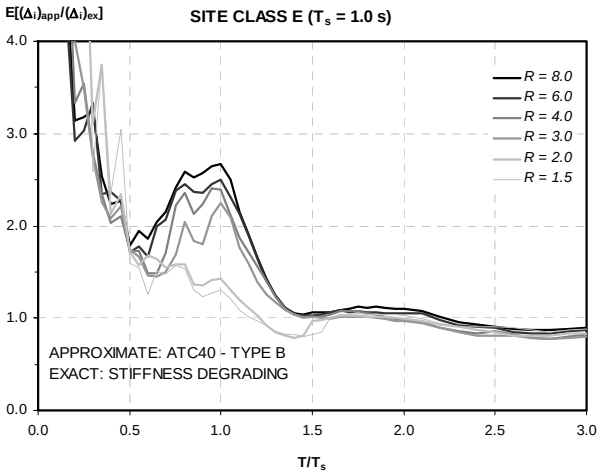


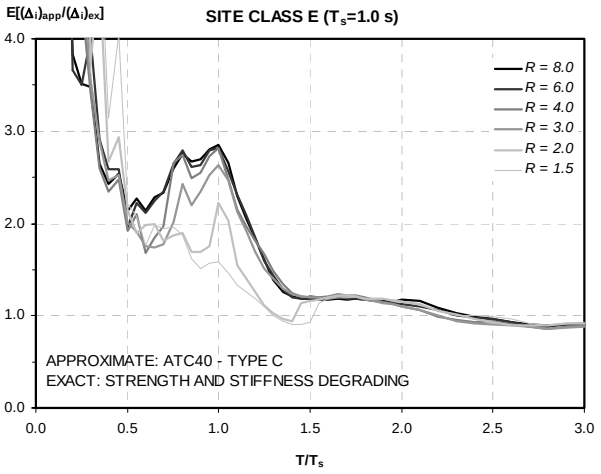


## ERROR DISPERSION

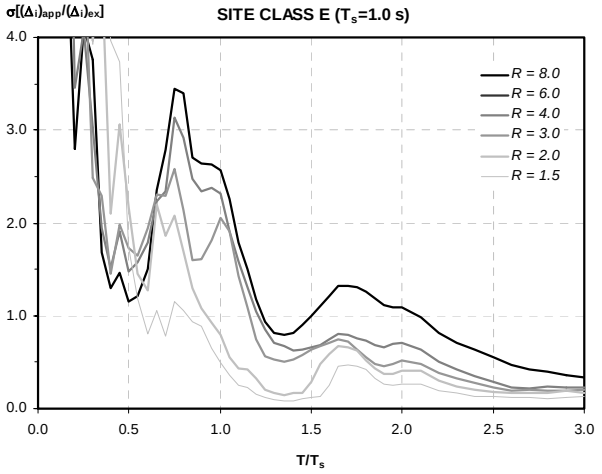


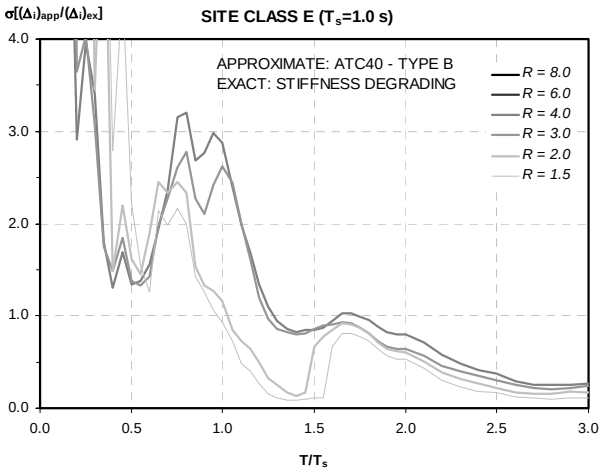


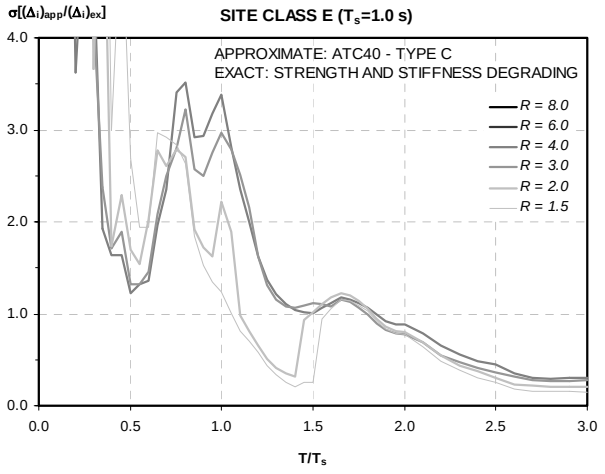

### *C.3.5 Comparisons for Near-Fault Ground Motions:*

## MEAN ERROR

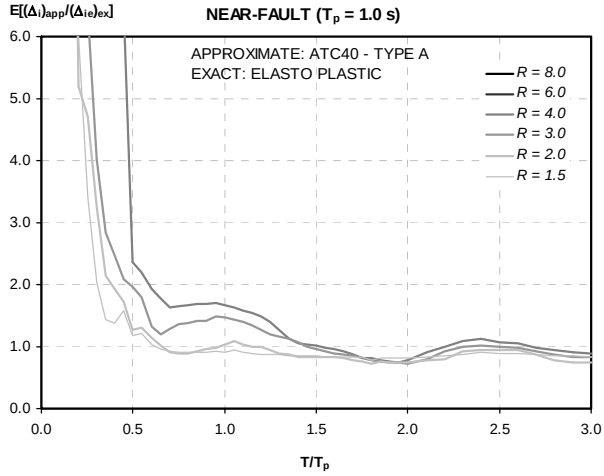


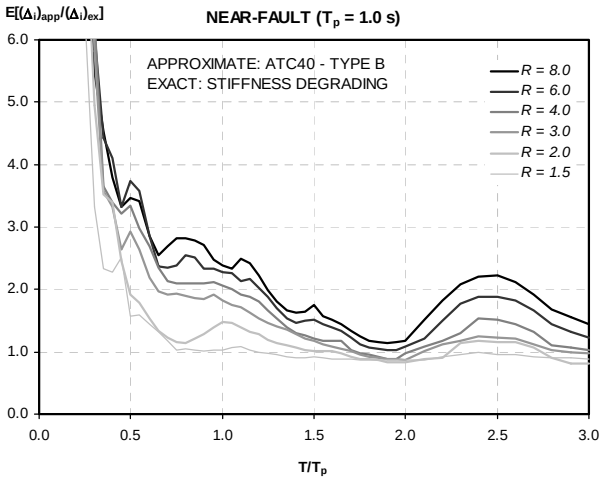


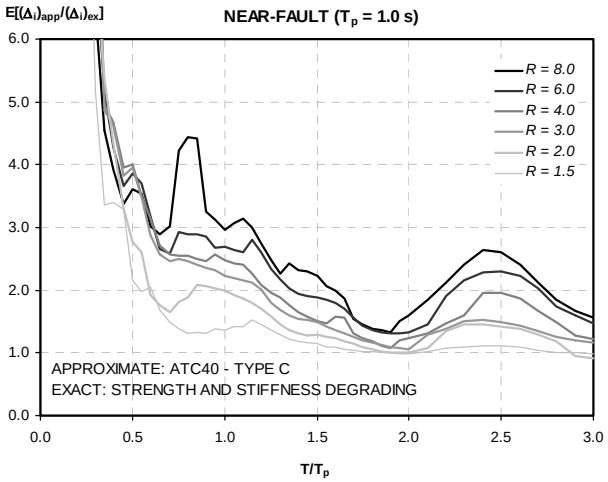


## ERROR DISPERSION

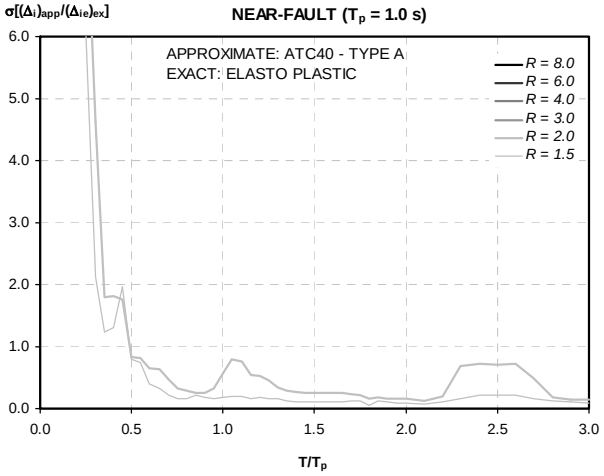


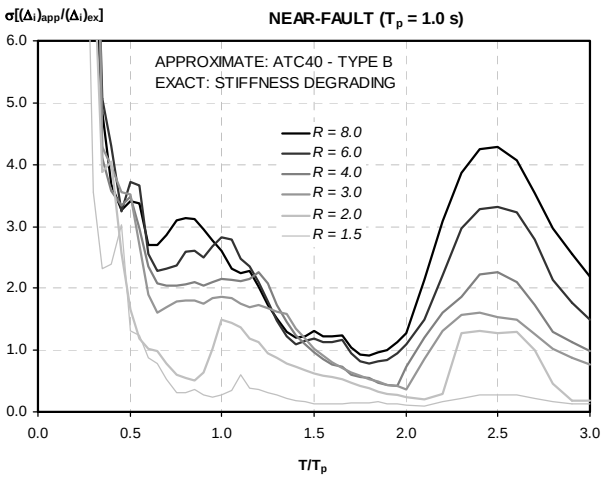


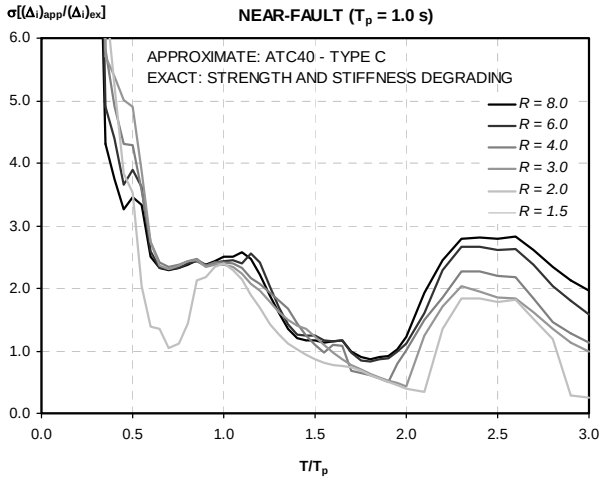

## C.4 Evaluation of the Coefficient Method of FEMA 356: Summary Results

### *C.4.1 FEMA 356 Nonlinear Static Procedure (NSP) $C_1$ Values for Different $T_s$ Values:*

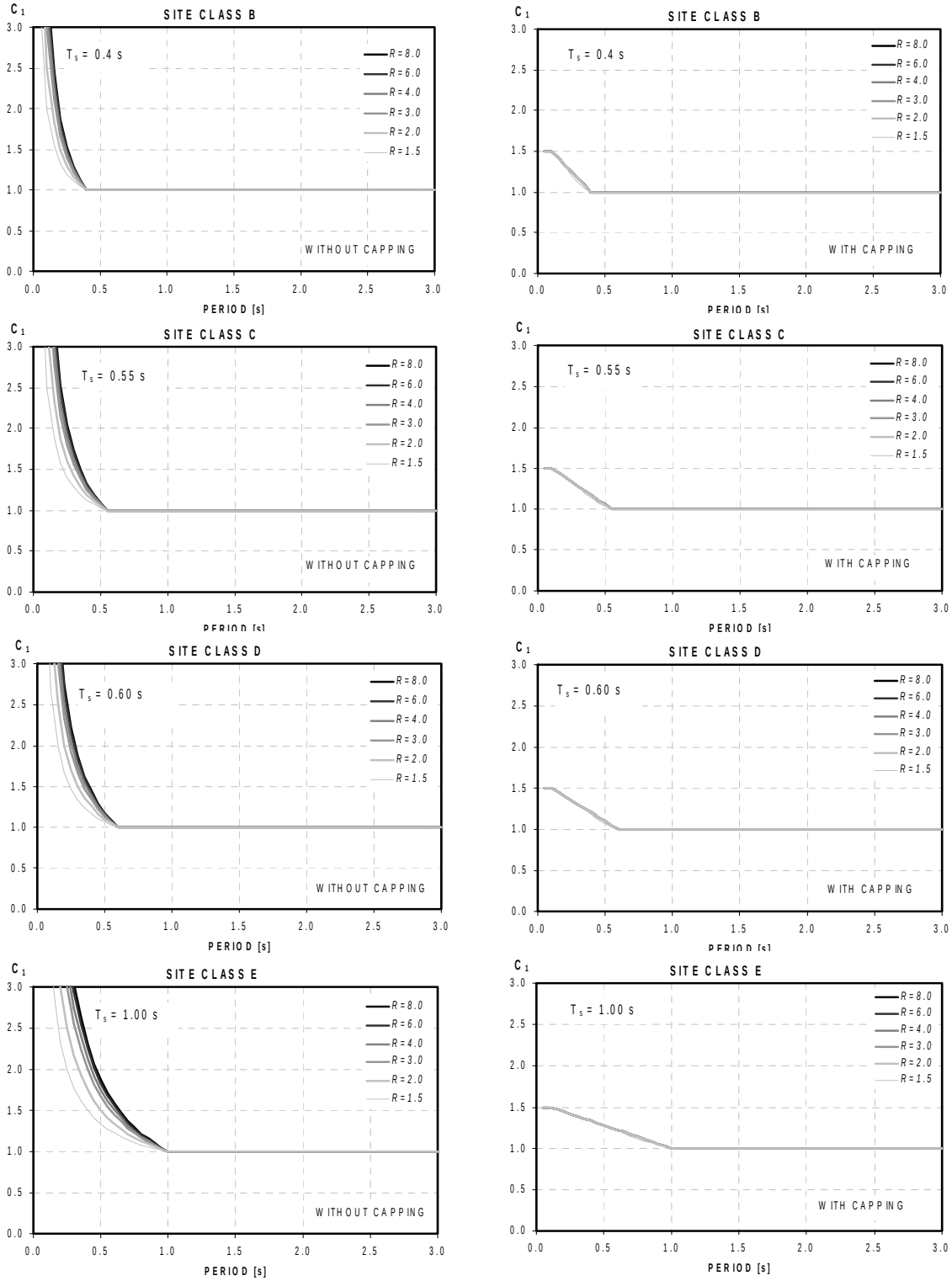

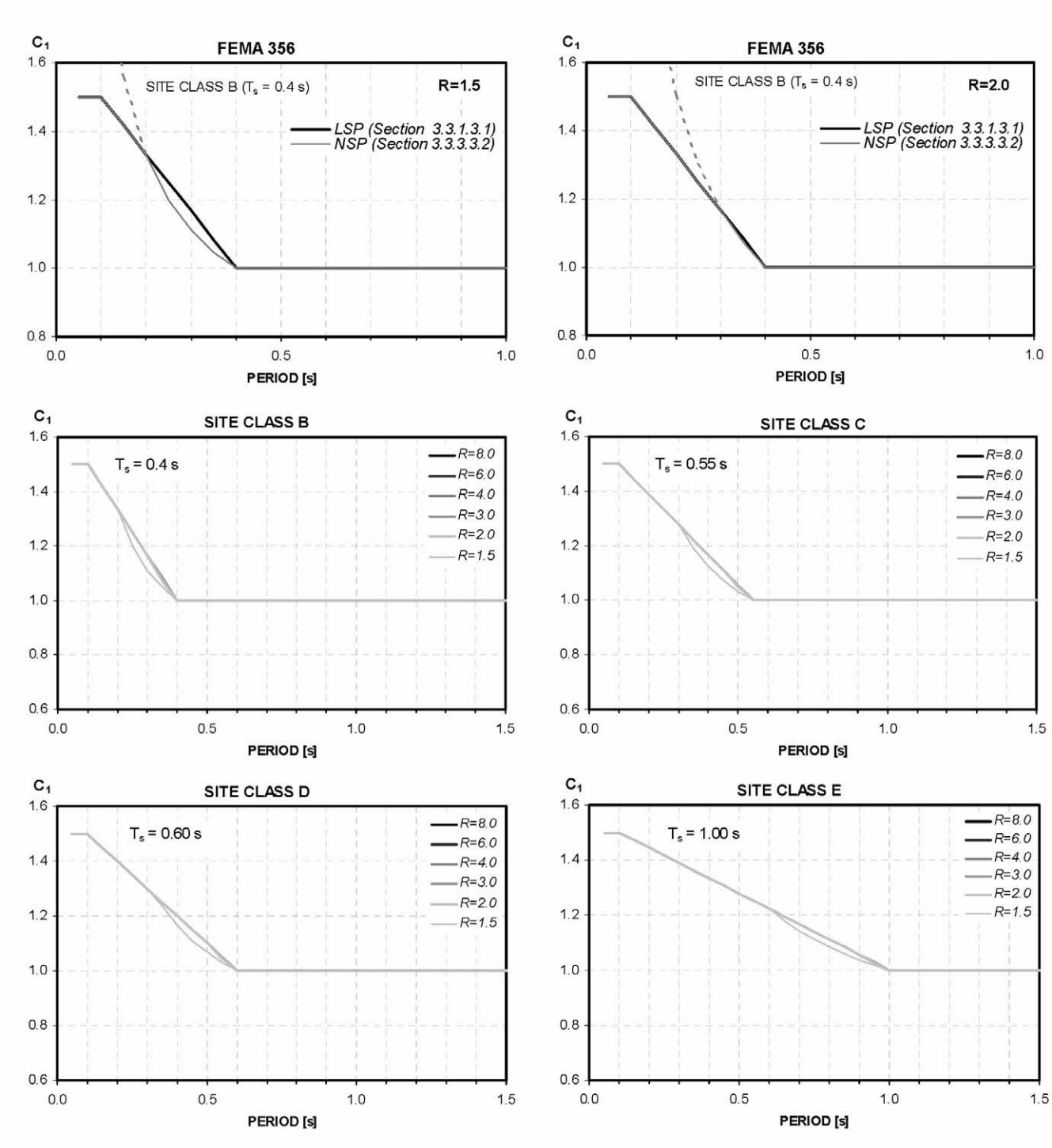
C1
FEMA 356
SITE CLASS B (Ts = 0.4 s)
R=1.5
LSP (Section 3.3.1.3.1)
NSP (Section 3.3.3.3.2)
PERIOD [s]
C1
FEMA 356
SITE CLASS B (Ts = 0.4 s)
R=2.0
LSP (Section 3.3.1.3.1)
NSP (Section 3.3.3.3.2)
PERIOD [s]
C1
SITE CLASS B
Ts = 0.4 s
R=8.0
R=6.0
R=4.0
R=3.0
R=2.0
R=1.5
PERIOD [s]
C1
SITE CLASS C
Ts = 0.55 s
R=8.0
R=6.0
R=4.0
R=3.0
R=2.0
R=1.5
PERIOD [s]
C1
SITE CLASS D
Ts = 0.60 s
R=8.0
R=6.0
R=4.0
R=3.0
R=2.0
R=1.5
PERIOD [s]
C1
SITE CLASS E
Ts = 1.00 s
R=8.0
R=6.0
R=4.0
R=3.0
R=2.0
R=1.5
PERIOD [s]

### *C.4.2 FEMA 356 NSP $C_2$ Values for Different $T_s$ Values:*

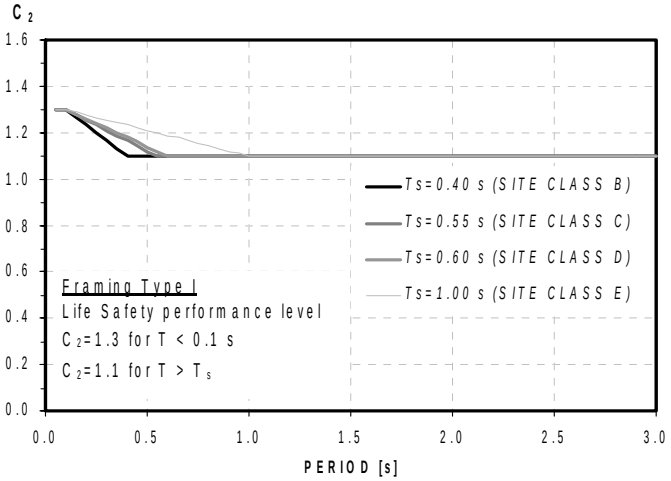


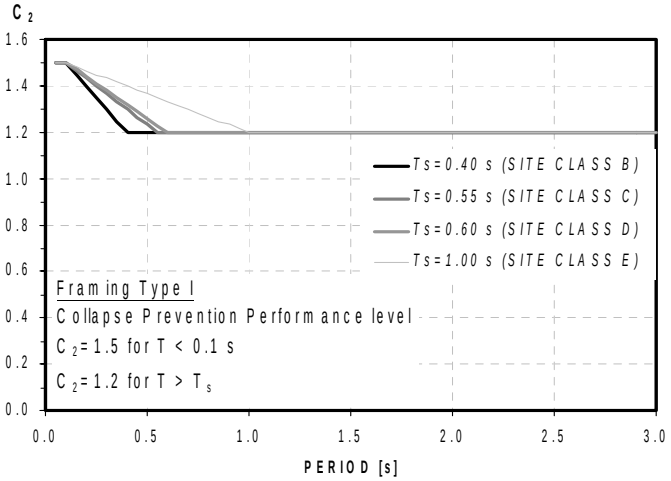

### *C.4.3 Mean Error of FEMA 356 NSP (Mean of Approximate to Exact Maximum Inelastic Displacements):*

#### C.4.3.1 Comparison with Elastic Perfectly Plastic Hysteretic Behavior:

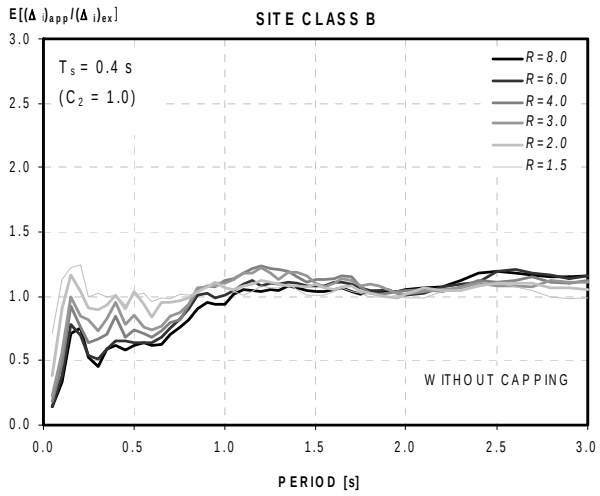


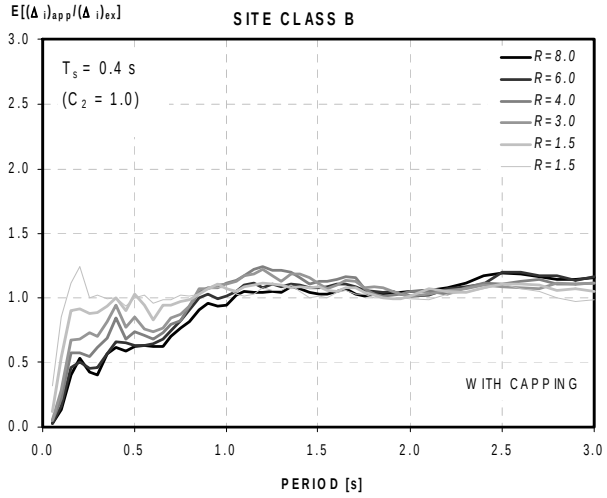


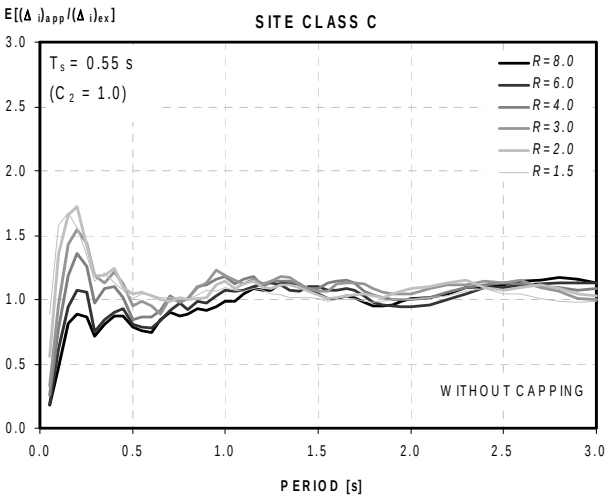


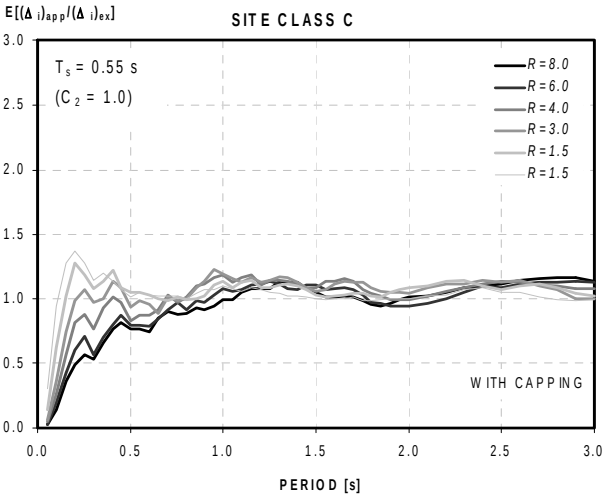


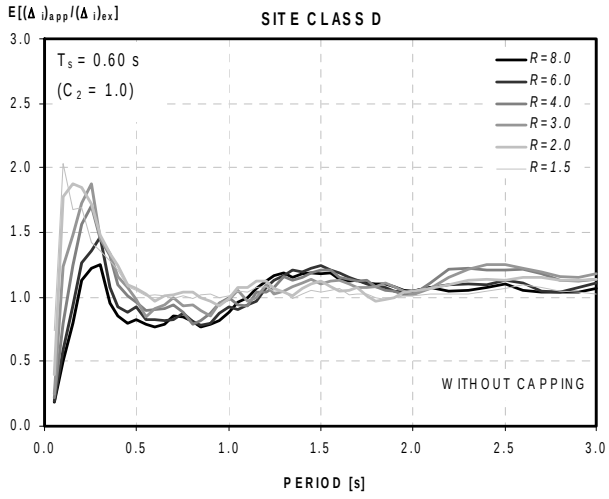


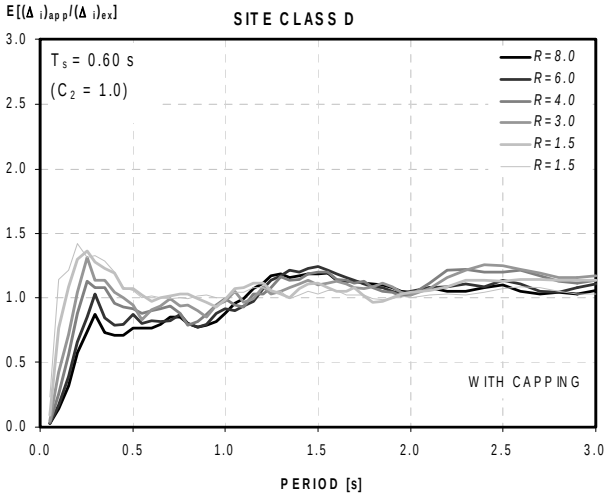

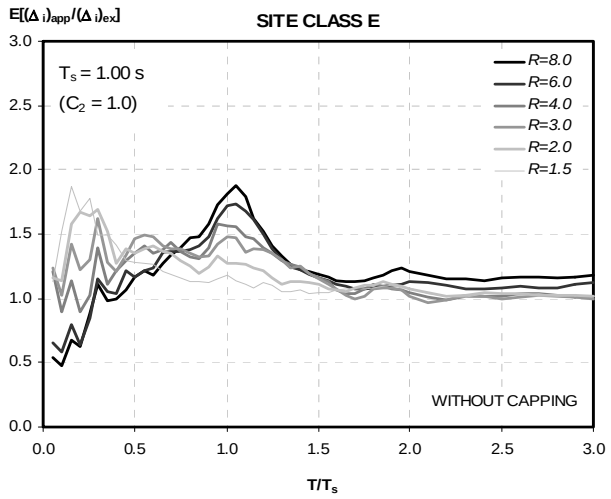
E[(Δ i)app/(Δ i)ex]
SITE CLASS E
Ts = 1.00 s
(C2 = 1.0)
R=8.0
R=6.0
R=4.0
R=3.0
R=2.0
R=1.5
WITHOUT CAPPING
T/Ts

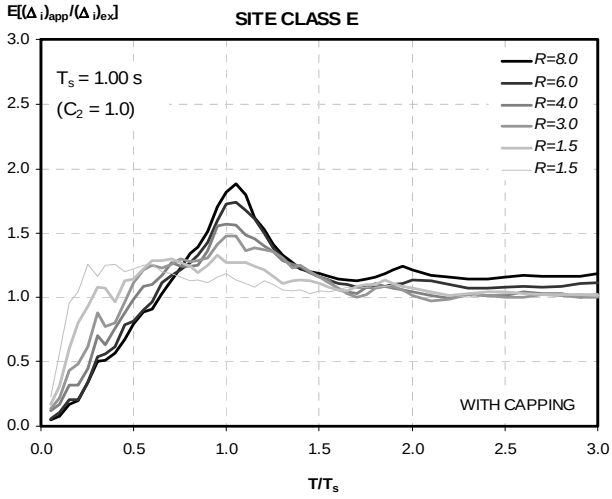
E[(Δ i)app/(Δ i)ex]
SITE CLASS E
Ts = 1.00 s
(C2 = 1.0)
R=8.0
R=6.0
R=4.0
R=3.0
R=1.5
R=1.5
WITH CAPPING
T/Ts

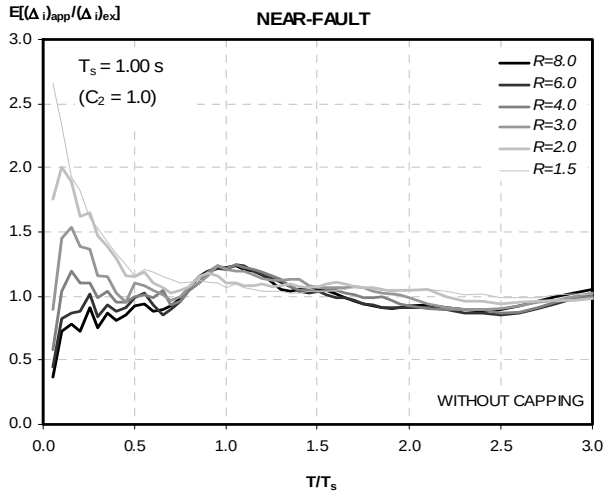
E[(Δ i)app/(Δ i)ex]
NEAR-FAULT
Ts = 1.00 s
(C2 = 1.0)
R=8.0
R=6.0
R=4.0
R=3.0
R=2.0
R=1.5
WITHOUT CAPPING
T/Ts

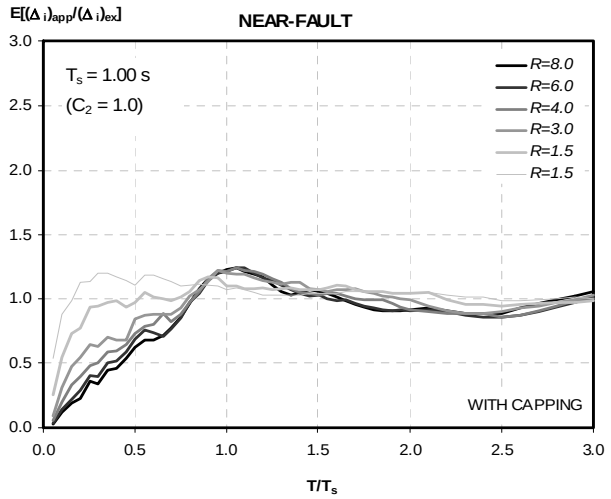
E[(Δ i)app/(Δ i)ex]
NEAR-FAULT
Ts = 1.00 s
(C2 = 1.0)
R=8.0
R=6.0
R=4.0
R=3.0
R=1.5
R=1.5
WITH CAPPING
T/Ts

### C.4.3.2 Comparison with Stiffness Degrading Hysteretic Behavior:

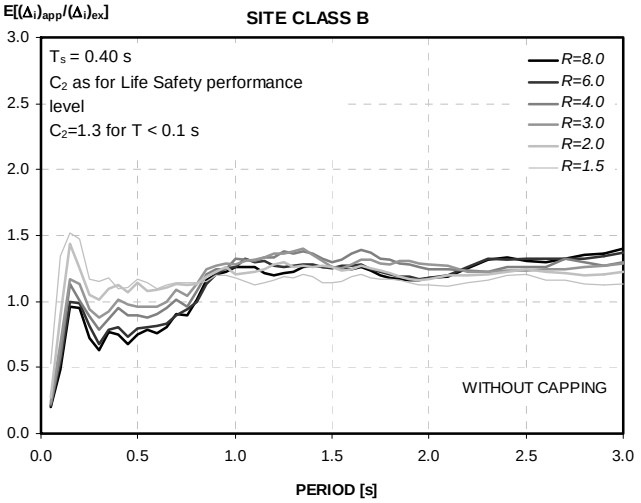


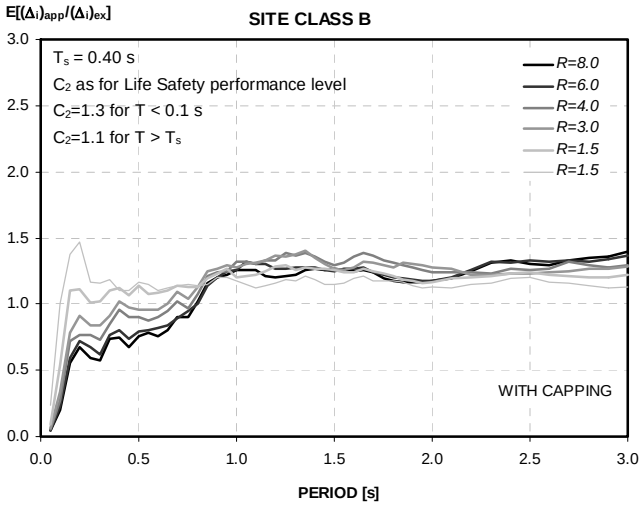


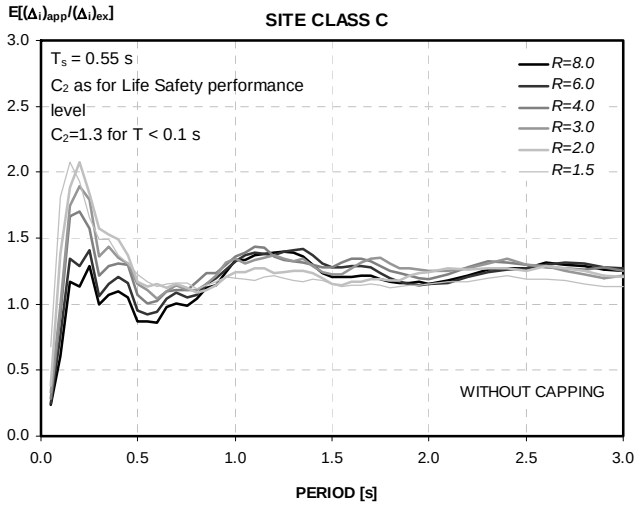


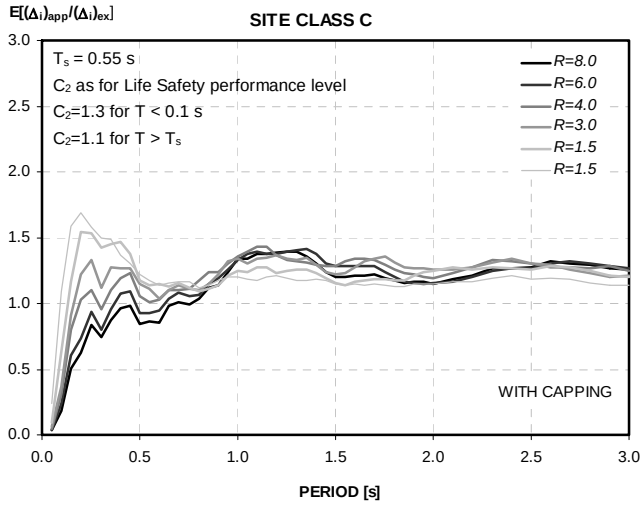


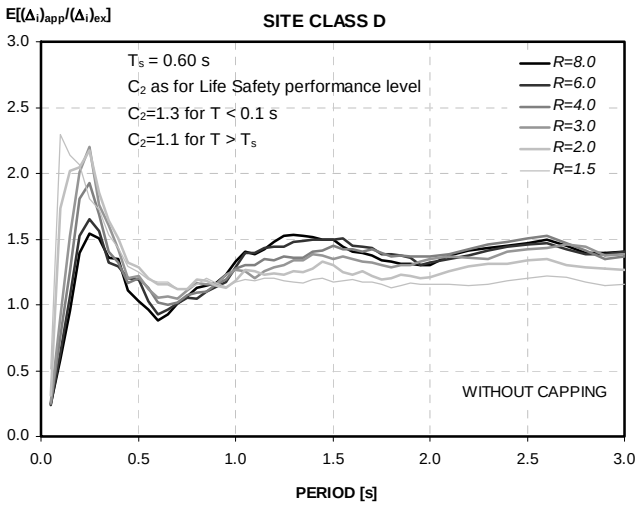


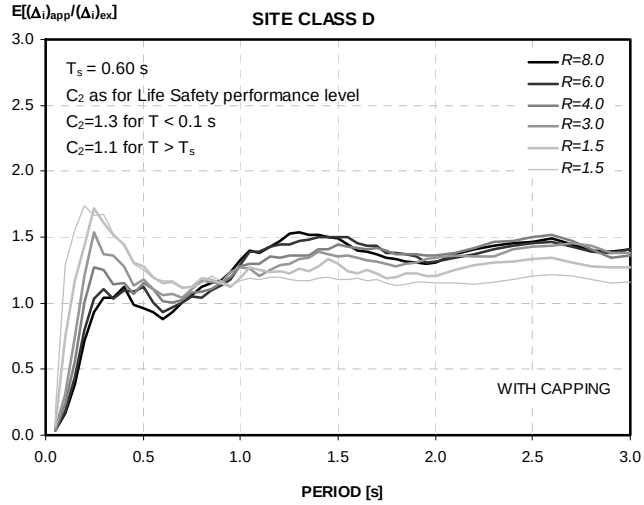

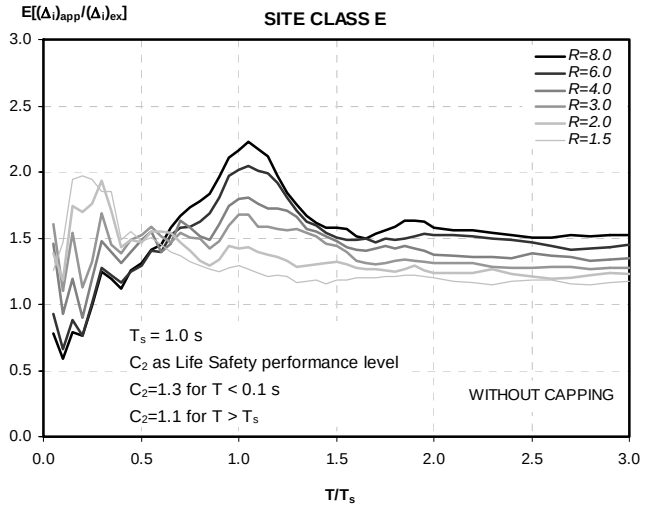
E[(Δi)app/(Δi)ex]
SITE CLASS E
R=8.0
R=6.0
R=4.0
R=3.0
R=2.0
R=1.5
Ts = 1.0 s
C2 as Life Safety performance level
C2=1.3 for T < 0.1 s
C2=1.1 for T > Ts
WITHOUT CAPPING
T/Ts

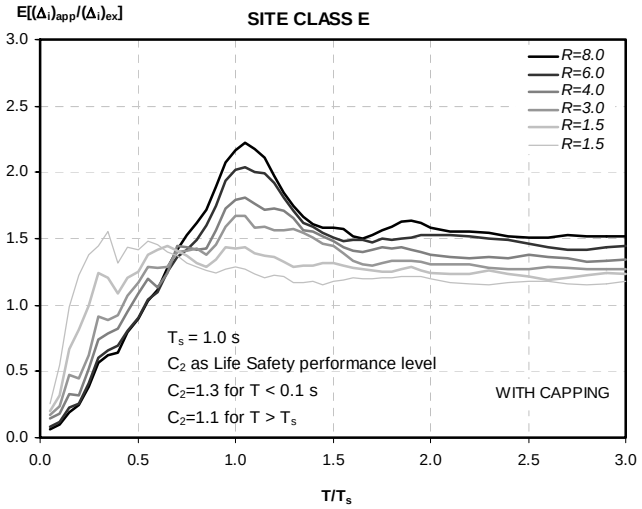
E[(Δi)app/(Δi)ex]
SITE CLASS E
R=8.0
R=6.0
R=4.0
R=3.0
R=1.5
R=1.5
Ts = 1.0 s
C2 as Life Safety performance level
C2=1.3 for T < 0.1 s
C2=1.1 for T > Ts
WITH CAPPING
T/Ts

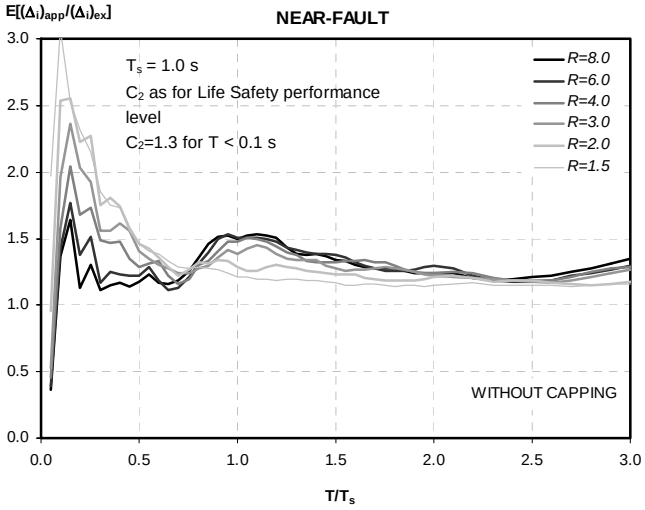
E[(Δi)app/(Δi)ex]
NEAR-FAULT
Ts = 1.0 s
C2 as for Life Safety performance level
C2=1.3 for T < 0.1 s
R=8.0
R=6.0
R=4.0
R=3.0
R=2.0
R=1.5
WITHOUT CAPPING
T/Ts

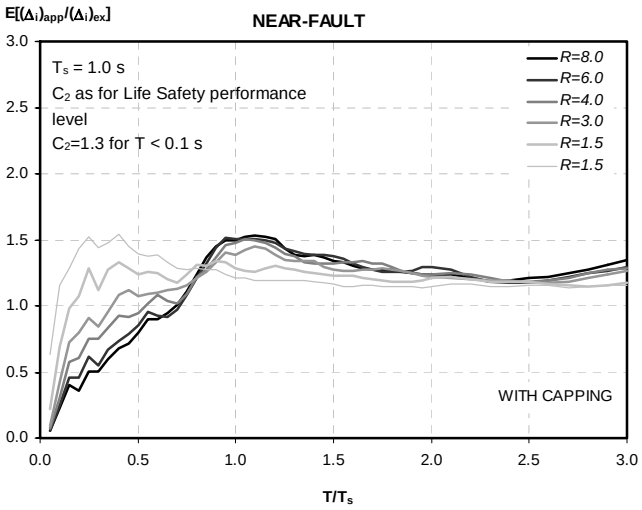
E[(Δi)app/(Δi)ex]
NEAR-FAULT
Ts = 1.0 s
C2 as for Life Safety performance level
C2=1.3 for T < 0.1 s
R=8.0
R=6.0
R=4.0
R=3.0
R=1.5
R=1.5
WITH CAPPING
T/Ts

### C.4.3.3 Comparison with Stiffness and Strength Degrading Hysteretic Behavior:

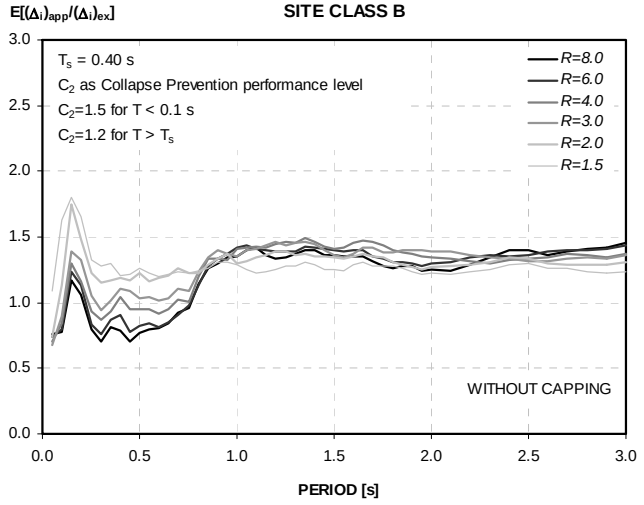


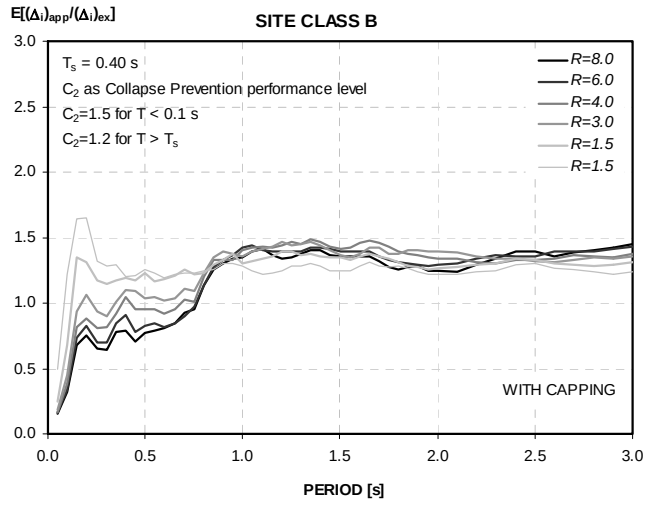


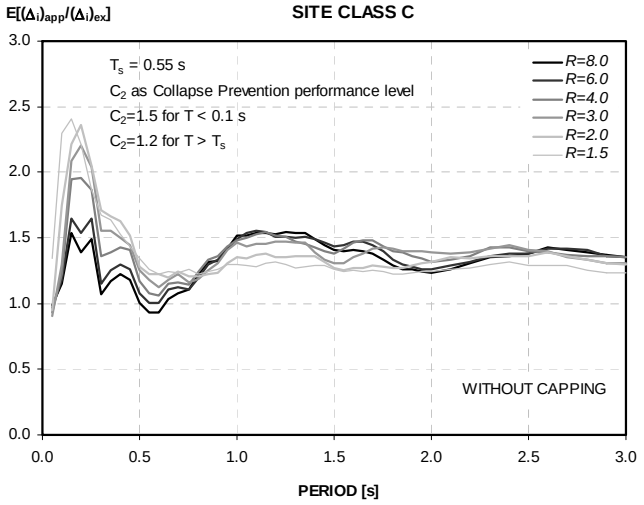


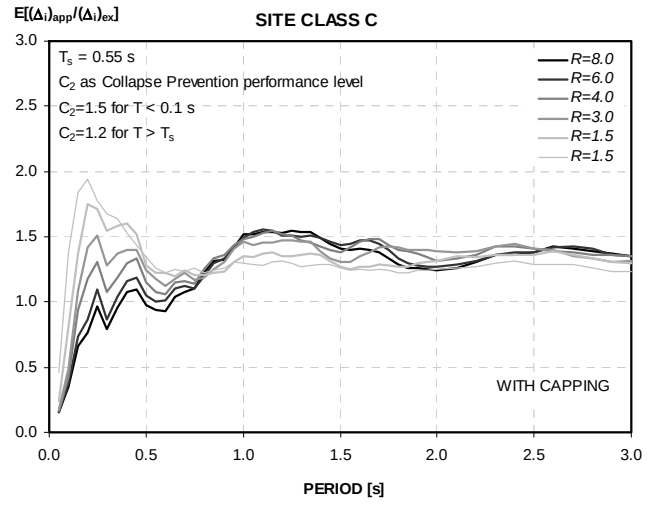


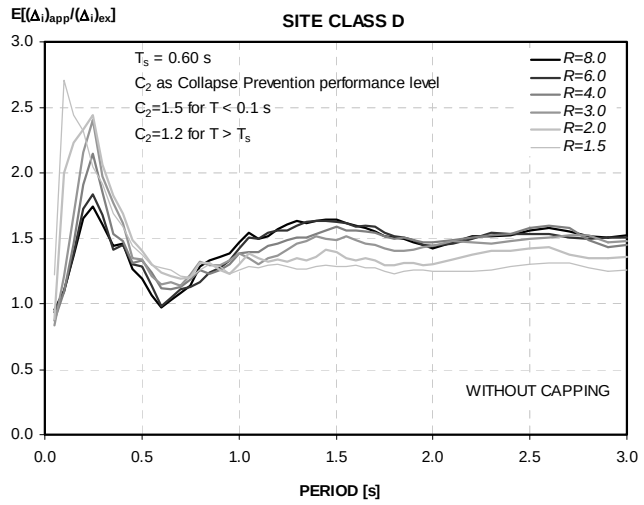


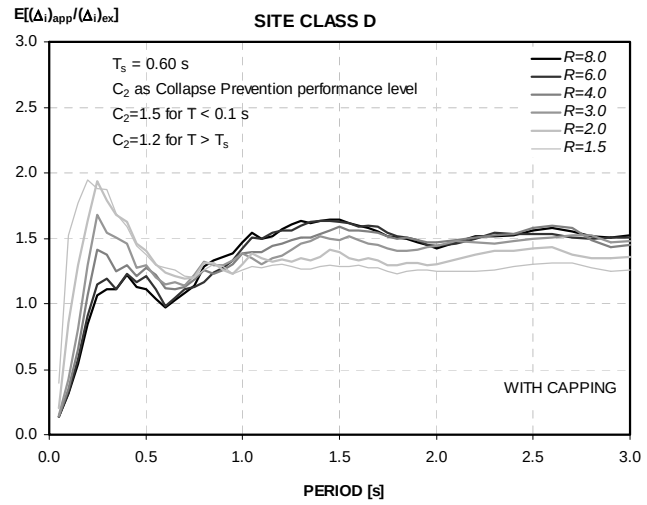

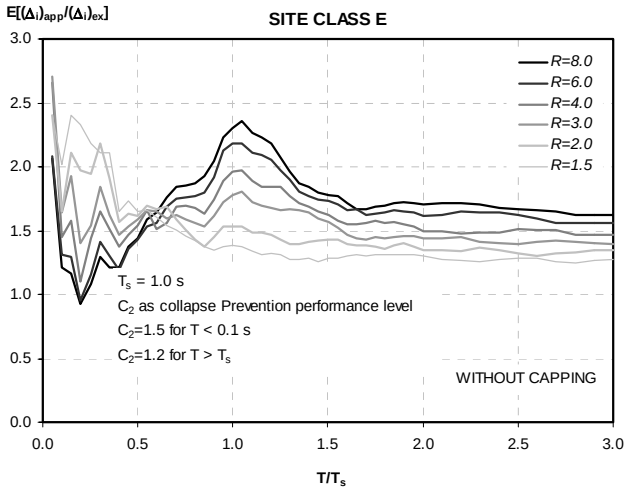
E[(Δi)app/(Δi)ex]
SITE CLASS E
R=8.0
R=6.0
R=4.0
R=3.0
R=2.0
R=1.5
Ts = 1.0 s
C2 as collapse Prevention performance level
C2=1.5 for T < 0.1 s
C2=1.2 for T > Ts
WITHOUT CAPPING
T/Ts

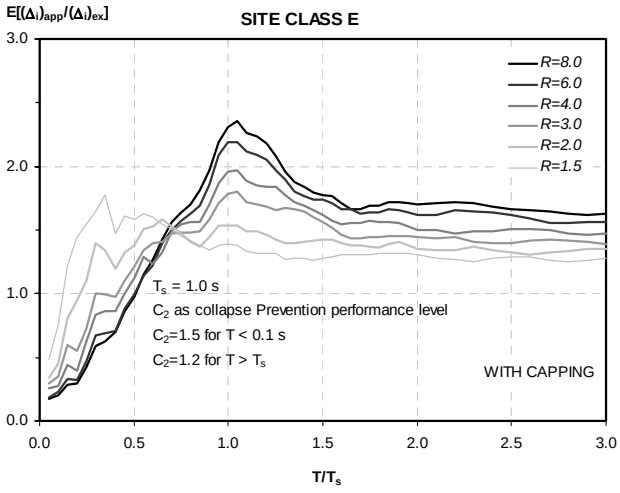
E[(Δi)app/(Δi)ex]
SITE CLASS E
R=8.0
R=6.0
R=4.0
R=3.0
R=2.0
R=1.5
Ts = 1.0 s
C2 as collapse Prevention performance level
C2=1.5 for T < 0.1 s
C2=1.2 for T > Ts
WITH CAPPING
T/Ts

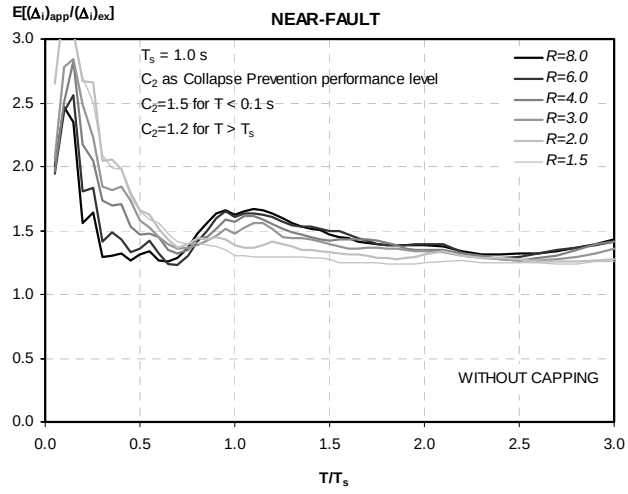
E[(Δi)app/(Δi)ex]
NEAR-FAULT
Ts = 1.0 s
C2 as Collapse Prevention performance level
C2=1.5 for T < 0.1 s
C2=1.2 for T > Ts
R=8.0
R=6.0
R=4.0
R=3.0
R=2.0
R=1.5
WITHOUT CAPPING
T/Ts

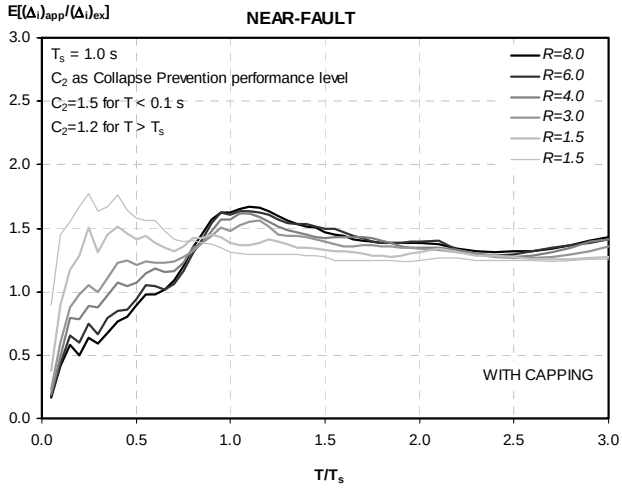
E[(Δi)app/(Δi)ex]
NEAR-FAULT
Ts = 1.0 s
C2 as Collapse Prevention performance level
C2=1.5 for T < 0.1 s
C2=1.2 for T > Ts
R=8.0
R=6.0
R=4.0
R=3.0
R=1.5
R=1.5
WITH CAPPING
T/Ts

### *C.4.4 Dispersion of the Error in FEMA 356 NSP (Standard Deviation of Approximate to Exact Maximum Inelastic Displacements):*

#### C.4.4.1 Comparison with Elastic Perfectly Plastic Hysteretic Behavior:

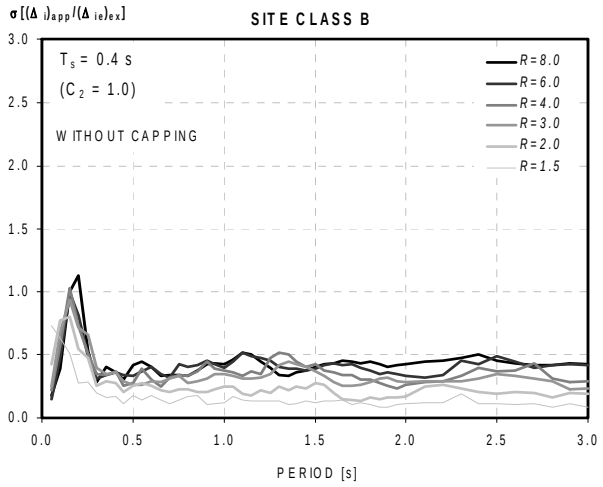


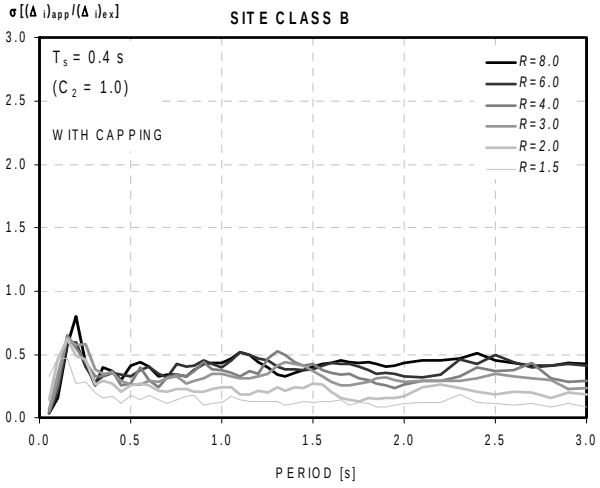


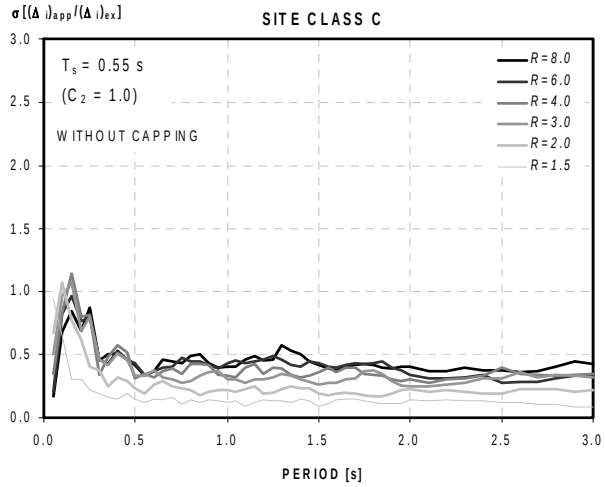


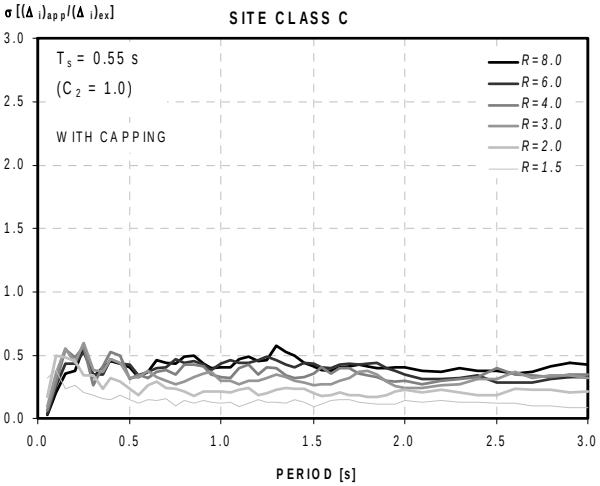


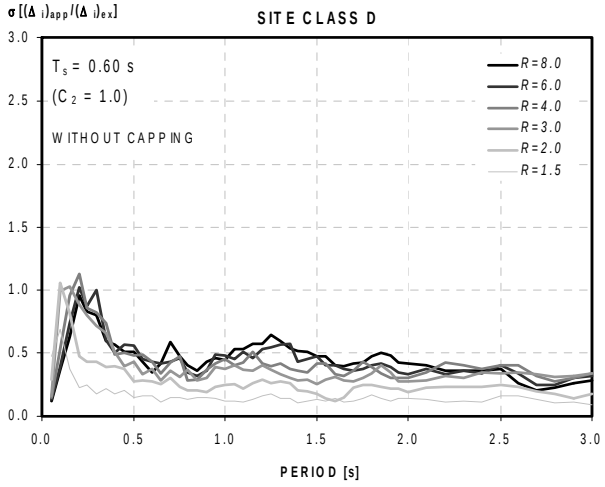


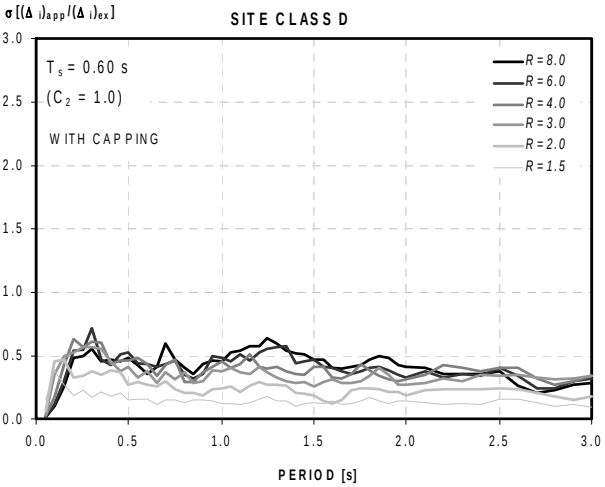

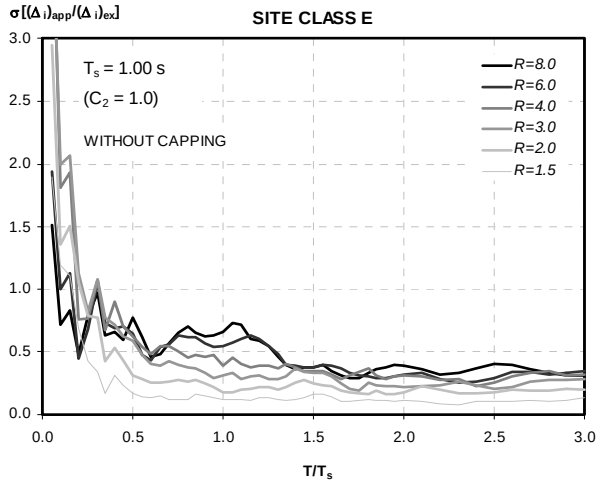
σ[(Δ i)app/(Δ i)ex]
SITE CLASS E
Ts = 1.00 s
(C2 = 1.0)
WITHOUT CAPPING
R=8.0
R=6.0
R=4.0
R=3.0
R=2.0
R=1.5
T/Ts

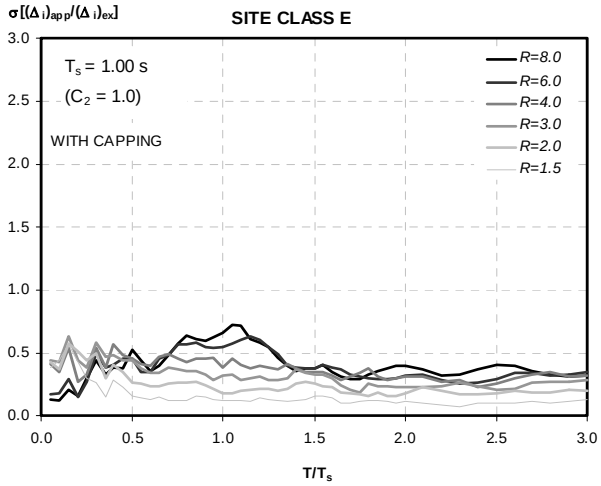
σ[(Δ i)app/(Δ i)ex]
SITE CLASS E
Ts = 1.00 s
(C2 = 1.0)
WITH CAPPING
R=8.0
R=6.0
R=4.0
R=3.0
R=2.0
R=1.5
T/Ts

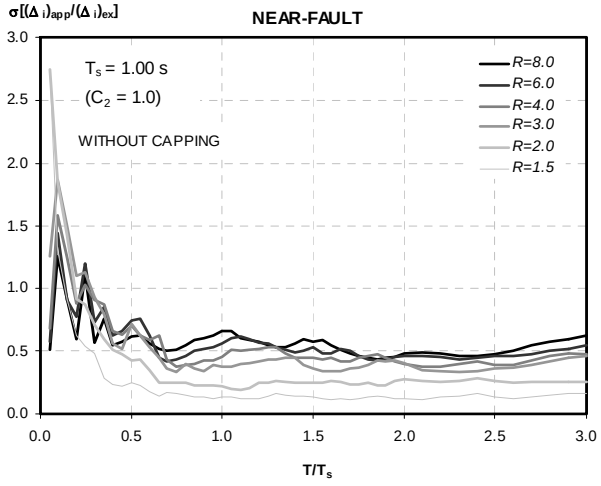
σ[(Δ i)app/(Δ i)ex]
NEAR-FAULT
Ts = 1.00 s
(C2 = 1.0)
WITHOUT CAPPING
R=8.0
R=6.0
R=4.0
R=3.0
R=2.0
R=1.5
T/Ts

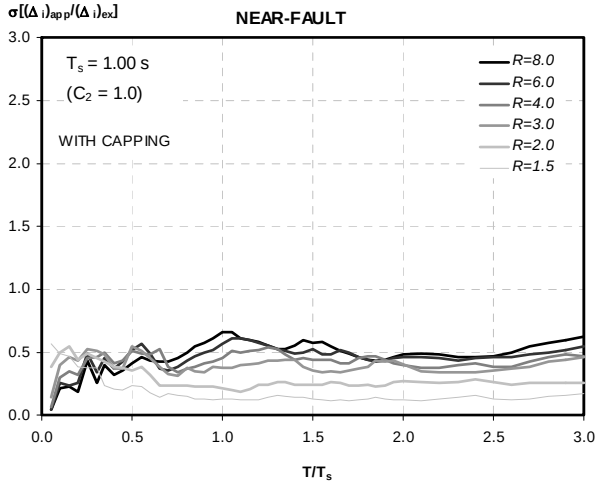
σ[(Δ i)app/(Δ i)ex]
NEAR-FAULT
Ts = 1.00 s
(C2 = 1.0)
WITH CAPPING
R=8.0
R=6.0
R=4.0
R=3.0
R=2.0
R=1.5
T/Ts

### C.4.4.2 Comparison with Stiffness Degrading Hysteretic Behavior:

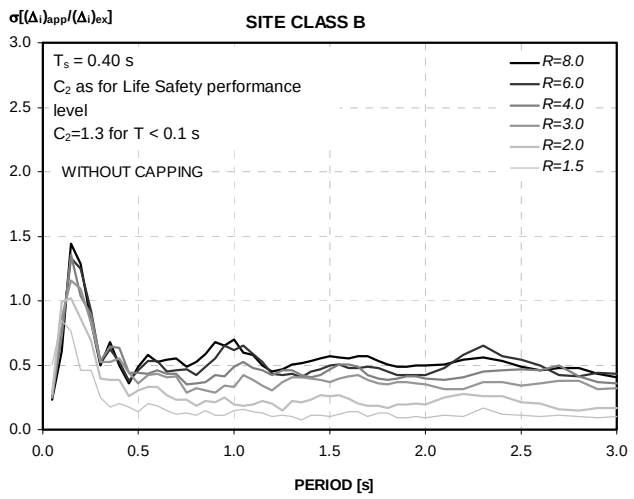


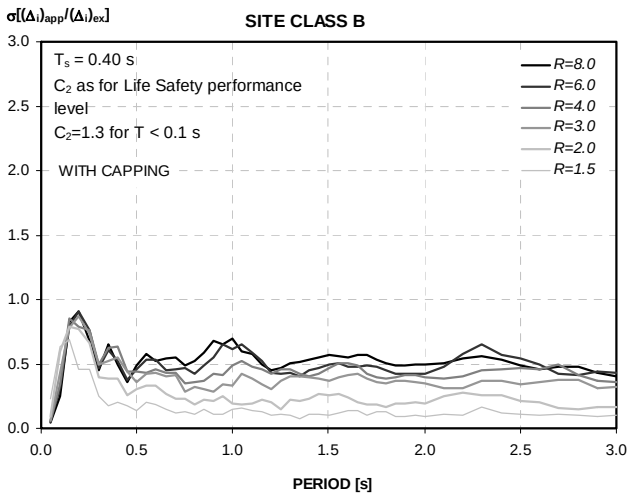


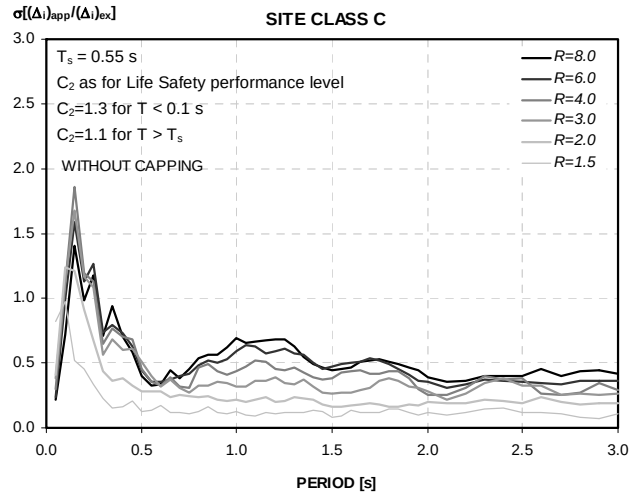


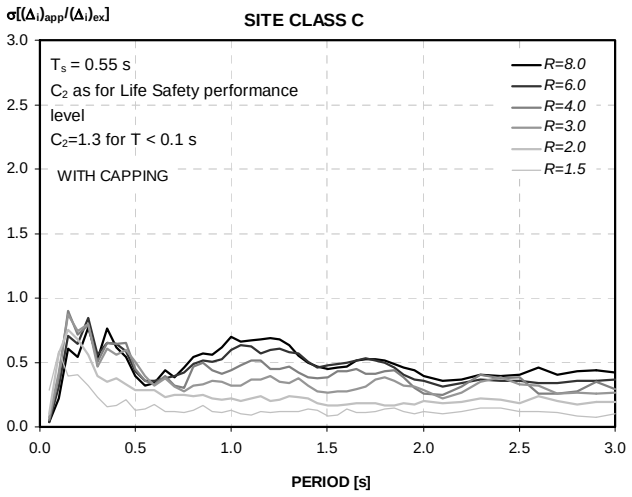


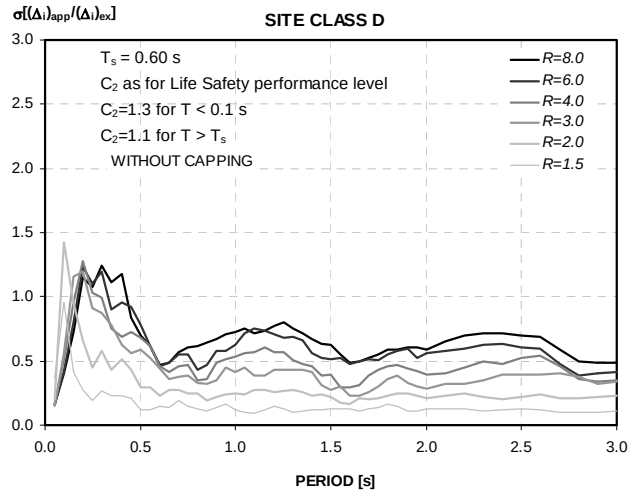


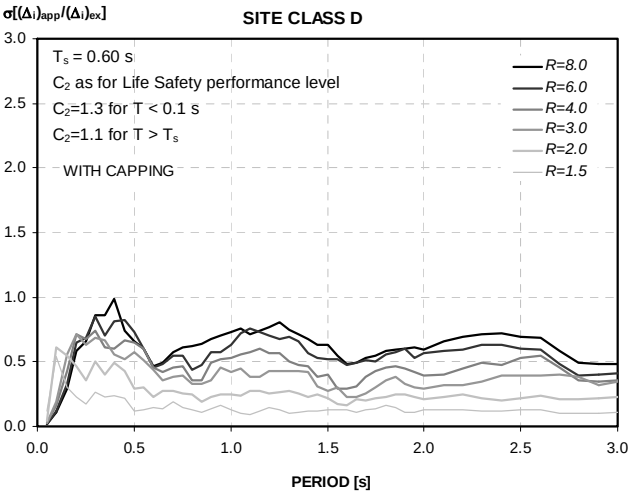

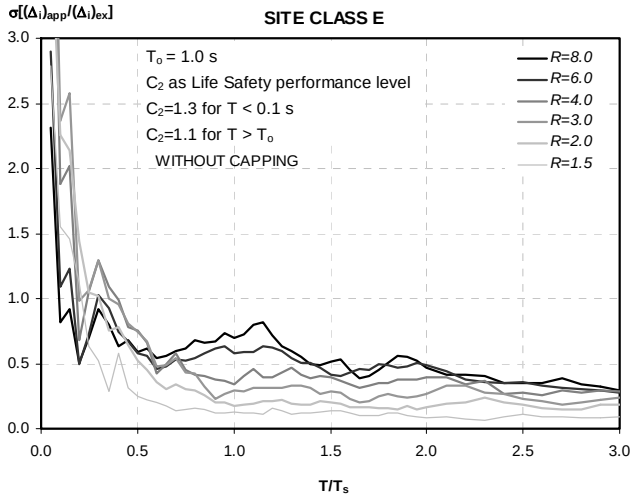
σ[(Δi)app/(Δi)ex]
SITE CLASS E
To = 1.0 s
C2 as Life Safety performance level
C2=1.3 for T < 0.1 s
C2=1.1 for T > To
WITHOUT CAPPING
R=8.0
R=6.0
R=4.0
R=3.0
R=2.0
R=1.5
T/Ts

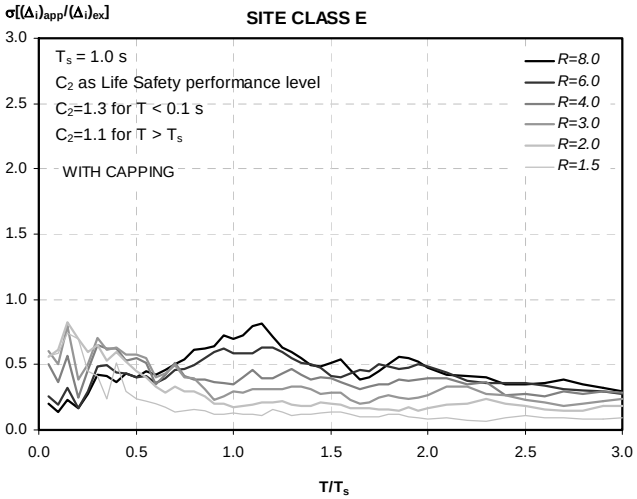
σ[(Δi)app/(Δi)ex]
SITE CLASS E
Ts = 1.0 s
C2 as Life Safety performance level
C2=1.3 for T < 0.1 s
C2=1.1 for T > Ts
WITH CAPPING
R=8.0
R=6.0
R=4.0
R=3.0
R=2.0
R=1.5
T/Ts

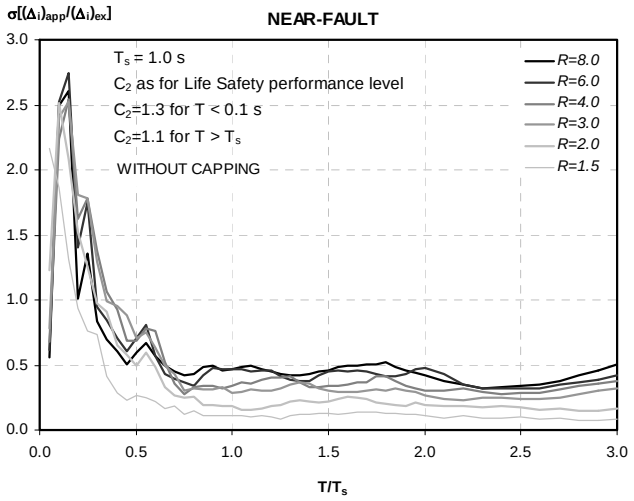
σ[(Δi)app/(Δi)ex]
NEAR-FAULT
Ts = 1.0 s
C2 as for Life Safety performance level
C2=1.3 for T < 0.1 s
C2=1.1 for T > Ts
WITHOUT CAPPING
R=8.0
R=6.0
R=4.0
R=3.0
R=2.0
R=1.5
T/Ts

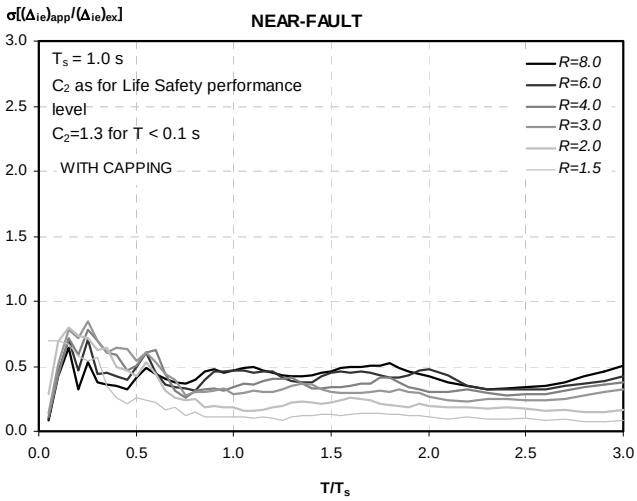
σ[(Δie)app/(Δie)ex]
NEAR-FAULT
Ts = 1.0 s
C2 as for Life Safety performance level
C2=1.3 for T < 0.1 s
WITH CAPPING
R=8.0
R=6.0
R=4.0
R=3.0
R=2.0
R=1.5
T/Ts

### C.4.4.3 Comparison with Stiffness and Strength Degrading Hysteretic Behavior:

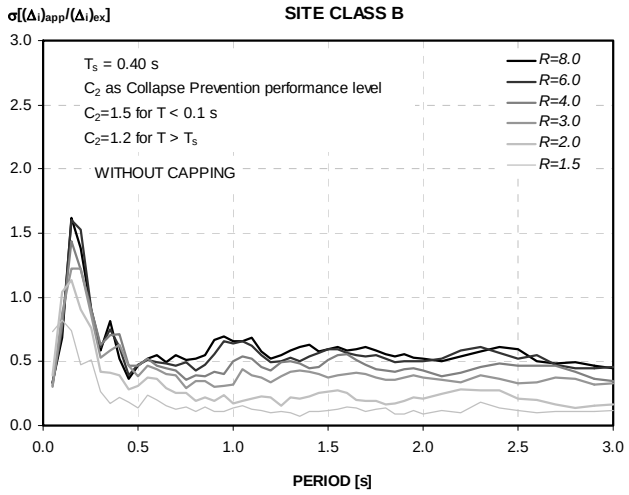


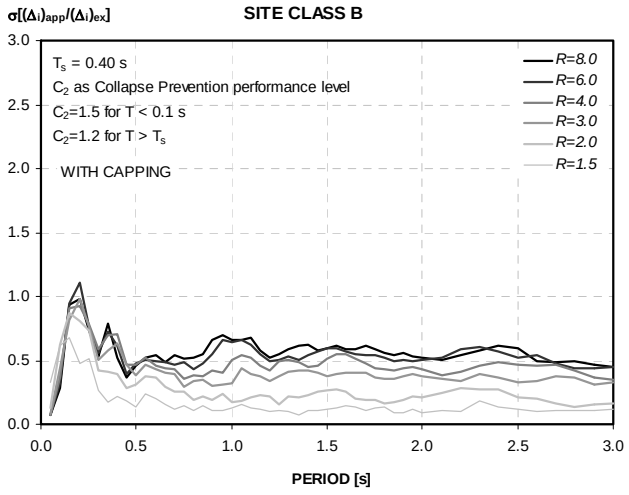


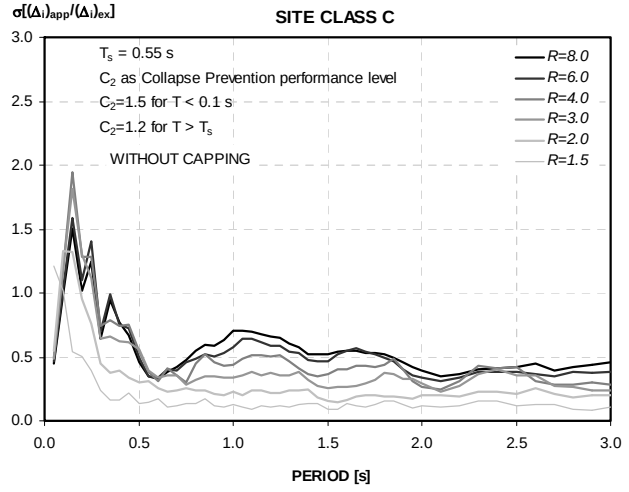


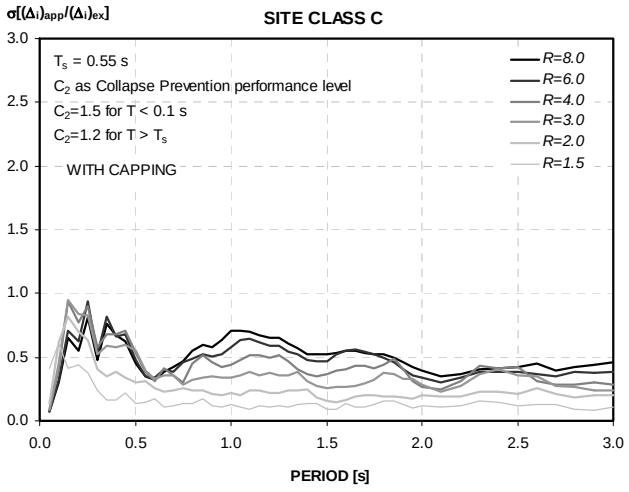


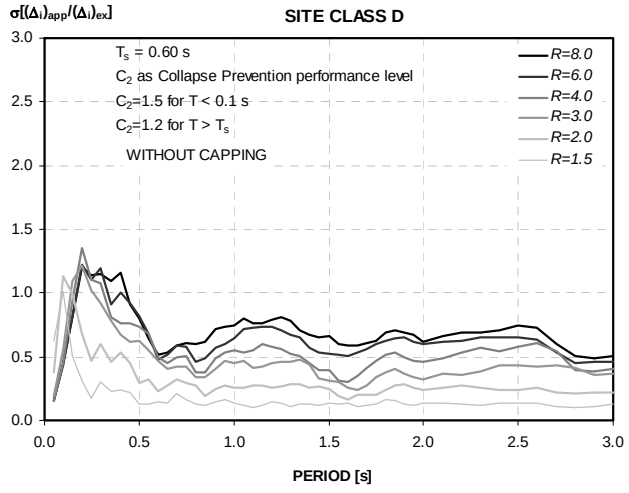


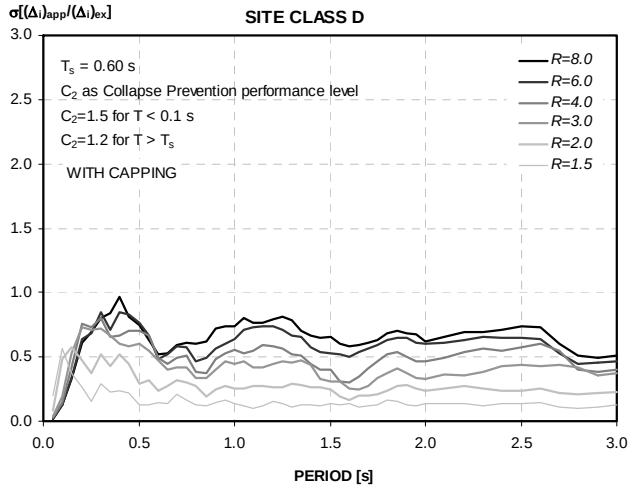

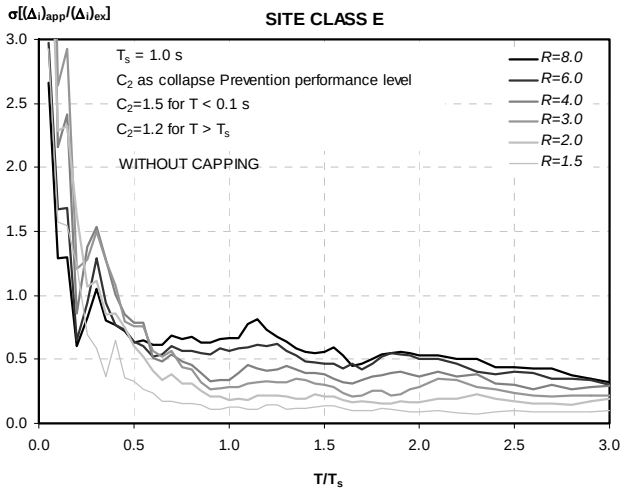
σ[(Δi)app/(Δi)ex]
SITE CLASS E
Ts = 1.0 s
C2 as collapse Prevention performance level
C2=1.5 for T < 0.1 s
C2=1.2 for T > Ts
WITHOUT CAPPING
R=8.0
R=6.0
R=4.0
R=3.0
R=2.0
R=1.5
T/Ts

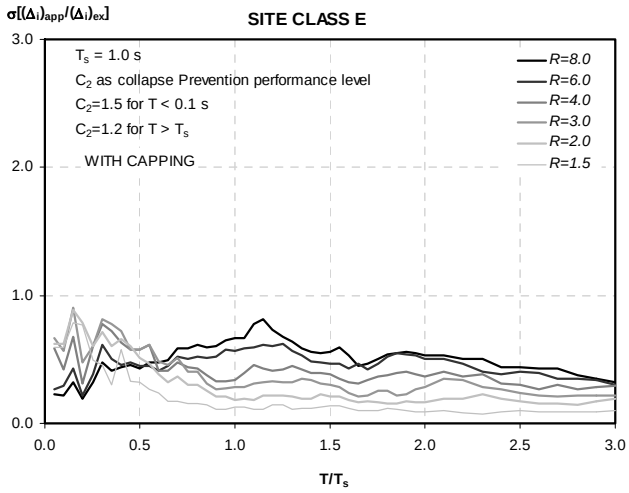
σ[(Δi)app/(Δi)ex]
SITE CLASS E
Ts = 1.0 s
C2 as collapse Prevention performance level
C2=1.5 for T < 0.1 s
C2=1.2 for T > Ts
WITH CAPPING
R=8.0
R=6.0
R=4.0
R=3.0
R=2.0
R=1.5
T/Ts

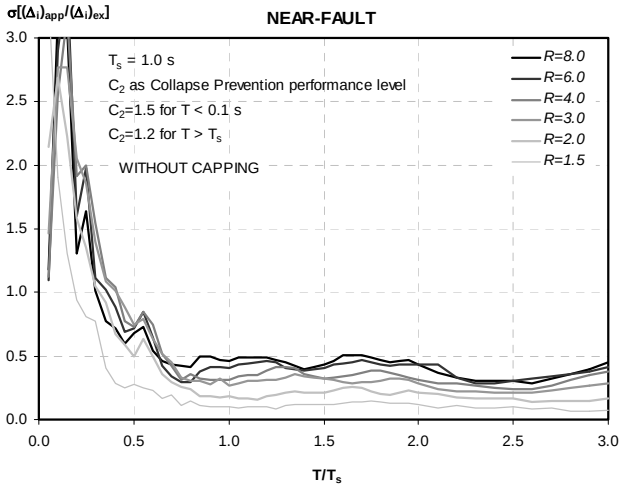
σ[(Δi)app/(Δi)ex]
NEAR-FAULT
Ts = 1.0 s
C2 as Collapse Prevention performance level
C2=1.5 for T < 0.1 s
C2=1.2 for T > Ts
WITHOUT CAPPING
R=8.0
R=6.0
R=4.0
R=3.0
R=2.0
R=1.5
T/Ts

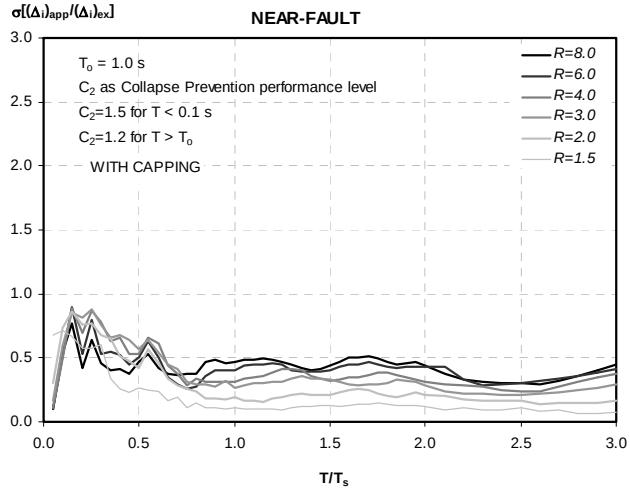
σ[(Δi)app/(Δi)ex]
NEAR-FAULT
To = 1.0 s
C2 as Collapse Prevention performance level
C2=1.5 for T < 0.1 s
C2=1.2 for T > To
WITH CAPPING
R=8.0
R=6.0
R=4.0
R=3.0
R=2.0
R=1.5
T/Ts

# D. Supplementary Information and Data on Equivalent Linearization

## D.1 Introduction

This appendix provides material supporting the improved procedures contained in Chapter 6. It provides a basic discussion of structural capacity and seismic demand for use with equivalent linearization procedures. It then reviews the theoretical underpinnings and past development of equivalent linearization procedures. It describes the new methodology for developing the improved effective period and damping equations found in Sections 6.2.1 and 6.2.2.

## D.2 Capacity-Spectrum Method

The Capacity-Spectrum Method (CSM) has rapidly grown in acceptance as a tool for determining the displacement response of structures in the inelastic response range. One of the attributes that makes the CSM appealing is its intuitive nature. It is relatively straightforward to think of an earthquake as presenting a demand on a structure and the structure as possessing a certain capacity to resist this demand. When the capacity and maximum demand are equal, the system can be considered to be in a state of "Equilibrium" that defines the expected performance of the structure.

The use of effective or equivalent linear parameters in the CSM is also appealing from an intuitive point of view. First, it seems reasonable that the period of a structure lengthens as it loses stiffness. Second, it seems logical that inelastic behavior and damage produce increased damping. The use of equivalent linear parameters also allows the CSM procedure to be applied with equal ease to cases where the earthquake demand is specified by a smooth design spectrum, a uniform hazard spectrum, some other form of site-specific design spectrum. Additionally, an extension of the conventional CSM solution procedure can provide the designer and researcher with useful information about the nature of the response beyond just the projected maximum amplitude of response.

The CSM approach was initially conceived using the secant stiffness as the effective linear stiffness along with various formulas or rules for effective viscous damping. However, from nonlinear vibration theory it is know that the secant stiffness is not an optimal equivalent linear stiffness parameter for defining the response of inelastic systems subjected to random-like excitations. Therefore, this and related elements of the CSM approach deserve re-examination with the goal of developing improved linearization procedures.

Herein, optimal equivalent linear stiffness and damping parameters are determined through a statistical analysis that minimizes the extreme occurrences of the difference (i.e., error) between the response of an actual inelastic system and its equivalent linear counterpart. The linear parameters are determined as functions of response ductility. Ductility is defined as the maximum inelastic response displacement divided by the yield displacement. A variety of different inelastic systems have been studied including bilinear hysteretic, stiffness degrading, and strength degrading behavior. It is found that the proposed linearization parameters provide a significant improvement over those employed in ATC-40, as judged by either response amplitude or performance point error measures.

### *D.2.1 Structural Capacity: Inelastic Pushover*

Nonlinear static procedures generally employ a "pushover" analysis to develop a representation of structural capacity. The ability to perform a nonlinear static analysis is based on the fundamental requirement that accurate information is obtainable about the structure, components, connections and material properties. These techniques are summarized in Section 2.4 and covered in detail in ATC-40 and FEMA 356.

The pushover curve is a structural surrogate for the actual multi-degree-of-freedom building model. The pushover curve characterizes the load versus deformation of cyclic structural response. It is generally taken to represent the backbone curve of the load-deformation hysteresis loops. From a pushover curve, the value of the initial elastic stiffness (elastic period) can be determined, as well as an estimate of the post- elastic stiffness.

The structural response behavior may also be categorized by hysteresis loop category. The backbone curve of response (from the push-over curve) does not fully specify how the building will respond to earthquake excitation. The hysteresis loop shape may be roughly bilinear and stable for subsequent cycles of response, or there may exhibit stiffness only or stiffness

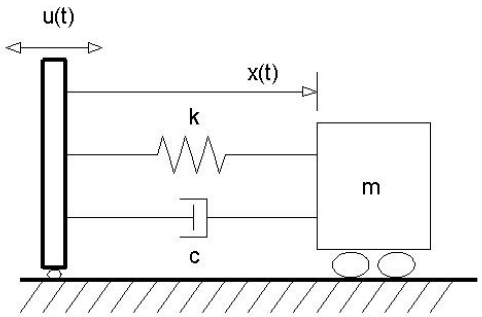


Figure D-1 SDOF oscillator model subjected to ground motion, u(t).

and strength degradation. Another type of hysteretic behavior is the "pinching" of the hysteresis loops that is associated with many concrete structures. However, this latter type of behavior has not been addressed in this document. Categorizing the hysteretic behavior as being of a certain type is left to the discretion of the engineer and usually requires considerable engineering judgment.

### *D.2.2 Seismic Demand: Response Spectra*

Traditional linear analysis methods use lateral forces to represent a design condition. For nonlinear methods it is easier and more direct to use a set of lateral displacements as a design condition. For a given structure and ground motion, the displacement demand is the maximum expected response of the building during the ground motion.

The differential equation of motion for the system in Figure D-1 is expressed as:

$$m\ddot{x}(t) + c\dot{x}(t) + kx(t) = -m\ddot{u}(t) \qquad \text{(D-1)}$$

Rearranging the equation and dividing through by the mass, *m*, results in:

$$(\ddot{x}(t) + \ddot{u}(t)) + 2\beta\omega\dot{x}(t) + \omega^2 x(t) = 0 \qquad \text{(D-2)}$$

where $\beta$ is the fraction of critical damping and $\omega$ is the natural frequency which is related to the natural period by $T = 2\pi/\omega$. Equation D-2 can be rearranged as:

$$\ddot{x}(t) + \ddot{u}(t) = -2\beta\omega\dot{x}(t) - \omega^2 x(t) \qquad \text{(D-3)}$$

Define Spectral Displacement (*SD*) and Pseudo-Spectral Acceleration (*PSA*) as follows:

$$SD = \max \forall t \left| x(t) \right| \qquad \text{(D-4)}$$

$$PSA = \max \forall t \left| \omega_n^{\,2} x(t) \right| \qquad \text{(D-5)}$$

where $\forall t$ has the mathematical meaning, "for all time." Although Spectral Acceleration (*SA*) may also be defined from Equation D-3 it is assumed in this document that *SA* is interchangeable with *PSA*. Therefore, no distinction will be made between *SA* and *PSA* and for consistency, only *SA* will be used in the remainder of this appendix.

In the ADRS format, a radial line represents a constant structural period, *T*, independent of the amount of damping present in the system. The relationship between *SA*, *SD* and *T* may be determined using Equations D-4 and D-5 which results in:

$$T = 2\pi\sqrt{SD/SA} \qquad \text{(D-6)}$$

An example of this is shown in Figure D-2 for 5% damping.

## D.3 Theoretical Basis for Equivalent Linearization

The general form of a SDOF oscillator equation of motion for the system shown in Figure D-3 can be expressed as

$$m\ddot{x}(t) + f(x(t), \dot{x}(t)) = -m\ddot{u}(t) \qquad \text{(D-7)}$$

where m is the mass of the system and $\ddot{u}(t)$ is the acceleration time history imparted to the oscillator. The term $f(x(t), \dot{x}(t))$ can have many forms. For this formulation, a linear system will be expressed as $f(x(t), \dot{x}(t)) = k_{eff}\, x(t) + c_{eff}\, \dot{x}(t)$ where $k_{eff}$ is the effective linear stiffness and $c_{eff}$ is the constant of proportionality for the effective viscous damping force,

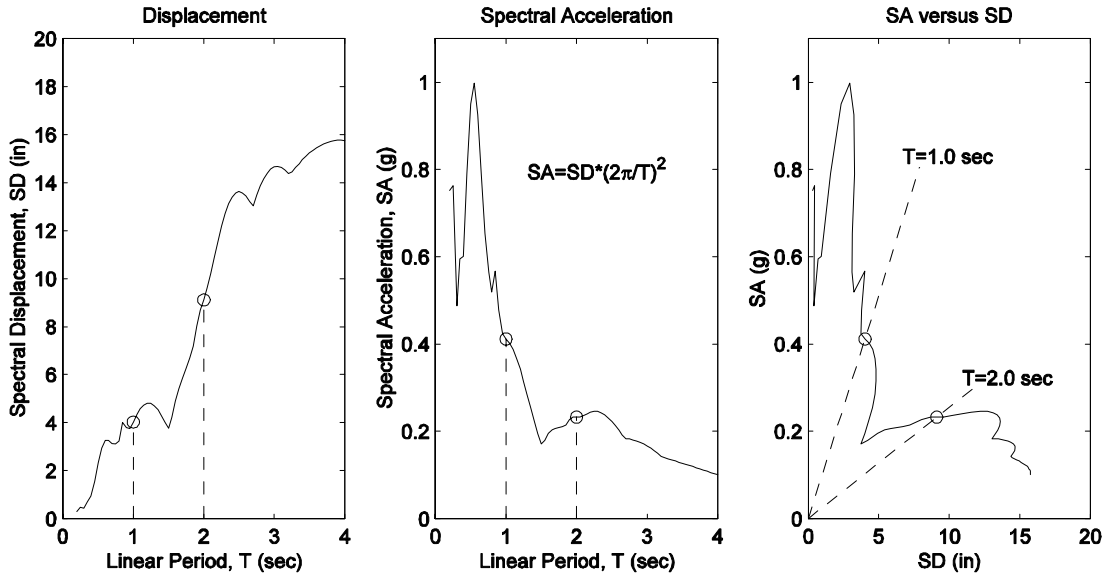


Figure D-2 Components of the ADRS format for representing Seismic Demand - *PSA* versus *SD*; left plot shows *SD* as a function of period, *T*; middle plot shows *PSA* as a function of period, *T*; right plot (ADRS format) is a compilation of the left and middle plots showing *PSA* versus *SD*, with period *T* defined by radial lines stemming from the origin.

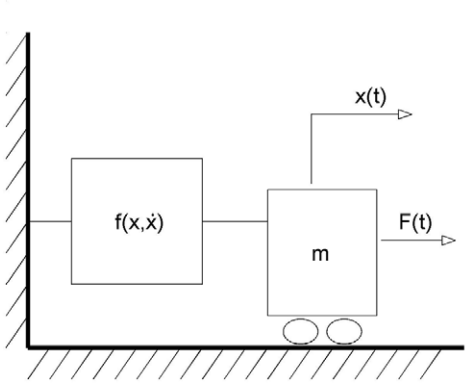


Figure D-3 SDOF oscillator model represented by Equation D-7.

$c_{eff}\,\dot{x}(t)$. Hysteretic systems, possess history dependent restoring forces that are non-separable functions of both displacement and velocity.

Equivalent linearization is an approximate technique for solving nonlinear differential equations. Equation D-7 may be rewritten as

$$m\ddot{x}(t) + c_{eff}\,\dot{x}(t) + k_{eff}\,x(t) + \varepsilon(x(t), \dot{x}(t)) = -m\ddot{u}(t) \quad \text{(D-8)}$$

where

$$\varepsilon(x(t), \dot{x}(t)) = f(x(t), \dot{x}(t)) - c_{eff}\,\dot{x}(t) - k_{eff}\,x(t) \quad \text{(D-9)}$$

The objective of equivalent linearization is to somehow select optimal values for the linear coefficients $c_{eff}$ and $k_{eff}$ such that the quantity $\varepsilon(x(t), \dot{x}(t))$ is in some sense minimized. Then, $\varepsilon(x(t), \dot{x}(t))$ is ignored and Equation D-8 is solved as an ordinary linear differential equation. The approximate linear system is shown in Figure D-4.

One possible approach is to minimize the mean square value of $\varepsilon$. The minimization criteria can be written as

$$\frac{\partial \overline{\varepsilon^2}}{\partial K} = 0 \quad \text{(D-10)}$$

$$\frac{\partial \overline{\varepsilon^2}}{\partial \gamma} = 0 \quad \text{(D-11)}$$

where the over bar represents an averaging operation.

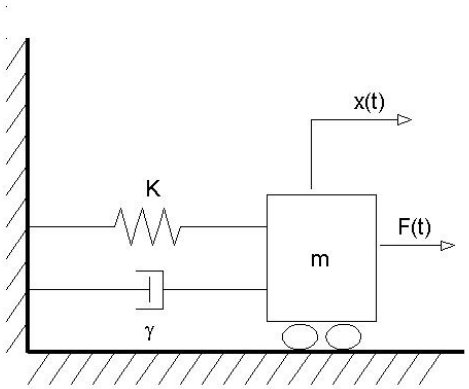


Figure D-4 Linear SDOF oscillator model with effective linear parameters as represented by Equation D-8.

If the excitation, $\ddot{u}(t)$, is a harmonic function of time, the steady-state solution can be assumed to be of the form

$$x(t) = x_{\max}\cos(\theta) \text{ where } \theta = \omega t - \phi \qquad \text{(D-12)}$$

Analyzing a single cycle of the steady state response leads to the following equation

$$\bar{\varepsilon}^2 = \frac{1}{2\pi}\int_0^{2\pi}(f(x_{\max},\theta) - c_{eff}\omega x_{\max}\sin\theta - k_{eff}x_{\max}\cos\theta)^2 d\theta \qquad \text{(D-13)}$$

Applying the minimization criteria in Equations D-10 and D-11 to Equation D-13 results in

$$c_{eff} = -\frac{1}{x_{\max}\omega\pi}\int_0^{2\pi} f(x_{\max},\theta)\sin\theta d\theta \qquad \text{(D-14)}$$

and

$$k_{eff} = \frac{1}{x_{\max}\pi}\int_0^{2\pi} f(x_{\max},\theta)\cos\theta d\theta \qquad \text{(D-15)}$$

This approach leads to an effective stiffness similar to what is seen in Figure D-5 where the effective stiffness is less than the secant stiffness, $K_{sec}$.

Another way to determine equivalent linear damping parameter is through energy balance. The energy dissipated by the hysteretic system may be equated to the energy dissipated by an equivalent viscous damper. Assume the response to be of a harmonic form over one full cycle of response expressed as

$$x(t) = x_{\max}\cos(\theta) \text{ where } \theta = \omega t - \phi \qquad \text{(D-16)}$$

Then, energy dissipated by a viscous damper over one cycle of response, *E*, can be expressed as

$$E = 2\pi^2 c_{eff} x_{\max}^2 / T \qquad \text{(D-17)}$$

where T is the period of cyclic motion.

For the bilinear hysteretic model seen in Figure D-5, the energy dissipated over one cycle of response, *E*, can be expressed as

$$E = 4x_y(k_o - \alpha k_o)(x_{\max} - x_y) \qquad \text{(D-18)}$$

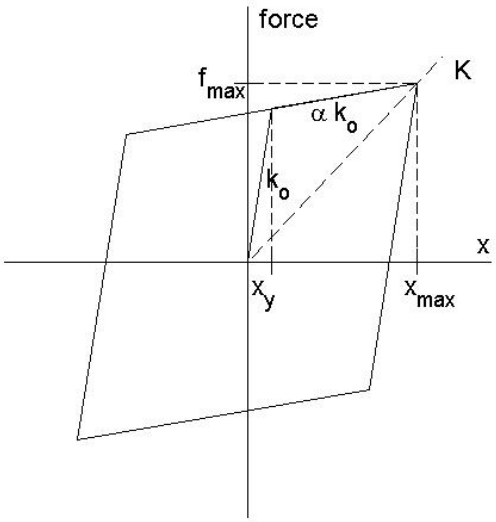


Figure D-5 Bilinear hysteretic system.

Equating energies from Equations D-17 and D-18 leads to

$$c_{eff} = 4(k_o - \alpha k_o)x_y(x_{\max} - x_y)T/(2\pi^2 x_{\max}^2) \quad \text{(D-19)}$$

In Figure D-5, the secant stiffness is labeled $K_{\sec}$ and can be expressed as

$$K_{\sec} = k_o(x_y + \alpha(x_{\max} - x_y))/x_{\max} \quad \text{(D-20)}$$

If the secant period, $T_{\sec}$, is assumed to be the period of structural response, then

$$k_{eff} = K_{\sec} \quad \text{(D-21)}$$

The secant stiffness can be related to the secant period and substituting Equation D-20 into Equation D-19 leads to the following expression for $c_{eff}$.

$$c_{eff} = 4(k_o - \alpha k_o)x_y(x_{\max} - x_y)\sqrt{\frac{m}{K_{\sec}}}/(\pi x_{\max}^2) \quad \text{(D-22)}$$

Equation D-22 corresponds to the equivalent viscous damping equation found in ATC-40 (Section 8.2.2.1). However, the response of inelastic systems to earthquake ground motions is not the same as the steady-state response to a constant amplitude sinusoidal forcing function as assumed in the above equivalent linearization formulation. Repeated full hysteresis loops with constant amplitude occur infrequently for inelastic systems subjected to earthquake time histories. Furthermore, partial and one-sided loops are likely to occur.

## D.4 Starting Point For Optimization

The ductility demand, $\mu$, is defined as the maximum displacement of the inelastic system divided by its yield displacement. For the bilinear hysteretic system shown in Figure D-5, the ductility demand is $x_{max}/x_y$. In 1980, an optimal set of equivalent linear parameters for earthquake excitation was defined based on making an adjustment to the linear response spectrum. In that study (Iwan, 1980) ductility dependent inelastic response spectra were compared with elastic response spectra, and displacement preserving shifts of the inelastic spectra were determined which minimized the average absolute value difference between the inelastic and equivalent linear spectra over a range of periods. A family of hysteresis behavior was considered including

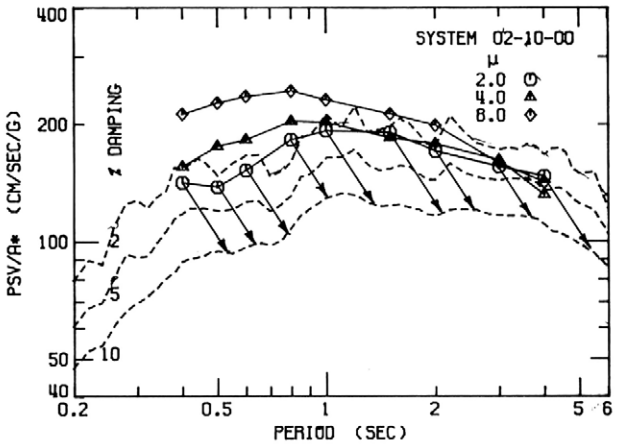


Figure D-6 Early effort to define optimal equivalent linear parameters (Iwan, 1980).

bilinear hysteretic as well as pinching hysteretic models. Figure D-6 shows a typical set of inelastic and elastic response spectra and indicates the manner in which the spectra were adjusted.

Using the stated procedure, the following relationships were obtained for the optimal effective linear parameters:

$$T_{eff}/T_0 - 1 = 0.121(\mu - 1)^{0.939} \quad \text{(D-23)}$$

$$\beta_{eff} - \beta_0 = 5.87(\mu - 1)^{0.371} \quad \text{(D-24)}$$

It is easily shown that the optimal effective period defined by the above relationship is significantly *less* than the period associated with the secant stiffness that is employed in the conventional CSM approach found in ATC-40 (or, the optimal stiffness is significantly *greater* than the secant stiffness). Indeed, the secant stiffness may overestimate the optimal effective period by more than 50% for larger values of ductility. It is also observed that the damping value used in the conventional CSM approach is significantly greater than the optimal damping parameter in Equation D-24. Thus, the conventional CSM approach significantly overestimates both the effective period and damping of inelastic systems. In some regions of response, these two overestimates combine in such a manner that the resultant response prediction is not much different from the prediction obtained from the optimal parameters. However, these two overestimates do not always counteract each other to produce reliable estimates of displacement.

Even though the conventional and some more optimal set of equivalent linear parameters may predict about the same average response for some range of cases, that does not mean they are equally effective. This may be illustrated by considering the distribution of the error for the two different approaches. Figure D-7shows the distribution of the Performance Point displacement error that is obtained using the early optimal parameters and the conventional CSM parameters for an elastoplastic system. It is evident from the figure that there is only a modest difference between the mean values of the error for the two approaches. The optimal parameters give a mean Performance Point error of -4.4% while the conventional CSM approach gives a mean error of -9.5%. However, there is a very substantial difference in the standard deviation of the error for the two approaches. The optimal approach error has a standard deviation of 21.2% while that of the conventional CSM approach is 68.7%. As seen from the figure, the conventional CSM approach has a much greater probability of exhibiting extreme over prediction errors than does the optimal approach, even though the mean error of the conventional approach is less conservative than the optimal approach. Hence, it is clear that it is inadequate to merely minimize the mean value of the displacement error when defining an optimal set of effective linear parameters. It is necessary to simultaneously minimize *both* the mean and standard deviation in some sense.

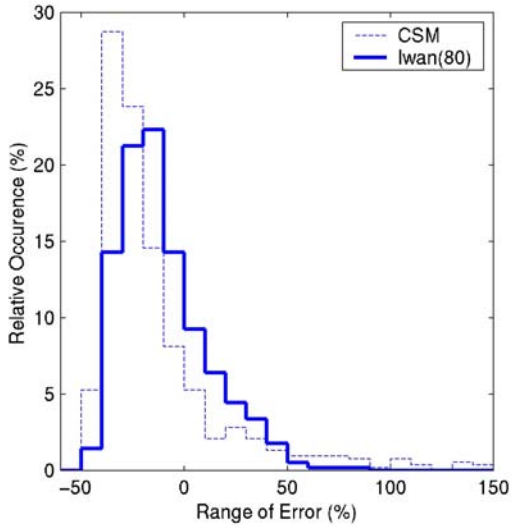


Figure D-7 Distribution of percent error in Performance Point displacement. Bilinear system with alpha=0, $T_0$ = 0.1-2.0 sec (0.1 sec increments), μ=2, 28 far-field earthquakes.

## D.5 Alternative Statistical Analysis

The results of the early optimization study described above provide the motivation for a more comprehensive study of equivalent linearization for earthquake response prediction. In the earlier study, the error measure used for optimization was the mean of the absolute value of the displacement error. This is an intuitive error measure which leads to reasonable results. However, this error measure may not be as directly meaningful as other possible measures. In practice, it would seem to be more appropriate to have the measure of goodness of the optimal effective linear parameters based on some measure of engineering acceptability. This is the approach used in this study.

Recall the equation of motion for the single-degree-of-freedom system in Figure D-3. When $f(x,\dot{x})$ represents a linear viscous damped system, the equation of motion may be expressed as

$$m\ddot{x}_{lin} + c_{eff}\dot{x}_{lin} + k_{eff}x_{lin} = -m\ddot{u}(t) \qquad \text{(D-25)}$$

where $c_{eff}$ and $k_{eff}$ are the viscous damping coefficient and spring stiffness, respectively. For a given ground excitation, $\ddot{u}(t)$, the solution, $x_{lin}$(t), may be computed using any numerical solution procedure. For an inelastic system, the restoring force, $f(x,\dot{x})$, may take a variety of forms. The solution for the inelastic system will be designated as $x_{inel}$(t).

Many different approaches are available for making a comparison between the displacement time histories $x_{inel}$(t) and $x_{lin}$(t). These include, but are not limited to, a point by point comparison of the displacement, velocity or acceleration time histories, comparing the number of zero displacement crossing or comparison of the amplitude spectra from a Fourier Transform. However, to quantify a comparison, there must be a value assigned to the amount of similarity or difference. Within the framework of performance-based engineering, the key performance variable is the maximum relative displacement amplitude that a structure experiences from the demand earthquake. The relative displacements for the inelastic and linear single-degree-of-freedom systems are $x_{inel}$(t) and $x_{lin}$(t), respectively.

The effective linear parameters obtained based on a comparison of displacement values would not be appropriate to be used in a velocity or force-based

design procedure. For example, the maximum velocities or accelerations from the linear solution should not be used as estimates for the maximum values of $\dot{x}_{inel}(t)$ or $\ddot{x}_{inel}(t)$. The maximum acceleration or maximum pseudo-acceleration would be a much better comparison parameter for effective linear parameters intended for use in a force-based approach.

The maximum displacement amplitude of the nonlinear time history $x_{inel}$(t) will be designated as $D_{inel}$ and the maximum displacement amplitude of the linear time history $x_{lin}$(t) will be designated as $D_{lin}$. The effective linear parameters developed in this study will be used for estimating the response of structures subjected to earthquake excitations. Therefore, using real earthquake time histories as the model inputs is most logical.

The methodology developed in this study employs a search over a two-dimensional parameter space related to the linear system coefficients $c_{eff}$ and $k_{eff}$ in Equation D-25. One can expect to find a combination or combinations of $c_{eff}$ and $k_{eff}$ that give the best "match" with an inelastic system, in some sense. The terms $c_{eff}$ and $k_{eff}$ will be replaced by the fraction of critical damping, $\beta_{eff}$, and the natural period of oscillation, $T_{eff}$. Equation D-25 can be expressed as

$$\ddot{x} + \frac{4\pi\beta_{eff}}{T_{eff}}\dot{x} + \left(\frac{2\pi}{T_{eff}}\right)^2 x = -\ddot{u}(t) \qquad \text{(D-26)}$$

The system parameters $\beta_{eff}$ and $T_{eff}$ completely describe the linear single-degree-of-freedom system.

### *D.5.1 Error Measure*

In order to compare the maximum displacements, $D_{inel}$ and $D_{lin}$, an error measure must be defined. In engineering design, unconservative displacement predictions are generally less desirable than conservative predictions. Therefore, a fundamental requirement of any error measure is that it distinguish between a conservative displacement prediction and a non-conservative displacement prediction. An error measure that uses an absolute value of the difference between $D_{inel}$ and $D_{lin}$ would not satisfy this requirement.

A simple error measure satisfying the above requirement is the ratio of the difference between the linear system maximum displacement, $D_{lin}$, and the inelastic system maximum displacement, $D_{inel}$, to the inelastic system maximum displacement.

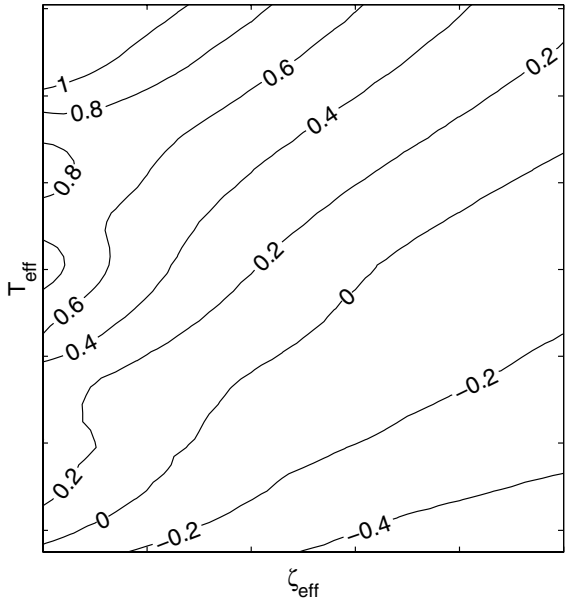


Figure D-8 Contour values of $\varepsilon_D$ over the two-dimensional parameter space of $T_{eff}$ and $\beta_{eff}$ for a single combination of inelastic system and ground excitation.

$$\varepsilon_D = \frac{D_{lin} - D_{inel}}{D_{inel}} \qquad \text{(D-27)}$$

Using this definition, a negative value of $\varepsilon_D$ reflects an unconservative displacement prediction while a positive value reflects a conservative displacement prediction. $\varepsilon_D$ might be considered to have a positive bias as it ranges from -1 to $\infty$. However, for the range of systems and excitations considered in this study, the slight positive bias in the statistical distribution of $\varepsilon_D$ is inconsequential.

For a given inelastic system and ground excitation, there will be a certain topology associated with the error, $\varepsilon_D$, as a function of linear system parameters $T_{eff}$ and $\beta_{eff}$ as shown in Figure D-8. Note that there exists a nearly diagonal contour of zero error. For any combination of $T_{eff}$ and $\beta_{eff}$ lying along this contour there will be a perfect match between $D_{lin}$ and $D_{inel}$.

For any specified ensemble of inelastic systems and ground excitations, distributions of $\varepsilon_D$ can be obtained for every combination of $T_{eff}$ and $\beta_{eff}$. This is illustrated in Figure D-9.

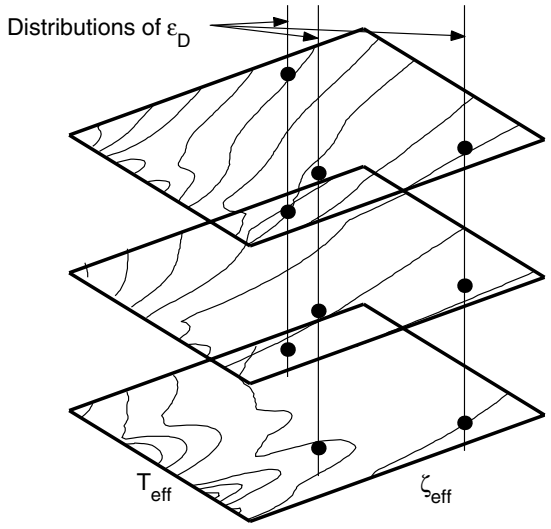


Figure D-9 Illustration of assembling $\varepsilon_D$ error distributions at every combination of $T_{eff}$ and $\beta_{eff}$ over an ensemble.

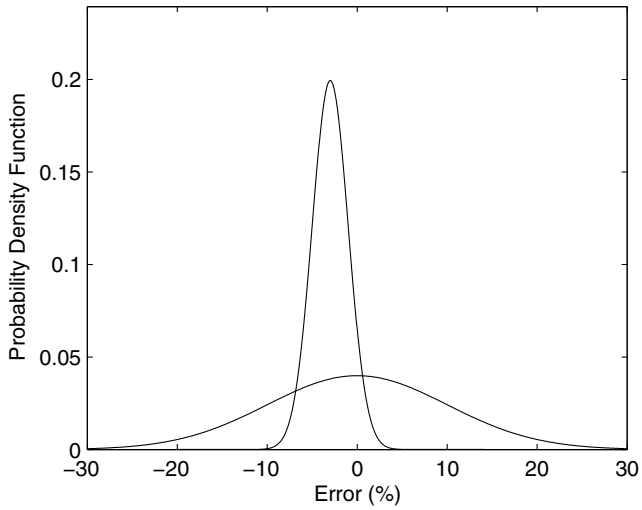


Figure D-10 Illustration of probability density functions of displacement error for a Normal distribution.

The importance of using the standard deviation as well as the mean of the error distribution is illustrated in the following example. Two hypothetical probability density functions are shown in Figure D-10. For the more widely spread error distribution, the mean error value is zero, while for the tighter distribution, the mean error value is -5%. Solely in terms of the mean value, the widely spread distribution is more accurate than the tighter distribution. However, a more insightful way to analyze the distributions would be in terms of an acceptable range of error values. In this example, an acceptable range of error values might be chosen to be from -20% to 20%. In this case, the distribution with the mean value of -5% would be both more "acceptable" compared to the distribution with a mean value of 0%.

Let $\Re$ be the probability that the error $\varepsilon_D$ lies outside the range from $a$ to $b$. Then, $\Re$ may be expressed as

$$\Re = 1 - \Pr(a < \varepsilon_D < b) \qquad \text{(D-28)}$$

If the distribution of $\varepsilon_D$ is assumed to be Normal, $\Re$ can be expressed as

$$\Re = 1 - \int_a^b \frac{1}{\sigma\sqrt{2\pi}} e^{\frac{-(x-m)^2}{2\sigma^2}} dx \qquad \text{(D-29)}$$

where $m$ is the mean value and $\sigma$ is the standard deviation of the distributions of $\varepsilon_D$ values. It will be assumed that the desirable range of error values, $\varepsilon_D$, from an engineering design point of view is between -10% and +20%. This assumption has been adopted after consultation with several members of the practicing structural engineering community. This range of error values will be referred to as the Engineering Acceptability Range (EAR). This range takes into account the general desire for a more conservative design rather than an unconservative design. That is, a 20% error is more acceptable than a -20% error.

### *D.5.2 Optimization Criterion*

The *optimum* point in the $T_{eff}$, $\beta_{eff}$ parameter space is chosen to be the point that minimizes the probability that the error, $\varepsilon_D$, will be outside the Engineering Acceptability Range. The *Engineering Acceptability Criterion* may therefore be defined as $\sigma$.

$$\Re_{EAR} \equiv 1 - \Pr(-0.1 < \varepsilon_D < 0.2) = \min \qquad \text{(D-30)}$$

Figure D-11 shows contours of $\Re_{EAR}$ as a function of $T_{eff}$ and $\beta_{eff}$. Also shown is the optimal point over the

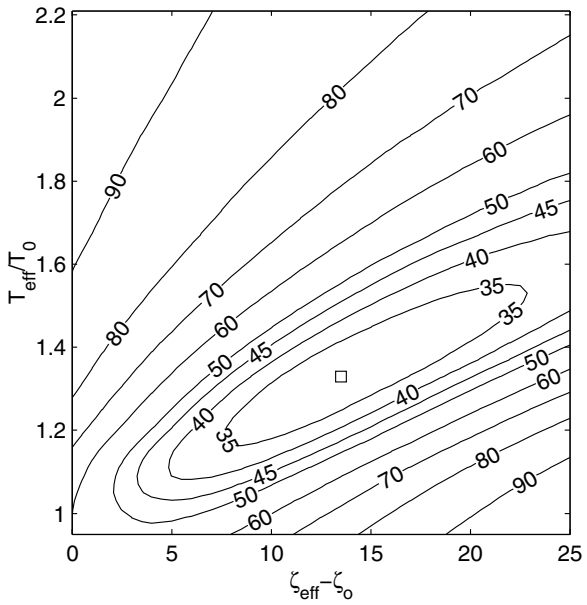


Figure D-11 Contours of $\Re_{EAR}$ over the $T_{eff}$, $\beta_{eff}$ parameter space. The optimum point is marked by a square.

two-dimensional parameter space which is denoted by a square.

The diagonal trend to the contours in Figure D-11 can be explained by the following physical reasoning. Consider the displacement response of a linear oscillator subjected to an earthquake excitation. Decreasing the system damping will always increase the displacement response. Generally speaking, decreasing the natural period will also decrease the displacement response. Although this is not true in all cases, especially for near-field ground motions, it is a general trend that by increasing period and damping in the correct proportion, a nearly constant maximum displacement can be achieved.

The size and shape of the contours in Figure D-11 give insight into the ramifications of using effective linear parameters that are different from the values at the optimal point. In Figure D-11, the contour closest to the optimum point has a value of 0.35 while the minimum value of $\Re_{EAR}$ ($\Re_{EAR_{min}}$) is 0.31. The gradient of the contours is more gradual along a line roughly from lower left to upper right. Therefore, if the effective period is under predicted, it is best to also have an under-predicted damping. If the effective period is over predicted, it is best to also have an over-predicted damping. In the general direction from lower right to upper left, the gradient of the contours is very large and the value of $\Re$ quickly increases for relatively small changes in the effective parameters. Over predicting one parameter and under predicting the other can have serious repercussions on the reliability of the displacement prediction.

## D.6 Effective Linear Parameters

The full explicit functional dependence of $\varepsilon_D$ may be indicated as follows

$$\varepsilon_D\left(\frac{T_{eff}}{T_o}, \beta_{eff} - \beta_o, \alpha, \mu, HYST\right) = \frac{D_{lin}(T_{eff}, \beta_{eff}) - D_{inel}(T_o, \beta_o, \alpha, \mu, HYST)}{D_{inel}(T_o, \beta_o, \alpha, \mu, HYST)} \quad \text{(D-31)}$$

The maximum displacement of the nonlinear system, $D_{inel}$, is a function of initial period, $T_0$, linear viscous damping, $\beta_0$, second slope ratio, $\alpha$, response ductility, $\mu$, and hysteretic model, denoted ``HYST''. The linear system response, $D_{lin}$, is a function of the two linear system parameters: period, $T_{eff}$, and damping, $\beta_{eff}$. It is desired to find effective linear parameters that are applicable over a range of $T_0$ and $\beta_0$ values. Therefore, multiple values of $T_0$ and $\beta_0$ will be included in the same ensemble. The two-dimensional $T_{eff}$, $\beta_{eff}$ parameter space is transformed into the $T_{eff}$ - $T_0$, $\beta_{eff}$ - $\beta_0$ parameter space.

The Engineering Acceptability Criterion is applied to the error distributions over the entire $T_{eff} / T_0$, $\beta_{eff} - \beta_0$ parameter space and the optimum combination of $T_{eff} / T_0$ and $\beta_{eff} - \beta_0$, is determined. Next, the ductility value is changed, and the entire process is repeated. The ductility values used in this study range from 1.25 to 6.5 in increments of 0.25. Additionally, ductilities of 8 and 10 are included.

The optimum values of $T_{eff} / T_0$ and $\beta_{eff} - \beta_0$ may be graphed as functions of ductility. Then, these results can be fitted with an analytical expression. Figure D-12 shows a typical example of the discrete optimum values of $T_{eff} / T_0$ and $\beta_{eff} - \beta_0$ graphed as a function of ductility along with a curve fit of the data. Information pertaining to the details of the curve fitting process may be found in Guyader, 2004.

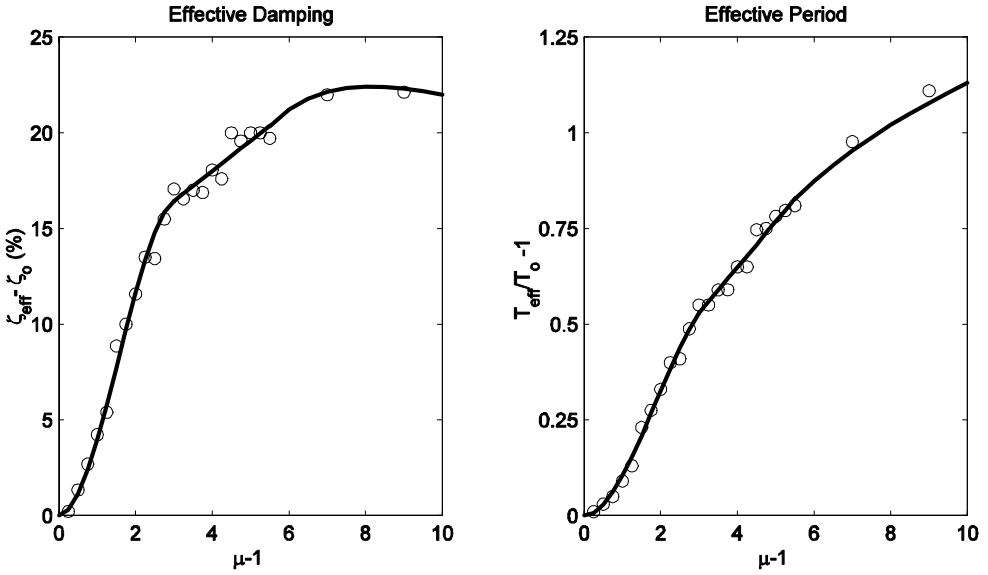


Figure D-12 Example of optimal effective linear parameters - discrete points and the curve fitted to the data

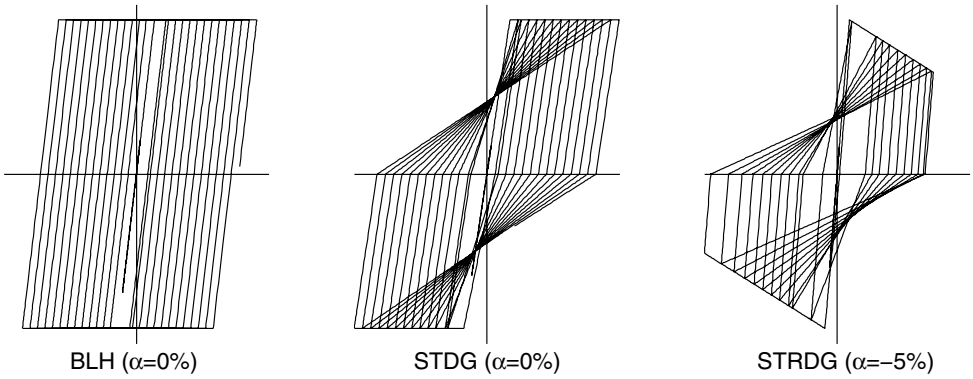


Figure D-13 Types of inelastic behavior considered. BLH=Bilinear hysteretic, STDG=Stiffness Degrading, and STRDG=Strength Degrading.

The new optimization criterion has been applied to the basic hysteretic models shown in Figure D-13. In each case, the basic model has been augmented by the addition of a linear spring element to create a non-zero second slope. $\alpha$ is the ratio of the post-yield stiffness to the elastic stiffness as seen in Figure D-6. The BLH and STDG models have been analyzed for alpha values of 0,2,5 and 10% while the STRDG model has been computed for alpha values of -3 and -5%. Results for all models and certain combinations of models are presented and discussed in Chapter 6. The elastoplastic system represents the greatest challenge in application of equivalent linearization due to the existence of long-period drifting displacement response in addition to the more quasi-harmonic motion (Paparizos and Iwan, 1988). It is noted that in general the results for the systems with alpha greater than zero are more favorable than for the systems with alpha equal to or less than zero.

## D.7 Performance Point Errors

The Capacity-Spectrum Method incorporates both structural capacity and seismic demand to determine a point where the demand and capacity are equal, referred to as the *Performance Point*. This point gives the expected displacement in the structure. The accuracy of the Capacity-Spectrum Method will be evaluated using a new error measure. For a given ground motion, the Performance Point Error, $\varepsilon_{D_{pp}}$, is defined as the difference between the displacement at the Performance Point, as determined using equivalent linear parameters, and the actual maximum inelastic displacement response divided by the maximum inelastic displacement. This can be expressed as

$$\varepsilon_{D_{pp}}(\alpha, \mu, HYST) = \frac{D_{lin}(T_{eff}(T_o, \alpha, \mu_{PP}), \beta_{eff}(T_o, \alpha, \mu_{PP}))}{D_{inel}(T_o, \beta_o, \alpha, \mu, HYST)} - \frac{D_{inel}(T_o, \beta_o, \alpha, \mu, HYST)}{D_{inel}(T_o, \beta_o, \alpha, \mu, HYST)} \quad \text{(D-32)}$$

Error statistics are created by combining all $T_0$ and $\beta_0$ values for a given hysteretic model, second slope ratio and ductility.

Several sources of error are introduced by the Capacity-Spectrum Method. Errors may arise in both the determination of structural capacity and seismic demand. To evaluate the error from the equivalent linear parameters alone, all other sources of error must either be eliminated or shown to be negligible.

In determining structural capacity, two sources of error exist: the capacity spectrum calculation and the hysteretic classification. A large source of error may come from representing a multi-degree-of-freedom building model by a single-degree-of-freedom system. This source of error is eliminated herein by considering only single-degree-of-freedom structures.

The second source of error in determining the structural capacity is the hysteretic classification. In what follows, errors associated with determination of the hysteretic model are eliminated since the actual hysteretic model is assumed apriori. In this way, both sources of error associated with the structural capacity have been removed.

In determining seismic demand, errors may be introduced through smoothing of the demand spectrum. A design spectrum that represents the effects of many possible earthquake sources is generally smooth and conservative. However, the spectrum of any actual earthquake ground motion is generally quite irregular. The potential errors associated with using a design spectrum instead of an actual earthquake response spectrum are eliminated in what follows by using actual earthquake response spectra. Demand spectra are calculated using the appropriate effective linear parameters. The only remaining source of error in the Capacity-Spectrum Method are errors associated with the effective linear parameters.

Performance Point Error results are presented for the bilinear hysteretic (BLH) and strength degrading (STDG) models with second slope ratios of 0% and 5% in Figures D-14 and D-15. The results clearly show an improvement using the new effective parameters as compared to the effective parameters used in ATC-40. For all cases, the probability of the Performance Point Error lying within the range of Engineering Acceptability is much higher for the new approach than for the current Capacity-Spectrum Method, especially for lower ductilities. This would appear to validate the use of higher order curve fitting for lower ductilities to help capture important local variations in the effective parameters.

At low values of ductility, the conventional Capacity-Spectrum Method approach is noticeably unconservative. Therefore, a building needing rehabilitated could be judged to not need an upgrade using the conventional Capacity-Spectrum Method approach. Within the framework of performance-based engineering, where Performance Objectives are very precise, accurate prediction at the lower ductility values can be quite important in terms of Immediate Occupancy and Operational building performance levels.

## D.8 References

Iwan, W.D., 1980, "Estimating inelastic response spectra from elastic spectra," *Earthquake Engineering and Structural Dynamics*, Vol. 8, pp. 375-388.

Guyader, A, 2004, *A Statistical Approach to Equivalent Linearization with Application to Performance-Based Engineering*, EERL 2004-04 Report, Pasadena, California.

Paparizos, L.G., and W.D., Iwan, 1988, "Some observations on the random response of an elasto-plastic system," *Journal of Applied Mechanics*, Paper No. 88-WA/APM-64, American Society of Civil Engineers.

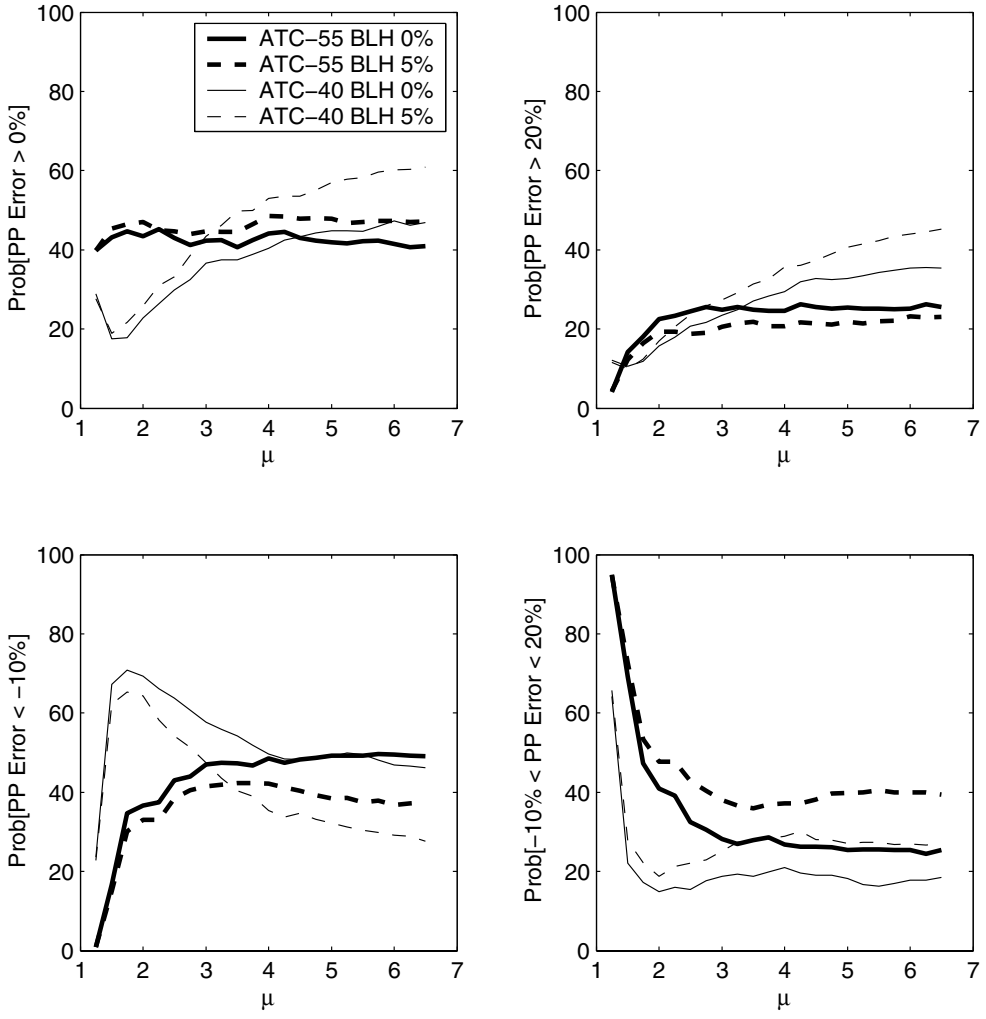


Figure D-14 Summary of Performance Point errors for bilinear hysteretic (BLH) model

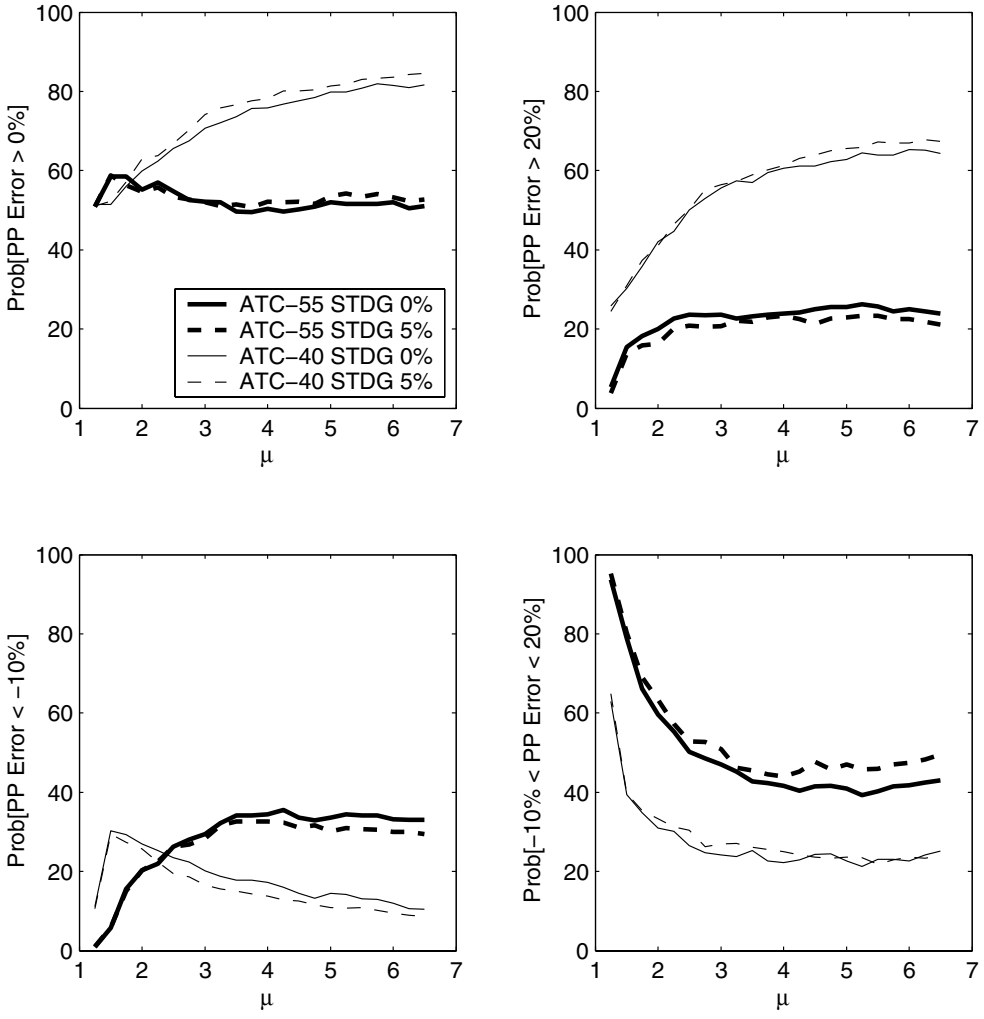


Figure D-15 Summary of Performance Point Errors for Strength Degrading (STDG) model

# E. Supplementary Information and Data on Soil-Structure Interaction Effects

## E.1 Introduction

This appendix provides detailed information on soil-structure (SSI) effects. The intent is to provide background information supporting the simplified design procedures presented in Chapter 8. Section E.2 describes kinematic interaction effects and engineering models used to describe these effects. Section E.3 describes foundation damping effects and how these effects contribute to the system damping ratio, which is the damping ratio for which the initial seismic demand spectrum should be computed. Reference citations are provided in Section E.4.

The soil-structure interaction effects described in this appendix are relevant at the stage of defining the elastic response spectrum, to be used during application of the Capacity-Spectrum Method of ATC-40, or the Coefficient Method of FEMA 356 (ASCE, 2000). The elastic spectra used during these procedures pertain to a free-field condition and for 5% damping. The spectral ordinates of the elastic spectra can be modified for kinematic interaction and foundation damping using the procedures presented in Sections E.2.4 and E.3.3, respectively (and summarized in Sections 8.2 and 8.3 of the main body of the report). The modified spectral ordinates can then be used in nonlinear static analyses of structural response and performance.

## E.2 Kinematic interaction

Kinematic interaction results from the presence of stiff foundation elements on or in soil, which causes foundation motions to deviate from free-field motions as a result of base slab averaging and embedment effects. The base slab averaging effect can be visualized by recognizing that the motion that would have occurred in the absence of the structure within and below the footprint of the building is spatially variable. Placement of a foundation slab across these variable motions produces an averaging effect in which the foundation motion is less than the localized maxima that would have occurred in the free-field. The embedment effect is simply associated with the reduction of ground motion that tends to occur with depth in a soil deposit.

The information provided in this section on kinematic interaction covers simple models for the analysis of ground motion variations between the free-field and shallow foundations at the ground surface (in which case kinematic interaction is dominated by base slab averaging) and embedded shallow foundations (in which case kinematic interaction can result from both base slab averaging and embedment effects). Kinematic interaction for pile-supported foundations is not covered. Theoretical models for kinematic interaction effects are expressed as frequency-dependent ratios of the Fourier amplitudes (i.e., transfer functions) of foundation input motion (FIM) to free-field motion. The FIM is the theoretical motion of the base slab if the foundation and structure had no mass, and is a more appropriate motion for structural response analysis than is the free-field motion.

In the following subsections, formulations for transfer functions that account for base slab averaging and embedment effects are presented. Recommendations are then provided regarding how transfer functions can be used to modify a free-field response spectrum or time history suite to estimate foundation input motions (FIMs) for use in nonlinear static procedures.

### *E.2.1 Shallow Foundations at the Ground Surface*

Base-slab averaging results from inclined or incoherent incident wave fields. Motions of surface foundations are modified relative to the free-field when incident waves impinge upon the foundation with an angle to the vertical axis, $\alpha_v$, or when the incident wave is incoherent. The first case is referred to as the wave passage effect and the second case as the ground motion incoherence effect. In the presence of these wave fields, translational base-slab motions are reduced relative to the free-field, and rotational motions are introduced. The reductions of base-slab translation, and the introduction of torsion and rotation in the vertical plane, are all effects that tend to become more significant with decreasing period. The period-dependence of these effects is primarily associated with the increased effective size of the foundation relative to the seismic wavelengths at low periods. In addition, ground motions are more incoherent at low periods.

Veletsos and Prasad (1989) and Veletsos et al. (1997) developed useful models for base slab averaging that combine an analytical representation of the spatial variation of ground motion with rigorous treatment of

foundation-soil contact. The models evaluate the response of rigid, massless circular and rectangular foundations on the surface of an elastic halfspace to incoherent SH waves propagating either vertically or at an angle $\alpha_v$ to the vertical. A result of the model is a transfer function between free-field motions and translational foundation motions (denoted with subscript '*u*').

The transfer function amplitudes computed by Veletsos and his co-workers are presented in Figure E-1 for circular and rectangular foundations subject to vertically incident incoherent SH waves. Similar curves are available for nonvertically incident coherent waves in the references. The transfer functions in Figure E-1 are plotted against the dimensionless frequency parameter $\tilde{a}_o$, defined as follows for circular and rectangular foundations, respectively,

$$\tilde{a}_0 = a_0\sqrt{\kappa^2 + \sin^2\alpha_v} \qquad \textbf{Circular}$$

$$\tilde{a}_o = \frac{\omega b_e}{2v_{s,r}}\sqrt{\kappa^2 + \sin^2\alpha_v\left(\frac{b}{b_e}\right)^2} \qquad \textbf{Rectangular} \qquad \text{(E-1)}$$

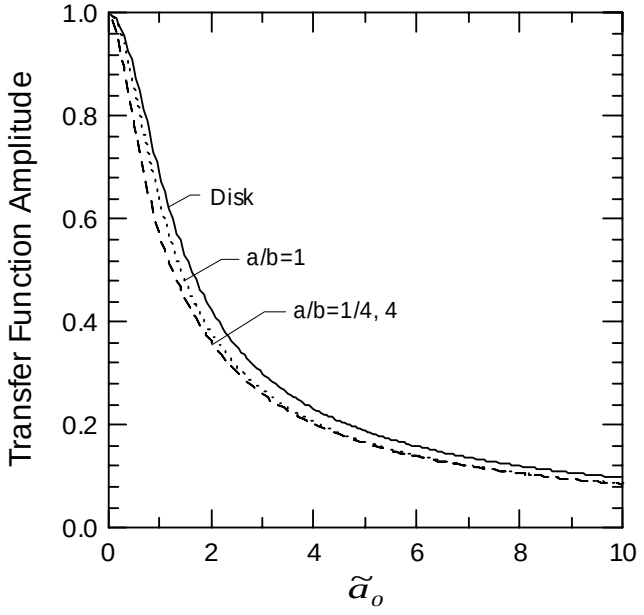


Figure E-1 Amplitude of transfer function between free-field motion and foundation input motion for vertically incident incoherent waves (Veletsos and Prasad, 1989; Veletsos et al., 1997).

where $a_0 = \omega r/V_{s,r}$, $V_{s,r}$ denotes a strain-reduced shear wave velocity, $r$ = radius of circular foundation, $a \times b$ = full footprint dimensions of rectangular foundation ($b$ being measured perpendicular to the direction of SH wave polarization), $b_e = \sqrt{ab}$ , and $\kappa$ = a ground motion incoherence parameter (information on the selection of $\kappa$ values are presented below).

Figure E-1 indicates that the transfer functions for circular and various rectangular geometries are similar to each other for small $\tilde{a}_o$. As noted by Veletsos et al. (1997), the near equivalence of the results for different aspect ratios ($a/b$=1/4 - 4) of rectangular foundations suggests that translational transfer functions primarily depend on foundation area. Given this near equivalence, the transfer function is principally a function of dimensionless frequency $\tilde{a}_o$. As shown in Equation E-1, $\tilde{a}_o$ is essentially the foundation dimension normalized by the wavelength (since wavelength is wave velocity divided by frequency), and then scaled by an incoherence/wave inclination term. When the foundation dimension is large relative to the wave length, $\tilde{a}_o$ is large and the transfer function ordinate is low. Conversely, small foundation dimensions relative to the wavelength produce transfer function ordinates near unity.

Kim and Stewart (2003) calibrated the above analysis procedure against observed foundation / free-field ground motion variations as quantified by frequency-dependent transmissibility function amplitudes, $|H|$. The above analytical models were fit to $|H|$ for the assumed condition of a rigid base slab and a vertically propagating, incoherent incident wave field. Calibrated from the fitting process was a ground motion incoherence parameter, $\kappa$. Since the limiting assumptions of the model were not strictly satisfied for actual structures, the results of the identification were denoted apparent $\kappa$ values ($\kappa_a$) that reflect not only incoherence effects, but also average foundation flexibility and wave inclination effects within the calibration data set. The foundation flexibility effects within the calibration data set generally correspond to shallow foundation conditions in which foundation components are inter-connected (i.e., continuous mats or footings inter-connected with grade beams). Parameter $\kappa_a$ was found to be correlated to average soil shear wave velocity as shown in Figure E-2. These values of $\kappa_a$ can be used with Figure E-1 (assuming $\alpha_v$ = 0) to define site-specific transfer functions given the foundation radius ($r$) and effective small-strain shear wave velocity ($v_s$). In these procedures, effective foundation radius is defined as $r = \sqrt{A_f/\pi}$ (where

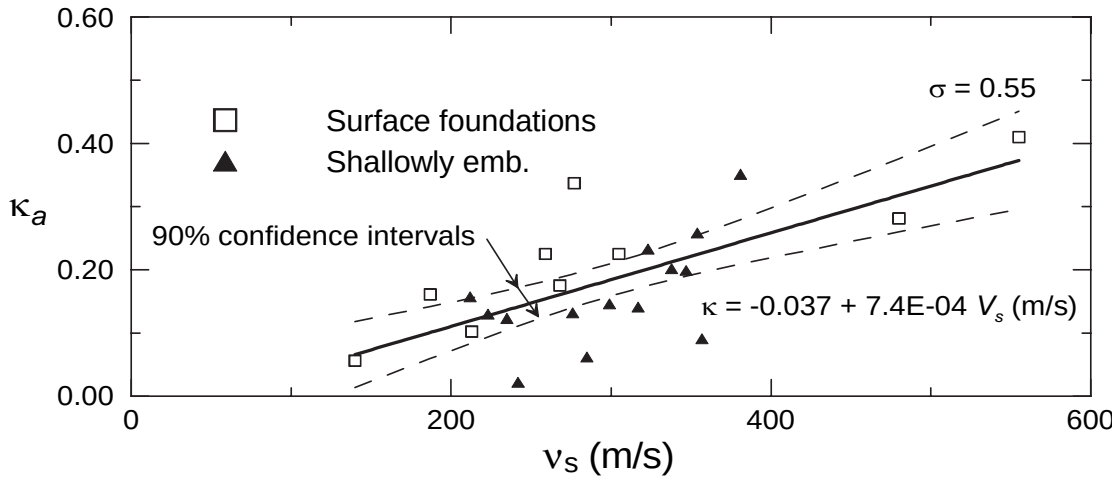


Figure E-2 Relationship between effective incoherence parameter $k_a$ and small-strain shear wave velocity $v_s$ from case histories (from Kim and Stewart, 2003).

$A_f$ = foundation area) and the effective $v_s$ for the site is defined as $r$ / (travel time for shear wave to travel from depth $r$ to ground surface). Depth is measured down from the base of the foundation.

The model has not been validated for foundations with low in-plane stiffness, buildings with large footprint dimensions (> 200 ft), and pile-supported foundations in which the cap and soil are not in contact. However, the judgment of the project technical team that developed this report is that the model can provide a reasonable first order estimate of the kinematic interaction effect for those conditions.

### *E.2.2 Embedded Shallow Foundations*

Foundation "embedment" refers to a foundation base slab that is positioned at a lower elevation than the surrounding ground, which will usually occur when buildings have a basement. When subjected to vertically propagating coherent SH waves, embedded foundations experience a reduction in base-slab translational motions relative to the free-field, and rotations in the vertical plane are introduced. The rotations are caused by incompatible shear strains along the sides of the excavation and the free-field.

Elsabee and Morray (1977) and Day (1978) have developed analytical transfer functions relating base-slab translational and rotational motions to free-field translations for an incident wave field consisting of vertically propagating, coherent SH waves. Base-slab averaging does not occur within this wave field, but foundation translations are reduced relative to the free-field due to ground motion reductions with depth and wave scattering effects. Day (1978) used finite element analyses to evaluate the base motions of a rigid cylindrical foundation embedded in a uniform elastic half space ($\beta = 0$, $\nu = 0.25$) and subjected to vertically incident, coherent SH waves. Elsabee and Morray (1977) performed similar studies but for the case of a visco-elastic soil layer of finite depth over a rigid base ($\beta = 0.05$ and $\nu = 0.33$). The amplitude of the halfspace and finite soil layer transfer functions are shown together in Figure E-3 for foundation embedment / radius ratio $e/r$ = 1.0. The primary difference between the two solutions is oscillations in the finite soil layer case at high frequencies. Also shown in Figure E-3a is the following approximate transfer function amplitude model developed by Elsabee and Morray (1977):

$$\left|H_u(\omega)\right| = \cos\left(\frac{e}{r}a_0\right) = \cos\left(\frac{e\omega}{v_s}\right) \quad [H_u \text{ must be} \geq 0.454] \qquad \text{(E-2)}$$

where $a_0 = \omega r/v_s$ and $e$ = foundation embedment. Figure E-3b shows the transfer function amplitude model is a somewhat more convenient form in which it is plotted as a unique function of $\omega e/v_s$.

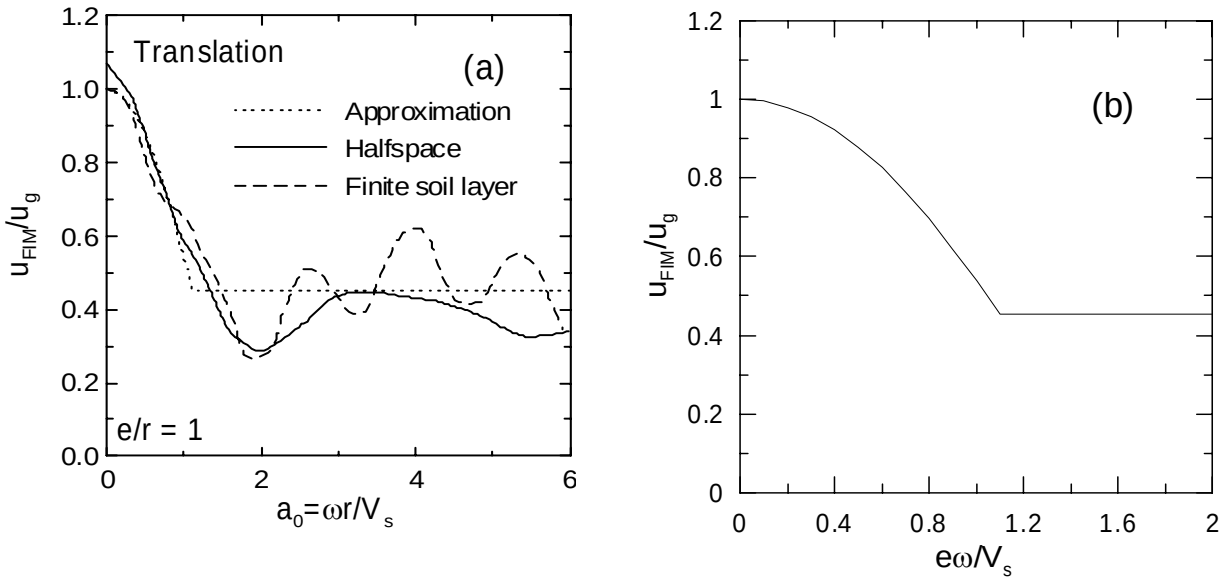


Figure E-3 (a) Transfer function amplitudes for embedded cylinders from Day (1978) and Elsabee and Morray (1977) along with approximate solution by Elsabee and Morray; (b) Transfer function amplitude model by Elsabee and Morray (1977).

The results in Figure E-3 can be contrasted with the behavior of a surface foundation, which would have no reduction of translational motions and no rotational motions when subjected to vertically incident coherent shear waves. Transfer function amplitudes in the presence of more realistic incident wave fields can be estimated at each frequency by the product of the transfer function ordinates from the previous section (for base slab averaging) and those from this section at the corresponding frequency.

Elsabee and Morray (1977) found these transfer functions to also be applicable to nonhomogeneous soil profiles, provided $v_{s,r}$ is averaged across the embedment depth. Mita and Luco (1989) found that solutions for circular foundations can be extended to square foundations, provided the radius of the equivalent cylinder is the average of the radii necessary to match the area and moment of inertia of the square base.

The analysis procedure described herein has been verified against recorded motions from two relatively deeply embedded structures with circular foundations having *e/r* = 0.9 and 2.9 (Kim, 2001). Embedment effects dominated the kinematic interaction for these deeply embedded foundations; for foundations with *e/r* < 0.5 Kim (2001) found that the embedment and base slab averaging models should be coupled by multiplying the respective transfer function ordinates from the two models to accurately simulate observed transfer functions.

### *E.2.3 Application of Transfer Functions to Calculation of Foundation Motions*

The analysis of free-field motions generally results in the specification of a design-basis acceleration response spectrum. Sometimes suites of time histories are specified that are compatible with this spectrum. The question addressed in this section is how this spectrum or time history suite should be modified once the transfer function amplitude for the site has been evaluated using the analysis procedures described above.

When free-field motions are specified only as response spectral ordinates, the evaluation of a modified response spectrum consistent with the FIM is needed. Veletsos and Prasad (1989) evaluated ratios of foundation / free-field response spectral ordinates (at 2% damping) for conditions where the corresponding transfer function ordinates could be readily determined. The transfer function ordinates and ratios of response spectra (RRS) were compared for an input motion with

specified power spectral densities and random phase. The results indicated that transfer function ordinates provide a reasonable estimate of response spectral ratios for low frequencies (e.g., < 5 Hz), but that at high frequencies (≥ 10 Hz) transfer function ordinates are significantly smaller than response spectrum ratios. The inconsistency at high frequencies is attributed to the low energy content of free-field excitation at high frequencies and the saturation of spectral ordinates at these frequencies.

The analytical results of Veletsos and Prasad were checked by (1) calculating the transfer function for a fixed set of conditions (surface foundation, $r$ = 50 m, $V_s$ = 250 m/s), (2) using this transfer function to modify a set of recorded free-field time histories to corresponding foundation-level time histories, and (3) evaluating the RRS using the two time histories. Representative results of these analyses are presented in Figure E-4. The left frame shows results for a time

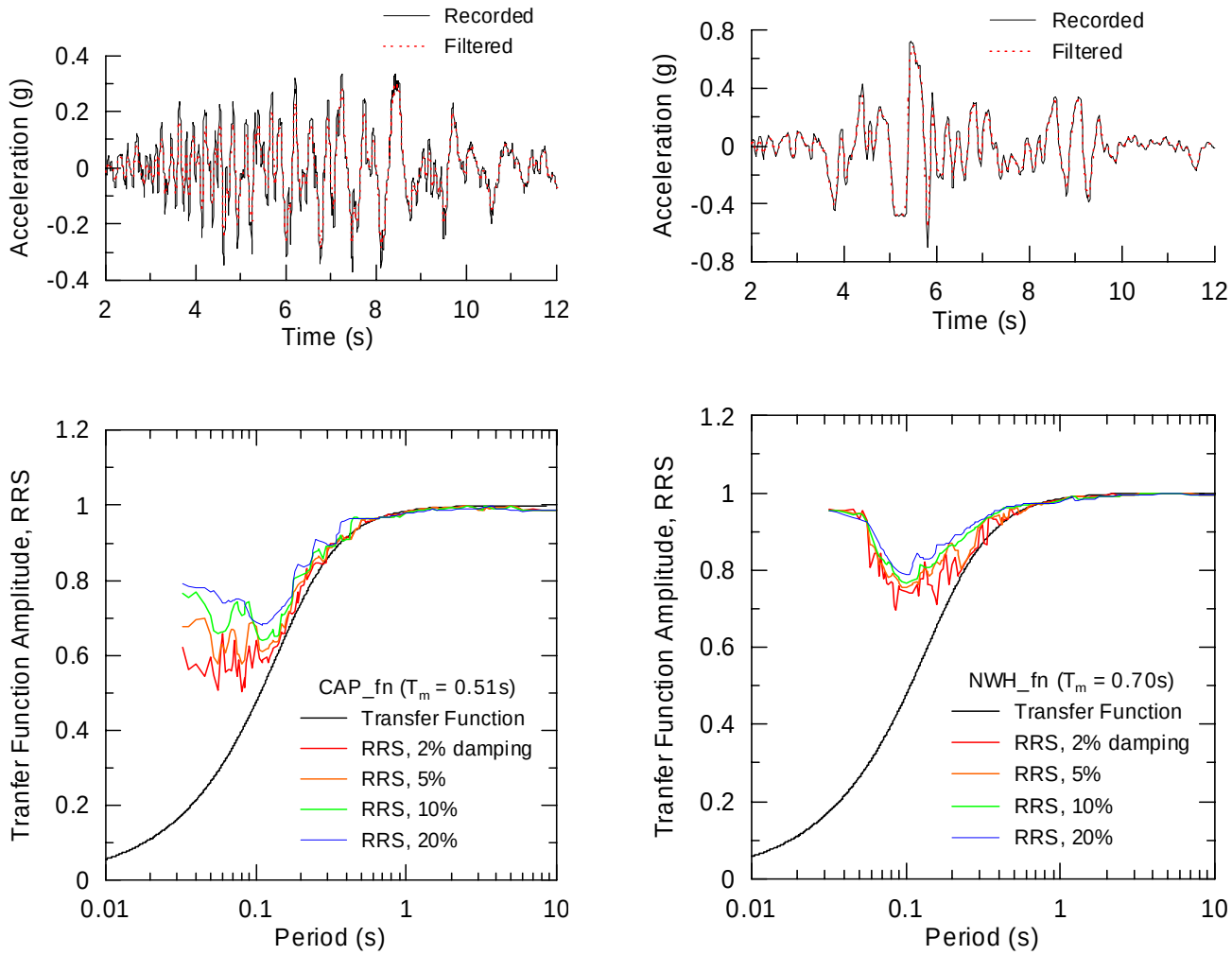


Figure E-4 Comparison of transfer function amplitude to ratios of response spectra (RRS) at different damping ratios. Left figure applies for time histories in which the spectral response is dominated by high-frequency spikes in the accelerogram, whereas in the right figure the response is dictated by lower frequency spikes.

history in which the spectral response is largely controlled by relatively high-frequency components of the waveform. The right frame shows results for a time history in which the peak response is associated with relatively low-frequency pulses. These types of low-frequency pulses are common for sites located on soft soils, but are also found in some sites subjected to significant near-fault, forward rupture directivity effects. The results suggest that for ordinary ground motions, RRS over a wide range of damping ratios can be reasonably estimated by transfer function ordinates for $T > 0.2$ s, but that some caution should be exercised for soft soil sites and perhaps for near-fault ground motions. It should be noted that only a few ground motion time histories were used in these analyses, and additional research is needed to evaluate the relationship between RRS and transfer function ordinates as a function of ground motion characteristics and damping ratio.

Based on the above, the following procedure is recommended for estimation of RRS from transfer function ordinates:

1. For periods > 0.2 s, estimate foundation response spectral ordinates as the product of free-field response spectral ordinates and the transfer function amplitude at the corresponding frequency.
2. For periods < 0.2 s, estimate foundation response spectral ordinates as the product of free-field response spectral ordinates and the transfer function amplitude at 0.2 s.

For structures on very soft soils (i.e., NEHRP Site Category E), no reductions of response spectra for kinematic interaction should be taken.

When free-field motions are specified as time histories for use in nonlinear time history analyses of structures, modified time histories representing the FIM can be evaluated as follows:

1. Calculate the Fourier transforms of the free-field time histories.
2. Multiply the amplitude of the free-field motions by the transfer function amplitude.
3. Use the amplitudes from (2) along with the phase angles of the free-field motions, and perform reverse Fourier transforms to estimate FIM time histories.
4. If needed, a revised response spectrum that accounts for kinematic interaction effects could be calculated from the FIM time histories.

It should be noted that maintaining the free-field phase angles in Step 3 is not strictly correct, especially for embedded foundations. If desired, phase shifts of $\omega e/V_s$ (in radians) could be introduced for motions of embedded foundations relative to ground surface motions. Models for phase adjustment are not available for kinematic interaction effects involving surface foundations, but the assumption of consistent phase should not significantly bias response spectral ordinates for estimated FIMs.

### *E.2.4 Simplified Procedure for Design*

The Kim and Stewart (2003) model for incoherence parameter $\kappa_a$ (presented in Section E.2.1), along with the procedure for converting transfer function ordinates to RRS (presented in Section E.2.3), enables the development of simplified design charts for kinematic interaction effects for non-embedded base slabs founded on alluvial soils. A significant simplification results from the fact that $\kappa_a$ is nearly proportional to $v_s$ (as seen in Figure E-2), which per Equation E-1 causes dimensionless frequency term $\tilde{a}_o$ to effectively reduce to a function of frequency and foundation size ($b_e$). This is shown below, written for vertically propagating waves ($\alpha_v = 0$):

$$\tilde{a}_0 = \frac{\omega b_e}{2V_{s,r}}\sqrt{\kappa^2 + \sin^2\alpha_v\left(\frac{b}{b_e}\right)^2} \approx \frac{\omega b_e \kappa}{2V_{s,r}} \approx \frac{\omega b_e n_1 V_s}{2n_2 V_s} = \frac{\omega b_e n_1}{2n_2} \quad \text{(E-3)}$$

where $n_1 \approx 6.5 \times 10^{-4}$ s/m and $n_2$ is the square root of the soil modulus reduction factor, which can be estimated as shown in Table E-1.

Figure E-5 shows the degree of approximation associated with taking $\kappa_a$ as proportional to $v_s$ (using

*Table E-1 Approximate values of n*

| | Peak Ground Acceleration (PGA) | | | |
|---|---|---|---|---|
| | 0.10 | 0.15 | 0.20 | 0.30 |
| n | 0.90 | 0.80 | 0.70 | 0.65 |

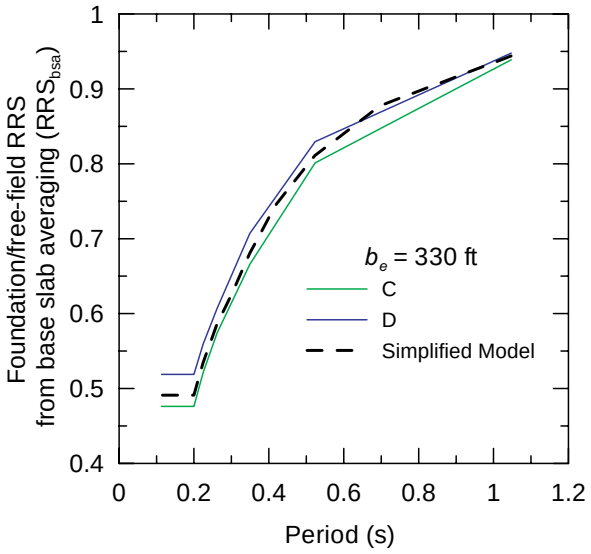


Figure E-5 RRS for foundation with $b_e$ = 330 ft. Simplified model ($\kappa_a / v_s = n_1$) vs. exact solution for $\kappa_a$

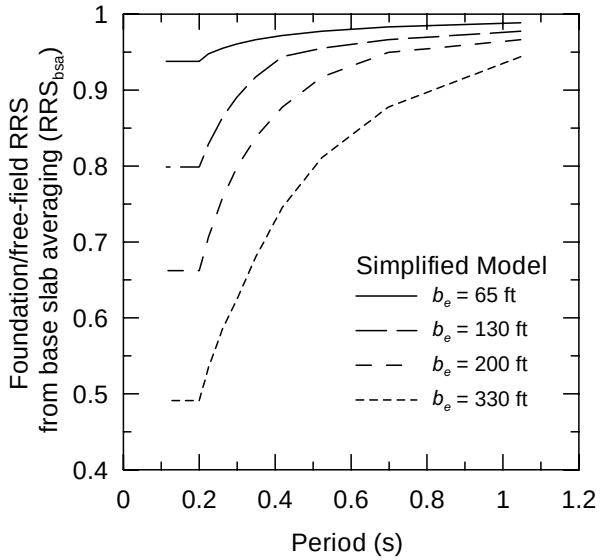


Figure E-6 RRS from simplified model as function of foundation size, $b_e$

proportionality term $n_1$). In this and subsequent figures, parameter $n_2$ = 0.65, which is the appropriate value for regions of high seismicity. The results for site classes C-D are shown for typical shear wave velocities within the categories based on borehole compilations. The difference between the simplified model and the result for individual site classes is small. Figure E-6 shows the resulting curves of RRS per Equation E-3 for foundations of various sizes. As expected, the kinematic interaction effect increases as the foundation size increases and as period decreases.

As with the base slab averaging model for surface foundations, simplified design charts for the RRS of embedded foundations can also be developed. These charts are based on the simplified model of Elsabee and Morray (1977) shown in Figure E-3b, but with the RRS interpreted from the transfer function amplitude as described in Section E.2.3. Figure E-7a presents RRS as a function of period in site categories A-D for a relatively large embedment depth of 30 ft. As can be seen in the figure, embedment effects are negligible at practical levels of embedment for firm rock site conditions (Site Categories A and B). Accordingly, Figure E-7b presents RRS values at three levels of embedment ($e$ = 10, 20, and 30 ft) only for Site Classes C and D.

Based on the above, the following simplified procedure is recommended for analysis of kinematic interaction effects:

1. Evaluate effective foundation size $b_e = \sqrt{ab}$, where $a$ and $b$ are the foundation dimensions in plan view.
2. Evaluate period-dependant RRS from base slab averaging ($RRS_{bsa}$) using Figure E-6. An approximate equation to the curves in Figure E-6 is presented below:

$$RRS_{bsa} = 1 - \frac{1}{14100}\left(\frac{b_e}{\tilde{T}_{eq}}\right)^{1.2} \qquad \text{(E-4)}$$

   where $b_e$ = effective foundation size (from Step 1) in feet, and $T$ = period in sec.

3. If the foundation is embedded a depth $e$ from the ground surface, evaluate an additional RRS from embedment ($RRS_e$) as a function of period due to embedment effects using Figure E-7. The equation of the curves in Figure E-7 is,

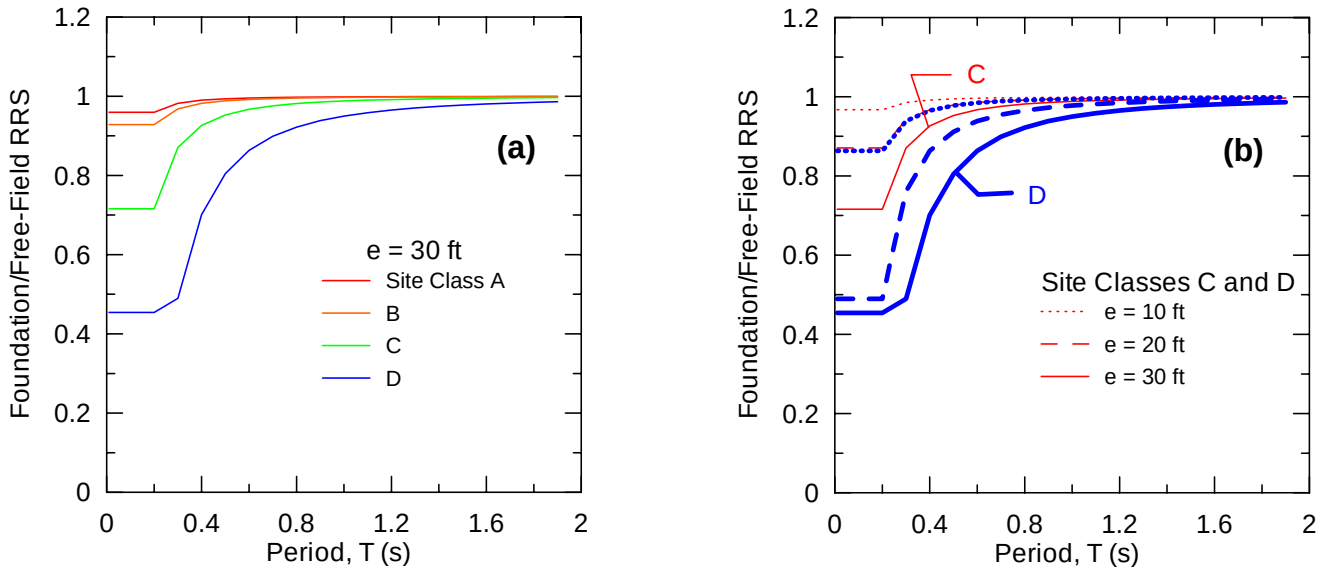


Figure E-7 (a) RRS for foundation embedded to depth e = 30 ft in different site categories; (b) RRS for foundations with variable depths in Site Classes C and D.

$$RRS_e = \cos\left(\frac{2\pi\, e}{\tilde{T}_{eq} v_{s,r}}\right) \geq \text{larger of 0.453 or the value of } RRS_e \text{ at } T = 0.2 \text{ sec} \qquad \text{(E-5)}$$

where $e$ = foundation embedment (in feet) and $v_{s,r}$ = effective strain-degraded shear wave velocity in the soil (in ft/s). Factors that can be used to estimate $v_{s,r}$ from small-strain shear wave velocity $v_s$ are given in Table E-1.

4. Evaluate the product $RRS_{bsa}$ times $RRS_e$ to obtain the total RRS. The spectral ordinates of the foundation input motion is the product of the free-field spectral ordinates and the total RRS.

Limitations associated with application of this approach include the following:

- Kinematic interaction effects should be neglected for soft clay sites, such as Site Class E.
- Embedment effects can be neglected for foundations embedded in firm rock (Site Classes A and B).
- The base slab averaging model has the following limitations:
  a) Underestimates ground motion reduction for sites on rock (i.e., use of the above formulation is conservative).
  b) The model has not been validated for foundations with low in-plane stiffness, buildings with large footprint dimensions (> 200 ft), and pile-supported foundations in which the cap and soil are not in contact. However, the judgment of the project technical team that developed this report is that the model can provide a reasonable first order estimate of the kinematic interaction effect for those conditions.
  c) The model should not be used for structures that have both foundations without significant connectivity of lateral elements and flexible floor and roof diaphragms.

## E.3 Foundation Damping

Inertia developed in a vibrating structure gives rise to base shear, moment, and torsion at the foundation soil interface, and these loads in turn cause displacements and rotations of the structure relative to the free field. These relative displacements and rotations are only possible because of compliance in the soil, which can significantly contribute to the overall structural flexibility in some cases. Moreover, the difference between the foundation input motion and free-field motion gives rise to energy dissipation via radiation damping and hysteretic soil damping, and this energy dissipation affects the overall system damping. Since these effects are rooted in the structural inertia, they are

referred to as *inertial interaction* effects, in contrast to the *kinematic interaction* effects discussed in the prior section.

The ATC-40 and FEMA 356 documents contain provisions for evaluating the properties of foundation springs (e.g., Sections 10.3 and 10.4 of ATC-40), and hence this aspect of inertial interaction is not emphasized here. Rather, the focus of this section is on the damping component of inertial interaction and the contribution of this damping to the overall system damping.

In the SSI literature, foundation stiffness and damping effects are often described in terms of an *impedance function*. The impedance function should account for the soil stratigraphy and foundation stiffness and geometry, and is typically computed using equivalent-linear soil properties appropriate for the in situ dynamic shear strains. Impedance functions can be evaluated for multiple independent foundation elements, or (more commonly) a single 6×6 matrix of impedance functions is used to represent the complete foundation (which assumes foundation rigidity).

In the following sub-sections, factors affecting foundation impedance functions are described, with an emphasis on those factors significantly affecting the damping component. The section is concluded with a discussion of how system damping ratios can be evaluated once factors affecting impedance functions and the fixed-based structural damping ratio are known.

### *E.3.1 Analysis of Impedance Functions*

#### E.3.1.1 Basic Case

Simplified impedance function solutions are available for rigid circular or rectangular foundations located on the ground surface and underlain by a uniform, visco-elastic halfspace. A thorough listing of impedance functions for these and other foundation shapes is provided in Gazetas (1991a, 1991b). A circular foundation shape with the above assumptions of foundation rigidity and soil uniformity comprise the "basic case" for foundation impedance considered here.

Terms in the complex valued impedance function are expressed in the form

$$\bar{k}_j = k_j(a_0, \upsilon) + i\omega c_j(a_0, \upsilon) \qquad \text{(E-6)}$$

where $j$ denotes either deformation mode $x$ (for translation) or $\theta$ (for rotation in the vertical plane), $\omega$ is angular frequency (radians/sec.), $a_0$ is a dimensionless frequency defined by $a_0 = \omega r/v_s$, $r$ = foundation radius, $v_s$ = soil shear wave velocity, and $\upsilon$ = soil Poisson ratio. Foundation radii can be computed separately for translational and rotational deformation modes to match the area ($A_f$) and moment of inertia ($I_f$) of the actual foundation (i.e. $r_x = \sqrt{A_f/\pi}$ , $r_\theta = \sqrt[4]{4I_f/\pi}$ ). There are corresponding $(a_0)_x$ and $(a_0)_\theta$ values as well.

The real stiffness and damping of the translational and rotational springs and dashpots are expressed, respectively, by

$$k_x = \alpha_x K_x \qquad c_x = \beta_x \frac{K_x r_x}{v_S} \qquad \text{(a)}$$

$$k_\theta = \alpha_\theta K_\theta \qquad c_\theta = \beta_\theta \frac{K_\theta r_\theta}{v_S} \qquad \text{(b)} \qquad \text{(E-7)}$$

where $\alpha_x$, $\beta_x$, $\alpha_\theta$, and $\beta_\theta$ express the frequency dependence of the impedance terms, and $K_x$ and $K_\theta$ are the static stiffness of a disk on a halfspace,

$$K_x = \frac{8}{2-\upsilon} G r_x \qquad K_\theta = \frac{8}{3(1-\upsilon)} G r_\theta^3 \qquad \text{(E-8)}$$

where $G$ = soil dynamic shear modulus. Additional solutions for $K_x$ and $K_\theta$ that take into account the foundation geometry in plan are presented in Table 10-2 of ATC (1996). Presented in Figure E-8 are the frequency-dependent values of $\alpha_x$, $\beta_x$, $\alpha_\theta$, and $\beta_\theta$ for a rigid circular foundation on the surface of a visco-elastic halfspace with soil hysteretic damping ratio $\beta_s$ (Veletsos and Wei, 1971; Veletsos and Verbic, 1973).

Validation studies for the above and similar impedance function formulations have been conducted by Lin and Jennings (1984) and Crouse et al. (1990) for small foundations (< 10 ft plan dimension), and by Luco et al. (1988), Wong et al. (1988), and DeBarros and Luco (1995) for larger scale building foundations (up to 80 ft plan dimension). These studies have generally found reasonably good agreement between experimental observations and analytical predictions, although the fit is usually markedly better for rotation vibration modes than for translation. The improved fit for rotation likely results from the relative ease of identifying impedance functions from rotation data as compared to relative

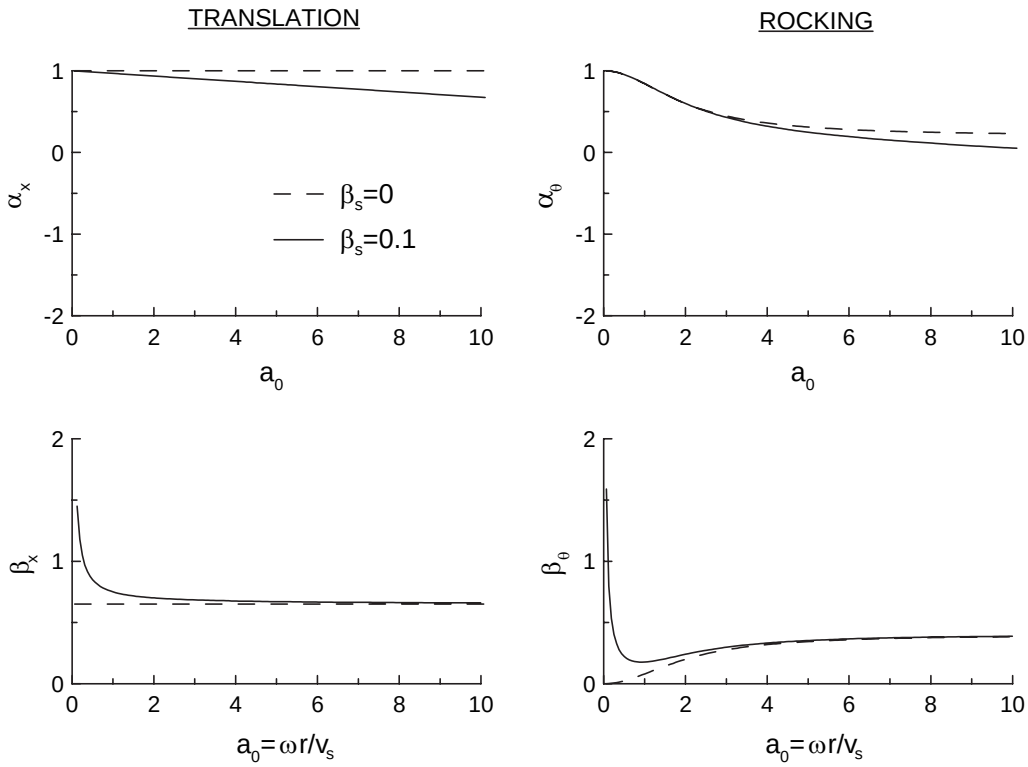


Figure E-8 Foundation stiffness and damping factors for elastic and viscoelastic halfspaces ($\upsilon = 0.4$). After Veletsos and Verbic, 1973.

foundation/free-field translations, which have weaker signals.

The above solutions for rigid, circular foundations on a halfspace can provide reasonable estimates of foundation impedance in many cases. However, the potentially significant effects of non-uniform soil profiles, embedded foundations, non-circular foundation shapes, and flexible foundations should be accounted for in some cases. The following sections discuss the effects of these factors on the damping component of impedance functions.

#### E.3.1.2 Nonuniform Soil Profiles

Gazetas (1991b) provides solutions for the impedance of rigid foundations overlying soil for which the shear stiffness increases with depth according to prescribed functions. The damping components of these solutions are plotted in Figure E-9 in terms of the frequency-dependent and dimensionless $\beta_x$ and $\beta_\theta$ terms; actual dashpot coefficients can be computed using these terms in Equations E-7a and b. Also plotted for comparative purposes are the solutions for a halfspace presented previously in Figure E-8. Note that the damping values for non-uniform profiles are plotted for a zero hysteretic damping condition (radiation damping only) and that the normalizing shear modulus and shear wave velocity are the values at the ground surface ($G_0$ and $v_{s0}$, respectively).

From Figure E-9, radiation damping in translation for a nonuniform profile is seen to be less than that for a halfspace at low frequencies. For rotation, a small reduction can occur at low frequencies, but the effect is less significant than for translation. At large frequencies, the radiation damping for nonuniform profiles exceeds that for the halfspace.

The low-frequency reduction in damping is due to reflections of body waves emanating from the foundation; the frequency dependence of the reduction is related to the depth over which the shear modulus increases relative to wavelength. For short-period (and short-wavelength) body waves, the nonuniform soil medium is "seen" as being effectively uniform, whereas

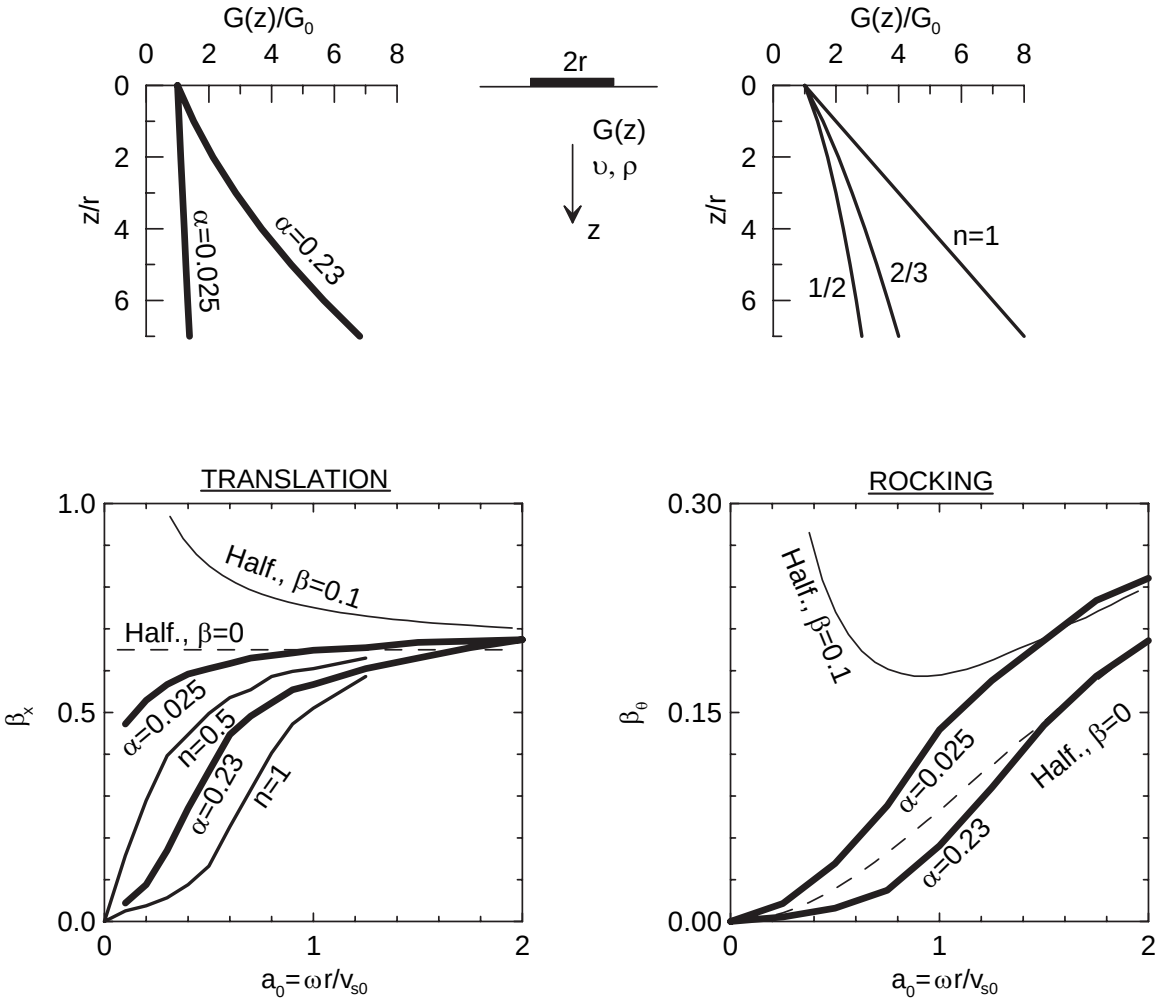


Figure E-9 Foundation damping factors for halfspace with and without hysteretic damping (Veletsos and Verbic, 1973) and for soil profiles with indicated shear modulus profiles and no hysteretic damping (Gazetas, 1991b).

long-period waves (with long wavelengths) "see" a much more nonuniform medium and wave transmission into the medium is impeded. The increase of radiation damping at high frequencies is due to the higher $v_s$ of the nonuniform profiles at depth as compared to the velocity of the halfspace model (for which $v_s$ was taken as $v_{s0}$).

The above effects on low-frequency damping can be contrasted with the effect of soil nonuniformity on foundation stiffness. A number of researchers (e.g., Roesset, 1980; Gazetas, 1991b; Stewart et al., 2003) have suggested that effective foundation stiffnesses can be computed from an average $v_s$ value over a specified depth range. For the common case in which soil stiffness increases with depth, this averaging will result in an effective $v_s$ value that is larger than $v_{s0}$. The use of this averaged $v_s$ would be unconservative in the case of damping, as the low-frequency damping is overpredicted by a halfspace model even when the halfspace velocity is taken as $v_{s0}$. Thus, different effective velocities of nonuniform soil profiles should be used for calculations of foundation stiffness and damping.

For the case of a finite soil layer overlying a much stiffer material, the key issue is a lack of radiation damping at periods greater than the fundamental period of the finite soil layer, $T_s = 4H/v_s$. Halfspace damping ratios can be used for periods less than the soil layer period. Above this period in materials with hysteretic damping, Elsabee and Morray (1977) developed the following damping recommendations:

$$\beta_x \approx 0.65\beta \frac{a_0/a_{01}}{1-(1-2\beta)(a_0/a_{01})^2} \text{ for } a_0/a_{01} \le 1 \quad \text{(E-9)}$$

$$\beta_\theta \approx 0.50\beta \frac{a_0/a_{01}}{1-(1-2\beta)(a_0/a_{01})^2} \le \frac{0.35a_0}{1+a_0^2} \quad \text{for } a_0/a_{01} \le v_p/v_s \quad \text{(E-10)}$$

where $a_{01} = 0.5\pi r/H$, $r$ = foundation radius, and $H$ = finite soil layer thickness.

In terms of practical application of the above results, the following observations are noted:

- For translational damping, profile non-uniformity is not significant for $a_0=\omega r/v_s > 1$. Case history studies suggest that inertial soil-structure interaction is generally not important for $h/(v_sT) < 0.1$ (Stewart et al., 1999). Hence, for sites where SSI is important, profile non-uniformity need not be considered if $h/r < 2\pi h/(v_sT)$. The value on the right hand side of the inequality will generally be more than 2/3 for cases where inertial SSI is important, which is larger than the aspect ratios for many short-period buildings. Accordingly, it is often justified to treat the nonuniform soil as a halfspace, taking the halfspace velocity as the in situ value immediately below the foundation. Note that the above inequality to allow profile non-uniformity effects to be neglected can be re-written as $v_sT/r < 2\pi$.
- Rotational damping for a non-uniform profile can generally be reasonably well estimated by a halfspace model, with the halfspace velocity taken as the in situ value immediately below the foundation.
- The use of halfspace models is unconservative for sites with a finite soil layer overlying a very stiff layer, if the structural system period is greater than the soil layer period. Alternative dashpot coefficients for such cases can be developed using Equation E-10.

#### E.3.1.3 Embedded Foundations

Foundation "embedment" refers to a foundation base slab that is positioned at a lower elevation than the surrounding ground, which will usually occur when buildings have a basement. The impedance of embedded foundations differs from that of shallow foundations in several important ways. First, the static stiffness of embedded foundations is increased, which is accounted for with the embedment factors given in Table 10.3 of ATC-40 (ATC, 1996). For circular foundations, these embedment terms are as follows:

$$\begin{aligned} (K_x)_E &= K_x\left(1+\frac{2}{3}\frac{e}{r_u}\right) \\ (K_\theta)_E &= K_\theta\left(1+2\frac{e}{r_\theta}\right) \end{aligned} \quad \text{(E-11)}$$

where $e$ = embedment depth. The second important difference between embedded and surface foundations is that embedded foundations can produce much larger damping due to the greater foundation-soil contact area.

An approximate and generally conservative approach for estimating the damping of embedded foundations consists of using the modified static stiffness terms from Equation E-11 coupled with the dynamic modifiers for a surface foundation in Figure E-8. This approach has been found to provide reasonable estimates of observed foundation damping in actual structures for embedment ratios $e/r_u < 0.5$ (Stewart et al., 1999). As short-period structures are seldom deeply embedded, this approximate approach will often suffice for practical applications. For more deeply embedded foundations, alternative formulations can be used such as Bielak (1975) or Apsel and Luco (1987). However, caution should also be exercised in the application of these approaches for embedded foundations with poor quality backfill against basement walls. For such foundations, gapping is likely and impedance functions should probably be formulated using the shallow foundation approach noted previously.

#### E.3.1.4 Foundation Shape

Impedance functions for foundations of arbitrary shape are commonly analyzed as equivalent circular mats (BSSC, 2001). As described previously, an equivalent

radius for translational stiffness is derived by equating the areas of the mats, while an equivalent radius for rotational stiffness is derived by equating the moments of inertia of the mats. The issue addressed in this section is the adequacy of this assumption for oblong foundations.

Combining a number of analytical impedance function solutions from the literature for foundations of arbitrary shape, Dobry and Gazetas (1986) found that the use of equivalent circular mats is acceptable for aspect ratios less than 4:1, with the notable exception of dashpot coefficients in the rotation mode. As shown in Figure E-10, dimensionless radiation damping coefficients $c_{rx}$ and $c_{ry}$ (for longitudinal and transverse rotations, respectively) are seen to be underestimated by the equivalent disk assumption at low frequencies. This is a consequence of the tendency for rotational vibrations to be dissipated into the soil primarily via the ends of the foundation. Hence, as aspect ratio increases, the two ends act increasingly as independent wave sources with reduced destructive interference between waves emanating from the foundation. For the case of longitudinal rotations, damping can be underpredicted by a factor of two or more for aspect ratios of L/B $\approx$ 4. For higher frequencies ($a_0$ > 3-4, not shown in figure), the results for the various aspect ratios converge to $c_{rx}$, $c_{ry}$ = ~1. This occurs because these high frequency waves have short wavelengths relative to the foundation dimension regardless of L/B, so destructive interference between the waves is small in all cases.

The use of dashpot coefficients for disk-shaped foundations can be used to provide conservative (lower-bound) estimates of the damping of oblong foundations. This approximation may be sufficient for many practical applications, especially given the relatively small influence of damping from rotations on system damping (damping from horizontal vibrations often contribute more significantly, see Section E.3.2). If more refined analysis of rotational damping is needed, rotational radiation dashpot coefficients for oblong, non-circular foundations can be calculated using procedures given in Gazetas (1991a, b).

#### E.3.1.5 Foundation Flexibility

This section addresses flexibility in the foundation structural system (i.e., the base mat, or assemblage of a base mat and grade beams/footings). The foundation flexibility referred to here is not associated with the soil.

Impedance functions for flexible circular foundation slabs supporting shear walls have been evaluated for a number of wall configurations, including: (1) rigid core walls (Iguchi and Luco, 1982), (2) thin perimeter walls (Liou and Huang, 1994), and (3) rigid concentric interior and perimeter walls (Riggs and Waas, 1985). These studies focused on the effects of foundation flexibility on rotation impedance; the horizontal impedance of flexible and rigid foundations are similar (Liou and Huang, 1994). Foundation flexibility effects on rotation impedance were found to be most significant for a rigid central core with no perimeter walls. For this case, the flexible foundation has significantly less stiffness and damping than the rigid foundation. The reductions are most significant for narrow central cores and large deviations between soil and foundation slab rigidity.

Significant additional work remains to be done on foundation flexibility effects on impedance functions because the existing research generally has investigated wall/slab configurations that are seldom encountered in practice for building structures. Nonetheless, based on the available studies and engineering judgment, the following preliminary recommendations are provided:

1. The rigid foundation assumption is probably generally acceptable for the analysis of damping associated with horizontal vibrations of reasonably stiff, inter-connected foundation systems.
2. For buildings with continuous shear walls or braced frames around the building perimeter, and continuous footing or mat foundations beneath these walls, the rigid foundation approximation can likely be used to provide a reasonable estimate of damping from rotation vibrations. In this case, the effective foundation radius ($r_\theta$) would be calculated using the full building dimensions. This recommendation also applies if continuous basement walls are present around the building perimeter. This case is referred to as stiff rotational coupling.
3. For buildings with a core of shear walls within the building, but no shear walls outside of this core, a conservative estimate of foundation damping can be obtained by calculating the effective foundation radius ($r_\theta$) using the dimensions of the wall foundations (which, in this case, would be smaller than the overall building plan dimensions). This is an example of soft rotational coupling between the shear walls and other load bearing elements.

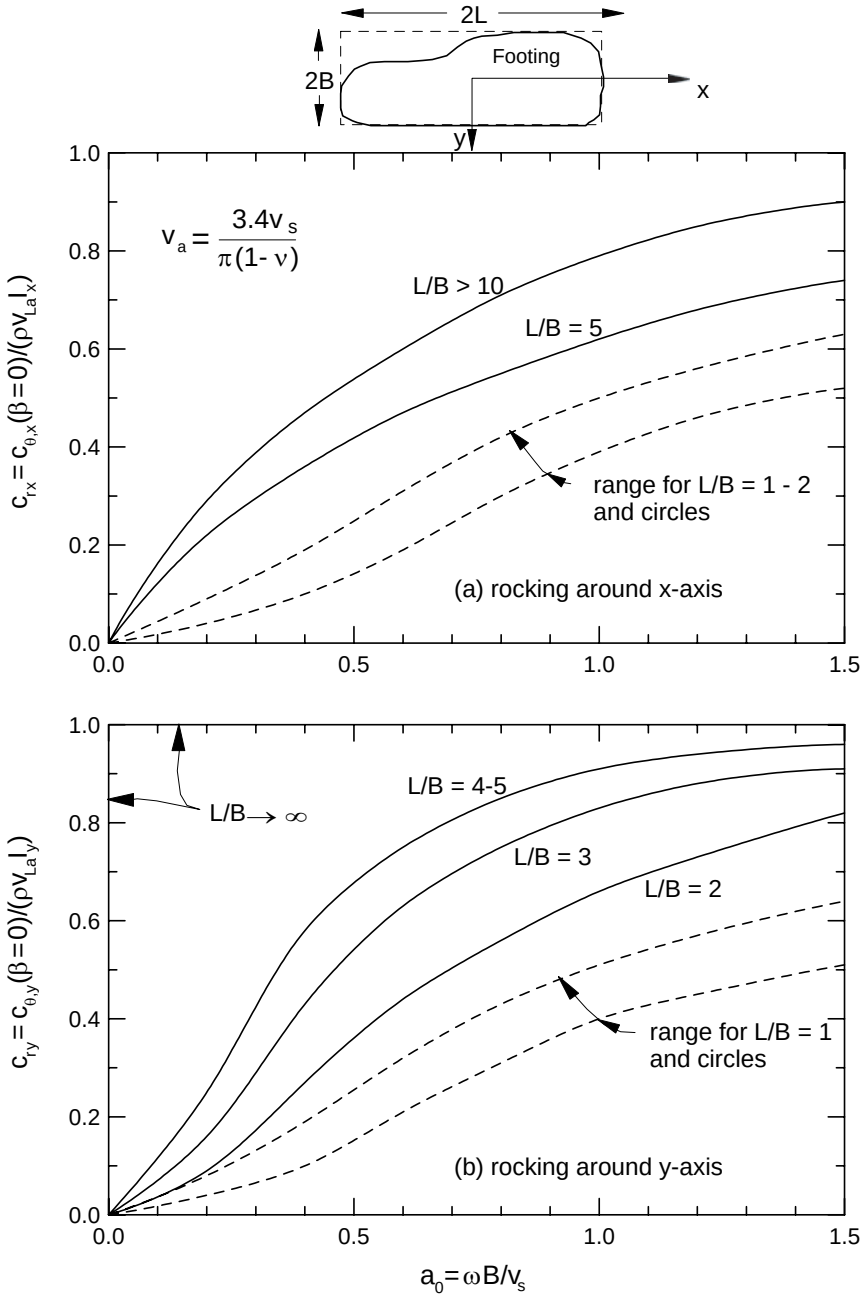


Figure E-10 Dashpot coefficients for radiation damping vs. normalized frequency for different foundation shapes (after Dobry and Gazetas, 1986).

4. For buildings with distributed shear walls at various locations around the building plan, the key issues are (1) the rotational stiffness of the building system as a whole (i.e., does the building tend to rotate as a single rigid block due to significant rotational stiffness coupling between adjacent elements, or do individual vertical components such as shear walls rotate independently of each other?), and (2) the degree to which destructive interference occurs between waves emanating from rotation of distinct foundation components.

In practice, it may sometimes be difficult to decide on the degree of rotational coupling between foundation elements. However, pushover analyses of the building with foundation springs utilized below foundation elements incorporate rotational coupling between foundation elements in a natural way. Hence, the results of such analyses can be used to infer the effective foundation size associated with the building's rotational impedance. This process is described in the following.

The derivation begins with the relationship between period lengthening and foundation spring stiffness values by Veletsos and Meek (1974):

$$\frac{\tilde{T}}{T} = \sqrt{1 + \frac{K^*_{fixed}}{k_x} + \frac{K^*_{fixed} h^2}{k_\theta}} \qquad \text{(E-12)}$$

In Equation E-12, the following quantities are known or can be estimated reliably:

- $T$ is the fixed base first mode period, and can be evaluated from the model of the structure utilized in pushover analyses, but with foundation spring stiffnesses set to infinity.
- $\tilde{T}$ is the flexible base first mode period, and can be evaluated from the model of the structure utilized in pushover analyses including foundation springs. The foundation spring stiffness should reflect strain-degraded soil properties.
- Stiffness parameter $K^*_{fixed}$ is the stiffness of the fixed-base structure, and can be evaluated as

$$K^*_{fixed} = M^* \left( \frac{2\pi}{T} \right)^2 \qquad \text{(E-13)}$$

  where $M^*$ is the effective mass for the first mode calculated as the total mass times the effective mass coefficient (see ATC-40, Equation 8-21).

- Foundation stiffness parameter $k_x$ represents the horizontal stiffness of the foundation system, and can be evaluated as described previously (Sections Sections E.3.1.1 – E.3.1.3). For the present application, a good approximation of $k_x$ is $K_x$.
- Height $h$ is the effective structure height taken as the full height of the building for one-story structures, and as the vertical distance from the foundation to the centroid of the first mode shape for multi-story structures. In the latter case, $h$ can often be well approximated as 70% of the total structure height.

Equation E-12 can then be re-arranged to estimate $K_\theta$ as follows:

$$K_\theta = \frac{K^*_{fixed} h^2}{\left( \frac{\tilde{T}}{T} \right)^2 - 1 - \frac{K^*_{fixed}}{K_x}} \qquad \text{(E-14)}$$

In the above, it has been assumed that $k_u \approx K_u$ and $k_\theta \approx K_\theta$, which is generally a reasonable approximation. The evaluation of an effective foundation radius from $K_\theta$ can be accomplished using Equation E-8, with the following result:

$$r_\theta = \left( \frac{3(1-\upsilon) K_\theta}{8G} \right)^{\frac{1}{3}} \qquad \text{(E-15)}$$

The value $r_\theta$ will decrease as the degree of rotational coupling decreases. For very stiff rotational coupling $r_\theta$ will approach the value that would be calculated from the moment of inertia derived from the full foundation dimension ( $r_\theta = \sqrt[4]{4 I_f / \pi}$ ).

A potential complication to the above may occur when foundations are closely spaced, and destructive interference occurs between waves emanating from adjacent foundation elements. If this occurred, the above formulation would be unconservative. Unfortunately, this topic has not been researched, and thus what footing separation distances constitute "close" and "widely spaced" is unknown, which in turn precludes the development of recommendations for the analysis of rotation damping for distributed walls.

Finally, it should be noted that for buildings with only moment resisting frames (no walls or braced frames), foundation rotation is not likely to be significant, and hence foundation flexibility effects on rotation damping are also likely insignificant.

### *E.3.2 Analysis of System Damping Ratios*

The effect of foundation flexibility on the response of a structure can be visualized using the single-degree-of-freedom oscillator depicted in Figure E-11. In the figure, displacement $u_g$ denotes the free-field ground motion, $u_f$ denotes foundation translation relative to the

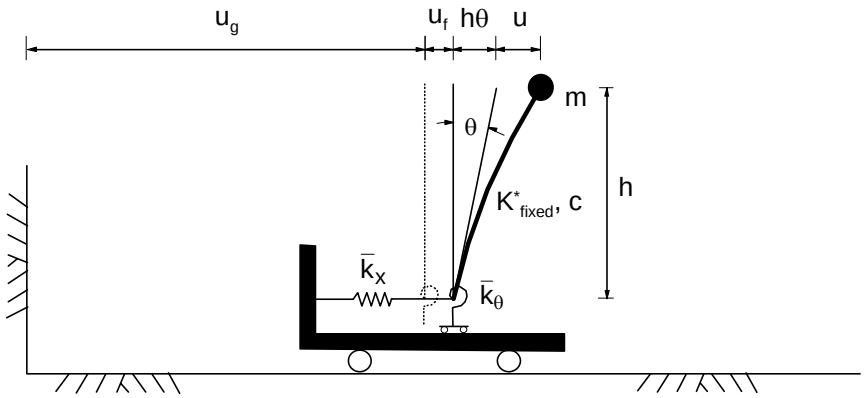


Figure E-11 Oscillator model for analysis of inertial interaction under lateral excitation.

free-field, $\theta$ denotes foundation rotation, and $u$ denotes displacement resulting from deformation within the structure with stiffness $K^*_{fixed}$ and dashpot coefficient $c$. SSI effects are manifested by a lengthening of the building period from the fixed-base case ($T$) to the flexible-base case ($\tilde{T}$), and by a change in the damping ratio (from $\beta_i$ to $\beta_o$). These effects have been evaluated as closed-form expressions for the simple oscillator configuration shown in Figure E-11. In this case, the impedance function is represented by complex-valued terms for the translation ($\bar{k}_x$) and vertical plane rotation ($\bar{k}_\theta$) foundation vibration modes. A vertical foundation degree-of-freedom also exists (impedance term $\bar{k}_v$), but does not affect $\tilde{T}$ or $\beta_o$.

The flexible-base damping ratio of the oscillator has contributions from the viscous damping in the structure as well as radiation and hysteretic damping in the foundation. Jennings and Bielak (1973), Bielak (1975, 1976) and Veletsos and Nair (1975) expressed the flexible-base damping $\beta_o$ as

$$\beta_0 = \beta_f + \frac{\beta_i}{\left(\tilde{T}_{eq}/T_{eq}\right)^3} \qquad \text{(E-16)}$$

where $\beta_f$ is referred to as the foundation damping and represents the damping contributions from foundation-soil interaction (with hysteretic and radiation components), and $\tilde{T}_{eq}$ and $T_{eq}$ represent the flexible- and fixed-base period of the structure accounting for the effects of yielding in the superstructure. From Equation E-16, it can be readily seen that the flexible-base damping, which is the damping ratio for which response spectra should be evaluated, is a function of fixed-base damping ($\beta_i$), the period lengthening ratio ($\tilde{T}_{eq}/T_{eq}$), and $\beta_f$. Parameter $\beta_i$ is generally assumed to be 5%. The period lengthening can be evaluated using the structural model used in pushover analyses as follows:

1. Evaluate the first-mode vibration period of the model, including foundation springs. This period is $\tilde{T}$. The period can be calculated using initial stiffness values for the structure and strain-degraded soil stiffness values.
2. Evaluate the first-mode vibration period of the model with the foundation springs removed (or their stiffness and capacity set to infinity). This period is $T$. As before, this period should correspond to pre-yield conditions.
3. Calculate the ratio $\tilde{T}/T$, which is the period lengthening under small-deformation (elastic) conditions.
4. Calculate $\tilde{T}_{eq}/T_{eq}$ using the following equation:

$$\frac{\tilde{T}_{eq}}{T_{eq}} = \left\{1 + \frac{1}{\mu_{sys}}\left[\left(\frac{\tilde{T}}{T}\right)^2 - 1\right]\right\}^{0.5} \qquad \text{(E-17)}$$

where $\mu_{sys}$ is the peak system ductility (including structure and soil effects).

With $\beta_i$ and $\tilde{T}_{eq}/T_{eq}$ known, the estimation of $\beta_o$ reduces to an analysis of foundation damping $\beta_f$. Graphical solutions and closed-form expressions for $\beta_f$

are available for the simple case of a circular foundation with radius $r$ on a uniform halfspace with velocity $v_s$ and hysteretic damping ratio $\beta_s$ (Veletsos and Nair, 1975). The expression for $\beta_f$ given by Veletsos and Nair is reproduced below,

$$\beta_f = \frac{\pi^4}{2}\frac{\gamma}{\sigma^3}\left(\frac{T_{eq}}{\tilde{T}_{eq}}\right)^3 \times \left\| \left[ \frac{(2-\upsilon)\beta_x}{\alpha(\alpha_x + ia_0\beta_x)}\frac{r^2}{h^2} + \frac{3(1-\upsilon)\beta\beta_\theta}{\alpha_\theta(\alpha_\theta + ia_0\beta_\theta)} \right] \right\| \quad \text{(E-18)}$$

where $\sigma = v_S T/h$, $\gamma = m/(\rho\pi r^2 h)$,

$\alpha = \alpha_x - \left(1/(\tilde{T}f_0)\right)^2$, $f_0 = \sqrt{K_x/m_f}\,/(2\pi)$, and

$$\beta = 1 - \frac{\left(1/(\tilde{T}_{eq}f_0)\right)^2}{\alpha_x - ia_o\beta_x}$$

The first term within the brackets in Equation E-18 is related to damping from foundation vibration in translation whereas the second term is related to foundation rotation. To develop approximate solutions for $\beta_f$ for non-circular foundations, Equation E-18 can be implemented with the radius and $a_0$ values in the first term taken as $r_x$ and $(a_0)_x$, respectively, and in the second term as $r_\theta$ and $(a_0)_\theta$.

Parameters $\sigma$ and $\gamma$ in Equation E-18 represent the ratio of the soil-to-structure stiffness and structure-to-soil mass, respectively. Most conventional short-period building structures have $\sigma$<10 and $\gamma \approx$ 0.1 to 0.2 [a representative value of $\gamma$ = 0.15 is recommended by Veletsos and Meek (1974)].

Due to the availability of these $\beta_f$ formulations for rigid circular foundations on a halfspace, it is convenient to idealize actual foundation and site conditions in terms of representative values of velocity and foundation radius. As described in Section E.3.1, this can generally be accomplished by taking the representative site shear wave velocity as the soil velocity immediately beneath the foundation ($v_{s0}$), and by calculating effective foundation radii for translational and vertical plane rotation vibration modes (i.e. $r_x = \sqrt{A_f/\pi}$, $r_\theta = \sqrt[4]{4I_f/\pi}$). As noted in Section E.3.1.5, special consideration may be required for oblong foundations and for the analysis of $r_\theta$ when shear walls or braced frames are distributed across the foundation plan.

Figure E-12 presents a customization of the Veletsos and Nair (1975) solution for $\beta_f$ in which different ratios of $r_\theta/r_x$ are used (the original solution applied for true circular foundations in which $r_\theta/r_x$ = 1.0) for three fixed values of $h/r_\theta$. Note that terms $v_{s,r}$ and $T_{eq}$ are used in the labeling of the horizontal axis to emphasize that strain-reduced shear wave velocities (evaluated from small-strain shear wave velocities using Table E-1) and ductility-reduced periods should be used in the analysis of $\beta_f$. Figure E-13 presents an identical set of plot to Figure E-12, but for a shallowly embedded foundation using the simplified approach for estimating embedment effects discussed in Section E.3.1.3.

In Figure E-12, $\beta_f$ is seen to increase with $h/(v_{s,r}T_{eq})$ and to decrease with $h/r_\theta$. The decrease of $\beta_f$ with $h/r_\theta$ indicates that lateral movements of the foundation (which dominate at low $h/r_\theta$) dissipate energy into soil more efficiently than foundation rotation (which dominates at high $h/r_\theta$). For a given $h/r_\theta$, the suites of curves within each frame indicate that $\beta_f$ increases with decreasing $r_\theta/r_x$ for $h/(v_{s,r}T_{eq}) < \sim 0.2$. This occurs because decreasing $r_\theta/r_x$ implies increasing foundation area ($r_x$), which provides additional damping from translational vibration. Note also the significantly higher damping when hysteretic damping is included ($\beta_s$=0.1) as opposed to radiation damping only ($\beta_s$ =0). Finally, a comparison of $\beta_f$ in Figures E-12 and E-13 indicates that additional foundation damping occurs for embedded foundations, as expected.

The above analysis procedure for $\beta_f$ has been found to reproduce reasonably accurately SSI effects on first-mode vibration properties of actual structures, as inferred from system identification analyses of recorded motions (Stewart et al., 1999). These case history studies revealed that the single most important parameter controlling the significance of inertial interaction is $h/(v_{s,r}T_{eq})$, and that inertial SSI effects are generally small for $h/(v_{s,r}T_{eq}) < 0.1$. This condition occurs for flexible structures such as moment frame buildings located on competent soil or rock. Conversely, SSI effects tend to be significant for stiff structures such as shear wall or braced frame buildings, particularly when located on soft soil.

To simplify the evaluation of foundation damping ratios in engineering practice, the fact that both $\beta_f$ and $\tilde{T}_{eq}/T_{eq}$ are strongly dependent on $h/(v_{s,r}T_{eq})$ is

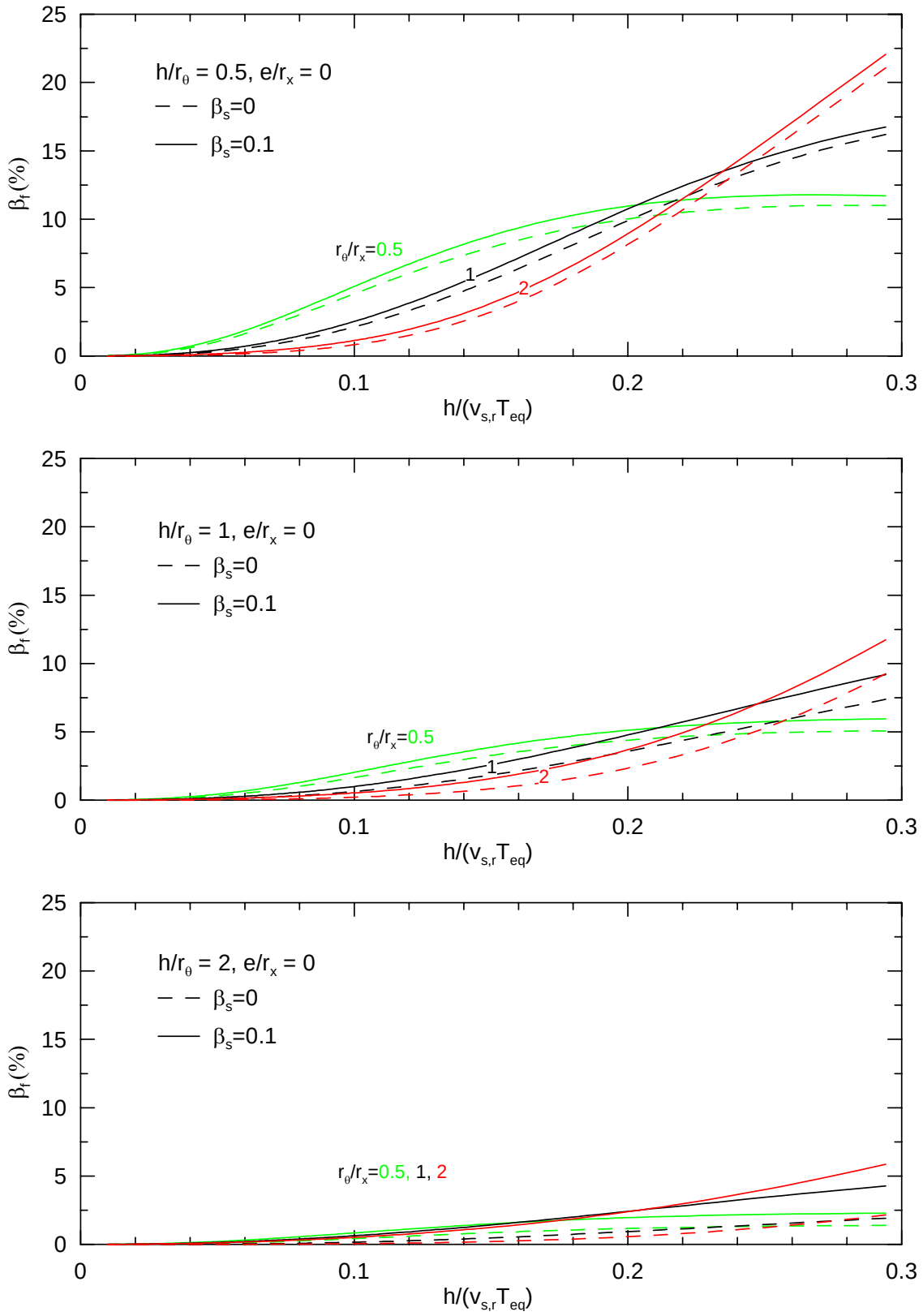


Figure E-12 Foundation damping for single degree-of-freedom structures on elastic halfspace with various aspect ratios ($h/r_\theta$) and foundation shapes ($r_\theta/r_x$), non-embedded foundation case ($e/r_x = 0$).

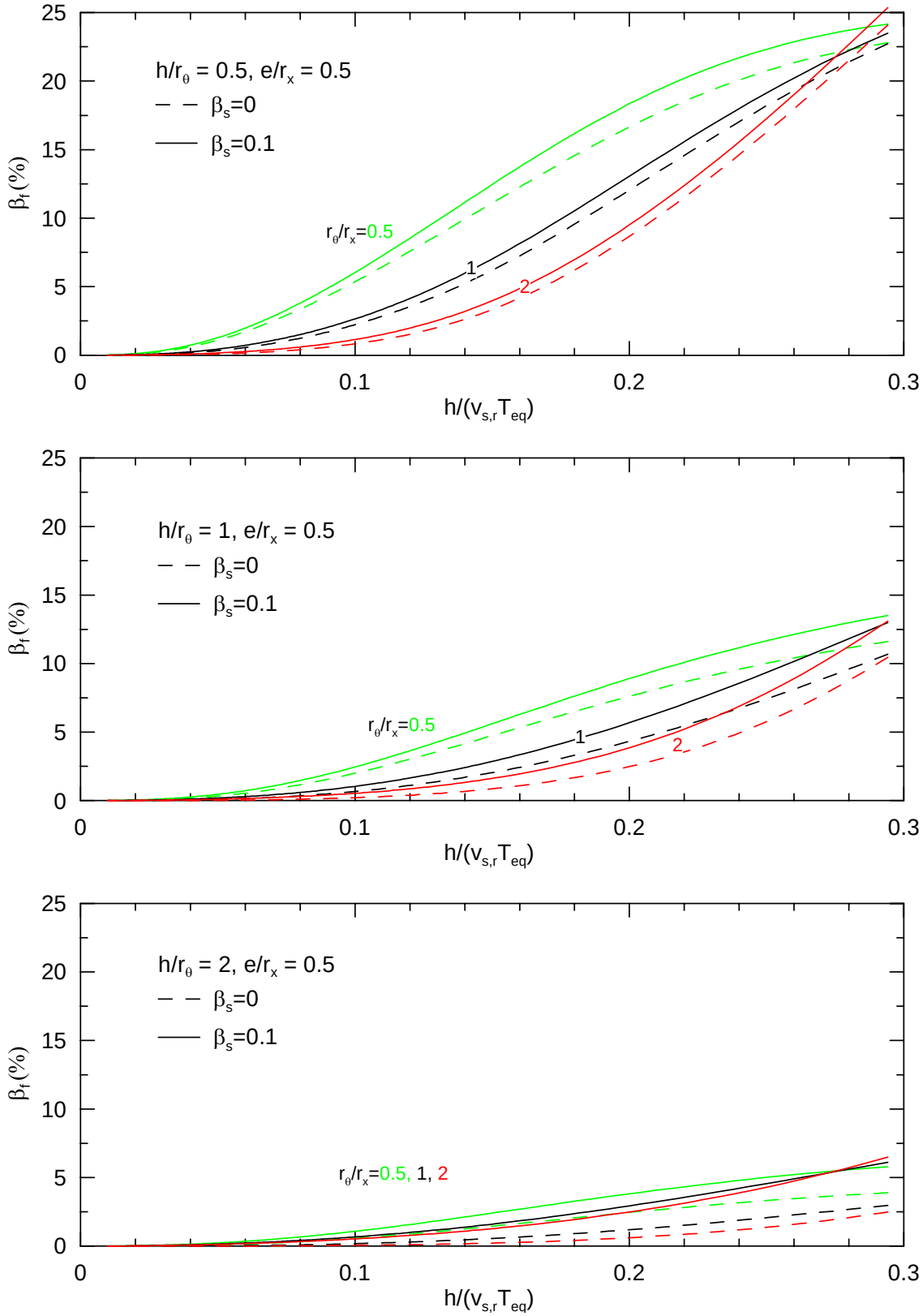


Figure E-13 Foundation damping for single degree-of-freedom structures on elastic halfspace with various aspect ratios ($h/r_\theta$) and foundation shapes ($r_\theta/r_x$), small foundation embedment case ($e/r_x = 0.5$).

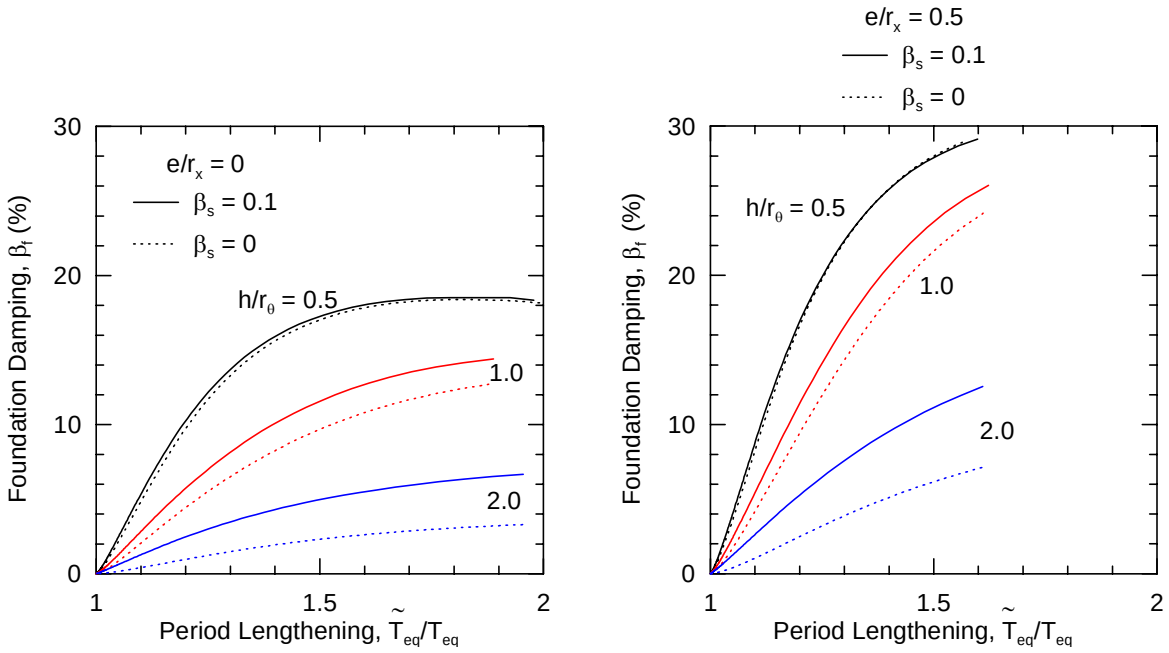


Figure E-14 Foundation damping factor $\beta_f$ expressed as a function of period lengthening $\tilde{T}_{eq}/T_{eq}$ for different building aspect ratios ($h/r_\theta$) and embedment ratios ($e/r_x$).

leveraged to generate curves relating $\beta_f$ to $\tilde{T}_{eq}/T_{eq}$ without the use of $h/(v_{s,r}T_{eq})$. The relationship was developed by also assuming equi-dimensional foundations ($r_\theta/r_x = 1.0$). Although results are shown for significant hysteretic soil damping ($\beta_s$=0.1) and zero hysteretic damping ($\beta_s$=0), use of the $\beta_s$=0 results is recommended because ductility in soil springs is already included as part of structural pushover analysis. The result is shown in Figure E-14, and requires the user only to know $\tilde{T}_{eq}/T_{eq}$ (easily obtained from a structural model, as described above) as well as $h/r_\theta$, and $e/r_x$. The damping ratios in Figure E-14 are conservative for $r_\theta/r_x < 1.0$, which is generally the case for buildings.

Another point that should be made in connection with the use of Figure E-14 is that the foundation spring stiffnesses used in the analysis of $\tilde{T}_{eq}/T_{eq}$ are based on average shear wave velocities to a depth of approximately $r_x$, whereas the velocity that should be used for the analysis of foundation damping at a non-uniform site is $v_{s0}$ (the velocity immediately below the foundation, which is typically smaller than the average $v_s$ over a depth range). The fact that $\beta_f$ is evaluated in terms of $\tilde{T}_{eq}/T_{eq}$ therefore introduces a bias, although the bias will generally result in underprediction of $\beta_f$, which is conservative and thus acceptable for a simplified design procedure.

Flexible base damping $\beta_o$ can actually increase or decrease relative to $\beta_i$ depending on $\tilde{T}_{eq}/T_{eq}$ and foundation damping $\beta_f$. The effect of the change in damping from $\beta_i$ to $\beta_o$ on spectral acceleration can be estimated using the procedures in Section 6.3.

### *E.3.3 Simplified Procedure for Design*

1. Evaluate the linear periods for the structural model assuming a fixed base, $T$, and a flexible-base using appropriate foundation modeling assumptions, $\tilde{T}$. Guidelines for the evaluation of soil spring stiffnesses are provided in FEMA 356 and ATC-40.
2. Calculate the effective structural stiffness for fixed base conditions, $K^*_{max}$ using Equation E-13.
3. Determine the equivalent foundation radius for translation, $r_x = \sqrt{A_f/\pi}$, where $A_f$ is the area of the foundation footprint if the foundation components are inter-connected laterally.
4. Calculate the translational stiffness of the foundation, $K_x$. This can be evaluated using the proce-

dures in FEMA 356 (Chap. 4) or ATC-40 (Chap. 10). For many applications, $K_x$ can be estimated using Equations E-8 and E-11.

5. Calculate the equivalent foundation radius for rotation, $r_\theta$, using Equations E-14 and E-15.
6. Determine the foundation embedment, *e*, if applicable.
7. Estimate the effective period lengthening ratio, $\tilde{T}_{eff} / T_{eff}$, for the nonlinear structure using Equation E-17.
8. Evaluate the initial fixed base damping ratio for the structure ($\beta_i$), which is often taken as 5%.
9. Using Figure E-14, determine foundation damping ($\beta_f$) based on $\tilde{T}_{eq} / T_{eq}$, $e/r_x$, and $h/r_\theta$. Intermediate values may be interpolated from these figures. An approximation to those curves is given by the following for the case without hysteretic soil damping (denoted $\beta_s = 0$):

$$\beta_f = a_1 \left( \frac{\tilde{T}_{eq}}{T_{eq}} - 1 \right) + a_2 \left( \frac{\tilde{T}_{eq}}{T_{eq}} - 1 \right)^2 \qquad \text{(E-19)}$$

where $\beta_f$ is in percent and

$$a_1 = c_e \exp\left(4.7 - 1.6 h / r_\theta\right) \qquad \text{(E-20)}$$

$$a_2 = c_e \left[ 25 \ln\left(h / r_\theta\right) - 16 \right] \qquad \text{(E-21)}$$

$$c_e = 1.5\left(e / r_x\right) + 1 \qquad \text{(E-22)}$$

The above equations are most applicable for $\tilde{T}_{eff} / T_{eff} < 1.5$, and generally provide conservative (low) damping estimates for higher $\tilde{T}_{eff} / T_{eff}$.

10. Evaluate the flexible base damping ratio ($\beta_0$) from $\beta_i$, $\beta_f$, and $\tilde{T}_{eff} / T_{eff}$ using Equation E-16.
11. Evaluate the effect on spectral ordinates of the change in damping ratio from $\beta_i$ to $\beta_0$ in accordance with Section 6.3 then modify the spectrum for free-field motion or that for the foundation input motion if kinematic effects are being included.

The change in spectral ordinate computed above can be combined with the change in spectral ordinate from kinematic interaction.

Limitations on the damping analysis described above include the following:

- The analysis approach should not be used when shear walls or braced frames are spaced sufficiently closely that waves emanating from distinct foundation elements will destructively interfere with each other across the period range of interest. Further discussion is presented in Section E.3.1.5.
- The analysis can be conservative (under-predicting the damping) when foundation aspect ratios exceed about 2:1. Further discussion is presented in Section E.3.1.4.
- The analysis is conservative when foundations are deeply embedded, $e/r_x > 0.5$. Further discussion is presented in Section E.3.1.3.
- The analysis is unconservative (over-predicting the damping) if $v_s T/r_x > 2\pi$ (where $v_s$ = average shear wave velocity to a depth of about $r_x$) and the foundation soils have significant increases of shear stiffness with depth. Further discussion is presented in Section E.3.1.2.
- The analysis is unconservative if the foundation soil profile consists of a soil layer overlying a very stiff material (i.e., there is a pronounced impedance contrast within the soil profile), and if the system period is greater than the first-mode period of the layer. Further discussion is presented in Section E.3.1.2.

## E.4 References

ASCE, 2000, *Prestandard and Commentary for the Seismic Rehabilitation of Buildings*, FEMA 356 Report, prepared by the American Society of Civil Engineers for the Federal Emergency Management Agency, Washington, D.C.

ATC, 1996, *Seismic Evaluation and Retrofit of Concrete Buildings*, ATC-40 Report, funded by the Seismic Safety Commission, published by the Applied Technology Council, Redwood City, California.

Apsel, R.J. and Luco, J.E., 1987, "Impedance functions for foundations embedded in a layered medium: an integral equation approach," *J. Earthquake Engrg. Struct. Dynamics*, Vol. 15, No. 2, pp. 213-231.

Bielak, J., 1975, "Dynamic behavior of structures with embedded foundations," *J. Earthquake Engrg. Struct. Dynamics*, Vol. 3, pp. 259-274.

Bielak, J., 1976, "Modal analysis for building-soil interaction," *J. Engrg. Mech.*, Vol. 102, American Society of Civil Engineers, pp. 771-786.

BSSC, 2001, *NEHRP Recommended Provisions for Seismic Regulations for New Buildings and Other Structures*, FEMA 368 Report, prepared by the Building Seismic Safety Council for the Federal Emergency Management Agency, Washington, D.C.

Crouse, C.B., Hushmand, B., Luco, J.E., and Wong, H.L., 1990, "Foundation impedance functions: Theory versus Experiment," *J. Geotech. Engrg.*, Vol. 116, No. 3, American Society of Civil Engineers, pp. 432-449.

Day, S.M.,1978, "Seismic response of embedded foundations," *Proc. ASCE Convention,* Chicago, Illinois, October, Preprint No. 3450.

de Barros, F.C.P. and Luco, J.E., 1995, "Identification of foundation impedance functions and soil properties from vibration tests of the Hualien containment model," *J. Soil Dyn. Earthquake Eng*., Vol. 14, pp. 229-248.

Dobry, R. and Gazetas, G., 1986, "Dynamic response of arbitrarily shaped foundations," *J. Geotech. Engrg.*, Vol. 112, No. 2, American Society of Civil Engineers, pp. 109-135.

Elsabee, F. and Morray, J.P., 1977, *Dynamic Behavior of Embedded Foundations*, Rpt. No. R77-33, Dept. of Civil Engrg., MIT, Cambridge, Massachusetts.

Gazetas, G., 1991a, "Formulas and charts for impedances of surface and embedded foundations," *J. Geotech. Engrg.*, Vol. 117, No. 9, pp. 1363-1381.

Gazetas, G., 1991b, *Foundation Vibrations, Foundation Engineering Handbook*, Chapter 15, H.-Y. Fang, ed., 2nd Edition, Chapman and Hall, New York, New York.

Iguchi, M. and Luco, J.E., 1982, "Vibration of flexible plate on viscoelastic medium," *J. Engrg. Mech.*, Vol. 108, No. 6, American Society of Civil Engineers, pp. 1103-1120.

Jennings, P.C. and Bielak, J., 1973, "Dynamics of building-soil interaction," *Bull. Seism. Soc. Am.*, Vol. 63, pp. 9-48.

Kim, S., 2001, *Calibration of Simple Models for Seismic Soil Structure Interaction from Field Performance Data*, Ph.D. Dissertation, University of California, Los Angeles.

Kim, S. and Stewart, J.P., 2003, "Kinematic soil-structure interaction from strong motion recordings," *J. Geotech. & Geoenv. Engrg.*, Vol. 129, No. 4, American Society of Civil Engineers, pp. 323-335.

Lin, A.N. and Jennings, P.C., 1984, "Effect of embedment on foundation-soil impedances," *J. Engrg. Mech.*, Vol. 110, No. 7, American Society of Civil Engineers, pp. 1060-1075.

Liou, G.-S. and Huang, P.-H., 1994, "Effect of flexibility on impedance functions for circular foundations," *J. Engrg. Mech.*, Vol. 120, No. 7, American Society of Civil Engineers, pp. 1429-1446.

Luco, J.E., Trifunac, M.D., and Wong, H.L., 1988, "Isolation of soil-structure interaction effects by full-scale forced vibration tests," *J. Earthquake Engrg. Struct. Dynamics*, Vol. 16, No. 1, pp. 1-21.

Mita, A. and Luco, J.E., 1989, "Dynamic response of a square foundation embedded in an elastic halfspace," *J. Soil Dynamics and Earthquake Engrg.*, Vol. 8, No. 2, pp. 54-67.

Riggs, H.R. and Waas, G., 1985, "Influence of foundation flexibility on soil-structure interaction," *J. Earthquake Engrg. Struct. Dynamics*, Vol. 13, No. 5, pp. 597-615.

Roesset, J.M., 1980, "A review of soil-structure interaction," in *Soil-Structure Interaction: The Status of Current Analysis Methods and Research*, J.J. Johnson, ed., NUREG/CR-1780 Report and UCRL-53011 Report, U.S. Nuclear Regulatory Com., Washington D.C., and Lawrence Livermore Lab., Livermore, California.

Stewart, J.P., Seed, R.B., and Fenves, G.L., 1999, "Seismic soil-structure interaction in buildings. II: Empirical findings," *J. Geotech. & Geoenv. Engrg.*, Vol. 125, No. 1, American Society of Civil Engineers, pp. 38-48.

Stewart, J.P., Kim, S., Bielak, J., Dobry, R., and Power, M., 2003, "Revisions to soil structure interaction procedures in NEHRP design provisions," *Earthquake Spectra*, Vol. 19, No. 3, pp. 677-696.

Veletsos, A.S. and Meek, J.W., 1974, "Dynamic behavior of building-foundation systems," *J. Earthquake Engrg. Struct. Dynamics*, Vol. 3, No. 2, pp. 121-138.

Veletsos, A.S. and Nair V.V., 1975, "Seismic interaction of structures on hysteretic foundations," *J. Struct. Engrg.*, Vol. 101, No. 1, American Society of Civil Engineers, pp. 109-129.

Veletsos, A.S. and Prasad, A.M., 1989, "Seismic interaction of structures and soils: stochastic approach," *J. Struct. Engrg.*, Vol. 115, No. 4, American Society of Civil Engineers, pp. 935-956.

Veletsos, A.S. and Verbic, B., 1973, "Vibration of viscoelastic foundations," *J. Earthquake Engrg. Struct. Dynamics*, Vol. 2, No. 1, pp. 87-102.

Veletsos, A.S. and Wei, Y.T., 1971, "Lateral and rocking vibrations of footings," *J. Soil Mech. and Foundations Div.*, Vol. 97, No. 9, American Society of Civil Engineers, pp. 1227-1248.

Veletsos, A.S., Prasad, A.M., and Wu, W.H., 1997, "Transfer functions for rigid rectangular foundations," *J. Earthquake Engrg. Struct. Dynamics*, Vol. 26, No. 1, pp. 5-17.

Wong, H.L., Trifunac, M.D., and Luco, J.E., 1988, "A comparison of soil-structure interaction calculations with results of full-scale forced vibration tests," *Soil Dyn. & Earthquake Engrg.*, Vol. 7, pp. 22-31.

# F. Supplementary Information and Data on Multi-Degree-of-Freedom Effects

## F.1 Introduction

### *F.1.1 Objectives*

The primary objective of the multi-degree-of-freedom (MDOF) studies is to illustrate the application of current nonlinear static procedures (proposed within ATC-40 and FEMA 356 and elsewhere) for estimating peak response quantities (floor and roof displacements, interstory drifts, story shears, and overturning moments) for a range of structural models/behaviors and for both ordinary and near-fault ground motions. The intention is to illustrate the range of results obtained with these procedures and their relationship to the results of nonlinear dynamic analysis. Secondary objectives include the identification of potential limitations of these procedures and the identification of possible improvements. The examples provide a uniform basis for evaluating the strengths and weaknesses of the various procedures in a single study, in which comparisons are made using a consistent framework and methodology. The study has a limited scope, and must be considered together with other, more detailed studies on the specific procedures.

### *F.1.2 Scope*

The evaluation of MDOF effects is divided into two portions. The first compares the response quantities determined in dynamic analyses with those estimated using various pushover procedures, for five building models subjected to both ordinary and near-fault ground motions. These comparisons are made assuming that the peak roof drift (or target displacement) is determined accurately by the pushover procedures. The second portion assesses the accuracy of the estimates of peak roof drift determined using "equivalent" single-degree-of-freedom (SDOF) systems.

Section F.2 describes the example buildings, analytical models and properties, and ground motions. Section F.3 describes the simplified inelastic analysis procedures. Section F.4 addresses the accuracy of the estimates of response quantities made using the simplified procedures for both regular and near-field ground motions. Section F.5 addresses the accuracy of "equivalent" SDOF estimates of peak roof displacement using relationships provided in ATC-40 and FEMA 356. Section F.6 provides information relating to a new approach for using scaled ground motion records in nonlinear response history analysis. Section F.7 reports some results obtained using an energy-based pushover procedure. Section F.8 contains (1) detailed descriptions of the ground motions used in the study, (2) detailed plots comparing the distributions of response quantities observed in the dynamic analyses with the deterministic values determined in the pushover analyses, (3) summary error statistics, and (4) plots of the observed coefficients of variation of the peak dynamic response quantities.

The ordinary ground motions were scaled to achieve predetermined values of peak roof drift. The peak roof drifts were selected to represent elastic response and two levels of nonlinear response. Thus, while the roof displacements achieved in the dynamic and static analyses were equal to the predetermined target values, the frequency content and timing of the ground motion records differed and introduced variability to the other peak response quantities. Of primary interest is the comparison of the deterministic estimates of the response quantities obtained using the simplified inelastic procedures to the statistical distributions of the peaks of these quantities determined by dynamic analyses.

The near-fault ground motions were applied at their natural (unscaled) intensities because of a concern that scaled near-fault records may be unrealistic. Thus, the target displacement used for each simplified inelastic procedure was set equal to the peak roof displacement observed for each near-fault ground motion. These results allow for comparisons of estimated and actual response quantities for individual records, as well as the determination of normalized errors. The small number of near-fault ground motions used and the lack of consistency in target displacements make the data less statistically meaningful than in the case of the ordinary ground motions. Consequently, the evaluation of the inelastic procedures for the near-fault motions is more qualitative, while the evaluation for the ordinary motions has a stronger quantitative basis.

## F.2 Example Buildings and Demand Parameters

Five example buildings were selected for study. These consist of two steel moment-resistant frame buildings designed as part of the FEMA-funded SAC joint

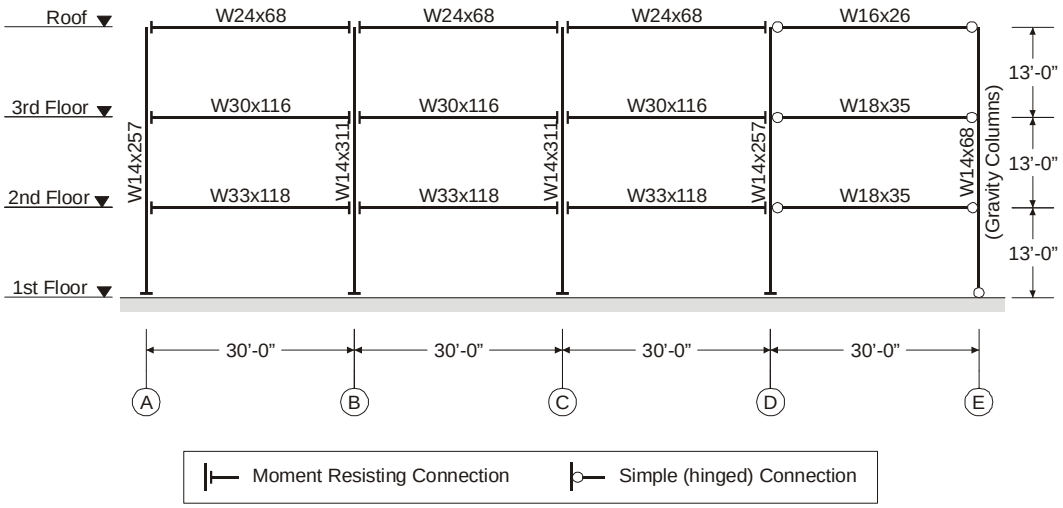


Figure F-1 Elevation view of the 3-story (regular and weak-story) steel frames used in the study.

venture project, modifications to each of these frames to induce weak story behavior, and a reinforced concrete shear wall building described in ATC-40.

The 3- and 9-story steel frames were designed and modeled in Drain-2DX as part of the SAC joint venture effort. The frames adopted in this study had been designed for Los Angeles using the 1994 *Uniform Building Code*, and employed "pre-Northridge" special moment-resistant frame connections along the building perimeter. The weak stories were introduced into the lowest story of the 3- and 9-story frames by reducing the flexural strengths of the columns, without changing their stiffnesses. This was done in order to affect the mechanism while keeping the elastic properties (e.g. periods of vibration) the same as for the regular frames. The lowest story column strengths were determined by trial and error to ensure that a weak story mechanism developed in dynamic analyses using records scaled to cause peak roof drifts equal to 4% of the building height.

The 8-story reinforced concrete wall building was based on the Escondido Village building that is described in ATC-40.

Detailed descriptions of these buildings follow.

### *F.2.1 Prototype Buildings*

#### F.2.1.1 Regular 3-Story Frame

The 3-story steel frame, as shown in Figure F-1, is the north-south lateral force-resisting system of a benchmark building for the SAC project. The building is 120 ft by 180 ft in plan and 39 ft in elevation, with a 2-ft extension from the perimeter column lines to the building edge. Typical floor-to-floor height is 13 ft. The building consists of four bays in the north-south direction and six bays in the east-west direction. As shown in Figure F-1, all connections are moment-resistant for the three left-most bays of the frame under consideration. The "gravity columns" on the right, labeled as such in the figure, are used to model *P*-delta effects, as described in Section F.2.2. The assumed gravity loading for the building is shown in Table F-1.

**Table F-1 Assumed Loading for the 3- and 9-Story Buildings**

| *Type* | *Intensity (psf)* |
|---|---|
| Floor dead load for weight calculations | 96 |
| Floor dead load for mass calculations | 86 |
| Roof dead load excluding penthouse | 83 |
| Penthouse dead load | 116 |
| Reduced live load per floor and for roof | 20 |

#### F.2.1.2 Regular 9-Story Frame

The 9-story steel frame is part of the lateral force-resisting system of another SAC model building. The building is 150 ft by 150 ft in plan and 122 ft in elevation with a 2 ft extension from the perimeter column lines to the building edge. As shown in

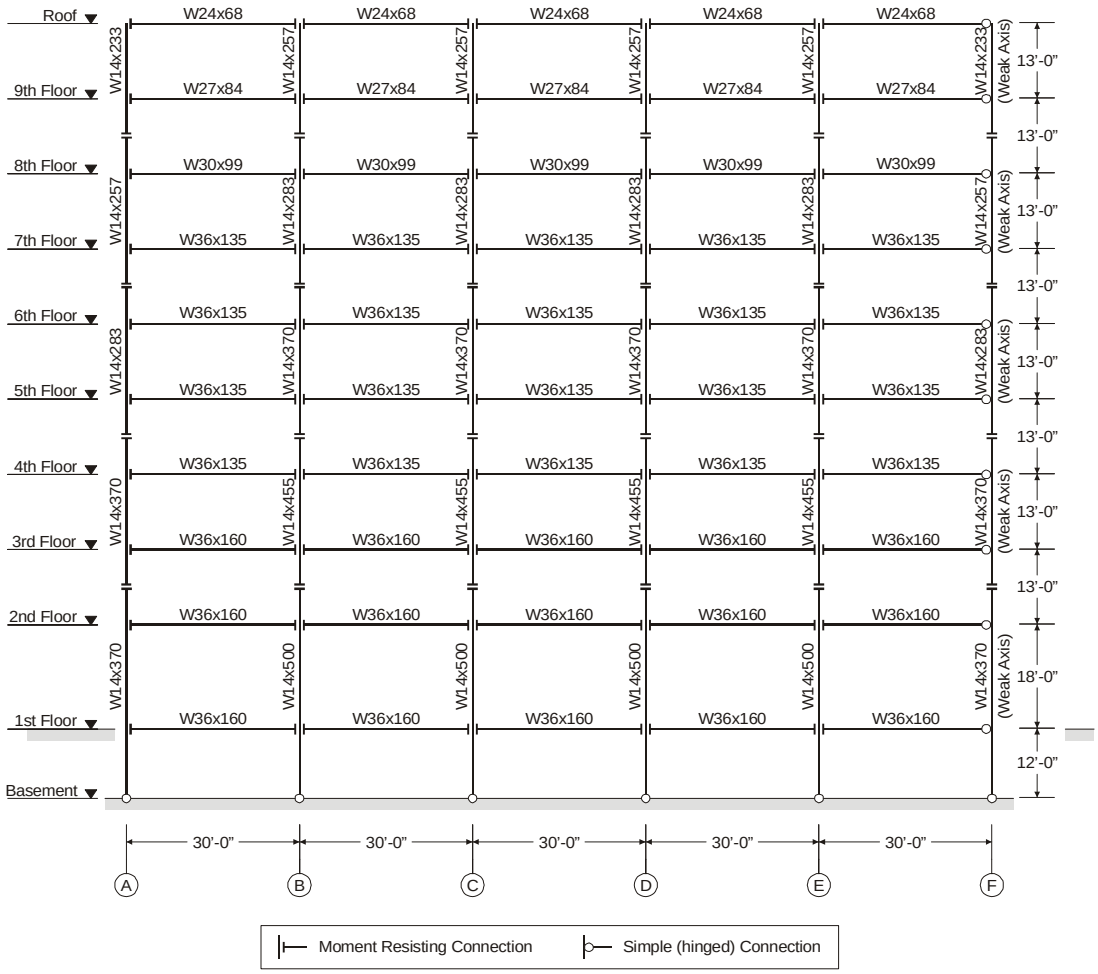


Figure F-2 Elevation view of the 9-story (regular and weak-story) steel frames used in the study.

Figure F-2, the frame considered in this study consists of five 30-ft long bays. The typical floor-to-floor height is 13 ft. The 1st story and basement floor-to-floor heights are 18 ft and 12 ft, respectively. The assumed gravity loading for this building is the same as that for the 3-story building.

#### F.2.1.3 3-Story Weak Story Frame

The strengths of the lowest story columns of the regular 3-story frame (Section F.2.1.1) were reduced to create the 3-story weak story frame. Based on the response observed in dynamic analyses, the lowest story column strength were reduced to 50% of their original values in order to develop weak-story behavior at a roof drift of 4% of the building height. No other changes were made.

#### F.2.1.4 9-Story Weak Story Frame

The strengths of the lowest story columns of the regular 9-story frame (Section F.2.1.2) were reduced to create the 9-story weak story frame. Based on dynamic response, the lowest story column strengths were reduced to 60% of their original values in order to develop weak-story behavior at a roof drift of 4% of the building height. No other changes were made.

#### F.2.1.5 8-Story Shear Wall

The 8-story shear wall represented in this study is one of the two longitudinal walls of the midrise building at Escondido Village, located at line A and between lines 4 and 6 of the as-built drawings of June 10, 1964. The wall is 8 stories in height, with a basement below. This structural wall was selected because it plays a substantial role in the lateral force resisting system for

**Table F-2 Properties of the 8-Story Reinforced Concrete Structural Wall**

| *Item* | *Gathered Information from ATC-40 Vol. 2 (ATC) and As-Built Drawings (DWG)* | | *Wall Used in this Study* |
|---|---|---|---|
| Typical floor height | 9 ' – 1" (Source: ATC and DWG) | | 9 ' – 1" |
| Basement height | 12' – 7" (Source: ATC and DWG) | | 12' – 7" |
| Wall length | 25' – 5" (Source: ATC and DWG) | | 25' |
| Wall thickness | Typical floor: | 10" (Source: ATC)<br>9 3/4" (Source: DWG) | 10" |
| | Basement | 12" (Source: ATC and DWG) | 12" |
| Boundary reinforcement | 7th floor to roof | 3 #6 (Source: DWG) | 3 #6 |
| | 5th floor to 7th floor | 3 #11 (Source: DWG) | 3 #11 |
| | 3rd floor to 5th floor | 6 #11 (Source: DWG) | 6 #11 |
| | Foundation to 3rd floor | 9 #11 (Source: DWG) | 9 #11 |
| Confinement reinforcement at boundary | #3 @ 12" with 135° hook (Source: ATC) | | #3 @ 12" with 135° hook |
| Distributed vertical reinforcement | Typical floor | $\rho = 0.0023$ (Source: ATC)<br>2 #4 @ 18" (Source: DWG, $\rho = 0.0023$) | 2 #4 @ 18" ($\rho = 0.0023$) |
| | Basement | 2 #5 @ 18" (Source: DWG, $\rho=0.00287$) | 2 #5 @ 18" ($\rho=0.00287$) |
| Horizontal reinforcement | Typical floor | $\rho = 0.0023$ (Source: ATC)<br>2 #4 @ 18" (Source: DWG, $\rho = 0.0023$) | 2 #4 @ 18" ($\rho = 0.0023$) |
| | Basement | 2 #4 @ 12" (Source: DWG, $\rho = 0.00278$) | 2 #4 @ 12" ($\rho=0.00278$) |
| Concrete strength | 3000 psi (Source: DWG)<br>3000 psi (Design) and 2470 psi (Test) (Source: ATC) | | 3000 psi |
| Reinforcing steel yield strength | 40 ksi (Source: ATC and DWG) | | 40 ksi |

the building and its location suggests that the degree of coupling is negligible. The information for this wall was gathered from ATC-40 Vol. 2 and the as-built drawings. Table F-2 summarizes the properties of the wall used in this study. Figure F-3 shows the elevation and cross sections of the wall. The assumed gravity loading is shown inTable F-3.

### *F.2.2 Modeling*

Two-dimensional models of the frame and wall buildings were prepared using standard elements that are available in Drain-2DX version 1.10. The models.. were subjected to horizontal excitation or lateral forces after the application of gravity loads. Inertial mass resisted horizontal excitations only. *P*-Delta effects were considered for all building models, using dead loads in combination with 40% of the design live loads. For the frame models, these loads were applied to a separate gravity column that was connected to the lateral force resisting system. The gravity column was pinned at each story, providing a "truss-bar" approximation of the effect of *P*-Delta on the global stiffness matrix. For the wall model, gravity loads attributary to the walls were applied. This induced compression in the concrete and steel fibers of the model, causing the wall to have an initial stiffness approximately equal to the gross section stiffness.

Fixed and variable time step solution schemes were employed, in all cases with events monitored. The default overshoot tolerances were used for members modeled with a plastic hinge beam-column element (Type 02). The overshoot tolerances for the members

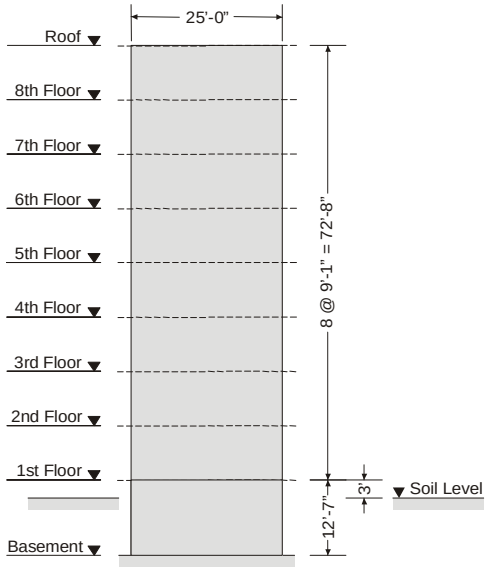


(a) Wall elevation

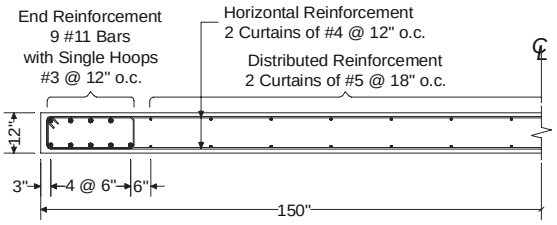


(b) Plan view of wall cross section: basement to 1st floor

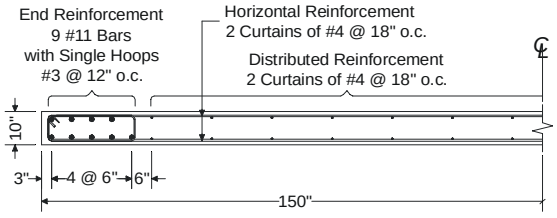


(c) Plan view of wall cross section: 1st floor to 3rd floor

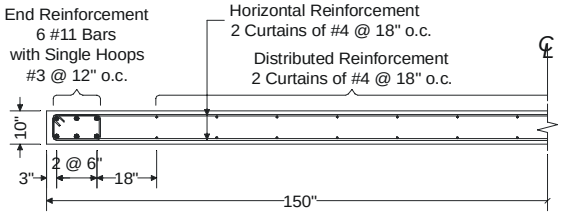


(d) Plan view of wall cross section: 3rd floor to 5th floor

Figure F-3 Elevation and plan views of the 8-story reinforced concrete shear wall used in the study

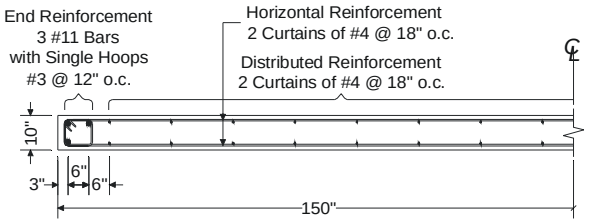


(e) Plan view of wall cross section: 5th floor to 7th floor

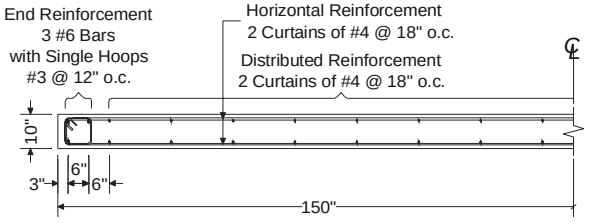


(f) Plan view of wall cross section: 7th floor to roof

Figure F-3 Elevation and plan views of the 8-story reinforced concrete shear wall used in the study (continued)

**Table F-3 Assumed Loading for the 8-Story Building**

| *Type* | *Intensity (psf)* |
|---|---|
| Floor dead load for weight calculations | 165 |
| Floor dead load for mass calculations | 165 |
| Roof dead load | 145 |
| Reduced live load per floor and for roof | 20 |

modeled with a fiber beam-column element (Type 15) were set to be 0.01% of the yield strengths of the fibers.

The steel frames were modeled using beam-column elements (Type 02), as illustrated in Figures F-4 and F-5. The SAC M1 model was used in this study, in which beams and columns span between nodes located at the intersections of the beam and column centerlines; rigid end offsets were set to zero and beam column joints were not modeled. Material yield strengths were 49.2 and 57.6 ksi, for the beams and columns respectively, and the post-yield stiffness of the moment-curvature relationship was set to 3% of the initial stiffness, as assumed in the SAC models. Gravity loads were applied along the frame elements as well as at the ends of these elements, at the nodes located where the

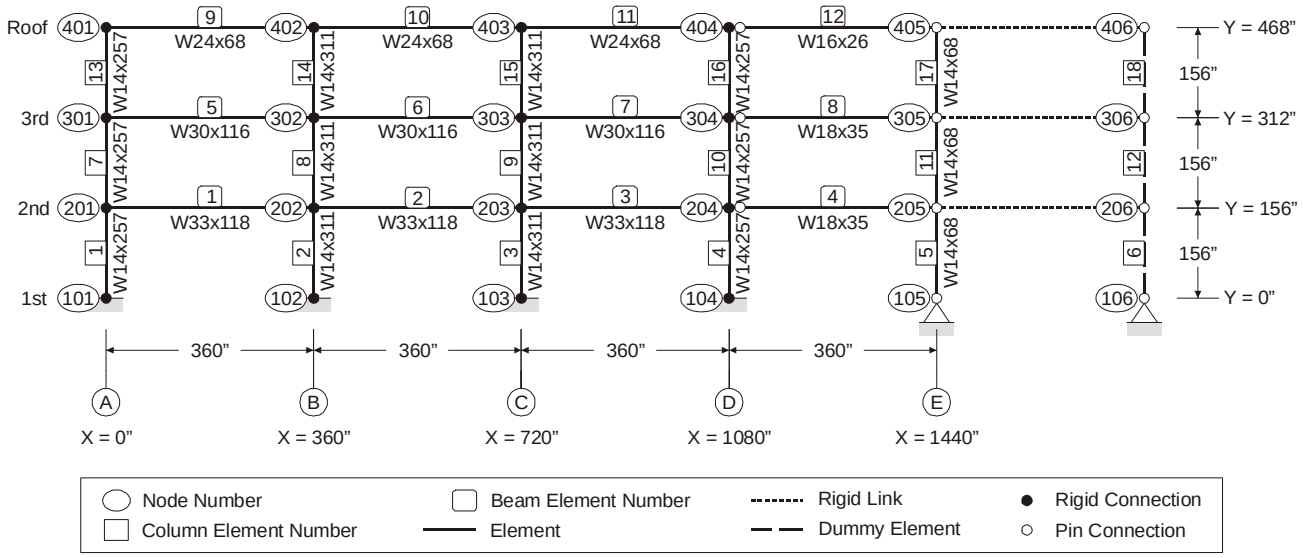


Figure F-4 Drain model of the 3-story (regular and weak story) steel frames.

beams and columns intersect. To avoid the possibility that overturning effects might influence the formation of column hinges, an effect that would be highly specific to the geometry and specific details of these particular frames, the flexural strengths of both beam and column elements were modeled to be independent of axial force. The strength and stiffness of the gravity column framing is neglected in the M1 model.

The reinforced concrete shear wall was modeled using a fiber element (Type 15), as illustrated in Figure F-6. The wall consists of nine elements, one element per story. Each element is divided into four segments along the element axis. The cross section of each segment is divided into 12 fibers. The base of the wall is assumed to be fixed, and a horizontal restraint is provided at the 1st floor. Inelasticity in flexure was modeled; it was assumed that the wall would have sufficient shear strength and that only elastic shear deformations needed to be represented. While the fibers had zero tensile strength, preloading by gravity ensured that all fibers contributed to the initial stiffness of the wall.

Because the degree of confinement at the wall boundaries is considered low, an unconfined concrete stress-strain relationship shown in Figure F-7(a) was used. For the longitudinal steel, a bilinear stress-strain relationship was employed [Figure F-7(b)].

The mass is lumped at the ends of the element. The mass contribution (assumed uniform) for the wall is calculated in such a way that the resulting fundamental period, based on effective stiffness, matches the elastic period reported in ATC-40, resulting in a mass contribution of 19.2% of the total floor mass. The resulting base shear coefficient at yield, obtained from a pushover analysis, is 0.129.

For the frame models, a Rayleigh damping ratio of 2% was applied to the first mode period and a period of 0.2 s, as assumed in the SAC models. For the wall model, 5% Rayleigh damping was set for the first and fourth mode periods corresponding to gross-section stiffness. In all models, the modal periods used to determine the damping ratios were those computed before gravity loading was applied.

#### F.2.2.1 Dynamic Characteristics of Models

The first three periods and mode shapes for the frame and wall buildings are provided in Table F-4. Because flexural cracking of the reinforced concrete wall was modeled, modal properties reported for the 8-story reinforced concrete shear wall (part b of Table F-4) are the properties determined based on the tangent stiffness of the cracked wall, determined in a first mode pushover analysis at a base shear equal to 60% of the base shear corresponding to yield of a bilinear curve that was fitted to the capacity curve.

To illustrate basic characteristics of each building model, capacity curves are presented for the five

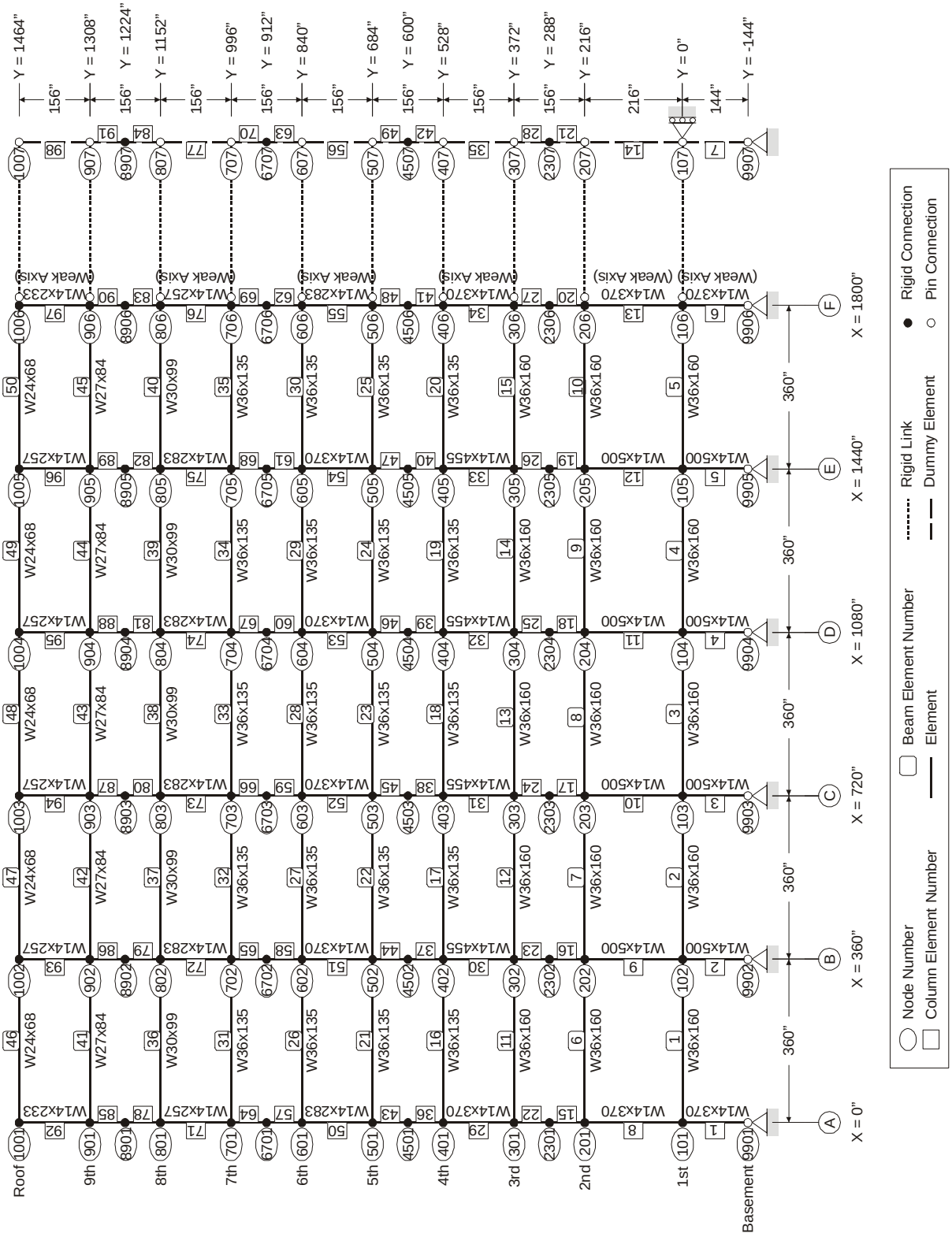


Figure F-5 Drain model of the 9-story (regular and weak-story) steel frames.

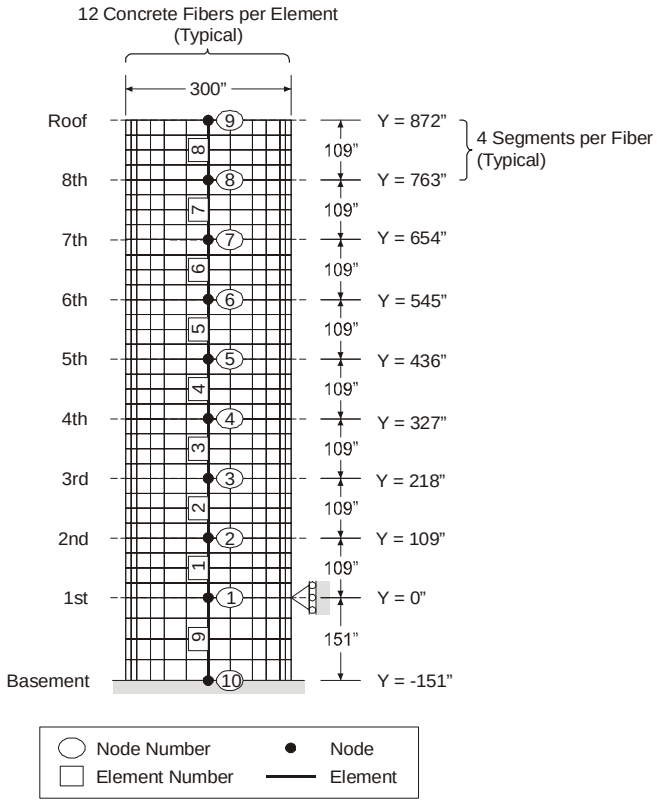


Figure F-6 Drain model of the 8-story reinforced concrete shear wall.

models in Figure F-8. The capacity curve represents the sum of the applied lateral forces at a given displacement,[1] as determined in a nonlinear static (pushover) analysis. In this case, the lateral forces were proportional to the amplitude of the first mode and mass at each floor level, where the modal amplitudes were determined with *P*-Delta effects considered. Based on a bilinear fit to the capacity curves, the base shear coefficient at yield and the drift at yield are as given in Table F-5.

#### F.2.2.2 Model Verification

Because the SAC frames have been the subject of prior research, the models could be validated by comparison to published research. The periods of the regular frames, reported in Table F-4, match those reported in FEMA 355C (SAC, 2000). The 9-story frame capacity curves (computed without *P*-Delta considered) are nearly the same as those published by Chopra and Goel (2002).

### *F.2.3 Ground Motions and Demand Intensities*

It was desired to assess the accuracy of the pushover procedures with respect to the results obtained from

1. When *P*-Delta is modeled, the element shear forces and base shear are increased by the *P*-Delta shears. The applied lateral force may be obtained equivalently as (1) the load factor times the sum of the components of the load vector or (2) the sum of the lowest story shears minus $P\Delta/h$, where $P$ = the gravity load on the lowest story, $\Delta$ = the displacement of the lowest story, and $h$ = the height of the lowest story.

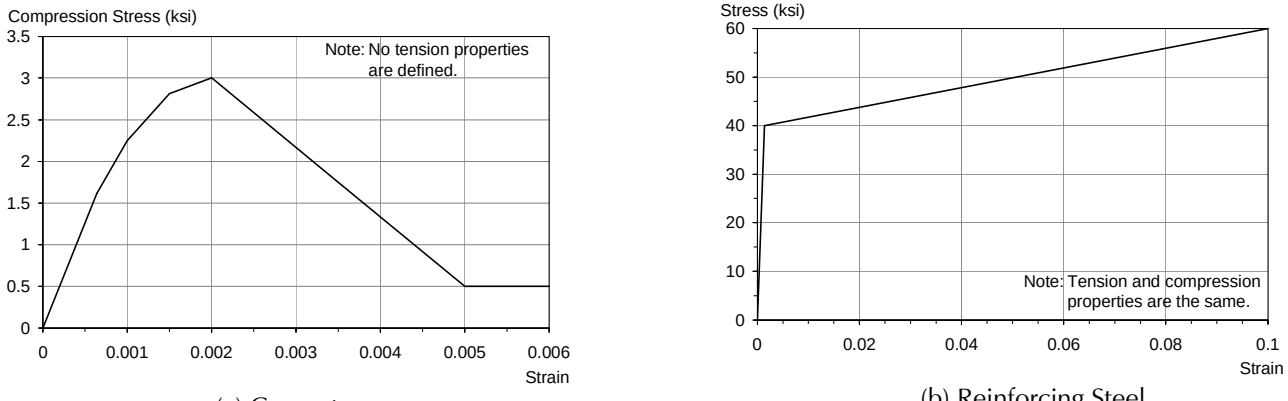


(a) Concrete

(b) Reinforcing Steel

Figure F-7 Idealized material stress-strain relationships used in drain model of the 8-story reinforced concrete shear wall

**Table F-4 Periods and Mode Shapes for the Frame and Wall Buildings**

| *Modal Properties* | | *Mode 1* | | *Mode 2* | | *Mode 3* | |
|---|---|---|---|---|---|---|---|
| | | *without P-Δ* | *with P-Δ* | *without P-Δ* | *with P-Δ* | *without P-Δ* | *with P-Δ* |
| Part a: 3-Story (Regular and Weak-Story) Frames | | | | | | | |
| Period (sec) | | 1.01 | 1.03 | 0.33 | 0.33 | 0.17 | 0.17 |
| Participation factor | | 1.27 | 1.27 | 0.33 | 0.33 | 0.06 | 0.06 |
| Modal mass coefficient | | 0.83 | 0.83 | 0.14 | 0.13 | 0.04 | 0.04 |
| Mode shape amplitude | 2nd floor | 0.27 | 0.28 | 1.20 | 1.21 | 4.07 | 4.04 |
| | 3rd floor | 0.66 | 0.66 | 1.14 | 1.14 | -3.34 | -3.33 |
| | Roof | 1.00 | 1.00 | -1.00 | -1.00 | 1.00 | 1.00 |
| Part b: 8-Story Reinforced Concrete Shear Wall | | | | | | | |
| Period (sec) | | 0.71 | 0.71 | 0.13 | 0.13 | 0.05 | 0.05 |
| Participation factor | | 1.49 | 1.49 | 0.71 | 0.71 | 0.34 | 0.34 |
| Modal mass coefficient | | 0.64 | 0.64 | 0.20 | 0.20 | 0.08 | 0.08 |
| Mode shape amplitude | 2nd floor | 0.03 | 0.03 | 0.15 | 0.15 | 0.44 | 0.44 |
| | 3rd floor | 0.09 | 0.09 | 0.42 | 0.42 | 0.98 | 0.98 |
| | 4th floor | 0.19 | 0.19 | 0.68 | 0.68 | 1.06 | 1.06 |
| | 5th floor | 0.31 | 0.31 | 0.84 | 0.84 | 0.47 | 0.47 |
| | 6th floor | 0.46 | 0.46 | 0.77 | 0.77 | -0.48 | -0.48 |
| | 7th floor | 0.63 | 0.63 | 0.42 | 0.42 | -1.09 | -1.09 |
| | 8th floor | 0.81 | 0.81 | -0.21 | -0.21 | -0.52 | -0.52 |
| | Roof | 1.00 | 1.00 | -1.00 | -1.00 | 1.00 | 1.00 |
| Part c: 9-Story (Regular and Weak-Story) Frames | | | | | | | |
| Period (sec) | | 2.27 | 2.34 | 0.85 | 0.87 | 0.49 | 0.50 |
| Participation factor | | 1.37 | 1.36 | 0.53 | 0.52 | 0.24 | 0.24 |
| Modal mass coefficient | | 0.83 | 0.84 | 0.11 | 0.11 | 0.04 | 0.04 |
| Mode shape amplitude | 2nd floor | 0.17 | 0.17 | 0.38 | 0.39 | 0.80 | 0.81 |
| | 3rd floor | 0.28 | 0.29 | 0.59 | 0.60 | 1.04 | 1.04 |
| | 4th floor | 0.39 | 0.40 | 0.72 | 0.72 | 0.84 | 0.83 |
| | 5th floor | 0.51 | 0.52 | 0.74 | 0.75 | 0.26 | 0.23 |
| | 6th floor | 0.62 | 0.63 | 0.64 | 0.63 | -0.49 | -0.51 |
| | 7th floor | 0.72 | 0.73 | 0.40 | 0.39 | -1.04 | -1.04 |
| | 8th floor | 0.83 | 0.83 | -0.01 | -0.02 | -0.96 | -0.94 |
| | 9th floor | 0.93 | 0.93 | -0.54 | -0.54 | -0.14 | -0.12 |
| | Roof | 1.00 | 1.00 | -1.00 | -1.00 | 1.00 | 1.00 |

**Table F-5 Base Shear Coefficient and Drift At Yield for Each Building Model**

| | Building | | | | |
|---|---|---|---|---|---|
| *Idealized Capacity Curve Properties* | *3-Story* | *3-Story Weak-Story* | *8-Story* | *9-Story* | *9-Story Weak-Story* |
| Yield drift (%) | 1.11 | 0.833 | 0.250 | 1.06 | 0.936 |
| Base shear coefficient | 0.329 | 0.247 | 0.129 | 0.177 | 0.156 |

**Table F-6 Ground Motions**

| # | *Identifier* | *Earthquake* | *Date* | *Magnitude* | *Station Location (Number* | *Component* | *PGA (g)* | *PGV (cm/ sec)* | *Char. Period (sec)* | *Source* |
|---|---|---|---|---|---|---|---|---|---|---|
| | | | | | Ordinary | | | | | |
| 1 | ICC000 | Superstitn | 11-24-87 | $M_s = 6.6$ | El Centro Imp. Co. Cent (01335) | 000 | 0.358 | 46.4 | 0.60 | CDMG |
| 2 | LOS000 | Northridge | 1-17-94 | $M_s = 6.7$ | Canyon Country – W Lost Cany (90057) | 000 | 0.41 | 43 | 0.59 | USC |
| 3 | G02090 | Loma Prieta | 10-18-89 | $M_s = 7.1$ | Gilroy Array #2 (47380) | 090 | 0.322 | 39.1 | 0.69 | CDMG |
| 4 | TCU122N | Chi-Chi, Taiwan | 9-20-99 | $M_s = 7.6$ | (TCU122) | N | 0.261 | 34 | 0.85 | CWB |
| 5 | G03090 | Loma Prieta | 10-18-89 | $M_s = 7.1$ | Gilroy Array #3 (47381) | 090 | 0.367 | 44.7 | 0.40 | CDMG |
| 6 | CNP196 | Northridge | 1-17-94 | $M_s = 6.7$ | Canoga Park – Topanga Can (90053) | 196 | 0.42 | 60.8 | 0.61 | USC |
| 7 | CHY101W | Chi-Chi, Taiwan | 9-20-99 | $M_s = 7.6$ | (CHY101) | W | 0.353 | 70.6 | 1.27 | CWB |
| 8 | ICC090 | Superstitn | 11-24-87 | $M_s = 6.6$ | El Centro Imp. Co. Cent (01335) | 090 | 0.258 | 40.9 | 1.03 | CDMG |
| 9 | CNP106 | Northridge | 1-17-94 | $M_s = 6.7$ | Canoga Park – Topanga Can (90053) | 106 | 0.356 | 32.1 | 0.45 | USC |
| 10 | E02140 | Imperial Valley | 10-15-79 | $M_s = 6.9$ | El Centro Array #2 (5115) | 140 | 0.315 | 31.5 | 0.29 | USGS |
| 11 | E11230 | Imperial Valley | 10-15-79 | $M_s = 6.9$ | El Centro Array #11 (5058) | 230 | 0.38 | 42.1 | 0.27 | USGS |
| | | | | | Near-Field (Maximum Velocity Direction) | | | | | |
| 1 | ERZMV1 | Erzincan | 3-13-92 | $M_s = 6.9$ | Erzincan Station | NA | 0.442 | 126 | 1.13 | EERL Caltech |
| 2 | RRSMV1 | Northridge | 1-17-94 | $M_s = 6.7$ | Rinaldi Receiving Station | 213 | 0.891 | 186 | 0.92 | EERL Caltech |
| 3 | LUCMV1 | Landers | 6-28-92 | $M_s = 7.3$ | Lucerne Valley Station | 280 | 0.732 | 147 | 0.52 | EERL Caltech |
| 4 | SCHMV1 | Northridge | 1-17-94 | $M_s = 6.7$ | Sylmar County Hospital Parking Lot | 190 | 0.865 | 138 | 0.51 | EERL Caltech |

CDMG: California Division of Mines and Geology
CWB: Central Weather Bureau, Taiwan
EERL Caltech: Earthquake Engineering Research Laboratory, California Institute of Technology
USC: University of Southern California
USGS: U.S. Geological Survey

nonlinear dynamic analyses and whether these procedures are suitable for the special case of near-fault ground motions. Accordingly, two sets of ground motions were used. The first set of motions was selected to represent the range of motion that may be expected at a specific building site. This range was established by selecting strong-motion records having a limited range of source distance for a specified site soil type. Site Class B motions had been proposed originally, but Site Class C motions were used because these soil conditions are more typical. The 11 motions in this set are referred to as "ordinary" motions in this report. The second set of motions consists of motions recorded close to the epicenter that contain very strong velocity pulses. The four motions in this set are referred to as "near-fault" motions in this report. The records are summarized in Table F-6; their acceleration, velocity, and displacement time histories are plotted in Section F.8.1. The characteristic periods identified in Table F-6 correspond approximately to the corner period at the intersection of the "constant acceleration" and "constant velocity" portions of the spectrum for the ordinary motions, and were computed as

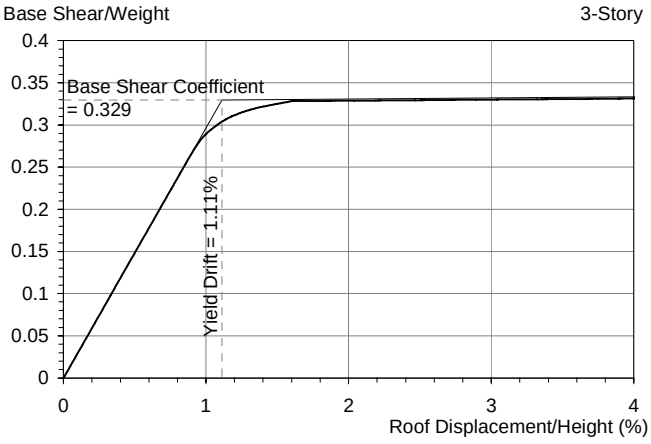


(a) 3-Story Steel Frame

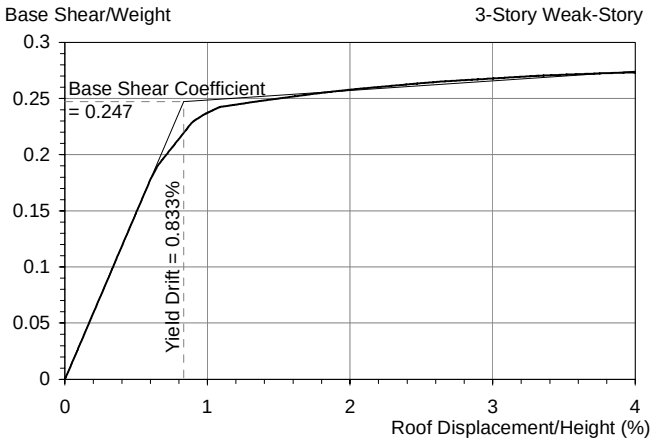


(b) 3-Story Weak-Story Steel Frame

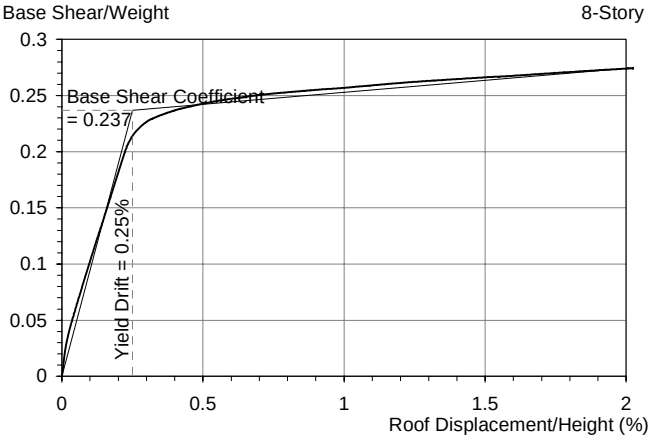


(c) 8-Story Reinforced Concrete Shear Wall

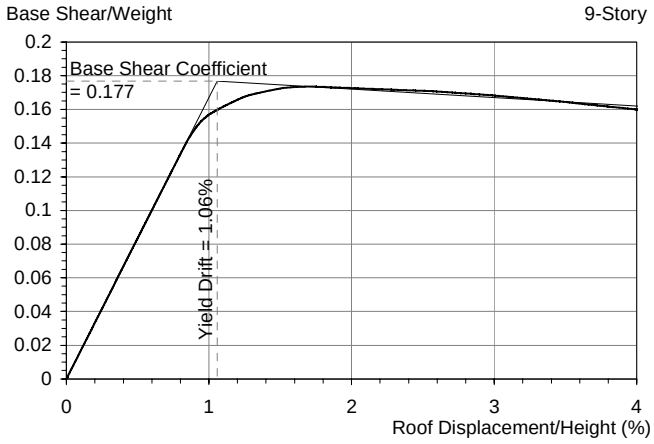


(d) 9-Story Regular Steel Frame

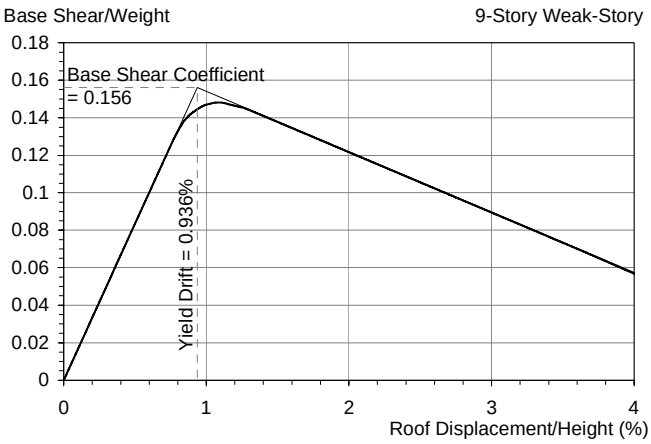


(e) 9-Story Weak-Story Steel Frame

Figure F-8 Capacity curves for the five model building examples.

$$T_g = 2\pi \frac{(S_v)_{\max}}{(S_a)_{\max}} \quad \text{(F-1)}$$

where $S_v$ and $S_a$ are the elastic pseudo-velocity and pseudo-acceleration spectra, respectively, for linear elastic systems having $\beta = 5\%$, as described by Cuesta and Aschheim (2001).

#### F.2.3.1 Ordinary (Site Class C) Motions

The Pacific Earthquake Engineering Research (PEER) Center strong-motion database[1] produced a set of over 50 strong ground motions in response to multiple queries in which magnitudes were restricted to the range $5.5 < M_s < 8.0$, the closest distance to fault rupture was restricted to 8 to 20 km, and site classification was restricted to Site Class C. Of these records, those with the largest elastic spectral displacements at a period of 1 second were retained, producing a set of 17 motions. Six of these were excluded based on (a) the presence of an identifiable strong velocity pulse early in the record, (b) the identification of the record as being "near-fault" or "near-field" in some research reports, and (c) a preliminary elimination of those records that would require the largest amplitude scale factors in order to achieve the drift levels described in Section 9.3. The 11 records that remain, listed in Table F-6, were generated from a number of events, with no event contributing more than 3 records.

#### F.2.3.2 Near-Field Motions

A variety of near-field motions was considered important for the example analyses. Recognizing that special processing is often necessary to accurately recover the record (Iwan and Chen, 1994), records were obtained from the Earthquake Engineering Research Laboratory at the California Institute of Technology (A. Guyader, personal communication). The component of near field motion used is oriented in the horizontal plane in the direction in which the maximum ground velocity occurs. These records are identified in Table F-6, and are not always aligned in the fault normal direction. The ground motion velocity histories (Section F.8.1) do show large velocity pulses. The near-field records were used without any further processing, and were applied at their natural intensities, that is, without scaling.

1. Available at http://peer.berkeley.edu/smcat/.

#### F.2.3.3 Drift Levels

The drift levels used for the ordinary ground motions were set to 0.5%, 2.0%, and 4.0% of the height of the building for the steel frames, and 0.2%, 1.0%, and 2.0% of the height of the building for the reinforced concrete structural wall building. These drift levels are referred to as "low," "moderate," and "high" in subsequent sections of this report. The low drift level results in elastic response. Because the regular 3- and 9-story steel frames have an effective yield drift of 0.83% and 1.1% of the height of the frame, the high drift levels cause system ductility demands of about 4.8 and 3.6, respectively, if response is predominantly in the first mode. The reinforced concrete wall building has a yield drift of approximately 0.25% and thus has system ductility demands of about 4 and 8 at the moderate and high drift levels, respectively.

These drift levels were used to illustrate the influence of yielding on the accuracy of the estimates obtained from the inelastic procedures for a range of response that is relevant for many buildings. For example, roof drifts of 2.5% and 5% of the height of the frame buildings and 1% and 2% of the height of the wall building correspond to the nominal Life Safety and Collapse Prevention performance limits, respectively, given in FEMA 356.

#### F.2.3.4 Ground Motion Scaling

The scale factors required to cause the peak roof drifts to be equal to the predetermined target values are reported for each building, drift level, and ground motion in Table F-7. These scale factors were used to determine mean elastic spectra for each building and drift level in order to determine relative contributions for the 2nd and 3rd modes as required for the square-root-of-the-sum-of-the-squares (SRSS) load vector and multimode pushover analysis (MPA) methods. This implementation detail is described more fully in Section F.3.1.6 and Section F.3.2.

### *F.2.4 Extensions to Address P-Delta*

Nearly all the pushover procedures have been presented in the literature without explicit treatment of *P*-Delta effects. Only in the Displacement Coefficient Method are *P*-Detla effects addressed, by modification of the SDOF displacement response using the term $C_3$.

*P*-Delta affects elastic and inelastic response. Elastic response is affected because the geometric stiffness causes an increase in the period of vibration and a change in the elastic mode shape. For inelastic systems,

**Table F-7 Scale Factors Applied to Each of the Ordinary Ground Motions for the Dynamic Analyses**

| | | Ground Motion | | | | | | | | | | |
|---|---|---|---|---|---|---|---|---|---|---|---|---|
| *Building* | *Drift* | *1 ICC000* | *2 LOS000* | *3 G02090* | *4 TCU122n* | *5 G03090* | *6 CNP196* | *7 CHY101w* | *8 ICC090* | *9 CNP106* | *10 E02140* | *11 E11230* |
| 3-story | 0.5% | 0.5281 | 0.4499 | 0.3675 | 0.4416 | 0.3934 | 0.2739 | 0.2827 | 0.6529 | 0.5243 | 0.5551 | 0.6335 |
| | 2% | 1.8493 | 1.6607 | 1.2930 | 1.5955 | 1.4885 | 1.4912 | 1.4255 | 2.9310 | 2.6645 | 2.8917 | 2.3071 |
| | 4% | 2.4626 | 2.6943 | 2.3852 | 2.2346 | 2.4672 | 2.0994 | 2.9252 | 3.6492 | 4.9953 | 6.2765 | 3.0257 |
| 3-story weak-story | 0.5% | 0.5281 | 0.4499 | 0.3690 | 0.4416 | 0.3934 | 0.2739 | 0.2827 | 0.6529 | 0.5243 | 0.5551 | 0.6335 |
| | 2% | 1.6962 | 1.4968 | 1.5223 | 1.4177 | 1.3330 | 1.3269 | 1.4034 | 2.3378 | 2.7180 | 2.7006 | 2.0535 |
| | 4% | 4.0050 | 2.4302 | 2.2434 | 2.1137 | 2.6378 | 2.6051 | 2.1937 | 3.4655 | 4.6072 | 5.3996 | 4.4179 |
| 8-story | 0.5% | 0.476 | 0.323 | 0.690 | 0.811 | 0.750 | 0.267 | 0.542 | 0.936 | 0.421 | 0.606 | 0.581 |
| | 1% | 1.957 | 1.858 | 2.246 | 2.480 | 2.396 | 2.162 | 2.530 | 3.889 | 2.084 | 3.069 | 3.412 |
| | 2% | 3.213 | 3.947 | 3.329 | 3.349 | 3.401 | 3.318 | 4.172 | 4.641 | 3.586 | 6.220 | 6.540 |
| 9-story | 0.5% | 0.4871 | 0.3133 | 0.5683 | 0.4237 | 0.3736 | 0.2348 | 0.2372 | 0.3243 | 0.4369 | 0.4844 | 0.8223 |
| | 2% | 3.0281 | 2.5204 | 4.0783 | 3.0244 | 3.2888 | 1.5376 | 1.4722 | 2.7696 | 3.9072 | 4.4352 | 2.9019 |
| | 4% | 5.4384 | 4.6774 | 6.3237 | 4.2556 | 5.6177 | 3.2536 | 3.2282 | 5.3885 | 9.4438 | 6.8838 | 7.6710 |
| 9-story weak-story | 0.5% | 0.4871 | 0.3133 | 0.5683 | 0.4237 | 0.3736 | 0.2348 | 0.2372 | 0.3243 | 0.4369 | 0.4844 | 0.8223 |
| | 2% | 2.8924 | 2.5527 | 4.0639 | 2.2949 | 3.2723 | 1.4242 | 1.8111 | 1.7457 | 2.7755 | 2.9933 | 4.5670 |
| | 4% | 3.6906 | 4.4874 | 6.3830 | 2.7551 | 4.9506 | 1.9801 | 1.9313 | 4.2350 | 3.4149 | 5.8639 | 5.0538 |

the geometric stiffness reduces the post-yield stiffness and may result in large increases in peak displacement or collapse. The predominant mechanism may change as well.

Chopra and Goel (2001) show for elastic response that independent pushovers in each mode are equivalent to conventional modal analysis, and that superposition in time, or by combination of individual peaks, is equivalent to modal superposition and response spectral analysis, respectively. A structure responding elastically in the presence of *P*-Delta responds with altered periods of vibration and mode shapes relative to those determined without *P*-Delta. Thus, theory indicates that the elastic portions of response should be determined using the modal properties considering *P*-Delta. Thus, for the pushover techniques that use elastic mode shapes (first mode, SRSS, and MPA), the mode shapes employed were those determined with *P*-Delta effects present.

The slope of the post-yield portion of the capacity curve determined by pushover analysis is reduced in the presence of *P*-Delta. This reduced slope, particularly when negative, can be expected to cause an increase in peak displacement response. Because ground-motion scale factors were adjusted to achieve predetermined target roof drifts, as described in Section F.2.3, this effect is subdued for the dynamic analyses using the ordinary ground motions.

## F.3 Simplified Techniques

Seven pushover methods were applied. In all methods, lateral forces are applied incrementally in a nonlinear static analysis to determine a capacity curve. The capacity curve represents the relationship between the applied lateral force and the displacement at the roof. The applied lateral force at any floor is proportional to the mass and displacement associated with a shape vector at the floor under consideration. The pushover methods differ in whether the shape vector remains proportional to an initial shape (which may be the first mode or another displacement pattern) or evolves as the onset of material nonlinearity causes softening of the structure, and in whether one or multiple modes are considered. These methods used in this study are summarized in the following sections. In addition, where specific assumptions or adaptations were required to implement these methods in this study, these implementation-specific details are also described.

### *F.3.1 Single Load Vectors*

#### F.3.1.1 First Mode

The first mode technique applies forces in proportion to the amplitude of the elastic first mode and mass at each

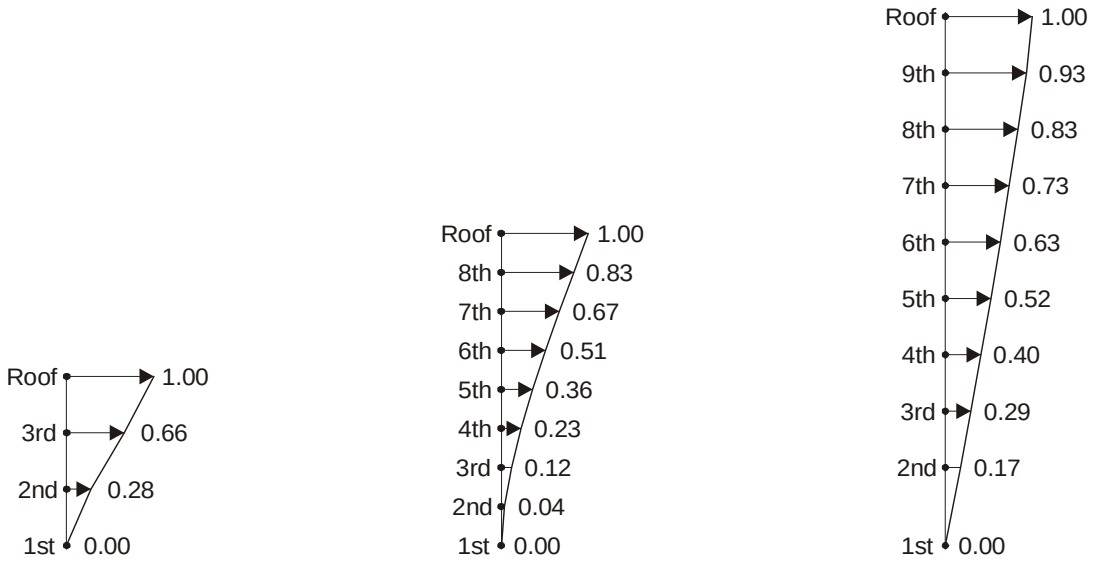


**(a) 3-story (Regular and Weak-Story) Steel Frames** **(b) 8-Story Reinforced Concrete Wall** **(c) 9-Story (Regular and Weak-Story) Steel Frames**

Figure F-9 Shape vectors of the 1st mode shape load pattern.

floor. The mode shapes of the five building models (Table F-4) are illustrated in Figure F-9, and the corresponding capacity curves, determined using this pushover technique, are illustrated in Figure F-8.

The capacity curve for the 8-story shear wall model (Figure F-8(c)) shows softening as cracks develop at the base of the wall. The shape vector used for this model was the elastic mode shape determined using the initial properties of the structure, after loading by gravity loads.

#### F.3.1.2 Inverted Triangular

The inverted triangular pattern uses a shape vector that increases linearly with height. This shape vector is also shown in Figure F-10 for the three building configurations.

#### F.3.1.3 Rectangular

The rectangular (or uniform) pattern uses a shape vector that is uniform with height. This shape vector is shown in Figure F-11 for the three building configurations.

#### F.3.1.4 Code Force Distribution

The "code" load pattern appears in many documents, including FEMA 368. The pattern varies from an inverted triangular shape for periods less than 0.5 s to a parabolic shape for periods greater than 2.5 s as a means to account for higher mode effects. The lateral force coefficient for floor $x$, $C_{vx}$, is given by

$$C_{vx} = \frac{w_x h_x^k}{\sum_{i=1}^{n} w_i h_i^k} \qquad \text{(F-2)}$$

where $w_x$ and $w_i$ are the weights of floor $i$ or $x$, $h_i$ and $h_x$ are the height of floor $i$ or $x$ above the base, and $k$ is an exponent that varies linearly with period from 1 for $T_1 < 0.5$ s to 2 for $T_1 \geq 2.5$ s. Since these forces are equal to the product of floor mass and the amplitude of a shape vector at each floor, the corresponding shape vectors are proportional to $h^k$. These shape vectors are illustrated in Figure F-12 for the three building configurations.[1] For the 8-story shear wall building, $k$ was determined based on the initial stiffness of the building, after gravity loading was applied.

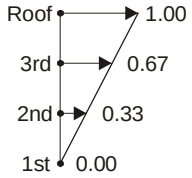


**(a) 3-story (Regular and Weak-Story) Steel Frames**

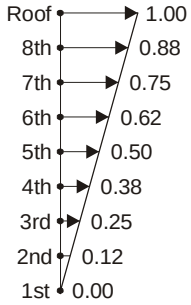


**(b) 8-Story Reinforced Concrete Wall**

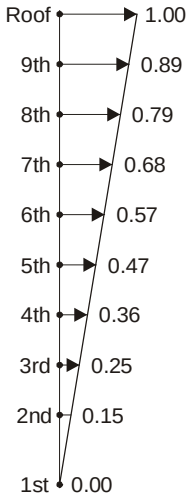


**(c) 9-Story (Regular and Weak-Story) Steel Frames**

Figure F-10 Shape vectors of the triangular load pattern.

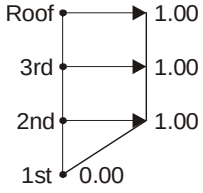


**(a) 3-story (Regular and Weak-Story) Steel Frames**

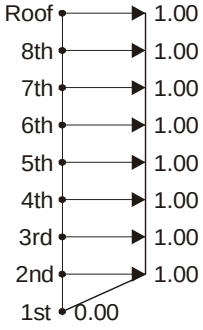


**(b) 8-Story Reinforced Concrete Wall**

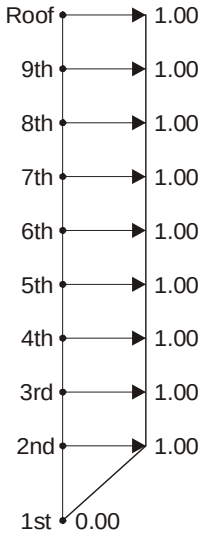


**(c) 9-Story (Regular and Weak-Story) Steel Frames**

Figure F-11 Shape vectors of the rectangular load pattern.

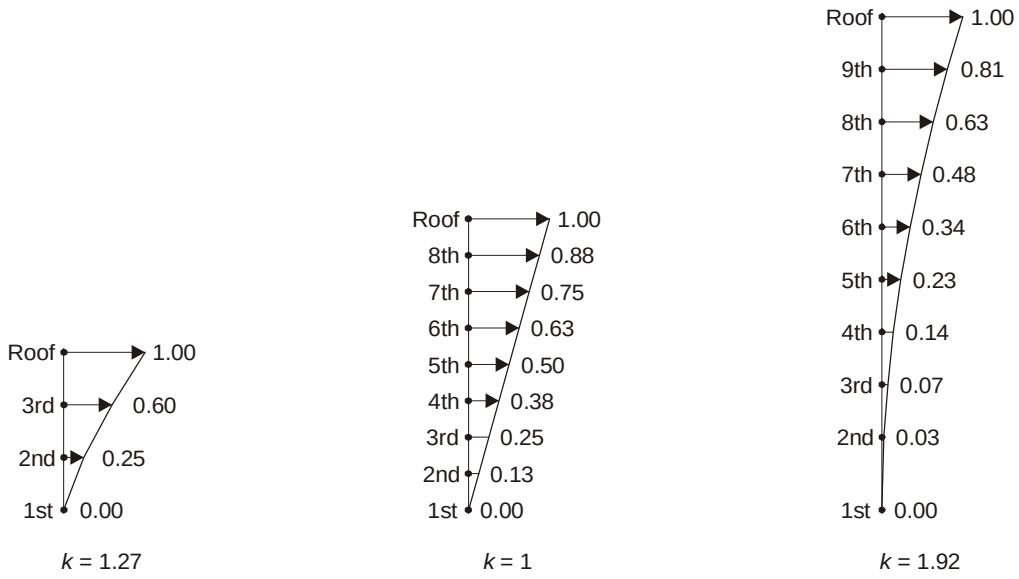


**(a) 3-story (Regular and Weak-Story) Steel Frames** **(b) 8-Story Reinforced Concrete Wall** **(c) 9-Story (Regular and Weak-Story) Steel Frames**

Figure F-12 Shape vectors of the code load pattern.

#### F.3.1.5 Adaptive First Mode

The adaptive first mode procedure recognizes that softening of the capacity curve reflects a reduction in stiffness, which, in turn, causes a change in the mode shape. Thus, lateral forces are applied proportional to the amplitude of an evolving first-mode-shape amplitude and mass at each floor.

The procedure was implemented as follows: the lateral load vector was adjusted at drift increments of 0.5% of the height of the building. The increment in lateral load for each interval (0% to 0.5%, 0.5% to 1.0%, 1.0% to 1.5% and so on) was based on the mode shape computed at the end of the preceding interval. The initial mode shape was used for the first interval.

The capacity curve of the 9-story weak story building develops a negative tangent stiffness as the roof displacement increases. Drain-2DX is not able to provide solutions to determine the free-vibration mode shapes when this occurs. Thus, the last computed mode shape was used for the subsequent steps

#### F.3.1.6 SRSS

The SRSS technique is based on a consideration of elastic modal responses. Associated with the response in each mode is a lateral force pattern, which can be summed to obtain story shears associated with each mode. An SRSS combination of the modal story shears results in a particular shear profile. The lateral forces required to generate the SRSS story-shear profile are applied in this pushover technique. The elastic spectral amplitudes are used to determine the modal story shears, even when nonlinear response is anticipated. A sufficient number of modes to represent at least 90% of the mass is included.

The first three modes were used for each building model. Because a single spectrum typically would be used for design, the SRSS procedure was applied to the mean of the scaled spectra used to achieve each predetermined drift level for each building. The mean elastic spectrum differed for each building and each drift level, because the scale factors used with each

1. Because the weak story frames have the same elastic properties as their SAC counterparts, the load vectors that are based on elastic properties are identical for the 3-story and 9-story frames.

record were specific to each building and drift level. Thus, a different SRSS load vector was determined for each structure and drift level. Because the load vectors are proportional to the product of the amplitude of a shape vector and mass at each floor level, the shape vectors corresponding to the SRSS distribution can be derived. These shape vectors are shown in Figure F-13 for the three building configurations and three drift levels.

For the near-fault motions, spectral amplitudes and SRSS combinations were determined for each near fault record. For the 8-story wall building, the periods used for the SRSS combinations were based on the initial stiffness, after gravity loading was applied.

### *F.3.2 Multiple Mode Pushover Analysis*

One approach to represent the influence of higher modes on response quantities combines peak response quantities determined in separate pushover analyses for the first several modes using an SRSS combination. The procedure proposed by Chopra and Goel (2001) considers the potential for nonlinear response in each

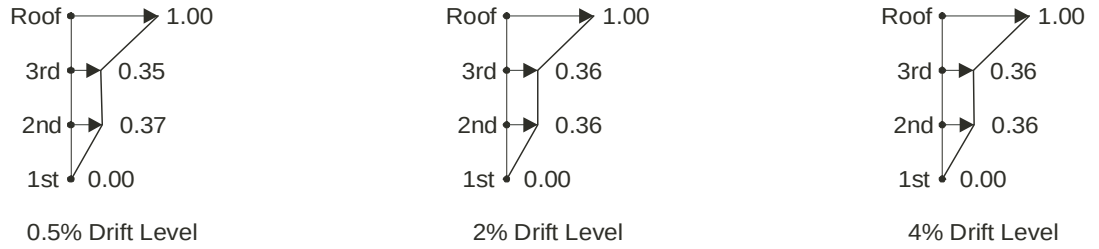


**(a) 3-Story Regular Steel Frame**

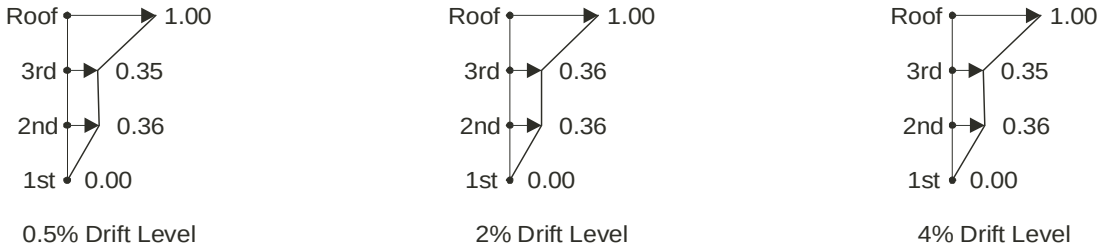


**(b) 3-Story Weak-Story Steel Frame**

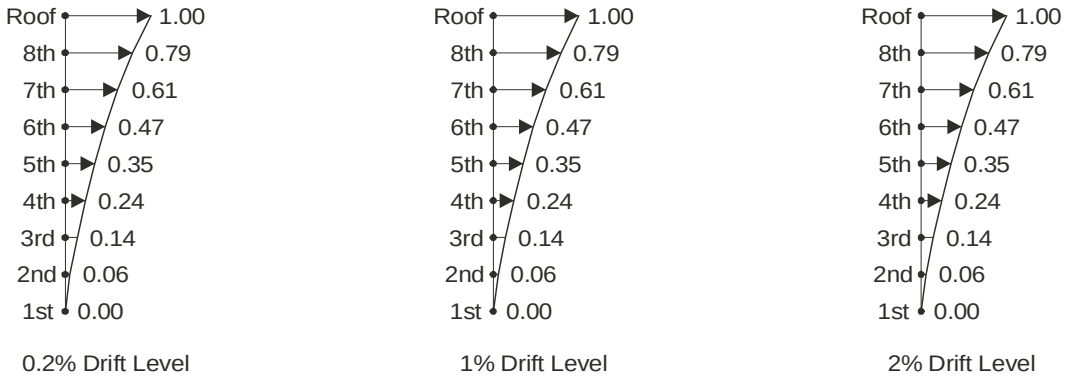


**(c) 8-Story Reinforced Concrete Wall**

Figure F-13 Shape vectors of the SRSS load pattern.

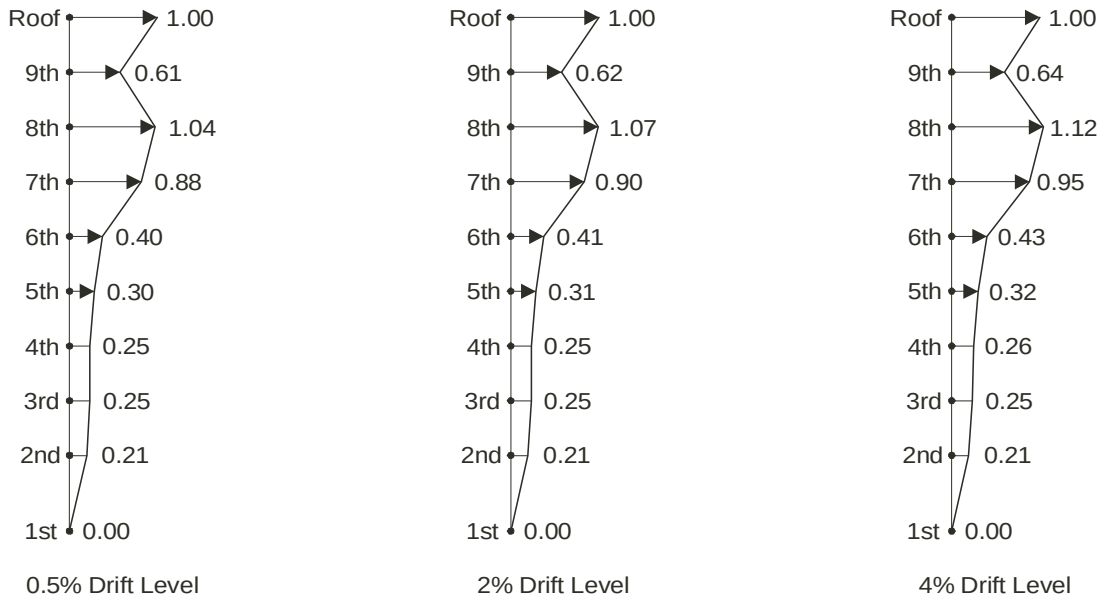


**(d) 9-Story Regular Steel Frame**

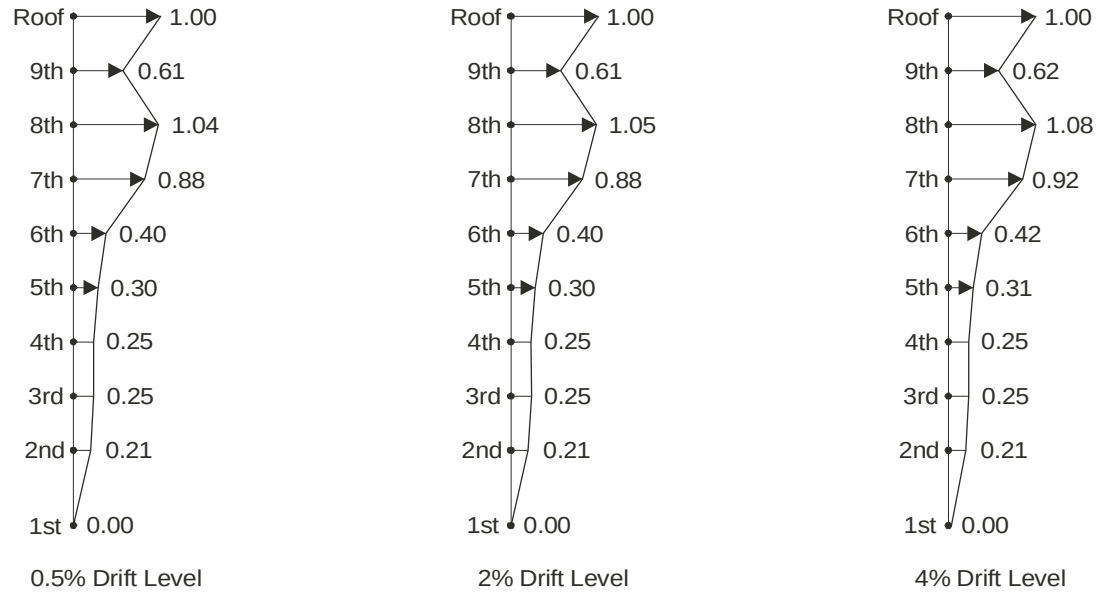


**(e) 9-Story Weak-Story Steel Frame**

Figure F-13 Shape vectors of the SRSS load pattern (continued).

independent modal analysis. According to their procedure, known as Multimode Pushover Analysis (MPA), capacity curves are developed for each "modal" response by applying lateral forces proportional to the mode shape amplitude and mass at each floor.

In the MDOF studies, capacity curves were determined by pushover analysis for each of the first three modes for each building model. In some cases the higher mode capacity curves displayed softening behavior similar to that observed in first mode pushover analyses. However, in other cases, the higher mode force patterns caused the roof displacement to reverse as inelasticity developed in the structure. Such reversals were observed for the 3rd mode pushover of the regular 3-story building (Figure F-14) and for the 2nd mode

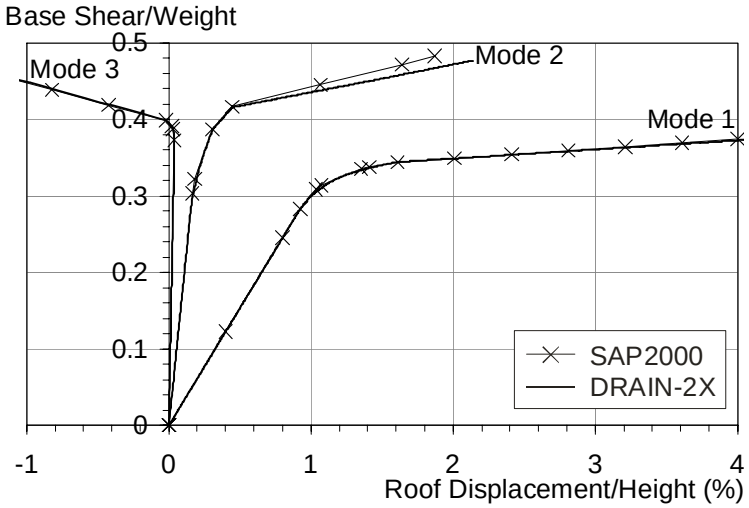


Figure F-14 First, second, and third mode pushover results for the 3-story regular steel frame.

pushover of the 3-story weak story building. Such reversals have also been observed by M. Aschheim and A. Chopra in previous analyses.

It is difficult to rationalize the use of a capacity-spectrum type procedure to identify a target displacement for capacity curves that do not display the usual softening behavior. Rather than making an *ad hoc* adjustment to the MPA method for just the 3-story buildings, a modified version of the MPA procedure capable of representing higher mode contributions was used for all five buildings. In the "modified MPA" procedure, elastic contributions associated with the 2nd and 3rd modes are combined with contributions from the 1st mode, which may be inelastic, using an SRSS combination.

For both the ordinary motions and the near-field motions, the target displacement used to determine the first mode contribution was the predetermined peak roof displacement, just as for the first mode pushover. In order to determine the higher mode contributions for the ordinary ground motions, mean spectra were computed for each building and drift level, using the ground motions as scaled to achieve the predetermined drifts. This allowed the contributions of the 2nd and 3rd modes to be determined directly from the mean spectra for the ordinary motions. For the near-field records, the elastic higher mode contributions were determined from the jagged elastic spectra associated with each unscaled near-field record. The higher-mode contributions were determined using spectra computed for viscous damping ratios of 2% and 5% for the frame and wall buildings, respectively.

For the 8-story shear wall building, the first mode capacity curve was determined by applying lateral forces proportional to the initial mode shape; a bilinear approximation to the capacity curve was then determined, having an intersection at $0.6V_y$, where $V_y$ is the yield strength of the fitted bilinear curve. The structure was pushed to the displacement corresponding to this point of intersection to determine the effective modal properties. The periods and modal participation factors associated with the tangent stiffness of the cracked wall at a base shear equal to $0.6V_y$ were used in the modified MPA procedure described above.

## F.4 Accuracy of Estimates Made Using Simplified Procedures

This section compares the estimates of response quantities obtained using the simplified inelastic procedures with the values obtained by nonlinear dynamic analysis. Comparisons for the ordinary motions are presented in Section F.4.2 and those for near-field motions are presented in Section F.4.3, after a discussion of error evaluation in Section F.4.1.

### *F.4.1 Error Measurement*

Two measures of error are used. For the ordinary motions, which were scaled to achieve predetermined target drifts, the error measure $E_1$ is defined as

$$E_1(i,j,k) = \left| \frac{Q_P(i,j,k) - \bar{Q}_D(i,j,k)}{\bar{Q}_D(i,j,k)} \right| \qquad \text{(F-3)}$$

where $Q_P(i,j,k)$ = pushover response quantity *i* at story/floor *j* for drift level *k*, and $\bar{Q}_D(i,j,k)$ = mean overall responses to the ordinary ground motions of the dynamic response quantity *i* at story/floor *j* at drift level *k*.

For the near-field motions, the peak roof drifts varied because the motions were used without scaling. For these motions, a second error measure, $E_2$, was defined as

$$E_2(i,j,k) = \left| \frac{\bar{Q}_P(i,j,k) - \bar{Q}_{D,l}(i,j,k)}{\bar{Q}_{D,l}(i,j,k)} \right| \qquad \text{(F-4)}$$

where $\bar{Q}_P(i,j,k)$ = mean overall near-fault responses of pushover response quantity *i* at story/floor *j* for drift level *k*, and $\bar{Q}_{D,l}(i,j,k)$ = mean overall near-fault responses of dynamic response quantity *i* at story/floor *j* at drift level *k* for record *l*.

### *F.4.2 Results for Ordinary Ground Motions*

Complete results for the five example buildings are provided in Sections F.8.2 and F.8.3.

The minimum, maximum, mean, median, and mean plus and minus one standard deviation values of the dynamic response quantities to the ordinary ground motions are plotted for each floor or story in Section F.8.2 (Figure F-32 through F-46). These plots include the deterministic results obtained using the various pushover techniques, plotted using various line styles. Errors in the pushover estimates relative to mean dynamic response quantities, calculated using the error measure $E_1$, are plotted as a function of drift level and pushover technique for each of the buildings in Section F.8.3 (Figures F-47 through F-51). The mean error is the mean of the errors calculated over the height of the building, and the maximum error is the maximum of the errors over the height of the building.

A summary of the results relating to peak responses, their estimates, and the errors of these estimates, is presented in the following subsections.

#### F.4.2.1 Floor Displacements

The peak displacement response showed the smallest variance relative to that observed for the other response quantities. Coefficients of variation are plotted in Section F.8.6 (Figures F-77 through F-81). The variance for the 8-story wall building was appreciably less than that of the frame buildings. The low variance in the displacement response of the five buildings is attributed to the relatively small contribution of higher modes to displacements, coupled with methodology of the study, in which the ordinary ground motions were scaled to obtain peak roof displacements equal to predetermined values.

The displacement response of the buildings generally followed an approximate first mode pattern. Exceptions to this pattern were noted as follows: (1) the response of the regular 9-story building to the CNP106 record appeared to be affected by higher modes at 4% drift; (2) substantial variability in the displacement pattern was observed for the 9-story weak story building at 2% drift, with a weak story developing for some motions but not others.

Peak displacement estimates were generally quite good for all load patterns. Differences occurred primarily with the rectangular load pattern, and for the 9-story frames, the code load pattern.

#### F.4.2.2 Interstory Drift Ratios

The peak interstory drifts of the 8-story shear wall building displayed little variance, in contrast to the larger variance evident in the interstory drifts of the frame buildings. All pushover techniques provided good estimates of the interstory drifts of the shear wall building at all drift levels, with slightly larger discrepancies occurring for the code and rectangular load patterns. This indicates that even the interstory drifts were dominated by response in a quasi-first mode for the shear-wall building.

The largest mean interstory drift ratios for the regular 3-story frame were about 20% greater than the average roof drift ratio at 0.5% drift, and decreased to about 10% greater than the average roof drift ratio at 4% drift. For the regular 9-story frame, the largest mean interstory drift ratios were about 35% greater than the average roof drift ratio at 0.5% drift, and increased to about 65% greater at roof drifts of 2% and 4%. Thus, while it appears that higher modes make larger relative contributions to the interstory drifts of frame structures, particularly longer period frame structures, the relative contribution may increase or decrease as drift levels increase and inelasticity develops.

Of the seven pushover methods considered, only the modified MPA procedure explicitly accounts for higher

modes. For the frame structures, this procedure often provided more accurate estimates of peak interstory drifts relative to the other pushover procedures. However, even the multiple mode estimates of frame interstory drifts were less than the mean dynamic values for the upper stories of the regular 9-story frame at the low and moderate drift levels and for several stories above the weak story of the 9-story weak-story frame at drifts of 2% and 4%.

The original MPA procedure and the modified MPA procedure used in the MDOF studies both use SRSS combinations and assume that there is no interaction of the modes, as is the case for elastic response. The SRSS combinations of response peaks, using the first three modes, nearly always underestimated the peak interstory drifts of the 3- and 9-story frames at 0.5% drift, suggesting that the SRSS estimates are not necessarily an upper bound to the mean dynamic peaks,[1] and that, in the case of the 9-story frames, consideration of additional modes may be required for improved estimates of interstory drift. Randomness in the timing of "modal" peaks generates variability in interstory drifts, limiting the potential accuracy of prospective estimates of interstory drift for individual events.

Interestingly, for each of the single mode load vectors except the rectangular load vector, the maximum of the interstory drifts determined over the height of the five buildings was a good estimate of the interstory drift that occurred in the nonlinear dynamic analyses at that story in the building. Furthermore, this maximum interstory drift provided a reasonable estimate of the largest interstory drifts that developed over the height of each structure. The weak story frames provide one illustration of this finding—each of these pushover methods provided good estimates of the interstory drifts that occurred at the weak stories of the 3- and 9-story weak story frames at drift levels of 2% and 4%. Of interest, this observation held even though the story at which the maximum interstory drift is calculated may vary with the choice of pushover load vectors.

#### F.4.2.3 Story Shears

The peak dynamic story shears begin with disproportionately large values at the uppermost story of all five buildings and increase monotonically towards the base. For the regular frames, peak dynamic story shears often exceeded pushover estimates, at all stories. For the regular 3-story frame, the modified MPA procedure underestimated story shears at 0.5% drift and significantly overestimated story shears at 4% drift. For the regular 9-story frame, the modified MPA procedure underestimated story shears over most of the building height at 0.5% drift, and overestimated story shears and 2% and 4% drift. The other pushover techniques generally had larger error.

For the weak story frames, all pushover techniques except for the modified MPA procedure provided good estimates of the lowest story shear at 2% and 4% drift. The dynamic shears in the remaining stories greatly exceeded the single-mode estimates at these drift levels. Estimates for these stories using the modified MPA procedure could be substantially more or less than the dynamic values, with the tendency to overestimate story shears becoming more pronounced with increasing drift levels. A possible improvement may be to include more modes, with each modal contribution reduced in some way as drift levels increase.

For the shear-wall building, the pattern of peak story shears changed with increasing drift. Response at 0.2% drift was marked by a quasi-first mode pattern, with a disproportionately large shear at the uppermost story. With increasing drift, the shears at the uppermost two stories and lowest three stories increased disproportionately, particularly for the lowest two stories. At 0.2% drift, the pattern of the story shears was offset from the code pattern by a more or less constant amount that resembles the $F_t$ force used in the Equivalent Lateral Force procedure of earlier codes[2]. At 1% drift, the modified MPA procedure typically underestimated the story shears for the lowest stories, although the estimates improved at 2% drift. Estimates with the other procedures were not as good at the 1% and 2% drift levels. The rectangular load pattern, often used to bound wall shears for design, underestimated the shears over the entire height of the wall at the 1% and 2% drift levels, and underestimated the shears over the upper four stories at the 0.2% drift level.

#### F.4.2.4 Overturning Moments

The peak dynamic overturning moments displayed less variance than the story shears. The overall pattern of overturning moments was captured with the single-load

1. This may be because the modal peaks were estimated with a 2% damped spectrum, but the damping present in the nonlinear dynamic analyses may have been lower for some modes, thus leading to underestimates of higher mode contributions to drift.

2. Perhaps a better correlation would have been observed if the exponent k had been determined based on the effective period of the structure rather than the initial period.

**Table F-8 Peak Roof Drift Ratios for the Five Building Models (%)**

| *Building Model* | *Near-Fault Record* | | | |
|---|---|---|---|---|
| | *ERZMV1* | *RRSMV1* | *LUCMV1* | *SCHMV1* |
| 3-story frame (regular) | 4.07 | 4.96 | 1.79 | 2.62 |
| 3-story frame (weak story) | 2.95 | 3.62 | 2.13 | 2.12 |
| 8-story wall | 1.24 | 2.06 | 0.64 | 0.73 |
| 9-story frame (regular) | 1.91 | 1.84 | 1.69 | 1.82 |
| 9-story frame (weak story) | 1.88 | 1.85 | 1.71 | 2.13 |

vector techniques except for the 9-story weak story building, and the single-load vector techniques gave similar estimates, with the exception of the rectangular and code load vectors. Although the overall pattern was captured, the dynamic values were substantially underestimated in some cases, particularly at the upper stories and for the higher drift levels. The modified MPA procedure was inconsistent, sometimes providing accurate estimates and sometimes severely overestimating or underestimating the peak overturning moments.

### *F.4.3 Results for Near Field Motions*

Sections F.8.4 and F.8.5 (Figures F-52 through F-71, and Figures F-72 through F-76) provide complete results of the analyses of the response of the examples to the near-field ground motions. Peak roof drift ratios obtained with the unscaled near-field motions were generally within or close to the ranges of predetermined drifts used with the ordinary ground motions (Table F-8), ranging between 1.79% and 4.96% for the 3-story frames, 1.69% and 1.88% for the 9-story frames, and 0.64% and 2.06% for the 8-story wall building.

For the near field motions, peak interstory drifts for the regular frames were at most about 25% higher than the average roof drift for the 3-story frame and were at most about 110% higher than the average roof drift for the 9-story frame. While these values are larger than the mean values reported in Section F.3.1 for the ordinary motions, they are not inconsistent with the peak values of interstory drift observed for the ordinary motions.

Errors in the estimates of the response quantities for both the ordinary and near fault ground motions are presented in Figures F-72 through F-76 for all buildings and pushover load vectors. The mean of the values of the error measure $E_2$ over the height of the buildings is plotted according to the drift level for the ordinary motions and is also plotted for the near-fault motions.[1] Maximum values of this error measure over the height of each building are also plotted. Note that the error measure $E_2$, when applied to the ordinary motions, is equivalent to the error measure $E_1$, because the mean of the pushover estimates is simply the single estimate obtained at a predetermined drift level.

A review of Figures F-72 through F-76 shows that the quality of the estimates is, in general, as good or better than the estimates made for the ordinary ground motions, with the exception of displacement estimates of the 9-story weak-story building. In some cases the weak-story frame showed a clear weak story response (RRSMV1 and LUCMV1 ground motions), while in other cases, peak interstory drifts in the weak story were only moderately elevated over those occurring in the regular frames for the same motion (ERZMV1 and SCHMV1 ground motions). These differences occurred even though the peak roof drifts of the 9-story weak-story frame (1.71% to 2.13%) were similar to those of the regular 9-story frame (1.69% to 1.91%). For those cases in which weak story responses occurred, the pushover methods provided good estimates of displacement response. Only for the two near-fault motions that did not generate a weak-story response were the estimates poor.

## F.5 Equivalent SDOF Estimates of Peak Roof Displacement Response

The preceding analyses of the example buildings for MDOF effects focused on the accuracy of estimates made using various load vectors for building models subjected to prescribed peak drift levels. Underlying this approach was the assumption that accurate estimates of the peak roof displacement can be obtained using the simplified inelastic procedures. Work by many researchers, including Chopra et al. (2003), Miranda (1991), Collins et al. (1995), Seneviratna and Krawinkler (1997), and Cuesta and Aschheim (2001), indicates a tendency for the equivalent SDOF models to overestimate peak roof displacements of inelastic structures, by up to 20% or more, depending on the level of nonlinearity in the system. To illustrate this

1. The $E_2$ error measure is defined in Section F.4.1.

tendency, estimates were made for the five example buildings based on their first mode capacity curves. The estimates were made using the ATC-40 and FEMA 356 relationships for establishing the yield-strength coefficient of the equivalent SDOF system.

### *F.5.1 Analysis Details*

Peak roof displacement estimates were made for the five example buildings subjected to the 11 ordinary ground motion records scaled to achieve the predetermined drift levels and for the unscaled near-field ground motions. Estimates were made for cases in which *P*-Delta effects were included as well as for cases in which *P*-Delta effects were excluded. Results are reported in detail for cases in which the bilinear curve, fitted to the capacity curve obtained from a first mode pushover analysis, displayed a positive post-yield stiffness. *P*-Delta effects were included for the 3-story frames and the 8-story wall (Figure F-8). However, to avoid a negative post-yield stiffness for the 9-story frames, *P*-Delta effects had to be excluded for the analyses of these frames.

In cases in which *P*-Delta effects were considered, the mode shape and the nonlinear static analysis were determined with *P*-Delta effects included, and the applied lateral force is plotted rather than the base shear (which is amplified due to *P*-Delta). In cases in which *P*-Delta effects were not considered, the mode shape and nonlinear static analysis were determined without considering *P*-Delta effects. For each case considered, ground motions were scaled to obtain the predetermined target drift levels for the MDOF models. If *P*-Delta effects were included, they were included in the nonlinear MDOF dynamic analyses and were represented using bilinear hysteretic models for the steel frame buildings and a stiffness degrading model for the concrete shear-wall building, with initial- and post-yield stiffnesses adjusted to reflect the effects of *P*-Delta on the MDOF capacity curves. Similarly, if *P*-Delta effects were not considered, they were excluded from both the MDOF and SDOF analyses.

"Equivalent" SDOF (ESDOF) systems were determined according to the methods of ATC-40 and FEMA 356. For both methods, the yield displacement $\Delta_y$ of the ESDOF system is determined as

$$\Delta_y = \frac{\Delta_{y,roof}}{\Gamma_1} \qquad \text{(F-5)}$$

where $\Delta_{y,\,roof}$ = the roof displacement at yield, and $\Gamma_1$= the first mode participation factor (given by $\phi^T M1/\phi^T M\phi$)[1].

In the ATC-40 method, the yield strength coefficient of the ESDOF system is given by

$$C_y = \frac{S_a}{g} = \frac{V_{y,mdof}/W}{\alpha_1} \qquad \text{(F-6)}$$

where $S_a$ = the pseudo-acceleration associated with yield of the ESDOF system, $g$ = the acceleration of gravity, $V_{y,\,mdof}$ = the yield strength of the MDOF system, $W$ = the weight of the MDOF system, and $\alpha_1$ = the modal mass coefficient (given by $\Gamma_1(\phi^T M1/1^T M1)$).

In the FEMA 356 method, the yield strength coefficient of the ESDOF system is approximated as

$$C_y = \frac{S_a}{g} = \frac{V_{y,mdof}}{W}\Gamma_1 \qquad \text{(F-7)}$$

which relies on the approximation $\Gamma_1 \approx 1/\alpha_1$.

If $\phi$ is set equal to an elastic mode shape, the ATC-40 method produces an ESDOF system that has a period of vibration equal to the period associated with the mode shape. However, the approximation in Equation F-7 causes the period of vibration and the yield strength coefficient of the FEMA 356 ESDOF system to deviate slightly from the corresponding period of the MDOF system.[2]

The ESDOF systems resulting from the ATC-40 and FEMA 356 methods were subjected to the scaled ground motion records, determined for each building model and drift level. A bilinear hysteretic model was used for the frames, and a simple stiffness degrading model was used for the ESDOF system representing the 8-story wall building. The resulting peak displacement was scaled by $\Gamma_1$ to obtain the estimated peak roof displacement.

---

1. For simplicity in presentation, this document presumes that $\phi$ has been normalized to unit amplitude at the roof.

2. Note that if higher modes are to be considered, $\Gamma_i$ is a poor approximation to $1/\alpha_i$, for $i > 1$.

### *F.5.2 Analysis Results*

The ratio of the roof displacement estimated with the ESDOF system and the peak roof displacement that developed in the nonlinear dynamic analysis of the MDOF system was determined for each building model and each ground motion record. Statistics of this ratio, termed the "displacement ratio," were determined for each building model at each drift level and for the set of near fault motions. The minimum, maximum, mean, median, and standard deviation of this ratio were computed. Detailed results for the ordinary motions are summarized for the ATC-40 formulation (Equation F-6) in Figure F-15.

Mean displacement ratios for the ordinary motions were between approximately 0.95 and 1.25 for the five buildings (Figure F-15), with a tendency to increase with increasing roof drift. Similar means were obtained with the FEMA 356 formulation (Equation F-7), although dispersions were larger for this formulation. Accuracy was similar for the near-field motions. The ATC-40 formulation is preferred because it resulted in smaller dispersions, accurately reflects the frequency content of the excitation for elastic response, and is consistent with common derivations of "equivalent" SDOF systems.

Accuracy was compromised in cases in which the post-yield stiffness of the ESDOF system was negative. In such cases, there was a tendency for the displacements of the equivalent SDOF systems to be exaggerated, with some SDOF systems collapsing, although the MDOF systems simply reached their predetermined drifts. For such cases, nonlinear dynamic analyses may be preferred, given the potential for ESDOF systems to significantly overestimate the roof displacement.

## F.6 Scaled NDP Analysis Method

### *F.6.1 Background*

The ATC-55 MDOF studies were conducted to illustrate the accuracy of several available pushover methods for estimating peak response quantities, by comparison with results obtained from nonlinear dynamic analyses. The pushover techniques were not consistently able to provide accurate estimates of response quantities (interstory drifts, story shears, and overturning moments) for many of the example buildings. The difference between the pushover estimates and the results from nonlinear dynamic analyses is attributed primarily to the presence of higher modes or MDOF effects. Although scatter is to be expected in the results from nonlinear dynamic analyses, the dispersion in the peak dynamic values of interstory drifts, story shears, and overturning moments was relatively small, and the values of these quantities could differ significantly from the estimates obtained using the various pushover methods.

The Scaled NDP is based on the idea that a relatively small number of nonlinear dynamic analyses can be used to estimate the response quantities of interest. In the Scaled NDP (described in Section 9.5.2), the ground motion records are scaled so that the peak roof displacement matches the target displacement determined from nonlinear static analysis. Each dynamic analysis contributes positively to the estimate of the central tendency and range of dynamic response values. In contrast, none of the pushover methods was able to consistently provide reliable estimates of the peak interstory drifts, story shears, and overturning moments, for the example buildings considered.

### *F.6.2 Elaboration of Step 3 and Examples*

Step 3 of the basic procedure described in Section 9.5.2 suggests that estimates of a response quantity at the mean plus $\kappa$ standard deviation level can be determined by multiplying the mean of the response quantity observed in the $n$ dynamic analyses by a coefficient. Let the sample mean of the response quantity of interest be designated by $\bar{x}_n$. As shown in Section F.6.3, if the response quantities are normally distributed, the quantity $c(1+\kappa COV)\bar{x}_n$ exceeds the true mean plus $\kappa$ standard deviations with confidence level $\alpha$. In the preceding, $c$ is given by

$$c = \frac{1}{1 - \left(\Phi^{-1}(\alpha)\right)\dfrac{COV}{\sqrt{n}}} \qquad \text{(F-8)}$$

where $\Phi^{-1}_{t,n-1}(\alpha)$ represents the value of the variate of the Student's t-distribution with $n$-1 degrees of freedom at a confidence level of $\alpha$, and COV represents the coefficient of variation determined for the sample of $n$ observations of the response quantity $x$.

Equation F-8 simplifies to $c$ = 1 for a confidence level, $\alpha$, of 50%. For a confidence level of 90%, Equation Equation F-8 can be solved to obtain the values of $c$ given in Table F-9.

Thus, the quantity $c(1+\kappa COV)\bar{x}_n$ is said to exceed the true mean plus $\kappa$ standard deviation value with confidence level $\alpha$. The quantity $\kappa$ assumes a value of zero where estimates of the true mean are sought.

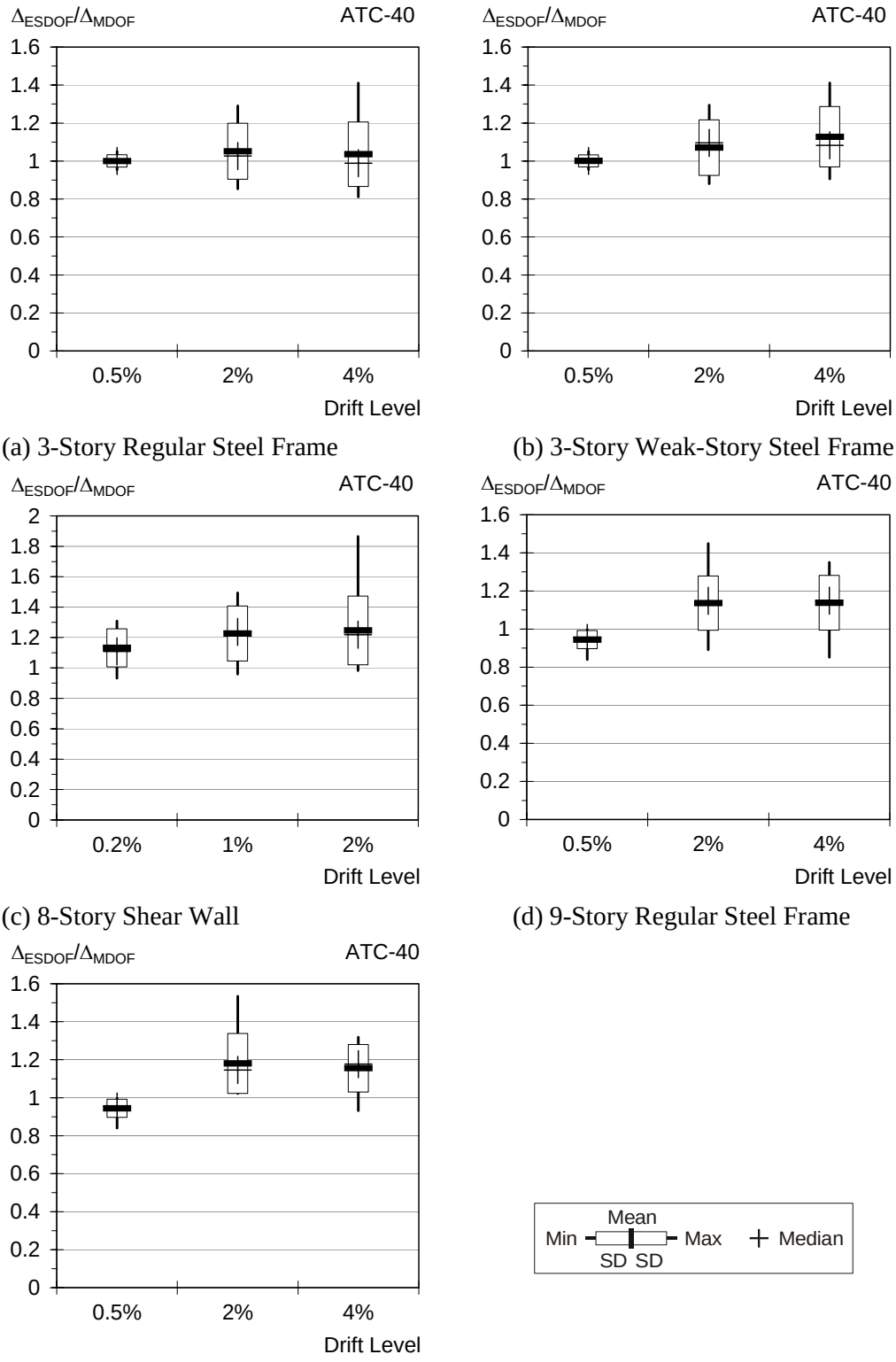


Figure F-15 Example statistical distributions of displacement ratios for the ordinary ground motions.

**Table F-9 Values of *c* at the 90% Confidence Level**

| *n* | $\Phi_{t,n-1}^{-1}(\alpha)$ | *Coefficient of Variation* | | | | | | | | | |
|---|---|---|---|---|---|---|---|---|---|---|---|
| | | 0.05 | 0.10 | 0.15 | 0.20 | 0.25 | 0.30 | 0.35 | 0.40 | 0.45 | 0.50 |
| 3 | 1.886 | 1.06 | 1.12 | 1.20 | 1.28 | 1.37 | 1.48 | 1.62 | 1.77 | 1.96 | 2.19 |
| 5 | 1.533 | 1.04 | 1.07 | 1.11 | 1.16 | 1.21 | 1.26 | 1.32 | 1.38 | 1.45 | 1.52 |
| 7 | 1.440 | 1.03 | 1.06 | 1.09 | 1.12 | 1.16 | 1.20 | 1.24 | 1.28 | 1.32 | 1.37 |
| 10 | 1.372 | 1.02 | 1.05 | 1.07 | 1.10 | 1.12 | 1.15 | 1.18 | 1.21 | 1.24 | 1.28 |
| 20 | 1.328 | 1.02 | 1.03 | 1.05 | 1.06 | 1.08 | 1.10 | 1.12 | 1.13 | 1.15 | 1.17 |
| 50 | 1.299 | 1.01 | 1.02 | 1.03 | 1.04 | 1.05 | 1.06 | 1.07 | 1.08 | 1.09 | 1.10 |
| 100 | 1.290 | 1.01 | 1.01 | 1.02 | 1.03 | 1.03 | 1.04 | 1.05 | 1.05 | 1.06 | 1.07 |

Table F-9 also can be used to indicate the number of analyses to run—that is, the point at which additional analytical data are of negligible benefit. The derivation of Equation F-8 is provided in Section F.6.3 below.

#### F.6.2.1 Example Illustrations

*Interstory Drift Estimate:* The sample mean of the peak values of interstory drift at the lowest story of the 9-story frame at a predetermined roof drift of 4% is $\bar{x}_n = 6.5\%$ . The true COV is estimated from the 11 peak dynamic responses to be 0.16. For this COV, Equation F-8 results in $c = 1.05$. The true mean value of peak interstory drift is estimated to not exceed $c\bar{x}_n$ = 1.05(6.5%) = 6.8% at the 90% confidence level. That is, there is a 90% probability that the true mean peak interstory drift at the lowest story is less than 6.8% at the hazard level that produces a roof drift of 4%.

*Story Shear Estimate:* The sample mean of the peak story shears at the lowest story of the 8-story wall at a predetermined roof drift of 2% is $\bar{x}_n$ = 1070 kips. To guard against the potential for shear failure, an "upper bound" limit on shear demands is desired. Based on the 11 analyses, the true COV of the peak story shears is estimated to be 0.22. Using Equation F-8, $c = 1.10$. Therefore, there is a 90% probability that the true mean plus one standard deviation peak story shear is less than $(1 + \kappa\text{COV})\, c\bar{x}_n$ = 1.10(1 + 0.22)(1070 kips) = 1440 kips, for the hazard that produces a roof drift of 2%.

Note that the numerical values determined by this approach should be considered estimates rather than exact values. The estimates are considered to be more reliable, in general, than those determined using only static analysis techniques.

### *F.6.3 Statistical Basis*

Equation F-8 was derived assuming that the response quantities are normally distributed, an assumption that is approximately applicable even for log-normally distributed data if the dispersion in the data is not large.

**Problem Statement:** A response quantity $X$ has peak values $x_1, x_2, \ldots x_n$ in $n$ dynamic analyses of a structure. The mean of the $n$ responses is $\bar{x}_n$ . The responses are assumed to be normally distributed, with mean $\mu$ and standard deviation $\sigma$. What is the scale factor $c'$ such that $c'\bar{x}_n$ exceeds $\mu + \kappa\sigma$ with a specified level of confidence $\alpha$?

**Answer:**

1. $X$ is normally distributed with true mean $\mu$ and standard deviation $\sigma_x$. That is, $X \sim N(\mu, \sigma)$.
2. The sample mean of $X$ is given by $\bar{x}_n$ where

$$\bar{x}_n \sim N\left(\mu, \frac{\sigma}{\sqrt{n}}\right) \qquad \text{(F-9)}$$

3. If the standard deviation $\sigma$ is estimated by the sample standard deviation $s$, then the sample mean has the Student's $t$-distribution with $n$-1 degrees of freedom:

$$\bar{x}_n \sim t_{n-1}\left(\mu, \frac{s}{\sqrt{n}}\right) \tag{F-10}$$

This can be expressed as

$$\frac{\bar{x}_n - \mu}{s/\sqrt{n}} \sim t_{n-1}(0,1) \tag{F-11}$$

4. We seek to establish *c'* such that

$$P(c'\bar{x}_n > \mu + \kappa\sigma) = \alpha \tag{F-12}$$

which can be restated as

$$P\left(\bar{x}_n < \frac{\mu + \kappa\sigma}{c'}\right) = 1 - \alpha \tag{F-13}$$

5. Given Equation F-10, this probability can be re-expressed as

$$\Phi_{t,n-1}\left(\frac{\frac{\mu + \kappa\sigma}{c'} - \mu}{s/\sqrt{n}}\right) = 1 - \alpha \tag{F-14}$$

where $\Phi_{t,n-1}$ is the cumulative distribution function for the Student's *t*-distribution with *n*-1 degrees of freedom. Thus,

$$\Phi_{t,n-1}^{-1}(1-\alpha) = \left(\frac{\frac{\mu + \kappa\sigma}{c'} - \mu}{s/\sqrt{n}}\right) \tag{F-15}$$

6. Algebraic manipulation allows *c'* to be expressed as

$$c' = \frac{1 + \kappa\sigma/\mu}{1 + \Phi_{t,n-1}^{-1}(1-\alpha)\frac{s/\mu}{\sqrt{n}}} \tag{F-16}$$

or equivalently as

$$c' = \frac{1 + \kappa COV}{1 - \Phi_{t,n-1}^{-1}(\alpha)\frac{COV}{\sqrt{n}}} \tag{F-17}$$

where σ/μ is approximated by the sample coefficient of variation, COV. For convenience, we may express $c' = c(1 + \kappa COV)$ where

$$c = \frac{1}{1 - \Phi_{t,n-1}^{-1}(\alpha)\frac{COV}{\sqrt{n}}} \tag{F-18}$$

where $\Phi_{t,n-1}^{-1}(\alpha)$ is the value of the variate of the Student's *t*-distribution with *n*-1 degrees of freedom at a confidence level of α.

### *F.6.4 Observed Coefficients of Variation*

The coefficients of variation (*COV*) of the response quantities determined in the MDOF studies are plotted in Section F.8.6 (Figures F-77 through F-81). The COVs are plotted for each response quantity at each floor or story for each of the five building models, at each of the three drift levels. In general, the COVs are highest at the upper stories and near the base of each model, and differ for each response quantity. The COVs for floor displacements diminish to zero at the top, due to the methodology employed in the study.

Approximate upper bounds to the COVs are tabulated in Table F-10, where "approximate" indicates that the limit was exceeded by a small amount at a limited number of locations. The COVs appear to increase with the number of stories (or period) and appear to be larger

**Table F-10 Approximate Upper Bounds to the COVs over the Height of each Building Model**

| *Building Model* | *Interstory Drift* | *Story Shear* | *Overturning Moment* |
|---|---|---|---|
| 3-story frame | 0.15 | 0.15 | 0.15 |
| 3-story frame (weak story) | 0.20 | 0.15 | 0.15 |
| 8-story wall | 0.10 | 0.20 | 0.15 |
| 9-story frame | 0.20 | 0.20 | 0.20 |
| 9-story frame (weak story) | 0.30 | 0.25 | 0.25 |

for buildings with weak story behavior. It is suggested that a COV of 0.25 to 0.30 may be appropriate for all quantities in cases where a sufficient number of analyses are not available for establishing an accurate estimate of the COV.

## F.7 Energy-based Approaches for Pushover Analysis

Motivated by the difficulties associated with reversals of the higher mode capacity curves (see Figure F-14), Hernández Montes et al. (2003) formulated an energy-based pushover analysis approach, in which a displacement is derived that represents the work done by the lateral forces acting through the floor displacements during the pushover analysis. The energy-based displacement is derived to coincide with the spectral displacement of conventional pushover approaches in the elastic portion of the response. However, the resulting capacity curves do not display the reversals observed in some conventional higher mode pushover analyses. The energy-based pushover approach was applied to the five example buildings to estimate (1) roof displacements based on response in the first mode and (2) other response quantities using a multiple mode procedure. Results are reported in the following.

### *F.7.1 Peak Displacement Response*

As described in Section F.5, many research studies have reported a tendency for conventional procedures to overestimate peak roof displacement of structures responding inelastically by up to 20% or more. This tendency is illustrated for the five example buildings in Figure F-15. These results are compared with estimates made using the energy-based first mode capacity curve in Table F-11.

The data in Table F-11 suggest that the energy-based approach provides an improvement in roof displacement estimates for the four frames. Note that the same hysteretic model was used for the frame elements and for the corresponding equivalent SDOF systems. Results for the wall building are more difficult to interpret because SDOF responses were computed using a simple stiffness-degrading model, while the MDOF responses were computed using a fiber element. Nevertheless, the energy-based displacement may be capable of providing improved estimates of roof displacement response.

**Table F-11 Means of the Ratio of Roof Displacements: SDOF Estimate / Actual MDOF**

| *Building* | *Roof Drift Level* | *Conventional First Mode* | *Energy-Based First Mode* |
|---|---|---|---|
| 3-story frame (with *P*-Delta) | 0.5% | 1.00 | 1.00 |
| | 2% | 1.05 | 1.03 |
| | 4% | 1.04 | 1.02 |
| 3-story weak story frame (with *P*-Delta) | 0.5% | 1.00 | 1.00 |
| | 2% | 1.07 | 0.94 |
| | 4% | 1.13 | 0.98 |
| 8-story wall (with *P*-Delta) | 0.2% | 1.13 | 1.16 |
| | 1% | 1.23 | 1.20 |
| | 2% | 1.25 | NA[1] |
| 9-story frame (without *P*-Delta) | 0.5% | 0.94 | 0.95 |
| | 2% | 1.14 | 1.03 |
| | 4% | 1.14 | 1.02 |
| 9-story weak-story frame (without *P*-Delta) | 0.5% | 0.94 | 0.95 |
| | 2% | 1.18 | 1.05 |
| | 4% | 1.16 | 1.03 |

[1] NA: the nonlinear static analysis failed to converge.

### *F.7.2 Multiple Mode Estimates of Response Quantities*

As described in Section F.3.2, the contributions of higher modes to response quantities were evaluated using a modified MPA procedure in which only elastic contributions of the higher modes were used, because the conventional multimode pushover procedure could not be used due to reversals of some higher mode capacity curves. The development of the energy-based pushover method provides a way to account for the potentially inelastic response associated with each of the modes, because the pushover curves obtained with the energy-based approach display the usual softening behavior. One concern with such a procedure is that responses in each mode are determined independently, and hence, estimates of response quantities computed by SRSS combinations can exceed capacity limits on force and moment. Results obtained with the modified

MPA procedure, used in the first portion of the MDOF studies, are compared in this section with the results obtained using a modified MPA procedure in which potentially inelastic responses are considered using the energy-based pushover curves.

In the energy-based modification to the multimode pushover analysis procedure, independent pushover analyses are done in each of the first three modes. For consistency, the target displacement for the first mode was set equal to the predetermined roof drift. The target displacements of the second and third modes were determined by application of an $R$-$C_1$-$T$ relationship to the mean spectrum, which was determined for the scaled ground motions used for each building and drift level. The $R$-$C_1$-$T$ relationship that was applied is given by Equation 5-1. Response quantities were determined for each of these modal pushover analyses at the corresponding target displacements. SRSS combinations of these quantities were then taken.

Figure F-16 compares results obtained with the modified MPA and energy-based multiple mode procedures against the backdrop of results obtained in the dynamic responses. A sampling of results are plotted that correspond to those presented in Section F.8.2. In some cases the results obtained with the energy-based multiple mode procedure are improvements, but the estimates still are not consistently reliable.

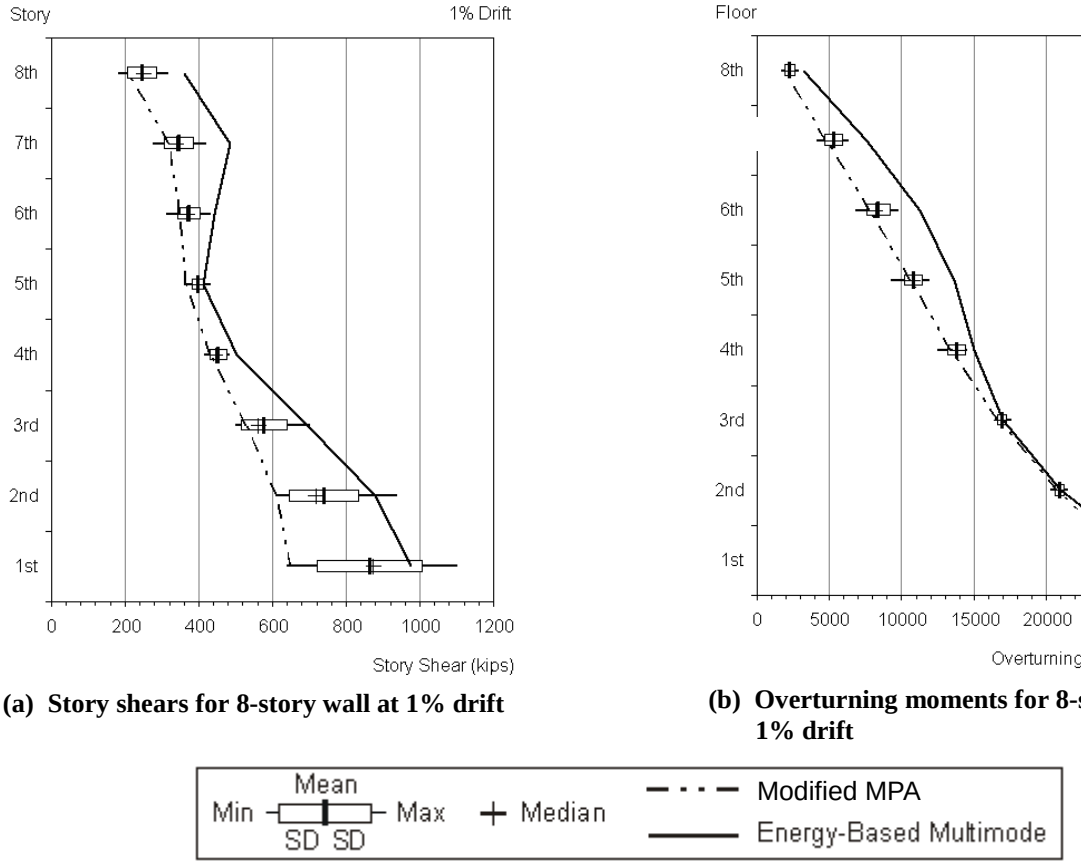


**(a) Story shears for 8-story wall at 1% drift**

**(b) Overturning moments for 8-story wall at 1% drift**

Figure F-16 Example comparisons of energy-based and conventional multiple mode calculations.

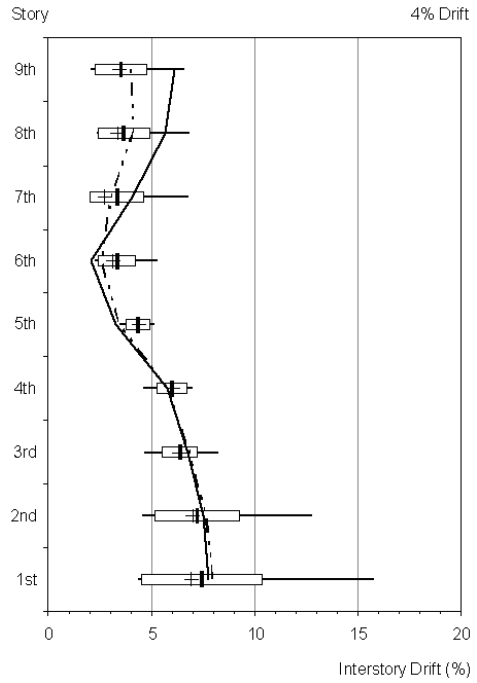


**(c) Interstory drifts for 9-story frame at 4% drift**

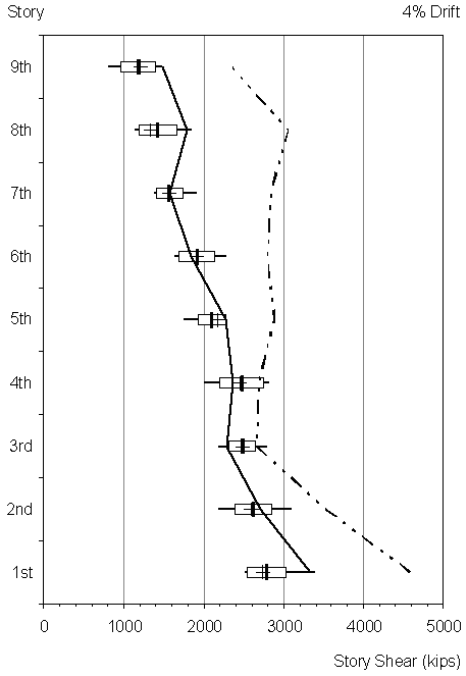


**(d) Story shears for 9-story frame at 4% drift**

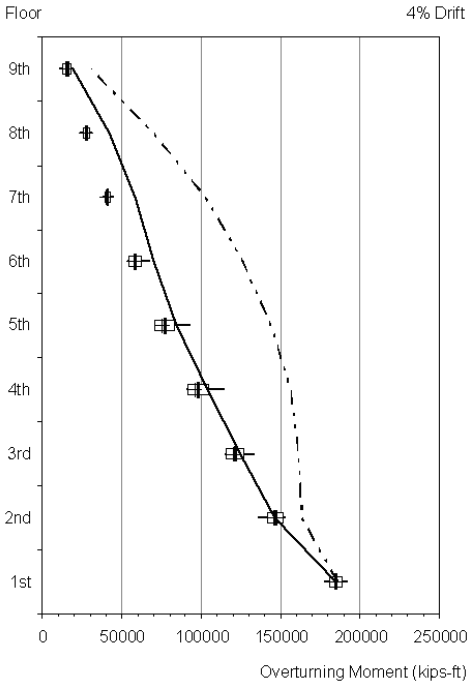


**(e) Overturning moments for 9-story frame at 4% drift**

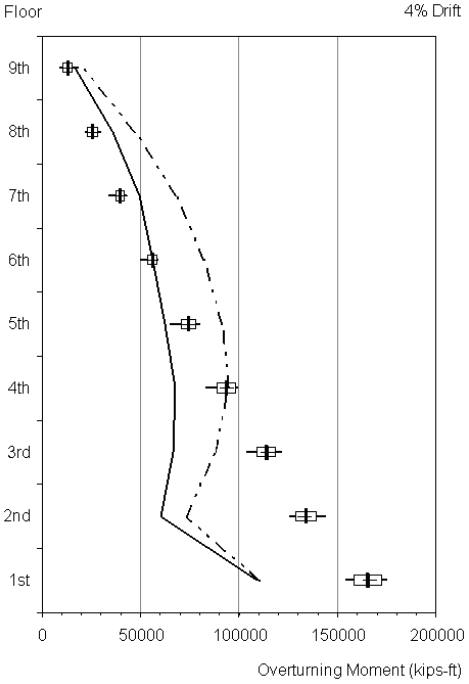


**(f) Overturning moments for 9-story weak story frame at 4% drift**

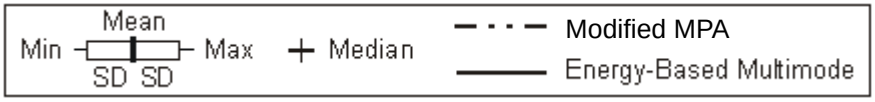


Figure F-16 Example comparisons of energy-based and conventional multiple mode calculations (continued).

## F.8 Detailed Figure Sets for the MDOF Examples

This section contains detailed figure sets resulting from the analyses described earlier in this Appendix. Section F.8.1 provides details of the ground motions, and includes plots of spectral acceleration and spectral displacement in addition to acceleration, velocity, and displacement time histories for the unscaled ground motions.

Section F.8.2 presents plots that compare the deterministic response quantities obtained in the static pushover analyses with the statistical distributions obtained in the dynamic analyses for the 11 ground motions. Results are presented for the peak values of each response quantity over the height of each building model, for the five building models, each at three predetermined values of roof drift.

Section F.8.3 presents an evaluation of mean and maximum errors in the static analysis estimates of the mean dynamic results presented in Section F.8.2. Mean and maximum errors in these estimates over the height of each building model are plotted, for each static analysis method, for each response quantity, and for each building model at each of three predetermined drift levels. See Section F.4.1 for further information.

Section F.8.4 presents plots that compare the deterministic response quantities obtained in the static pushover analyses with the peak values obtained in the dynamic analyses, for each building model subjected to each near-field ground motion. The peak roof drift obtained in the dynamic analysis and used in the static pushover analysis is shown.

Section F.8.5 presents an evaluation of mean and maximum errors in the static analysis estimates of the near-field response values, as described in Section F.4.1 These errors are plotted together with those obtained for the ordinary ground motions for comparison purposes.

Section F.8.6 presents observed coefficients of variation of the response quantities determined for the ordinary (Site Class C) motions.

### *F.8.1 Ground Motion Details*

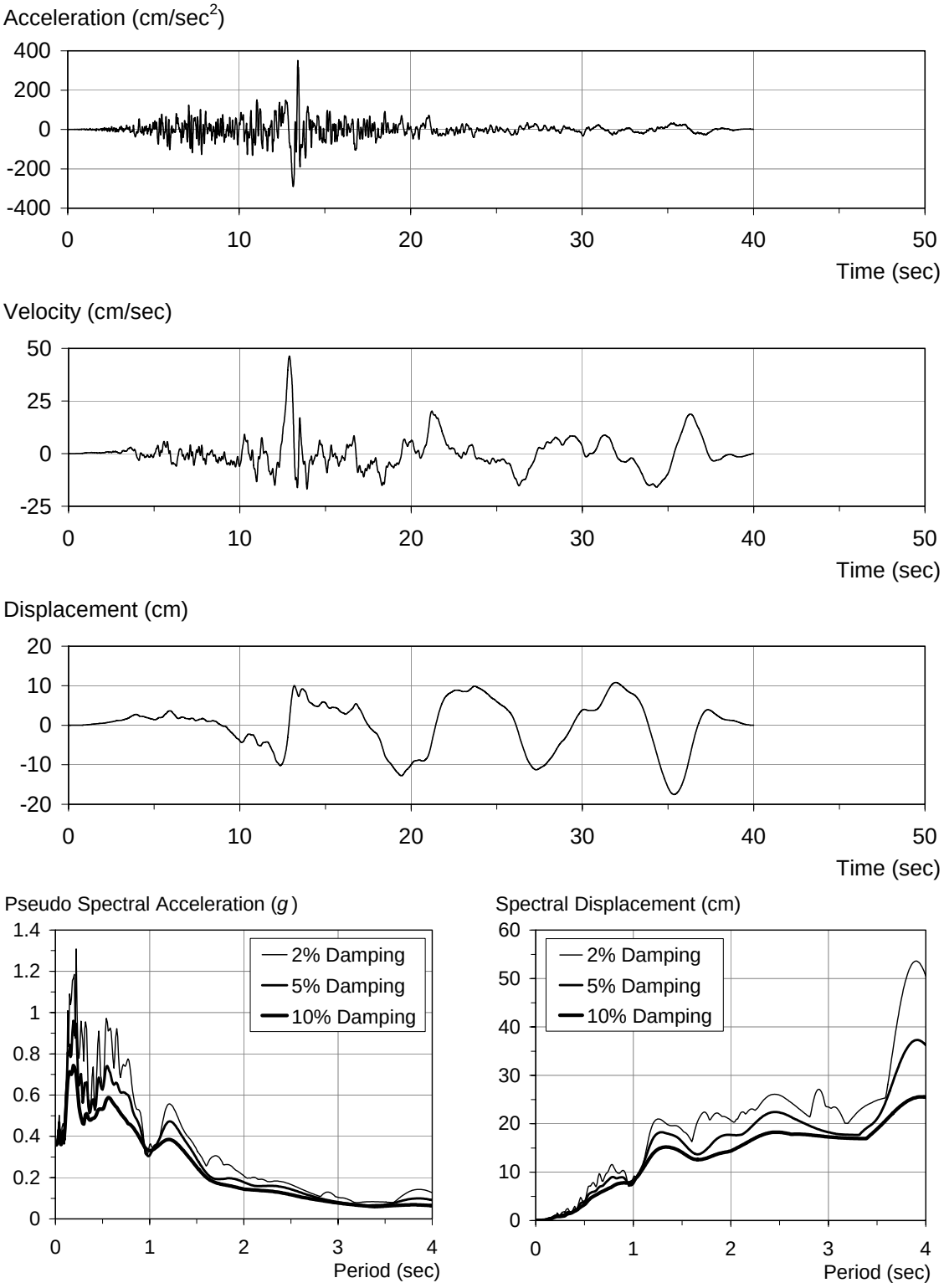


Figure F-17 Characteristics of the ICC000 ground motion

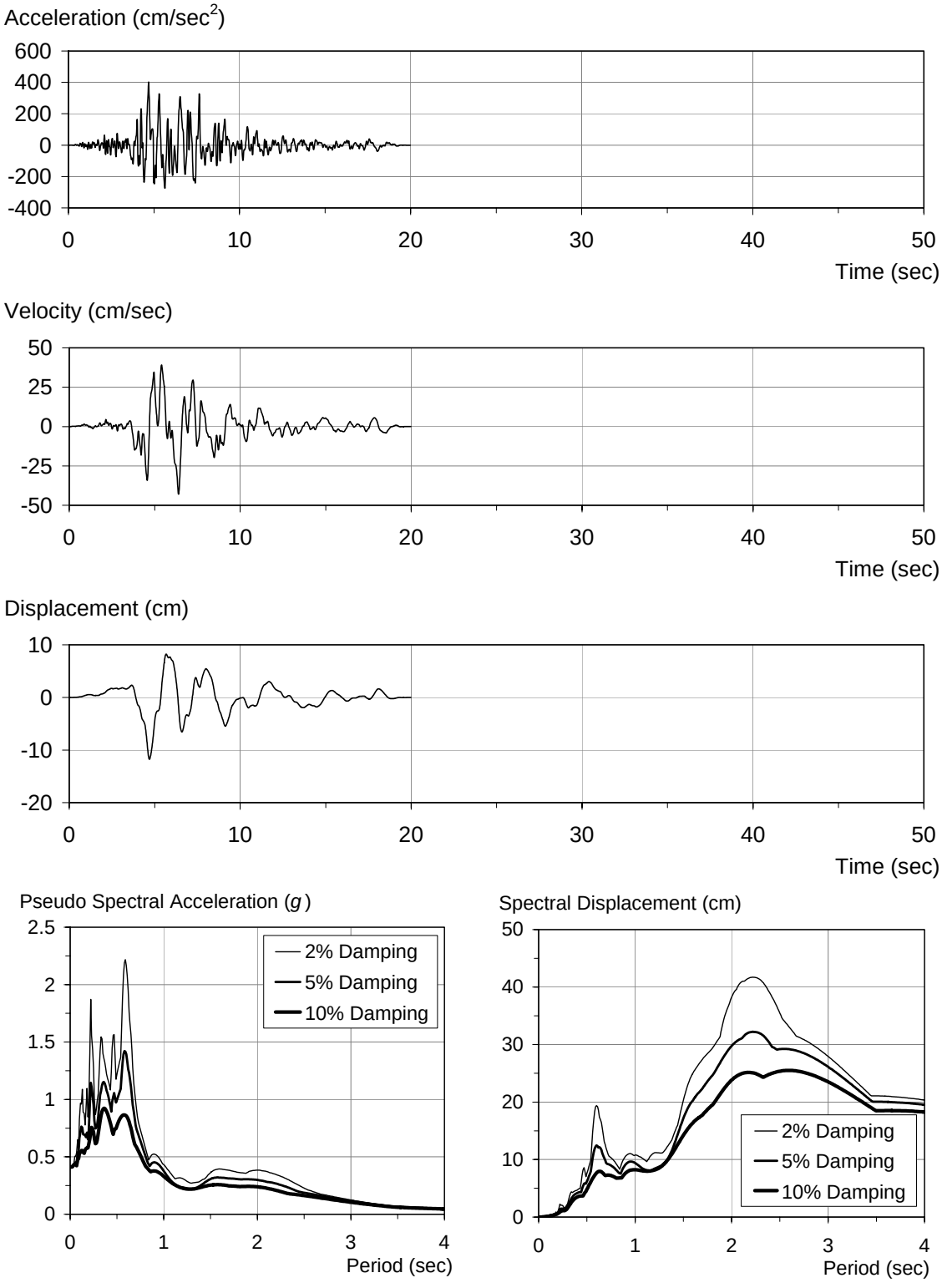


Figure F-18 Characteristics of the LOS000 ground motion

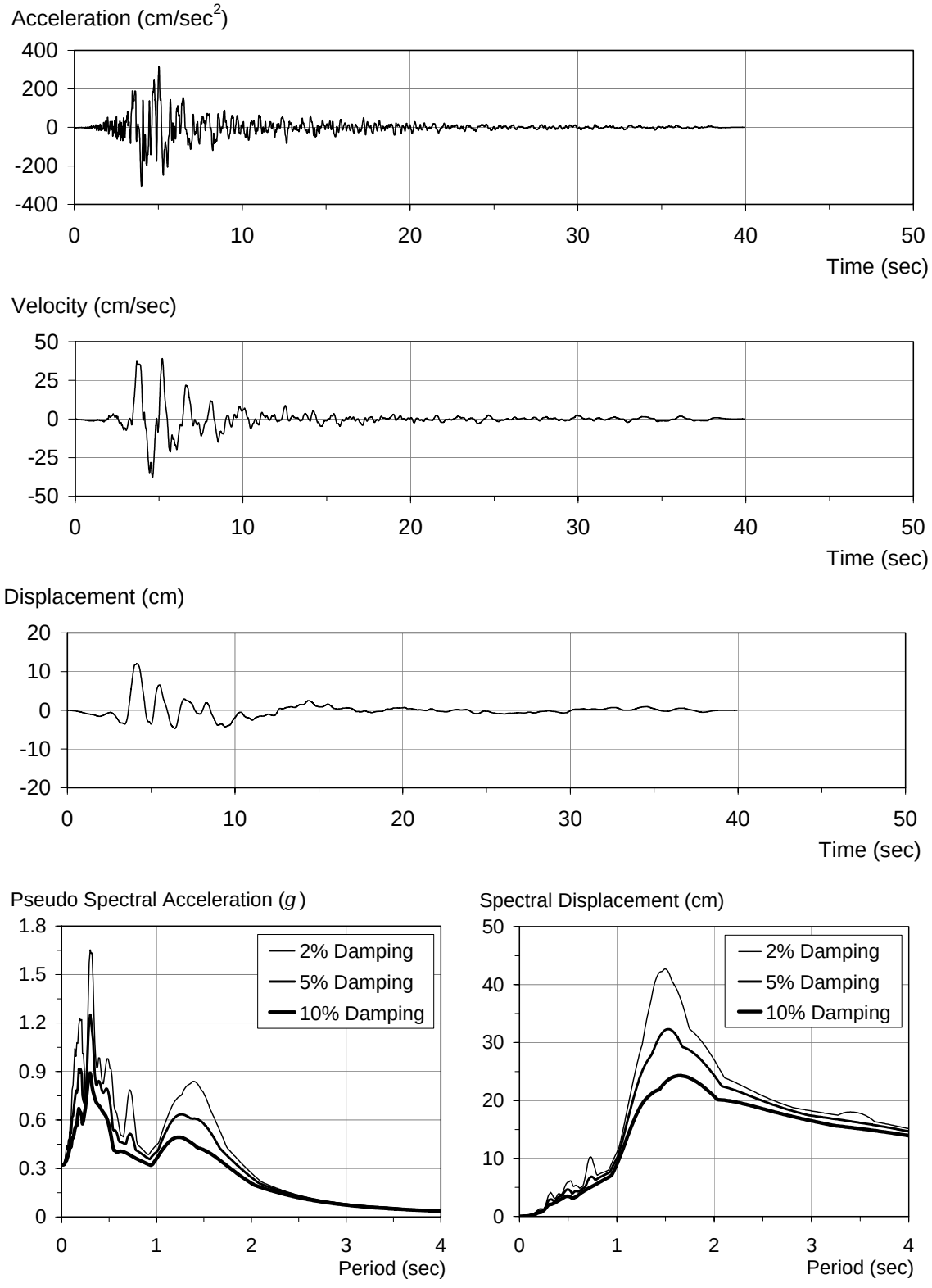


Figure F-19 Characteristics of the G02090 ground motion

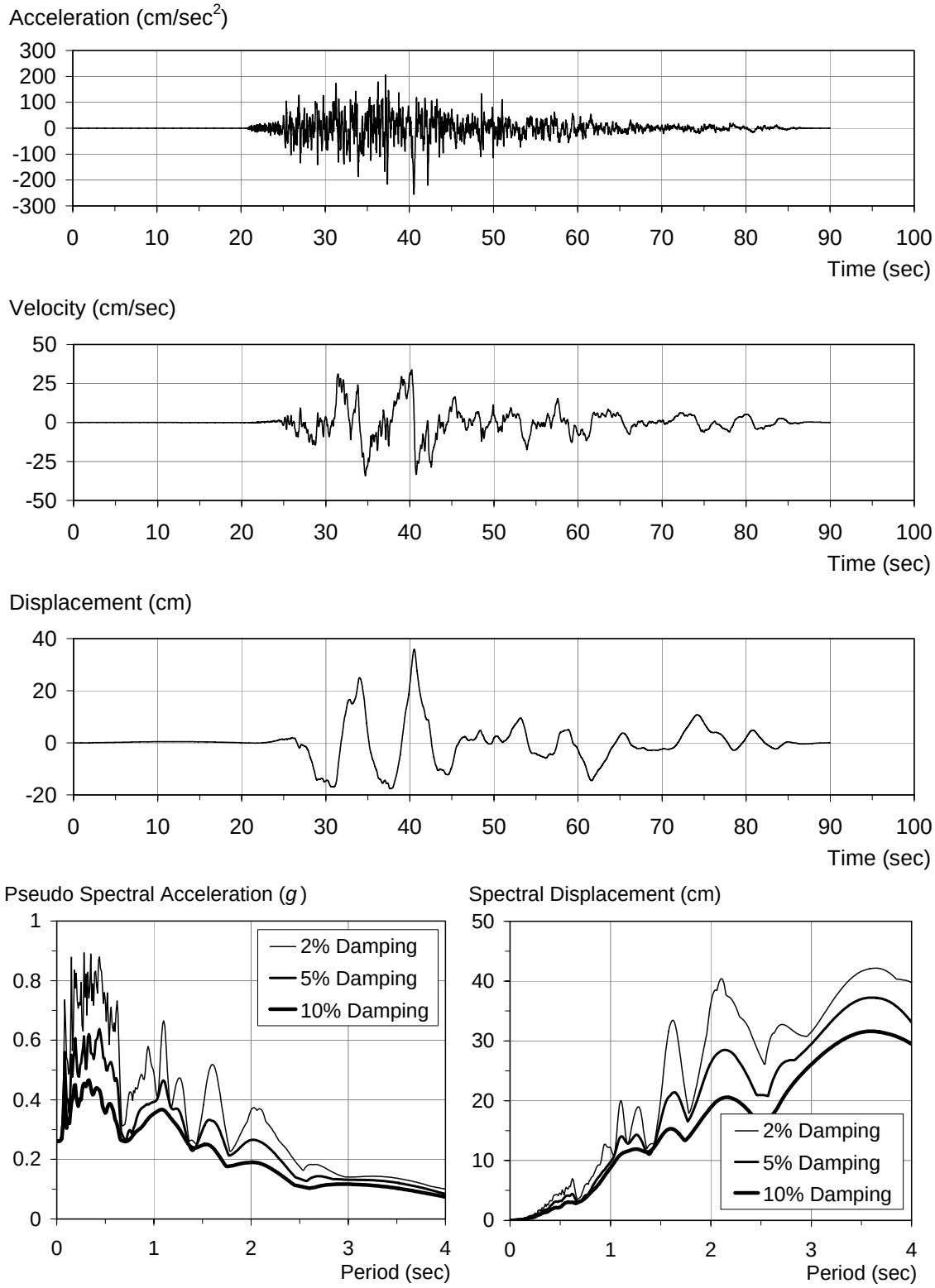


Figure F-20 Characteristics of the TCU122N ground motion

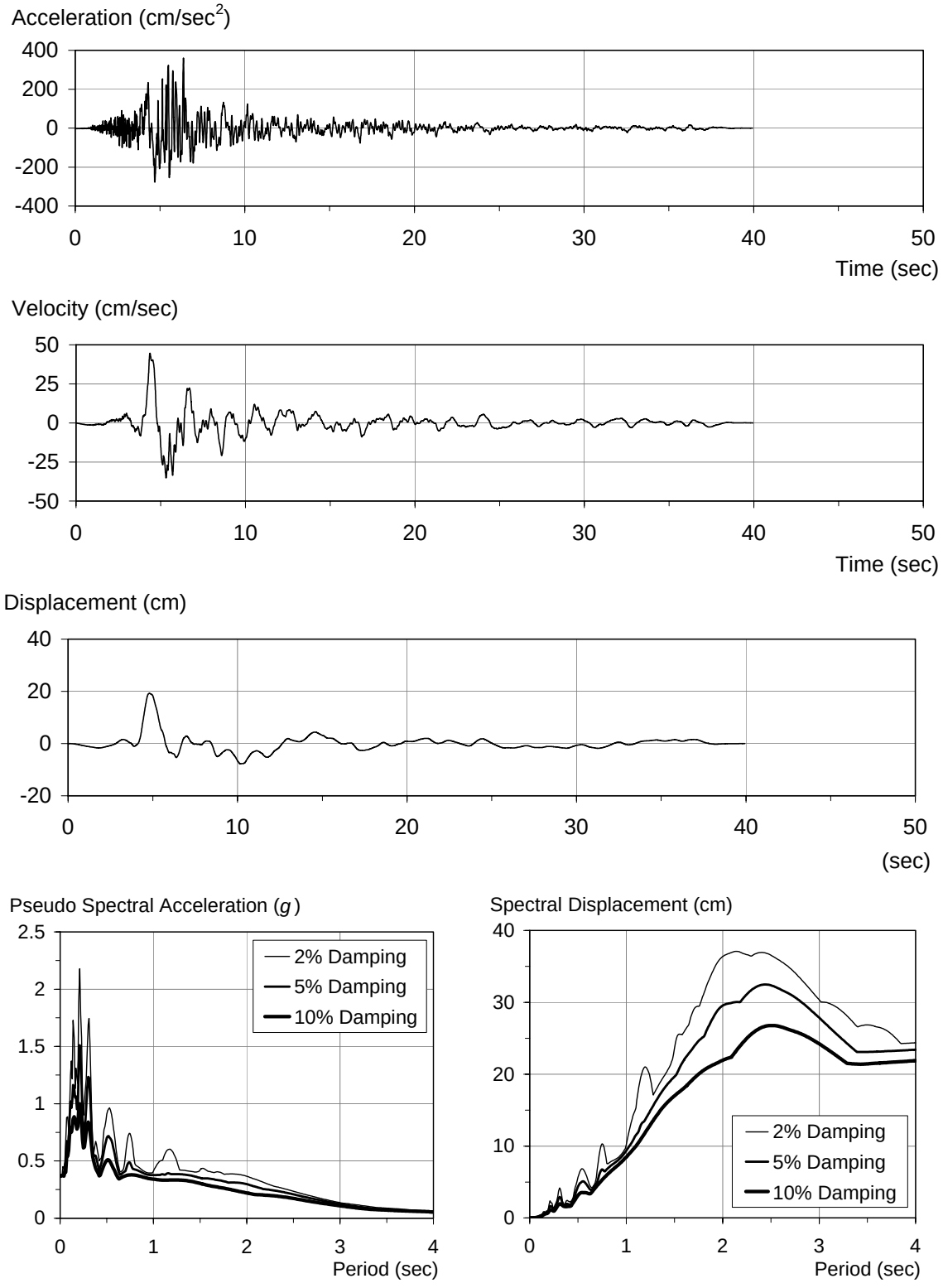


Figure F-21 Characteristics of the G03090 ground motion

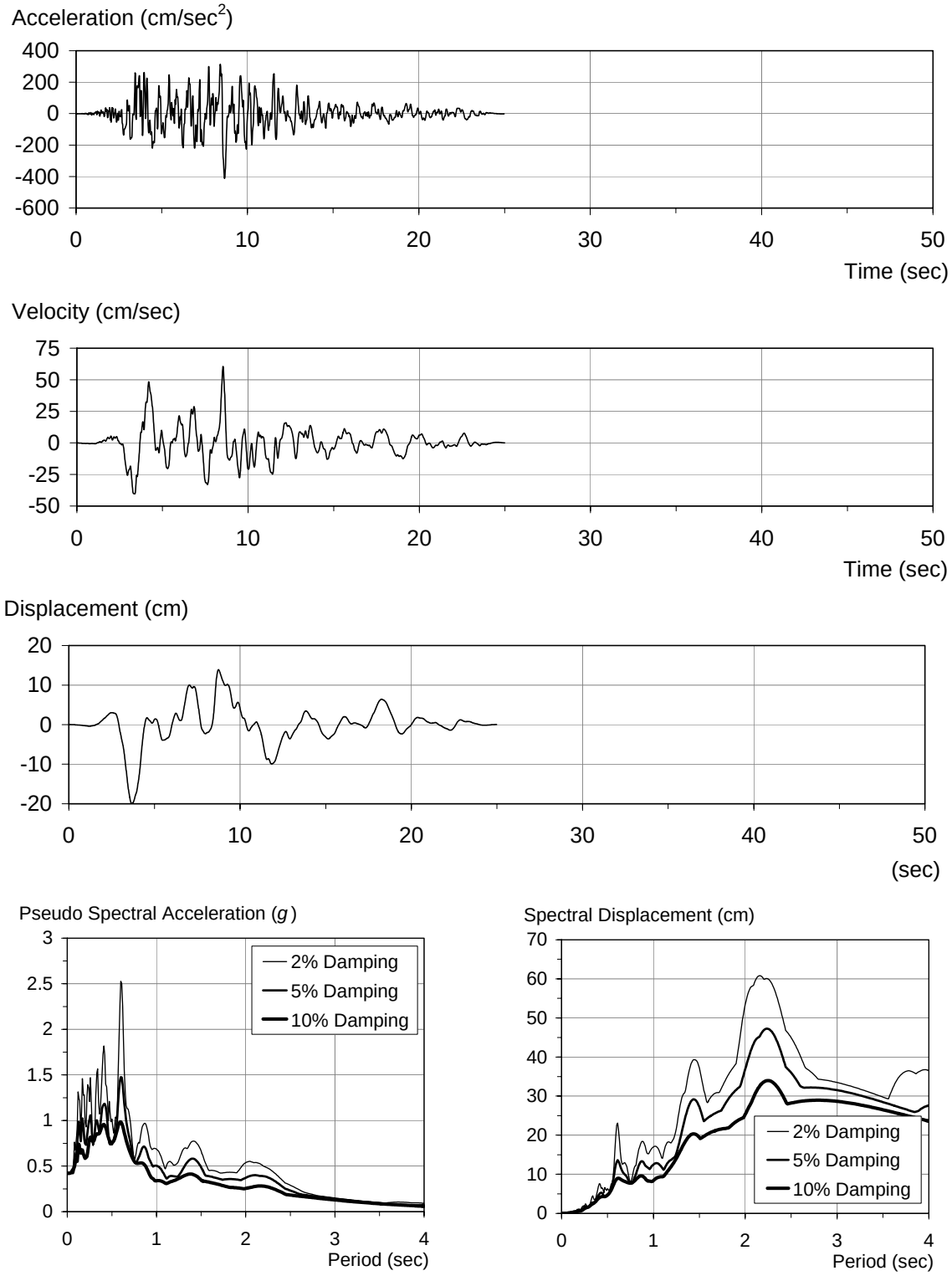


Figure F-22 Characteristics of the CNP196 ground motion

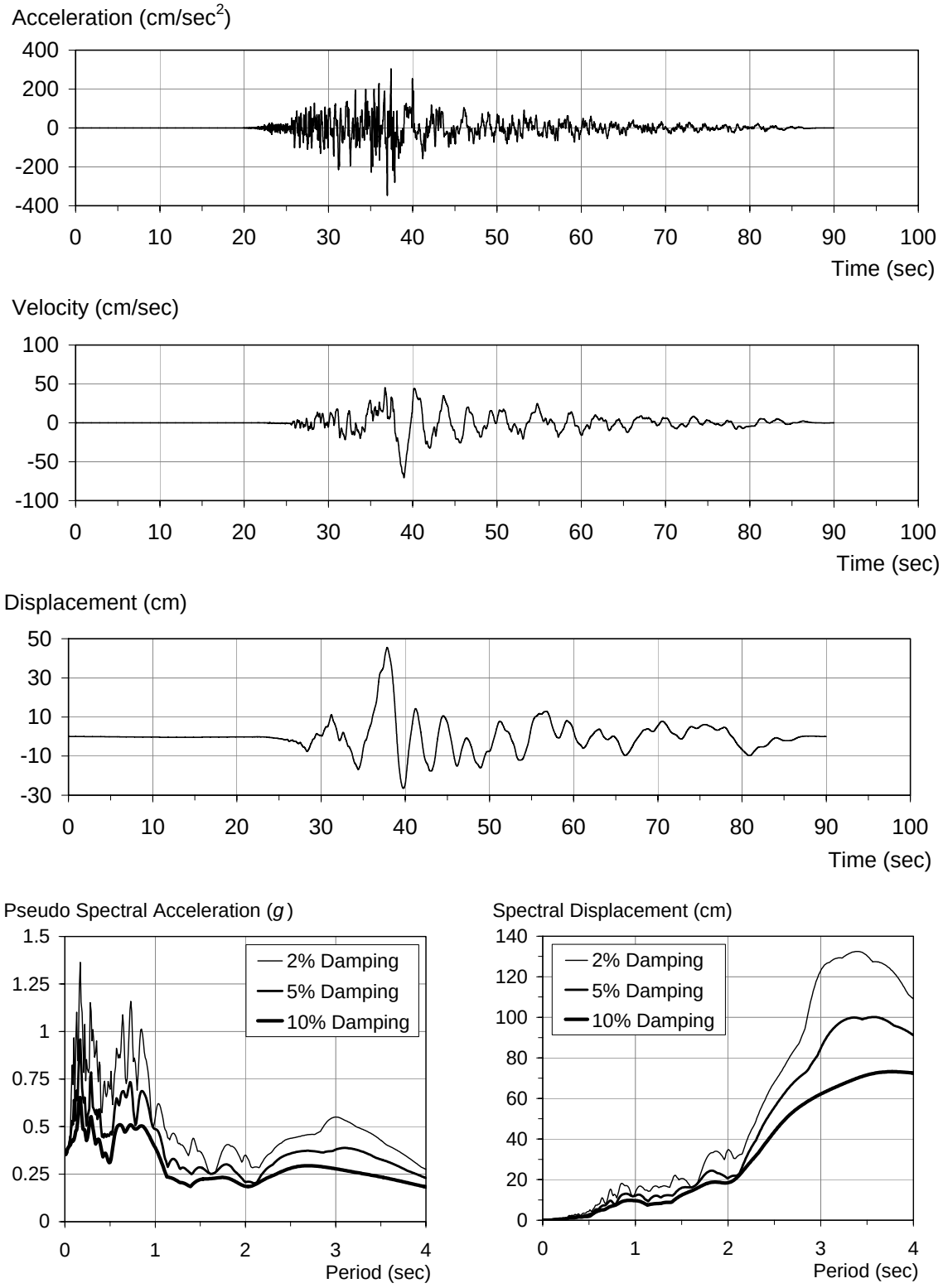


Figure F-23 Characteristics of the CHY101W ground motion

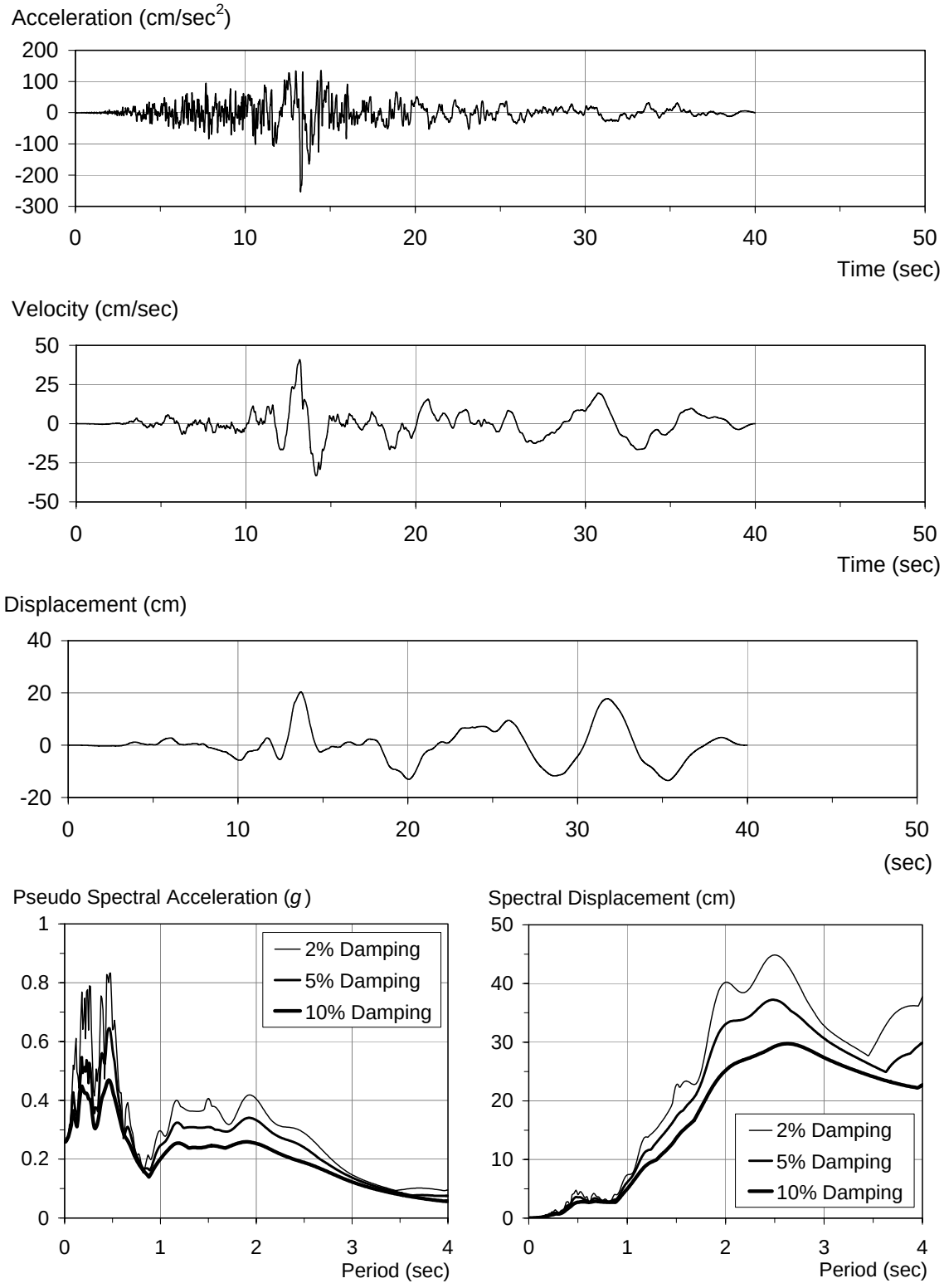


Figure F-24 Characteristics of the ICC090 ground motion

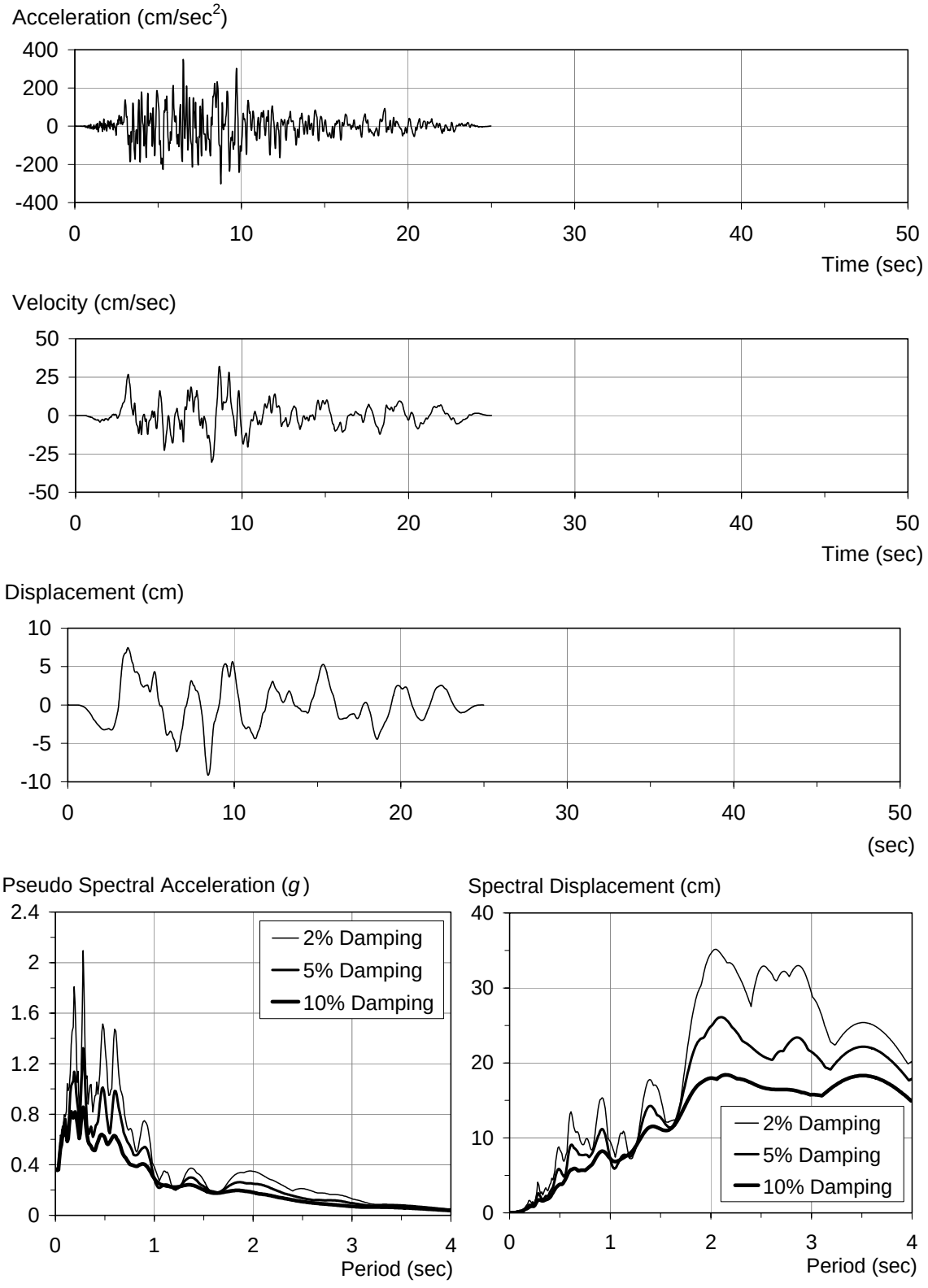


Figure F-25 Characteristics of the CNP106 ground motion

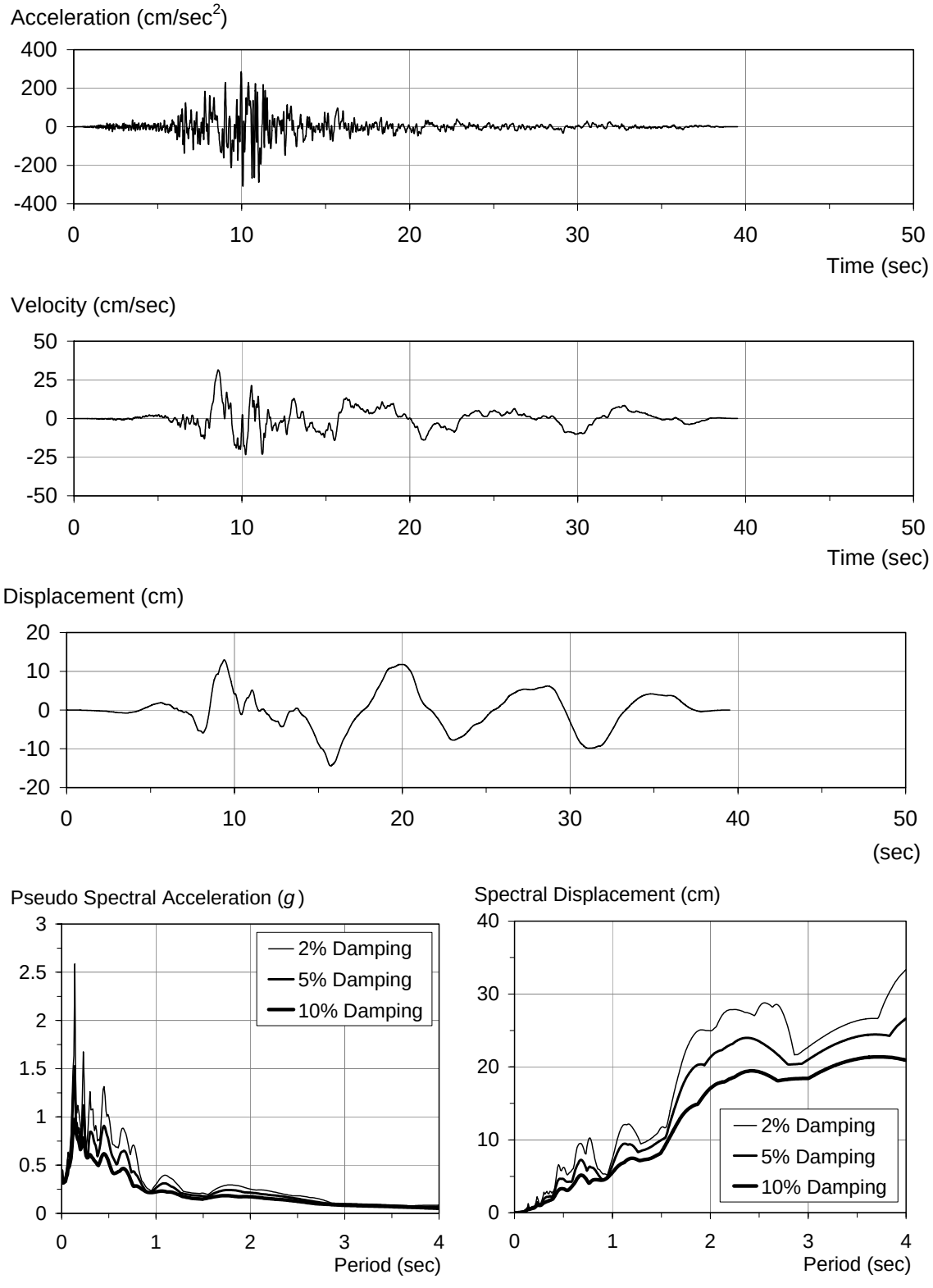


Figure F-26 Characteristics of the E02140 ground motion

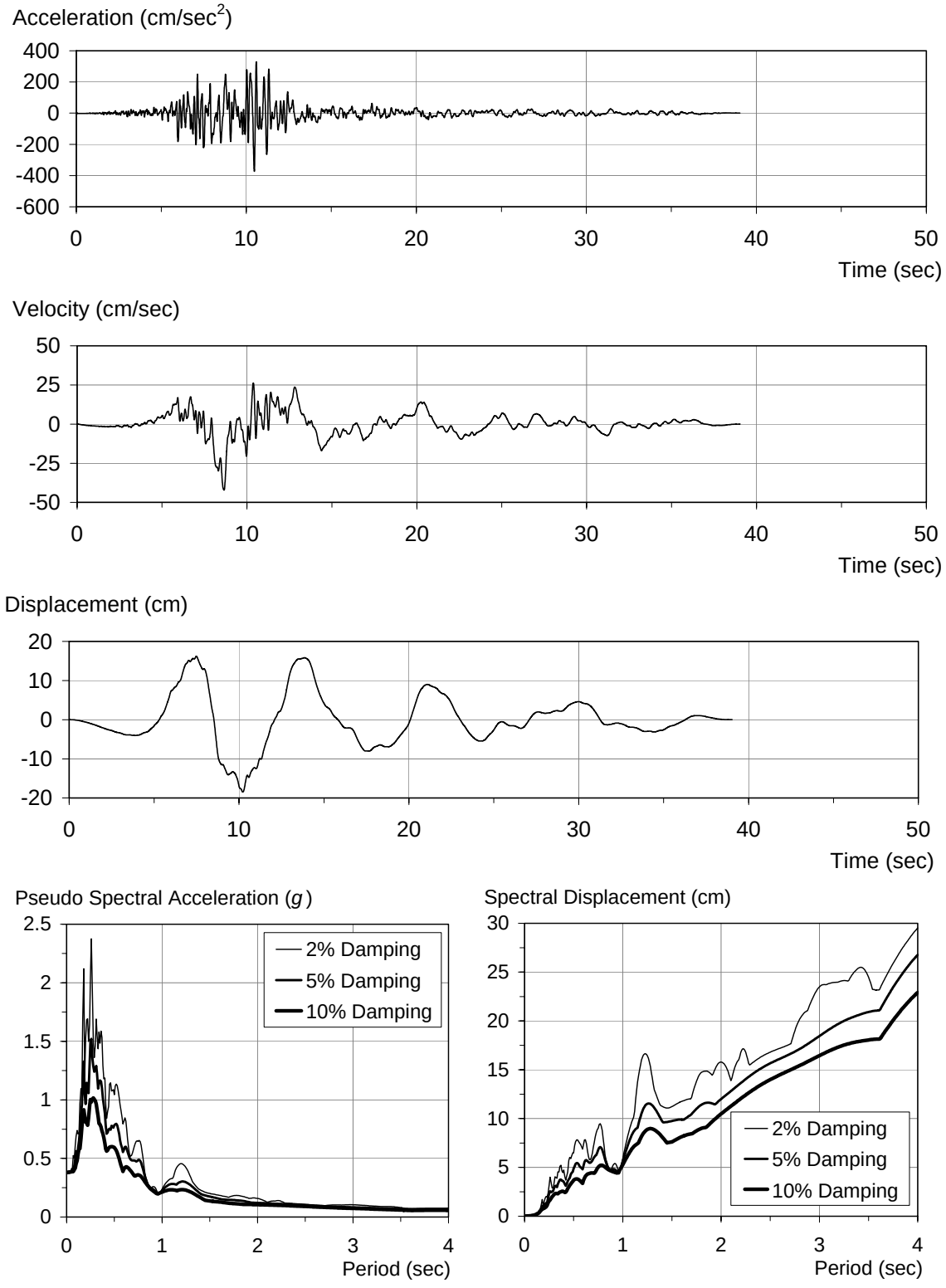


Figure F-27 Characteristics of the E11230 ground motion

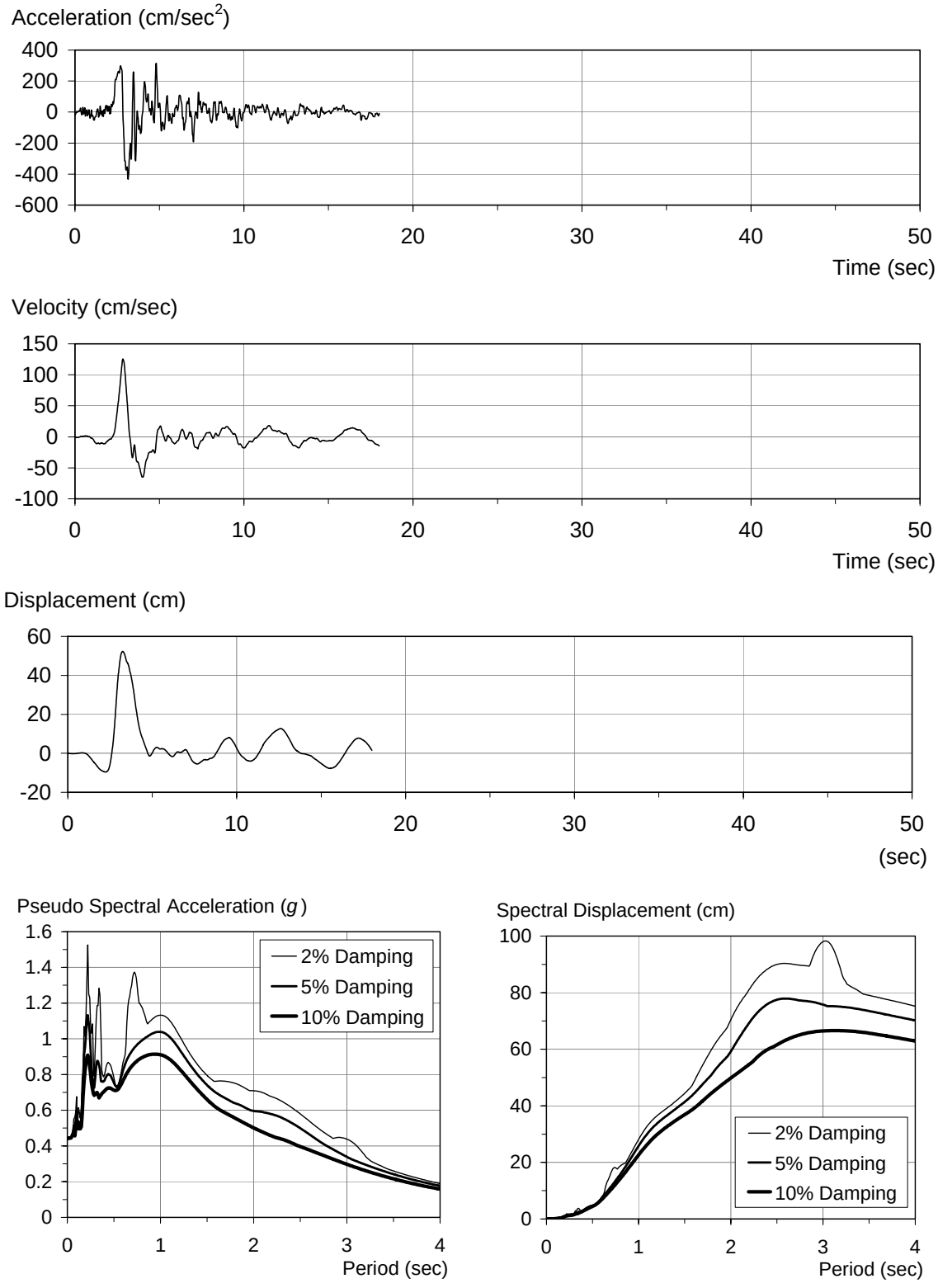


Figure F-28 Characteristics of the ERZMV1 ground motion

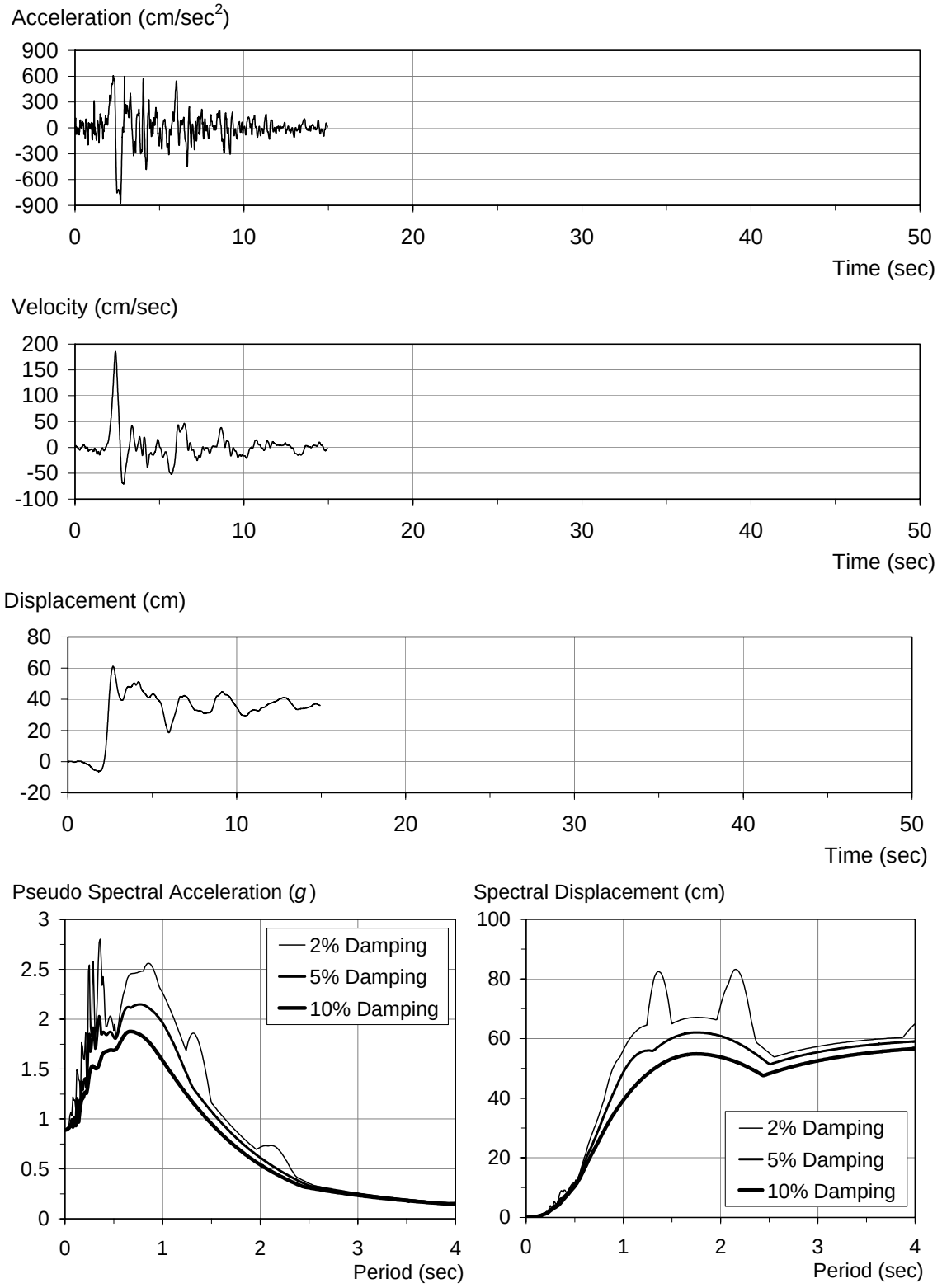


Figure F-29 Characteristics of the RRSMV1 ground motion

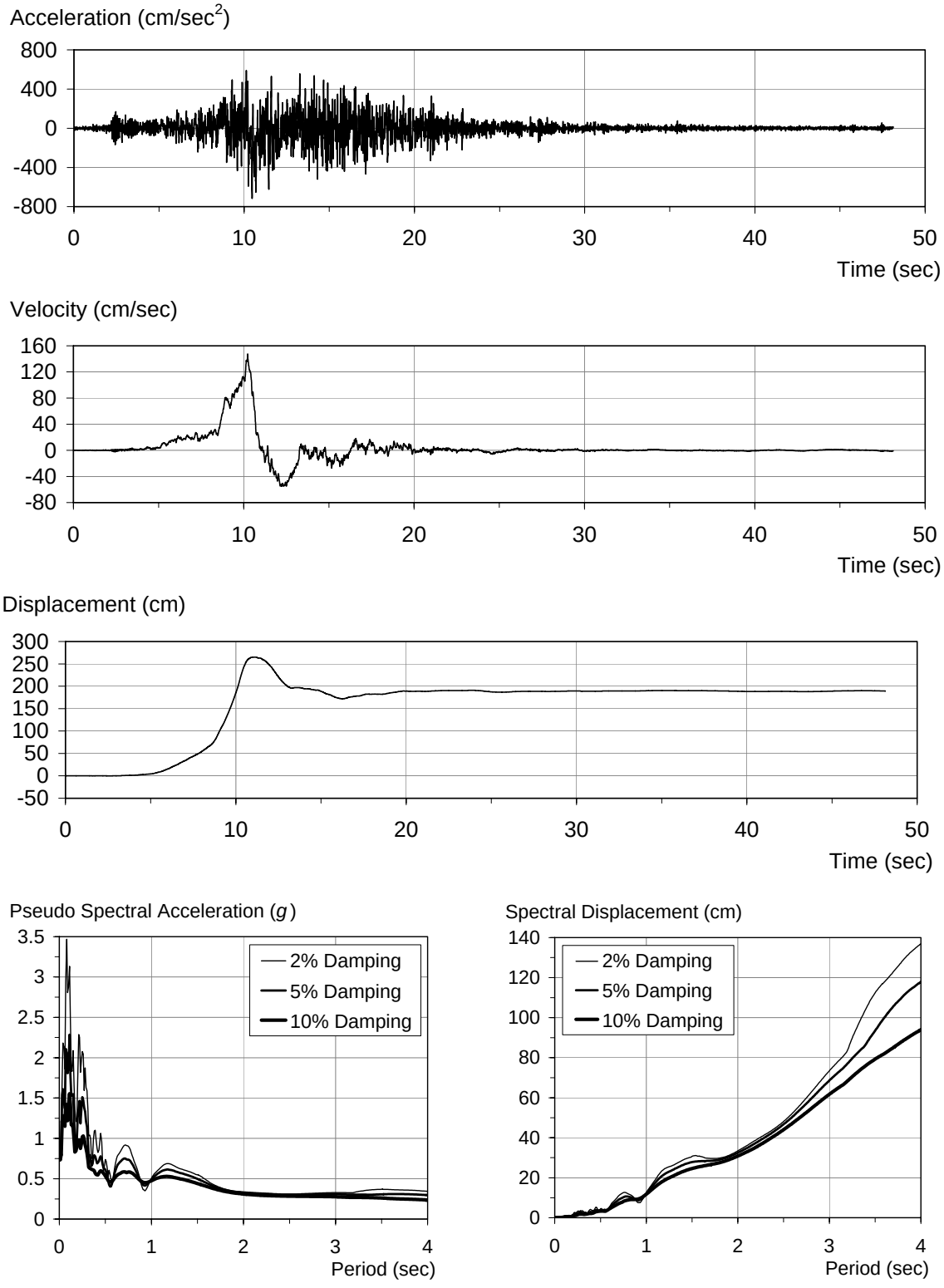


Figure F-30 Characteristics of the LUCMV1 ground motion

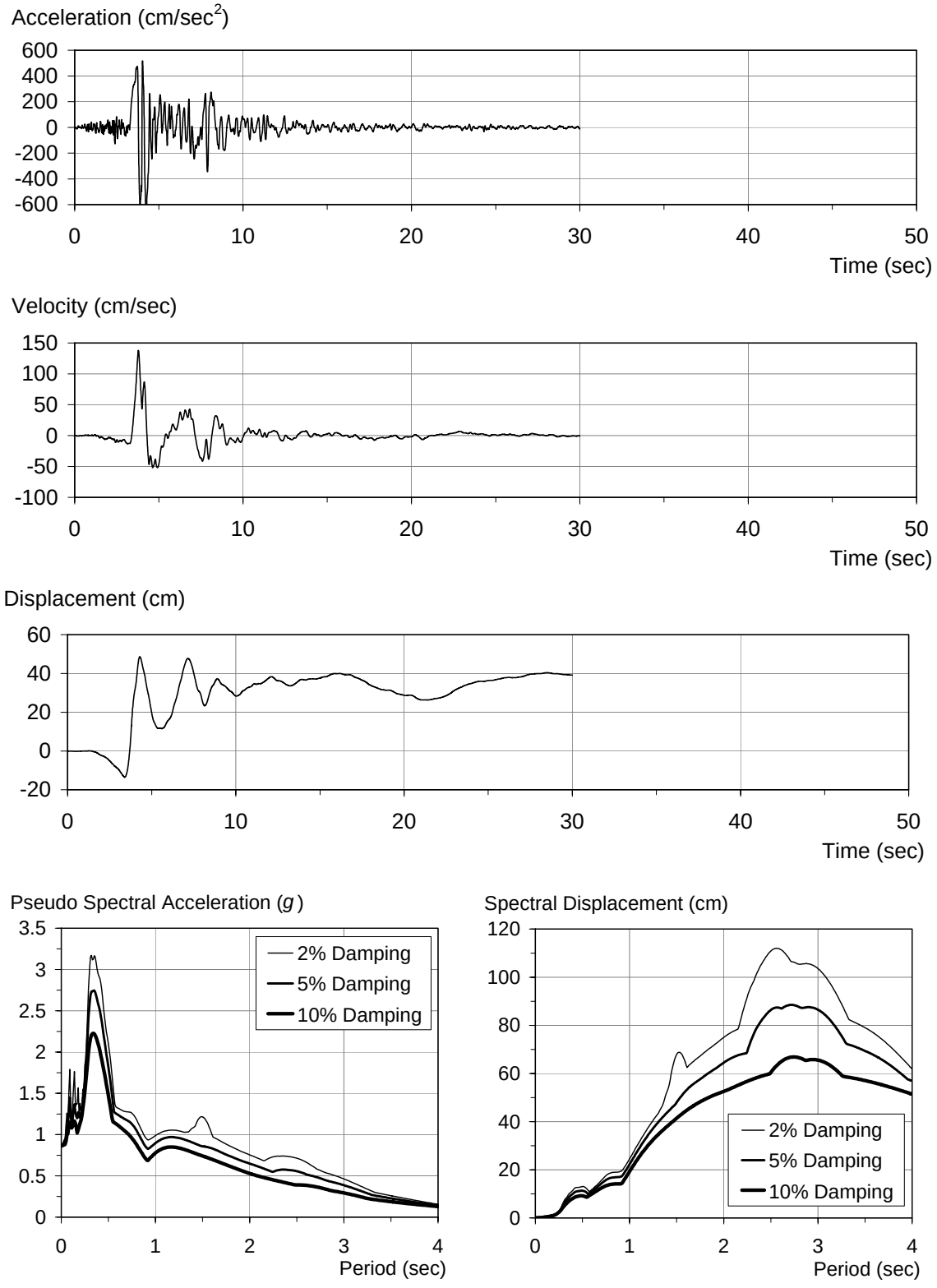


Figure F-31 Characteristics of the SCHMV1 ground motion

### *F.8.2 Responses to Ordinary (Site Class C) Motions*

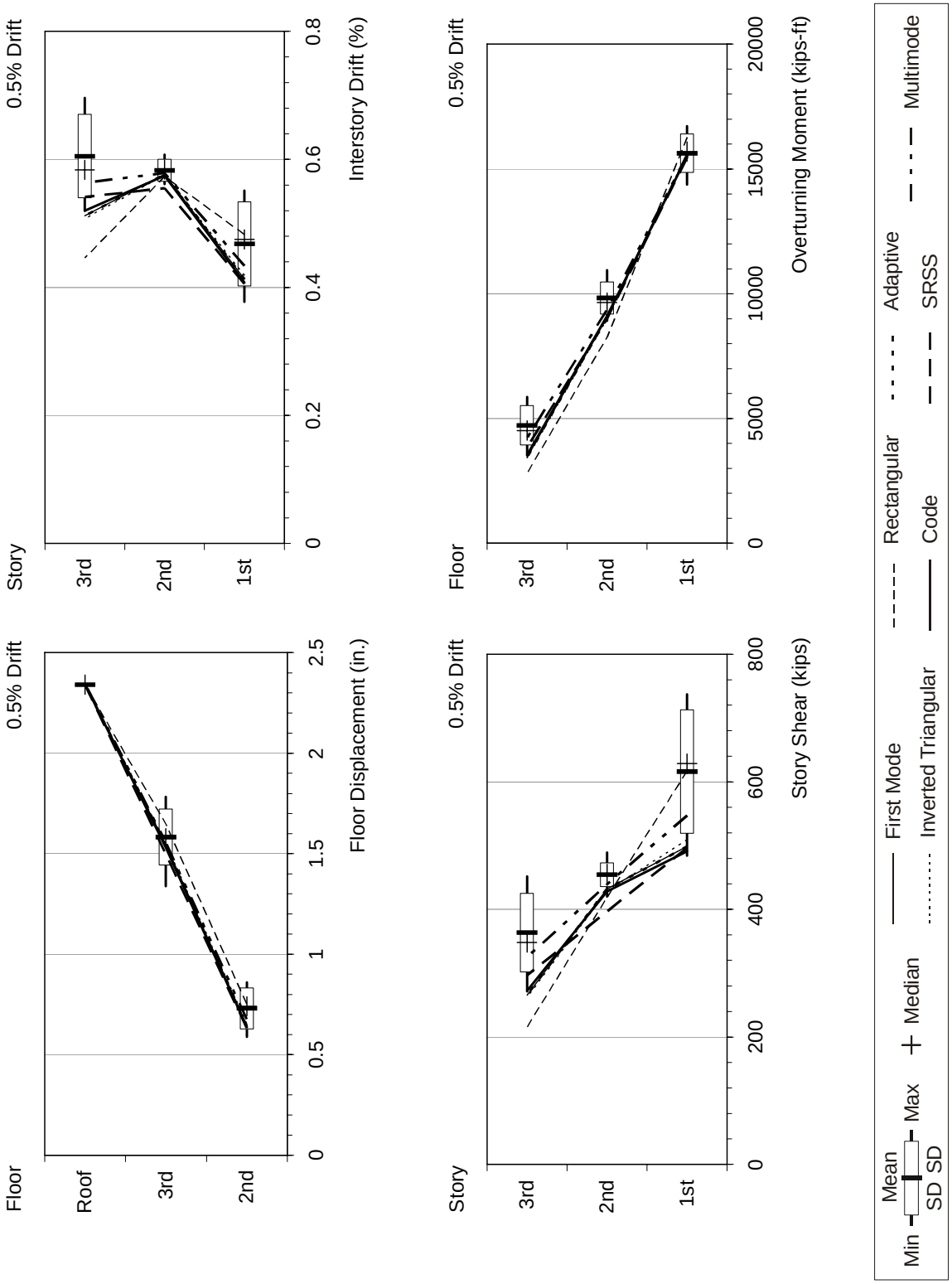


Figure F-32 Response quantities of the 3-story building for 0.5% drift level

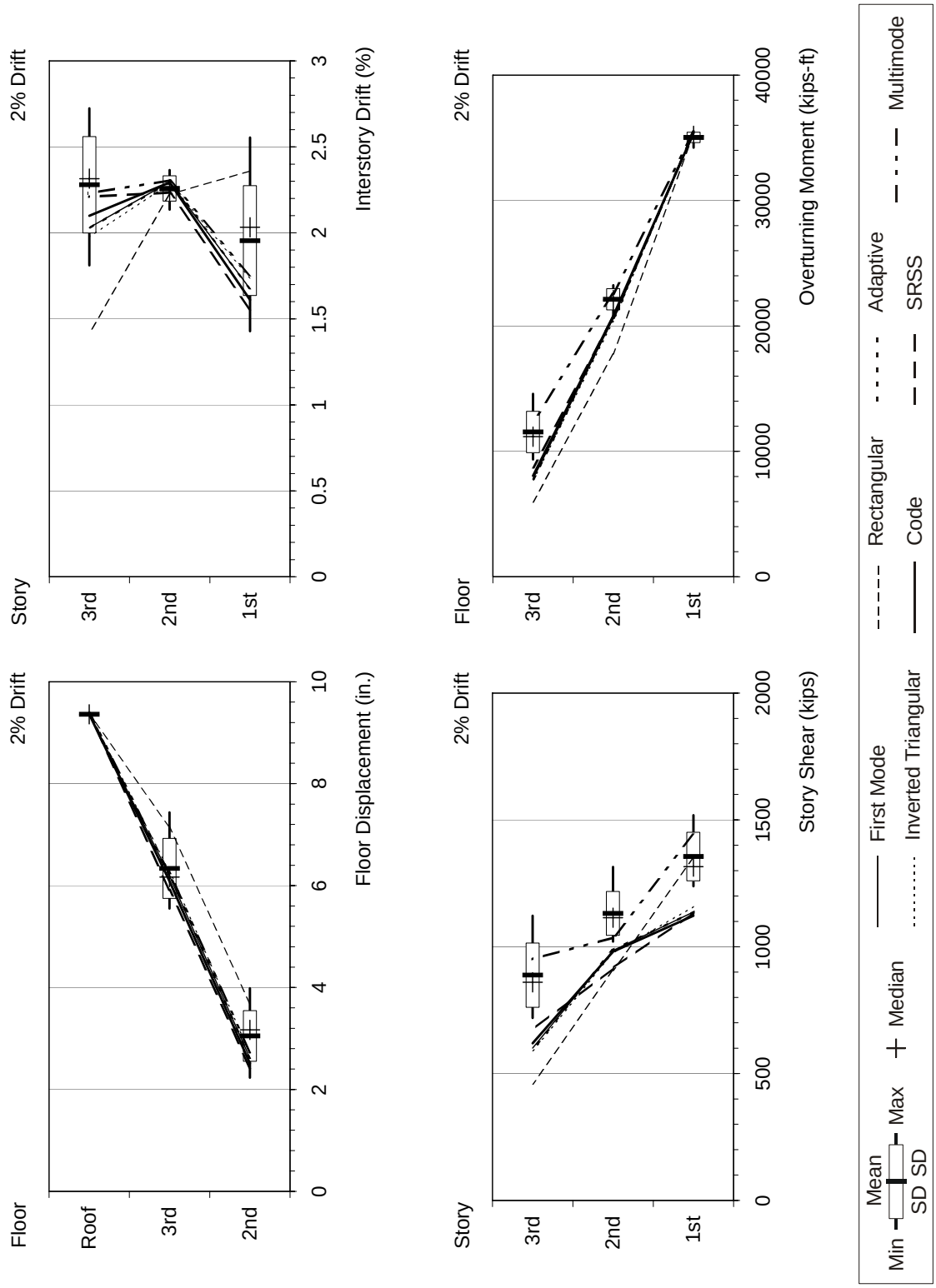


Figure F-33 Response quantities of the 3-story building for 2% drift level

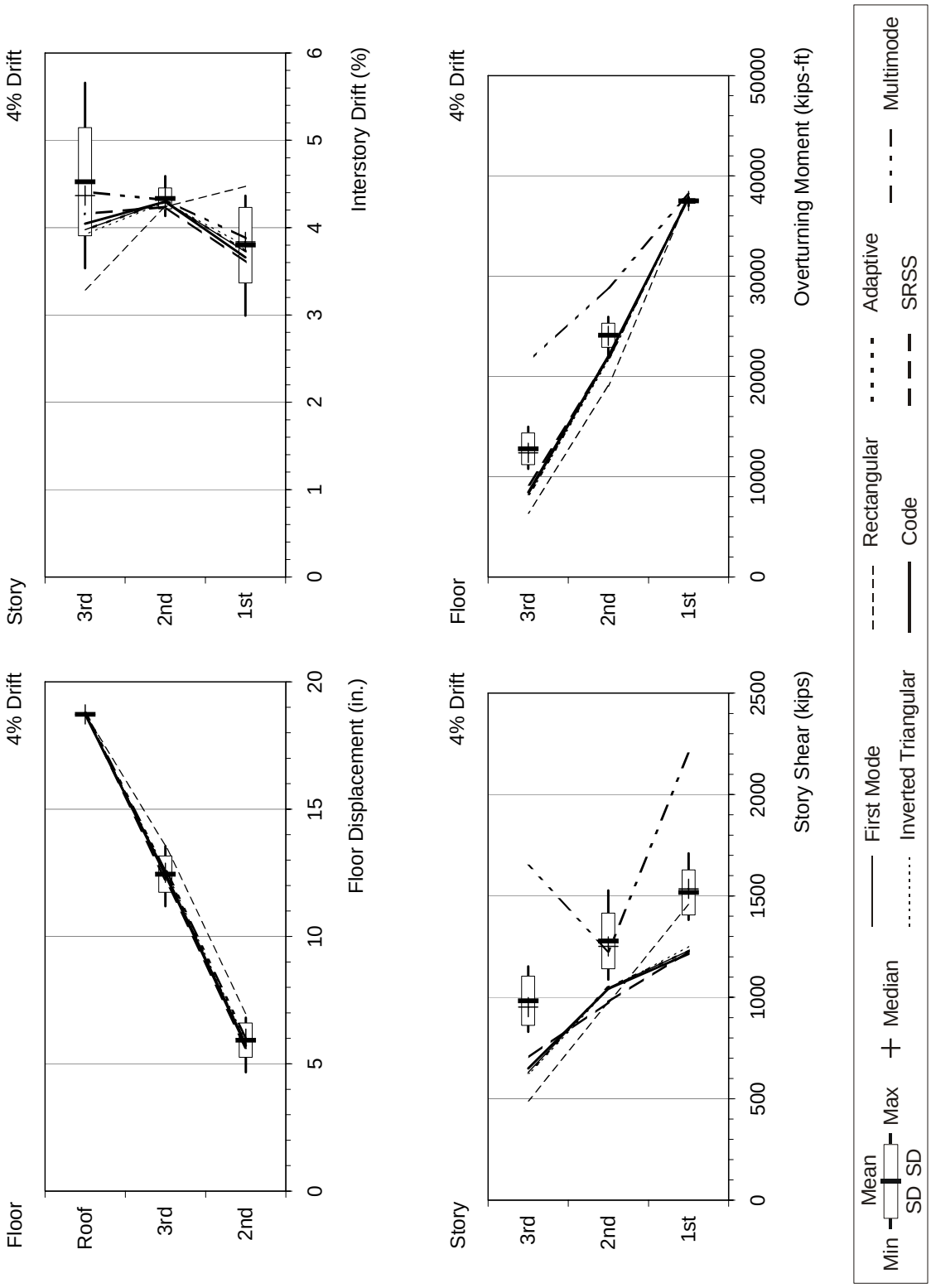


Figure F-34 Response quantities of the 3-story building for 4% drift level

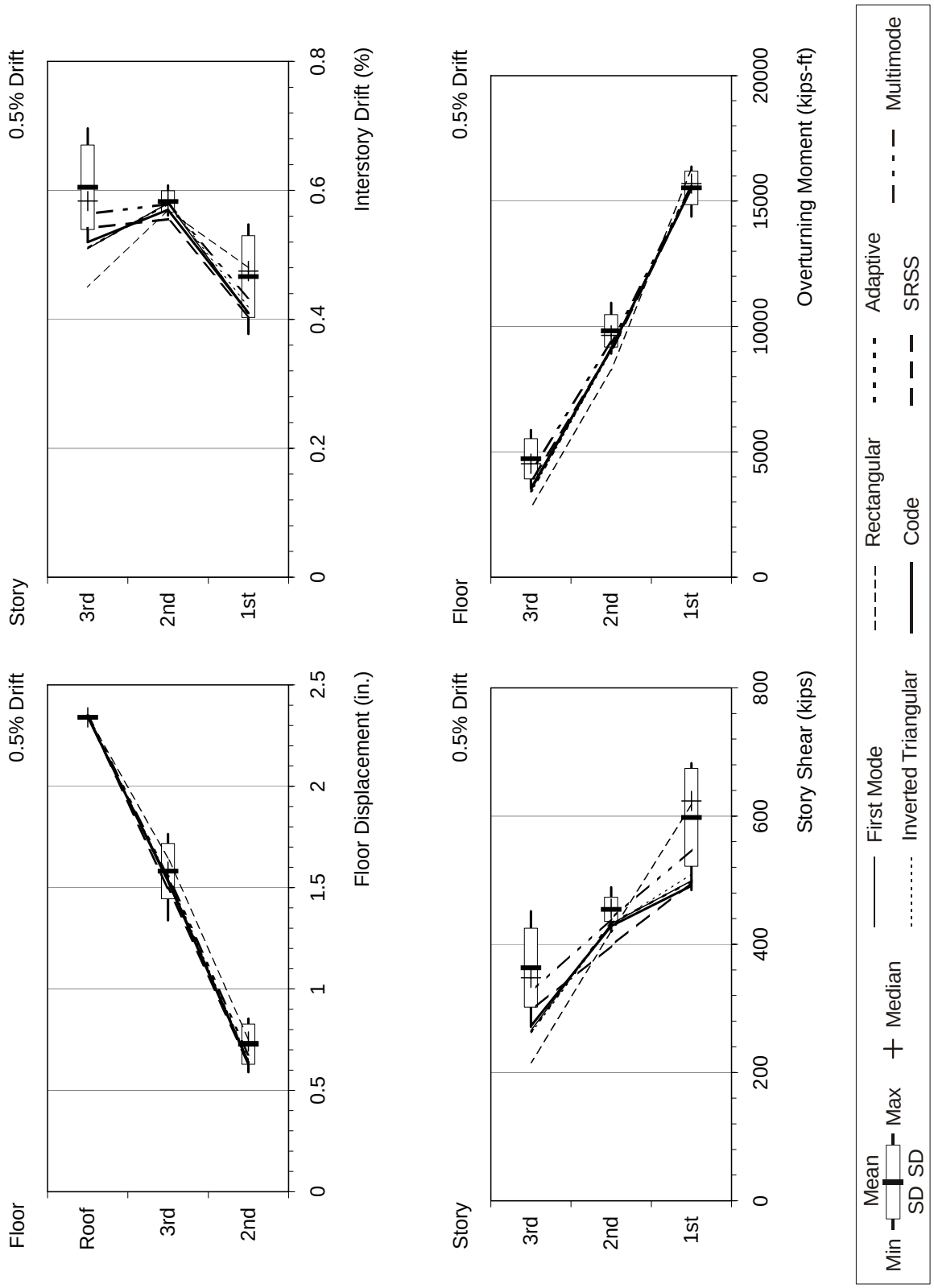


Figure F-35 Response quantities of the 3-story weak-story building for 0.5% drift level

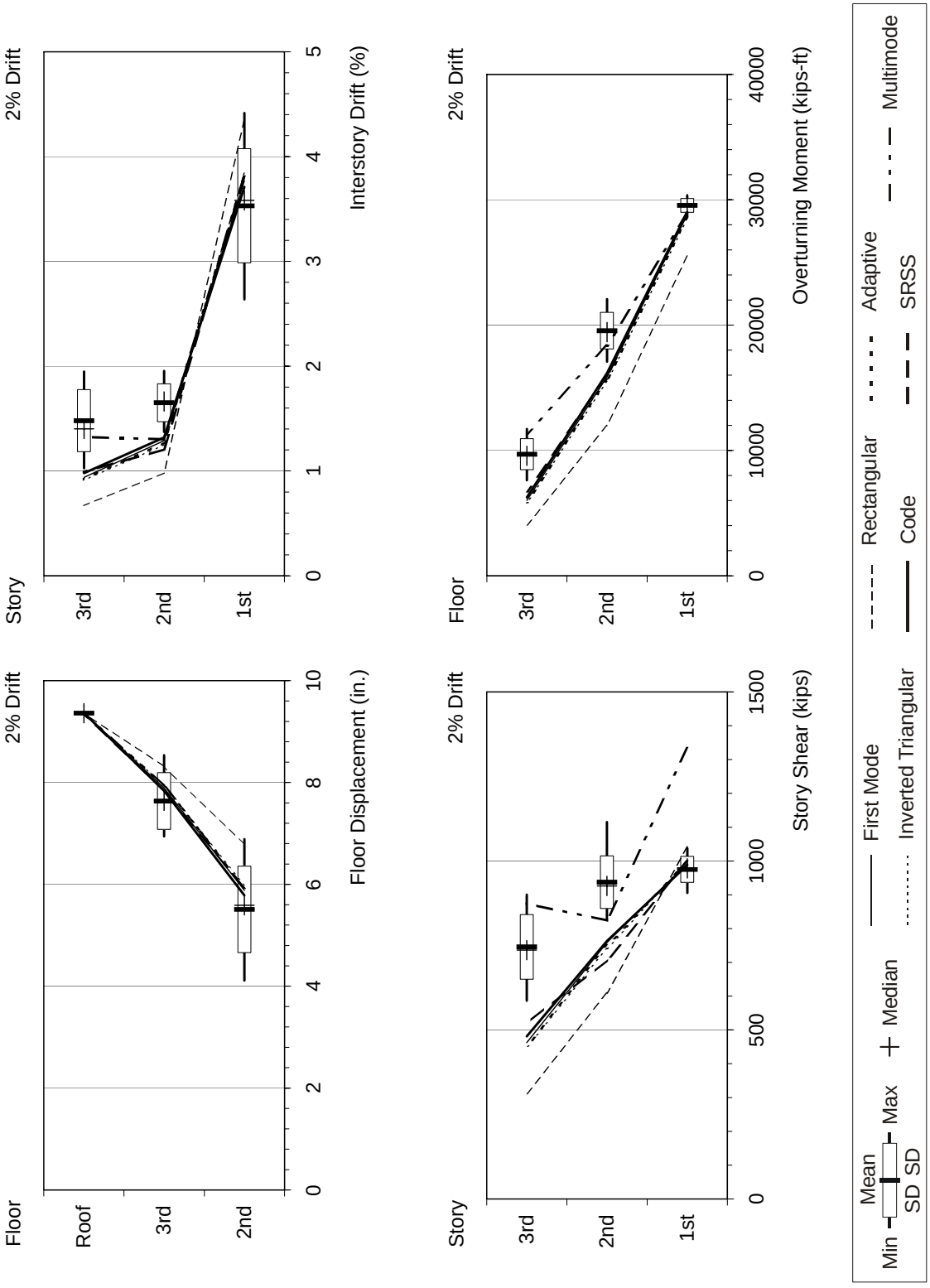


Figure F-36 Response quantities of the 3-story weak-story building for 2% drift level

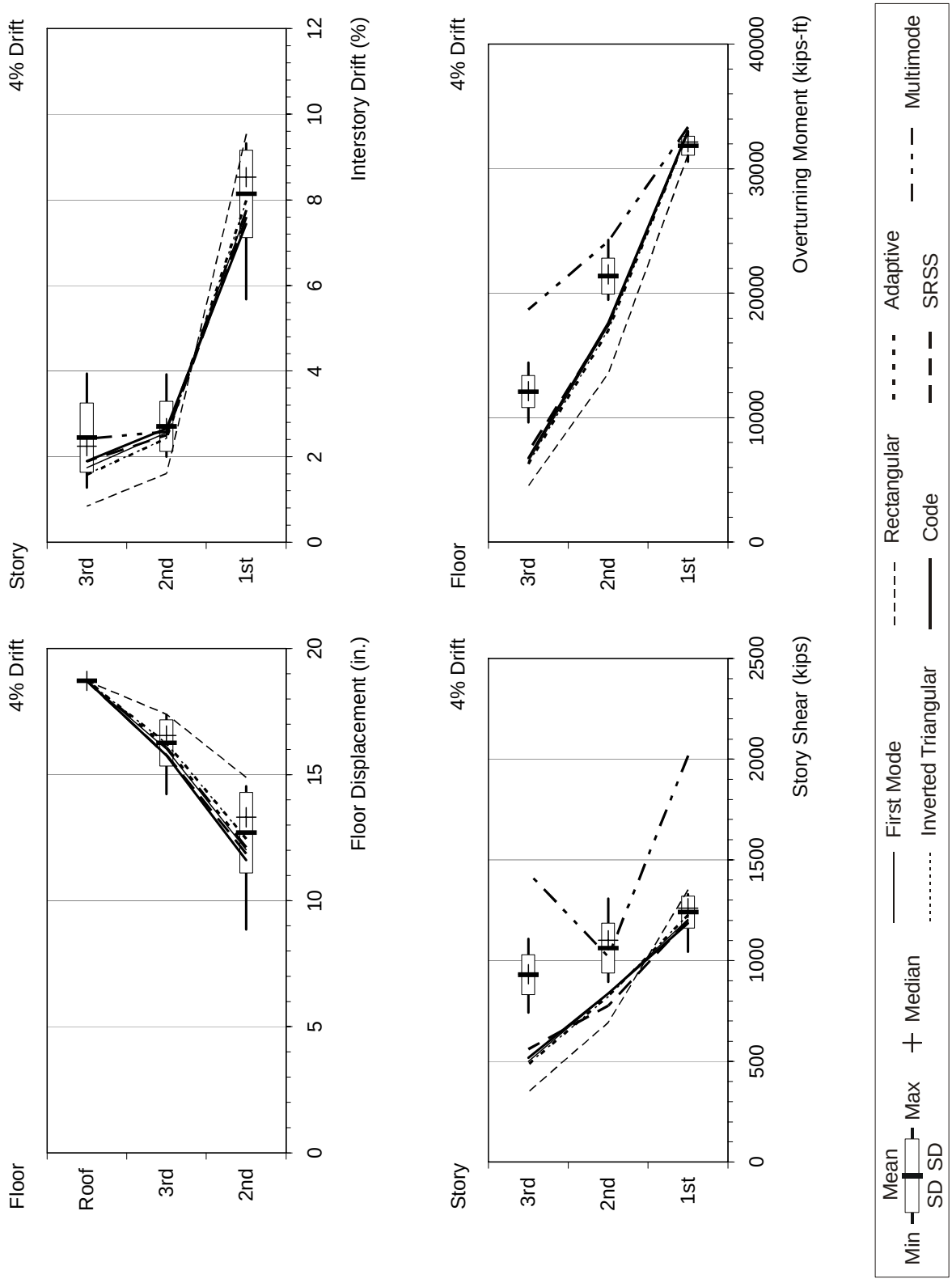


Figure F-37 Response quantities of the 3-story weak-story building for 4% drift level

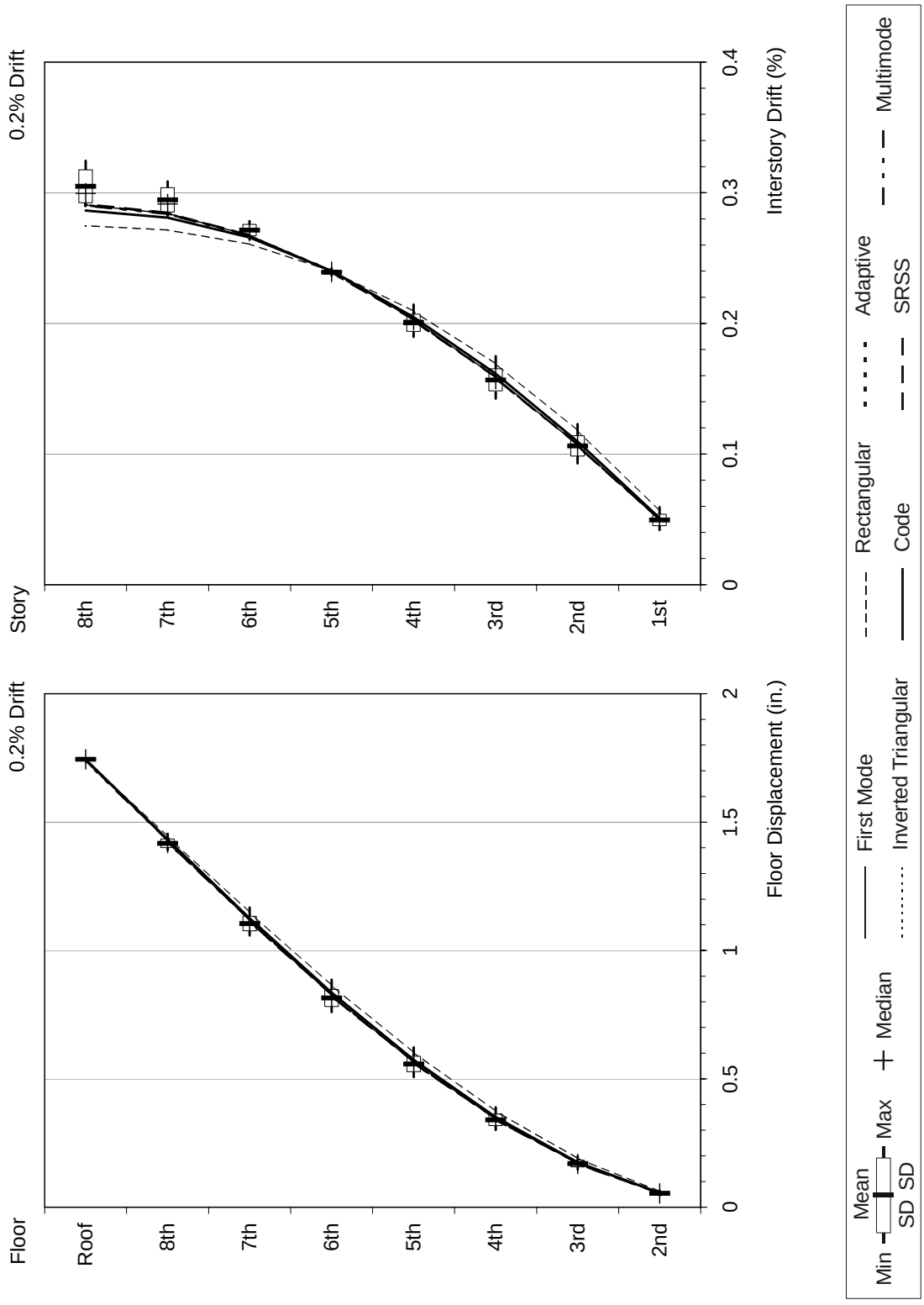


Figure F-38 Response quantities of the 8-story building for 0.2% drift level

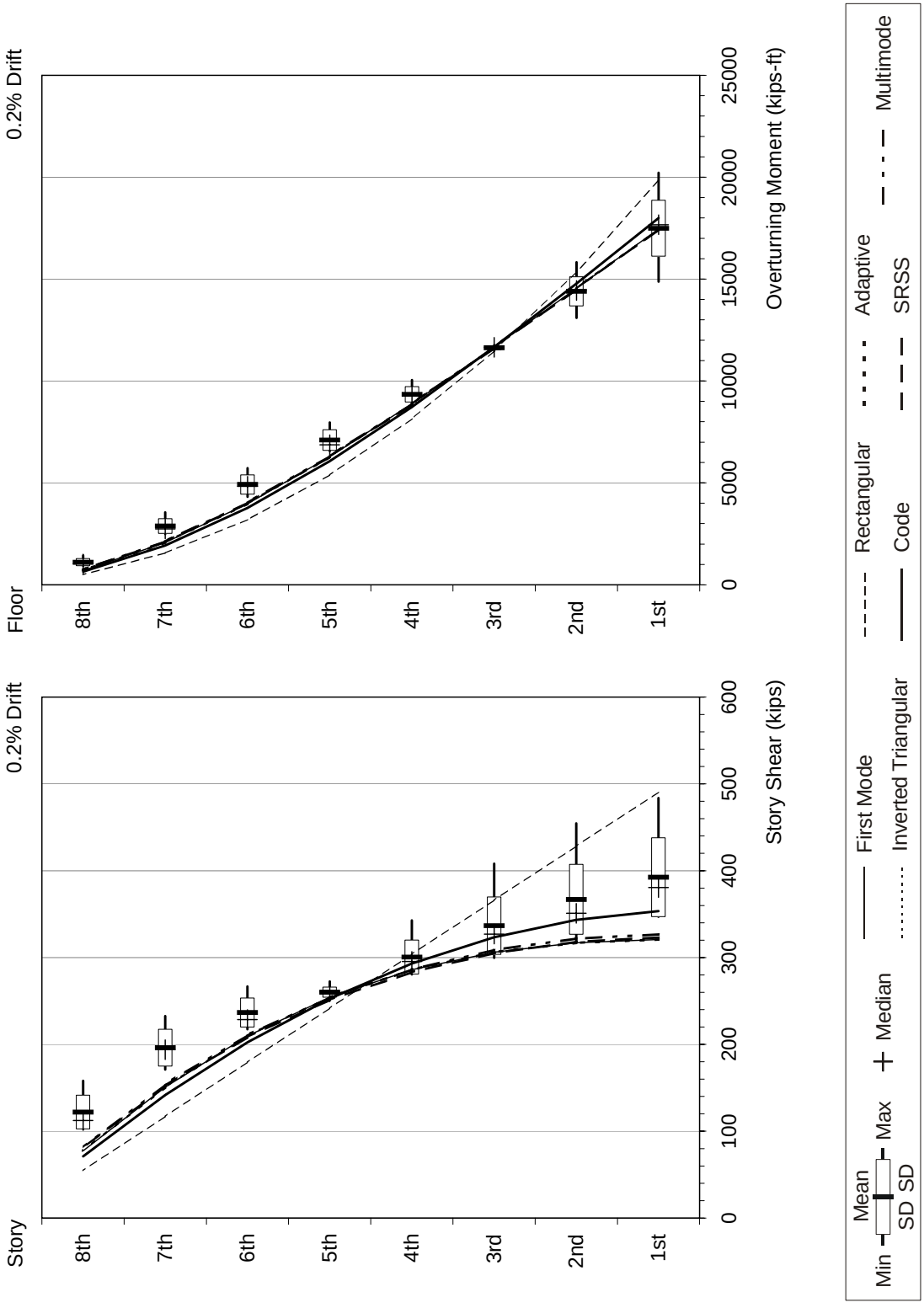


Figure F-38 Response quantities of the 8-story building for 0.2% drift level (continued)

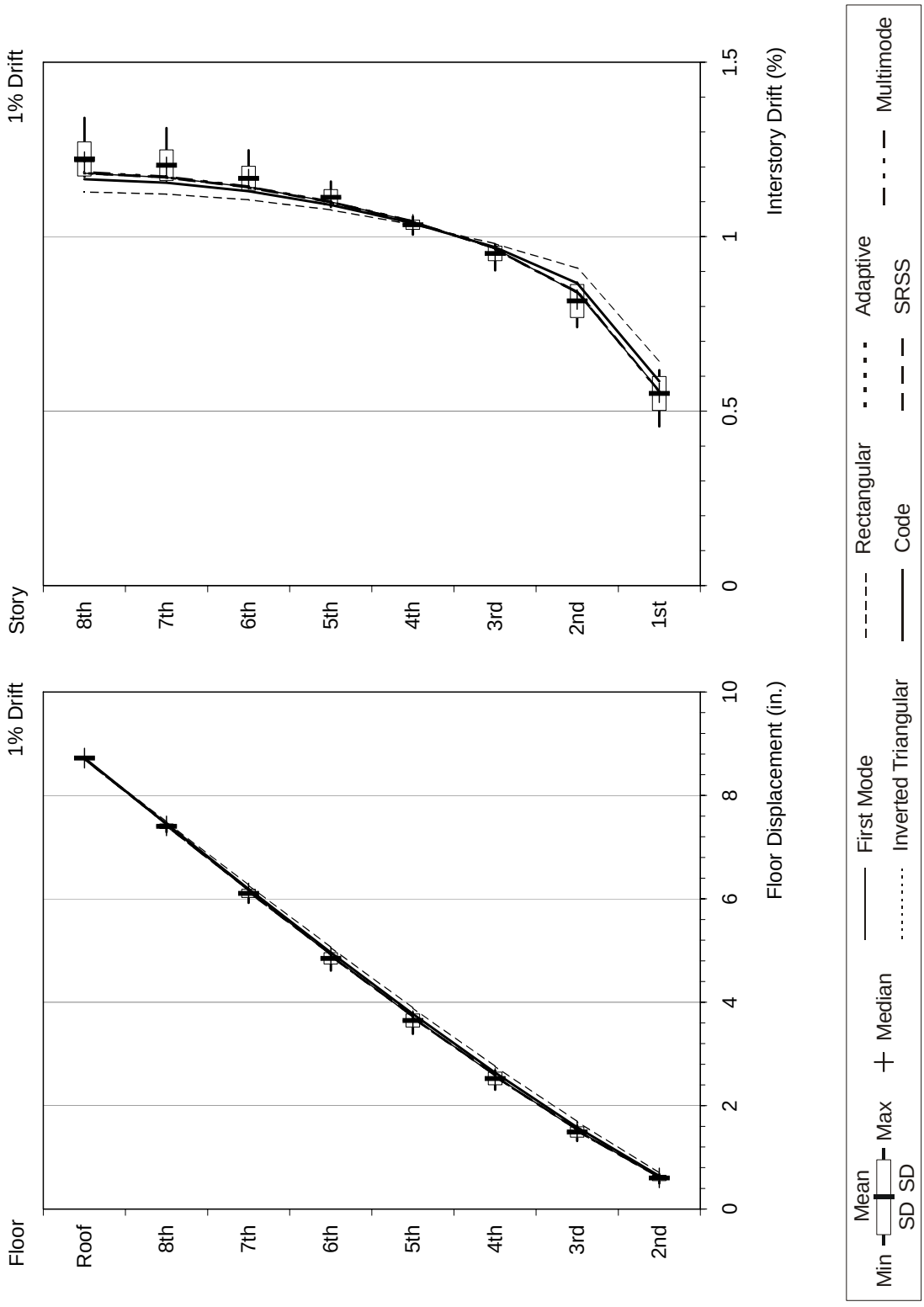


Figure F-39 Response quantities of the 8-story building for 1% drift level

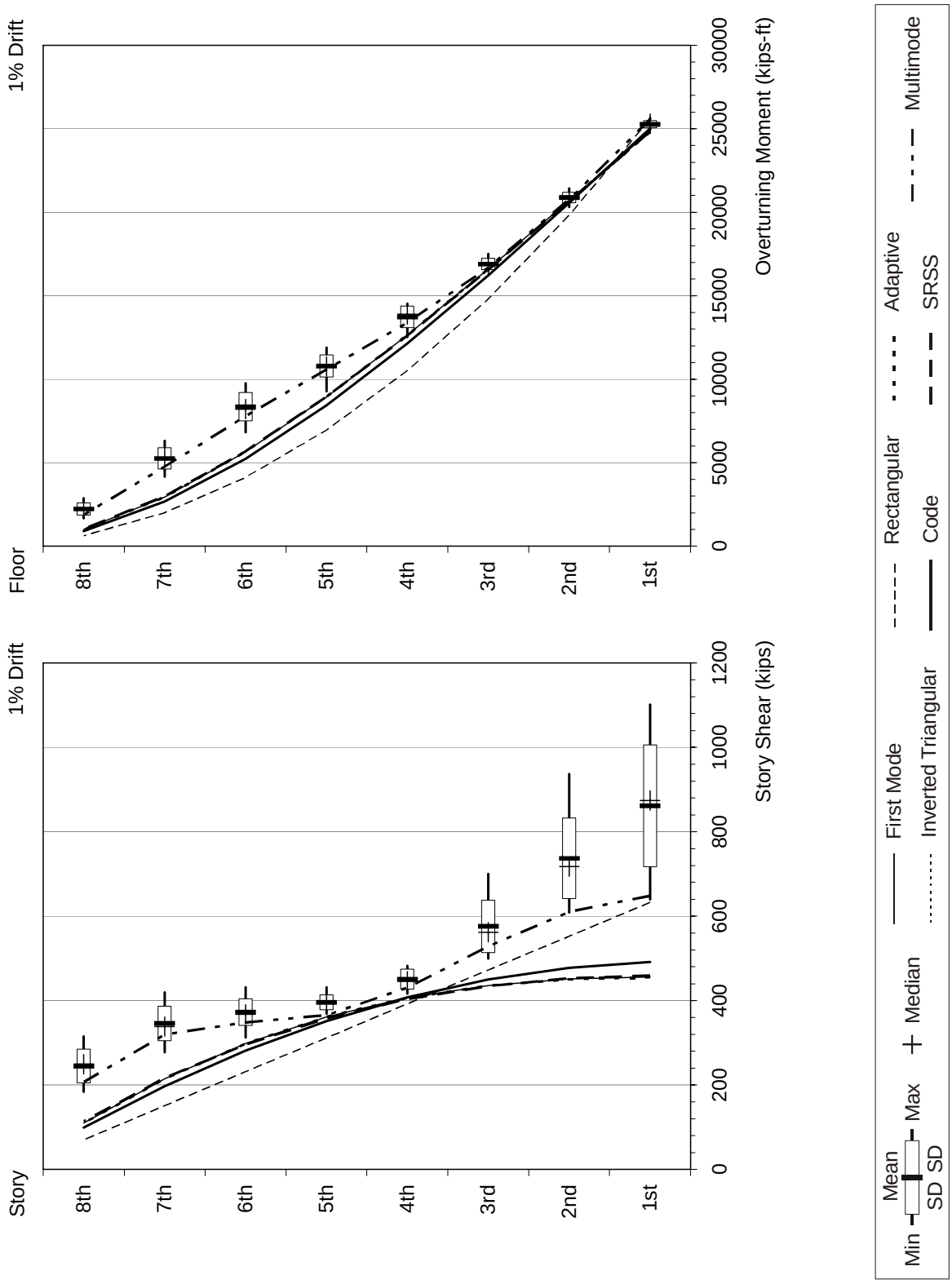


Figure F-39 Response quantities of the 8-story building for 1% drift level (continued)

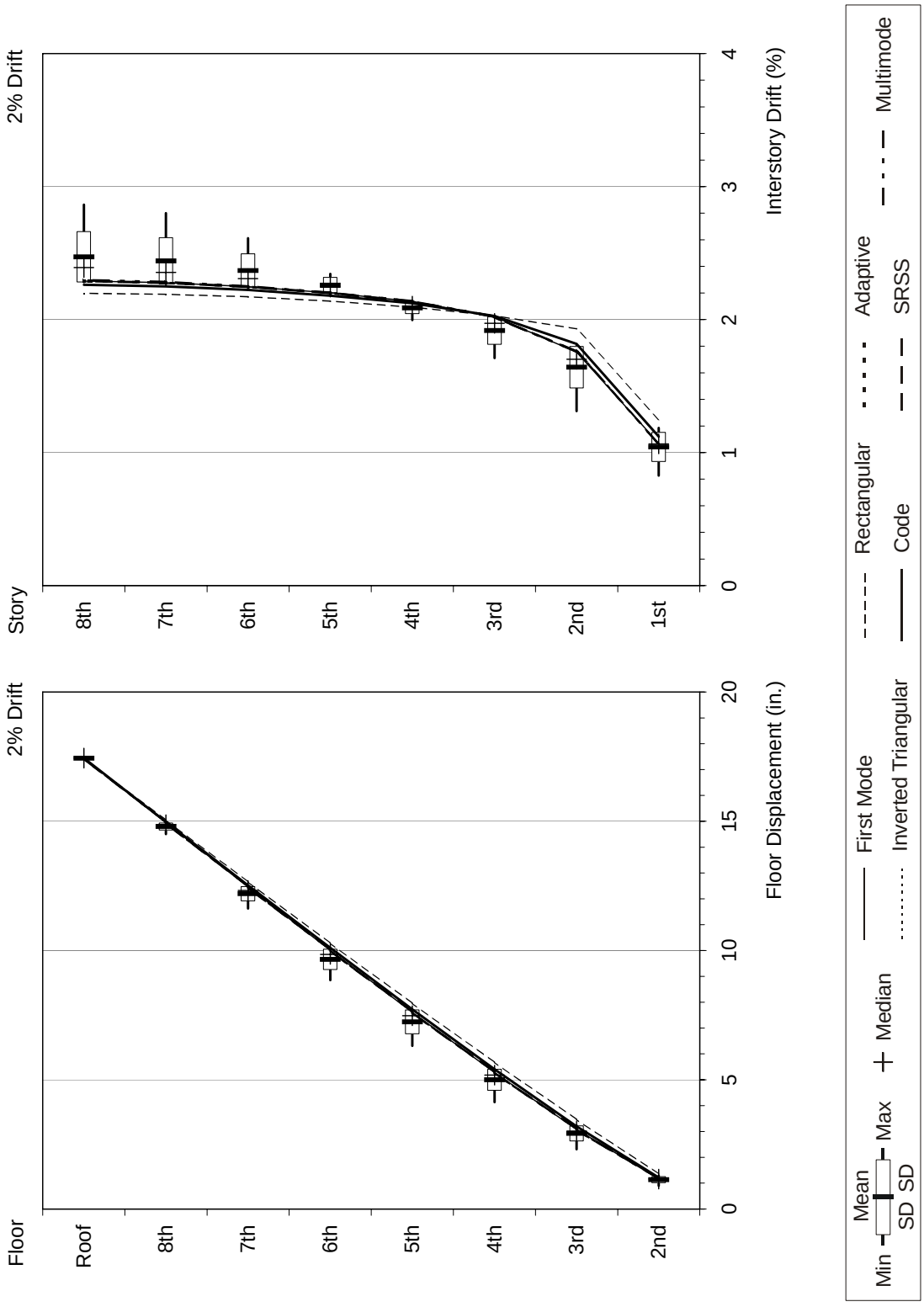


Figure F-40 Response quantities of the 8-story building for 2% drift level

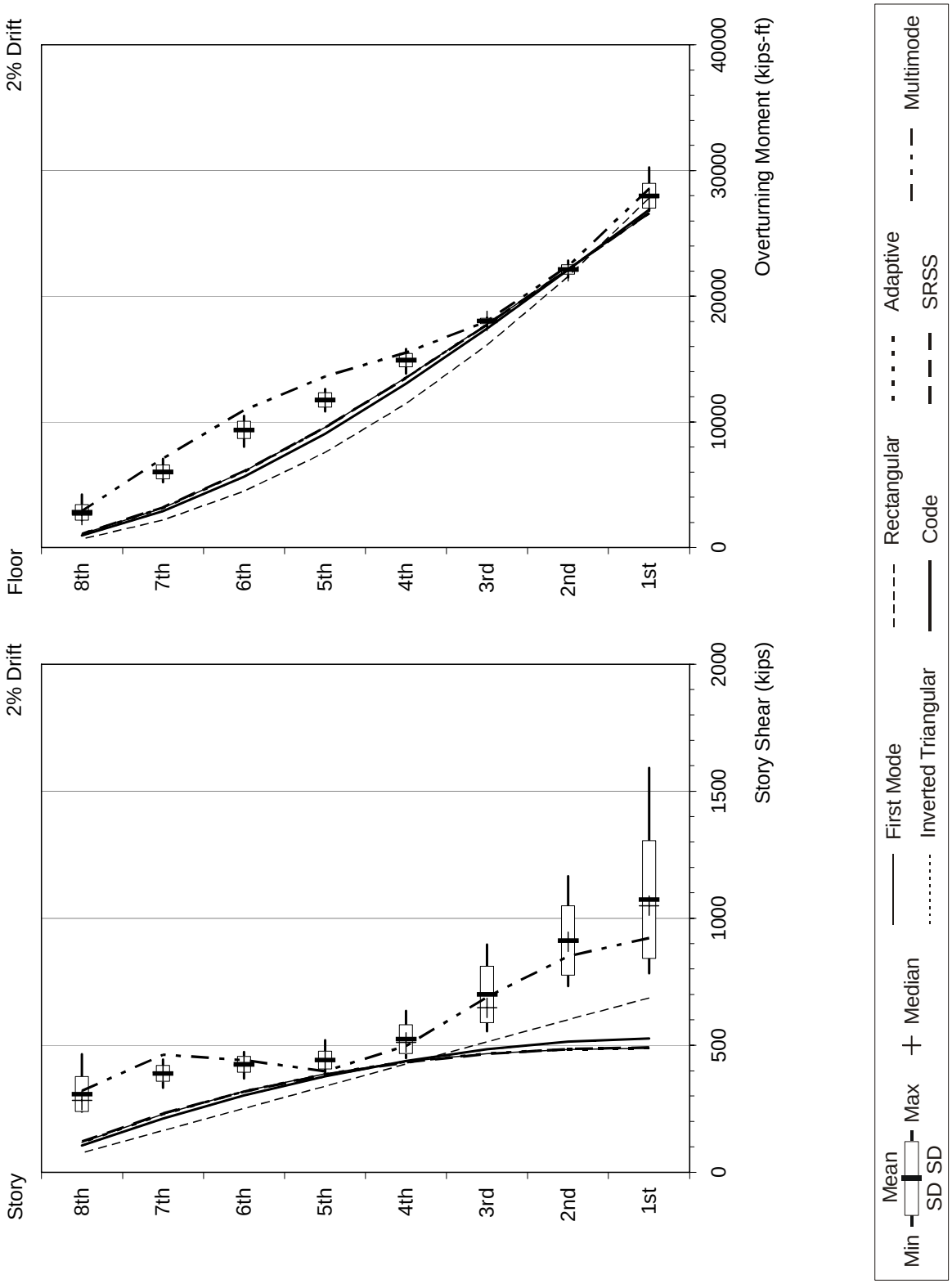


Figure F-40 Response quantities of the 8-story building for 2% drift level (continued)

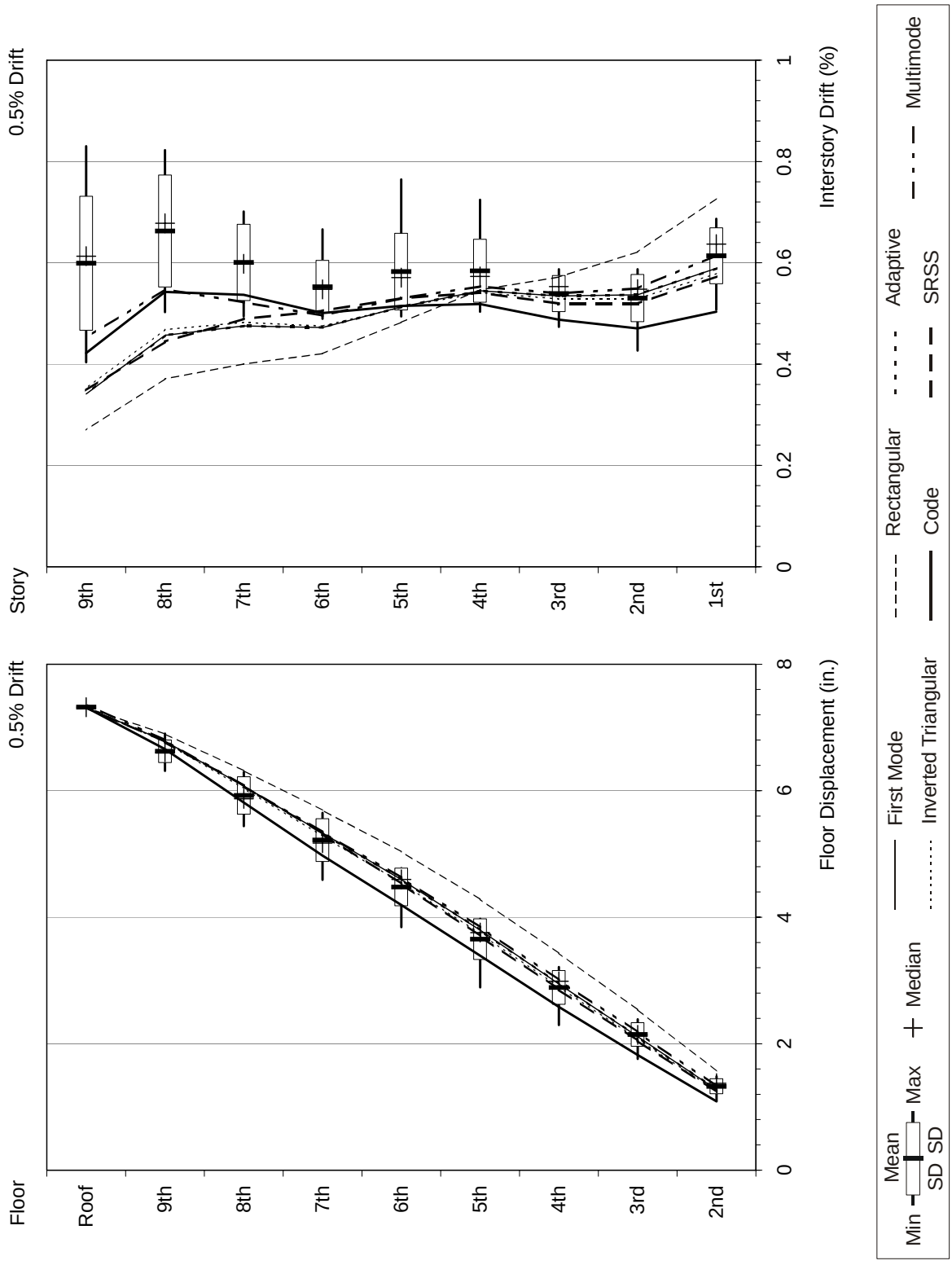


Figure F-41 Response quantities of the 9-story building for 0.5% drift level

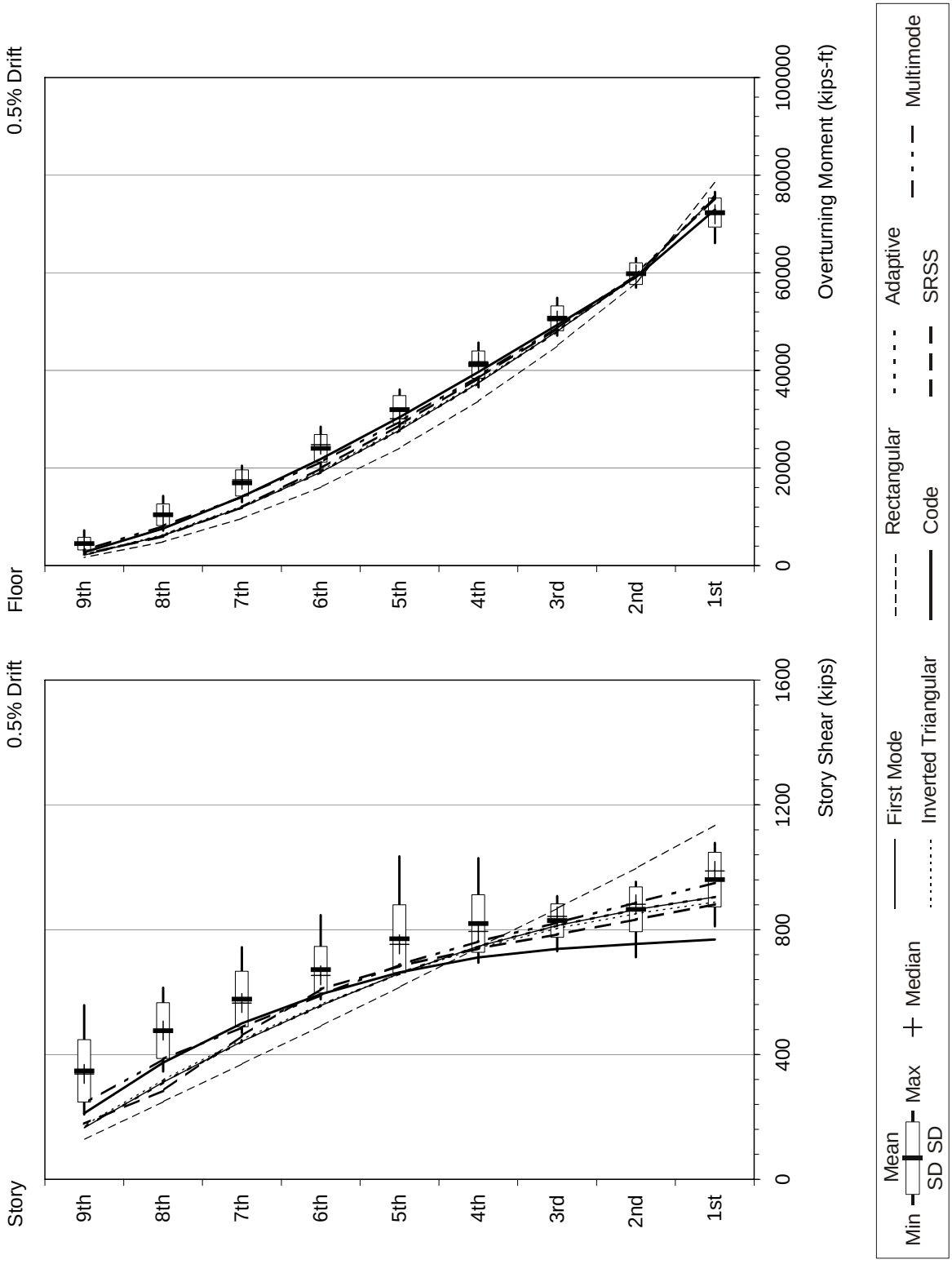


Figure F-41 Response quantities of the 9-story building for 0.5% drift level (continued)

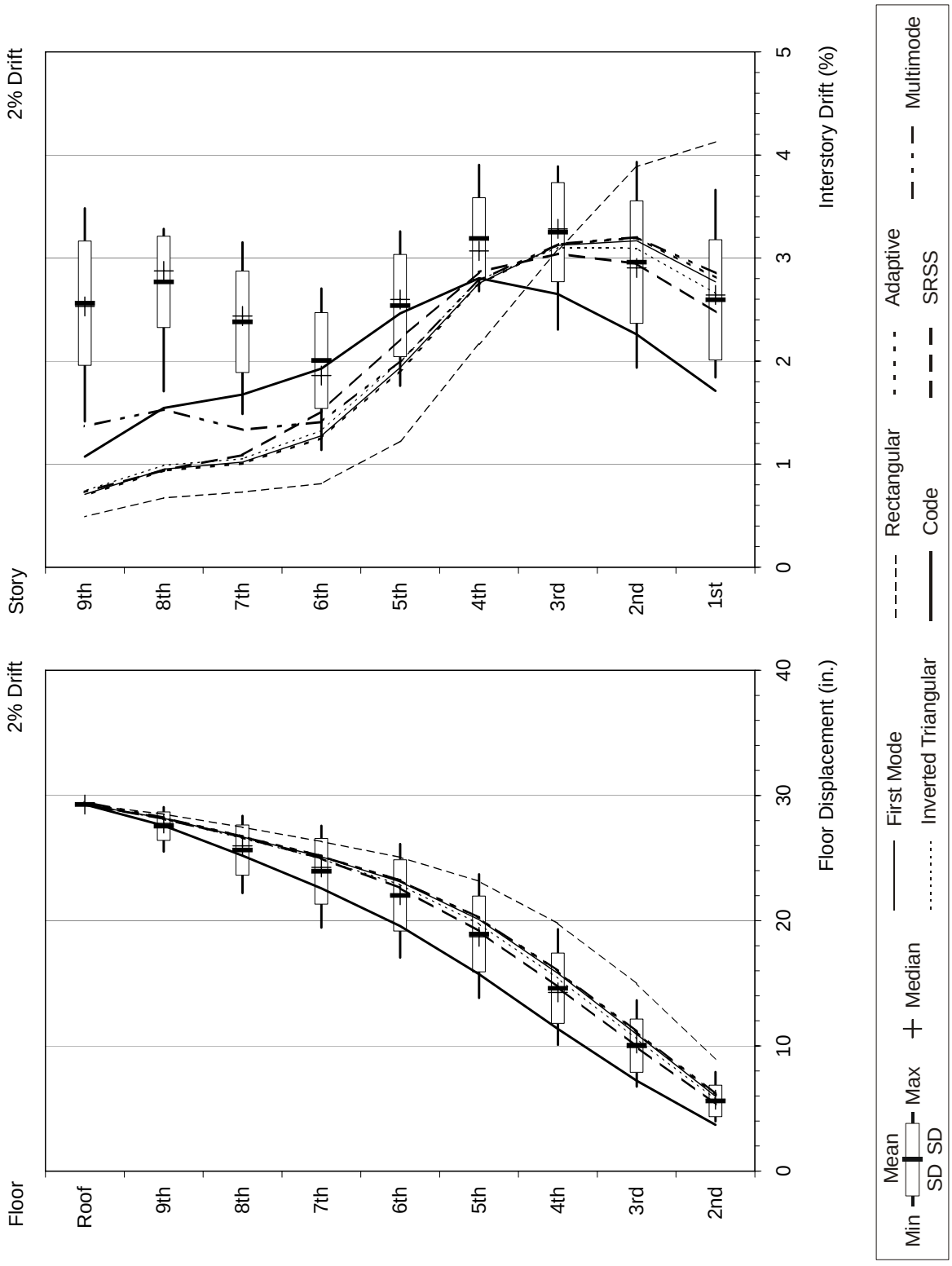


Figure F-42 Response quantities of the 9-story building for 2% drift level

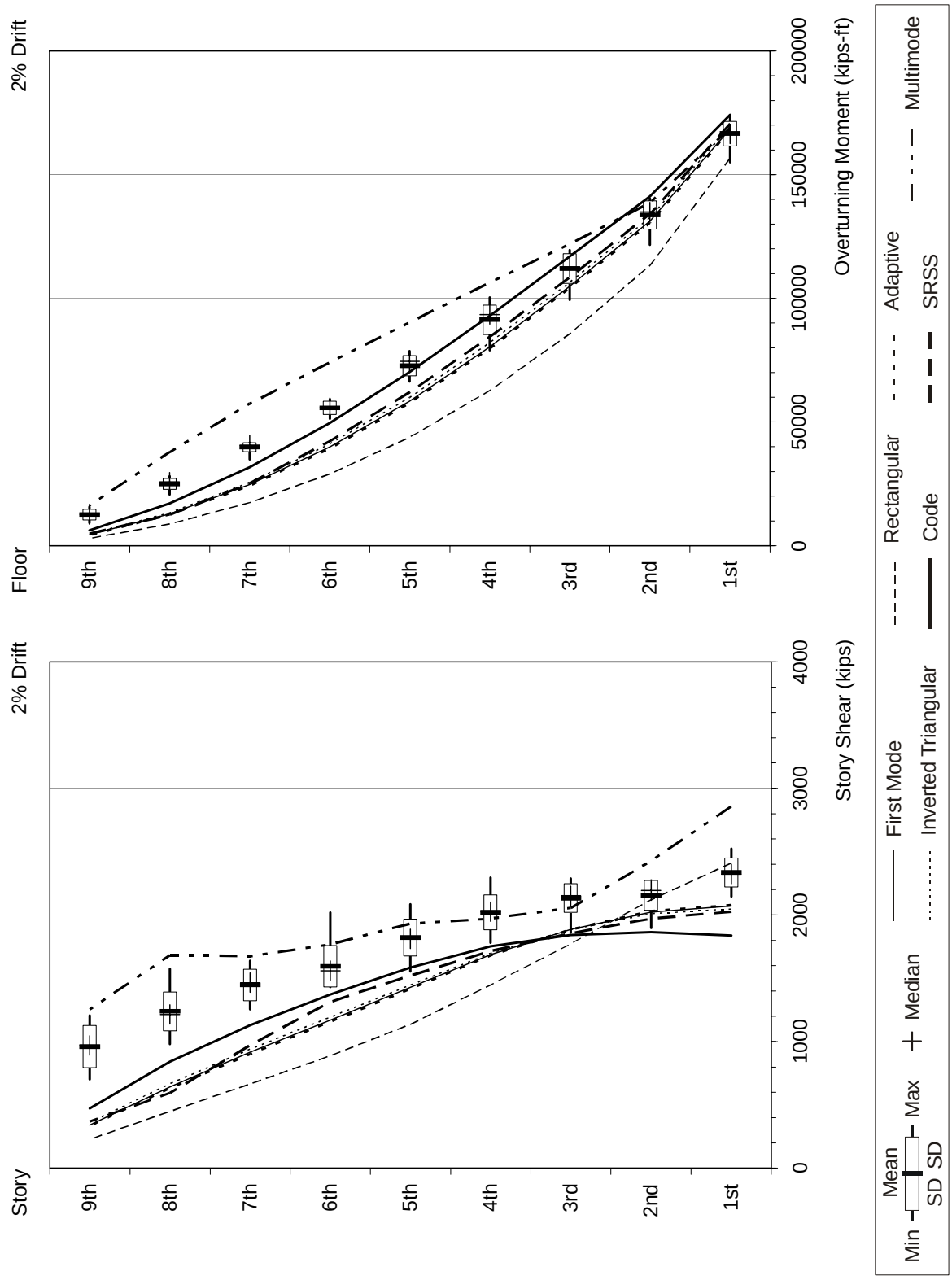


Figure F-42 Response quantities of the 9-story building for 2% drift level (continued)

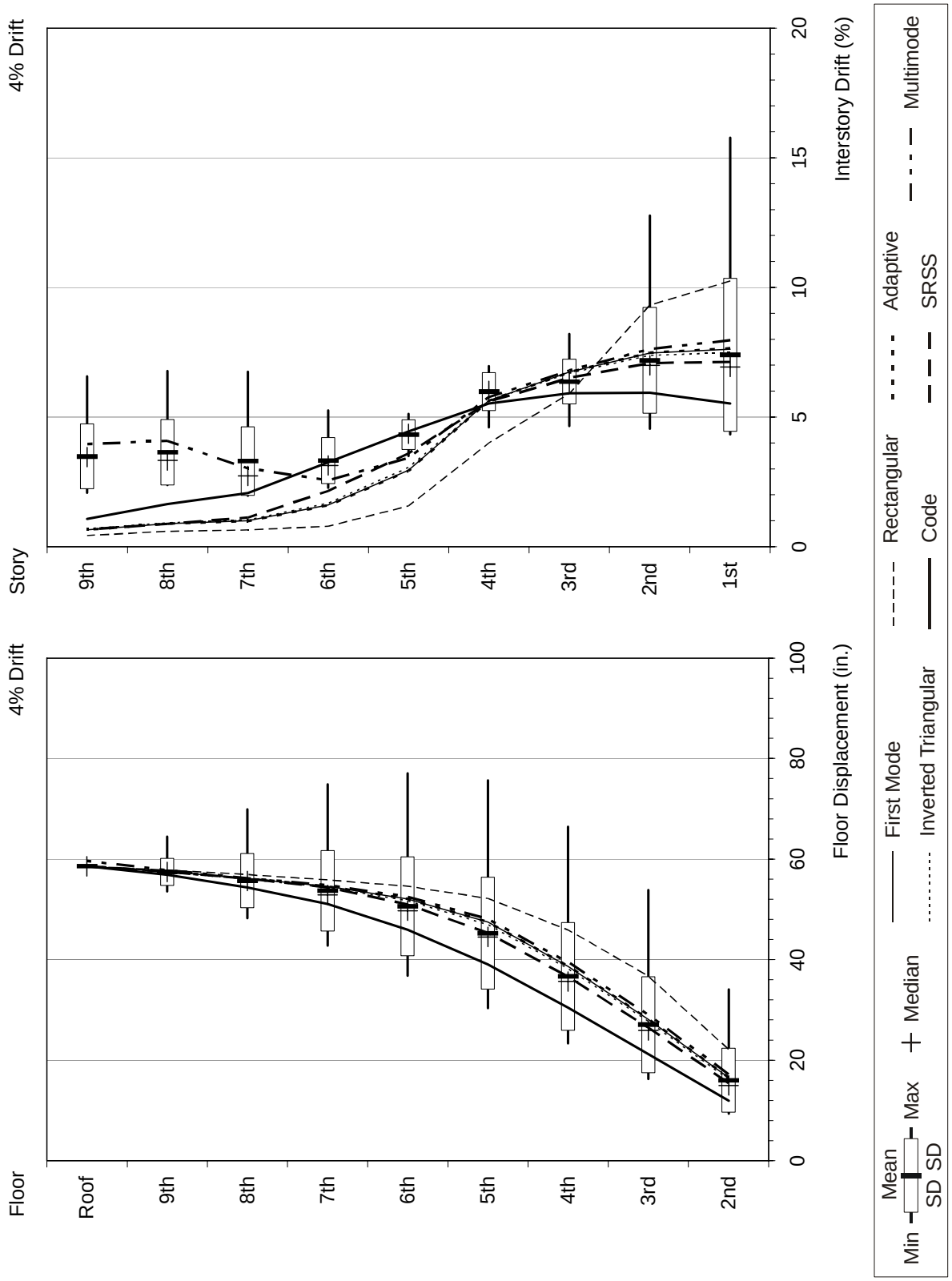


Figure F-43 Response quantities of the 9-story building for 4% drift level

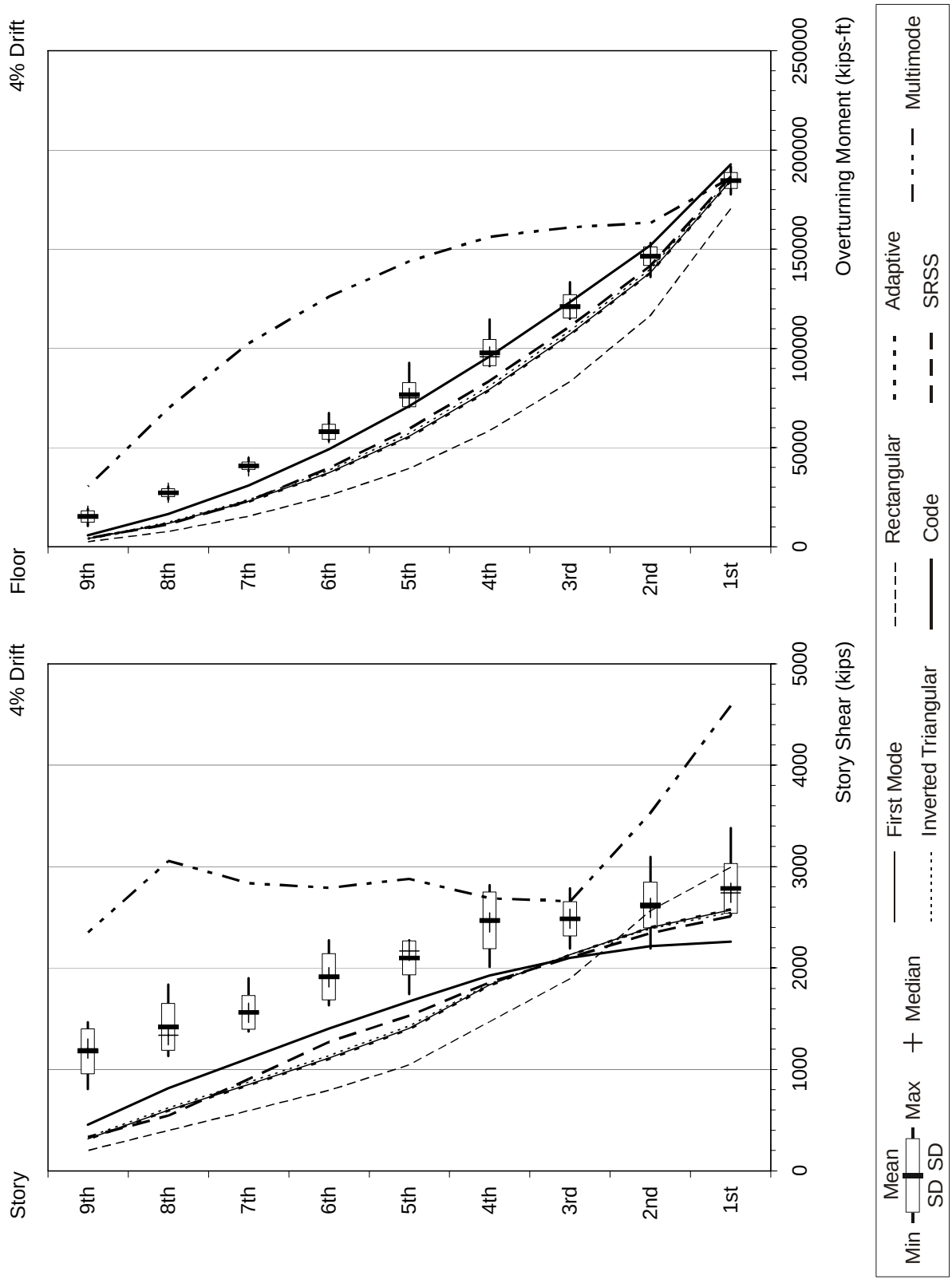


Figure F-43 Response quantities of the 9-story building for 4% drift level (continued)

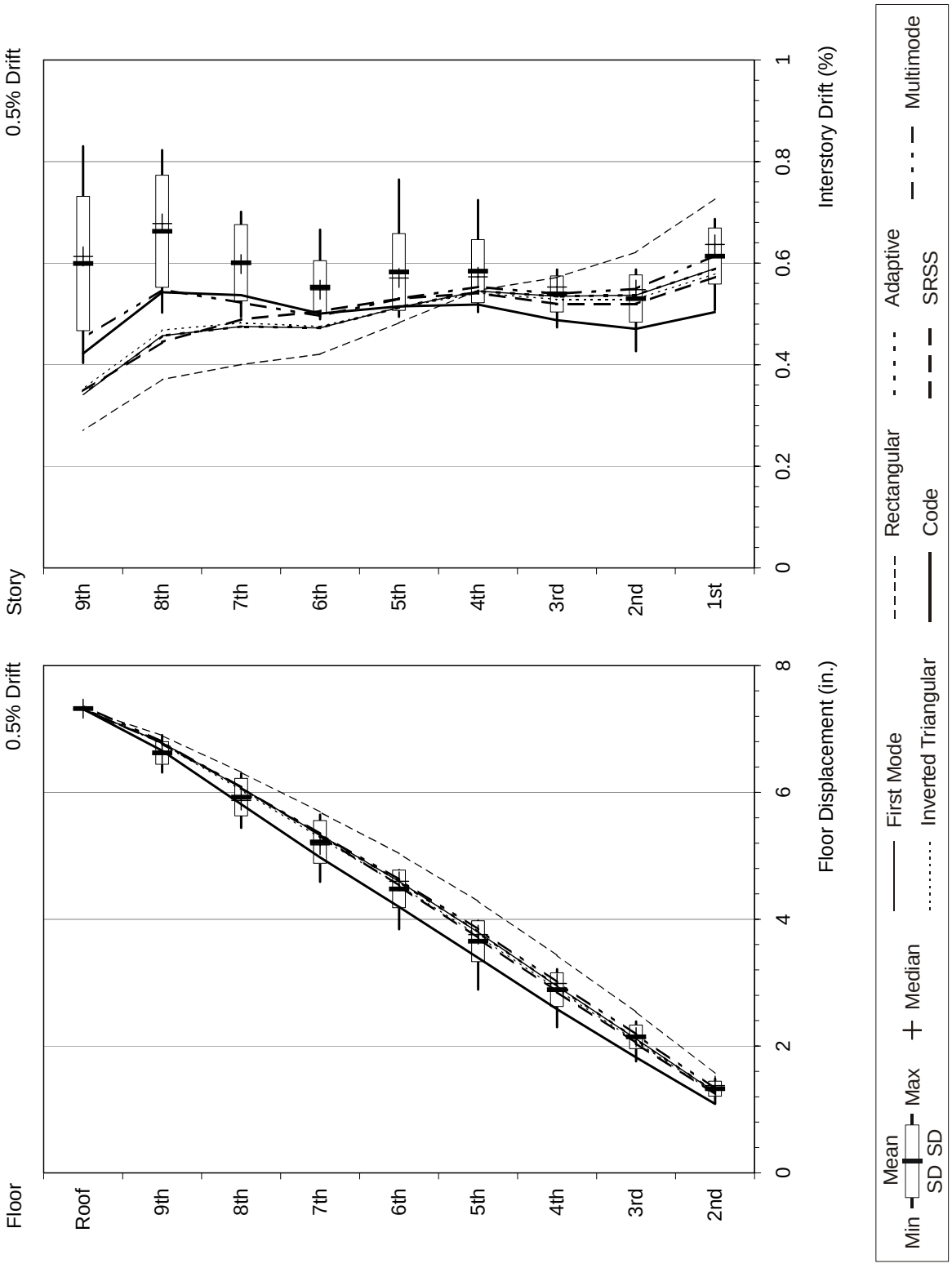


Figure F-44 Response quantities of the 9-story weak-story building for 0.5% drift level

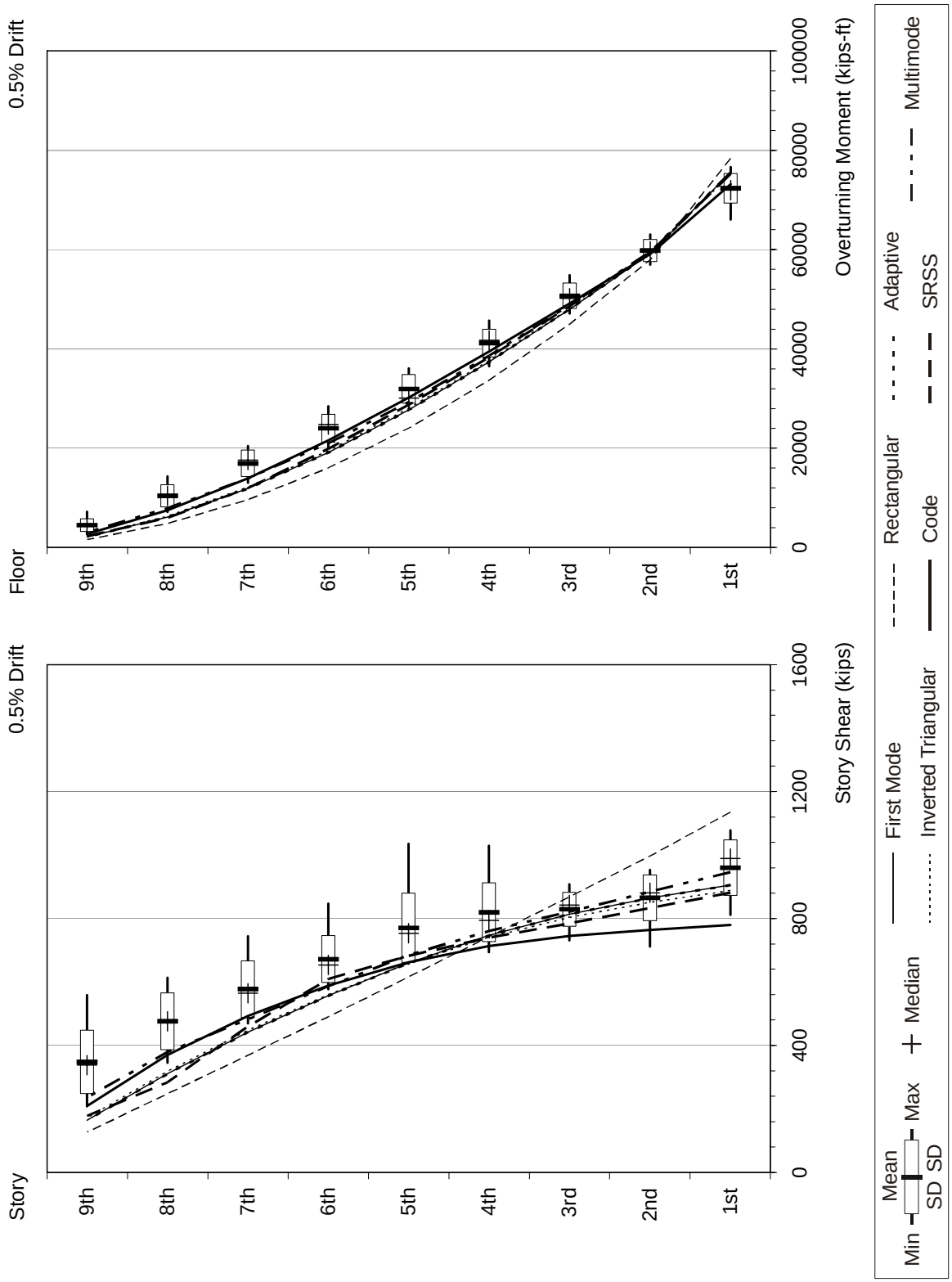


Figure F-44 Response quantities of the 9-story weak-story building for 0.5% drift level (continued)

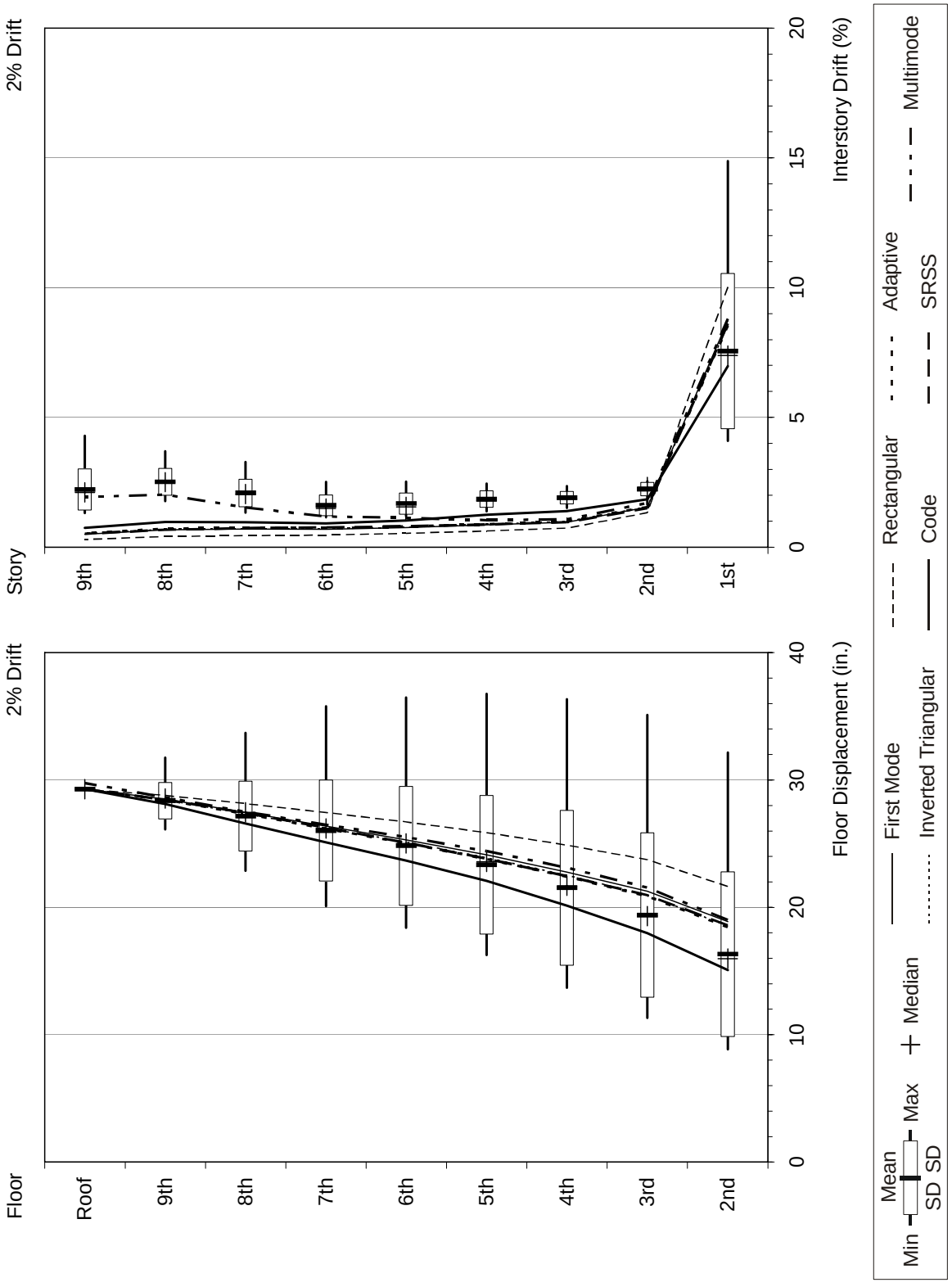


Figure F-45 Response quantities of the 9-story weak-story building for 2% drift level

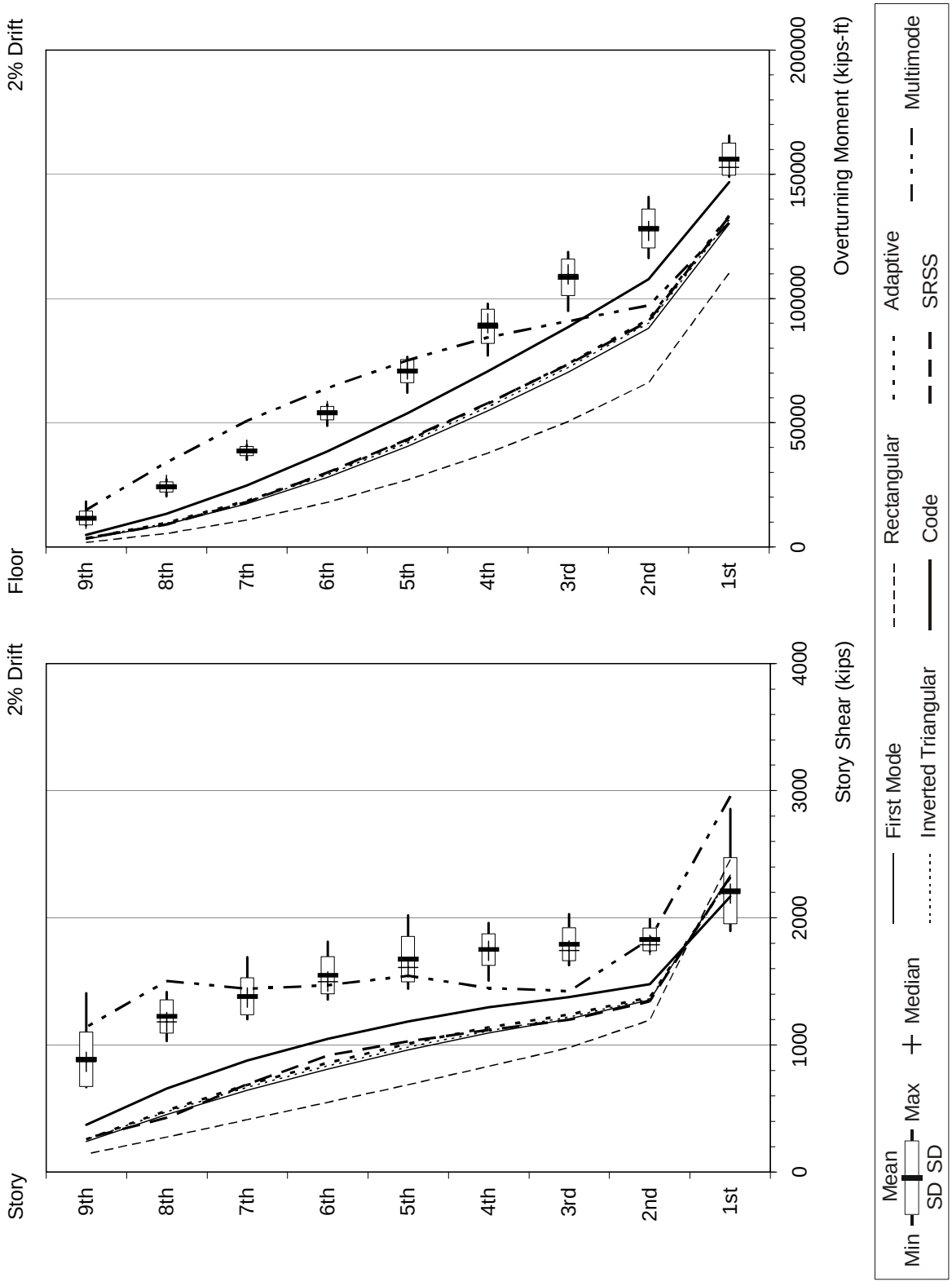


Figure F-45 Response quantities of the 9-story weak-story building for 2% drift level (continued)

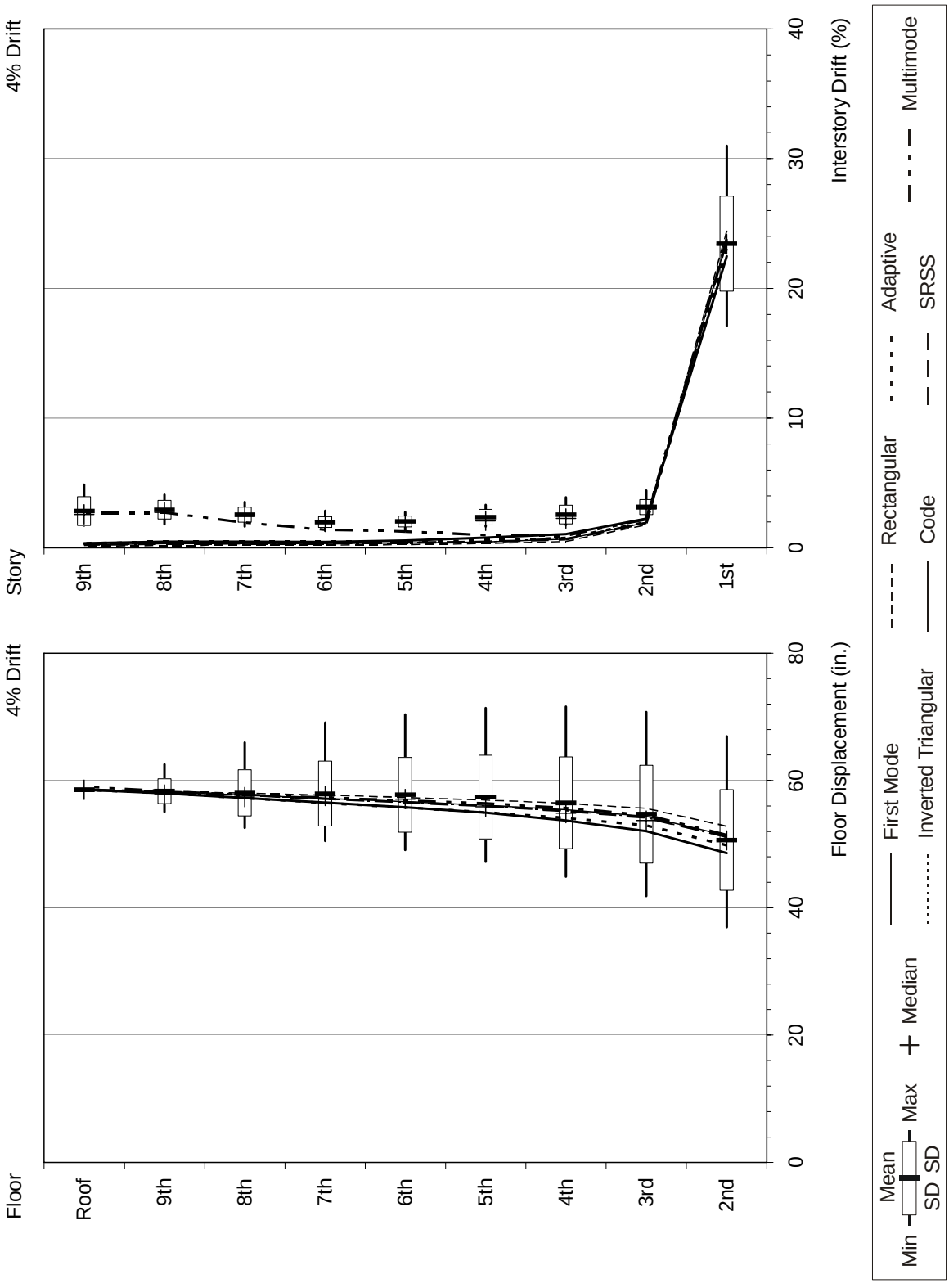


Figure F-46 Response quantities of the 9-story weak-story building for 4% drift level

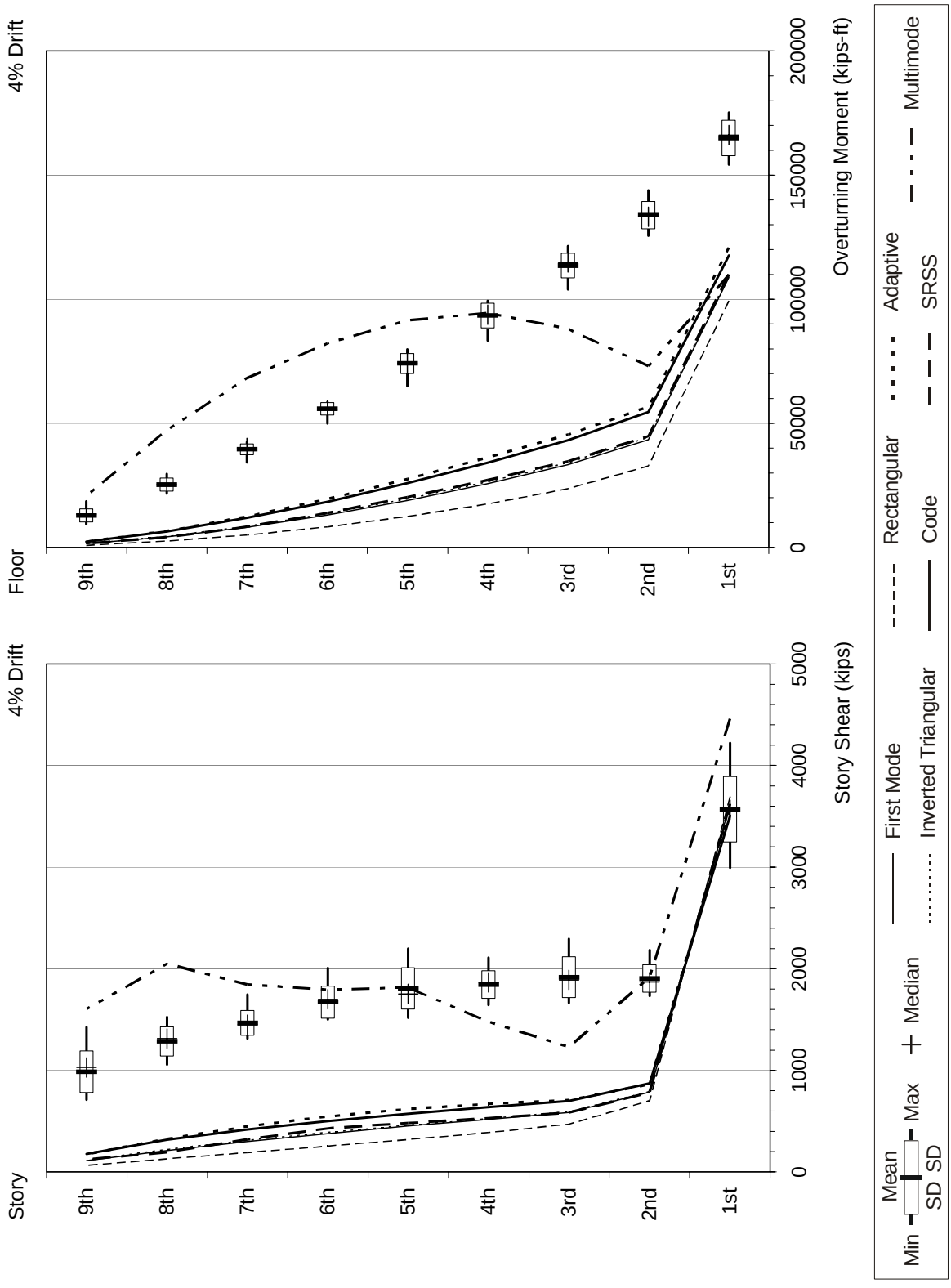


Figure F-46 Response quantities of the 9-story weak-story building for 4% drift level (continued)

### *F.8.3 Errors Associated with Ordinary (Site Class C) Motions*

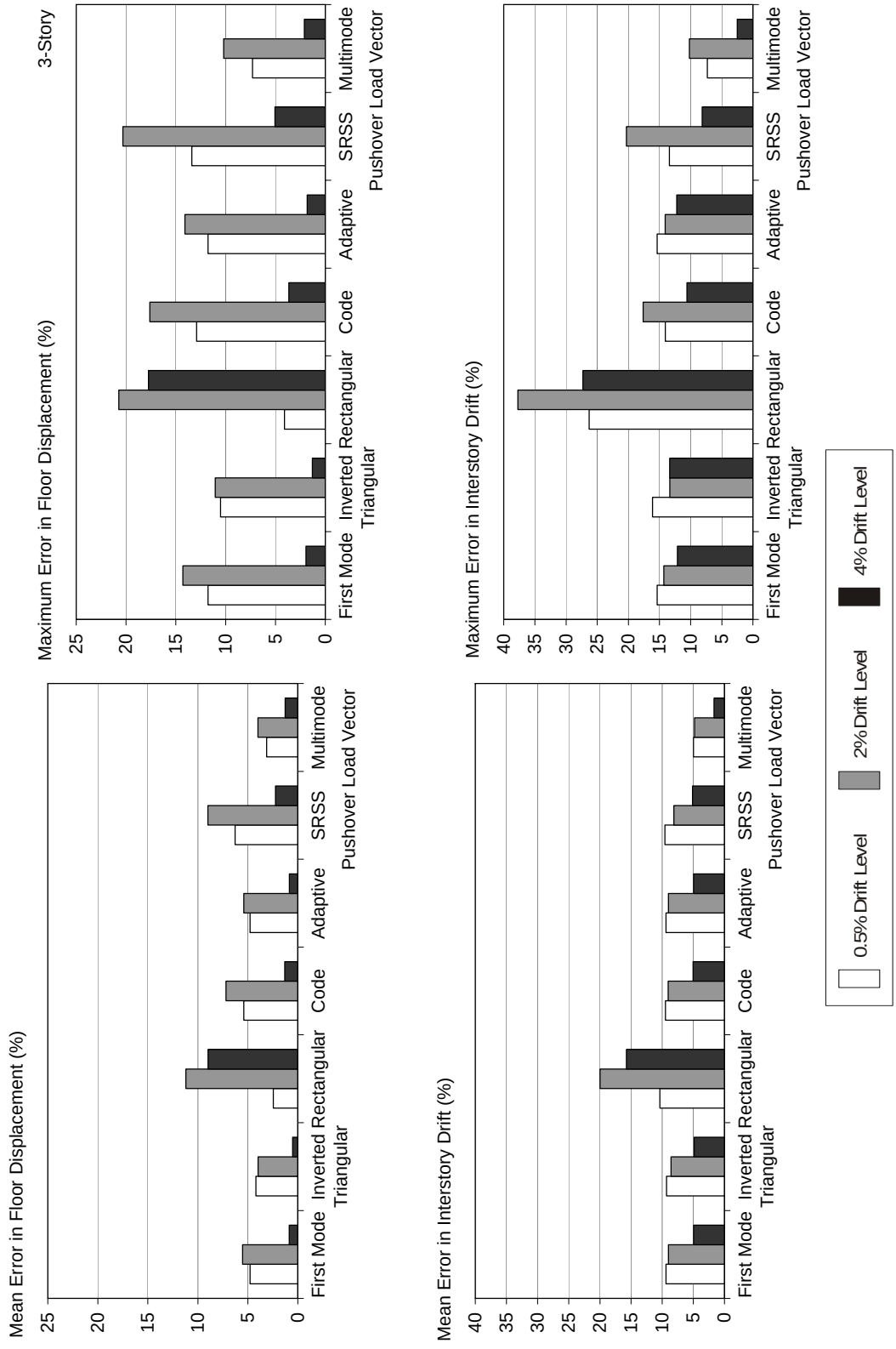


Figure F-47 Mean and maximum errors for the 3-story building

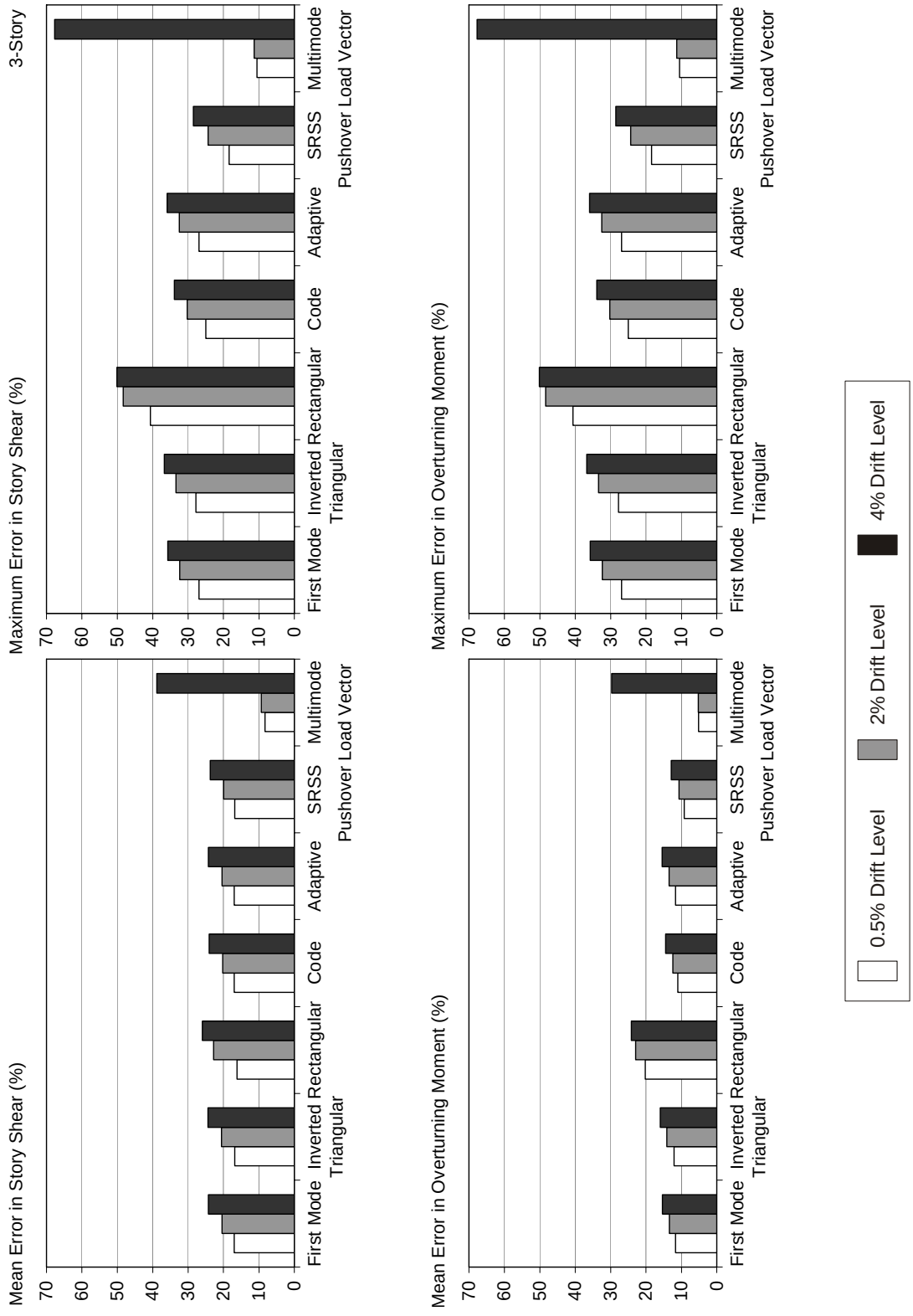


Figure F-47 Mean and maximum errors for the 3-story building (continued)

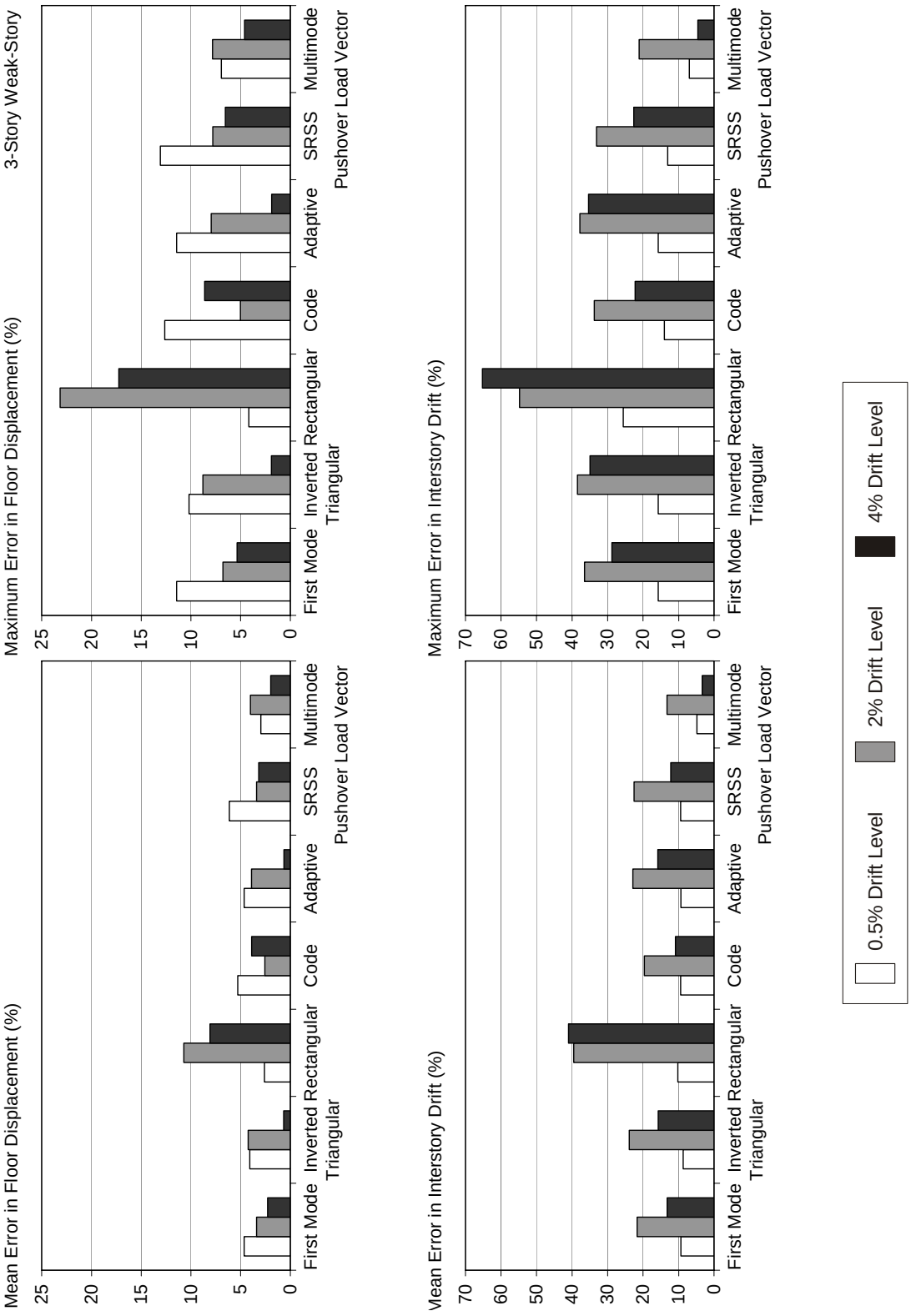


Figure F-48 Mean and maximum errors for the 3-story weak-story building

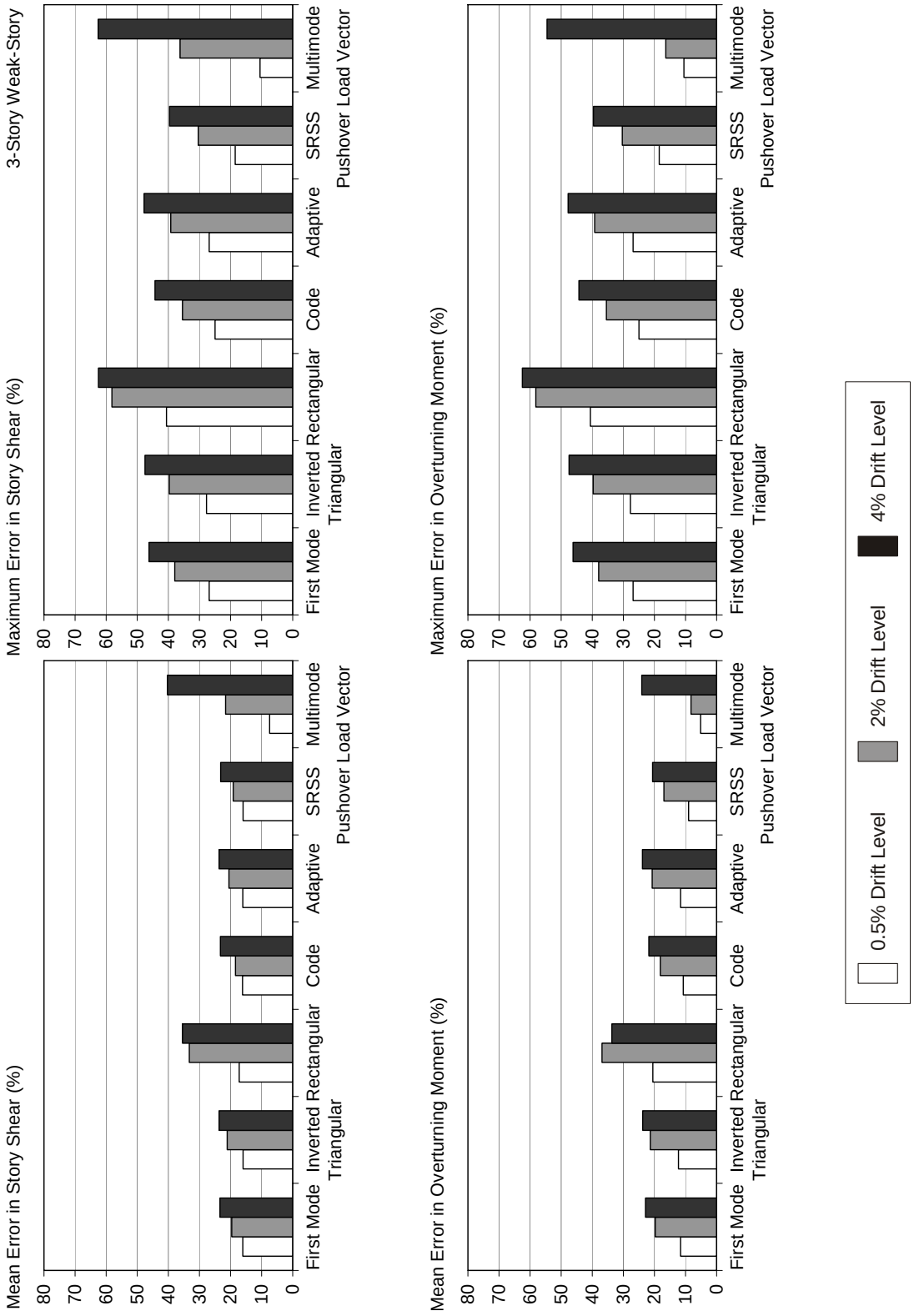


Figure F-48 Mean and maximum errors for the 3-story weak-story building (continued)

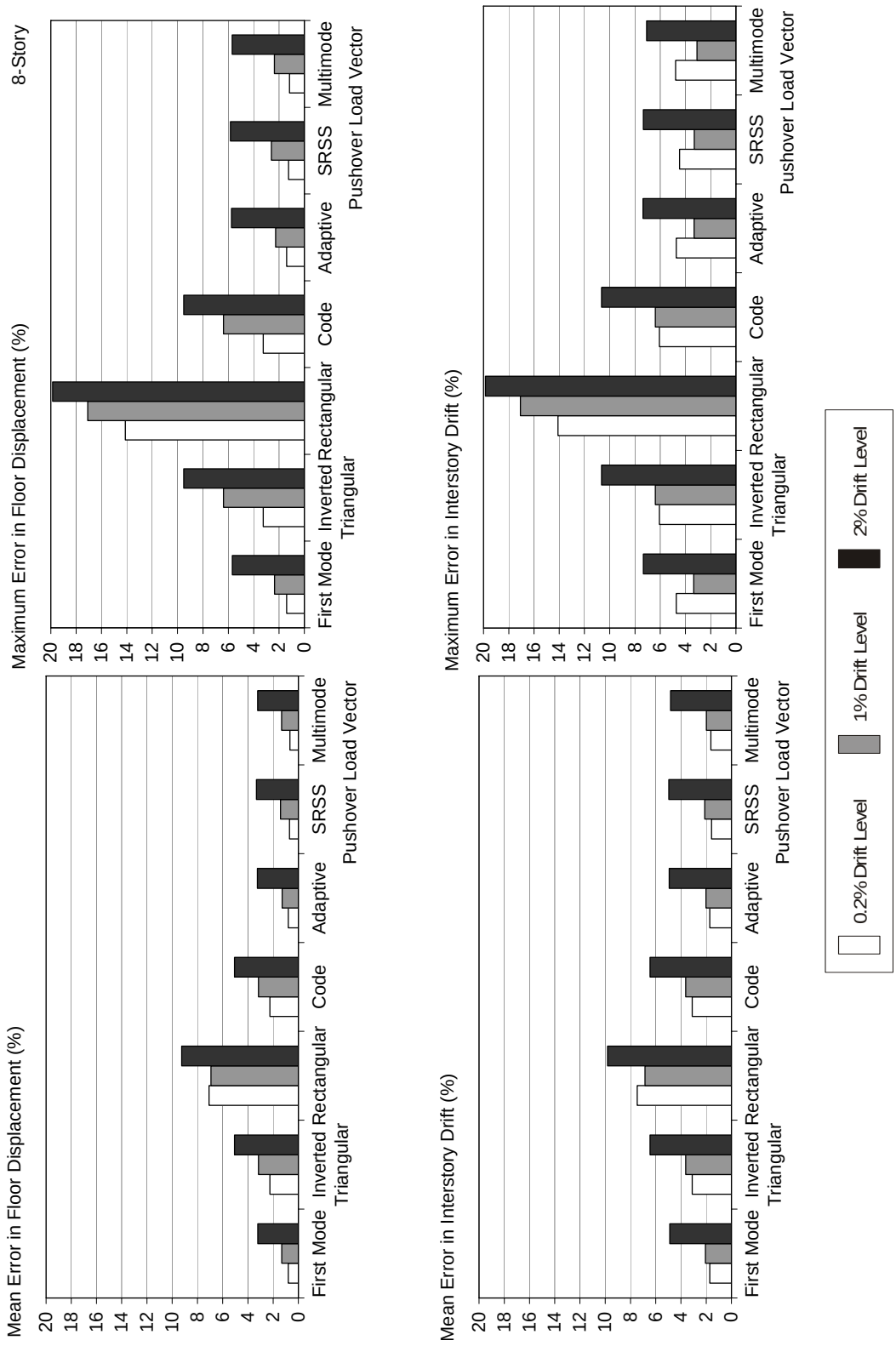


Figure F-49 Mean and maximum errors for the 8-story building

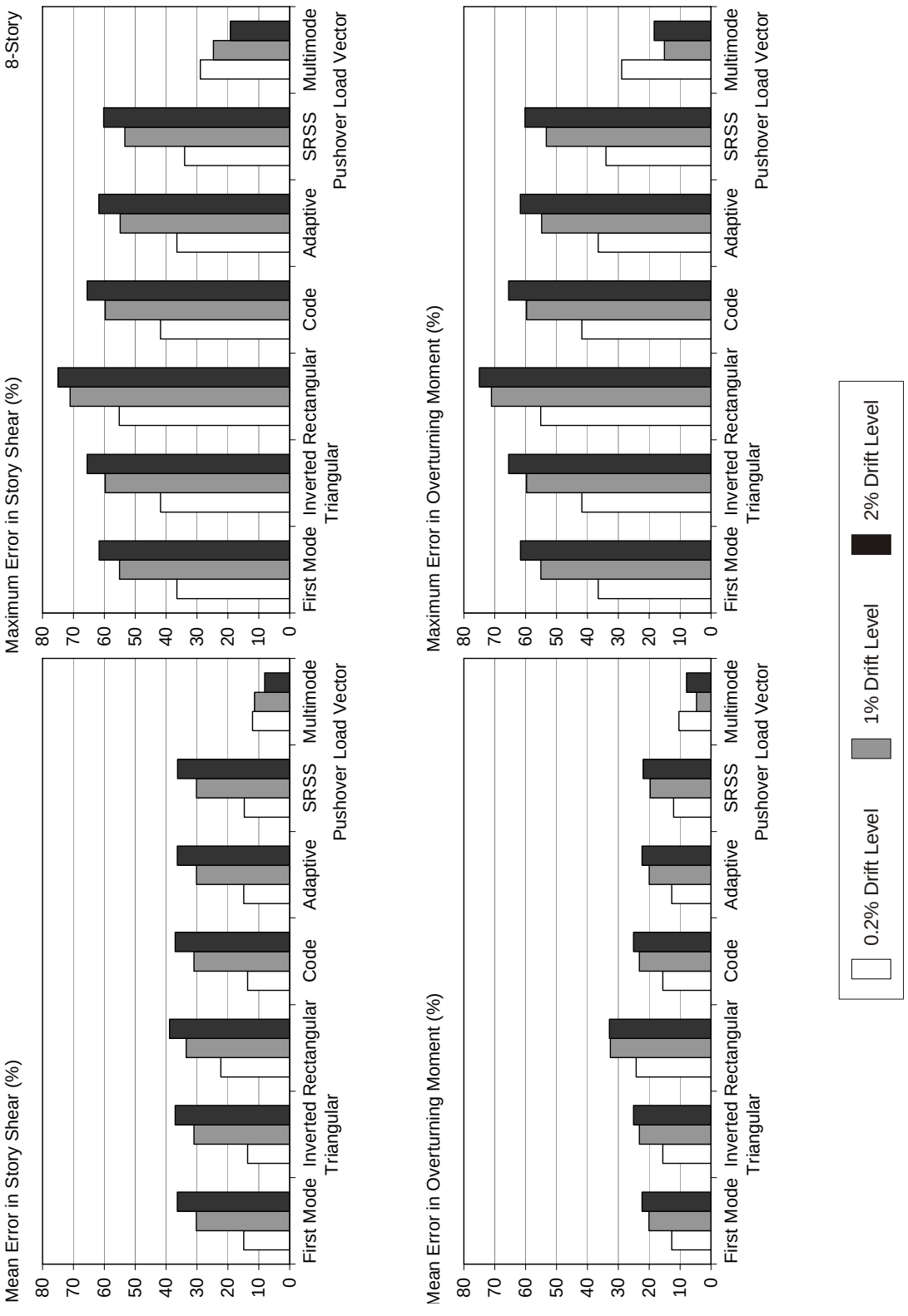


Figure F-49 Mean and maximum errors for the 8-story building (continued)

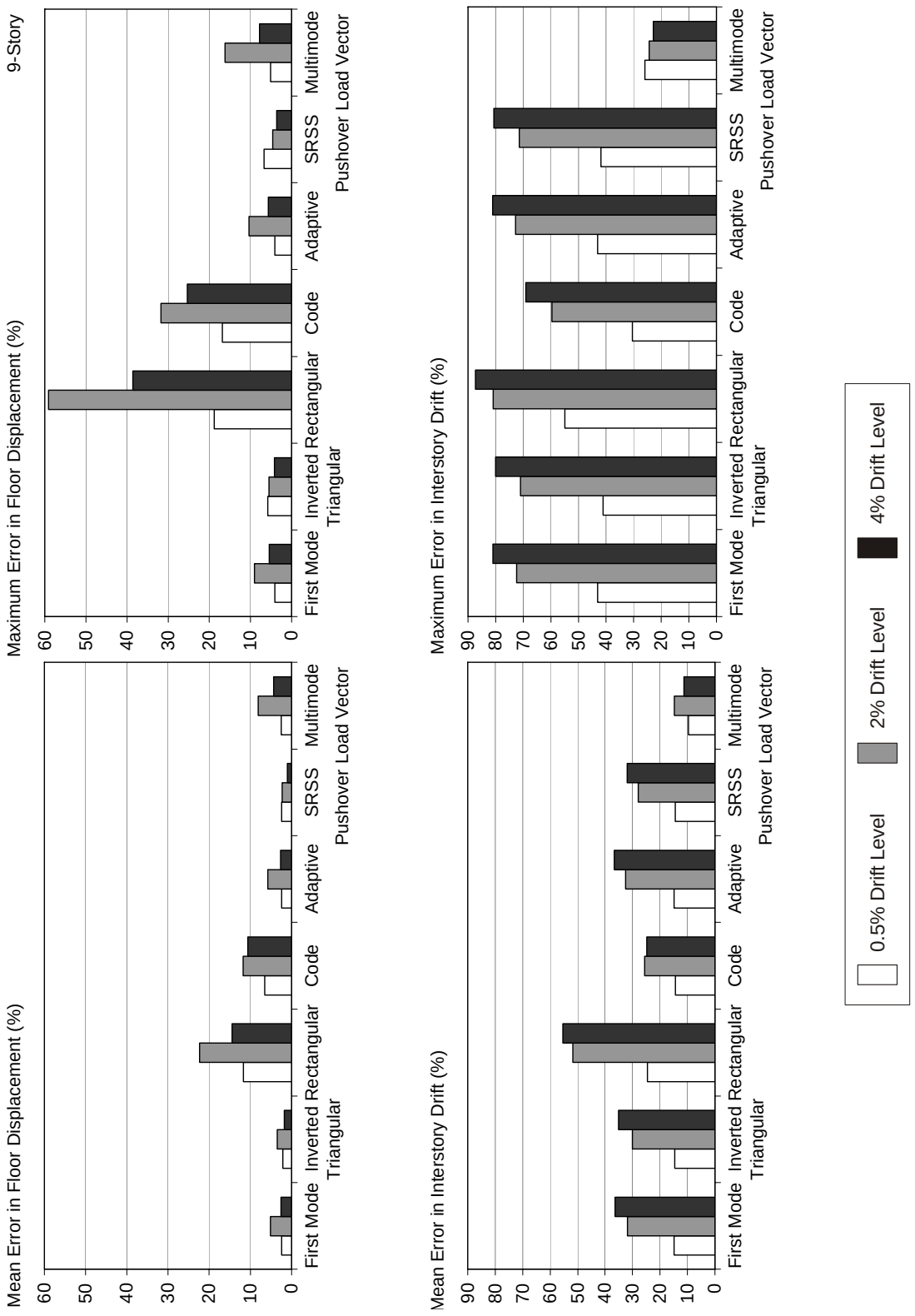


Figure F-50 Mean and maximum errors for the 9-story building

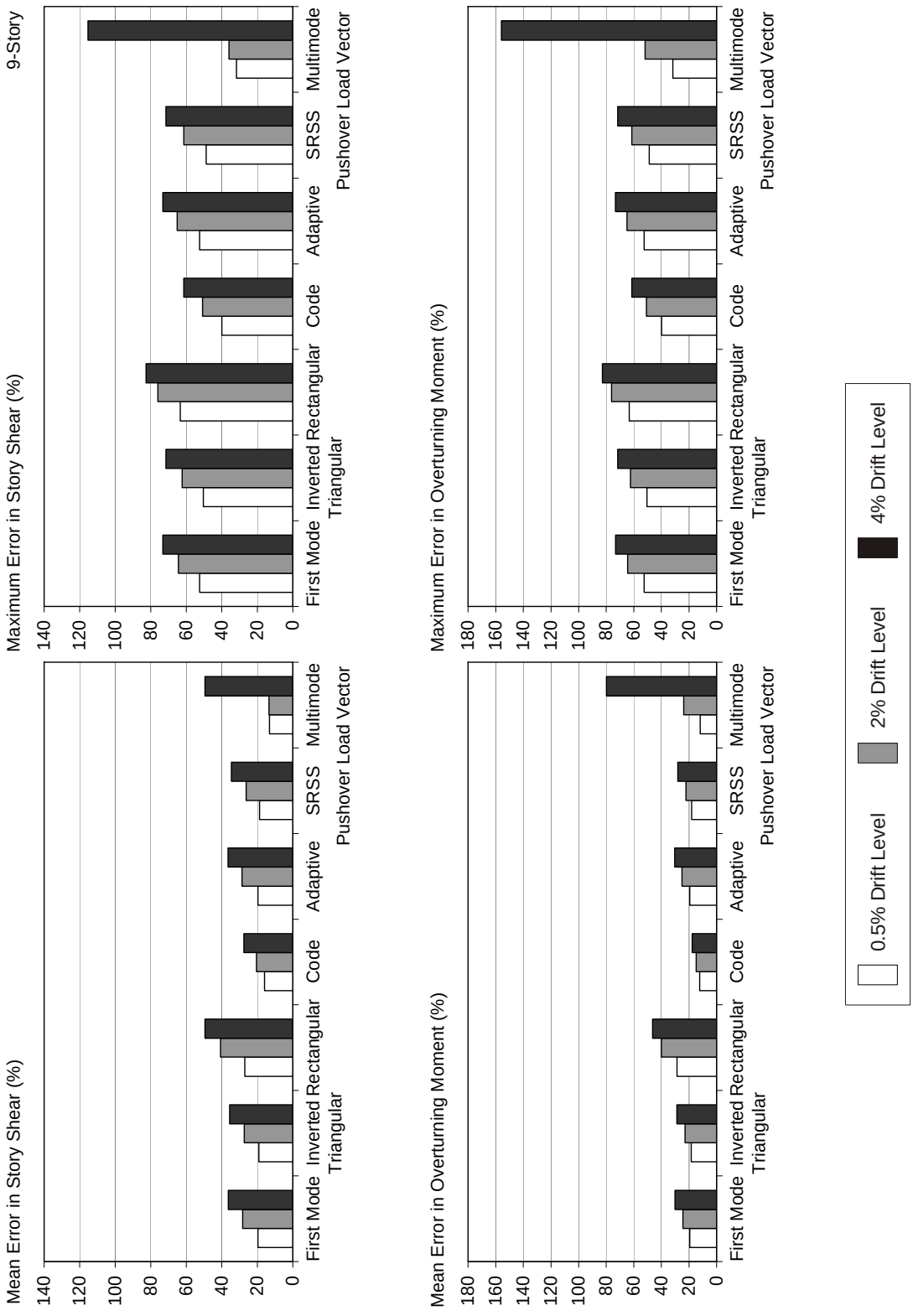


Figure F-50 Mean and maximum errors for the 9-story building (continued)

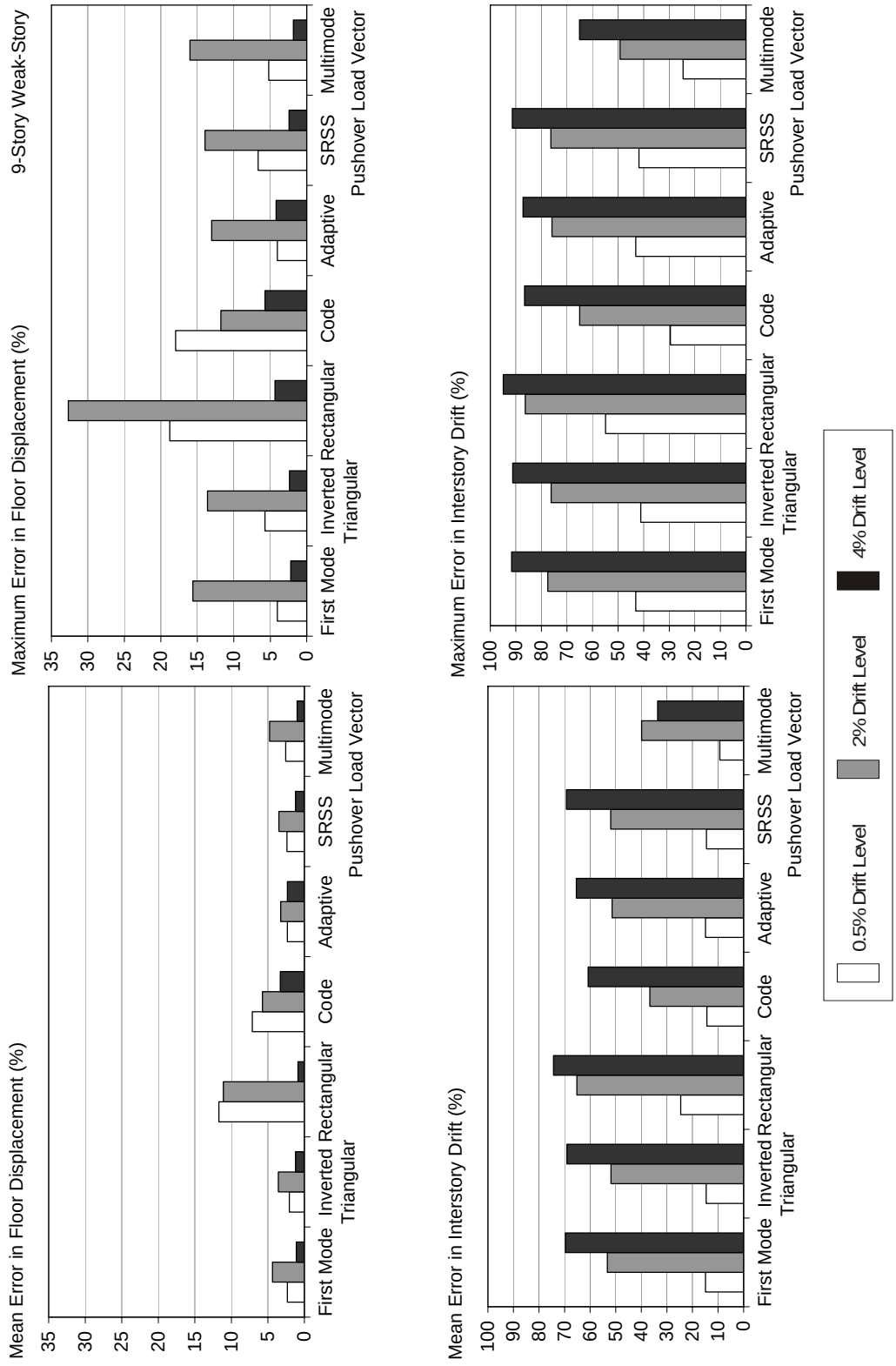


Figure F-51 Mean and maximum errors for the 9-story weak-story building

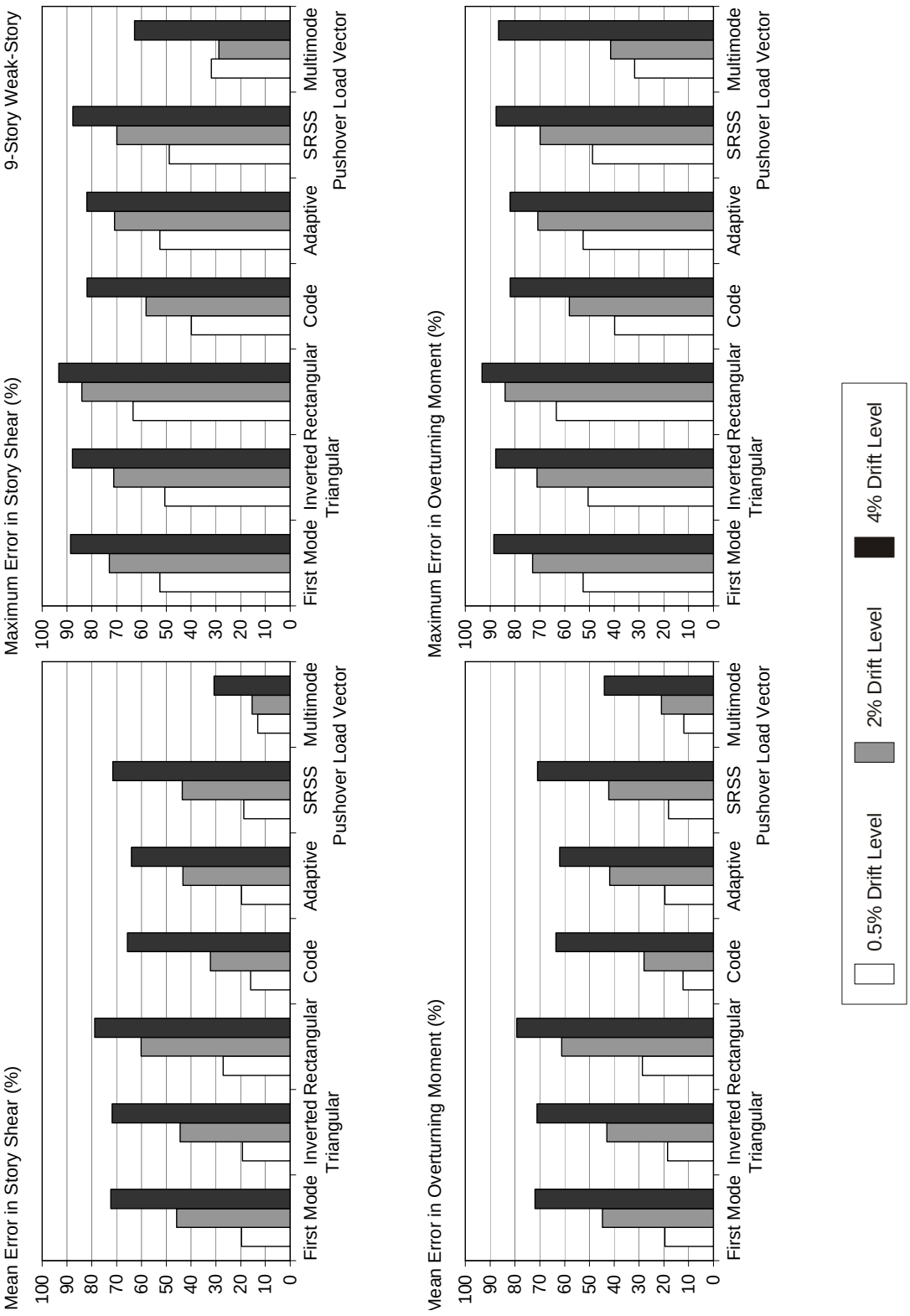


Figure F-51 Mean and maximum errors for the 9-story weak-story building (continued)

### *F.8.4 Responses to Near Fault Motions*

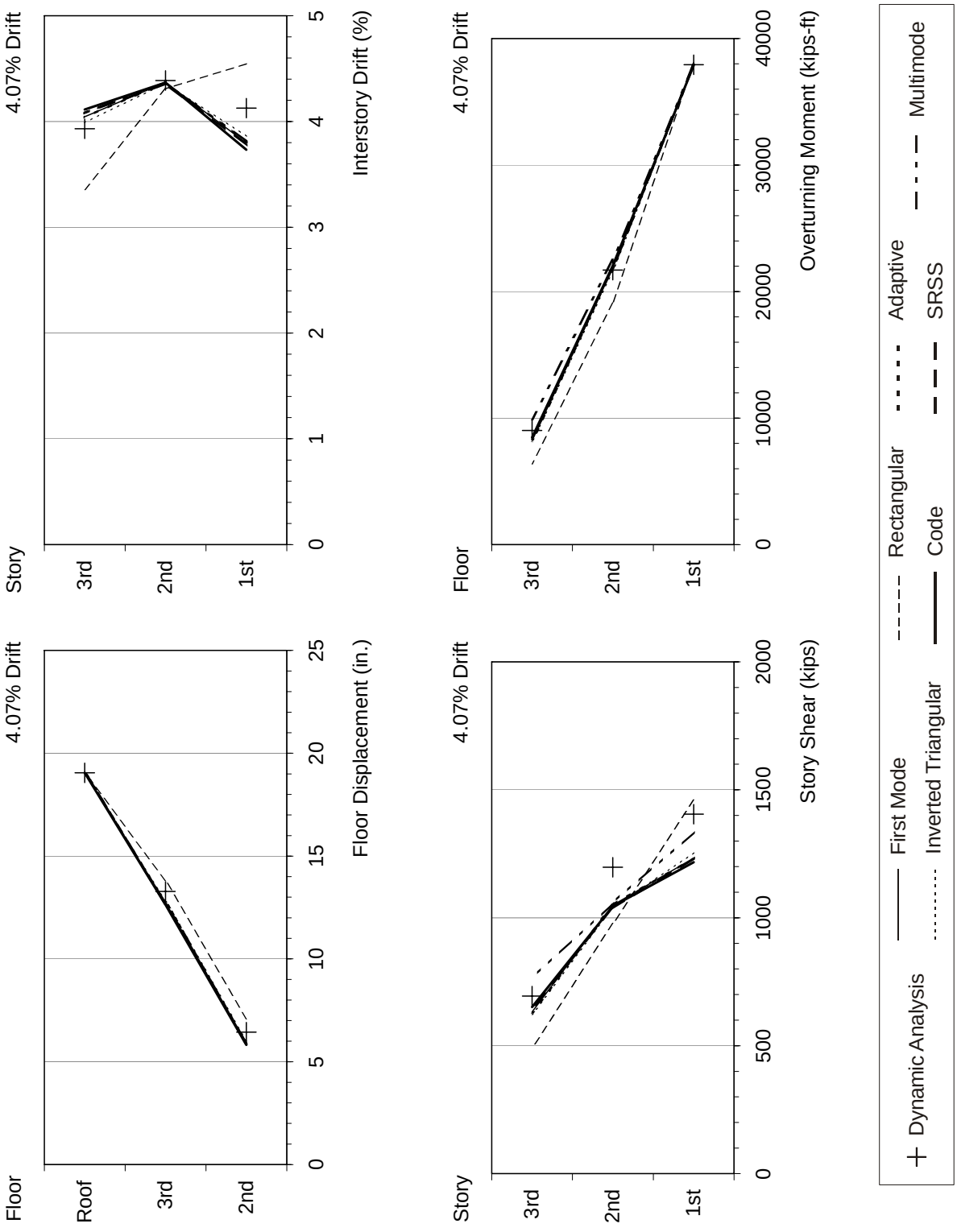


Figure F-52 Response quantities of the 3-story building under ERZMV1 ground motion

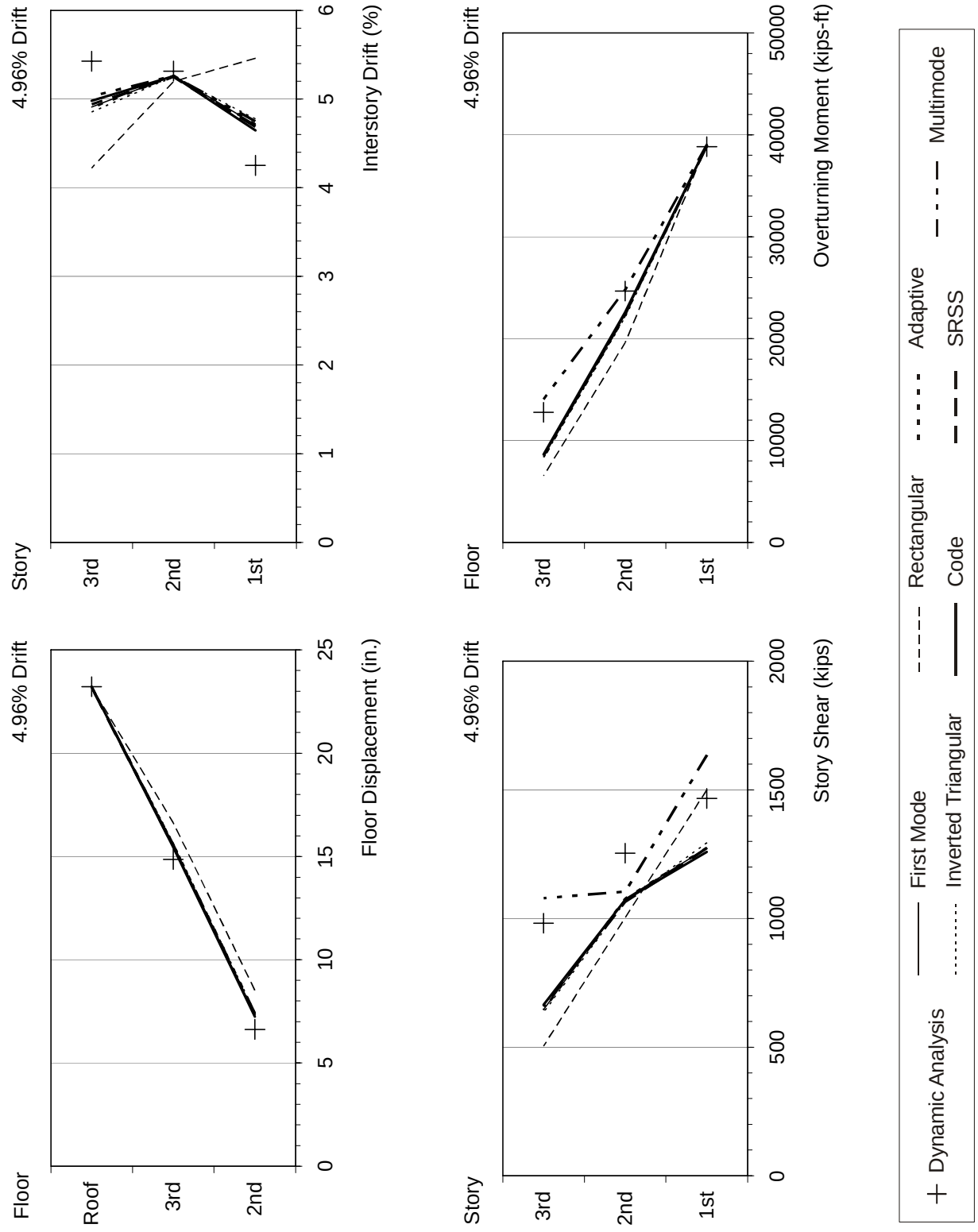


Figure F-53 Response quantities of the 3-story building under RRSMV1 ground motion

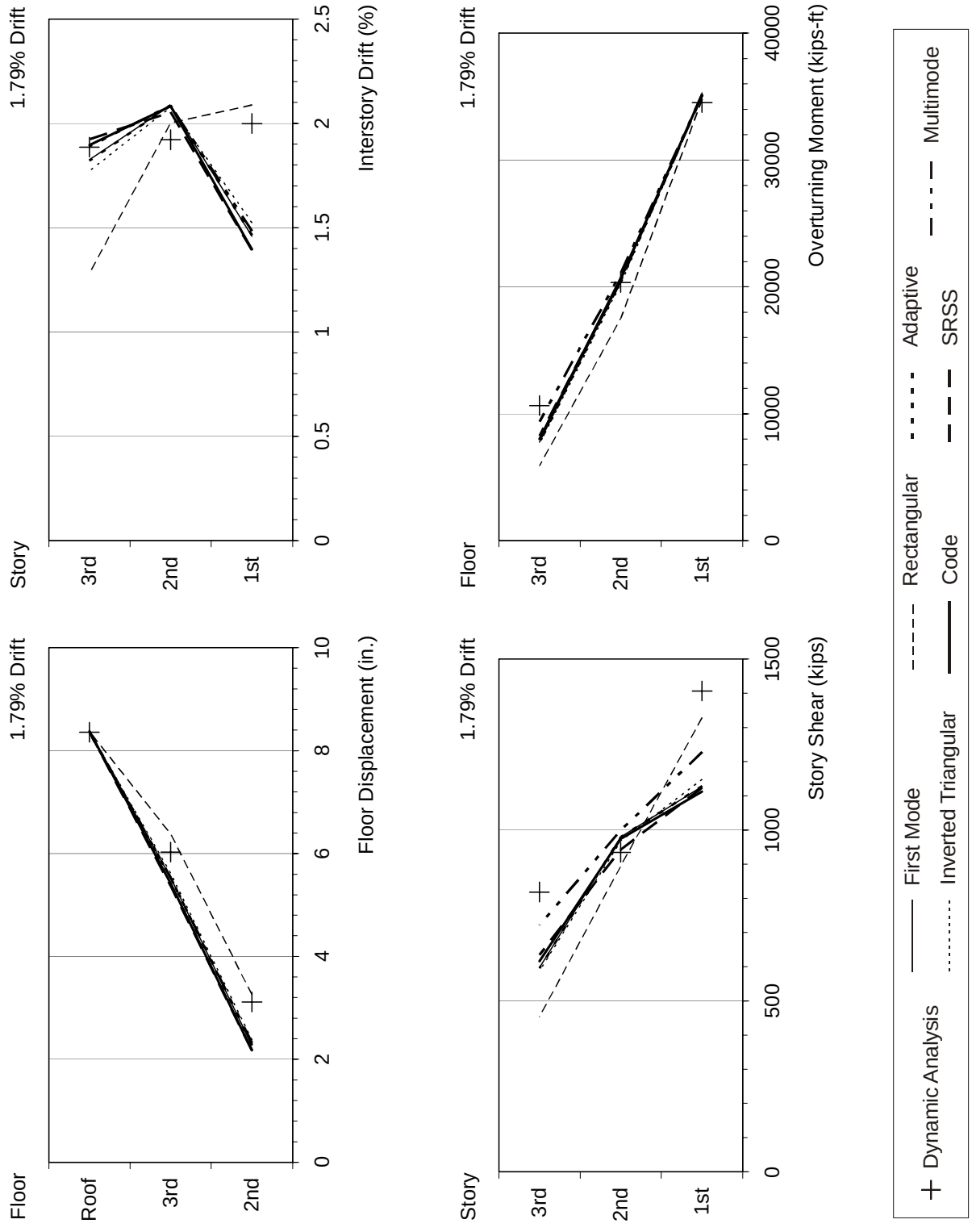


Figure F-54 Response quantities of the 3-story building under LUCMV1 ground motion

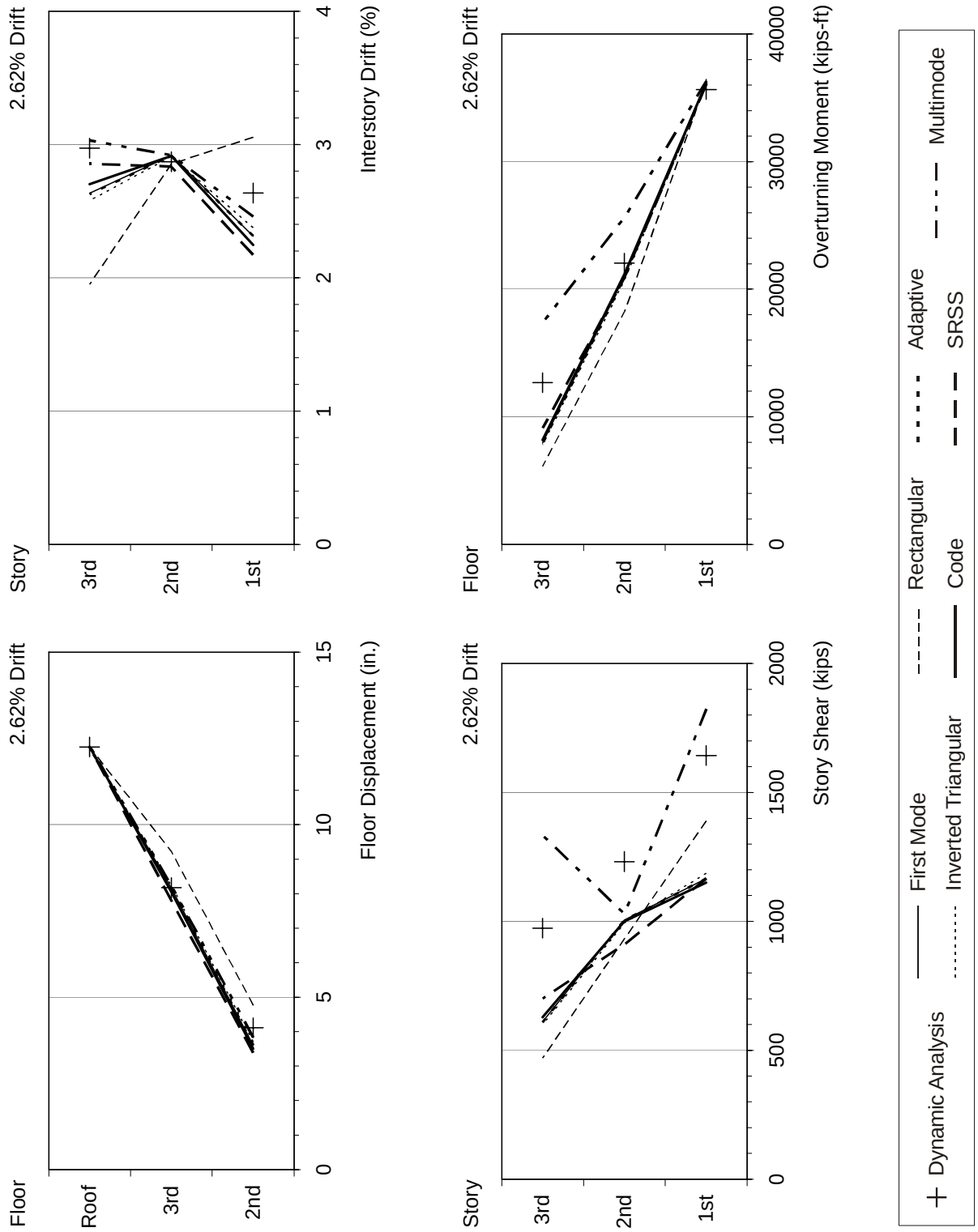


Figure F-55 Response quantities of the 3-story building under SCHMV1 ground motion

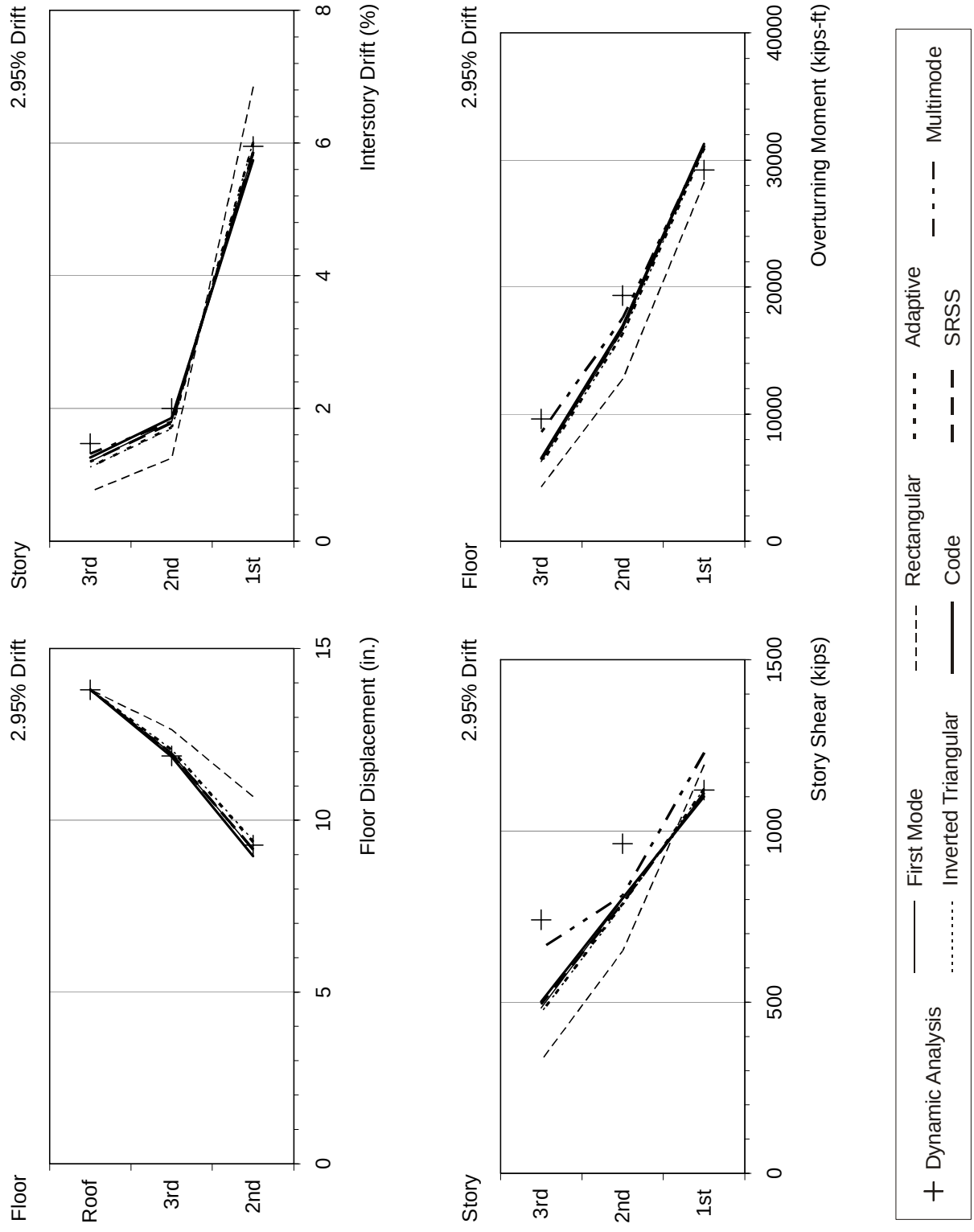


Figure F-56 Response quantities of the 3-story weak-story building under ERZMV1 ground motion

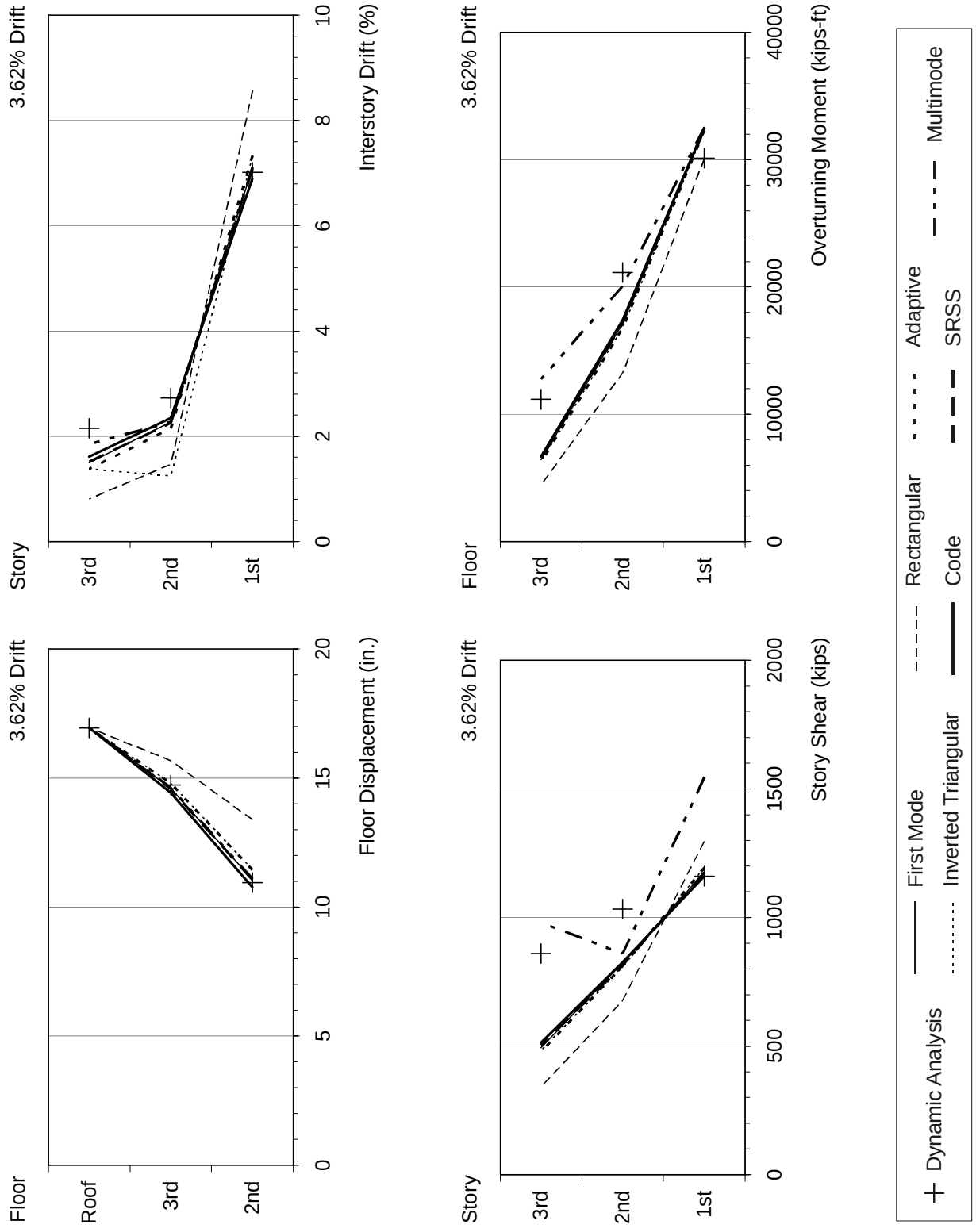


Figure F-57 Response quantities of the 3-story weak-story building under RRSMV1 ground motion

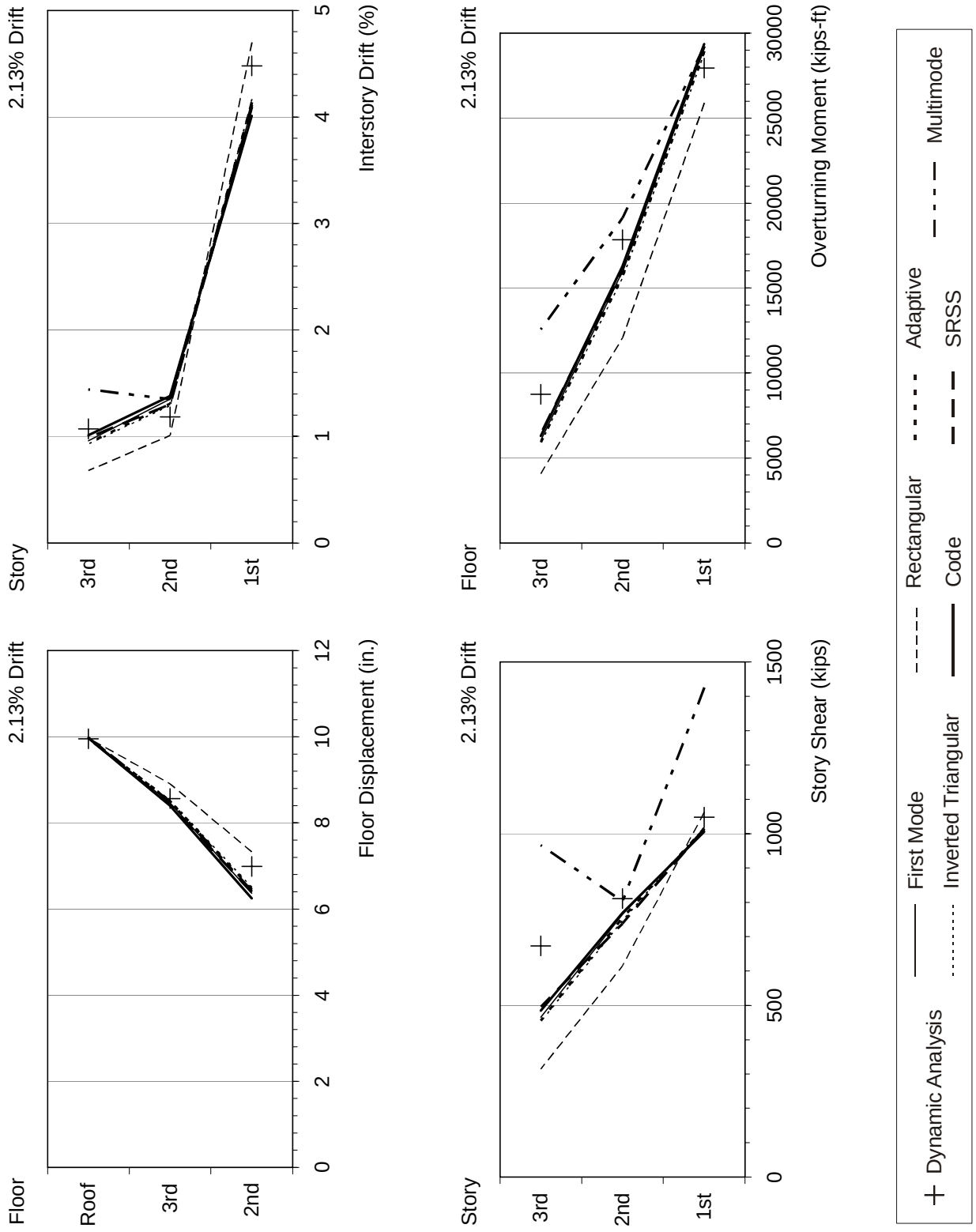


Figure F-58 Response quantities of the 3-story weak-story building under LUCMV1 ground motion

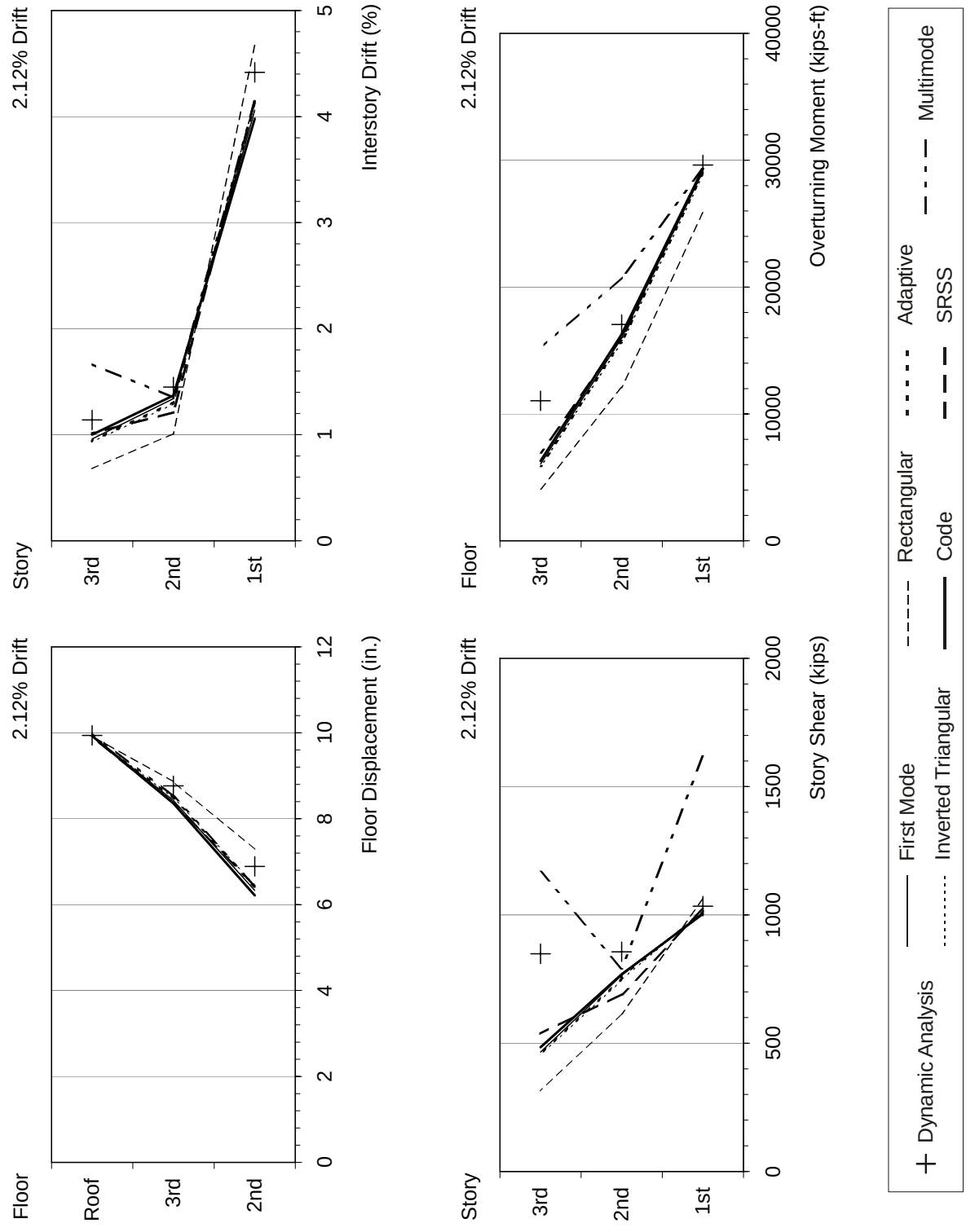


Figure F-59 Response quantities of the 3-story weak-story building under SCHMV1 ground motion

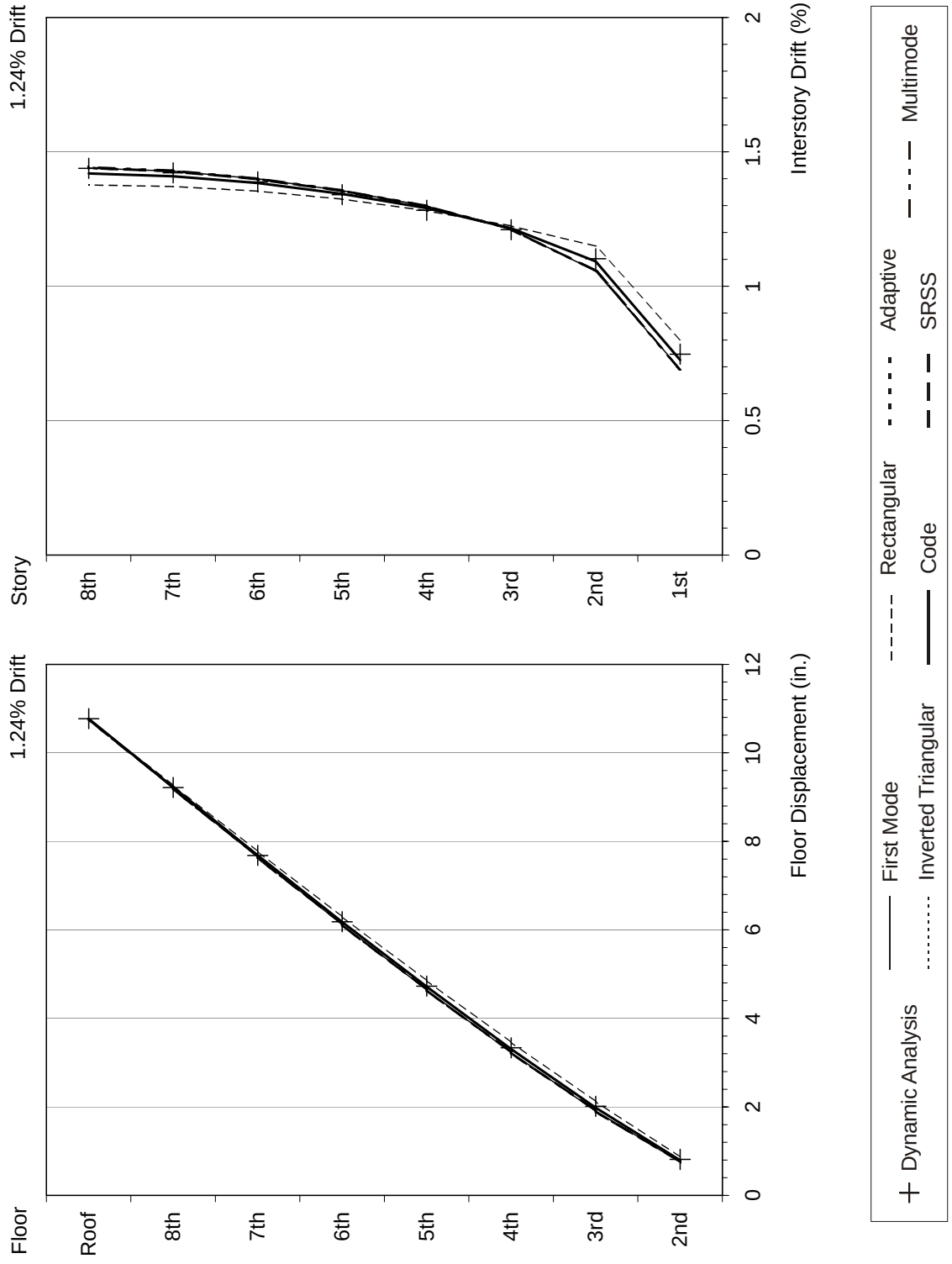


Figure F-60 Response quantities of the 8-story building under ERZMV1 ground motion

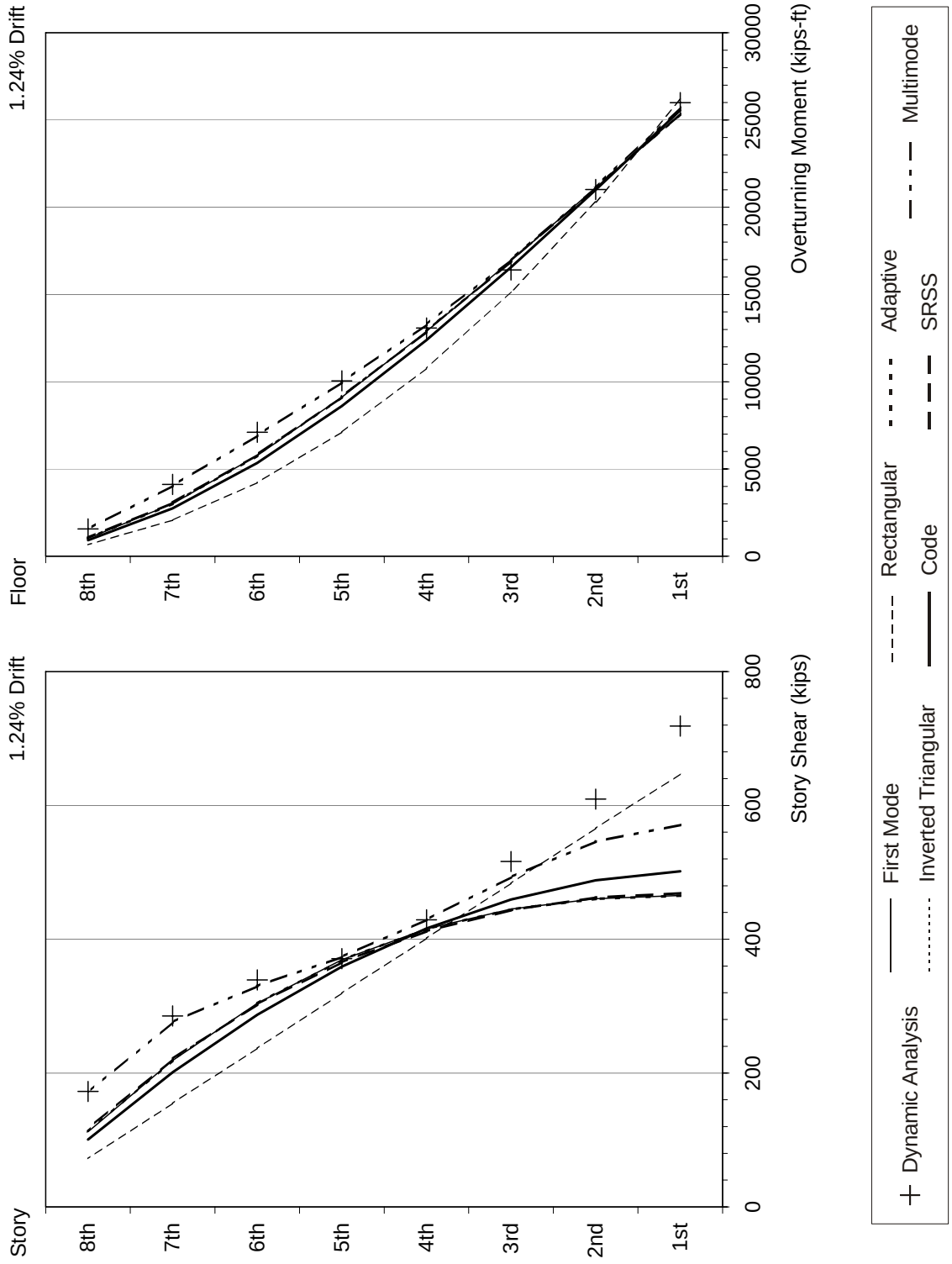


Figure F-60 Response quantities of the 8-story building under ERZMV1 ground motion (continued)

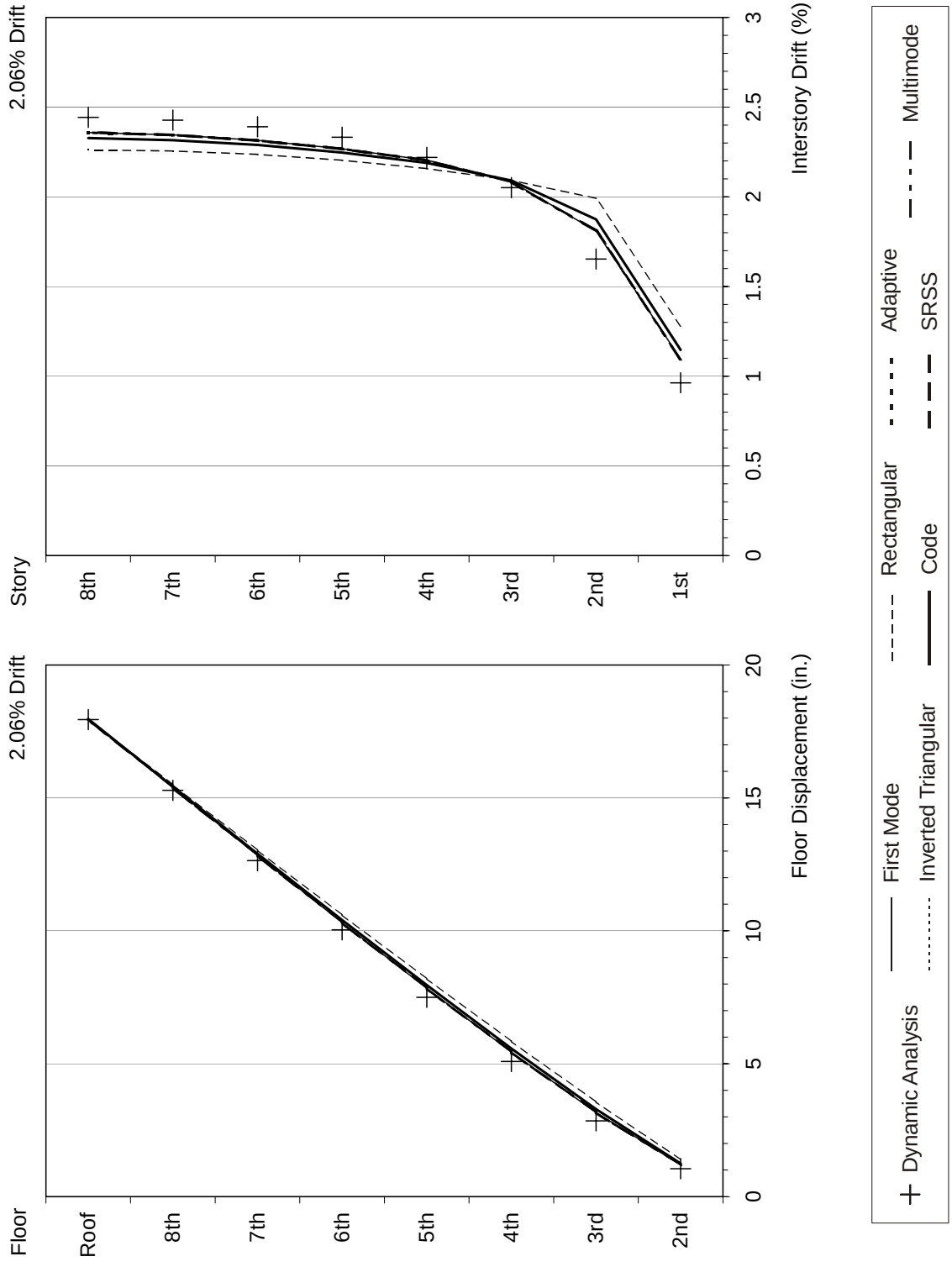


Figure F-61 Response quantities of the 8-story building under RRSMV1 ground motion

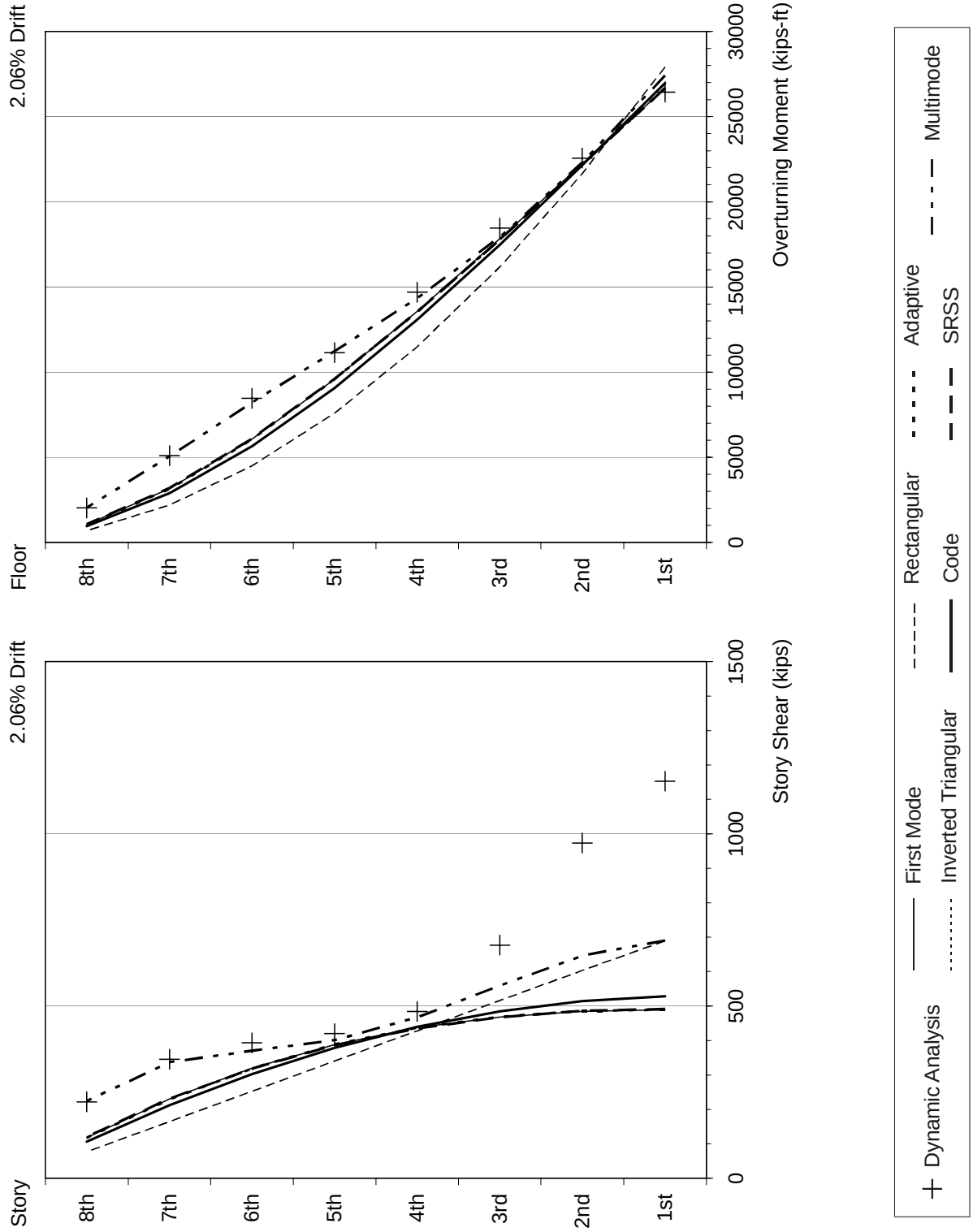


Figure F-61 Response quantities of the 8-story building under RRSMV1 ground motion (continued)

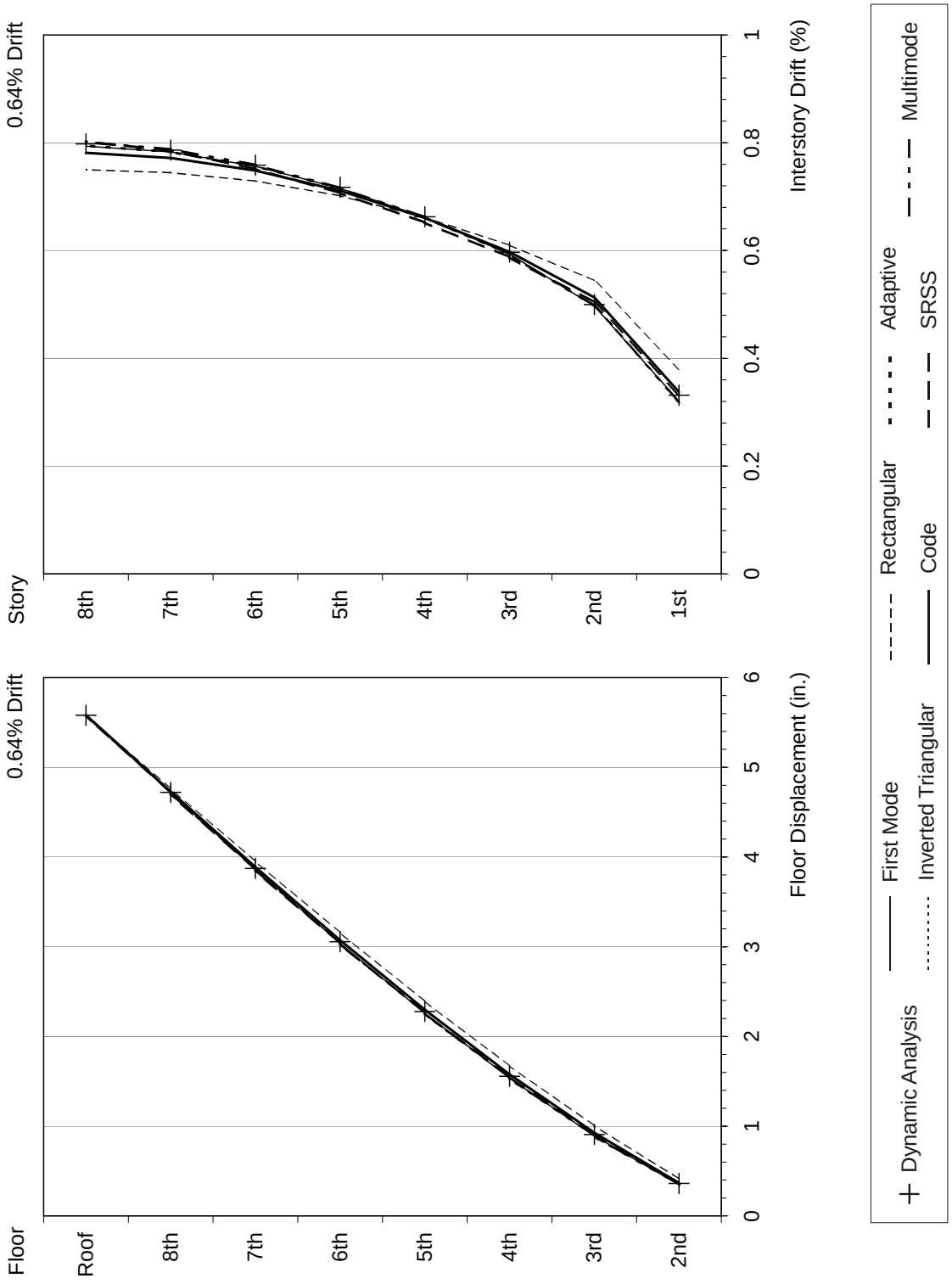


Figure F-62 Response quantities of the 8-story building under LUCMV1 ground motion

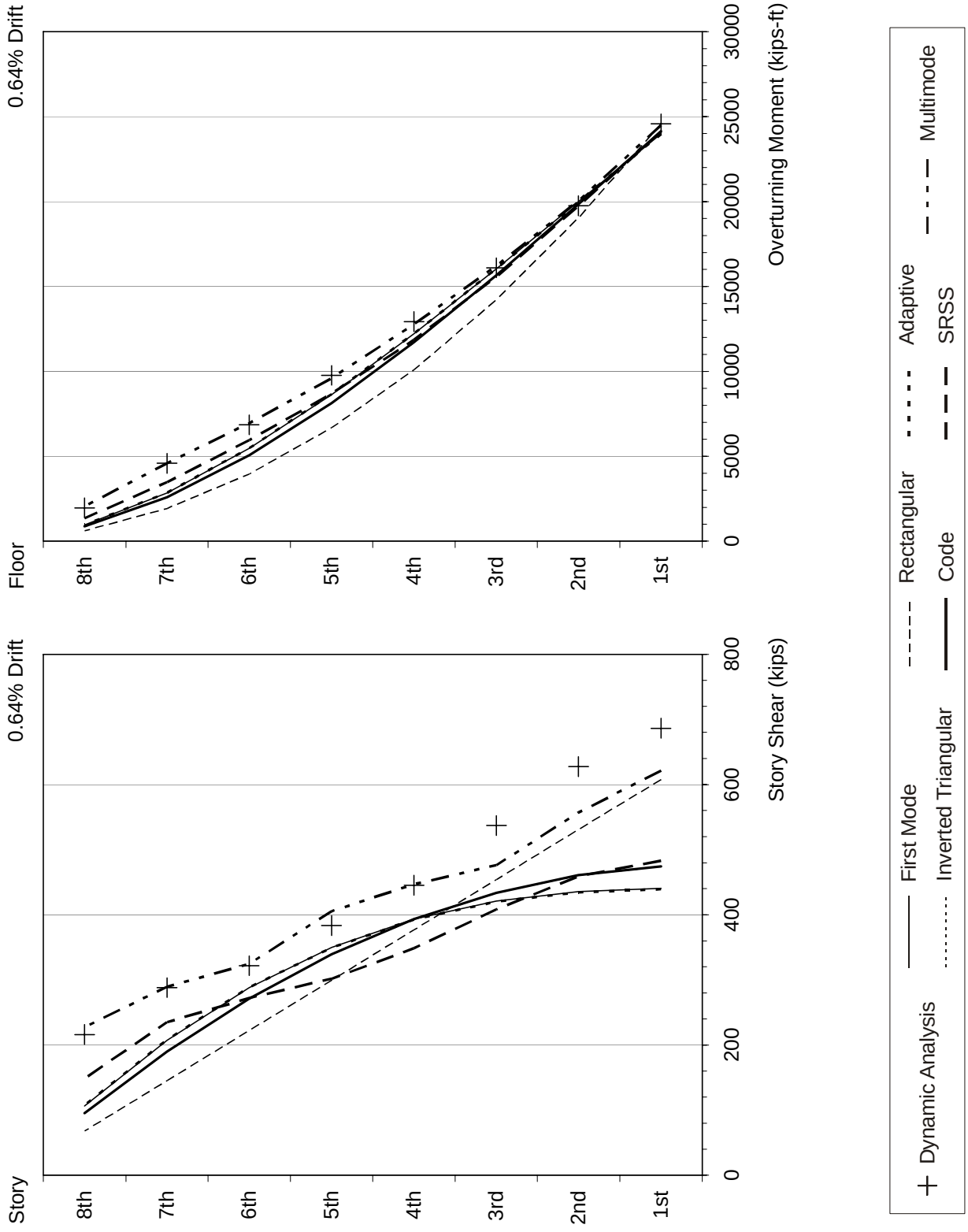


Figure F-62 Response quantities of the 8-story building under LUCMV1 ground motion (continued)

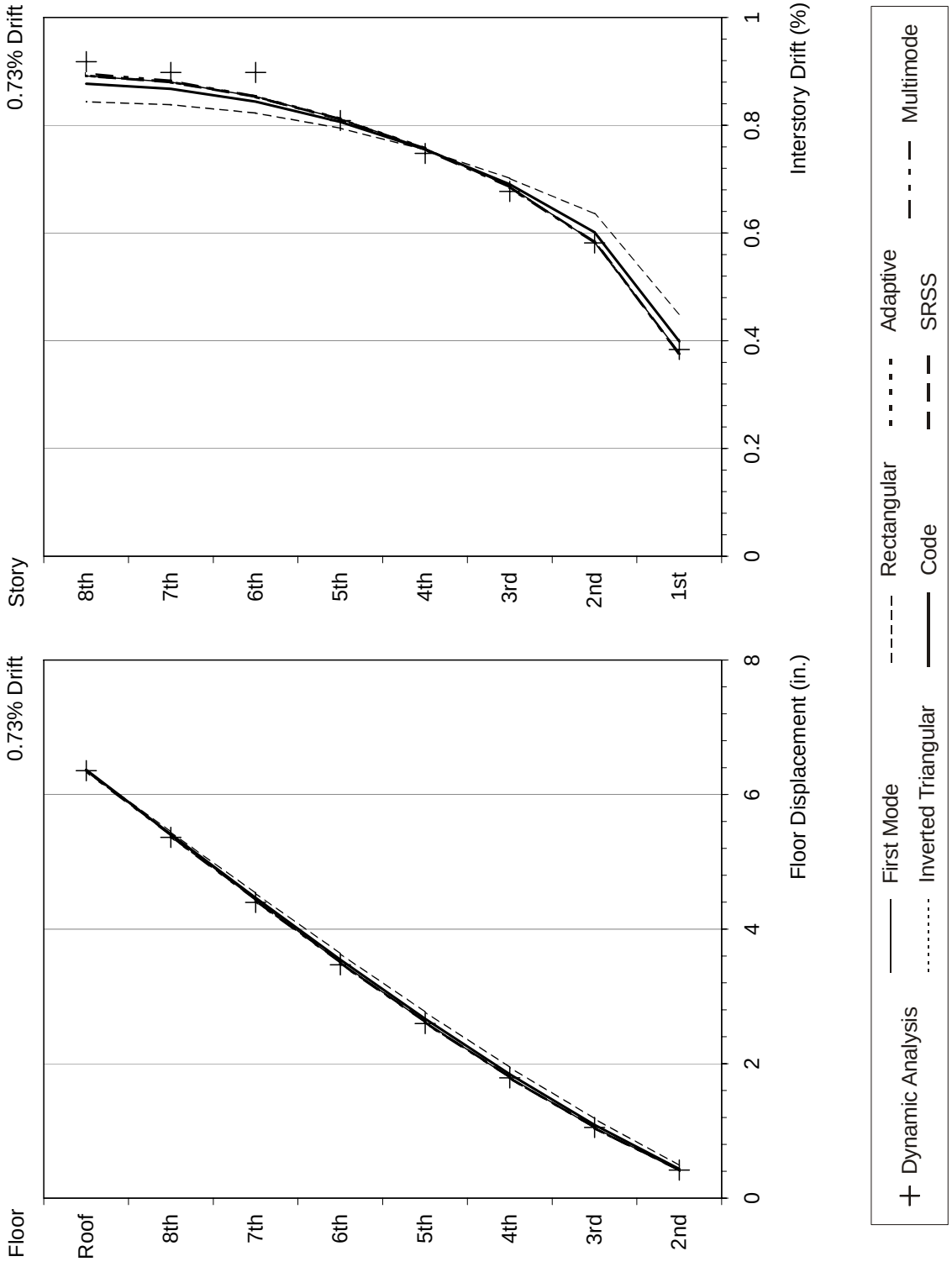


Figure F-63 Response quantities of the 8-story building under SCHMV1 ground motion

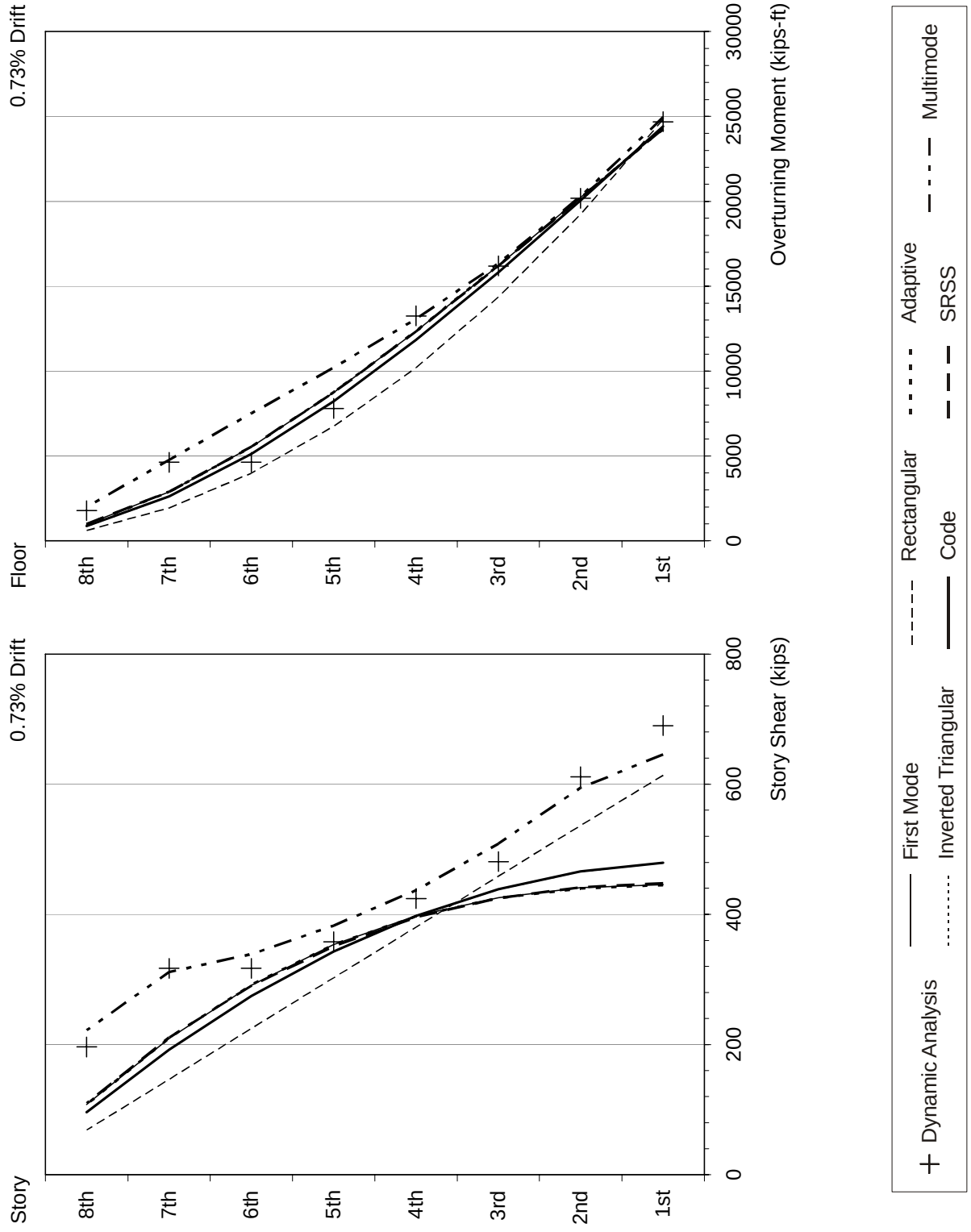


Figure F-63 Response quantities of the 8-story building under SCHMV1 ground motion (continued)

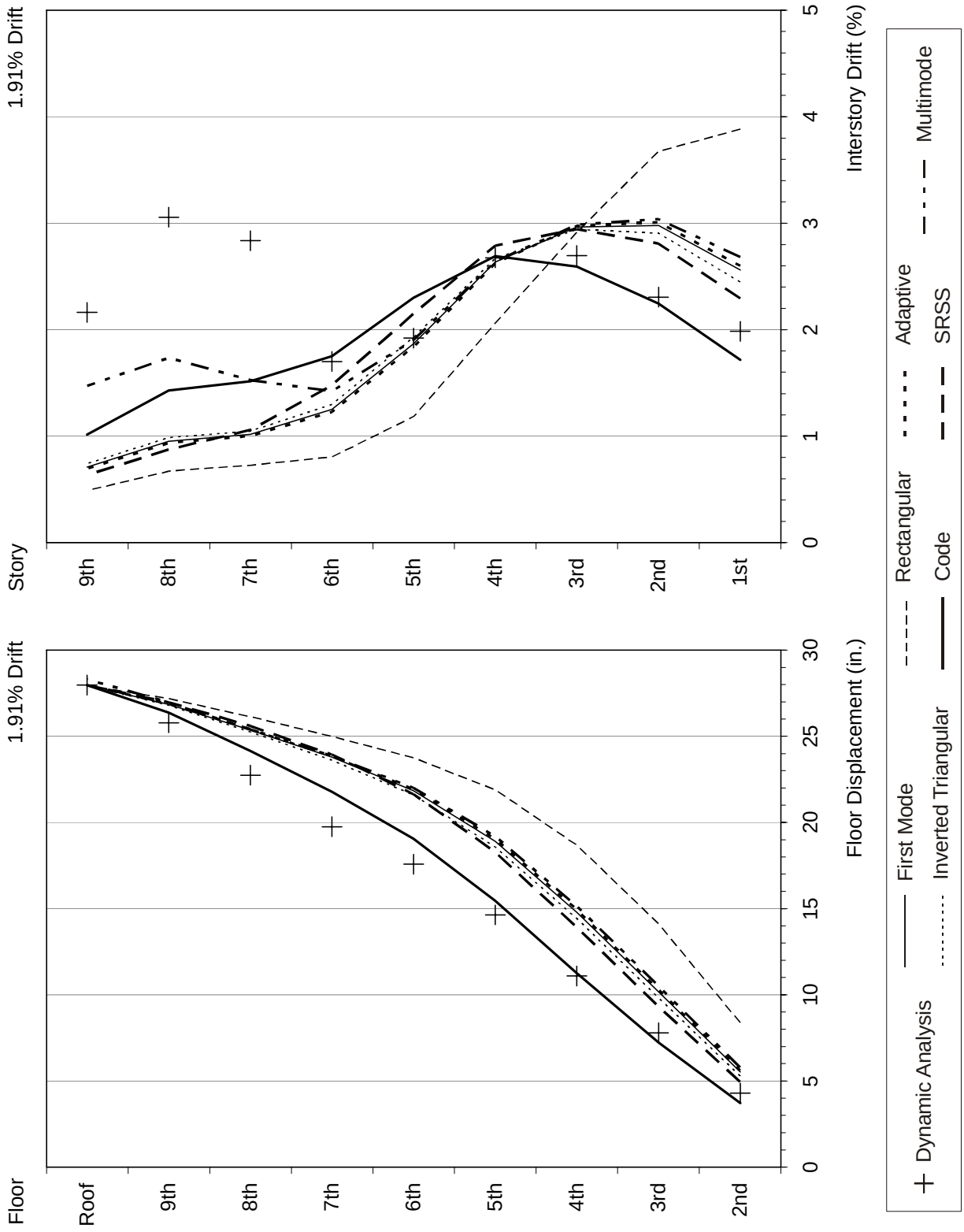


Figure F-64 Response quantities of the 9-story building under ERZMV1 ground motion

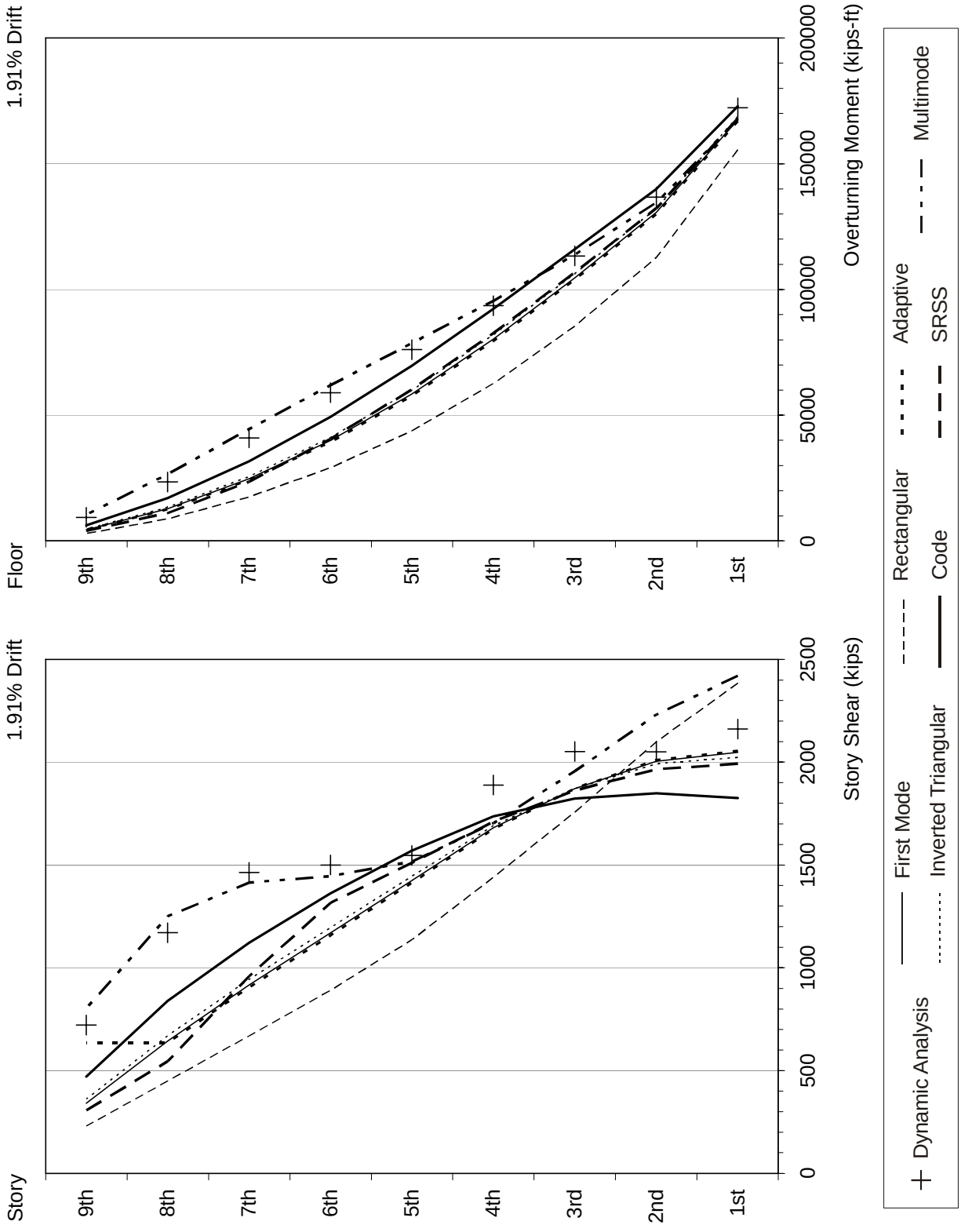


Figure F-64 Response quantities of the 9-story building under ERZMV1 ground motion (continued)

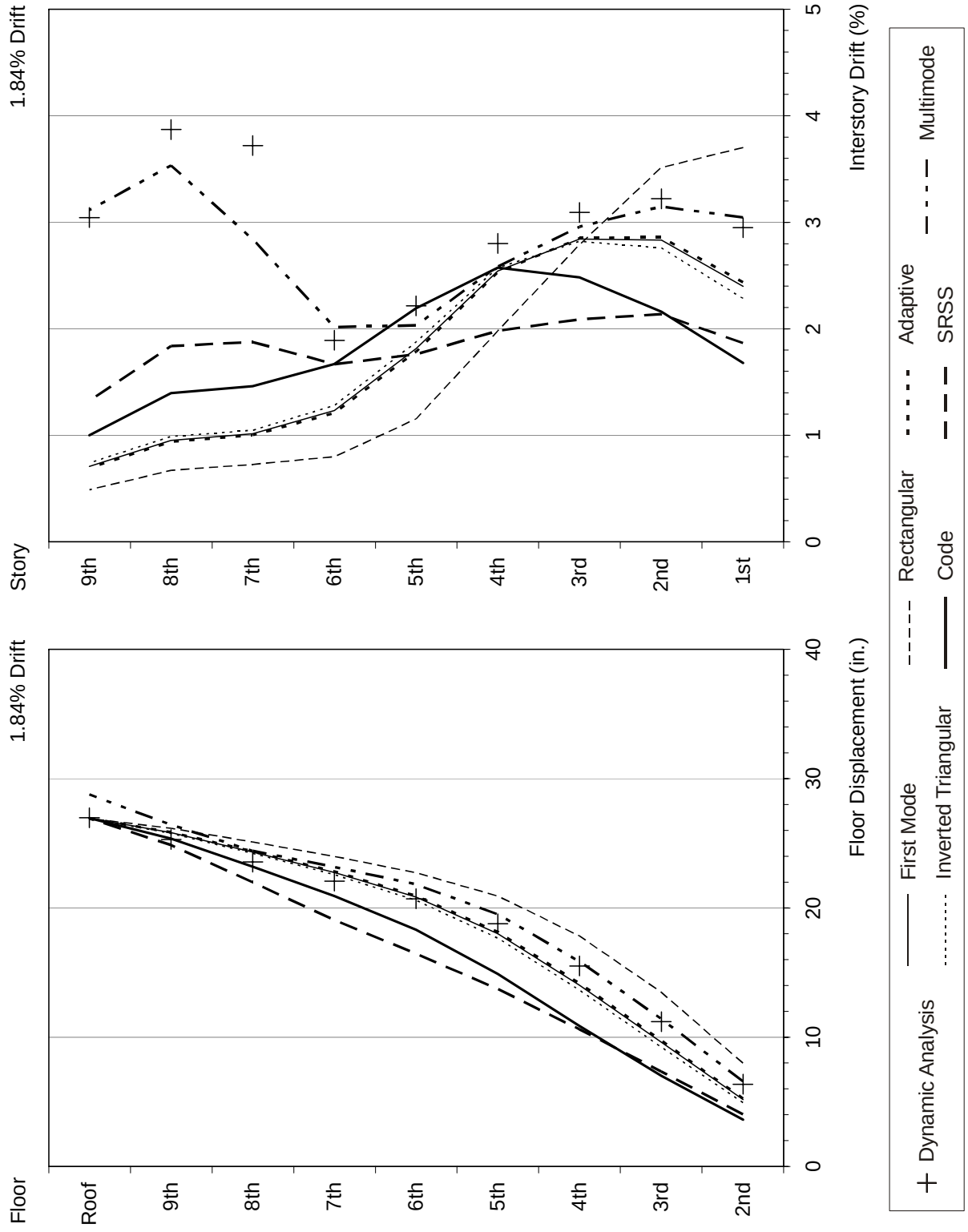


Figure F-65 Response quantities of the 9-story building under RRSMV1 ground motion

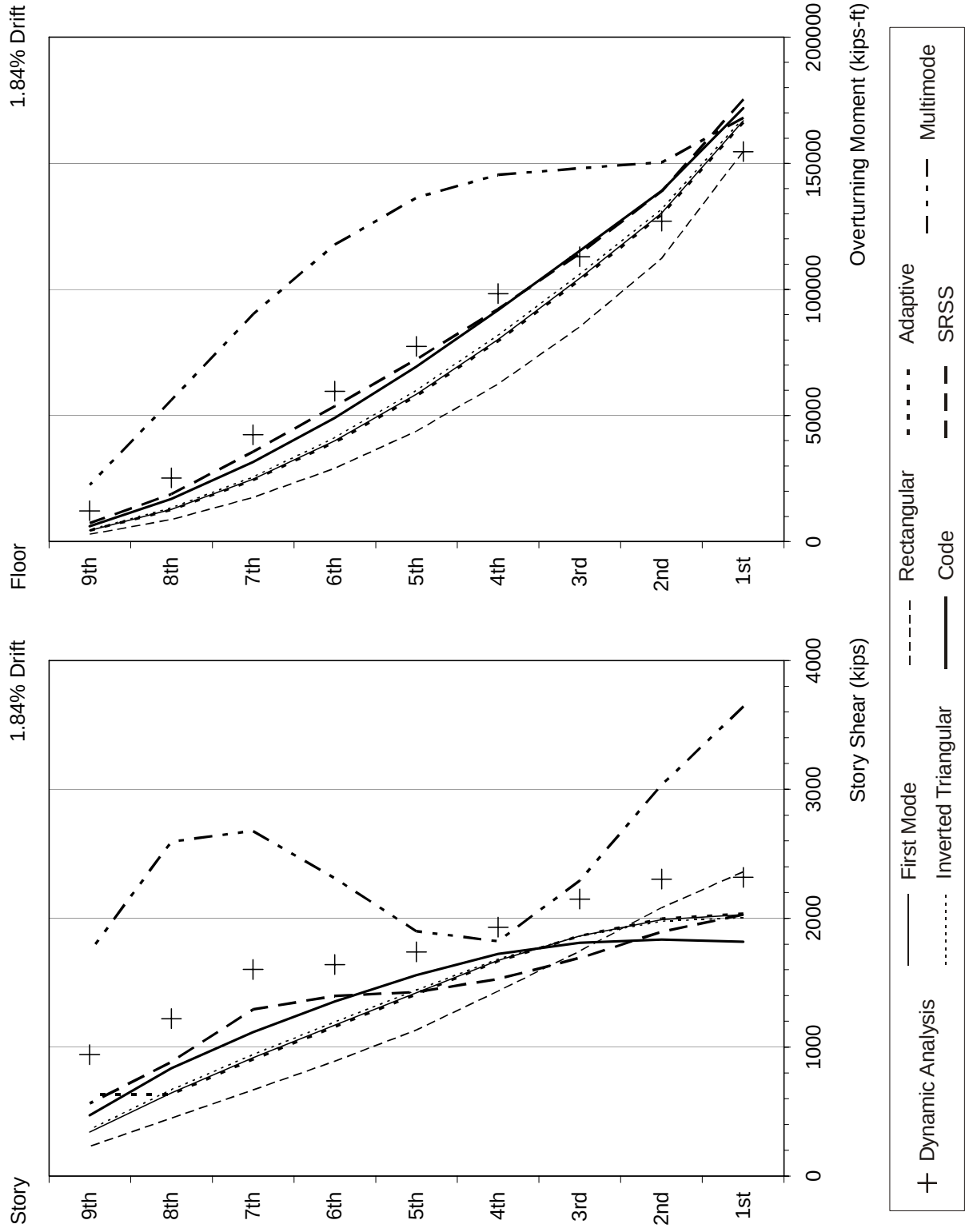


Figure F-65 Response quantities of the 9-story building under RRSMV1 ground motion (continued)

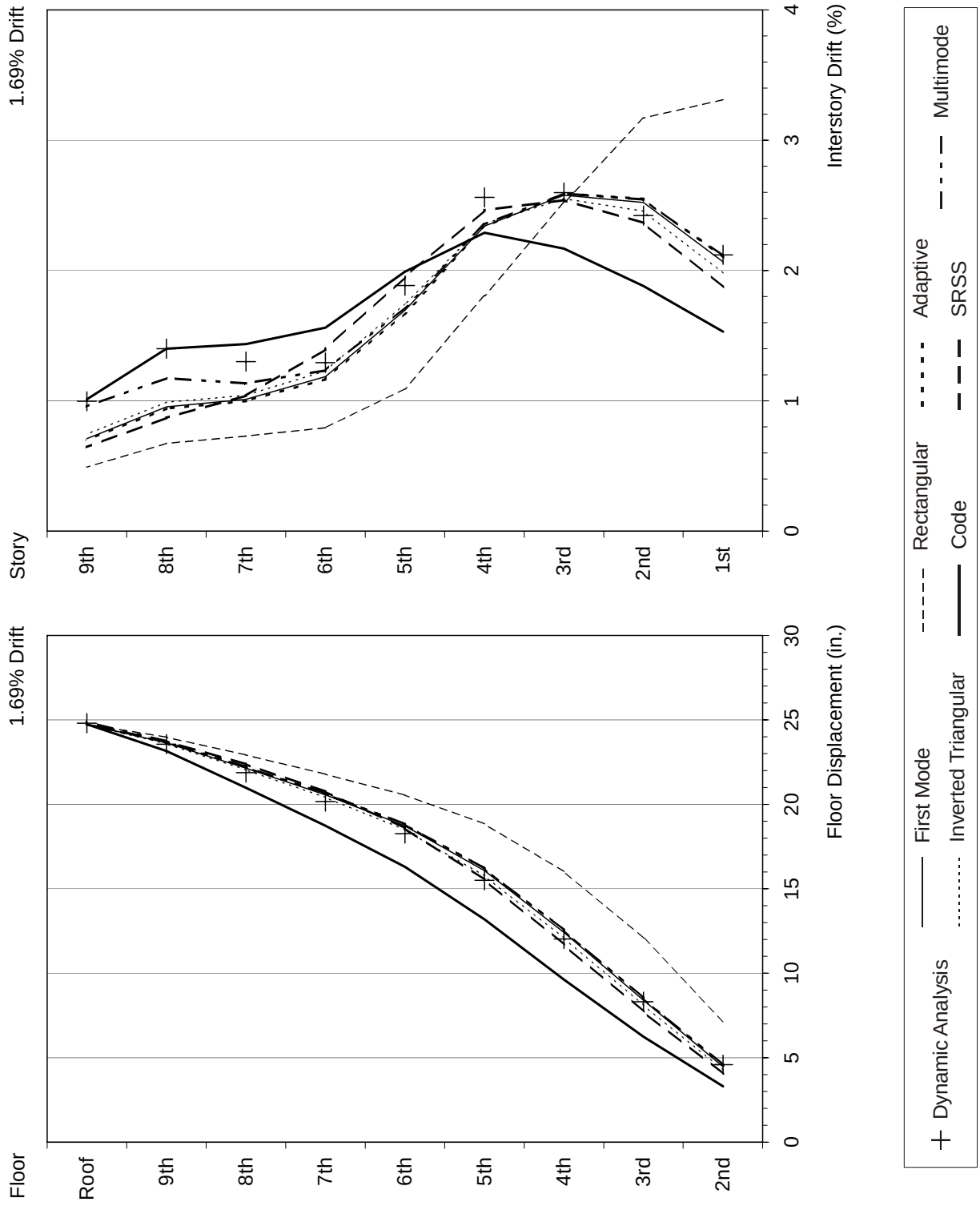


Figure F-66 Response quantities of the 9-story building under LUCMV1 ground motion

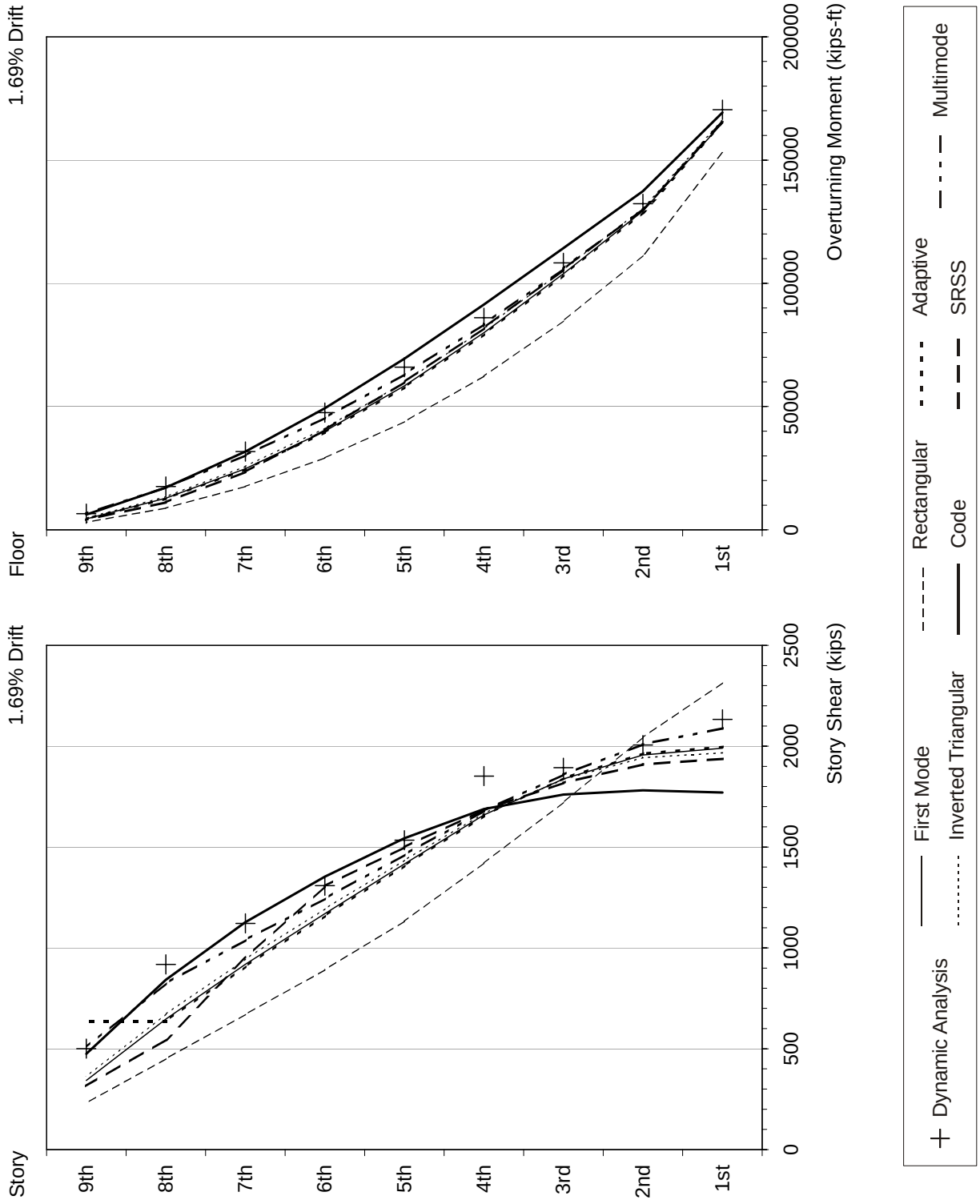


Figure F-66 Response quantities of the 9-story building under LUCMV1 ground motion (continued)

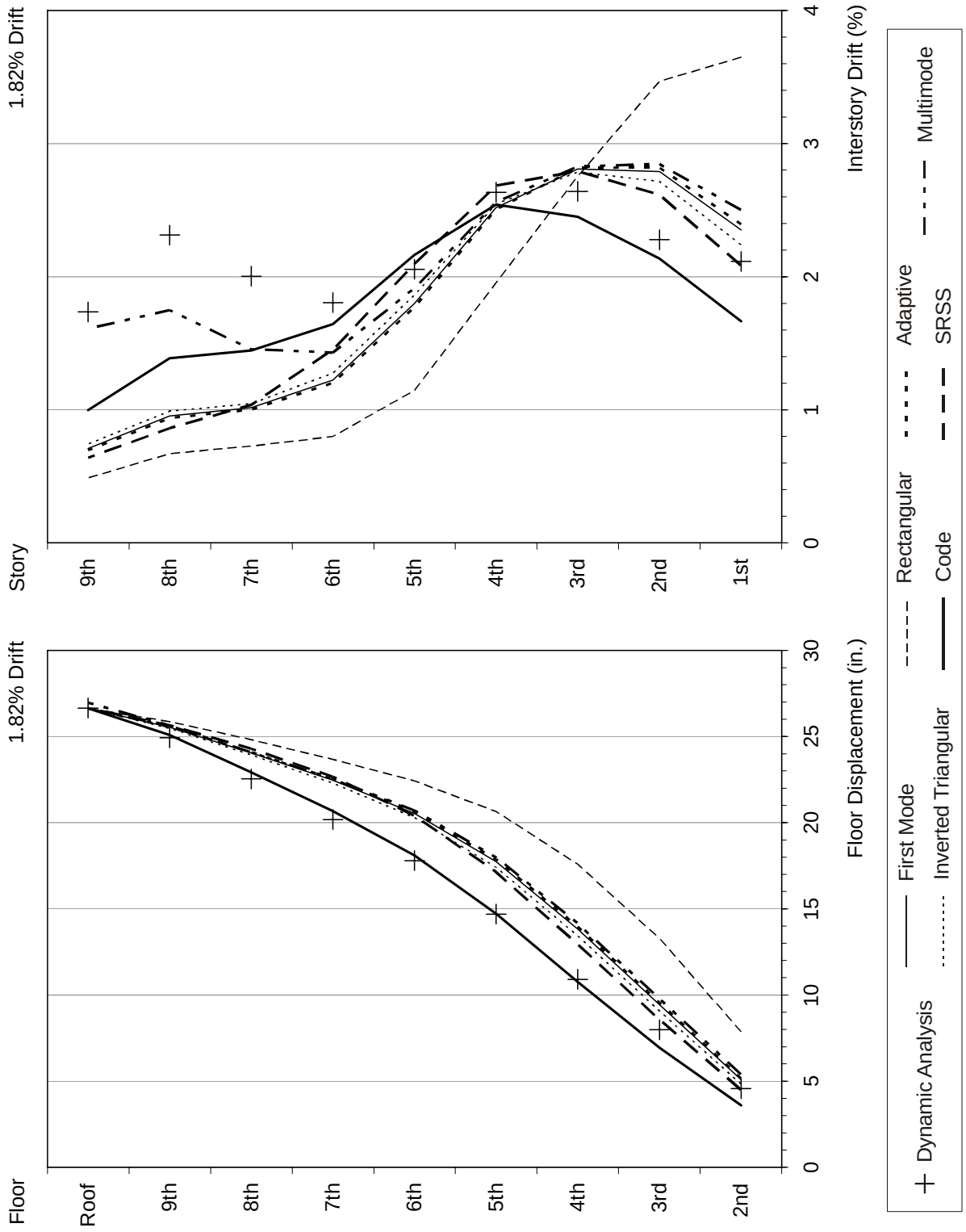


Figure F-67 Response quantities of the 9-story building under SCHMV1 ground motion

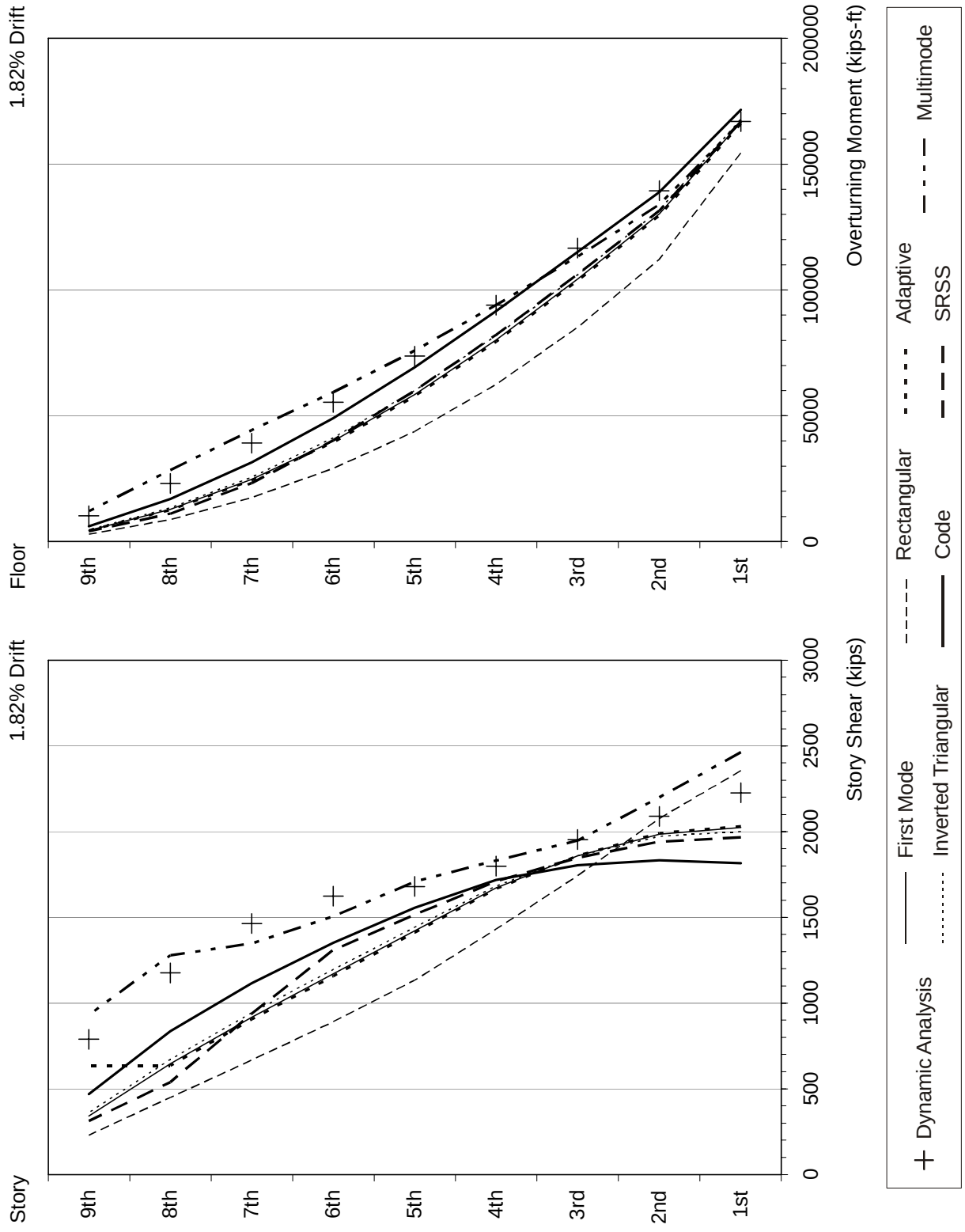


Figure F-67 Response quantities of the 9-story building under SCHMV1 ground motion (continued)

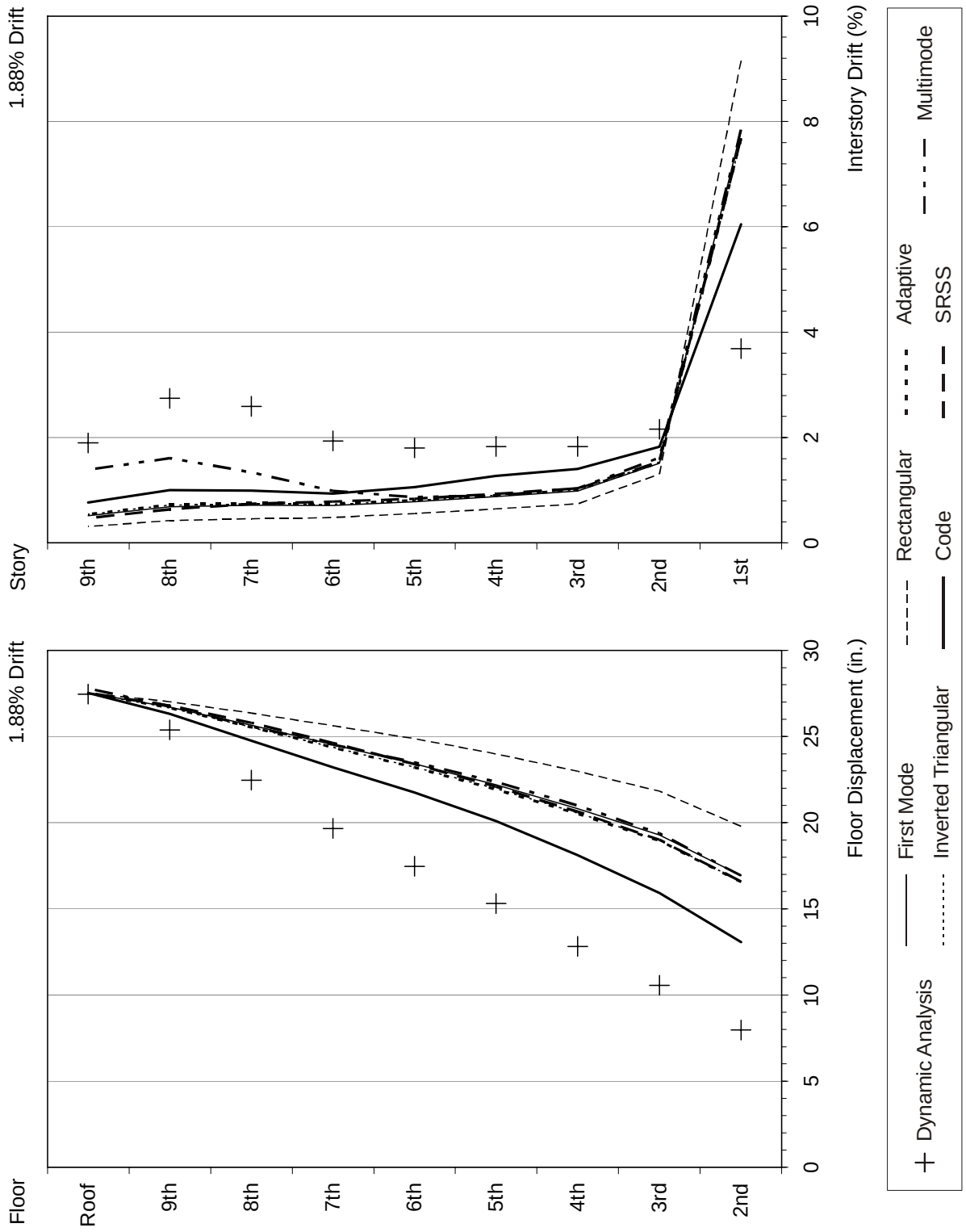


Figure F-68 Response quantities of the 9-story weak-story building under ERZMV1 ground motion

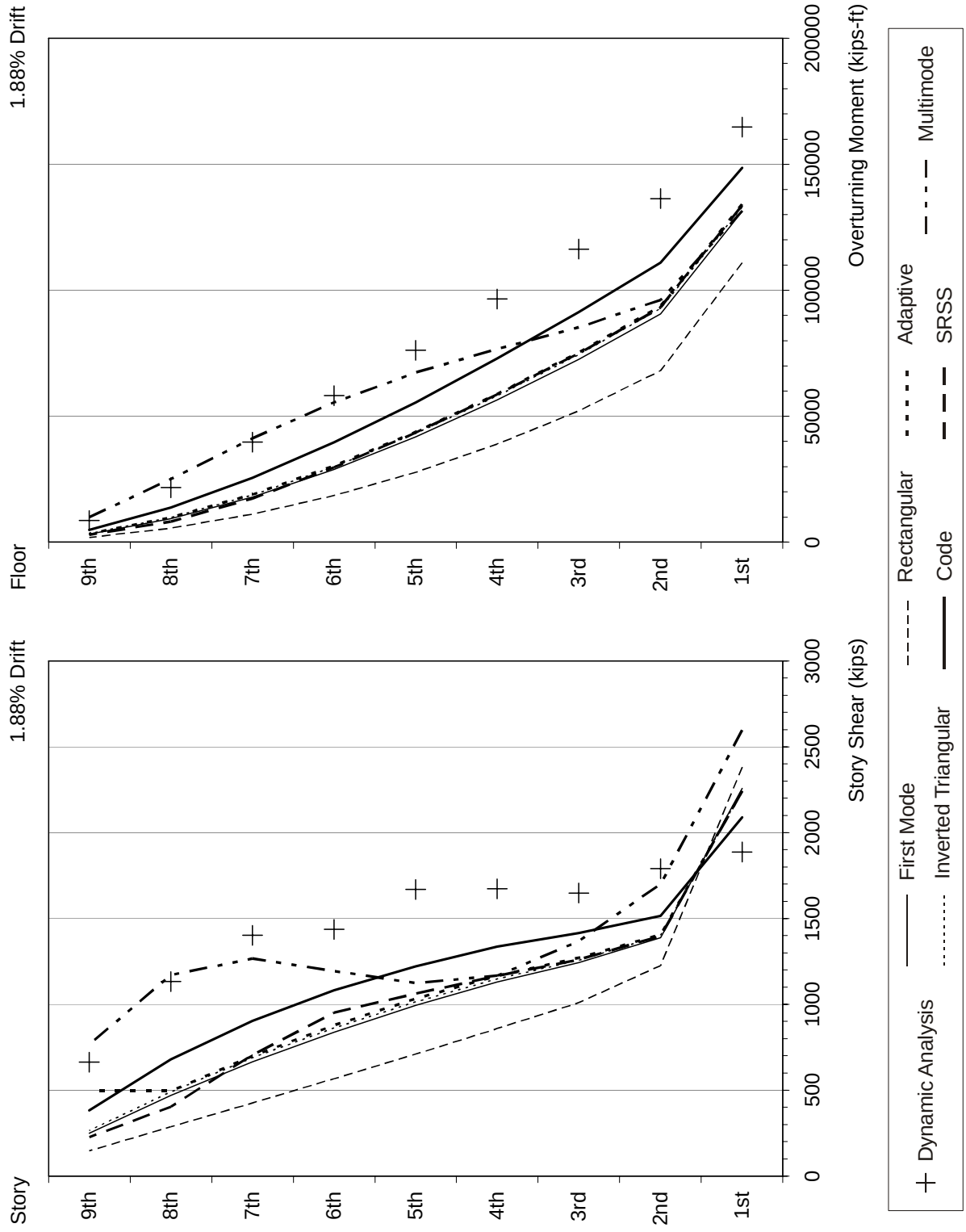


Figure F-68 Response quantities of the 9-story weak-story building under ERZMV1 ground motion (continued)

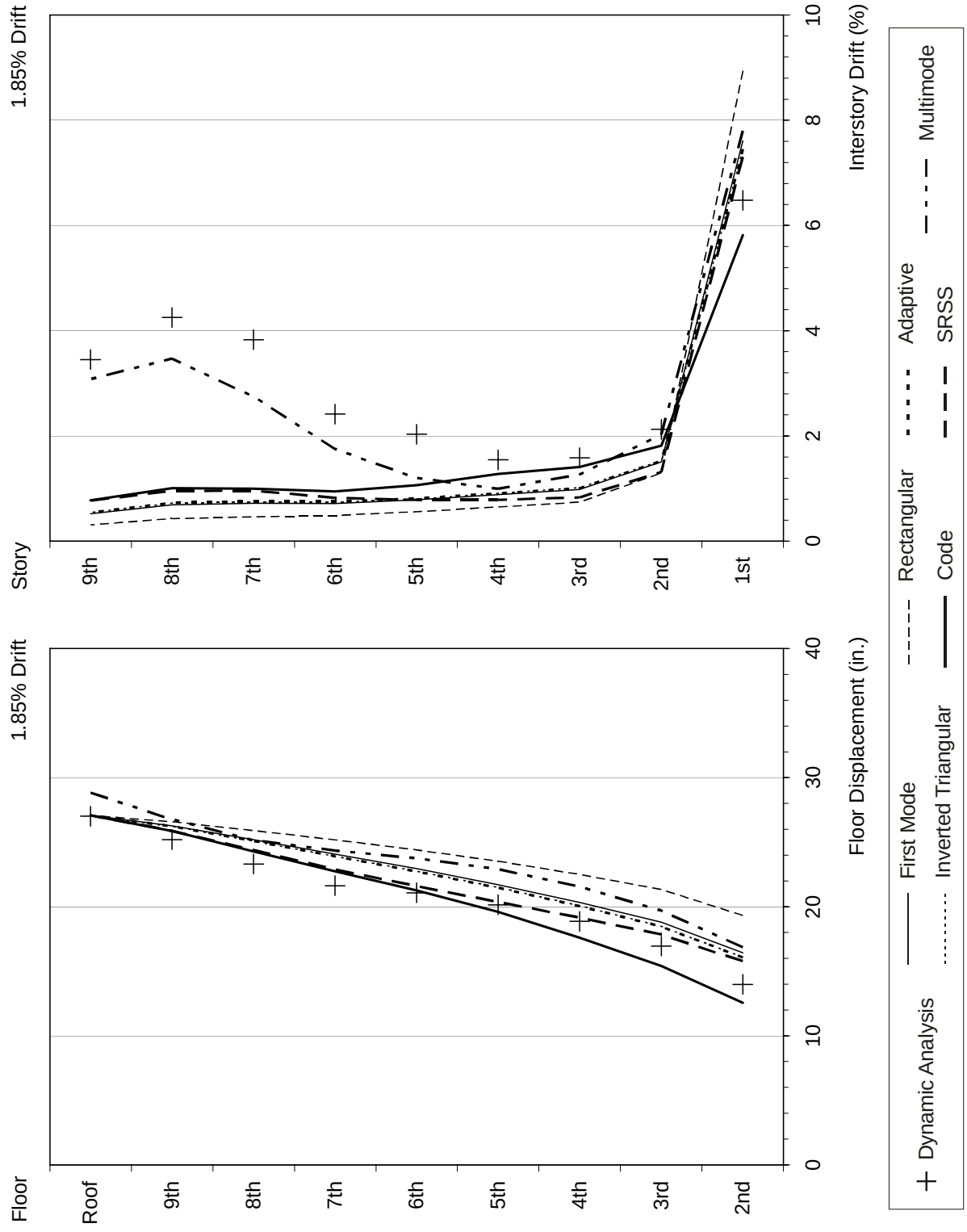


Figure F-69 Response quantities of the 9-story weak-story building under RRSMV1 ground motion

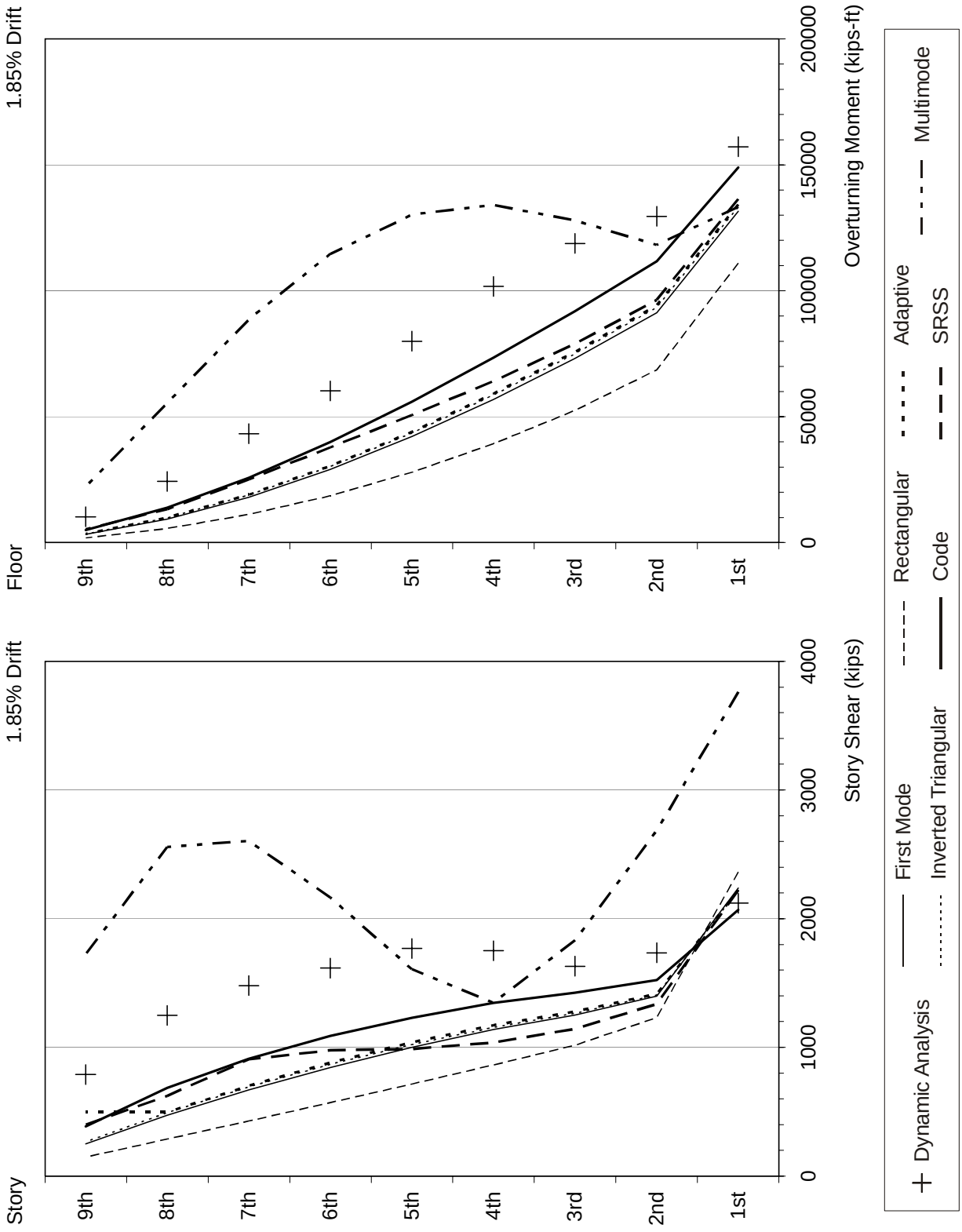


Figure F-69 Response quantities of the 9-story weak-story building under RRSMV1 ground motion (Continued)

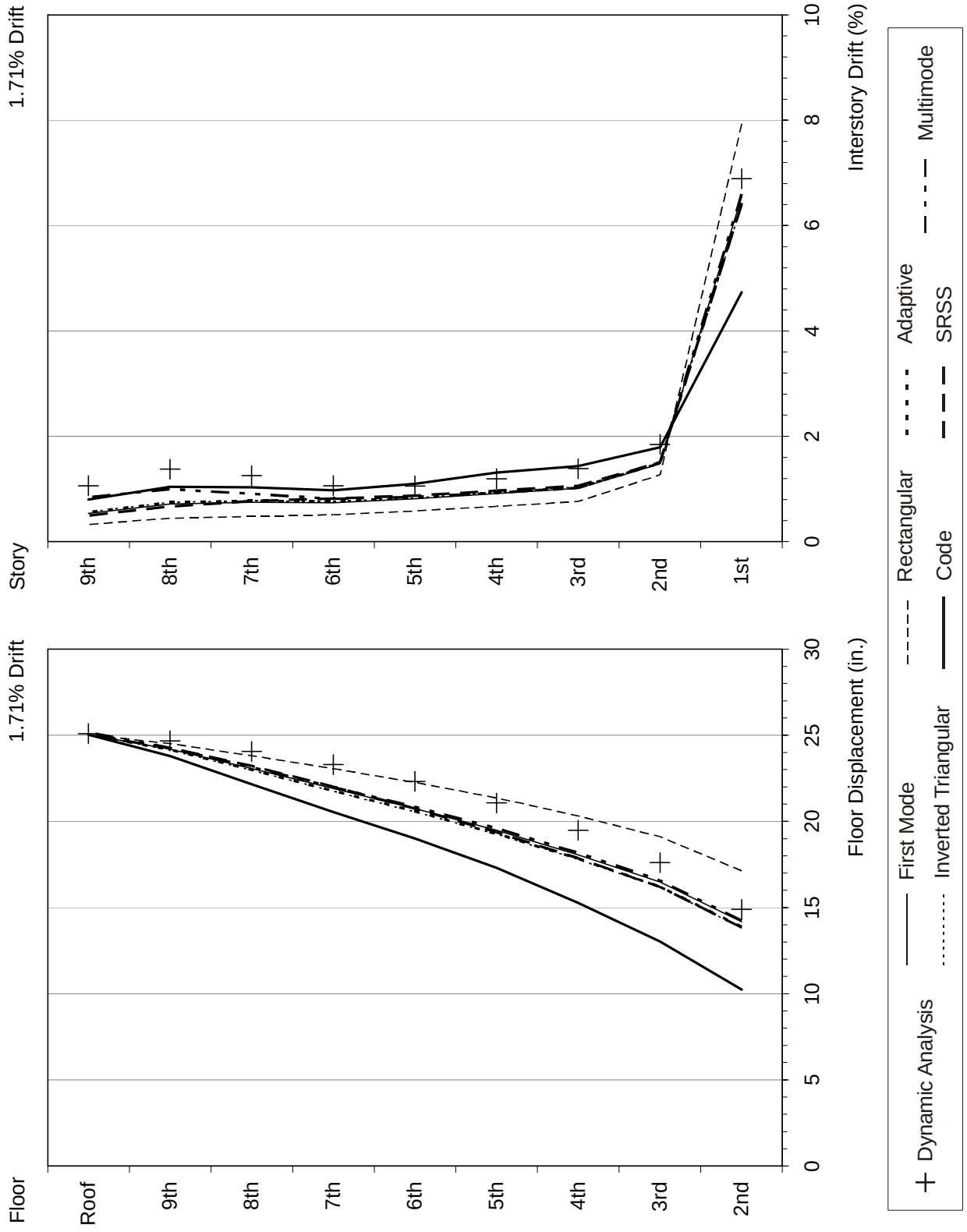


Figure F-70 Response quantities of the 9-story weak-story building under LUCMV1 ground motion

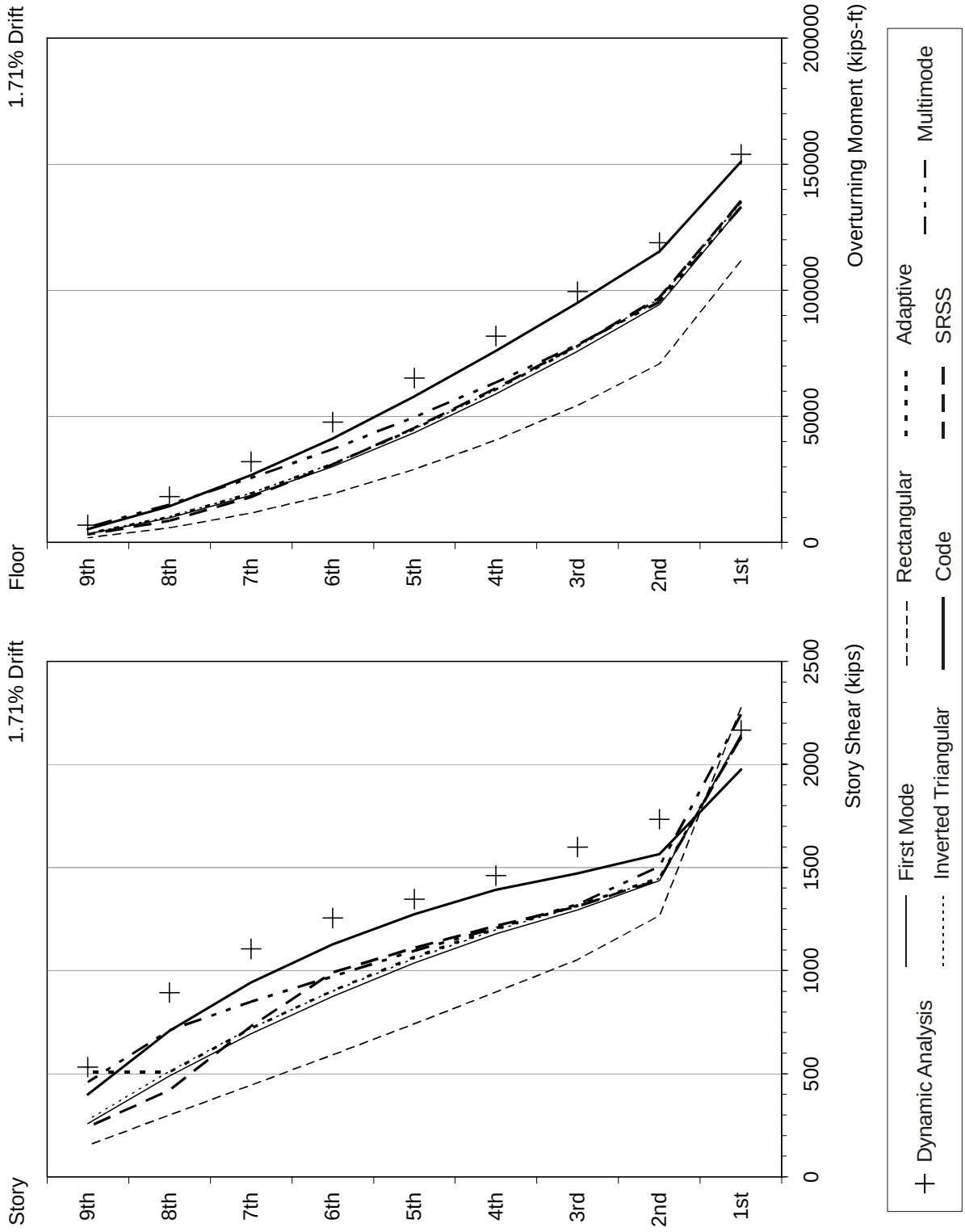


Figure F-70 Response quantities of the 9-story weak-story building under LUCMV1 ground motion (continued)

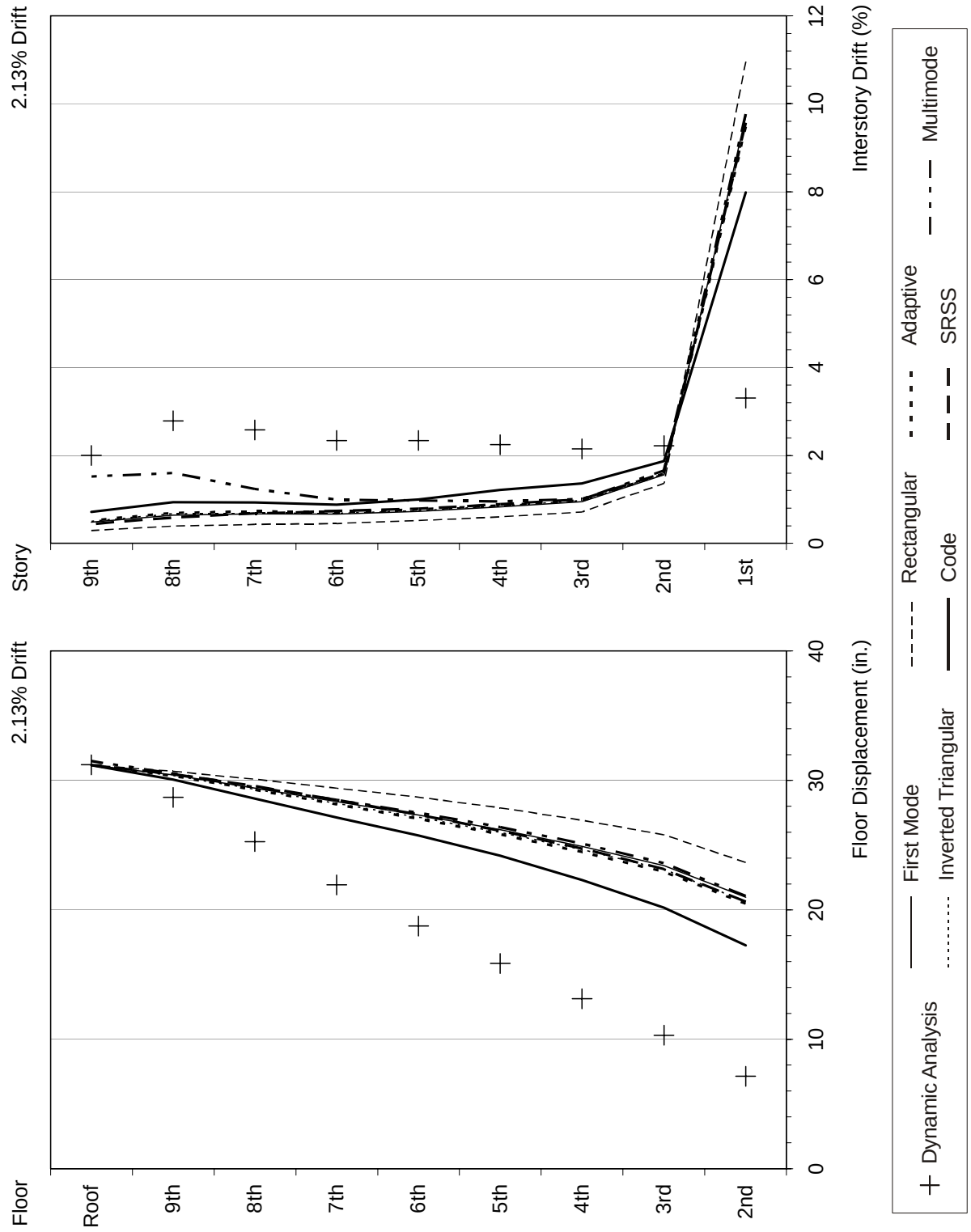


Figure F-71 Response quantities of the 9-story weak-story building under SCHMV1 ground motion

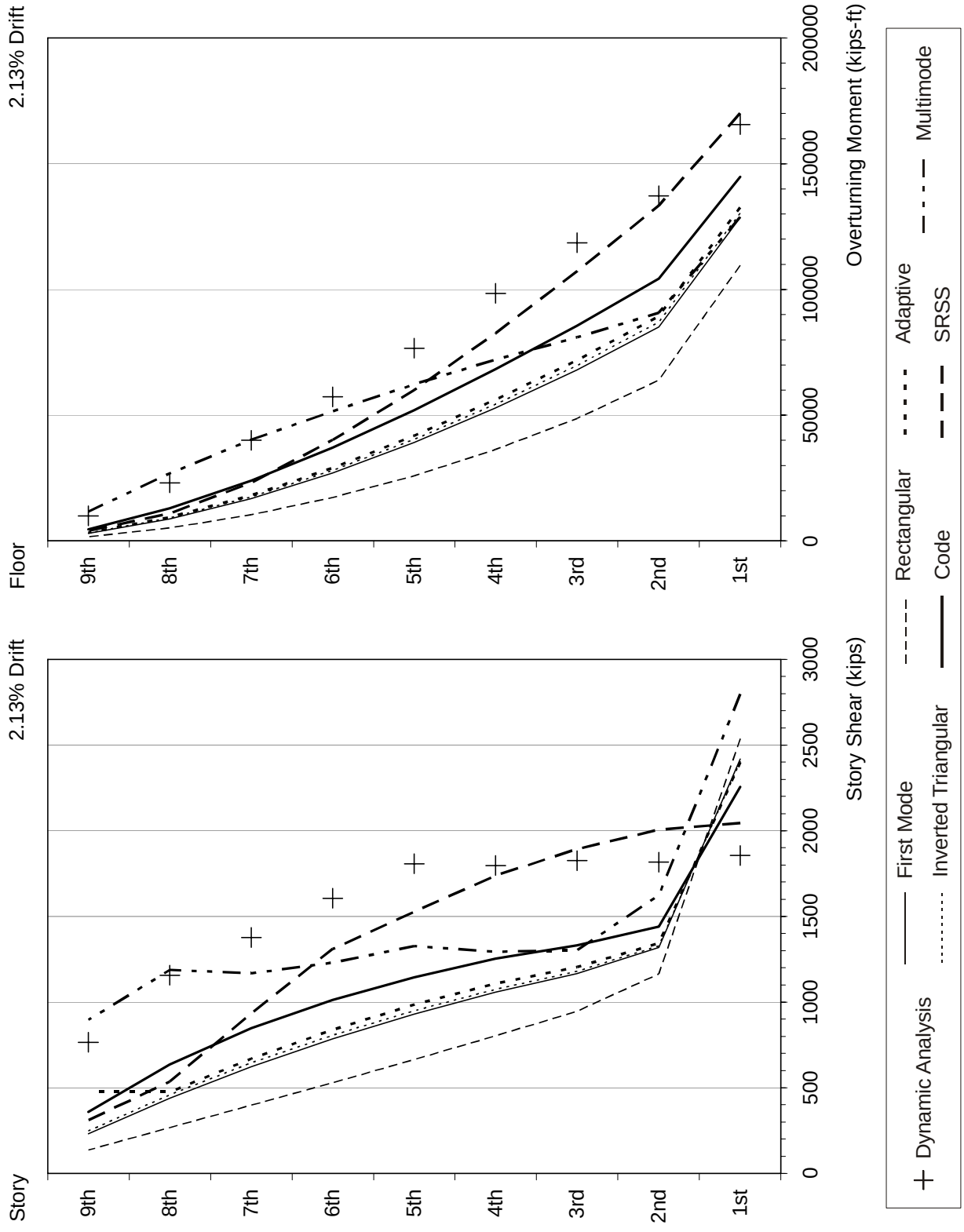


Figure F-71 Response quantities of the 9-story weak-story building under SCHMV1 ground motion (continued)

### *F.8.5 Errors Associated with Near Fault Motions*

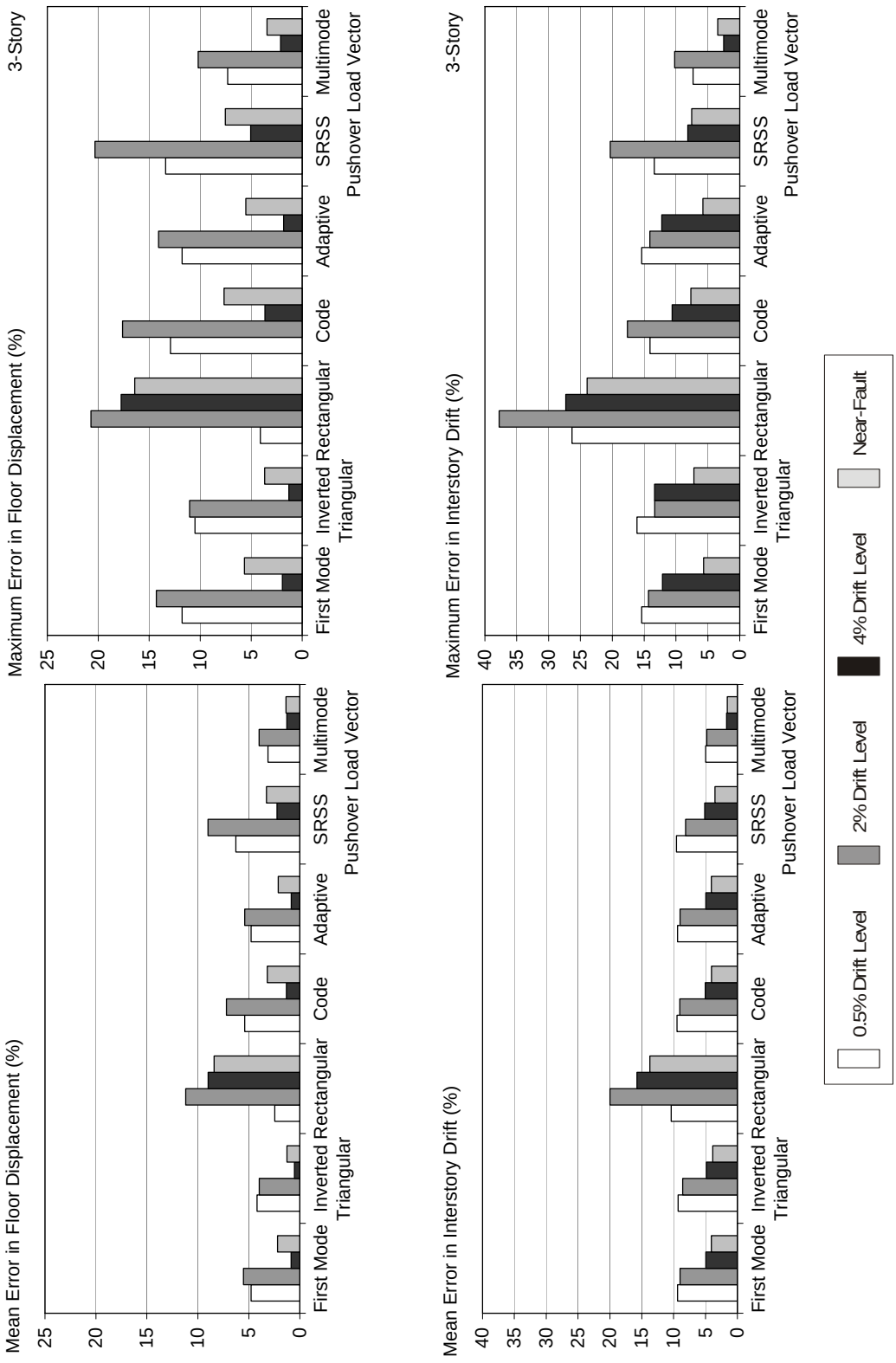


Figure F-72 Mean and maximum errors for the 3-story building

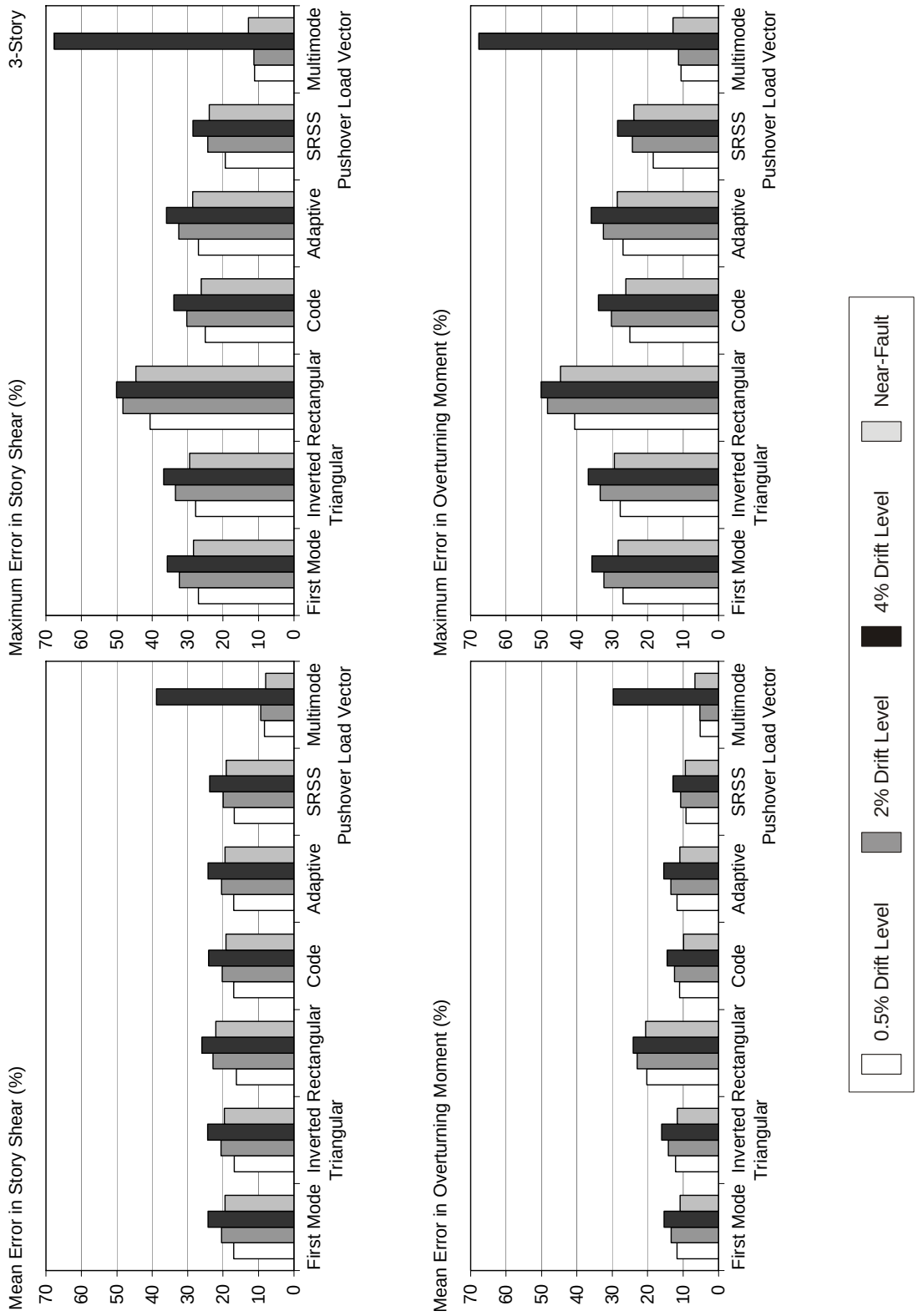


Figure F-72 Mean and maximum errors for the 3-story building (continued)

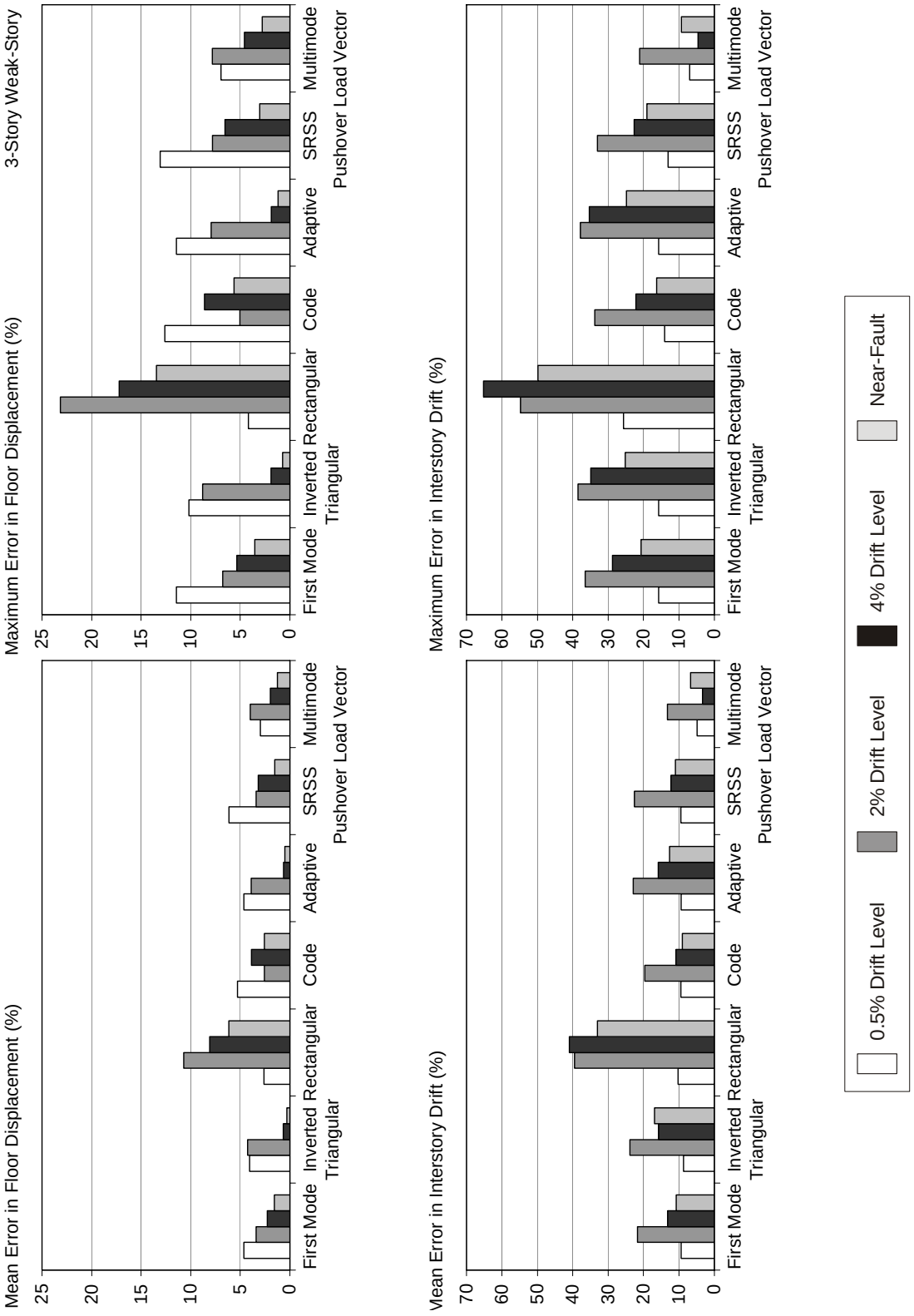


Figure F-73 Mean and maximum errors for the 3-story weak-story building

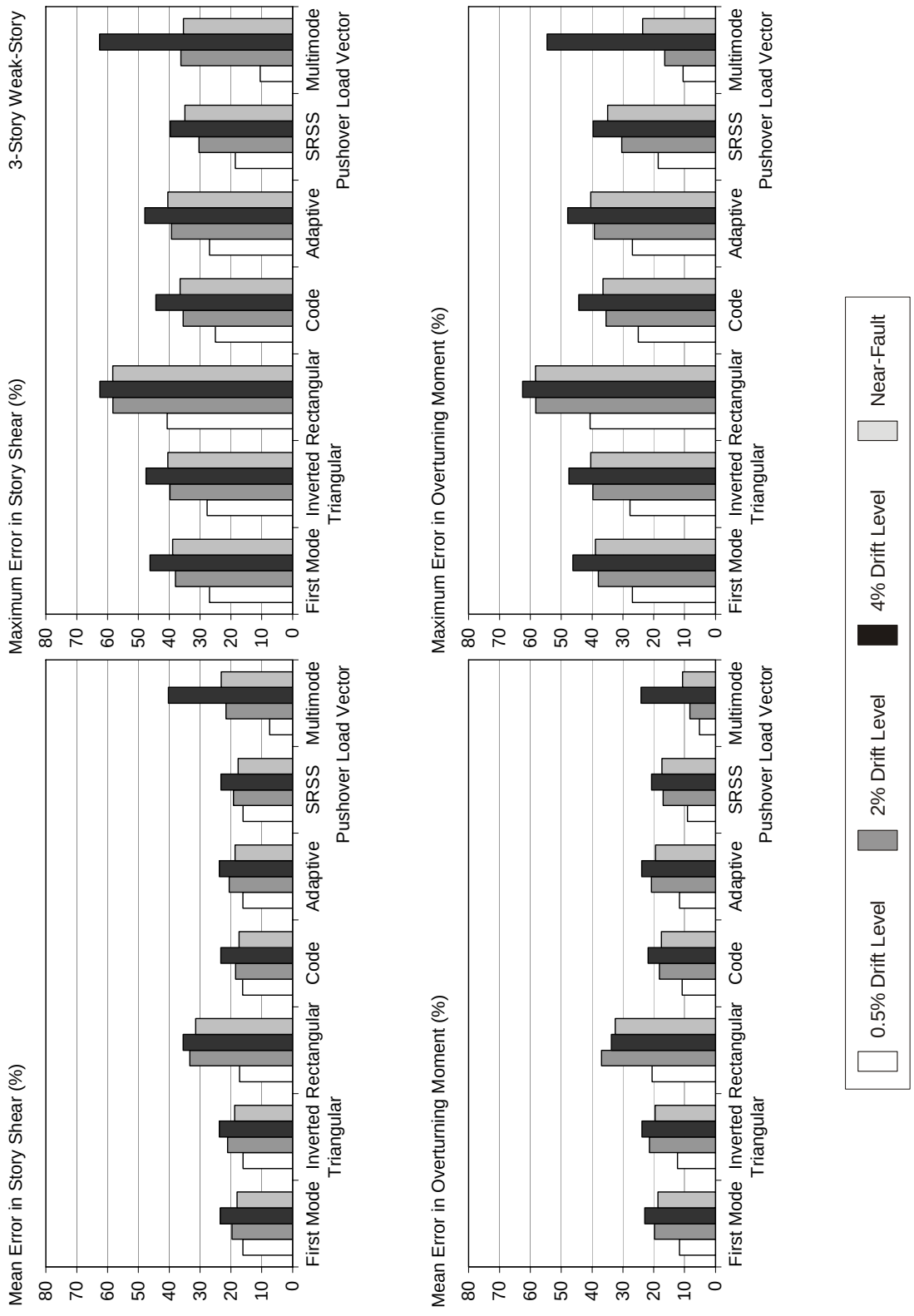


Figure F-73 Mean and maximum errors for the 3-story weak-story building (continued)

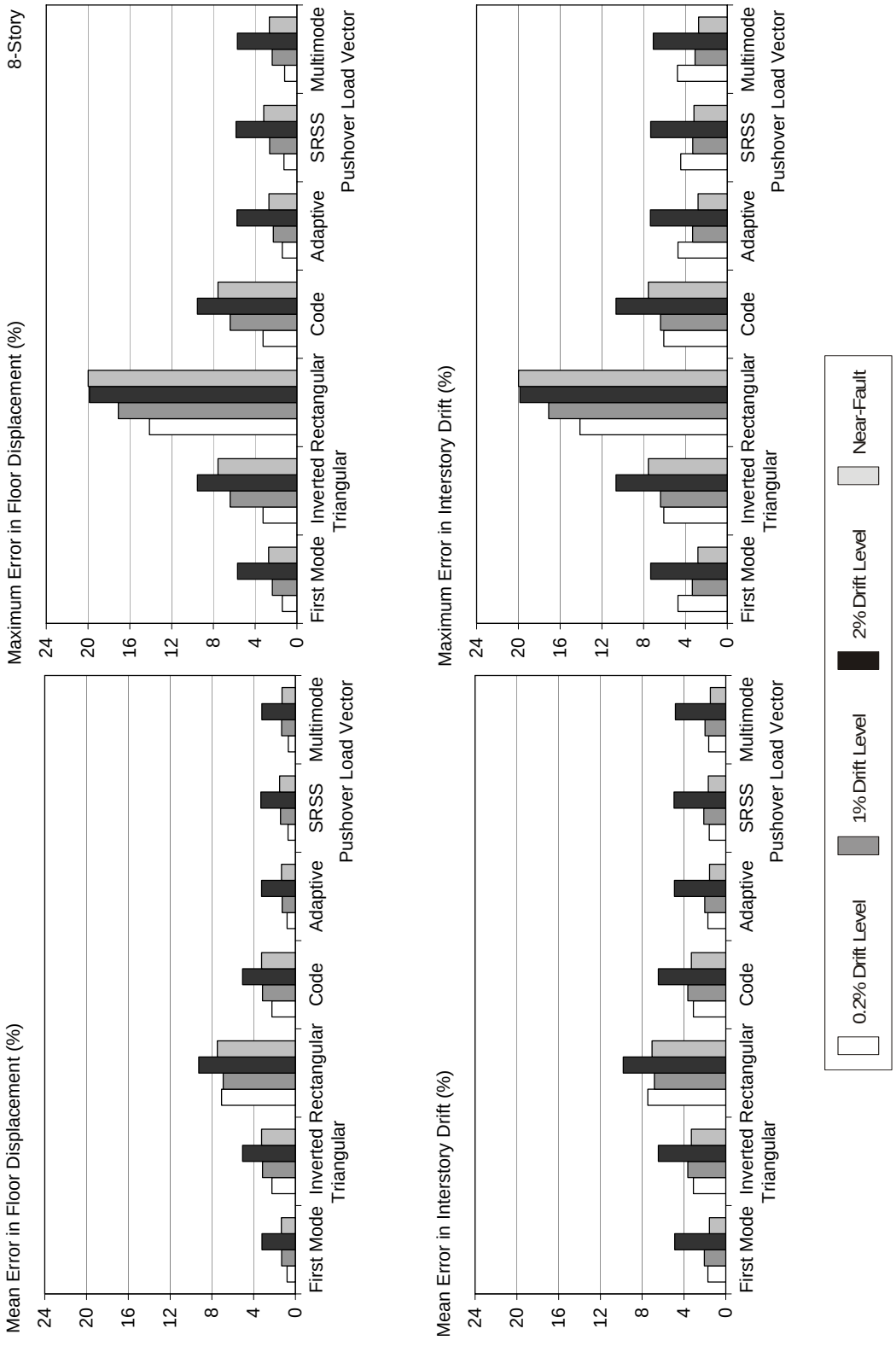


Figure F-74 Mean and maximum errors for the 8-story building

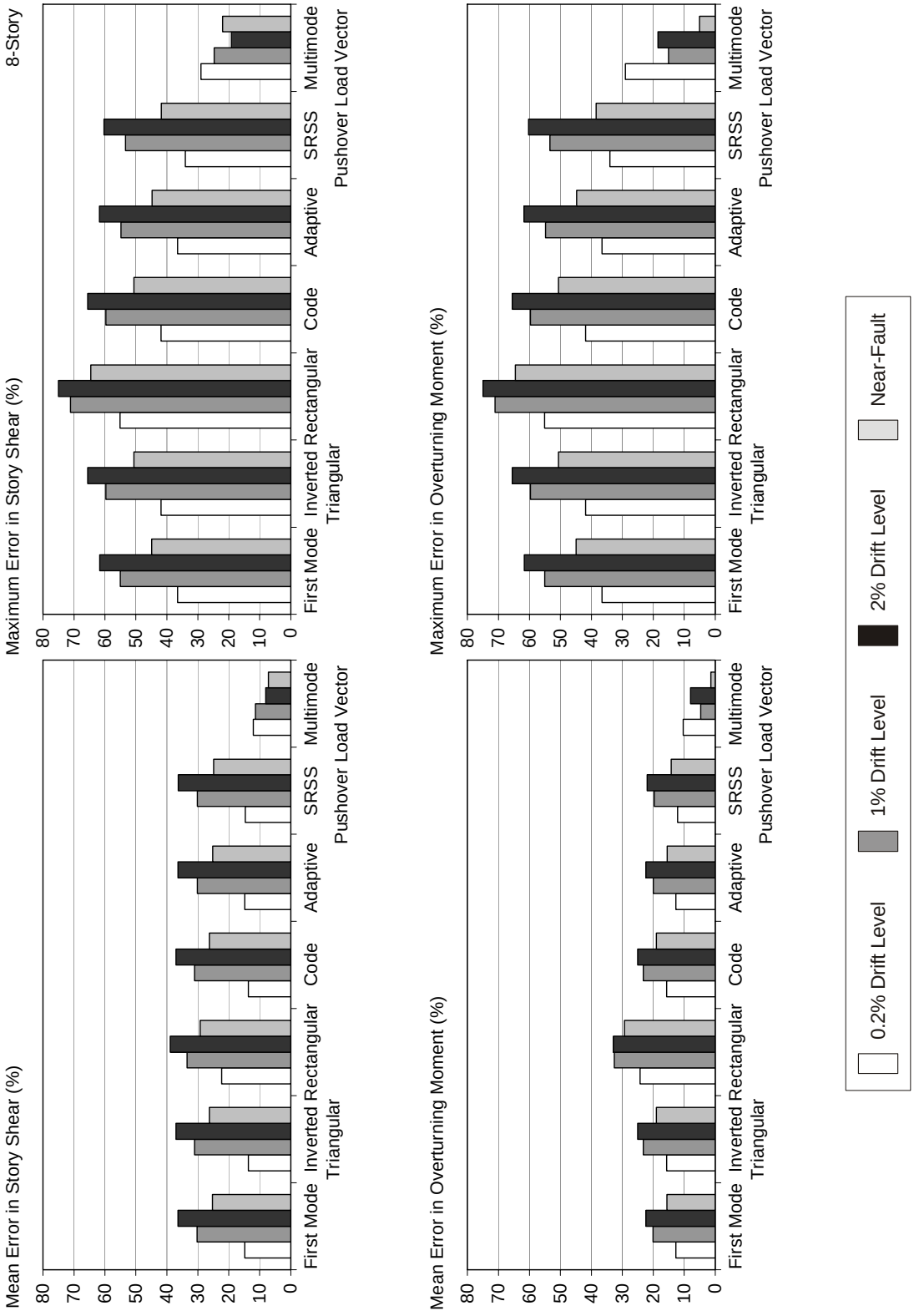


Figure F-74 Mean and maximum errors for the 8-story building (continued)

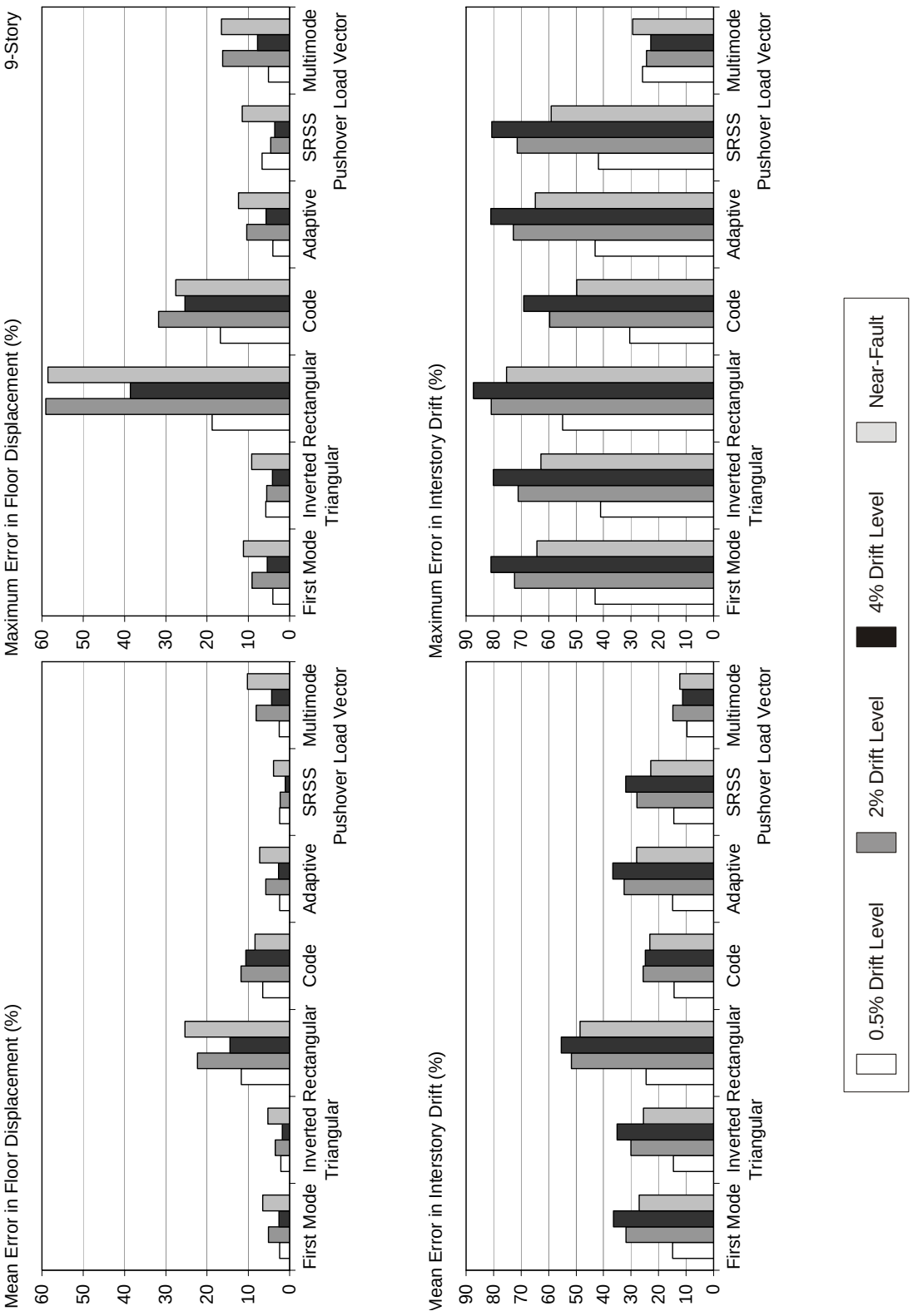


Figure F-75 Mean and maximum errors for the 9-story building

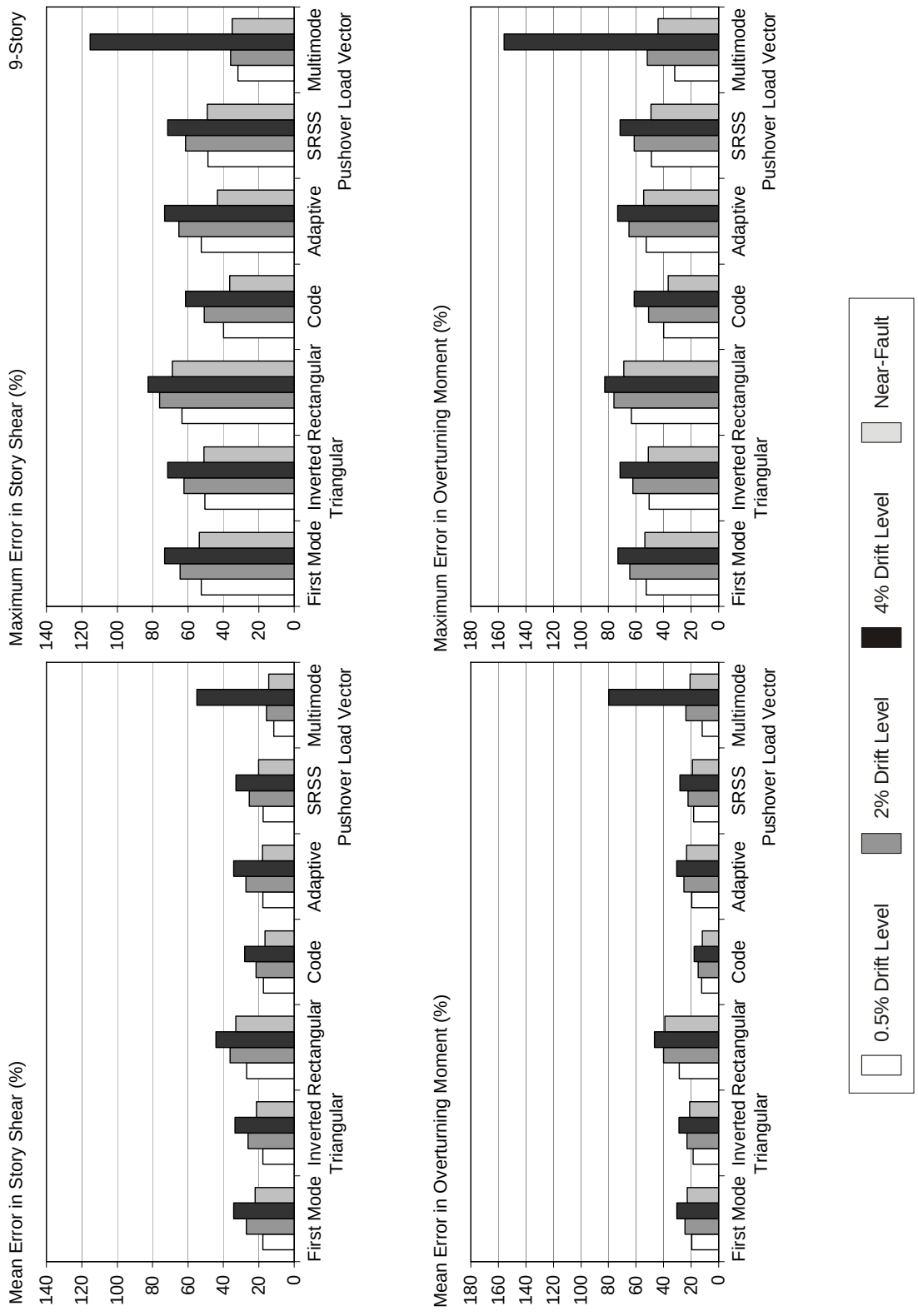


Figure F-75 Mean and maximum errors for the 9-story building (continued)

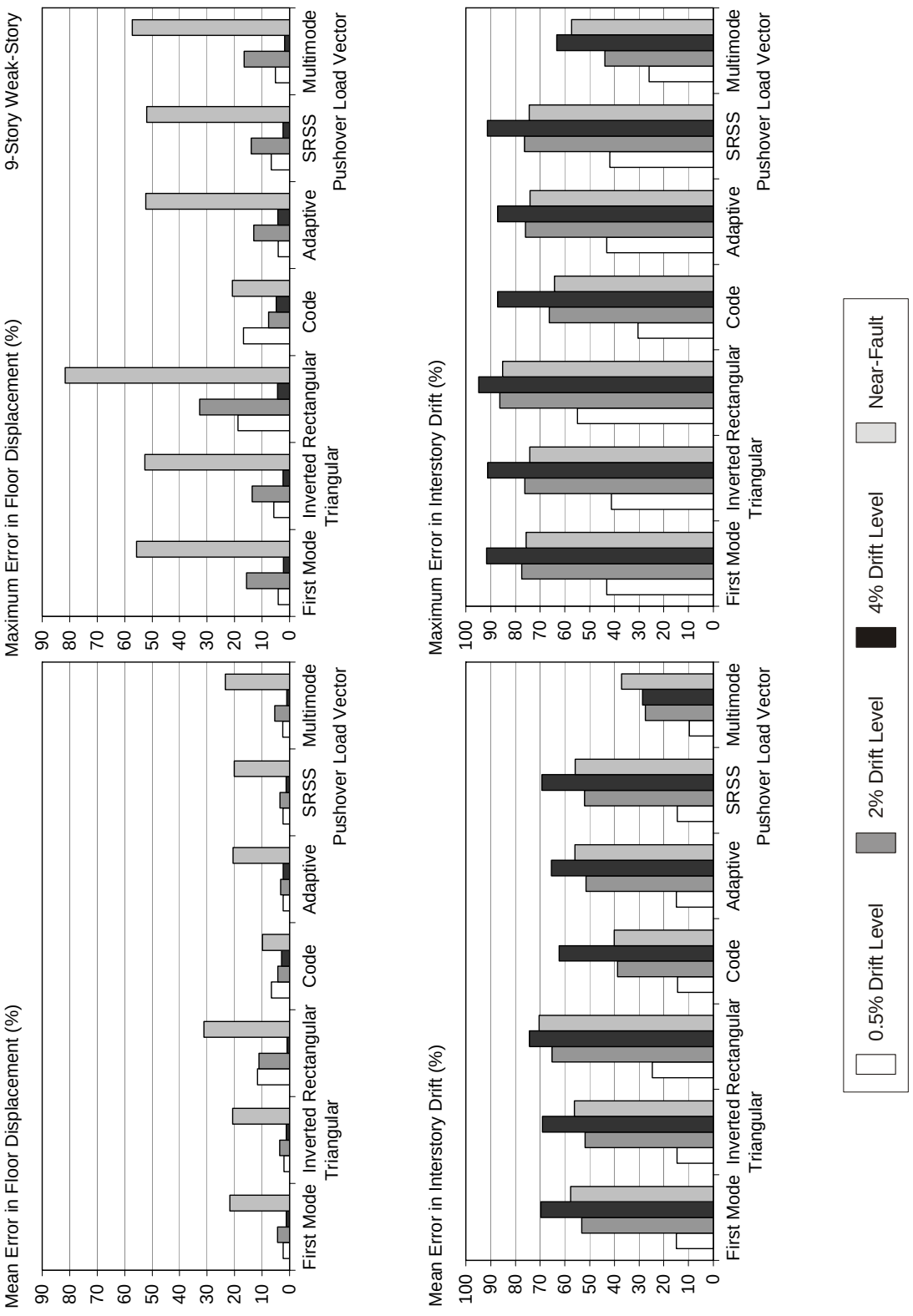


Figure F-76 Mean and maximum errors for the 9-story weak-story building

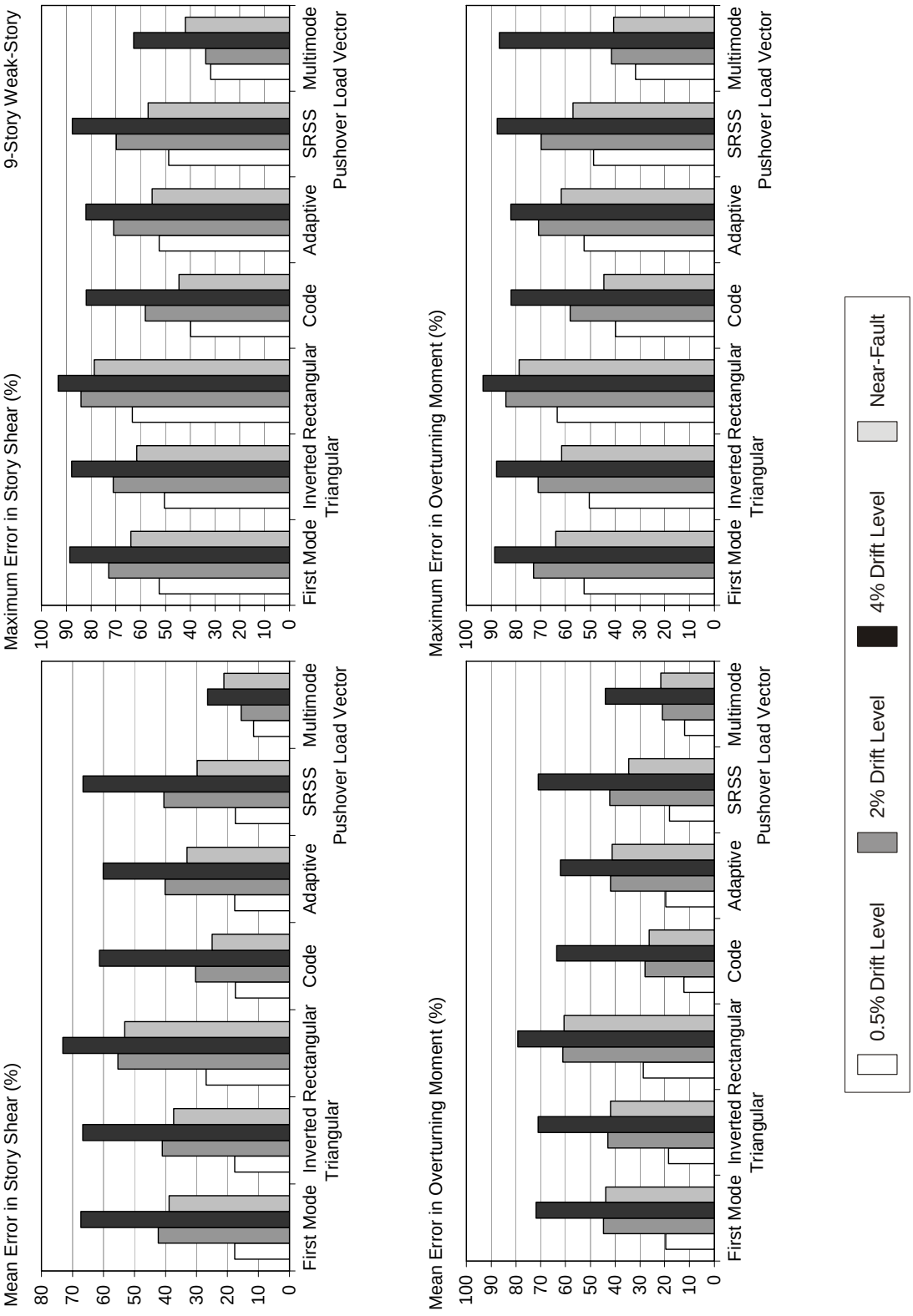


Figure F-76 Mean and maximum errors for the 9-story weak-story building (continued)

### *F.8.6 Observed Coefficients of Variation of the Response Quantities Determined for the Ordinary (Site Class C) Motions*

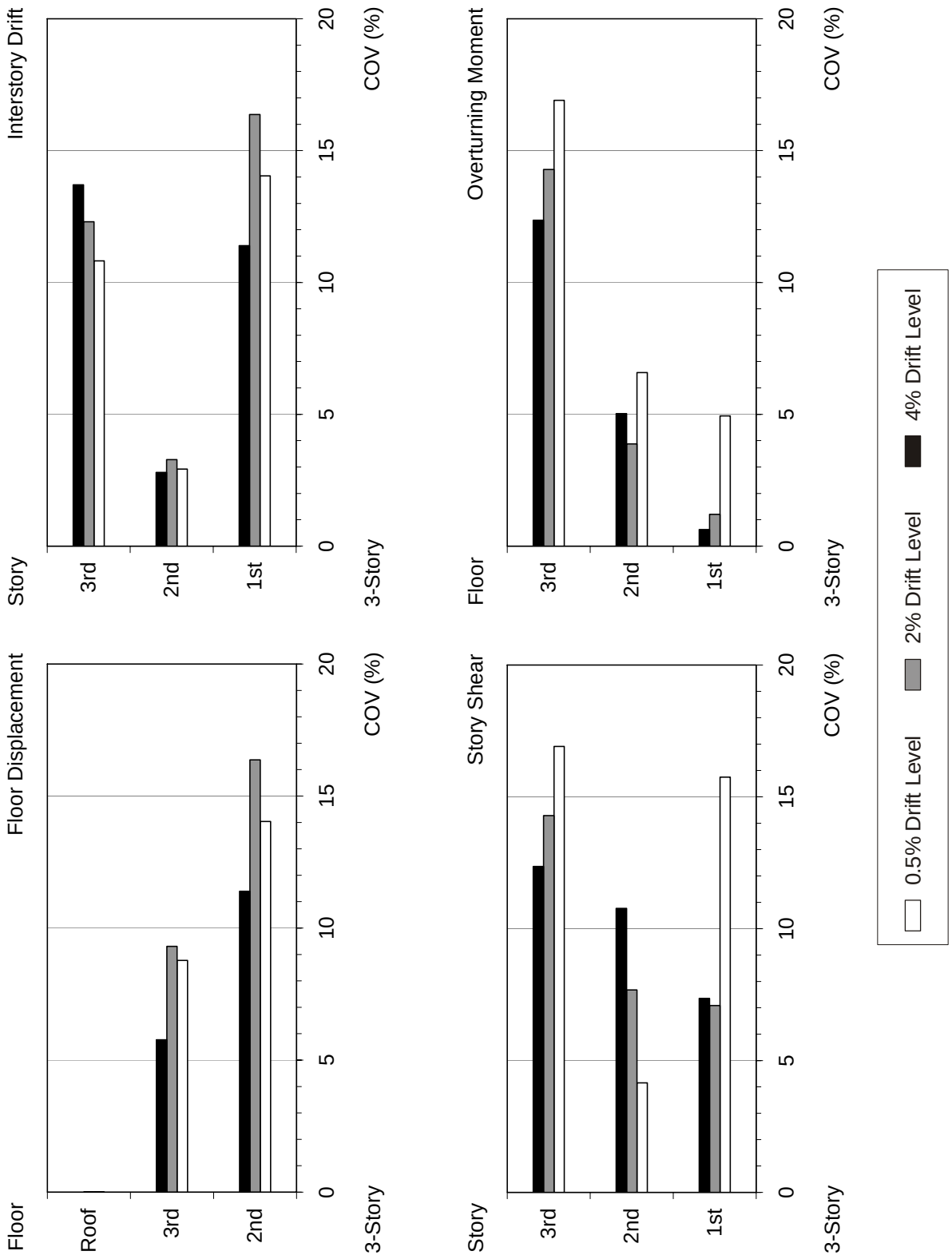


Figure F-77 Observed COVs for the 3-story frame building.

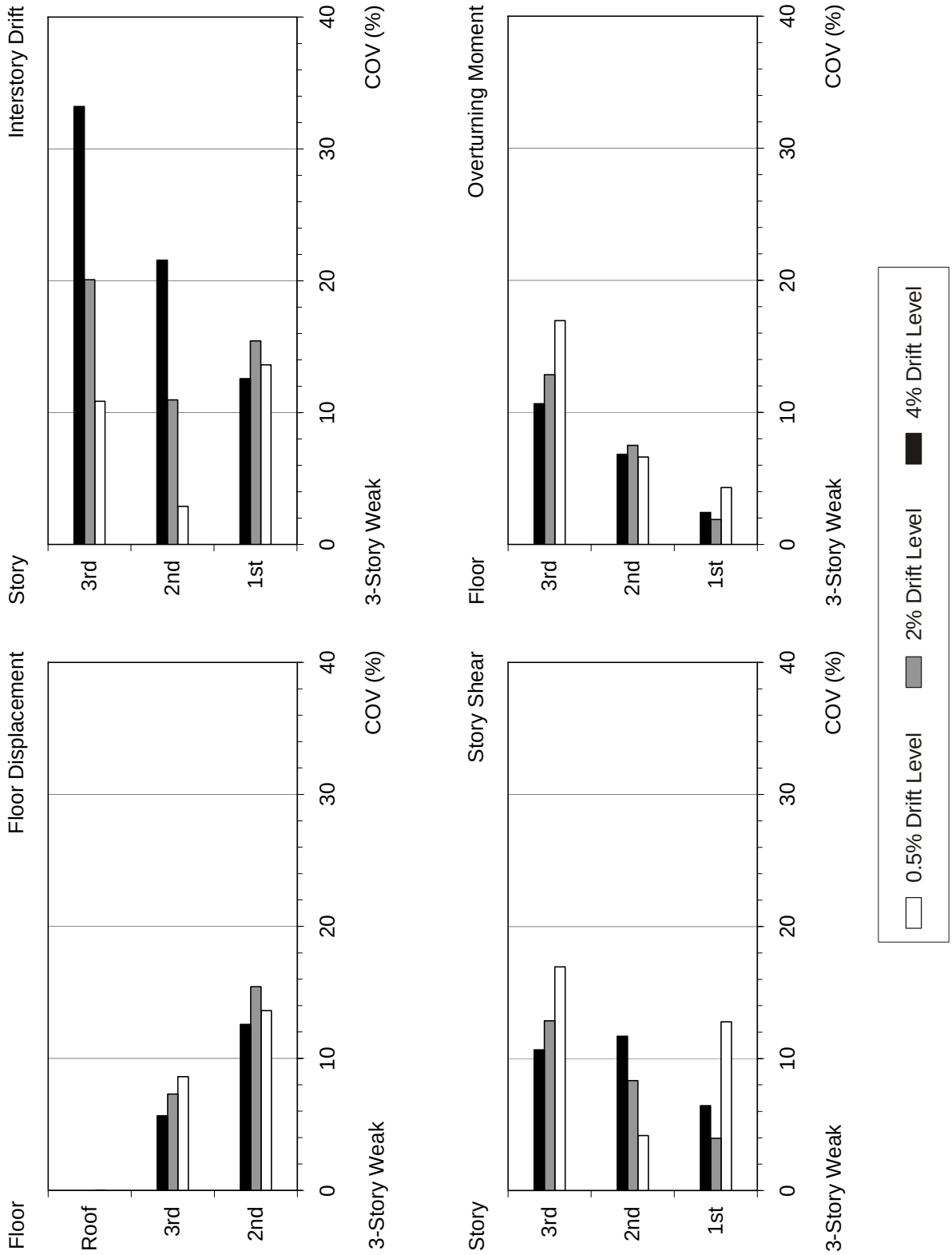


Figure F-78 Observed COVs for the 3-story weak story frame building

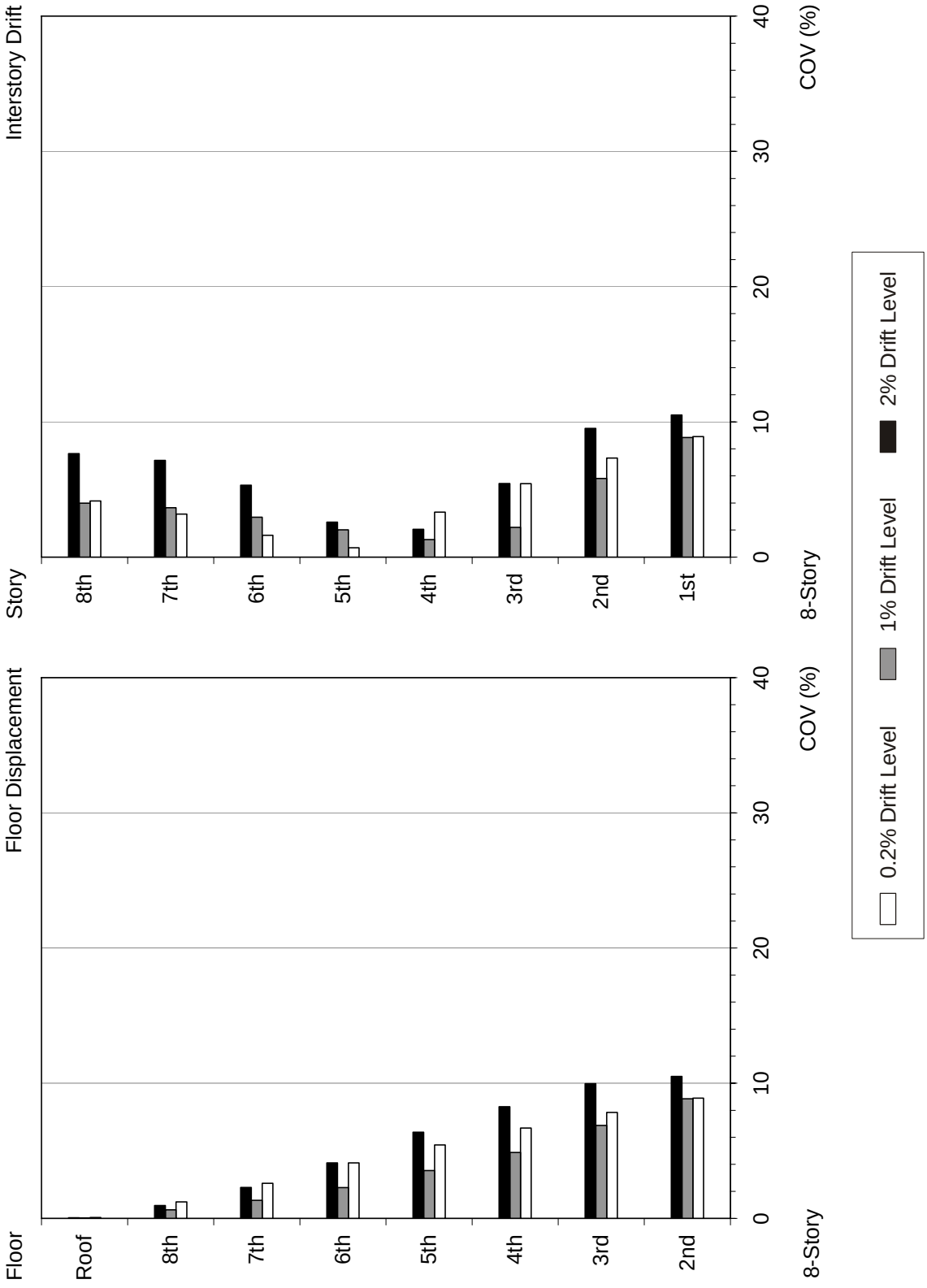


Figure F-79 Observed COVs for the 8-story wall building

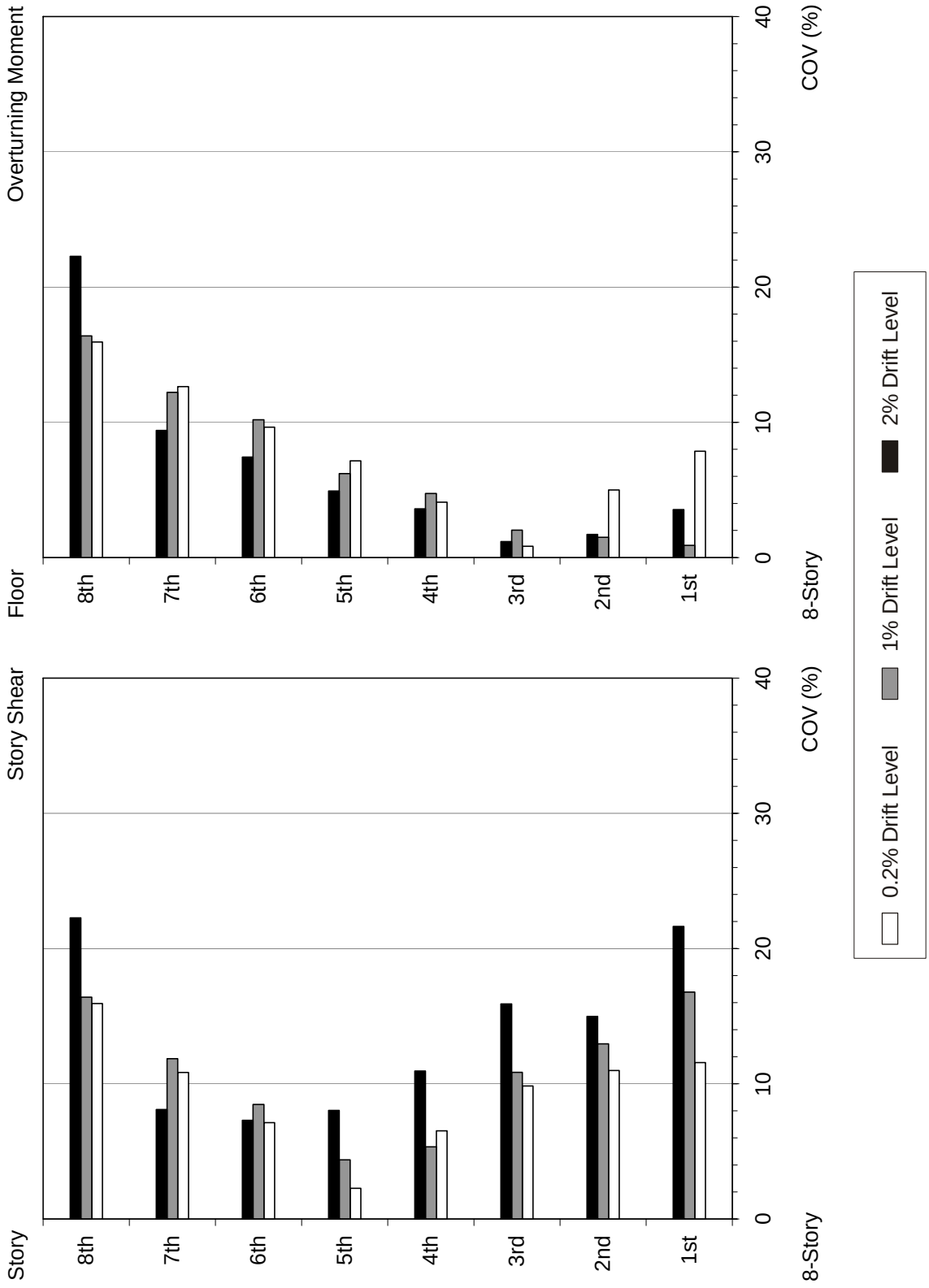


Figure F-79 Observed COVs for the 8-story wall building (continued)

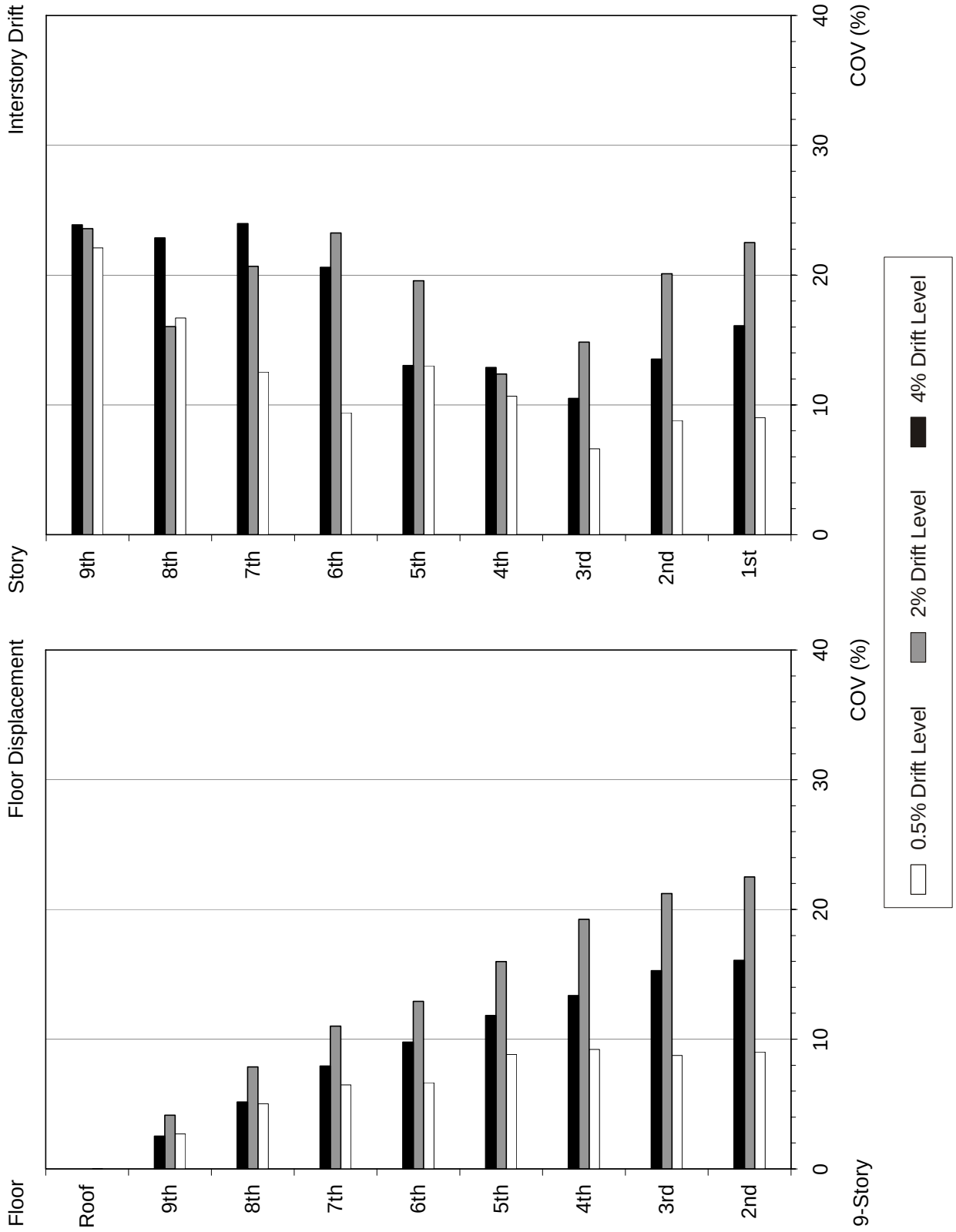


Figure F-80 Observed COVs for the 9-story frame building

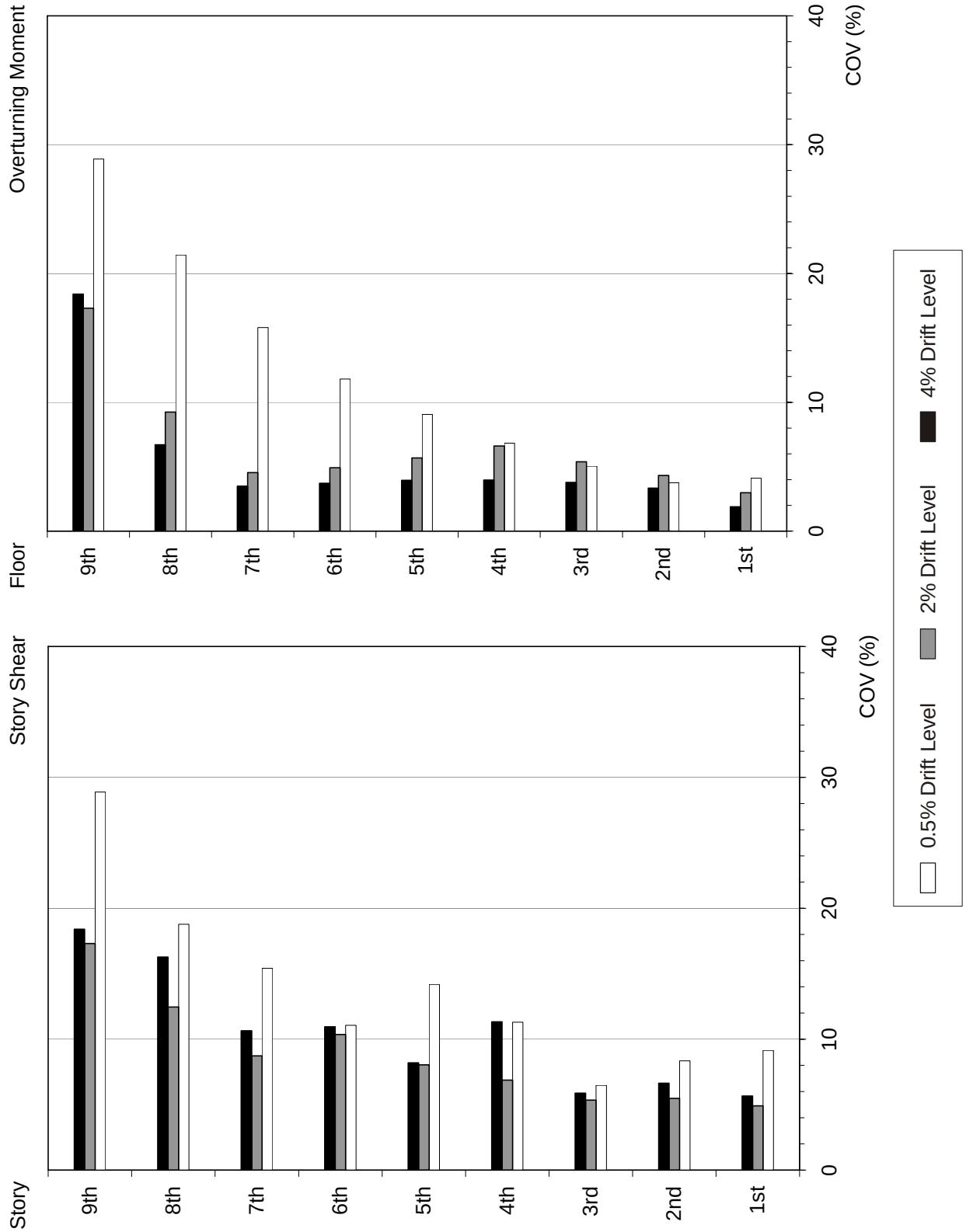


Figure F-80 Observed COVs for the 9-story frame building (continued)

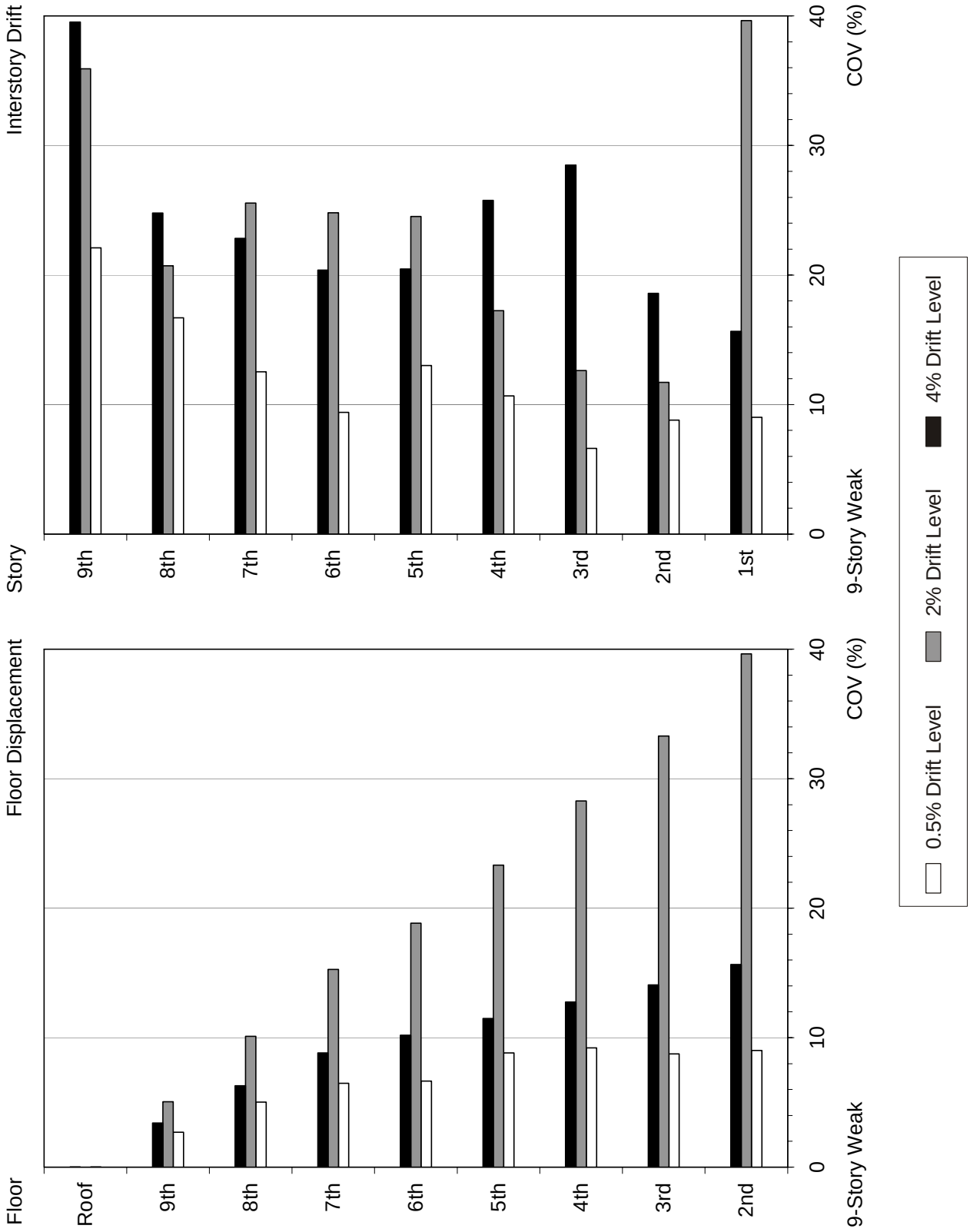


Figure F-81 Observed COVs for the 9-story weak story frame building

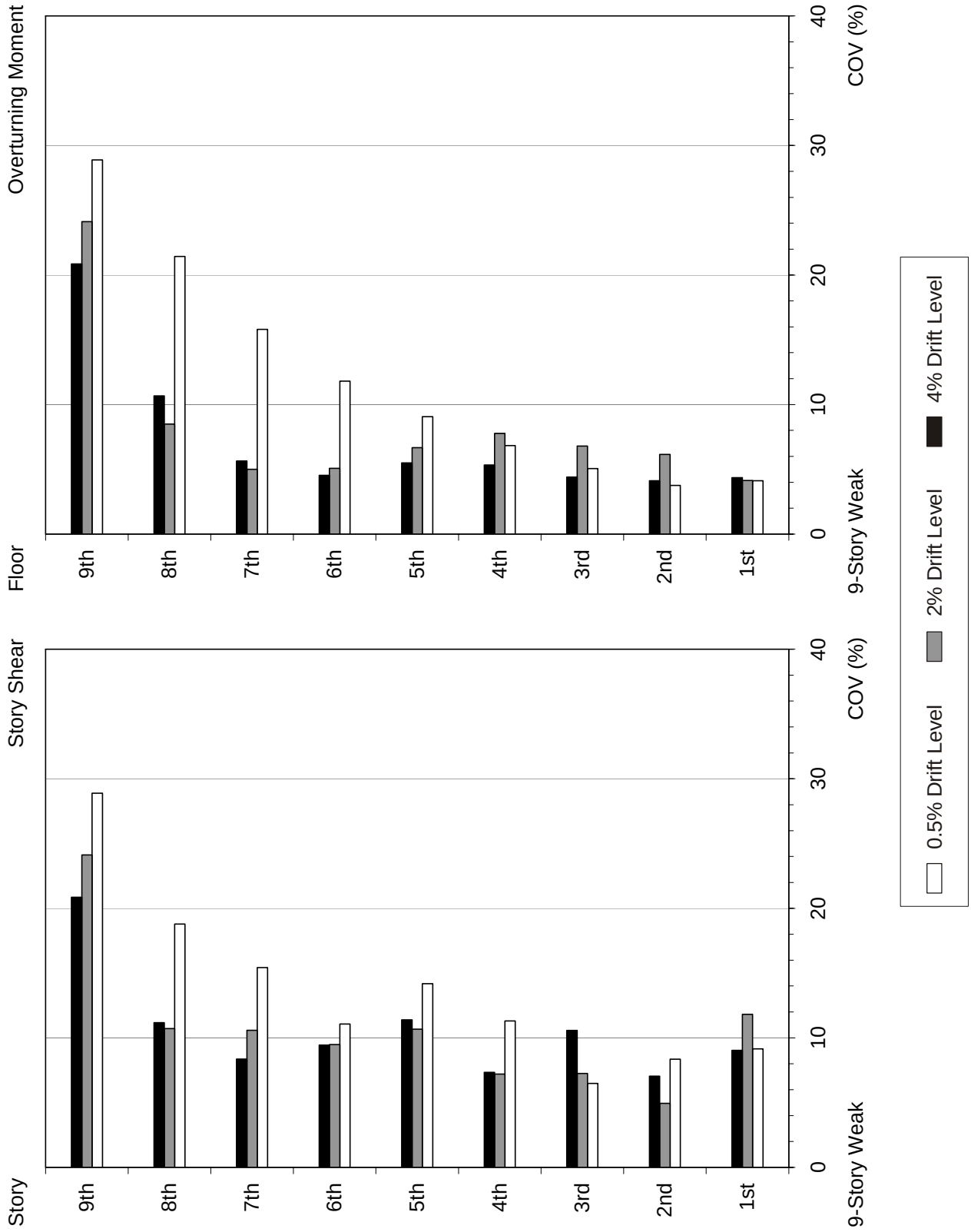


Figure F-81 Observed COVs for the 9-story weak story frame building (continued)

## F.9 References

Chopra, A., and Goel, R., 2001, *A Modal Pushover Analysis Procedure to Estimate Seismic Demands for Buildings: Theory and Preliminary Evaluation* PEER Report No. 2001/03, Pacific Earthquake Engineering Research Center, University of California, Berkeley.

Chopra, A.K., and Goel, R.K., 2002, "A modal pushover analysis procedure for estimating seismic demands for buildings," E*arthquake Engineering and Structural Dynamics*, Vol. 31, pp. 561-582.

Chopra, A.K., Goel, R.K., and Chintanapakdee, C., 2003, "Statistics of single-degree-of-freedom estimate of displacement for pushover analysis of buildings," *Journal of Structural Engineering*, Vol. 129, No. 4, pp. 459-469.

Collins, K.R., Wen, Y.K., and Foutch, D.A., 1995, *Investigation of Alternative Seismic Design Procedures for Standard Buildings*, UILU-ENG-95-2003 Report, Civil Engineering Studies, Structural Research Series No. 600, Dept. of Civil Engineering, University of Illinois at Urbana-Champaign, 187 pages.

Cuesta, I., and Aschheim, M.A., 2001, *Using Pulse R-Factors to Estimate Structural Response to Earthquake Ground Motions*, CD release 01-03, Mid-America Earthquake Center, Urbana, Illinois.

Hernández Montes, E., Kwon, O-S, and Aschheim, M., 2004, "An energy-based formulation for first- and multiple-mode nonlinear static (pushover) analyses," *Journal of Earthquake Engineering*, Vol. 8, No. 1, pp. 69-88.

Iwan, W.D., and Chen, X.D., 1995, "Important near-field ground motion data from the Landers earthquake," *Proceedings 10th European Conference on Earthquake Engineering*, Vol. 1, A.A. Balkema, Rotterdam, pp. 229-234.

Miranda, E., 1991, *Seismic Evaluation and Upgrading of Existing Buildings*, Ph.D. thesis, University of California at Berkeley.

SAC, 2000, *State of the Art Report on Systems Performance of Steel Moment Frames Subject to Earthquake Ground Shaking*, FEMA 355C Report, prepared by the SAC Joint Venture (a partnership of the Structural Engineers Association of California, the Applied Technology Council, and California Universities for Research in Earthquake Engineering) for the Federal Emergency Management Agency, Washington, D.C.

Seneviratna, G. D.P.K., and Krawinkler, H., 1997, *Evaluation of Inelastic MDOF Effects for Seismic Design*, BLUME-120 Report, John A. Blume Earthquake Engineering Center, Stanford, California, 177 pages.

### FEMA Reports

FEMA 368, 2000, *NEHRP Recommended Provisions for Seismic Regulations for New Buildings and Other Structures, Part 1 - Provisions*, prepared by the Building Seismic Safety Council for the Federal Emergency Management Agency, Washington, D.C.